THE UNIVERSITY
of EDINBURGH

Metabolic Regulators of Inflammation in Acute Pancreatitis

Alastair John Hayes

PhD thesis

Supervisor: Professor Damian J Mole

Submission Date: 30-April-2020

Word Count: 60,000

Table of Contents

DECLARATION

I, Alastair John Hayes, declare that the work detailed and described in this thesis has been written by myself and represents my own work. Any contributions from the published or unpublished work of others have been fully acknowledged in the proper manner. This work has not been submitted for any other degree or professional qualification.

Signature: Date of signature:

Mr. Alastair John Hayes BSc Med Sci (Hons), MBChB, MRCS(Ed), MSc

ACKNOWLEDGEMENTS

A very special thank you to my primary supervisor, Professor Damian Mole, who was a constant source of inspiration, enthusiasm and support. I am deeply indebted to Professor Mole for offering me this unique opportunity to undertake my studies in this fascinating field of inflammation, metabolism and drug discovery, and for his support and friendship during the big challenges I encountered. I am most grateful for the guidance, encouragement and inspiration given to me by my other supervisors, Professor John Iredale and Professor Sarah Howie.

An enormous thank you to Dr Xiaozhong Zheng who helped tremendously with many daily aspects of the project and laboratory work. Your great wisdom helped avoid many difficulties, and your experience was indispensable. Another special thank you to Dr Toby Murray who also was a fantastic support, and helped integrate me into the mass spectrometry lab and assisted with the tracer experiments in particular during his year with us as a Masters in Scientific Research student. I would also like to express my gratitude to many others in the University of Edinburgh who helped my overcome many of the technical challenges, including Mrs Shonna Johnston & Dr Will Ramsay (flow cytometry), Mr George Just, Mrs Margaret Binnie, and Dr Natalie Homer (mass spectrometry core facility), colleagues in the centre for

biological services and veterinary colleagues, in particular William Mungall, as well as Dr Forbes Howie (biochemical scientist) Dr James Bailey (murine histology). From the University of Edinburgh department of surgery, a particular thank you to Mr Christos Skouras and Professor James Garden for their support. Thank you to Miss Luclie Neyton and Dr Kenneth Baillie (University of Edinburgh) for sharing their analysis of the transcriptomics data. Although not included in this thesis, a big thank you is due to Dr Natalia Bochkina (University of Edinburgh) for her mathematical expertise with the telemetry data analysis as we complete the write up of this research for peer review publication.

More widely, a big thank you to Dr Iain Uings from GlaxoSmithKline, and his colleague Dr John Liddle, for their great insights into pharmacodynamics/pharmacokinetics, offering very helpful advice, and who supplied the KMO inhibitor compound, GSK898. I would like to thank my peers from the European Pancreatic Club Pancreas 2000 project, were a great source of encouragement and inspiration as many of these friends had either completed or were completing their own doctoral thesis as I was staring my own: Dr Sven-Petter Haugvik, Dr Per Hedenström, Dr Darko Siuka, Dr Roberto Valente, Dr Bjorn Lindkvist and Dr Gabriele Capurso.

I am deeply grateful to my funders, Guts UK (formerly Core), for the Amelie Waring Fellowship award. Without their support none of this would have been feasible and their constructive feedback on progress reports was also very helpful as an external opinion. A particular acknowledgement and thank you to the surviving family members of Amelie Waring, who established this fellowship that supports young investigators in studying pancreatitis. The Amelie Waring Fellowship helps nurture ground breaking pancreatitis research within the UK which is helping develop new ideas and potential treatments that offers hope for this most unfortunate group of patients who develop severe acute pancreatitis.

A particular thank you to my thesis examiners who gave of their time and expertise to digest and assess my work, with helpful comments and suggestions.

Lastly, I would like to express my enormous thanks to my family for their help in so many different ways. My brother, Stuart, helped introduce me to scientific Python computer programming which was a tremendously helpful skill to learn given the large datasets generated by the telemetry data. A special thank you to my parents for their love and support. Thank you to my father for his inspirational enthusiasm for biomedical science, wisdom and advice. Lastly, to my wonderful wife, Karen, a special thank you for all your support and love to get me through.

LAY SUMMARY OF THESIS

The pancreas gland sits behind the stomach and helps with the digestion of food. Acute pancreatitis occurs when the pancreas becomes inflamed, usually after irritation by bile stones from the gallbladder, or excessive consumption of strong alcohol. It is a common reason to be admitted to hospital with abdominal pain. One in five patients will experience a serious attack which involves damage to vital organs, characterised by a dangerous response by the body's immune system. The treatment for those with severe pancreatitis usually consists of supportive therapy in critical care, with intravenous fluids and strong pain killers, but there is currently no specific treatment that can improve the body's response to pancreatitis. The burden on healthcare resources from pancreatitis is substantial and expensive. Despite modern medical practice, at least one in twenty patients die from an attack of acute pancreatitis. Those who are sickest have been shown to have increased blood levels of a potentially harmful bodily chemical called '3HK', which stands for 3-hydroxykynurenine, a breakdown product tryptophan, which is an essential dietary nutrient. The chemical 3HK is made by an enzyme called 'KMO', which stands for kynurenine-3-monooxygenase.

Before starting my project, our research group discovered that blocking the enzyme activity of KMO reduced the harmful effects in a laboratory test model of severe pancreatitis. This potential breakthrough had only been studied at an early stage in the disease, and it was unknown whether KMO blockade could improve recovery beyond 24 hours, and reduced the risk of death.

My research, therefore, focussed on the early disease recovery phase from 24 hours to 7 days. Using experimental models of pancreatitis, I found that artificially increasing blood levels of the 3HK increased susceptibility to critical illness but that blocking the KMO enzyme which produces 3HK, critical illness could be delayed and potentialy reduced. When working with cells in the test tube, bodily inflammation signalling molecules increased cell death when tested with 3HK, but not so with other chemicals related to 3HK. This information supports the theory that 3HK is most toxic during severe inflammation, such as acute pancreatitis. Together these results support the concept that blocking KMO enzyme would reduce the sensitivity of bodily vital organs to inflammation in acute pancreatitis and may improve recovery by reducing multiple organ failure.

ABSTRACT OF THESIS

Acute pancreatitis (AP) is a common inflammatory disease with multiple aetiological triggers, most commonly gallstones and alcohol consumption, but with no specific treatment. One in four patients with AP develop organ dysfunction, requiring critical care support and have a high risk of death. During systemic inflammation, and specifically during AP, there is increased flux through the kynurenine pathway of tryptophan metabolism due to induction of rate-limiting enzymes by inflammatory mediators, leading to elevated circulating 3-hydroxykynurenine (3HK) levels. In clinical AP in humans, plasma 3HK levels correlate with clinical severity. 3HK is hazardous to many cell types, principally through the generation of reactive oxygen species. Production of 3HK can be blocked by inhibiting kynurenine 3-monooxygenase (KMO), the enzyme which catalyses kynurenine hydroxylation. KMO has a prominent role in regulating the systemic inflammatory response during severe AP, but the mechanisms that link metabolism through KMO and systemic inflammation have eluded discovery, until now.

In this thesis, I firstly show that the KMO blockade in genetically-altered mice protects against critical illness and improves recovery in an experimental model of severe AP. This more severe model consisted of 2% sodium taurocholate retrograde ductal infusion along with simultaneous implantation of a moderately invasive telemeter device with chest leads, which monitored heart rate, locomotor activity and body temperature. The telemetry system was required to continuously monitor for clinical signs of recovery and deterioration in this potentially lethal model, and because the pancreatic ductal infusion after the device implantation would not be technically feasible, the device had to be implanted at the same time as pancreatitis induction. I discovered a hepatocyte-restricted role for KMO, where mice generated to lack *Kmo* solely in hepatocytes ($Kmo^{alb\text{-}cre}$) showed elevated plasma kynurenine and 3HK levels, reduced $^{13}C_6$-3-hydroxykynurenine tracer clearance, and transcriptomic alterations in key innate immunity pathways in liver tissue, specifically modulating expression of canonical toll-like receptor pathway signalling genes. Although $Kmo^{alb\text{-}cre}$ mice with elevated 3HK did not significantly differ in pancreas injury metrics, multiple-organ neutrophilia infiltrate or routine biochemistry at an early timepoint (24-hr) using, these mice succumbed fatally earlier and more readily to experimental AP over 7-days using a less severe recovery telemetered model of AP, thus indicating an impaired recovery and increased susceptibility for critical illness. The less severe, recovery model, also utilised 2% sodium taurocholate infusion, but the telemeter device was smaller, lighter and faster to implant and only measured locomotor activity and temperature. Therapeutically reducing 3HK to undetectable levels through

systemic blockade using a highly-specific KMO inhibitor rescued the phenotype, protecting against critical illness and early mortality in the 7-day recovery telemetered model of AP. In vitro, interleukin-1β was found to synergise with 3HK to cause cellular apoptosis, a mode of cell death previously shown to occur in multiple organ failure during experimental severe AP by our research group, thereby demonstrating a cytotoxic effect by 3HK and innate immune mediators.

Together, these findings establish the KMO product 3HK as a modulator of innate immunity that exhibits a complex interaction with inflammatory cytokines during critical illness to promote excess morbidity and death from multiple organ failure that may be rescued by systemic KMO blockade.

ABBREVIATIONS

3HAA	3-hydroxyanthranilic acid
3HK	3-hydroxykynurenine
^{13}C6-3HK	^{13}C6 isotope-labelled 3-hydroxykynurenine
^{13}C6-Kyn	^{13}C6 isotope-labelled kynurenine
AA	Anthranilic acid
AANAT	Aralykylamine N-acetyltransferase
AAs	Amino acids
ACh	Acetylcholine
AhR	Aryl hydrocarbon receptor
AIM2	Absent in melanoma 2
AP-1	Activator protein 1
APACHE II score	Acute physiology and chronic health evaluation II score
ALRs	Absent in melanoma 2-like receptors
ATP	Adenosine 5'-triphosphate
BAPTA	1,2-Bis(2-aminophenoxy)ethane-N,N,N',N'-tetraacetic acid
βME	β-mercaptoethanol
cADPr	Cyclic ADP-ribose
CARS	Compensatory, anti-inflammatory response syndrome
CBT	Core body temperature
CCK1R	Cholecystokinin type 1 receptor
CFTR	Cystic fibrosis transmembrane conductance regulator
CLRs	C-type lectin receptors
CMV	Cytomegalovirus
CNS	Central nervous system
CRP	C-reactive protein
CTRC	Chymotrypsin C
CYP2E1	Cytochrome P450 family 2 subfamily E member 1
D5-KA	Deuterated (3,5,6,7,8-d5) kynurenic acid
DAMPs	Danger associated molecular pattern molecules
DB	Double blank
DHQCA	Dihydroxyquinolinequinonecarboxylic acid
DMEM	Dulbecco's modified eagle medium
DMSO	Dimethyl sulphoxide
EBM-2	Endothelial cell growth basal medium 2
EDTA	Ethylenediaminetetraacetic acid
eIF2α	Eukaryotic translation initiation factor 2 subunit 1
ELAM-1	Endothelial leukocyte adhesion molecule 1
EPI	Exocrine pancreatic insufficiency
ERCP	Endoscopic retrograde cholangiopancreatography
FADD	Fas associated via death domain
FAEEs	Fatty acid ethyl esters
FLP	Flippase
FRT	Flippase recognition target
GABA	Gamma aminobutyric acid

GCN2	General control nonderepressible 2
GPR35	G protein-coupled receptor 35
GSK	GlaxoSmithKline
HAPS	Harmless acute pancreatitis score
HMVEC-L	Human lung microvascular endothelial cells
HPLC	High performance liquid chromatography
HSPs	Heat shock proteins
ICAM-1	Intercellular adhesion molecule 1
ICD-10	10th revision of the international statistical classification of diseases and related health problems
IFNγ	Interferon gamma
IFNβ	Interferon beta
IκB kinase	Inhibitor of NF-κB kinase
IL1β	Interleukin 1β
IP_3R	Inositol 1,4,5-triphosphate receptor
KA	Kynurenic acid
KAT	Kynurenine aminotransferase
KMO	Kynurenine 3-monooxygenase
KP	Kynurenine pathway
LPS	Lipopolysaccharide
Ly6C	Lymphocyte antigen 6 complex, locus C
mAChR	Muscarinic acetylcholine receptor
MIP2	Macrophage inflammatory protein 2
MOF	Multiple organ failure
MPTP	Mitochondrial permeability transmembrane pore
MSD	Meso Scale Discovery
MyD88	Myeloid differentiation primary response protein 88
NAADP	Nicotinic acid adenine dinucleotide phosphate
NAD^+	Nicotinamide adenine dinucleotide (oxidized)
NADH	Nicotinamide adenine dinucleotide (reduced)
$NADP^+$	Nicotinamide adenine dinucleotide phosphate (oxidized)
NADPH	Nicotinamide adenine dinucleotide phosphate (reduced)
NaMN	Nicotinic acid mononucleotide
NaTCA	Taurocholic acid sodium
NEFAs	Non-esterified fatty acids
NF-κB	Nuclear factor kappa-light-chain-enhancer of activated B cells
NLRs	Nucleotide-binding oligomerization domain-like receptors
NNK	Nicotine-derived nitrosamine ketone
NMDA	N-methyl-D-aspartic acid
OHXan	Hydroxyxanthommatin
$P2RX_7$	Purinergic receptor 2X ligand-gated ion channel 7
PANCREA	Pancreatitis across nations clinical research and education alliance
PBS	Phosphate buffered saline
PCR	Polymerase chain reaction
PEG	Polyethylene glycol
PGAM5	Phosphoglycerate mutase family member 5

PLAs	Platelet-leukocyte aggregates
PLP	Pyridoxal 5′-phosphate (active form of vitamin B_6)
PMCA	Plasma membrane Ca^{2+} ATPase
PRRs	Pattern recognition receptors
PRSS1	Protease, serine 1
PSTI	Pancreatic secretory trypsin inhibitor
RIPK1	Receptor-interacting serine/threonine-protein kinase 1
RLRs	Retinoic acid-inducible gene (RIG)-I-like receptors
RM1	Rat and mouse number 1 maintenance
RNA	Ribonucleic acid
RYR	Ryanodine receptor
SLC6A19	Solute carrier family 6 member 19
SLC16A10	Solute carrier family 16 member 10
SLE	Systemic lupus erythematosus
SNP	Single nucleotide polymorphism
SPINK1	Serine protease inhibitor, Kazal type-1
TIRAP	Toll/interleukin-1 receptor domain-containing adaptor protein
TLRs	Toll-like receptors
TRAM	TRIF-related adaptor molecule
TRIF	TIR-domain-containing adaptor inducing IFNβ
TRP	Tryptophan
TDO	Tryptophan 2,3-diozygenase
WHO	World Health Organization
XA	Xanthurenic acid
Xan	Xanthommatin
ZT	Zeitgeber Time

1. INTRODUCTION

1.1. Acute pancreatitis

1.1.1. History of the pancreas gland and pancreatitis

1.1.1.1. Ancient observations of the pancreas

The term 'pancreas', originates from the ancient Greek term 'πᾶν' (meaning '*pan'*, or 'all' in English) and κρέας ('*kreas'*, or 'flesh') meaning '*all flesh'*, on account of the absence of hard matter such as bone or cartilage (1, 2). The term was in use during Aristotle's era (384-322 B.C.), who referred to the gland as the 'so-called pancreas' in his pioneering zoology writings '*Historia Animālium*' (3). The earliest detailed anatomical description of the pancreas is attributed to another Greek scholar, the anatomist Herophilus of Chalceodon (c. 335-280 B.C.), who studied many human and animal organs and is accredited with naming of the duodenum which means 'twelve fingers long'. The pancreas is common to all vertebrates, but the form by which it takes in different species is variable, and can consist of anatomically separate pancreata. The human pancreas is a relatively distinct elongated gland located in the retroperitoneal region of the upper abdomen, with distinct parts referred to as the head, body, and tail. The pancreatic head is in direct contact with the duodenum, whilst the tail abuts the hilum of the spleen (**Figure 1**). For centuries after its identification, the functions of the pancreas remained mysterious, with theories relating to its proximity to the stomach; as a cushion function for the stomach, or that it served to close the pyloric sphincter.

1.1.1.2. Modern-day understanding of the pancreas gland

Under the microscope, the pancreas can be seen to be structurally arranged into distinct lobules composed primarily of the digestive enzyme-producing cells of the exocrine pancreas, named 'acinar cells'; there are also ducts which transmit digestive enzymes into the intestines; and distinct clusters of endocrine cells can also be seen, described as 'islets of Langerhans' (P. Langerhans 1869), that secrete many important hormones including insulin by beta cells. The acinar cells produce pancreatic amylase and an array of lipases and proteases (4). Pancreatic amylase and lipases and are synthesized as active enzymes which catalyse the initial breakdown of carbohydrates and triglycerides, respectively duodenum (5). Trypsinogen is the most important of the protease enzymes because of its central role in regulating all of the others. There are 3 well defined forms of this enzyme: cationic trypsinogen (encoded by *PRSS1* gene), anionic trypsinogen (encoded by *PRSS2* gene), and mesotrypsinogen (encoded by *PRSS3* gene) (4). Cationic and anionic trypsinogens are the major forms with respect to trypsin activity, and these are co-synthesised with pancreatic secretory trypsin inhibitor (PSTI), also known as serine protease inhibitor, Kazal-type 1

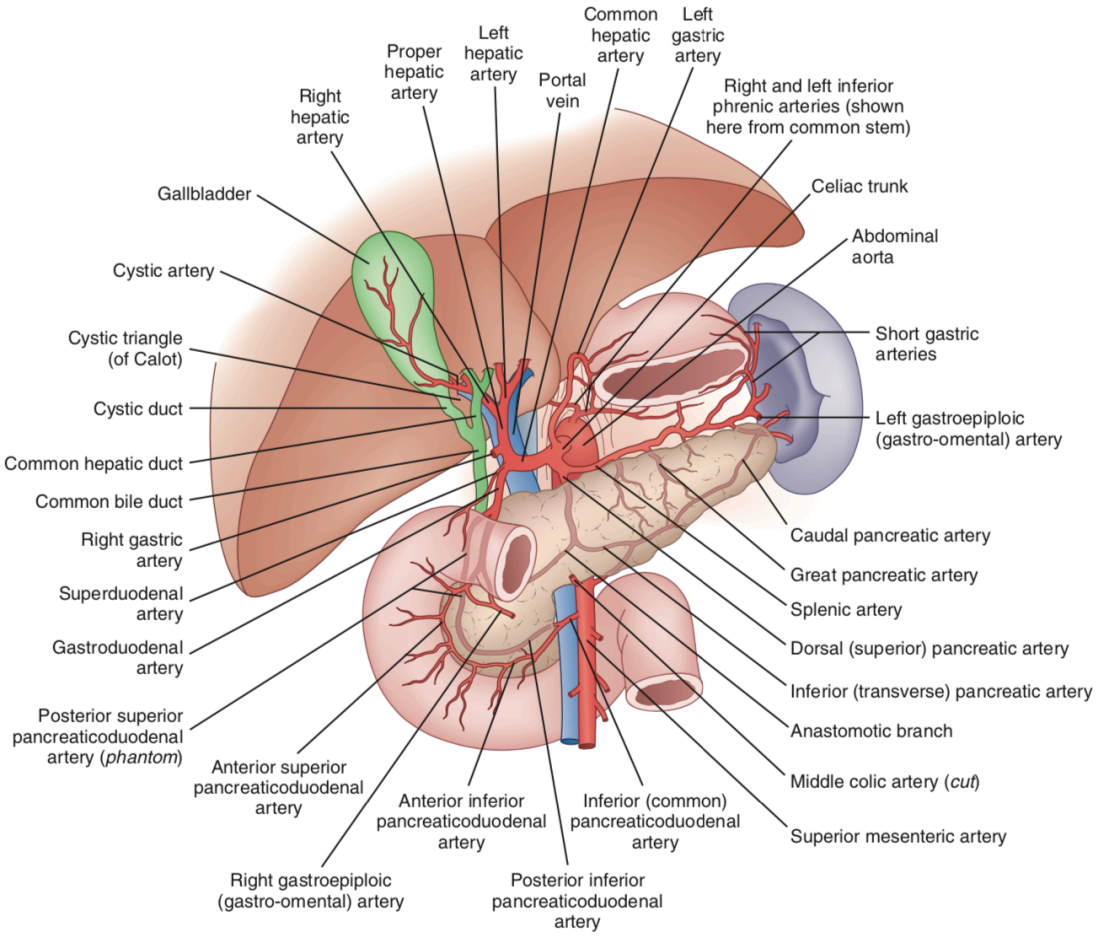

Figure 1. **The human pancreas and its anatomical relations**
The majority of the stomach has been removed in this illustration to give a view of the pancreas gland (centre of image). The duodenal loop surrounds the head of the pancreas and the spleen is adjacent to the tail of the gland. The gallbladder and the proximal part of the common bile duct can be seen below the liver. The plentiful blood supply to the pancreas, spleen and liver is well illustrated in this image from Sabiston Textbook of Surgery, 20th Edition: Chapter 55 'Exocrine pancreas', Figure 55-1 (5). The image was originally from Netter illustration, www.netterimages.com Elsevier Inc.

(SPINK1) (4). Trypsinogens are normally activated in the duodenum thereby producing trypsin, a process which was traditionally thought to be performed by enterokinase (also called enteropeptidase), but controversy exists (4). Activation occurs by cleavage of the trypsinogen activation peptide which then alters the molecular structure and stabilises the trypsin active site; a process that is regulated by feedback control mechanisms and biochemical conditions - principally pH and [Ca^{2+}] (4). Once activated, trypsin catalyses the activation of protease zymogens (i.e. chymotrypsinogen, proelastase, carboxypeptidase) within the duodenum and jejunum by engaging its activation site with the zymogen activation peptide sequence (4). Pancreatic lipase, more precisely known as pancreatic triglyceride lipase (PTL), is also indirectly controlled by trypsin because an enzyme which promotes PTL activity within the duodenum, called 'colipase', is thought to be secreted as a pro-enzyme and converted by

trypsin to its active form in the duodenum. The pancreas also contains connective tissue, derived from the embryonic mesenchyme, which forms the septa that separate the many lobules of the organ and the gland is surrounded by a very thin connective tissue capsule.

Acinar cells are pyramidal in shape, which allows them to cluster around drainage acini and ducts. The acinar cells are responsible for the synthesis, storage and secretion of pancreatic digestive zymogens into the ductal lumen, along with chloride and these cells comprise the majority of the pancreas parenchyma (6). Acinar cells have a high secretory turnover heavily dependent on mitochondrial production of adenosine triphosphate (ATP). The ductal cells produce bicarbonate-rich fluid which help transport the enzymes through the ductal system and into the duodenum (5). The primary functions of the pancreatic ductal cells are to provide the water (H_2O) and electrolytes, including bicarbonate (HCO_3^-), required to dilute the pancreatic digestive enzymes and deliver these into the duodenum (5). Intracellular carbonic anhydrase catalyses the conversion of H_2O and CO_2 into HCO_3^- and H^+ within pancreatic ductal cells, and from the apical membrane of the ductal cells HCO_3^- is secreted into the ductal lumen (5). The delivery of bicarbonate into the duodenum is important for neutralisation of hydrochloric acid secreted by gastric parietal cells, because the pancreatic digestive enzymes require an alkaline environment for catalytic activity (5). The complex neurohormonal mechanisms which control activity of the exocrine pancreas starts with the cephalic phase, whereby upon sight and smell of food the brainstem stimulates the pancreas to secrete, which is followed by stimuli from gastric distension and duodenal stimulation from secretin and cholecystokinin release.

1.1.1.3. Historical descriptions of the inflamed pancreas

The earliest surviving description of an acutely inflamed pancreas is often attributed to a Huguenot doctor, Iacobo A Vindone, who when living in Basel, Switzerland in 1579 reported his post-mortem findings in an alcoholic with pancreatic necrosis (7). Much later, the famous Dutch surgeon, anatomist, writer and politician, Nicolaes P Tulp, published in 1652 in his '*Observationes medicae*' a clinicopathological report of a pancreatic abscess (7). In 1815, G Fleischmann reported his autopsy findings linking pancreatitis and alcohol. In 1887, Reginald Fitz from Boston, USA delivered a lecture reporting the systematic review of 53 patients with pathologically documented acute pancreatitis, entitled "*A consideration of Pancreatic Hemorrhage, Hemorrhagic, Suppurative, and Gangrenous Pancreatitis, and of Disseminated Fat-Necrosis*" (2). W. Korte (1899), was the first to consider gallstones as a trigger of pancreatitis, although EL Opie (1901), a pathologist at Johns Hopkins Hospital in Baltimore, proposed the that reflux of bile into the pancreatic duct induced AP (7).

1.1.2. Pathobiology of acute pancreatitis (AP)

Investigation into the initial molecular events which lead to human AP is inherently problematic, but nonetheless several noteworthy discoveries have been made. Evidence of pathological events are based upon data derived from *in-vitro* cell-based studies (mostly investigating acinar physiological mechanisms), models of the disease in laboratory animals (mostly rodents), which are informed by clinical observations.

1.1.2.1. Experimental AP

The four most frequently used acute pancreatitis model-types in rodents comprise: i) secretagogue hyperstimulation; ii) retrograde pancreatic ductal infusion; iii) nutrient-induced pancreatitis and; iv) the amino acid induction models (e.g. L-arginine) (8-10). The intra-ductal infusion models commonly consist of a dilute bile acid infusate containing taurolithocholate, taurodeoxycholate or taurocholate (11-14). The commonly utilised experimental models of AP are listed in **Table 1**. The choice of AP model for any given study will not only depend on scientific issues, but any given laboratory group may have preferences influenced on prior experience and indeed by animal licencing regulations. The severity of each model can be quite variable depending on the animal species used, any genetic alteration in the host animal, the dosing protocol and the use of adjunct sensitizer treatments. There is a catalogue of genetically engineered mouse models which can produce inflammatory changes targeted to the pancreas, using various genetic engineering systems, but which lack the systemic proinflammatory effects that are more commonly seen in the above four listed AP model-types (15). With the retrograde pancreatic ductal infusion models, increased concentrations of

Model type	Example	Severity	Refs
Secretagogue hyperstimulation +/- sensitizer	Cerulein injections (CCK analogue) +/- alcohol, LPS, obesity, GDOC, duct obstruction	Mild to lethal depending on cerulein and sensitizer dosing	(16)
Bile acid infusion of pancreatic duct	Glycodeoxycholic acid (GDOC) Sodium taurocholic acid (NaTCA)	Potentially lethal*	(11-14, 17)
Diet-induced AP	Choline-deficient ethionine (CDE) diet	Potentially lethal*	(17)
Amino acid-induced AP	L-arginine, L-lysine, L-ornithine	Potentially lethal*	(9, 10)
Pancreatic duct obstruction +/- secretagogue	Ligation of common biliopancreatic duct +/- caerulin	Mild to moderate - variable due to species used & duration of ligation	(17)

Table 1: Commonly used experimental AP rodent models
*potentially lethal at high doses.

infused bile acids and flow rates are associated with increased pancreatic and extra-pancreatic organ injury which can produce severe disease with multiple-organ injury and lethality. Given Professor Mole group's considerable experience with the intraductal infusion model, with its capacity to induce extra-pancreatic organ injury but with the option to adjust the severity of the model, this was the chosen model for my work.

1.1.2.2. Acinar cell events in physiology and disease

During the past half-century, many fascinating discoveries have been made which give mechanistic insights into the physiological workings of the pancreas. Whilst pancreatic ductal cells have a recognised contributory role in AP (see Hegyi *et al.* (6)), here I focus upon the acinar cells, as these are the dominant cell-type in the pathogenesis of AP.

1.1.2.2.1. Acinar cell physiology

Other than the transport of chloride into the ductal system, the biological activity of acinar cells is to synthesise and secrete digestive enzymes and pro-enzymes. In eukaryotic cells, exocytosis is generally activated by a spike in cytosolic Ca^{2+} concentrations ($[Ca^{2+}]i$). Because pancreatic acinar cells do not possess voltage-gated plasma membrane channels, such as those on neural and endocrine cells, the large and rapid Ca^{2+} cytosolic concentration spikes required for stimulus-secretion coupling is mostly delivered from cytoplasmic Ca^{2+} storage compartments (**Figure 2**). Additionally, one research group have recently reported their novel and very interesting findings of a plasma membrane mechanoreceptor, Piezo1, which upon mechanical stimulation forms a pore that facilitates acinar cell Ca^{2+} influx (18). The initial stimulatory response spike in $[Ca^{2+}]i$ is independent of extracellular Ca^{2+}, but as intracellular stores are depleted, and cytosolic Ca^{2+} having been extruded (in order to avoid cytotoxic levels) extracellular Ca^{2+} supply becomes increasingly critical in order to sustain secretion (19). Acinar cells have a special type of store-operated channel (SOC) called a Ca^{2+} release-activated Ca^{2+} (CRAC) channel which allows Ca^{2+} entry into the cells to replenish cytoplasmic stores (20). $[Ca^{2+}]i$ also regulates chloride channel opening and repeated Ca^{2+} spikes are important for efficient mitochondrial generation of ATP (21). Both chloride transport and zymogen granule exocytosis occur through the apical plasma membrane where they are secreted into the acinar lumen and ductal system.

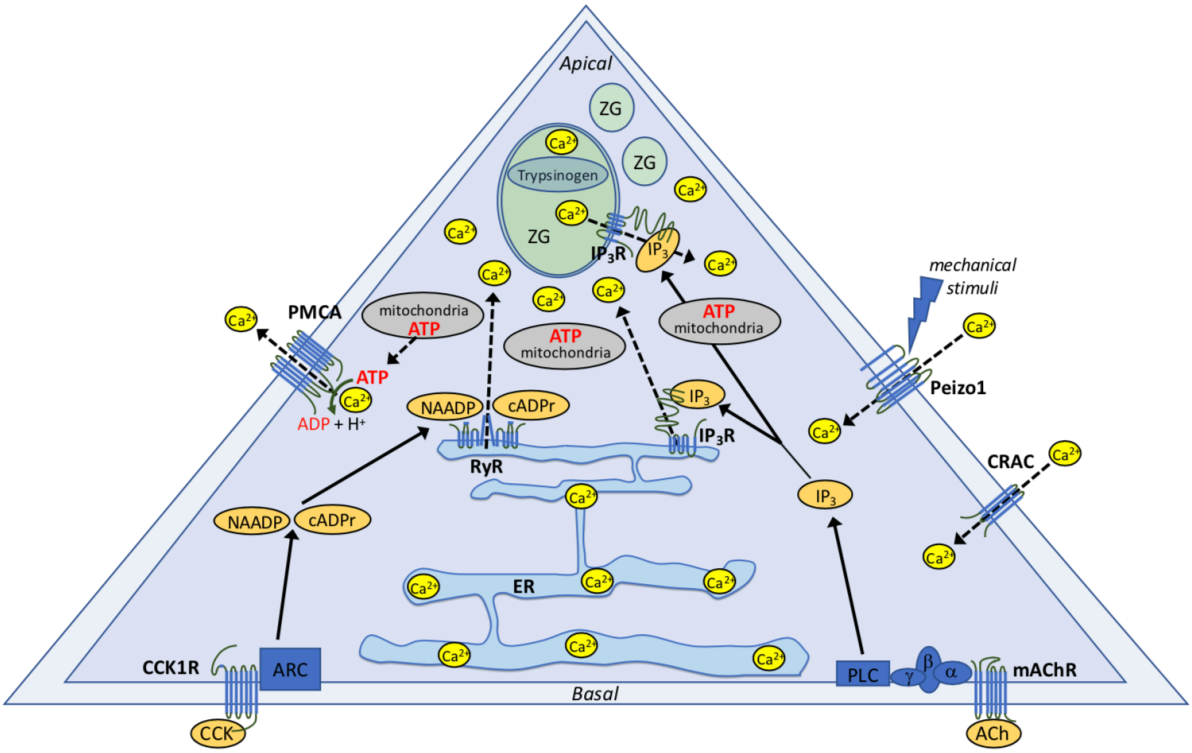

Figure 2: Overview of calcium signalling in pancreatic acinar cells
Movement of Ca^{2+} is indicated by dotted arrows. Abbreviations: ACh: acetylcholine; ADP: adenosine diphosphate; ATPase: adenosine triphosphate; CCK1R: cholecystokinin 1A receptor; CRAC: Ca^{2+} release-activated Ca^{2+}; mAChR: muscarinic acetylcholine receptor; PLC: phospholipase C; PMCA: plasma membrane Ca^{2+}-activated ATPase. Copyright © 2020 AJ Hayes.

The main site of cytoplasmic Ca^{2+} storage is the endoplasmic reticulum (ER), but other organelles, such as zymogen granules (ZGs), also contribute Ca^{2+} to the cytosol (**Figure 2**) (22). Although the ER is mostly located in the basolateral area of the acinar cells, it has long, thin extensions which extend into apex where the secretory ZGs are located. There are two well characterised Ca^{2+} channels which mediate Ca^{2+} release from cytoplasmic stores (e.g. ER) into the apical area of the acinar cell – inositol triphosphate receptor (IP3R) (23) and the ryanodine receptor (RYR) channel (24). Nicotinic acid adenine dinucleotide phosphate (NAADP) from NADP and cyclic ADP-ribose (cADPR) from NAD activate RYR channels, and this is typically initiated by the hormone cholecystokinin binding the CCK1 receptor on the acinar plasma membrane (25). Inositol triphosphate (IP3) is a water-soluble messenger compound generated by receptor-activated phospholipase C that binds the IP_3R, and this is typically initiated by the neurotransmitter acetylcholine (ACh), from vagal stimulation, which binds the plasma membrane muscarinic ACh receptor (23, 26).

Acinar cells contain high numbers of mitochondria, which supply ATP for critical functions including secretory processes and for the plasma membrane Ca^{2+}-activated ATPase (PMCA) pumps which allow acinar cells to extrude toxic levels of Ca^{2+}. Importantly, acinar mitochondria are distributed in a very specific 'belt-like' manner that creates a diffusion barrier between the apex where the cytosolic Ca^{2+} concentrates spike, and the basal part of the cell that contains the nucleus. Another noteworthy factor which protects against cytotoxic Ca^{2+} levels is Calmodulin, which is a protein that binds calcium and organelle release of Ca^{2+} through its inhibitor effect on calcium releasing channel, the aforementioned IP3R (20, 26, 27).

The human pancreas secretes three isoforms of trypsinogen, encoded by the *serine protease* (PRSS) genes 1, 2 and 3 (28). Trypsinogen is normally inactive until it is cleaved by enterokinase in the intestinal lumen to make active trypsin in the duodenum by proteolysis of its 8 amino acid-long N-terminal activation peptide (29). Acinar cells have a number of inbuilt protective mechanisms to avoid excessive intracellular trypsin activity; namely: i) Synthesis of trypsin in the inactivated form (trypsinogen); ii) Compartmentalisation of trypsinogen in zymogen granules (ZGs); iii) Autolysis of activated trypsin; iv) Synthesis of specific trypsin inhibitors which delay trypsinogen autoactivation (e.g. serine protease inhibitor Kazal type 1: encoded by *SPINK1* gene) or can catalyse trypsinogen breakdown (e.g. chymotrypsin C) (29); and v) Prevention of globally elevated cytosolic Ca^{2+} concentrations which promote trypsinogen activation. The second of these, isolation of trypsinogen in ZGs, protects trypsinogen from Cathepsin B which is a lysosomal enzyme that can activate trypsinogen to trypsin (30). With respect to iv), active chymotrypsin C (CTRC) (activated by trypsin from chymotrypsinogen C) and trypsin can act in concert to irreversibly degrade trypsinogen thereby mitigating the development of trypsin activity, but paradoxically they can both also activate trypsinogen to trypsin depending on the particular peptide bonds which are cleaved (29, 31).

1.1.2.2.2. Acinar cell injury

Before considering the he earliest molecular events that are specific to various aetiologies, it is helpful to review the core biological acinar features which appear to be common to all initiating causes of AP. There are three key pancreatic acinar cell mechanisms implicated in the pathogenesis of AP, which consist of:

i) Abnormal elevations in cytosolic Ca^{2+} concentrations
ii) Mitochondrial dysfunction
iii) Intra-acinar conversion of digestive proteases from inactive zymogens into their active forms (32, 33).

As discussed above (1.1.2.2.1.), spikes in the concentrations of cytosolic Ca^{2+} within the apical area of the acinar cell are physiological, but Ca^{2+} overload results in cellular dysfunction which may lead to cell death. The generation of excessive $[Ca^{2+}]i$ signalling has been shown to be elicited by unphysiologically elevated concentrations of ACh or CCK, by long-chain fatty acids (FAs) or fatty acid ethyl esters (FAEEs), or by bile acids (34). The central importance of Ca^{2+} in the pathogenesis of AP has been demonstrated by treatment with a selective Ca^{2+} chelator agent which prevents many of the features of AP (26, 35-38). Additionally, pharmacological inhibition of plasma membrane Ca^{2+} entry channel, CRAC, has been demonstrated to be cytoprotective for acinar cells exposed to experimental AP stimuli (39). Mitochondrial Ca^{2+} overload reduces ATP production, the energy substrate for Ca^{2+} pump activity at the ER and plasma membrane (i.e. PMCA pumps), thereby disarming the protective defences and further elevating $[Ca^{2+}]i$ (6). The vicious cycle of increasing $[Ca^{2+}]i$ leads to acinar cell toxicity, large endocytic vacuolization, intracellular trypsinogen activation and cell necrosis (6, 32).

Secondly, mitochondria play at least 2 vital physiological roles for the acinar cells (detailed in 1.1.2.2.1.); i) The biosynthesis of ATP and ii) As a chain, the mitochondria act as a Ca^{2+} diffusion barrier 'fire-wall' preventing cytotoxic global cytoplasmic elevations in Ca^{2+}. A non-specific mitochondrial channel that traverses the outer and inner mitochondrial membranes, called the mitochondrial permeability transition pore (MPTP), is known to open during high $[Ca^{2+}]i$, especially when accompanied by oxidative stress, which causes loss of mitochondrial membrane potential, termed 'depolarisation', which causes ATP depletion and necrosis (33, 40-43) . MPTP opening promotes cleavage of phosphoglycerate mutase family member 5 (PGAM5) from the inner mitochondrial membrane which also activates necrosis (40). Additionally, a heme protein normally located between the inner and outer mitochondrial membranes that functions in the electron transport chain, called Cytochrome c, is also released in response to elevated $[Ca^{2+}]i$ and activates a series of caspases which induce apoptosis. MPTP inhibitors such as cyclosporin A, are able to prevent cytochrome c release thus inhibiting caspase activation and apoptosis (44).

Cyclophilin D is a mitochondria-specific peptidyl-prolyl isomerase plays a negative role in the production and efficient transmission of mitochondrial energy to the cytoplasm, though a number of mechanisms, including MPTP regulation (45, 46). Although mitochondrial dysfunction results from unphysiologically elevated $[Ca^{2+}]i$, this is not the sole mechanism in AP, however, and cyclophilin D is another important factor. The formation of a complex

between cyclophilin D and ATP synthase, a mechanism that does not require [Ca^{2+}] overload, has also been observed in AP (47). Impaired autophagy, endoplasmic reticulum (ER) stress and deregulated acinar lipid metabolism which are all found in acinar cells in AP are all mediated by mitochondrial dysfunction and can be normalised by cyclophilin D knockout (47). Cyclophilin D inhibitors have shown promise as a potential pancreatitis drug target to reduce acinar cell damage by mitochondrial protection (40, 46). Trypsin-mediated trypsinogen activation within the pancreas is referred to as 'autoactivation' and increases acinar trypsin activity. Inappropriately high levels of trypsinogen autoactivation within the acinar cell can precipitate activation of several enzyme types, as well as the complement and kinin pathways, resulting localised acute inflammatory changes (48). Intra-pancreatic trypsin activity is highly regulated and failure of the various protective mechanisms contribute of the development of AP.

Starting with trypsinogen, the strongest disease-causing mutations are in the cationic trypsinogen gene (*PRSS1*) and are more typically associated with chronic pancreatitis than AP, as autosomal dominant hereditary pancreatitis (28, 49). Briefly, functional mutations in *PRSS1* are known to give rise to acinar cell injury and pancreatitis by increasing intracellular trypsin activity in 3 ways (**Table 2**). In light of CTRC's important role in trypsin activity regulation, it is not surprising that loss-of-function *CTRC* gene mutations may increase risk of pancreatic inflammation (52). Such mutations have one of three functional defects in CTRC activity: i) impaired CTRC protein secretion (and causing ER stress); ii) impaired catalytic activity; and iii) impaired proteolytic stability (50). The CTRC-independent mechanism was discovered most recently, and has been re-created as a genetically-altered mouse model with mutant D23A of the murine T7 gene, which is analogous to the D22G mutation in human *PRSS1* (51). Although trypsinogen-trypsin dynamics are more relevant to chronic AP, there is likely a contributory role in acute inflammation given that protection is observed in experim-

Primary mechanism	**CTRC**	**Effect of mutations**	**Mutant examples***	**Refs.**
Increase trypsinogen	Involved	Block CTRC-dependent trypsinogen degradation	N29I, N29T, V39A, R112C, R122H	(31)
Increase trypsin	Involved	Increase autoactivation by CTRC-mediated cleavage of the trypsinogen activation peptide (at the N terminus)	A16V, N29I	(31, 51)
Increase trypsin	Independent	Directly stimulate autoactivation independent of CTRC	D19A, D20A, D22G, K23R	(52)

Table 2: Functional genetic mutations in *PRSS1* which increase trypsin activity
*human mutations

-ental AP with absent trypsinogen isoform-7 gene (mouse cationic trypsinogen) from supramaximal caerulein-induced acinar injury (53). SPINK1 binds trypsin and thereby prevents the latter from interacting and potentially activating further trypsinogen (although trypsin also contributes to trypsinogen degradation). Trypsinogen autoactivation is thereby delayed until the SPINK1 is saturated and newly formed trypsin is free to potentially autoactivate trypsinogen. Functional mutations in the *SPINK1* gene have also been found to impair SPINK1 function leading to increased intra-acinar trypsin activity and such mutations are well known for their prevalence in hereditary forms of chronic pancreatitis (see section 1.1.4.3.)

Additionally, impaired autophagy, ER stress and dysregulated acinar cell lipid metabolism are also known to contribute to acinar cell stress and promote the three key pathological hallmarks described above (47, 54). Beyond these recognised acinar hallmarks, other harmful features have been observed in AP, most notably the autodigestive dysfunctional processing of secretory granules with the release of endocytic vacuole content into the cytosol or abnormal basolateral membrane exocytosis (into the gland!), as opposed to physiological secretion through the apical membrane and onwards into the ducts and duodenum (55).

1.1.3. Epidemiology and demographics of acute pancreatitis

The estimated worldwide incidence of acute pancreatitis (AP) has been calculated to be 34 cases [95% confidence interval (CI) 23-49] per 100,000 general population per year (56). The disease predominantly affects middle-aged or older people. Amongst children, the incidence stands at 3-13 cases per 100,000 population per year (57). Pooled analyses of global data found equivalent incidence of AP between adult men and women (56). However, with increase age, there is an increasing preponderance towards males (58). Across the globe differences exist in regard to incidence of AP, with North America and Western Pacific regions having a higher incidence (58). Europe has a relatively low incidence (29 cases per 100,000 general population per year), but Northern and Eastern parts of Europe have higher rates (58). In the United Kingdom, the reported incidence of AP has ranged from 5 to 42 cases per 100,000 general population, and has been slowly increasing over recent decades (59-62). Similar to other countries, the overall gender distribution for AP is approximately equal (47% female) in Scotland, but there is slight male preponderance for those with severe AP (63). As with other diseases provoked by an array of inducers, the population's epidemiological characteristics are defined by the aetiological factors (63).

1.1.4. Aetiology of acute pancreatitis

There are great number of published clinical reports that allege possible causes of AP. The identification and isolation of aetiology, particularly in humans, has many challenges and studies often have many limitations. Moreover, the distinction between inducers of AP, as opposed to risk factors becomes increasingly less distinct where aetiological factors are rare. A mnemonic frequently cited in undergraduate textbooks (e.g. The Oxford Handbook of Clinical Medicine, 5th edition) or other educational materials which serves as memory-recall aid for the aetiological factors in AP is 'I GET SMASHED'. I have adopted this mnemonic here for two reasons. Primarily it is easily remembered, and will best help the reader recall the details which follow. Secondly, I have used this mnemonic in a modified fashion, with the addition '& Smoke' (**Table 3**) to underline the contribution of cigarette smoking as a modifiable aetiological factor for recurrent AP, and the synergistic effect between smoking and alcohol for non-gallstone AP. Prior to reviewing the individual aetiological factors sequentially using the mnemonic as a framework, the descriptive epidemiological factors (i.e. age, sex, ethnicity and geographical location), can be helpful to understand at the outset, and are therefore separately discussed first.

I: Idiopathic

G: Gallstones (especially calculi ≤ 5 mm) & Genetic mutations (64)
E: Ethanol/ alcohol (especially spirits) (65)
T: Trauma (66) & obstructing Tumours of the pancreas

S: Surgery & Steroids (67)
M: Mumps & other infectious triggers (68-70)
A: Autoimmune
S: Scorpion stings
H: Hypercalcaemia / Hyperlipidaemia (metabolic) (71)
E: ERCP-induced pancreatitis
D: Drug side-effect (69, 70, 72)
&
Smoke (duration of cigarette smoking associated with increased non-gallstone AP risk) (73)

Table 3. Aetiology of acute pancreatitis – I GET SMASHED & Smoke
A popular mnemonic often cited in undergraduate textbooks (e.g. The Oxford Handbook of Clinical Medicine, 5th Edition; pg 466) to recall the causes of acute pancreatitis is 'I GET SMASHED'. This is extend here to include '& Smoke' to highlight the aetiological importance of cigarette smoking with regards to AP, recurrent AP and chronic pancreatitis (74), and the synergistic detrimental effects of alcohol ('getting smashed') together with smoking.

1.1.4.1. Descriptive epidemiology of AP

In adult populations, the most frequent triggers of AP are gallstones or alcohol consumption, whilst amongst children non-malignant biliary tract diseases are the most frequent cause of AP, accounting for ~1/3rd of cases (57, 75). Unlike adults, alcohol is rarely reported as a trigger in paediatrics (57, 75). Blunt abdominal trauma, systemic diseases (e.g. autoimmune), infections, drugs, and genetic causes are other frequent causes within the paediatric population which are described in the relevant sections below (57).

Most studies report an increased proportion of gallstone aetiology amongst females, and a higher proportion of alcohol-related AP amongst males (63, 76). Females also appear to be at slightly increased risk of AP after ERCP compared to males (77). There does not appear to be sex preponderance in drug-induced AP or genetic causes (78). However, primary hyperparathyroidism (pHPT) is more prevalent amongst females, and there is considerable evidence that pHPT is a risk factor for AP (79).

With regards to ethnicity, a large (n = 70,231 hospitalised AP patients) observational epidemiological study from California, USA showed statistically significant differences between ethnic groups (76). After data standardisation, African Americans had a higher incidence of alcohol-related AP, and a lower biliary AP rate compared to white Americans (76). Asians had a very low standardized incidence rate of alcohol-related AP, and Hispanics had the highest rates of biliary AP (76).

Geographical differences in AP aetiology relate to complex interactions between many aetiological factors including population demographics, alcohol consumption, ethnicity, immunisation programs (e.g. Mumps), and local prevalence of AP-related infectious diseases (particularly parasitic causes) (68, 80). Limitations in access to diagnostic services, such as radiological and endoscopic ultrasound technologies, in some parts of the world likely bias the aetiological classifications reported.

1.1.4.2. Gallstone-related AP

Across Europe, ~10% adult males and ~20% adult females have calculi in the gallbladder or biliary tract (81). For those with asymptomatic gallstones, it has been estimated that over a 30-year period, the risk of biliary pancreatitis would be no more than 2% (82). The prevalence of gallstones increases with age, and is higher in women than in men across all age groups (81). There are many recognised risk factors for gallstone disease besides sex and ethnicity, include genetic risk factors, metabolic syndrome, physical inactivity, rapid weight loss, dietary factors, gallbladder hypomotility, drugs, liver cirrhosis, Crohn's disease (81, 83). The accessibly of surgical services to removal of the gallbladder (cholecystectomy) or

endoscopically extract ductal stones by endoscopic retrograde cholangiopancreatography (ERCP), is an important factor for reducing the incidence of biliary AP, particularly rates of recurrent biliary AP. Gallstones may be asymptomatic but can be complicated by biliary colic, cholecystitis, jaundice and AP. Despite the higher female : male ratio of gallstone prevalence (~2-fold), the rate of biliary pancreatitis amongst patients at risk of biliary pancreatitis (i.e. non-cholecystectomy cohort with gallstones) was 20% higher for males than females (82). Small gallstones (i.e. <5 mm) pose an increased risk of AP (84), as large stones which form within the gallbladder may be too big to pass through the cystic duct and into the common bile duct. Reported in 1974, Acosta *et al.* tested his hypothesis that calculi migrating through the ampulla induced AP by systematically examining the faeces of AP and acute biliary patients, looking for gallstones (85). 34 pancreatitis patients had faecal gallstones (94%), as compared to only three biliary controls (8%) (85). The proportion of AP cases attributable to gallstones reported in European national studies has been just less than half of all pancreatitis patients (44% in Sweden, Hungary and Scotland) (63, 65, 86). Large-scale AP studies often do not specify what proportion of gallstone-related pancreatitis patients were or were not induced by ERCP, which is a well-recognised complication of the procedure. AP complicates 5-10% of ERCP procedures, but there are recognised risk factors related to the procedure or patient, such as difficult cannulation, multiple injections; patients who are young, female or have previously had pancreatitis (8, 87).

It is widely accepted that biliary pancreatitis is initiated by the migration of stones through the ampulla of Vater (85), but the underlying mechanism has been heavily debated. Since the presence and passage of bile duct stones, without pancreatitis, is not an uncommon clinical situation there must be specific requirements, or additional factors, necessary to potentiate acinar cell injury sufficient to cause clinical pancreatitis (e.g. stone/duct features, duct occlusion time, sphincter of Oddi function, pancreas health, smoking etc). The three configurations by which a migrating gallstone could theoretically induce pancreatic injury are well-illustrated in a review by Lerch and Gorelick (reproduced in **Figure 3**) which shows:

A. Isolated pancreatic duct obstruction
B. Common channel theory
C. Dual ductal obstruction (9)

It has been shown that in addition to passive diffusion, bile acids can be taken up by acinar cells via bile acid transporters or G-protein-coupled, cell surface bile acid receptor (Gpbar1) (88). With the presumption that refluxing bile acids reach the ductal and acinar cells, investigators have reported several interesting mechanisms demonstrating how bile-acids can

induce pancreatic cellular damage (6). Low dose luminal administration of bile acids can stimulate a protective bicarbonate and fluid secretion effect, which is calcium dependent (38). High concentrations of luminal bile acid inhibit ductal secretion and induce toxic elevations in Ca^{2+} concentrations (38). On reaching acinar cells, bile acids mobilise Ca^{2+} from endoplasmic reticulum (36, 90), and apical acidic Ca^{2+} stores (91) increasing cytosolic Ca^{2+} concentrations.

There are notable objections to the simplistic assertion that contaminating biliary reflux up the pancreatic ductal system induces pancreatitis when considering the real-life human situation. Specifically, because the pancreatic secretory pressure is physiologically higher than that of the bile duct, pancreatic secretions would preferentially enter the biliary tree, and not the other way around, at least for the first few hours after ampullary obstruction should a common biliopancreatic channel exist (92, 93).

Any bile that would enter the pancreatic ductal tree must overcome the stimulatory 'flushing away' effect which bile acids are known to induce in ductal cells (at low but not high concentrations) (38), before the bile acids can reach the acinar cells (6, 11). It has been shown that elevated pancreatic ductal pressures can cause upstream impaired acinar cell zymogen granule exocytosis resulting in granules to coalesce with intracellular lysosomes resulting in autodigestive pancreatic injury (94). After prolonged obstruction at the ampulla, pancreatic ductal pressures begin to fall and by 24 hours may be equivalent to biliary pressures. By which time, the obstructed bile-pancreatic juice mixture may become activated (i.e. bile salts activation of trypsinogen) with enhanced toxicity to the pancreas (93).

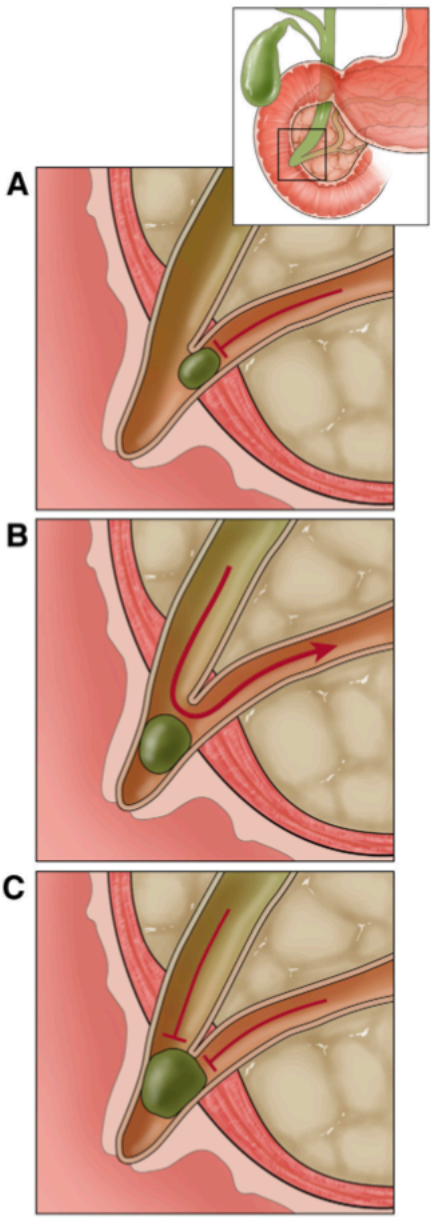

Figure 3. Theoretical mechanisms by which gallstone migration might induce acute pancreatitis

A) Pancreatic duct outflow obstruction.

B) Common channel theory with a channel between the common bile duct and the pancreatic duct.

C) Calculus obstructing both ducts.

The literature favours theories A & C, as there is compelling evidence that undermines the requirement for a common channel as shown in B. Figure is from Lerch and Gorelick *Gastroenterology*, 2013 [Figure 4] (89).

1.1.4.3. Genetic-related AP

Known genetic mutations which increase the rise of pancreatitis arise in genes which code for digestive proteases or trypsin inhibitor proteins. Patients with such mutations typically present to paediatric services with early onset of recurrent AP which progress to chronic pancreatitis by adulthood. Genetic mutations in *PRSS1* gene have been discussed in relation to acinar cell physiology and give rise to increased intracellular trypsin activity by impaired trypsinogen degradation, or increased trypsin formation by CTRC-dependent, or (rarely) by CTRC-independent mechanisms (see section 2.2.1.1.1. and Table 2) (29, 31). The clinically most frequent mutations involve R122H (~70%), and N291 (~20%) sites (31). Such mutations have a high penetrance, of up to 80%, and are associated with recurrent AP from a young age (31, 95). Additionally, a genome-wide association study (GWAS) found that two common genetic variants in *PRSS1*, at *CLDN2* and *PRSS1-PRSS2* loci, significantly increase the risk for alcohol-related pancreatitis (96).

Unlike *PRSS1* mutations, known functional mutations in the *CTRC* gene are all loss-of-function in nature. *CTRC* mutations are classified as impairing either secretion, catalytic activity, or proteolytic stability (29). These were also discussed in some detail above (section 2.2.1.1.1.), and are of particular relevance to chronic pancreatitis. Mutations in *CTRC* alone are not thought to be sufficient to cause pancreatitic inflammation without additional genetic predisposition or other risk factors (97).

During inflammation of the pancreas, *SPINK1* gene expression is increased to minimize the presence of active trypsin (97). Therefore, loss-of-function mutations in *SPINK1* reduce the effectiveness of this protective mechanism increasing susceptibility to recurrent AP and progression to chronic pancreatitis (97). Indeed, mutations in *SPINK1* (typically N34S, which is common, affecting ~2% of people in populations across the world) can present with AP, but similar to *PRSS1*- and *CTRC*-related AP, cases present at a young age (median ~20 yrs old in *SPINK1*) (97, 98). *SPINK1* mutations are not a risk factor for an initial attack of AP, and it is very infrequently associated with organ failure, however, it is strongly associated with recurrent AP (Odds ratio = 19) (98, 99).

Cystic fibrosis transmembrane conductance regulator (*CFTR*) is a cyclic adenosine monophosphate-regulated chloride-bicarbonate channel which is localised to the apical plasma membrane of epithelial cells such as pancreatic ductal cells (100). *CFTR* gene mutations disrupt activity of the channel with variable phenotypes. Such mutations are typically associated with chronic pancreatitis. Lastly, mutations in the calcium-sensing receptor gene, *CASR*, are rare and are more typically related to chronic pancreatitis (100).

1.1.4.4. Ethanol / Alcohol-related AP

Alcohol consumption behaviour varies widely across the world for cultural, religious, and socioeconomic reasons, as well as reasons related to farming and production. Considering that heavy alcohol consumption (e.g. >60 g/day) is far more common in any given population than the incidence of alcohol-related AP, with <10% of heavy drinkers developing clinically relevant AP, this suggests that there are undetermined environmental or genetic factors which may be protective for many heavy drinkers, or else factors which increase susceptibility for the subgroup who develop alcoholic pancreatitis (33, 101). Indeed, as mentioned above (section 1.1.4.3.), a recent GWAS study found two common genetic variants in *PRSS1* gene to significantly increase the risk for alcohol-related pancreatitis (96). It is important, therefore, not to overlook other causes of AP simply because a patient consumes alcohol (102). Different types of alcoholic drink are likely to differ with respect to pancreas toxicity, as the risk of AP is increased by the amount of spirits consumed on single occasion (65). The amount of wine, beer or average amount of monthly alcohol ingestion was not significant (65). Smoking is associated with a younger age of first episode of AP in both alcohol drinkers and non-alcohol drinkers, and is associated with recurrence of non-gallstone-related AP (73, 103).

The main difficulty in studying the underlying mechanisms of alcohol-induced pancreatitis in rodents has been that alcohol consumption alone (i.e. alcohol diet +/- gastric infusion) does not reliably cause AP (8). This has been the experience of researchers using wildtype mice, but genetically altered mice [e.g. nuclear factor erythroid 2 like factor 2 (*NRF2*) gene knockout mice] have been shown to develop pancreatic (and liver) injury with alcohol ingestion (104).

Researchers have found that chronic alcohol ingestion primes the rodent pancreas to sensitizer co-treatments (e.g. cholecystokinin analogue cerulein) which can be given at very low, physiological doses to induce AP (8). Lipopolysaccharide (LPS) is a component of the gram-negative bacterial cell membrane which can induce AP when co-administered to rats with prolonged ethanol feeding (8). Because alcohol is known to increase gut permeability, and increased serum LPS levels are found in humans with high chronic alcohol consumption due to translocation of enteric gram-negative bacteria, this is a clinically relevant model (105). Furthermore, gut barrier failure has been observed in experimental AP, with increased gut mucus oxidative stress which is thought to promote the development of multiple organ failure (106).

Alcohol is metabolised by both oxidative and non-oxidative pathways in humans and rodents (107). With oxidative metabolism, ethanol is converted to acetaldehyde and acetate, principally by alcohol dehydrogenase and also by cytochrome P450 family 2 subtype E

member 1 (CYP2E1), with generation of reactive oxygen species as a by-product which can cause oxidant stress. Fatty acid ethyl esters (FAEEs) are formed by non-oxidative metabolism, the products of alcohol and fatty acids catalysed by fatty acid ethyl ester synthases (FAEE synthases) (107). Oxidative metabolism of ethanol mostly occurs in the liver, and in the pancreas metabolism is dominantly by non-oxidative pathways (6, 107). The toxic effects of FAEEs on pancreatic acinar cells include toxic Ca^{2+} signalling, mitochondrial dysfunction, trypsinogen activation, induction of transcription factors nuclear factor kappa B (NF-κB) and activator protein 1 (AP-1), leading to apoptosis and necrosis (22, 107-111). Additionally, alcohol has harmful effects upon ductal and pancreatic stellate cells (94).

1.1.4.5. Trauma- and Tumour-related AP

Injuries to the pancreas following abdominal trauma are relatively rare, particularly after blunt injury, but are more frequent with penetrating injuries. Elevations in serum amylase after major trauma, however, are relatively common, particularly involving severe craniofacial injuries due to circulating salivary gland-type α-amylase. In abdominal trauma specifically, hyperamylasaemia is associated with pancreatic injuries and can serve as a screening test, particularly in children where a large radiation dose from CT scanning may seem unjustifiable. However, hyperamylasaemia can also result from an injury to the small bowel due to systemic absorption of α-amylase from an intestinal perforation (112). Additionally, hyperamylasaemia has been found to be unreliable in excluding pancreatic injuries within 6-hrs from the time injury (112). Therefore, considered interpretation of amylase results in trauma patients is required in light of the pancreatic specificity of the α-amylase assay, the injury pattern and the time interval since the injury. Pancreatic trauma is associated with significant morbidity and mortality particularly especially when the duct is damaged (AAST grades III to V), and the American Association for the Surgery of Trauma (AAST) have produced a pancreatic injury grading system which guides assessment (by CT/MRI, ERCP or operative), management, prognostication and trauma research (113, 114). Besides the in increasingly severe grades of haematoma and laceration describe by AAST with gland injury, abdominal trauma can also induce acute pancreatitis which is thought result from ischaemia or activation of acinar cell mechanical stress sensors, Piezo1 ion channels, which are described in more detail in the above section ‘acinar cell physiology’ (see 1.1.2.2.1) (18). Whilst some classifications incorporate post-ERCP pancreatitis within ‘trauma’, it is addressed separately bellow (see 1.1.4.11).

The other ‘T’ in this mnemonic represents pancreaticobiliary ‘Tumours’. It is thought that AP arises in these patients because of elevated ductal pressures resulting from

obstructing. It has been estimated that 5-14% of patients with pancreaticobiliary mass lesions (malignant or benign) present with idiopathic AP (115). For this reason, it has been recommended that a pancreaticobiliary mass be excluded in any patient over 40 years old with idiopathic AP by contrast-enhanced CT, MRI or endoscopic ultrasound (115).

1.1.4.6. Surgery- and Steroid-related AP

Following on from pancreatic tumours is major 'Surgery'. Indeed, the most frequently cited surgical inducer of AP has been surgery pancreatic surgery, which can be understood in mechanistic terms when considering the tissue damage and ischaemia involved, and activation of the acinar cell mechanoreceptors, Piezo1 ion channels, which allow Ca^{2+} influx into acinar cells [Piezo1 channels have been discussed above (sections 1.1.2.2.1 and 1.1.4.5)]. Other major operations, particularly aortic, cardiopulmonary bypass and liver transplantation have been recognised as an inducers of AP, likely due to pancreatic ischaemia (67, 116).

The other 'S' in this mnemonic stands for 'Steroids' – which have been recognised as potential inducers of AP since the 1950s (117). However, cases of steroid-induced AP in the literature do not meet the criteria for class 1a level of evidence described by for drug-induced AP Badalov *et al.* (see section 1.1.4.12 and Table 4, below), so it must be highlighted that whilst steroids are considered separately from other medications in this aetiological mnemonic system, the evidence for AP-induction is not higher for steroids than other drugs (78). That said, cases of steroid-related AP that have been published do show a particularly severe disease course with high lethality (78).

1.1.4.7. Mumps & other infectious triggers of AP

Infectious agents are rare but potentially preventable and curative inducers of AP. Aetiologically, the best understood are parasitic causes which appear to trigger AP through obstruction of the ductal system and may require decompressive endoscopic sphincterotomy in addition to anti-parasitic therapy (118). Of these, the best recognised are the nematode *Ascaris lumbricoides* and the trematode *Clonorchis senensis* (popularly known as the Chinese liver fluke) (68, 118).

The mechanisms by which viral infections induce AP are less clear despite the induction of pancreatic inflammation in laboratory mice using single stranded-RNA picornavirus, *Coxsackievirus type B*, having been first demonstrated 70-years ago (119). The other viruses which have reportedly induced AP have all been DNA viruses, and are supported by case report level evidence only. Specifically, single stranded-DNA viruses: paramyovirus *Mumps orthorubulavirus* (which causes Mumps), and orthohepadnavirus *Hepatitis B virus*.

Double-stranded-DNA viruses include: herpesviridae *Cytomegalovirus* (CMV) and *Herpes simplex virus* (HSV), as well as alphaherpesvirus *Varicella-zoster virus* (VZV). AP is not uncommon in HIV/AIDS since immuno-compromised patients are susceptible to opportunistic infections which may trigger AP and anti-retroviral drugs can induce AP (80).

The body of evidence to support the aetiology of bacterial infections in AP is less than that for viral infections and there is also no established pathological mechanism to support this possible cause. Even if such micro-organisms are cultured directly from sampling th pancreas, a critic could reasonably suggest that such infections could be secondary rather than a primary aetiological factor. Those bacterial which are cited in the literature as potential inducers of AP by more than one case report include *Mycoplasma pneumoniae*, *Salmonella typhi* (68, 80).

Lastly, whilst fungal infections can arise within the pancreas parenchyma as micro- or macro-abscesses, these generally do not cause AP (68, 80). The relevance of fungal infections in AP is that they arise as a complication by causing infection of necrotic pancreatic tissue (e.g. Candida) (80).

1.1.4.8. Autoimmune-related AP

Disease of the adaptive immune system which involves the pancreas is termed auto-immune pancreatitis (AIP). It is a pancreatic manifestation of a multi-organ inflammatory disease which is now termed IgG4-related disease (120). It is a chronic fibroinflammatory disease which is distinct from classical chronic pancreatitis. Current classifications distinguish two subtypes which have several opposing features, but for simplicity Type 1 can be remembered as having elevated serum IgG4 levels, whilst Type 2 patients have levels within normal limits (121). Type 1 typically involves extra-pancreatic organs, whilst Type 2 is more confined to the pancreas. Both types response well to steroid challenge. Histologically there are lymphoplasmacytic infiltration with fibrotic changes which are very different to chronic pancreatitis and AP. Systemic lupus erythematous (SLE), which is characterised by immune complex deposition in multiple organ systems, is also associated with AP, albeit rarely, and authors often report a favourable response to steroids in these patients (122). Another autoimmune disease with upregulation of interferon type-1 inducible genes which has an increased risk of AP is Sjogren's syndrome, although pathobiological connections between AP and Sjogren's are not currently defined (123).

1.1.4.9. Scorpion sting-induced AP

Venomous stings can induce a wide array of acute critical illness. Besides the few cases of snake bite-induced AP, scorpion stings are the main venomous inducers of AP. Scorpions are predatory arachnids with >1000 species. The genera, *Tityus*, are a subgroup of scorpions with thick-tails. The species *Tityus trinitatis* (**Figure 4**), which is endemic to Trinidad and Tobago, possess an especially pancreatotoxic venom that induces AP, which was first highlighted in 1970 by C Bartholomew who reported 24 cases of scorpion-induced AP encountered in just a 2-month period (125)! AP is not the only effect on humans from this venom, as is has cardiotoxic effects too. Additionally, other scorpions of this genus also have pancreaticotoxic effects, such as the venom of the *Tityus serrulatus*, which can be found in Brazil (126). Mechanistically, such *Tityus* venom has been shown to profoundly induce exocrine secretion and contraction of the sphincter of Oddi, which is likely mediated by muscarinic cholinergic mechanisms (127-129).

Figure 4: *Tityus trinitatis* scorpion (male)
Picture is from textbook 'Scorpion Venoms' Springer Science, 2015 [Chapter 10, pg 224, Figure 2 B]. Photograph taken by Jan Ove Rein. (124)

1.1.4.10. Hypercalcaemia, hyperlipidaemia and metabolism-related AP

There are two main chronic metabolic associated with the occurrence and recurrence of AP; namely hypercalcaemia (which is often the result of primary hyperparathyroidism) and hyperlipidaemia.

Several observational studies from many groups around the world have found a significant association between hypercalcaemia and AP (79). There are notable exceptions, however, which allow for ongoing debate. In particular, the *JAMA* 1980 paper from Mayo Clinic denounced this association based on a large dataset of >1000 cases of surgically confirmed hyperparathyroidism with only 1.5% having had evidence of pancreatitis, and of these, more than half had other more compelling aetiological factors, such as high alcohol intake or gallstones (130). However, given the central role of calcium signalling in both acinar cell physiology and in AP pathogenesis (26), it seems biologically plausible that there would be a causal association to some degree as the data overall appears to suggest. Interestingly, it should be noted that severe AP and admission to critical care, as opposed to mild disease, is associated the use of calcium-altering drugs, previous parathyroid surgery as well as hypocalcaemia found on admission bloods (63).

Another chronic metabolic disorder associated with the occurrence of AP is hyperlipidaemia. Required serum levels are thought to be very high, however, with guidelines suggesting an arbitrary cut-off of serum triglyceride >1000 mg/dl (11.2 mmol/l) (115). The condition may be primary, such as inherited disorders of lipoprotein metabolism which may be detected in childhood, or secondary disorders of lipoprotein metabolism (e.g. diabetes mellitus, obesity, hypothyroidism) which may also require an additional underlying mild form of genetic dyslipidaemia (48). The treatment is with standard supportive measures, anti-lipid drugs and the consideration of plasma electrophoresis and heparin (131, 132). Mechanistically, fatty acid esters are known to contribute to dysregulated Ca^{2+} signalling within acinar cells so there is a plausible association between elevated lipids and the induction of AP.

1.1.4.11. ERCP-related AP

Whilst the pathogenesis of acute pancreatitis has mostly focussed upon gallstone and alcohol-induced aetiologies, post-ERCP pancreatitis presents the opportunity to administer drugs prophylactically or very early in the disease course, which would not be feasible with other aetiologies. Experimental ERCP-pancreatitis models using rodents consist of pressure-controlled pancreatic ductal infusion (133). The pressure effect of ductal infusion has been shown to induce transient pancreatitis changes in rats, where saline was used as the infusate at high pressures (134). In the human therapeutic ERCP situation, luminal pressures are a likely contributing factor for post-ERCP pancreatitis, which is the rationale for inserting a plastic stent into the pancreatic duct in challenging cases (135). However, additional factors, such as luminal acidity, are also known to be important in the pathogenesis of post-ERCP AP (133), with the supporting evidence that release of inflammatory mediators can be induced by low pH stimulus of transient receptor potential neuronal ion channels (133). Whilst understanding of the specific molecular events which trigger acinar cell injury and pancreatitis by animal models would seem important, it is noteworthy that use of rectal NSAIDs, as evidenced by clinical studies, has not undergone confirmation animal study (8, 136, 137).

1.1.4.12. Drug induced-AP (other than steroids)

The diagnosis of drug-induced AP is not easily established but a thorough review of this topic was published in 2007 by Badalov *et al*. (78). Herein the authors classify alleged pharmacological inducers of AP by levels of evidence from Class I to IV (**Table 4**), with the strongest evidence being Class Ia in which 'at least 1 case report is that of a positive challenge, excluding all other causes, such as alcohol, hypertriglyceridaemia, gallstones and other drugs' (78).

Class	Definition	Drug
1a	• At least 1 case report with positive re-challenge test, **excluding all other causes**	Methyldopa, Azodisalicylate, Bezafibrate, Cannabis, Carbimazole, Codeine, Cytosine, Dapsone, Enalapril, Furosemide, Isoniazid, Mesalazine, Metronidazole, Pentamidine, Pravastatin, Procainamide, Pyritinol, Simvastatin, Stibogluconate, Sulfamethoxazole, Sulindac, Tetracycline, Valproic acid
1b	• At least 1 case report with positive re-challenge test; *however* **other causes were not ruled out**	Tretinoin, Amiodarone, Azathioprine, Clomiphene, Dexamethasone, Ifosfamide, Lamivudine, Losartan, Lynesterol, 6-mercaptopurine, Meglumine, Methimazole, Nelfinavir, Norethindronate/Mestranol, Omeprazole, Premarin, Co-Trimoxazole
II	• At least 4 cases in the literature • Consistent latency (≥75% of cases)	Paracetamol, Chlorthiazide, Clozapine, Didanosine, Erythromycin, Estrogen, Asparaginase, Pegasparagase, Propofol, Tamoxifen
III	• At least 2 cases in the literature • No consistent latency among cases • No re-challenge test	Alendronate, Atorvastatin, Carbamazepine, Captopril, Ceftriaxone, Chlorthalidone, Cimetidine, Clarithromycin, Cyclosporin, Gold, Hydrochlorothiazide, Indomethacin, Interferon/ribavirin, Irbesartan, Isotretinoin, Ketorolac, Lisinopril, Metolazone, Metformin, Minocycline, Mirtazapine, Naproxen, Paclitaxel, Prednisone, Prednisolone
IV	• Drugs not fitting into the earlier-described classes, **single case report** published in medical literature, without re-challenge test	Adrenocorticotropic hormone, Ampicillin, Bendroflumethiazide, Benazepril, Betamethasone, Capecitabine, Cisplatin, Colchicine, Cyclophosphamide, Cyproheptadine, Danazol, Diazoxide, Diclofenac, Diphenoxylate, Doxorubicin, Ethacrynic acid, Famciclovir, Finasteride, 5-fluorouracil, Fluvastatin, Gemfibrozil, Interleukin-2, Ketoprofen, Lovastatin, Mefenamic acid, Nitrofurantoin, Octreotide, Oxyphenbutazone, Penicillin, Phenolphthalein, Propoxyphene, Ramipril, Ranitidine, Rifampin, Risperidone, Ritonavir, Roxithromycin, Rosuvastatin, Sertraline, Strychnine, Tacrolimus, Vigabatrin/lamotrigine, Vincristine

Table 4: Drug-induced AP based on drug classes (78).

1.1.4.13. Smoking-related AP

Whilst cigarette smoking is a recognised risk factor for both acute and chronic pancreatitis, experimental animal models of cigarette-smoke toxicity are lacking (8). Liquid extracts of cigarette tobacco, especially nicotine metabolite nicotine-derived nitrosamine ketone (NNK), have been demonstrated to cause mild pancreatic injury. *In vivo*, NNK was found to activate trypsinogen and vacuolization, whereas NNK pre-treatment prior to induction

of acute pancreatitis with cerulein heightened its effects upon the pancreas (138). Chronic nicotine exposure (as well as NNK exposure) impairs thiamine (vitamin B_1) uptake from the circulation by decreasing expression of cell thiamine transporters. Deficiency of thiamine results in mitochondrial dysfunction, a hallmark of pancreatitis pathogenesis (139, 140). Chronic alcohol use is frequently associated with inadequate thiamine absorption from the diet, which likely compounds acinar cell thiamine depletion amongst smokers.

1.1.5. Clinical definitions and scoring systems for acute pancreatitis

1.1.5.1. Diagnostic criteria for acute pancreatitis

The internationally agreed diagnostic features for AP require at least two of the following criteria (115, 141):

1) Characteristic abdominal pain
2) Serum pancreatic enzyme levels (i.e. amylase or lipase) 3-fold greater than the upper limit of normal range values
3) Radiological evidence of AP.

Plasma pancreatic enzyme levels (i.e. amylase) are useful for diagnostic purposes, but a higher plasma concentration does not reliably correlate with worse disease severity (142). The diagnosis is usually reached without the need for radiological imaging, but where it is required, contrast-enhanced computed tomography (CT), magnetic resonance cholangiopancreatography (MRCP) or transabdominal ultrasonography have been recommended (141, 143).

1.1.5.2. Fatal acute pancreatitis

The clinical outcomes in AP are remarkably heterogenous, ranging from mild and self-limiting to multiple organ failure and death. Deaths are typically due to extra-pancreatic organ failure and usually arise in the first 2 weeks, as evidenced by national studies consisting of >1000 AP deaths (59, 144) (**Figure 5**). Indeed, the median duration from hospital admission to death amongst AP patients admitted to critical care was found in one national study to be just 82-hrs (n = 54 AP deaths) (63). Prior to these reports, smaller studies (<20 AP deaths) advocated a theory that there is a second peak of deaths from AP that arise later (>3 weeks) due to infected pancreatitis necrosis. This debunked theory highlights the limitations of conclusions drawn from small data series from specialist units, rather than taking a broad population-based approach (145, 146). This distinction is important when directing finite

research resources with the aim of reducing lethality in AP. These larger, population-based studies support the concept that deaths typically arise in the first 2 weeks and are due to overwhelming multiple organ failure, rather than from septic complications thereafter. Additionally, studies from specialist units typically overlook prehospital AP fatalities which were found to comprise 17% of nation-wide deaths from AP in Sweden at that time (147). The proportion of fatal prehospital cases for any given country will differ depending upon the availability of access to emergency medical services, social care systems, levels of societal levels of alcohol dependence and the size of homeless populations. Better characterised are the inpatient fatal AP cases amongst adults, which most large series report this figure at approximately 4% [of 70231 in California, USA (76)] to 5% amongst adults [of 2053 in Scotland (63)]. Mortality amongst paediatric populations has been reported between 0-11% (75). This broad range in mortality reflects the small sample size of each study. However, taken together, from available reports, the collective paediatric AP mortality was 4.7% (43 of 922) (148-153). The key interventions to reduce AP fatalities apart from prevention strategies, are rapid access to diagnostics and effective treatments which ameliorate the systemic inflammatory response and organ failure.

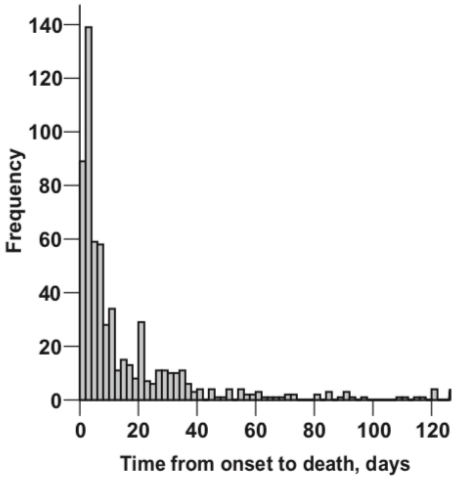

Figure 1 Histogram depicting time from onset of acute pancreatitis to death

Figure 5: Deaths arise early in AP, no delayed second peak from sepsis

Histogram depicts right-skewed data with the majority of deaths arising early in AP (<3 weeks) from a large, national population-based study (n = 1024 AP deaths). Notably, there is no large delayed second peak after 3 weeks, a notion that has been advocated by smaller studies from specialist units. Figure is from Mole *et al. HPB*, 2009 [Figure 1] (144).

1.1.5.3. Nature and duration of organ dysfunction in acute pancreatitis

Acute inflammation which leads to the systemic inflammatory response syndrome (SIRS) can be caused by other non-infective conditions besides AP, such as major burns, trauma, surgery, ischaemia-reperfusion and haemorrhagic shock. All of these conditions can be complicated by multiple organ dysfunction syndrome (MODS), which commonly involves severe pulmonary, cardiovascular, or renal function compromise. These bodily systems in particular typically struggle to meet the physiological requirements during a severe acute systemic inflammatory condition, and therefore malfunction to the point of 'critical illness'; the latter has been defined as '*life-threatening organ dysfunction which requires mechanical or*

pharmacological support to prevent imminent death' (154). In severe AP, pulmonary, cardiovascular, renal, haematological and hepatic systems are the most commonly affected (63, 144, 155). Failure of the more frequently affected organ systems (respiratory, cardiovascular, renal), are discussed in more details.

The duration of organ dysfunction in the first week of AP was the focus of UK clinical research groups at the start of the 20th century (156, 157), with the description of terms 'transient' (<48-hrs) and 'persistent' (>48-hrs) which are now ingrained in the international AP severity nomenclature (158). It has been firmly established that transient organ dysfunction has a distinctly better prognosis than persistent organ dysfunction (158).

1.1.5.3.1. Respiratory failure in AP

Acute respiratory distress syndrome (ARDS) is defined by a constellation of clinical and physiological criteria characterised by an acute, diffuse, inflammatory lung injury, leading to increased alveolar capillary permeability, increase lung weight, and loss of aerated lung tissue (**Figure 6**) (159). The term 'acute lung injury' (ALI) has dropped out of favour within the scientific community, and ARDS is now subclassified as mild, moderate and severe, with the 2012 Berlin definition having been widely endorsed by esteemed thoracic and critical care societies (159). Histologically, ARDS is characterized by an acute, exudative phase, combining diffuse alveolar damage and noncardiogenic oedema, followed later (amongst survivors) by a fibroproliferative phase (160). The injury process in ARDS involves diffuse alveolar damage with alarmin and proinflammatory mediator release, PRR activation, transcription of genes under NF-κB and activator protein-1 (AP-1) control, infiltration of activated macrophages and neutrophils, proliferation of fibroblasts all of which impair gas exchange and lung mechanics (160). A comprehensive review of the inflammatory and cellular components of ARDS in AP by Akbarshahi *et al.* is recommended for interested readers (161). ARDS is not the only thoracic complication of AP, however, and other potentially serious intrathoracic complications can give rise to cardiopulmonary failure, such as pleural, pericardial and mediastinal collections (effusion, pseudocyst, empyema), pneumonia, venous thromboembolism, pseudoaneurysm and cardiac arrhythmia (162).

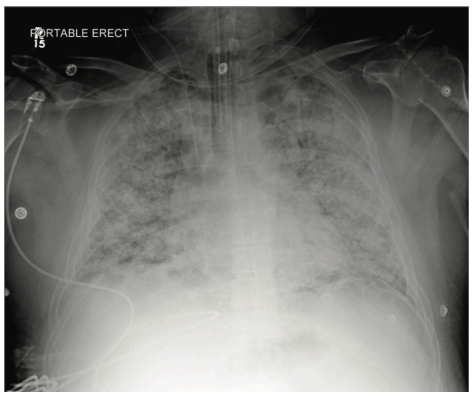

Figure 6. **Chest radiograph of a patient with acute respiratory distress syndrome (ARDS)**
Chest radiographic features demonstrating diffuse bilateral pulmonary infiltrates. Acute respiratory distress syndrome (ARDS) is a common complication in severe AP. Image from Fan et al. *JAMA*, 2018 [Figure 1A] (159).

1.1.5.3.2. Cardiovascular failure in AP

Cardiovascular dysfunction requiring inotrope or vasopressor support is very common in severe AP, affecting ~60% of patients (63). Bleeding in the context of AP (e.g. haemorrhagic pancreatitis) is exceptionally rare, and therefore cardiovascular dysfunction is typically due to 'vasoplegia'; a syndrome of pathologically low systemic vascular resistance (SVR), that is manifest as hypotension or the requirement for therapies to avoid this, in the presence of a normal or increased cardiac output (163). The contractile state of the vascular smooth muscle cells within the tunica media controls the arteriolar diameter and thereby modulates the systemic vascular resistance along with cardiac output (163).

As vasoplegia progresses to the point of tissue hypoperfusion and cellular hypoxia it is termed 'shock'. This form of shock is known by a few terms in the literature; namely, vasodilatory, distributive or vasoplegic shock. Treatment often requires vasopressor infusion, usually with catecholamines, with invasive blood pressure monitoring. Physiological regulators of arterial tone include endothelial secretions (e.g. nitric oxide, prostacyclin, endothelin), vasoactive metabolites (e.g. acidosis, hydrogen peroxide) and other autocoids (e.g. serotonin, prostaglandins, thromboxane A_2) (163). Extrinsic regulation of vascular resistance is largely mediated by neural sympathetic control and vasoactive hormones (e.g. adrenaline, angiotensin II and vasopressin) (163). In AP, circulating DAMPs and other proinflammatory mediators, together with altered neuro-endocrine hormone axes, disrupt the vascular tone by their effects on endovascular smooth muscle and endothelial cells.

1.1.5.3.3. Acute kidney injury in AP

Acute kidney injury (AKI) is a collection of extremely heterogenous clinical syndromes united by a sudden decrease in estimated glomerular filtration rate (164). AKI may manifest as changes in only serum creatinine, or just urine output, or both (164). The overall prevalence of acute kidney injury (AKI) in AP is not well defined, but appears to be in the region of 8-15% (165). From a detailed case-by-case review of AP clinical records (n = 2053 cohort), which included 0.3% patients already on renal dialysis prior to hospitalization, 4.8% of AP patients required renal replacement therapy during their admission (63). AKI typically develops late in the course of AP, usually after failure of other systems, with <10% of AP-MODS patients first developing AKI (155, 165). This explains why the mortality amongst AP patients who require renal replacement therapy is so very high (>75%), as it is a late occurrence in the sequence of failing organ systems (165). The pathophysiology of AKI in AP has received less attention than pulmonary complications in severe AP. From available studies, there is evidence that mediators absorbed into the circulation from necrotic acinar cells

and pancreatic ascites are pathogenic. Circulating proinflammatory cytokines, such as TNFα, are thought to have cytotoxic effects on glomeruli, tubular capillaries and endothelial cells, potentially leading to ischaemia, apoptosis and necrosis (165). Collectively AKI in AP appears to arise from the culmination of hypovolaemia from increased vascular permeability, inflammatory signalling, vasoconstriction, intravascular coagulation and the direct nephrotoxic effects of circulating endogenous mediators and DAMPs (165). For interested readers, a focussed review of AKI in AP by Nassar and Qunibi is recommended (165).

1.1.5.4. Severity predictor scoring systems in acute pancreatitis

There are many clinical scoring systems which have been designed to act as tools in the assessment of AP patients or else generic critical care tools which have been adopted by the pancreatitis scientific community. **Table 5** lists, in chronological order, the main scoring systems used to prognosticate AP severity. The output result for each score is listed is a separate column.

Score	Country (Year)	Factors	Disease	Tests	Output	Ref(s)
Ranson	NY, USA (1974 & 1977)	11	AP-specific	Repeated	Number (0-11) Severe (≥3)	(166, 167)
Glasgow	UK (1978)	9	AP-specific	Single	Number (0-8) Mild (0-2) or Severe (≥3)	(168-170)
Balthazar	NY, USA (1985)	1	AP-specific	Single	CT grade of AP severity (A-E)	(171)
APACHE II	DC, USA (1985 & 1989)	12	Generic	Single	Number (0-71) Severe (≥10) or >8 in AP (143)	(172, 173)
Hong Kong	Hong Kong (1993)	2	AP-specific	Single	Severe (Urea >7.4 mmol/L and/or Glucose >100 mmol/L)	(174)
Japanese	Japan (2002)	18	AP-specific	Single	Number (0-27) Stage (0-4)	(175)
Panc 3	MA, USA (2007)	3	AP-specific	Single	Number (0-3) Mild (0) or Severe (≥1)	(176)
POP	UK (2007)	6	AP-specific	Single	Number (0-54)	(177)
BISAP	MA, USA (2008)	5	AP-specific	Single	Number (0-5) Mild (0-2) Severe (≥3)	(178)
HAPS	Germany (2009)	3	AP-specific	Single	Number (0-3) Mild (0) Severe (≥1)	(179)

Table 5: Severity prognosticator scores
APACHE II: Acute physiology and chronic health examination II; BISAP: Bedside index for severity in AP; HAPS: Harmless acute pancreatitis score; PASS: Pancreatitis activity scoring system; POP: pancreatitis outcome prediction.

1.1.5.4.1. The original AP severity prediction scores – Ranson & Imrie

The original scoring system by John Ranson and colleagues in New York, USA in the mid to late 1970s (166, 167), described 13 variables, which became 11 (having dropped the serum 'amylase' result and 'previous AP episodes'). Six of the 11 required a repeat assessment within 48-hrs: The decrease in haematocrit, increase in urea, the lowest serum calcium and arterial oxygen tension, and highest base deficit and estimated fluid deficit (166). The need for repeated tests, an estimation of fluid deficit and 48-hrs delay were practical limitations that other scoring system since have all avoided. Around the same time, across the Atlantic Ocean in Scotland, the surgical department in Glasgow produced their own scoring system for pancreatitis in 1978 using 8 factors, with the only new parameter being serum Albumin which was missing from Ranson's system. Professor Imrie and his Glasgow colleagues did not include haematocrit decrease or estimation of fluid sequestration, nor did they include acidaemia by way of base excess which Ranson had included (168, 169).

1.1.5.4.2. New AP scores between 1980-2000

In 1985, a New York radiologist Emil J Balthazar produced a CT-based 5-level scoring system to grade the severity of AP-related radiological changes (171). During the same year, a team of intensive care academics in Washington DC published the national validation results of a revised version of their original APACHE score, simply rebranded as APACHE II, which was found to be a robust prognosticator tool in for critical illness in general (173). APACHE II has 12 factors with graded scoring with a maximum of 71 points, and a score over 10 being considered as severe. The APACHE II score was found to be useful for AP patients in particular when tested in an UK population (172), and has since been adopted by into UK guidelines as a quantifier of severity, but using a slightly lower cut-off of >8 for severe AP (143). In 1992, a group from Hong Kong sought to focus severity prediction down to only 2 factors on admission for predicting severe AP; using elevated blood urea and glucose, but this system was criticised and not widely adopted (174).

1.1.5.4.3. The 21st century AP prediction scores

After the turn of the 21st century, in the 2000s, there was a global flurry of new AP scoring systems. A decade after the Hong Kong score, and in stark contrast, the Japanese developed the most sophisticate system employing 18 factors, which is more than any AP severity system before or since (175). Then in 2007, in line with the Hong Kong efforts to produce a rapid and simple score, a group from Harvard, Boston in the USA produced the 3-point Panc 3 score. In keeping with the origin American score by Ranson, Panc 3 also used

haematocrit, but used two novel parameters: body mass index (BMI) and evidence of pleural effusion on chest radiograph (176). At the same time, a group in London developed a new predictive score, called the Pancreatitis Outcome Prediction (POP) score for severe AP with the premise that a new AP-specific score was worthy of investigation given the considerable advances in critical care medicine over the 30 years since the Glasgow and Ranson scores were developed (177). The POP score utilised 6 parameters, of which 4 were largely unchanged: Age, urea, calcium and arterial oxygenation. As in Ranson's score, POP quantified acidaemia, using arterial pH as opposed to base excess. The only new factor not included in either the Glasgow or Ranson scores was mean arterial blood pressure (177). Curiously, less than a year after the Panc 3 score was published a separate group of authors also affiliated with Harvard, Boston published the Bedside Index Severity in Acute Pancreatitis (BISAP) score (178). This was an easy-to-use 5-factor score which for the first time incorporated impaired mental status as a prognostic indicator. As with the other Harvard score (i.e. Panc 3), the BISAP also scored pleural effusion on chest radiograph. In 2009, a group from Germany with the collaborations of Italian clinical epidemiologist P Mainsoneuve and pancreatologist AB Lowenfels from New York, took a refreshing and novel approach to AP severity scoring by producing the Harmless Acute Pancreatitis Score which used just three factors to exclude a severe episode; namely: Absence of rebound tenderness, normal haematocrit, and normal serum creatinine (**Table 5**, above) (179).

Whilst APACHE II is not disease-specific, it has the unique advantage in that it is designed to be repeatedly recalculated during intensive care therapy and given that the linear range is from 0 to 71, it can be used as a daily, dynamic surrogate marker of clinical improvement, in a similar fashion to the organ failure severity scores.

1.1.5.4.4. Organ failure scores

The scoring systems listed above are used to prognostically stratify acutely ill patients, which is subtly different from quantifying actual severity. The risk of fatal AP relate to the duration of organ failure in the first week, and the most widely utilised tool for assessing organ failure is the Marshall score which is a generic critical care tool which measures 6 factors (180):

- Respiratory: PO_2/FiO_2 ratio
- Renal: Serum creatinine
- Hepatic: Serum bilirubin
- Cardiovascular: Pressure adjusted heart rate
- Haematologic: Platelet count
- Neurologic: Glasgow coma score (GCS).

When studying patients with AP in particular, the hepatic dysfunction component is omitted to avoid confounding effects of biliary obstruction, and even the haematological and neurological components were dropped by the 2012 revised Atlanta classification, which is interesting in light of the 2008 BISAP score that incorporates mental status. Another system used to score organ failure which is very similar to the Marshall system is the sepsis-related organ failure assessment (SOFA) tool which also uses a 6-factor score: PO_2/FiO_2 ratio, creatinine, bilirubin, hypotension, platelet count, and GCS (**Table 6**). Thus, the only difference between Marshall and SOFA is the cardiovascular quantification, with the Marshall system using a pressure-adjusted heart rate [PAR = (Heart rate x central venous pressure) / mean blood pressure], whilst the SOFA uses mean arterial pressure (with or without increasing quantities of vasopressors). The preference of 2012 revised Atlanta is the modified Marshall score (141).

System	Country (Year)	Factors	Disease	Detail	Ref(s)
Marshall OF	Canada (1995)	6	Generic	Number (0-24). Clinicobiochemical markers of OF	(180)
SOFA	International (1996)	6	Generic	Number (0-24). Clinicobiochemical markers of OF	(181)

Table 6: Organ failure severity systems
OF: Organ failure; SOFA: Sepsis-related organ failure assessment

1.1.5.4.5. Actual severity AP assessment systems

During the early 1990s, as multiple organ failure scoring tools were being developed, the need for clearer definitions in the literature for AP was met by an international consortium who assembled in Atlanta, USA. This was the start of improved uniformity in definitions in AP, to help with the development of international guidelines and in conducting clinical research. **Table 7** shows a chronological catalogue of publications which describe actual AP disease severity, which includes a column detailing definitions of severity groups. The evolution of expert opinion can be seen with the introduction of 'duration of organ failure' in 2005 from the UK guideline, to the inclusion of a moderate group from 2012 onwards.

More recently a more functional scoring system has been introduced by the Southern California Pancreas Study Group, called the Pancreatitis Activity Scoring System (PASS) (182, 183). PASS differs from the others in Table 7 in that it can be used to monitor a patient's condition during AP and chart progress, in a similar way that APACHE II can be used to chart physiological progress. The factors which comprise the PASS score are: i) organ failure (modified Marshall ≥2), ii) SIRS (≥2), iii) abdominal pain, iv) opiate requirement over 12-hrs, v) tolerance of oral intake over 12-hrs (182).

System	Country (Year)	Severity groups	Ref.
1992 Atlanta	International (1992)	Mild (no OF or complications) Severe (OF and/or complications)	(184)
Japanese	Japan (2002)	Number (0-27). Stage (0-4) Clinicobiochemical markers of OF.	(175)
UK	UK (2005)	Mild (OF lasting <48-hrs) Severe (OF >48-hrs, otherwise as per '92 Atlanta)	(143)
2012 Atlanta	International (2012)	Mild: No OF or complications Moderate: OF <48-hrs, local complications or exacerbated co-morbidities Severe: OF >48-hrs	(141)
Determinant-based	International (2012)	Mild: No OF and no (P)P necrosis* Moderate: OF <48-hrs and/or sterile (P)P necrosis* Severe: OF >48-hrs or infected (P)P necrosis* Critical: OF >48-hrs and infected (P)P necrosis*	(158)
ACG	USA (2013)	Mild: no OF and/or pancreatic necrosis Moderate: OF <48-hrs or complications (local or systematic) Severe: OF >48-hrs and/or death	(115)
PASS	CA, USA (2017)	5 factors: SIRS (x25 points/ criteria), mod Marshall (x100/ system of 3 – respiratory, cardiovascular, renal), Abdo pain (0-10 score x5), Morphine equivalent dose (number of mg x5), Tolerating diet (yes=0, no=1, x40). Number (0-450). Mild (<140)	(182, 183)
AAST EGS	USA (2018)	Grades 1 to 5 (guides to management) 1: Acute oedematous AP; 2: Pancreatic phlegmon or peripancreatic fluids collection or haemorrhage; 3: Sterile pancreatic necrosis 4: Infected pancreatic necrosis or abscess 5: Extrapancreatic extension of pancreatic necrosis (e.g. colonic necrosis)	(185)

Table 7: System of actual AP severity
AAST EGS: American association for the surgery of trauma emergency general surgery; ACG: American college of gastroenterology; IAP: International association of pancreatology; OF: Organ failure; SOFA: Sepsis-related organ failure assessment. *(P)P necrosis: (peri)pancreatic necrosis

1.1.5.4.6. Application of human AP severity systems to my experimental AP research

In the murine model of AP used in this PhD work, which is discussed later, I sought to apply the principles of AP scoring systems by using implantable telemetry to continuously monitor physiological changes, and I developed and used an experimental AP-specific cage-side clinical scoring sheet. This cage-side tool incorporated clinical signs of pain in rodents with analgesia administration protocols, and the parenteral administration and oral consumption of analgesia was monitored throughout these AP recovery studies. The total body weight loss was also recorded. All these measures were taken in an effort to monitor experimental AP disease activity under laboratory conditions.

1.1.5.5. Adverse risk factors for a severe episode of AP

The simplest surrogate clinical endpoints for an adverse outcome in AP are all physiologically based: i) organ dysfunction; ii) critical care admission; and iii) fatality. Published observational studies employing multivariate statistical analysis tools have can highlight adverse and protective factors of AP-MODS. **Table 8** outlines the main factors associated with critical illness in AP.

Adverse pre-existing factors for critical illness
Aged over 80 years (63)
Alcohol dependency (63, 147)
Calcium-altering medication use (63)
Chronic kidney disease (63)
COPD (63)
Coronary artery stent placement in previous 1 year (63)
Diabetes in the young (aged 30-39 years) (63)
Hyperlipidaemia (86)
IHD or hypertension (63)
Morbid obesity (186-188)
Smoking (63)
Thyroid or parathyroid surgical history (63)
Type 2 diabetes mellitus (if not taking insulin) (63)
Adverse factors on admission for critical illness
Organ dysfunction: Respiratory; Cardiovascular; Renal (63, 144, 158, 165)
Hypocalcaemia (63)
(Peri)pancreatic necrosis or infection on CT/MRI scan (158)
Protective pre-existing factors against critical illness
Previous hospitalization for AP (less likely to need CC admission) (63)
Table 8. Clinical features associated with critical illness in acute pancreatitis
Adverse and protective factors associate with critical care admission, organ support or death in acute pancreatitis. The adverse factors are shaded above in green with distinction between pre-existing factors and those on admission. Protective factors for multiple organ failure in AP are highlighted below in blue. This is not an exhaustive list, but covers the main factors evidenced by the literature.

Some findings by different studies have shown conflicting results, such as the protection or risk conferred by statin use prior to AP, which may relate to heterogenous statin prescribing practices across the world (63, 189). Some risk factors can be identified in one study, but found to be statistically insignificant in another, which may be explained by a number of factors such as the complex nature of the risk factor of interest with occult confounders, the study size, demographics or definitions. One example of this, is the increased risk of critical illness in AP associated with (morbid) obesity (186, 187), which is not seen in all studies (63, 190). However, there are good biological reasons to support the assertion that obesity is not only associated with the development of AP (i.e. cholesterol cholelithiasis), but contributes to the severity of AP by contributing to proinflammatory mediator production [e.g. damage-

associated molecular patterns (DAMPs) and adipokines (188, 191, 192)], and impairs inflammation resolution (193). Interestingly, a previous hospitalisation for AP is protective against the need for critical care support, which may relate to local pancreatic changes following a previous pancreatitis episode (i.e. fibrosis).

1.1.6. Systemic inflammatory response in acute pancreatitis

The clinical course of AP has been described in terms of the 'early' and late' phases. The 'early phase' (<2 weeks) is widely considered as a sterile inflammatory response, because activation of the innate immune system is driven by host cellular injury products [i.e. damage- (or danger-) associated molecular pattern molecules (DAMPs)] which engage many of the same receptors and signalling cascades that exogenous infectious agents activate [i.e. pathogen-associated molecular patterns (PAMPS)]. AP is frequently complicated by a systemic inflammatory response syndrome (SIRS), and clinical biochemical markers, most notably C-reactive protein (CRP) which is produced by hepatocytes in response to proinflammatory cytokines (e.g. interleukin-6), can aid clinicians in biochemically monitoring progression or resolution of the systemic inflammatory response. The term 'SIRS' has been in use for over 25 years as a non-specific human pathophysiological response, and is widely utilised in AP literature (194). The most common cause of SIRS is infection, which is termed 'sepsis', but there are other non-microbial drivers of SIRS besides AP; with major burns, trauma and major surgery being common examples in clinical practice. In adults, the criteria for SIRS are met when 2 or more of the following abnormal clinical features are met:

i) Abnormal body temperature >38^{o}C or <36^{o}C;
ii) Tachycardia, with heart rate greater than 90 beats per minute;
iii) Tachypnoea, with >20 breaths per minute and/or hyperventilation indicated by a blood partial pressure of carbon dioxide <32 mmHg (<4.27 kPa);
iv) Abnormal total white blood cell count >12,000 cells/mm^3 or <4,000 cells/mm^3 (194).

There is evidence to support impaired gut integrity in AP related to increased reactive oxygen species and reactive nitrogen intermediate-mediated mucous damage, which can exacerbate SIRS (106, 195). At its worst, SIRS can progress into functional failure of multiple organ systems – a state of affairs that was unsurvivable before the modern era of intensive care medicine. AP multiple organ failure (AP-MOF) often arises from a hyperinflammatory 'sterile' response, but may signify an overt septic complication, with common sources being infected pancreatic necrosis, cholangitis, or pneumonia. For those that survive the 'early phase' and

transition into the 'late phase', the SIRS is replaced by a prolonged hypo-inflammatory derangement of the immune system, which has been termed as the 'compensatory, anti-inflammatory response syndrome' (CARS) or 'persistent inflammation, immunosuppression and catabolism syndrome' (PICS). This can increase susceptibility to an array of diseases on account of a poorly functioning immune system for weeks or months. The altered immune function relates to changes in the innate and adaptive systems, including consumption of complement (196-199).

1.1.6.1. The innate immune system

The cellular components of the immune system are broadly divided into two complementary groups; the adaptive system (comprising T and B lymphocytes), and the innate cells (including macrophages, dendritic cells, neutrophils and mast cells). The innate immune system is characterized by its ability to quickly recognise and react to a wide array of stimuli, which activates a multitude of signalling pathways (e.g. induction of inflammatory genes, complement cascade activation), produces pro-inflammatory mediators (e.g. cytokines), stimulates leucocyte recruitment to the site of injury (e.g. chemokines and adhesion molecules), and is key to the acute phase response in inflammation (200). Regardless of the nature of pancreatic injury, the immune system response is initially activated by abnormal movement of intra-cellular contents (i.e. DAMPs) by dead, dying and injured pancreatic cells, predominantly acinar cells (43). The local and systemic production of proinflammatory mediators (e.g. inflammasomes, cytokines) is a key part of the systemic inflammatory response. Inflammasomes are innate immune complexes comprising nucleotide-binding oligomerization domain-like receptors (NLRs) or absent in melanoma 2 (AIM2) which can activate caspase-1, and can subsequently cleave pro-cytokines to secrete IL-1β and IL-18, and in-so-doing communicate inflammatory signalling to neighbouring cells (201). Consequently, the activation, recruitment and infiltration of leukocyte subsets proceeds with a neuro-endocrine stress response. Here I lay out some of the key factors which activate the host immune response in AP.

1.1.6.2. Damage-associated molecular pattern molecules (DAMPs)

1.1.6.2.1. Description and examples of DAMPs

DAMPs (also termed 'alarmins', originally by Dr. Joost J. Oppenheim) comprises a growing list of endogenous host molecules which can act as receptor agonists when they are released into intra- or extra-cellular compartments in which they do not normally traffic, where

they engage receptors which would otherwise bind microbe components, pathogen-associated molecular patterns (PAMPs), and thereby activate the innate immune signalling by 'sterile' means. Post-translational modification of DAMPs can affect their ability to bind receptors (43). The DAMPs best characterised include: high mobility group box 1 (HMGB1), histones, nucleic acids, adenosine triphosphate (ATP), oxidised-low density lipoprotein (LDL), amyloid-β, calcium-binding proteins of the S100 protein family, oxidised-phospholipid, degradation products of extra-cellular matrix (ECM) and heat shock proteins (e.g. Hsp60) (202). This assorted group of molecules is recognised as an important driver of SIRS and multiple organ dysfunction syndrome (MODS) (43, 202-205).

HMGB1 is one particular DAMP which has been the focus of considerable research activity, including in relation to AP. HMGB1 functions in the nucleus as a non-histone architectural chromatin-binding protein that bends DNA and promotes protein assembly on specific DNA targets, but it also has an extracellular role as an alarmin (206). It can be secreted by activated monocytes and macrophages, and passively released by necrotic cells (less so by apoptotic cells) and is recognised as an early mediator in sterile injuries (in contrast to a late mediator in sepsis) (202, 206-209). Circulating HMGB1 levels have been shown to be elevated in patients with AP, particularly in severe disease, and HMGB1 co-culture with select proinflammatory mediators, in particular IL-1β and LPS, causes a strong proinflammatory synergist effect, detected through highly elevated IL-6 synthesis (210, 211). Systemic HMGB1 blockage, by intraperitoneal anti-HMGB1 antibody, attenuates severe experimental AP (212). Interestingly, intra-acinar HMGB1 appears to protect against acinar damage in experimental AP, with loss of HMGB1 in the acinar cells substantially worsening the severity of experimental AP in terms of the pancreas injury and lung injury (213). This is in stark contrast to extracellular HMGB1 which acts as a pro-inflammatory cytokine (213).

1.1.6.2.2. Pattern recognition receptors (PRRs)

The detection and response to DAMPs is first mediated by membrane-bound as well as cytosolic pattern recognition receptors (PRRs) expressed by resident and circulating immune cells (e.g. monocytes), endothelial and epithelial cells (200). Additionally, DAMPs are also potent activators of complement, leading to rapid C3a and C5a generation (198, 214). PRRs are classified into several groups: AIM2-like receptors (ALRs), c-type lectin receptors (CLRs), NOD-like receptors (NLRs), purinergic receptor 2X ligand-gated ion channel 7 ($P2RX_7$), receptor for advanced glycation end products (RAGE), RIG-like receptors (RLRs), Toll-like receptors (TLRs). Some PRRs reside on the cell surface (e.g. TLRs-1,-2,-4,-5,-6,

PRR	Example	PRR site	Ligands include	Functions include	Refs
ALRs	AIM2	Cytosol	dsDNA	Caspase-1-activating inflammasome assembly	(215)
CLRs	Dectin-1	Cell surface (DCs)	Fungal	Antifungal immunity by lymphocyte function. IRF-1 activation, Ras/Raf-1, Ca2+/calcineurin/NFAR, NLRP3/caspase-1	(216)
NLRs	NLRP3	Cytosol	DAMPs, PAMPs	NOD1/2 RIP2, NF-κB, AP-1	(202)
$P2XR_7$	$P2XR_7$	Cell surface	Extracellular ATP	Proinflammatory mediator release, proliferation, cell death	(217)
RAGE	RAGE	Cell surface	HMGB1, S100s	HMGB1 uptake	(43)
RLRs	RIG-I	Cytosol	Viral PAMPs, other RNAs	Anti-viral IFN induction, caspase activation, IPS-1-dependent NF-κB	(218)
TLRs	TLR2	Cell surface or intracellular vesicles	DAMPs, PAMPs	Downstream transcription factor activation (e.g. MyD88-dependent NF-κB activation)	(202)

Table 9: Pattern recognition receptors (PRRs)
Abbreviations: ALRs: Absent in melanoma 2-like receptors; CLRs: C-type lectin receptor; NLRs: Nucleotide-binding oligomerization domain-like receptor; P2XR7s: Purinergic receptor 2X ligand-gated ion channel 7; RAGE: Receptor for advanced glycation end products; RLRs: Retinoic acid-inducible gene (RIG)-I-like receptors; RIG-I: Retinoic acid inducible gene-I; TLRs: Toll-like receptors.

$P2RX_7$), or on intracellular vesicles, such as the endoplasmic reticulum (e.g. TLRs-3,-7,-8,-9), whilst others are less constrained and found in the cytosol (e.g. NLRs) (**Table 9**) (202, 203).

1.1.6.2.3. PRR activation by location: Cell surface, Intracellular organelle, & Cytosolic

After DAMP ligand engagement of a PRR, various proinflammatory downstream signalling pathways are activated. For example, TLRs are known to recruit a variety of adaptor proteins such as Myeloid differentiation primary response protein 88 (MyD88), Toll/interleukin-1 receptor domain-containing adapter protein (TIRAP), TIR-domain-containing adapter-inducing interferon-beta (TRIF), TRIF-related adaptor molecule (TRAM) (207). MyD88 is used by all TLRs, except intracellular TLR3, and activates transcription factor NF-κB and mitogen-activated protein kinase (MAPK) pathways, releasing NF-κB for nuclear translocation and induction of proinflammatory cytokines and other mediators of inflammation (202).

Cell surface PRRs TLR2 and TLR4 are activated by HMGB1, heat shock proteins (HSPs) and histones (43, 219). Investigators have demonstrated that TLR4 signalling contributes to severity in experimental AP, in terms of injury to the pancreas and lung, by ameliorating pro-inflammatory signalling in TLR4-knockout mice with AP (220) or in wild-type mice with AP which are engrafted TLR4-deficient hematopoietic cells (221). Another important surface PRR is RAGE, which is known for RAGE-dependent uptake of HMGB1 by macrophages (43), and the 'HMGB1-self DNA' complex is internalised by RAGE and is recognised by TLR9 (202). In experimental AP, RAGE has been found to modulate

inflammasome activation in macrophages, by activating the immune sensor AIM2 which initiates AIM2-inflammasome assembly (222).

TLR9 is found on ER membrane, and can bind to histones and plays a role in DNA recognition which may be important in inflammation where self-DNA is incompletely digested during apoptosis (43, 201, 202). In AP, activation of TLR9 is known to induce expression of genes which encode pro-cytokines and mediates the innate immune responses to nuclear and mitochondrial DNAs, histone and HMGB1 (201, 223).

Cytosolic PRRs, nucleotide-binding oligomerization domain-like receptors (NLRs) and retinoic acid-inducible gene-I-like receptors (RLRs) perform cytosolic DAMP/PAMP surveillance in many cell types, not only immune cells (43, 202). The NLRs are noteworthy as they include NOD-like receptor protein 3 (NLRP3) which resides in the cytosol and can form the NLRP3-inflammasome (201). ATP-induced NLRP3/caspase-1 inflammasome activation is mediated via the plasma membrane purinergic receptor $P2RX_7$ and has been shown to have a contributory role in experimental AP (43, 201).

1.1.6.3. Cytokines and proinflammatory intracellular signaling

Cytokines are small protein signalling molecules (usually 16 to 25 kDa) produced by a wide variety of cells including leucocytes, endothelial cells, fibroblasts and stromal cells, which trigger a plethora of inflammatory effects. Chemokines are a subclass of the latter, which induce chemotaxis in nearby responsive cells. Several circulating cytokines are robustly elevated in the plasma of AP patients and positively correlate with disease severity; most notably cytokines tumour necrosis factor α (TNFα), interleukins 1β (IL-1β) and 6 (IL-6), interferon γ (IFNγ) and chemokines interleukin 8 (IL-8) and monocyte chemoattractant protein (MCP-1) (94, 224-230). These mediators are secreted by injured acinar cells and peripheral blood mononuclear cells (PBMCs) (227, 231).

TNFα is released from many cell types including activated monocytes/macrophages, endothelial cells and pancreatic acinar cells (48, 225, 228, 230-233). The precursor protein, pro-TNFα, is a transmembrane protein that requires cleavage by TNFα converting enzyme (TACE; also known as ADAM17) to allow extracellular release of soluble TNFα. TNF (~20 types known) binds TNF receptors (~30 types known) and activates important signalling pathways, which include NF-κB translocation to the nucleus, as well as c-Jun N-terminal kinase (JNK), and p38 MAPK signalling (231, 233). NF-κB plays an important role in various stages of AP by mediating the expression of many genes involved in inflammation, including intercellular adhesion molecule 1 (ICAM-1) adhesion molecule expression in acinar cells (234, 235). TNF can induce cell death by apoptosis or necroptosis, both of which depend on the

non-ubiquitinatylated status of receptor-interacting serine/threonine protein kinase 1 (RIPK1) and recruitment of caspase 8 by the death effector domain of Fas associated via death domain (FADD) (233).

Another robustly elevated circulating cytokine in AP is IL-6, which binds to its receptors which are membrane bound (IL-6R) or soluble (sIL-6R) (236). The membrane-bound receptors are mainly found on hepatocytes and leukocytes (236). IL-6 bound to its receptor activates Jak-2-dependent STAT3 pathway (236). STAT3 is involved in regulation of apoptosis, inflammation, and the acute phase response, which includes CRP expression in hepatocytes (236).

The orchestrated induction of cytokines is a highly complex process, and is not well characterised in AP principally because the disease course and severity are so variable from person-to-person and there is cross-talk between pathways depending upon the involved cell types (237). Cytokine knockout mice can throw up unexpected results, for instance IFNy which is elevated in AP, particularly in severe disease, was found to be protective against pancreatic injury and neutrophil recruitment in cerulein-induced AP by repressing NF-κB activation (238).

Furthermore, the gut microbiota can have profound effects on the circulating cytokine profile and systemic inflammatory response, even in sterile DAMP-driven inflammatory conditions (239). One notable function of circulating inflammatory cytokines is to activate the endothelium which becomes more porous, allowing mediators to gain access to the intercellular space and promote infiltration of leucocytes, which in the case of AP is mostly neutrophil infiltration into the pancreas (43, 198).

1.1.6.4. Endothelium, leukocytes and platelets

1.1.6.4.1. Endothelial cells

Endothelial cells are the interface between the inflamed pancreas and the circulation, which play an important role in inflammation (240). Several adhesion molecules are required to facilitate leucocyte recruitment which is a critical step in the inflammatory response: These include vascular cell adhesion molecule-1 (VCAM-1), intracellular cellular adhesion molecule-1 (ICAM-1), endothelial leukocyte adhesion molecule-1 (ELAM-1), and E-selectin are expressed on endothelial cells, smooth muscle cells and tissue macrophages (240). These adhesion molecules, together with other mediators (e.g. proinflammatory lipid mediators), allow leucocytes to roll and firmly attach, before trans-endothelial migration (240, 241).

1.1.6.4.2. Leukocytes - Neutrophils

The dominant leucocyte in AP in terms of peripheral blood counts during the initial stages of AP with and infiltration into the pancreas, is the neutrophil. In humans, neutrophils are the most abundant circulating leucocyte, with ~60% of bone marrow dedicated to neutrophil production. These phagocytic cells are highly motile, terminally differentiated, and short-lived (191). Circulating neutrophils are quiescent, but can be primed and activated, with IL8 an important neutrophil-activating CXC chemokine (191). Neutrophils express a vast array of PRRs, particularly TLRs, and are thus able recognised and react to PAMPs and DAMPs (191, 242). Neutrophils are highly effective pathogen killers during the early phase of infection due to their capacity to rapidly recruit at sites of infection (e.g. by MIP2) where they provide the first line of defence by phagocytosing, killing, and digesting bacteria and fungi. A hallmark of AP is the accumulation of neutrophils in the pancreas, which have been shown to modulate the severity of both the local changes (e.g. by trypsin activation through NADPH oxidase) as well as the systemic manifestations of pancreatitis (44, 243, 244). Necrotic cell death, such as acinar necrosis in AP, can generate a profound local inflammatory reaction characterised by accumulation of neutrophils which leak proteases and other noxious agents that can damage the surrounding viable tissue (245). Such responses are classically considered as 'wound healing' homeostatic reactions to tissue injury, in which the phagocytic functions of neutrophils contribute to the clearance of debris (245). However, neutrophils are capable of causing profound collateral tissue injury in the process of debris clearance, and this overexuberant neutrophil activity contributes to tissue damage in sterile inflammatory stimuli (246). With regard to other granulocytes, eosinophils have been shown to accumulate and degranulate in the pancreas and promote inflammation and fibrosis during experimental AP (247). Mast cells appear to contribute to pancreatic and lung injury in experimental AP, as demonstrated by the amelioration of AP using a mast cell stabilizer (248).

1.1.6.4.3. Leukocytes - Macrophages

Macrophages are the major resident immune cell in the normal pancreas (249, 250). However, in pancreatitis, there is an influx of monocytes/macrophages from the bone marrow (249, 251). In mice, these infiltrative monocyte/macrophages highly express cell surface lymphocyte antigen 6 complex locus C protein ($Ly6C^{hi}$) (249, 252), become activated (249), and release cytokines and HMGB1 (213, 251). Infiltrative macrophages also help with tissue healing by promoting DNA damage repair by making high levels of heparin-binding epidermal growth factor receptor-like growth factor (HB-EGF) (253). In general terms, dendritic cells (DCs) function as instructors for the T-cell response by antigen presentation. DCs are also

normally present in the pancreas, but in contrast to macrophages, DCs do not appear to be harmful, but have a protective role when examined in experimental AP, with protection from pancreatic injury and reduction in circulating proinflammatory cytokines (254). Besides the observed depletion of circulating natural killer (NK) cell numbers in severe AP in humans (255), investigators have not found any significant role in clinical or experimental AP for NK cells (197, 249).

1.1.6.4.4. Leukocytes - Lymphocytes

RAG2 knockout mice, lacking both B and T cells, are partially protected against pancreatic injury in cerulein-induced AP (249). In clinical studies, there is a decrease in total circulating lymphocyte (T & B cell) counts in AP, particularly with severe AP, which is likely due to increased apoptosis as well as migration to the site of inflammation, but does not appear to have been thoroughly investigated (197, 199, 255-257). This pattern of repressed lymphocyte counts is also seen in non-pancreatitis critical illness (258).

With regard to B cells, whilst there is an overall decrease in CD19+ B cell number (256, 257), there is a relative increase in CD19+ B cells amongst a pure lymphocyte population, particularly with severe AP (259, 260). This at first appears contradictory, but reflects the composition of the parent population pool from which the percentages are calculated. Anti-inflammatory IL-10 producing B cell subset populations are quantitively smaller in severe AP, as compared with mild AP (256).

With regard to T cells (CD4+ and CD8+), these known to be present in small numbers in the normal pancreas, but have been shown to be recruited into the pancreas in experimental AP (250). It is unknown to what extent T cell activity contributes to SIRS in pancreatitis but circulating concentrations of inflammatory mediators made by T cells (and other cells) are robustly elevated in the plasma (250). The CD4+ (helper) T cell subgroup contributes to pancreatic injury in experimental pancreatitis, whereas the cytotoxic (CD8+) subgroup do not (250). It is unclear how CD4+ cells induce acinar cell injury, particularly since the most likely culprit, the macrophage activator IFNγ, has surprisingly been found to be protective with regards pancreatic injury in experimental pancreatitis using a global IFNγ knockout (238). It might be postulated that HIV-induced CD4 cell depletion could clarify the importance of CD4+ lymphocytes in AP, but the clinical data are confounded by the use of anti-HIV medications which are known to be associated with AP and hypertriglyceridemia (70). Whilst there are increased circulating concentrations of CD4+ T helper cell type 1 (Th1) cytokines (ie. IFNγ, TNFα) as well as CD4+ Th2 cytokines (i.e. IL-4, IL-5, IL-10) in AP, there appears to be a robust asymmetrical suppression of CD4+ subgroup populations. Specifically, the Th1 subpopulation

seems to be more diminished than the Th2 subgroup and have altered inflammatory signalling profiles (199, 257, 261). It seems likely that altered lymphocyte transcriptome following and attack of AP affects the host's capacity to defend against opportunistic and nosocomial infections (199).

1.1.6.4.5. Platelets

Circulating platelets are known to be activated in AP patients (262). Platelet integrin glycoprotein IIb/IIIa (GPIIb/IIIa) is a receptor for fibrinogen and von Williebrand factor and contributes to platelet activation. Activated platelets typically secrete the arachidonic acid metabolite thromboxane A2, as well as an array of immunomodulatory mediators (e.g. histamine and serotonin), and undergo morphological changes. Activated platelets are known to engage with, and activate, neutrophils by forming platelet-leukocyte aggregates (PLAs). A platelet-activating factor antagonist, Lexipifant, was tested in a large-scale multi-centred double-blinded randomized trial in the UK examining its clinical effect on reducing SIRS and AP-MODS in acute pancreatitis (263). The treatment arm was associated with repression of circulating proinflammatory inflammatory mediators, inferring an immunological benefit, but did not demonstrate improvements in preventing organ dysfunction, which was the main study outcome. This was in part due to the unexpectedly high proportion of included participants with established organ dysfunction prior to drug delivery (263). It is most likely that platelet activation does contribute to SIRS/MODS given some of the improvements in soft end-points in the Lexipifant study and from experimental data showing that platelets promotes neutrophil accumulation in pancreas and lung in pancreatitis, which is in part mediated by platelet production of MIP-2 and CXC chemokines (264-266).

1.1.6.5. Neuro-endocrine stress response

Critical illness is characterized by alterations in the hypothalamic—anterior pituitary—peripheral hormone axes, which profile changes between the 'acute', 'chronic' and 'recovery' phases of critical illness survivors (267). In contrast to cytokines which are produced by a variety of cells and have effects on a large spectrum of effector cell types, hormones are distinctly produced by select specialist cells and have more restricted target effects. The early acute phase response (first hours to a few days) involves increased systemic cortisol availability, elevations in catecholamines, growth hormone, and altered thyroid axis function, due to complex mechanisms involving increased pituitary secretion, altered peripheral endocrine organ sensitivity and activity, altered plasma protein binding, and reduced hormone clearance (154, 267-269). There is activation of the sympathetic nervous system, and other

neuro-hormones vasopressin and dopamine are also elevated in critical illness and AP (154, 267, 269, 270).

The situation is complicated by target tissue resistance to circulating hormones, in part due to proinflammatory cytokine effects on hormone receptor expression (267). The stress-induced hypercortisolism observed in critically ill patients has many profound physiological effects from stimulating catabolism, supporting cardiovascular function and immunomodulatory effects. All of the aforementioned acute phase hormones, plus glucagon from the pancreas, collectively help maintain tissue perfusion and release rapid provision of energy substrates (e.g. glucose, fatty acids, and amino acids) from body stores (271). The stress hormone profiles change substantially, however, over the duration of the disease course. The most dramatic clinical presentation of this change is the onset of adrenal insufficiency, which may require therapeutic supplementation with catecholamines and hydrocortisone infusions in the critical care department. In experimental AP in rats, hydrocortisone showed beneficial effects in relation to reduced early mortality and suppression of cytokines and arachidonic acid breakdown products (272). Dopamine, which is often used in critical care for its vasopressor effects, appears to have anti-inflammatory effects in the context of experimental AP (270). Other important hormone systems may dysregulate during critical illness, such as insulin resistance and sick euthyroid syndrome (271).

Additionally, heavy alcohol consumption, a frequent inducer of AP, has complicated effects upon the hypothalamic and extrahypothalamic stress regulation pathways, with acute binge intoxication driving blood cortisol and norepinephrine levels, whilst chronic consumption causes neuroendocrine tolerance and blunted stress responses (273). Finally, heavy alcohol consumption can give rise to sympathetic dominance and repressed parasympathetic activity with altered cardiovascular effects (274).

1.1.6.6. Resolution of the systemic inflammatory response and organ failure in AP

1.1.6.6.1. The proinflammatory response in microbial invasion versus sterile inflammation

The acute inflammatory response is an important protective mechanism against host attack, such as infection or injury, but must be switched off to avoid the ill effects from nonresolving inflammation when the offending insult is neutralized (275). The need for a local inflammatory response is most apparent in cases of microbial invasion, as opposed to a sterile insult, and the SIRS response, particularly multiple organ dysfunction, appears to be have no clear benefit in sterile inflammation.

1.1.6.6.2. Resolution of inflammation

Uncontrolled inflammation, in terms of magnitude and duration, is potentially very damaging for the host, and to avoid excessive inflammation there exists inbuilt endogenous control mechanisms (276). In self-limiting inflammation, the host inflammatory response actively participates in successful resolution, which requires more than simply passive dilution of proinflammatory mediators (276). Resolution is a complex orchestrated process which involves actions by leukocytes, cytokines, hormones and specialised proresolving mediators. Anti-inflammatory lipid mediators include eicosanoids and 'specialized pro-resolving lipid mediators' (SPMs), which are known to be key signalling molecules in the resolution of inflammation, play a pivotal role in regulating the inflammatory profile and return to homeostasis. SPMs thwart inflammation by chemokine sequestering and eliminating chemoattractant gradients thereby inhibiting neutrophil chemotaxis, promoting leukocyte engulfment, and stimulating resolution through the recruitment and differentiation of macrophages to clear cell debris and apoptotic neutrophils from inflamed tissue (241). SPM comprise lipoxins, resolvins, protectins, and maresins which are biosynthesized from arachidonic acid and omega-3 fatty acids (241, 277).

1.1.6.6.3. Resolution in acute pancreatitis

Failure to resolve inflammation can lead to excess tissue damage, such as persistent multiple organ dysfunction in AP, or the development of chronic inflammation in the form of chronic pancreatitis. It is known that neutrophil extracellular traps (NETs) are used to degrade cytokines and chemokines, thereby disrupting neutrophil recruitment and activation (278). And together with macrophages, neutrophils also appear to have a regulatory role in pancreatic regeneration (279). With regard to systemic inflammation and proresolving lipid mediators, observational studies have shown that impaired clinical recovery amongst major trauma patients is associated with higher ratios of proinflammatory leukotriene pathway gene expression to resolvin pathway genes, which begs the question as to whether this balance could be pharmacologically tipped in favour of proresolution, and if doing so could expedite recovery (241). Indeed, manipulation of resolution-regulating lipid mediators might be of benefit to patients of all-cause critical illness and lipid mediator resolution therapies may become part of a multimodal immunomodulatory approach (277). Whilst SPMs have received little clinical study in AP, there has been encouraging research activity with SPMs in experimental AP, which have shown to ameliorate injury to both pancreas and lung (280, 281).

1.1.7. Long-term sequelae of acute pancreatitis

Of those who survive an attack of AP, there are potential sequelae which may arise long after apparent clinical resolution (282). Transition from AP to clear-cut chronic pancreatitis occurs in ~4% of cases (282), and transition to recurrent episodes of AP in ~20% (58). Those who get recurrent AP are then at higher risk of subsequently developing chronic pancreatitis (58, 282). Endocrine and exocrine and dysfunction are far more common after AP than in the general population (87). With regard to the former, newly diagnosed diabetes mellitus (DM) is much higher after AP (23%) than in the general population (4-9%) (283). Following discharge from hospital after AP, the prevalence of DM is two-fold at 5 years compared with rates at 12 months (283). Post-pancreatitis diabetes mellitus is more common amongst those who had severe AP and in alcohol-related pancreatitis (58, 284). Steatorrhoea, the main symptom of exocrine dysfunction, is common after substantial pancreatic necrosis (58). Pancreatic exocrine insufficiency can lead to maldigestion and malabsorption and there is an increased risk of developing osteoporosis years after AP, particularly amongst females aged 50-64 years old, and with recurrent AP (58, 285).

Following AP, cross sectional imaging may reveal anatomical abnormalities of the gland such as pseudocysts and peripancreatic vascular complications (e.g. splenic vein thrombosis or splenic artery aneurysm). In the longer term, pancreatic atrophy, ductal changes or parenchymal calcification are well recognised. There is little clinical evidence that AP, unlike chronic pancreatitis, is a risk factor for pancreatic cancer, however occult pancreatic cancer should be considered as a possible trigger of AP in patients aged over 50 years old if no aetiology factor is identified (286).

As is generic amongst surviving critical care patients, AP hospital survivors with persistent early organ dysfunction, as compared to those who had mild disease, have been shown to have a reduced life expectancy upon hospital discharge (287). Severe AP patients were more likely than match controls to develop cardiovascular, gastrointestinal, pulmonary and neoplastic disease (288). More specifically, these consisted of myocardial infarction, congestive cardiac failure, DM, liver disease, peptic ulcer disease, peripheral vascular disease, pulmonary disease, cancers and renal disease (288). As for actual cause of death amongst AP hospital survivors, the most common fatal conditions were neoplasia, vascular, digestive/metabolic and respiratory causes (288). The biggest difference between the general population and was the 3-fold increase in proportion of digestive/metabolic deaths in ccAP survivors, classified by the 10th revision of the international statistical classification of diseases and related health problems (ICD-10) chapters III, IV, XI, XVIII (288).

1.1.8. Potential treatments for acute pancreatitis

1.1.8.1. Previously tested targeted AP drugs have failed

A high-quality systematic review of pharmacological interventions for AP tested in randomised controlled trials has been published by the Cochrane Library in 2017 (289). The investigators analysed 78 trials which met inclusion criteria, to assess the effects firstly on short-term mortality for a vast array of treatments in AP patients: antibiotics, antioxidants, aprotinin, atropine, calcitonin, cimetidine, EDTA, gabexate, glucagon, iniprol, platelet activating factor receptor antagonist (Lexipafant), NSAIDs, octreotide, oxyphenonium, probiotics, activated protein C, somatostatin, somatostatin plus omeprazole, somatostatin plus ulinastatin, thymosin, ulinastatin, and inactive control (289). This extensive list included protease inhibitors (gabexate, aprotinin and ulinastatin), an anticholinergic drug (oxyphenonium), hormones (thymosin, calcitonin, octreotide) and acid suppressants (cimetidine and omeprazole). The authors had several other outcomes of interest besides short term mortality, including as 'serious adverse events', 'adverse events', 'organ failure' and 'sepsis'; please see publication for definitions on 'adverse' and 'serious adverse' events (289). The authors summarised their findings by concluding that there:

"***was no evidence of difference in short-term mortality between the groups in any of the comparisons****. However, the confidence intervals were wide and consistent with significant benefits or harms of interventions"*.

Of all the interventions, Lexipafant appeared to be the most promising agent. The last clinical trial by Johnson *et al.* was hoped to demonstrate an improved short-term mortality but the results were not consistent with survival benefit (263). An independent critical appraisal of the Lexipafant AP studies has been published and is recommended for interested readers (290).

1.1.8.2. Benefits of organ support

However, there are many therapies and interventions offered by modern critical care departments which have been shown to optimize organ function (e.g. low tidal volume ventilation and prone positioning in moderate/severe ARDS) which likely extend to AP-MODS patients, and offer a survival advantage. In particular, a critical review of the evidence of certain pulmonary interventions (which is the most frequent extra-pancreatic organ to fail in AP-MODS) can be can be sourced from the Intensive Care society website <www.ics.ac.uk> (e.g. Guidelines on the management of acute respiratory distress syndrome, V1, 2018).

1.1.8.3. Potential new AP-specific pharmacological therapies

Despite the concerns that AP research is dramatically on the decline relative to research activity in other areas of gastroenterology (291), there is a raft of exciting new possibilities on the horizon, and interested readers can interrogate ClinicalTrials.gov or the ISRCTN registry websites for the latest registered trials. Some of the upcoming pharmacological therapies entering clinical trials have been captured by PJ Lee and GI Papachristou in a recent review published in *Nat Rev Gastroenterol Hepatol.*, with diverse drug targets such as: calcium release-activated channel (CRAC), mitochondrial permeability transition pore (MPTP), HMG-CoA, G protein-couples receptor 81 (GPR81), TNF synthesis, unsaturated free fatty acids and IL-6 (292). Additionally, new technologies have emerged from the pharmaceutical industry, such as the CytoSorb® which aims to remove cytokines from the circulation by extracorporeal cytokine adsorption (293). Meanwhile some investigators have adopted a different approach to organ dysfunction and are focussed on the restoration of cellular ATP levels with the hope of enhancing the functional recovery of tissues, akin to recharging 'flat batteries', with restoration of cellular ATP levels by nutrition, to protect acinar cells and vital organ function (294-296).

One novel avenue for modulating the systemic inflammatory response and multiple organ dysfunction in AP is the kynurenine pathway of tryptophan metabolism (297) which has been the focus of this PhD thesis.

1.2. The kynurenine pathway of tryptophan metabolism

1.2.1. Essential nutrients, including B-vitamins and amino acids

All organisms, not least humans, require micronutrients for healthy metabolic functioning. Essential micronutrients are particularly important biochemical compounds which cannot be synthesized at sufficient quantities within an organism, if at all, and therefore must be externally sourced from the diet to maintain health. In disease states, such as acute inflammation and critical illness, concentrations of many micronutrients alter, having many systemic repercussions on metabolism and inflammation (298).

1.2.1.1. Vitamins

Essential micronutrients for human health fall into four categories: minerals, essential fatty acids, essential amino acids and vitamins. The latter group was originally termed '*vitamine*', by Polish chemist Casimir Funk (1884-1967), because they were 'vital' for health

and, on account of their nitrogenous content, were mistakenly thought to include an amine group, which is of course true of amino acids (299). However, the term was popularised and remains today as '*vitamin'*. There are 13 vitamins required by humans for metabolic functions, which comprise the four fat-soluble vitamins A, D, E, K, as well as water-soluble vitamin C and the 8 B-vitamins (B_1, B_2, B_3, B_5, B_6, B_7, B_9, B_{12}). The term '*vitamer*' refers to a chemical compound which has a similar molecular structure to a particular vitamin and shows vitamin activity in a biological system. With regard to the metabolism of amino acid tryptophan, which is discussed later, there are three notable B-vitamins which play important roles in the oxidat--ive kynurenine pathway: these are B_2 (riboflavin and associated vitamers), B_3 (niacin and nicotinamide) and B_6 (pyridoxine and vitamers) (**Figure 7**). The numbers within the B-vitamin category are not sequential as others have come and gone, having been debunked as vitamins and lost their status. These include, choline/adenine (formally B_4), adenosine monophosphate (formally B_8), para-aminobenzoic acid (formally B_{10}), pteryl-hepta-glutamic acid (formally B_{11}). B_6 comprises of six vitamers: pyridoxal (PL), pyridoxamine (PM), pyridoxine (PN), and their corresponding phosphorylated forms (300). Pyridoxal 5'-phosphate (PLP) is the active coenzyme form of vitamin B_6, which is an important cofactor for many metabolic enzymes, including those which metabolise amino acids. Further details can be found below regarding particular vitamers: PLP (section 1.2.6.2.) and FAD (section 1.2.7.2).

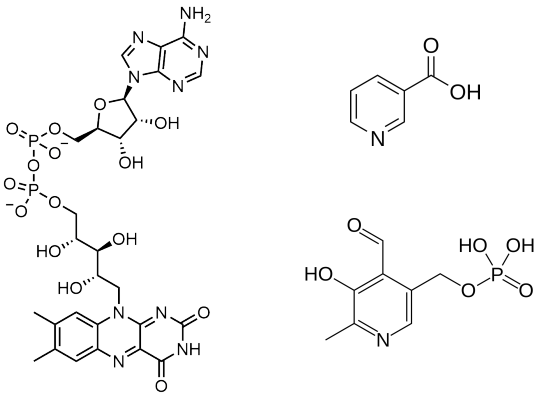

Figure 7. B-vitamins necessary in the kynurenine pathway
Left: Flavin adenine dinucleotide (B_2 vitamer). Top right: Nicotinic acid (B_3). Bottom right: Pyridoxal 5-phosphate (B_6 vitamer). Images from Wikipedia.

1.2.1.2. Amino acids

Amino acids are defined as structural organic units, or monomers, that contain basic amine ($-NH_2$) and acidic carboxyl (-COOH) groups, centralised on a carbon atom. By way of comparison, ketoacids similarly contain a carboxyl (-COOH) group but contain a ketone ($RC(=O)R^1$) group, rather than an amine. Integral to their function, each amino acid possesses a unique organic *R* group (or side chain) appendage (**Figure 8**). When the latter is an aryl group, also called an aromatic ring, such amino acids are termed 'aromatic'. Aromatic molecules have low tendency for reactivity and are thus

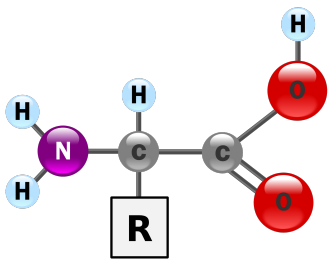

Figure 8. Amino acid structure
Each amino acid has an $-NH_2$ amine group, and a -COOH carboxyl group, and an individual -R side chain. Image from Wikipedia.

chemically very stable. With the exception of glycine (because of its structural simplicity), all amino acids have L- (*laevorotatory*) and D- (*dextrorotatory*) stereochemical isoforms, with a mirror-image structural orientation, akin to the similarities between left and right feet. This structural distinction is important, since the difference of L- or D-isomeric configuration can have functional biological implications. For example, L-tryptophan, which has a strong bitter flavour has a 100-fold greater affinity to bind albumin than D-tryptophan, which cannot easily cross the blood brain barrier and is sweeter than sucrose to taste (301, 302). However, across all the kingdoms of life, cells predominantly use L-amino acids (303).

There are over 140 known amino acids which are component residues of naturally occurring proteins (304, 305). Few amino acids independently enact biological activities, rather they tend to function as proteins by forming peptide chains ('polypeptides'). There are 22 amino acids that are naturally incorporated into polypeptides, and therefore described as natural, or 'proteinogenic', amino acids (304). Two of these, selenocysteine and pyrrolysine, are incorporated into proteins by unique synthetic mechanisms, whilst 20 amino acids are encoded by genetic codes of living organisms and are called 'canonical' amino acids. Of these 20 protein-forming amino acids, nine are commonly termed 'essential' with regard to human health (i.e. His, Ile, Leu, Lys, Met, Phe, Thr, Trp and Val). Because the human body cannot synthesize them *de novo*, they must be externally sourced, normally by dietary ingestion. Additionally, other amino acids are described as semi-essential depending on the stage of growth and development. In mammals, skeletal muscle is the largest reservoir of both peptide-bound and free amino acids (306).

1.2.1.2.1. An overview of amino acid functions

Amino acids have diverse roles which include cellular fuel, signalling, regulators of gene expression, precursors for synthesis of hormones and small-molecule nitrogenous substances with enormous biological importance. Plasma amino acid concentrations are maintained at relatively constant levels in the post-absorptive state in health, but can alter with pathophysiological conditions such as disease, lactation and pregnancy (304). Altered levels of amino acids and their products can have pathological consequences (304). Interestingly intra-peritoneal dosing of rodents with arginine, ornithine and lysine have been shown to induce experimental acute pancreatitis, but the primary biological mechanism is unclear (10). There are a small number of amino acids which have profound neurophysiological effects; some are inhibitory neurotransmitters (e.g. GABA) whilst others are excitatory (e.g. Glutamine/Glutamate).

Genes encoding enzymes to metabolise arginine and tryptophan are known to respond to pro-inflammatory mediators, a key feature that distinguishes them from other amino acids. Inflammatory cues induce expression of inducible nitric oxide synthase (iNOS) and two arginase isoforms (*ARG1*, *ARG2*) which metabolise the former, whilst isoforms of indoleamine 2,3-dioxygenase (*IDO1*, *IDO2*) catabolised tryptophan (307).

1.2.2. Tryptophan

1.2.2.1. L-tryptophan overview

The aromatic amino acid L-tryptophan (tryptophan), is required by all forms of life for protein synthesis and is a precursor for several bioactive compounds that are known to be important for mammalian physiology, such as the neurotransmitter serotonin (5-hydroxytryptamine), the hormone melatonin, the immune-modulatory kynurenines, and nicotinamide adenine dinucleotide (NAD^+). Tryptophan has vitamin-like properties through its ability to replace pellagra-preventing dietary factor niacin (vitamin B_3) at times of dietary niacin shortage. In the plant kingdom, where tryptophan is biosynthesised, tryptophan has several important biological roles in pollination, development, and plant-pathogen interactions. Tryptophan is incorporated into polypeptides or metabolized into auxin, glucosinolates, phytoalexins, alkaloids, and other important indolic compounds (308, 309). Polypeptide amino acids translated from human genes are exclusively in the L-isomer configuration. In recent years it has been established that D-amino acids can in rare instances be post-translationally introduced into polypeptides, however D-tryptophan occurs exceptionally rarely amongst the appearance of D-amino acids (303, 310, 311). Indeed, only the L-isomer (i.e. L-tryptophan) can cross the blood-to-brain barrier (306).

1.2.2.2. Discovery and naming of tryptophan

Tryptophan was first isolated in the early 1900s by British biochemists FG Hopkins and SW Cole (312). Hopkins, along with Christiaan Eijkman of Holland, was later a recipient of the 1929 Nobel Prize in Physiology or Medicine for the discovery of vitamins. Hopkins and Cole digested the phosphoprotein milk extract, casein, with pancreatic secretions [liquor pancreaticus (Benger)] in the presence of glyoxylic acid. The name tryptophan, appears to have come from the fact that it is 'revealed by tryptic digestion of a protein' (302). Additionally, the term 'tryp-', seems to have originated from Greek 'τρῖψις' ('*trîpsis'*, or 'rubbing') referring to the yield of digestive fluid released from rubbing of the pancreas. Of the 20 canonical amino acids, tryptophan is the largest by molecular weight, but is the least chemically abundant

canonical amino acid in proteins and cells. As with the other aromatic amino acids (tyrosine and phenylalanine), tryptophan is naturally fluorescent (313), but possesses some unique features which include the possession of an indole structure, and the ability to bind serum albumin. Other amino acids, such as glutamine or cysteine are naturally linked in plasma to metals, such as copper (314, 315). Indeed only ~10% of tryptophan is freely diffusible, ensuring that there is a storage pool of circulating tryptophan awaiting release (301, 302, 316). Non-esterified fatty acids, and a small number of drugs, are known to be able to displace circulating tryptophan from its bond with albumin (302, 314).

1.2.2.3. Biosynthesis of tryptophan

Humans lack the biochemical pathways to produce tryptophan, the costliest amino acid to synthesise, it is therefore derived from the diet and microbiome. Tryptophan biosynthesis is performed by lower organisms including most plants, algae, bacteria, and fungi, as well as some parasitic protozoans, utilising the shikimate pathway in the initial steps. This pathway is also responsible for the synthesis of other aromatic amino acids; namely phenylalanine and tyrosine (317). The shikimate-chorsimate pathway is a seven-step biosynthetic metabolic route

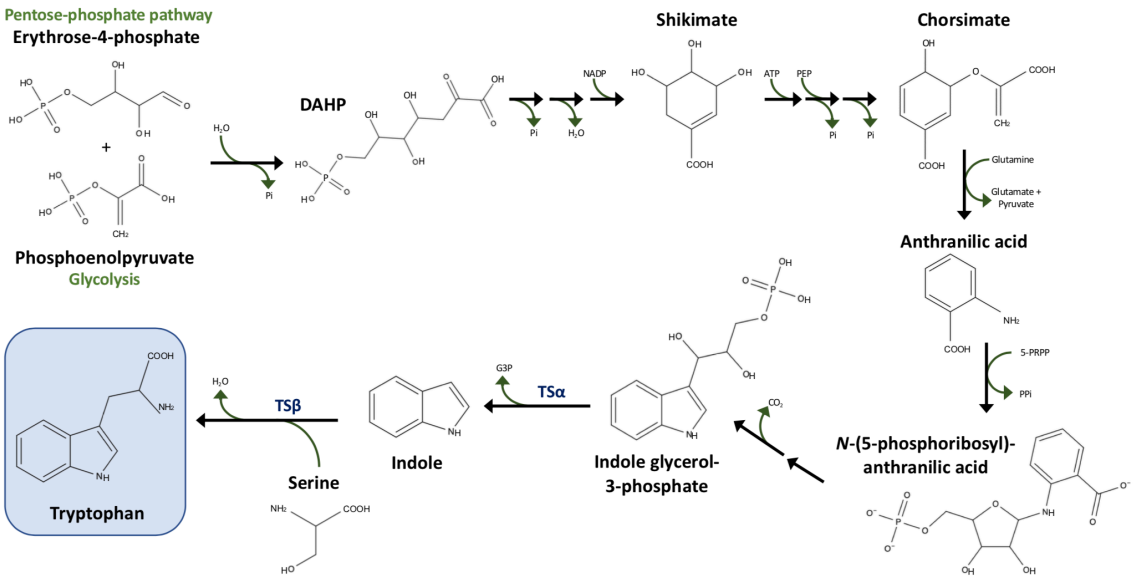

Figure 9. **Tryptophan biosynthesis by the shikimate and the tryptophan pathways**
Tryptophan biosynthesis starts through the seven-step shikimate pathway. The shikimate pathway produces chorismate, a common precursor for aromatic amino acids, at which point the biosynthesis of tryptophan diverges from that of tyrosine and phenylalanine. The tryptophan pathway converts chorismite to tryptophan via six enzymatic steps. These pathways are present in lower organisms e.g. plants, bacteria. Abbreviations: ATP: adenosine triphosphate; DAHP: 3-deoxy-*D*-arabiono-heptulosonate-7-phosphate; G3P: glyceraldehyde 3-phosphate; PEP: phosphoenolpyruvate; 5-PRPP: 5-phosphoribosyl pyrophosphate; Pi: inorganic phosphate; PPi: inorganic pyrophosphate; NADP: nicotinamide adenine dinucleotide phosphate; TSα: tryptophan synthase α subunit; TSβ: tryptophan synthase β subunit.

which starts with intermediates from glycolysis and the pentose-phosphate pathway, the 3-carbon phosphoenolpyruvate (PEP), and the 4-carbon erythrose-4-phosphate (E4P), respectively, which are condensed into the 7-carbon compound, 3-deoxy-*D*-arabino-heptulosonate-7-phosphate (DAHP) (**Figure 9**, above). The end product of the shikimate pathway is chorismite, which requires an ATP-dependent phosphorylation step (shikimate to shikimate 3-phosphate) (318, 319).

After the formation of chorismite, tryptophan synthesis diverges from that of phenylalanine and tyrosine: The initial enzymatic step converts chorismite to anthranilate. Three mores intermediate steps are involved, before the final two steps which are both catalysed by the $\alpha_2\beta_2$ tetramer bi-enzyme complex, called tryptophan synthase. The α-subunit cleaves indole glycerol-3-phosphate into separate indole and glyceraldehyde-3-phosphate, and transports the indole through a molecular tunnel before the β-subunit can complete a condensation reaction by coupling of serine with indole, resulting in tryptophan formation (317, 320-322).

A group of genes called the *trp* operon encode a cluster of enzymes for the biosynthesis of tryptophan in organisms that can make tryptophan. Regulation of the *trp* operon is interesting and complex, with different mechanisms amongst bacterial genera (323). High and low intracellular tryptophan concentrations modulate *trp* operon transcription through a complex gene regulatory negative feedback loop. A *trp* repressor reduces expression of the *trp* operon, whilst attenuation promotes termination of *trp* operon transcription (324). Because tryptophan biosynthesis is costly process in terms of energy consumption, many gut-commensal bacteria (e.g. *E. Coli*) preferentially transport tryptophan intra-cellularly from their environment by way of specialised permeases transmembrane transport proteins for nitrogenous and tryptophan metabolites needs and resort to *de novo* biosynthesis only when the environment is tryptophan deficient (325, 326).

1.2.2.4. The fate of dietary tryptophan

Besides aforementioned milk as a source of tryptophan, other natural food types rich in this amino acid include poultry, egg, soy, bean, tuna fish, oats, bananas, dried prunes, rice, cheese, bread, peanuts and chocolate (327, 328). The World Health Organisation (WHO) report in 2007, set the recommended tryptophan intake at 4 mg kg^{-1} day^{-1} for healthy metabolism (329), supported by original work from Lazaris-Brunner *et al.* (330). The necessary quantity of tryptophan is less than the other eight essential amino acids which ranges from 10 mg kg^{-1} day^{-1} (Histidine and Methionine) to 39 mg kg^{-1} day^{-1} (Leucine) (329).

After a meal, proteins are digested into di- and tri-peptides, referred to as oligopeptides, as well as single amino acids, by the action of pancreatic proteases (trypsin, chymotrypsin, elastase, and carboxypeptidases) (4, 331). Oligopeptides absorbed from the intestinal lumen do so along the brush border via oligopeptide transporters, and are cleaved by intracellular peptidases into single amino acids (331). There are general ubiquitously expressed neutral amino acid transporters, as well as high-affinity and highly-selective transporters which are important for efficient uptake when concentrations are low (332, 333). Local mediators such as cytokine IFNγ can induce tryptophan-selective uptake which is important since IFNγ regulates indoleamine 2,3-dioxygenase (IDO) activity and depletes intracellular tryptophan levels (334). Tryptophan and other aromatic amino acids that are not immediately metabolised, are transported through intestinal enterocytes by amino acid transporter SLC6A19 (B^0AT1), and exit the basolateral side via SLC16A10 (TAT1) towards the portal blood (331). Recently tryptophanyl-tRNA synthetase has also been found to play an important role in high-affinity intra-cellular transport of tryptophan, possibly by secretion of TrpRS into the extracellular space where it binds tryptophan and re-enters the cell (335). Mutations in genes encoding specialised transporters can result in systemic disorders, for example Hartnup disease results from functional mutations in *SLC6A19* (331, 336). Not all dietary tryptophan directly absorbed by the human host, but is instead metabolised within the gut by three major pathways (328):

i) Gut microbiota can directly metabolise tryptophan to indole, indicant, tryptamine, and skatole, and indole derivatives (337). These are ligands of the aryl hydrocarbon receptor (AhR) and have important roles in gut immune homeostasis (325, 338-341).
ii) Serotonin is generated from tryptophan by specialised host intestinal enterochromaffin cells and by gut-resident bacteria. Serotonin plays an important role in modulating gut motility, sensation and secretion. Gut serotonin does not ordinarily cross the blood-to-brain barrier, but rather is metabolised and excreted in the urine as 5-hydroxy-indoleacetic acid (5-HIAA). Normally ~2% of ingested tryptophan is metabolised to 5-HIAA, which can increase to as much as 60% in patients with malignant carcinoid syndrome (342-345).
iii) The human gut immune and epithelial cells can metabolise gut tryptophan through the kynurenine pathway via enzymatic action of indoleamine 2,3-dioxygenase (IDO) (346).

In circulating blood, ~90% of total plasma tryptophan is albumin-bound, with the remainder as a free, unbound form. The two states exist in equilibrium, and concentrations together alter with light-dark cycle circadian rhythms (347-349). Tryptophan is not biologically inert, and suppresses gluconeogenesis by the inhibition of phosphoenolpyruvate

carboxykinase, so tryptophan depletion tends to increase plasma glucose levels (350). Nitrogen-balanced healthy adults use less than 1% of dietary tryptophan for anabolic protein synthesis, because the amount of protein degradation and synthesis is well matched (351) (302). Where tryptophan is utilised in the biosynthesis of proteins, the action of tryptophanyl tRNA synthetase is necessary to catalyse the addition of tryptophan. The plasma concentration of tryptophan is ~40-80 μM in humans and slightly higher in mice (~60-100 μM) (352), and levels negatively correlates with increased biological age (353).

Tryptophan can only be transported across the blood-to-brain barrier in its free form by neutral amino acid transporters (354). A major determinant of the ratio of free tryptophan to albumin-bound tryptophan is the plasma concentration of non-esterified fatty acids (NEFAs), which also bind to albumin and by doing so displace tryptophan from its binding site (355), resulting in an elevation of plasma free tryptophan (356, 357). In pregnancy, free plasma tryptophan levels are elevated by a combination of albumin depletion and NEFA elevation, however the total tryptophan levels are actually reduced (351). Clinical studies have shown that tryptophan restriction increases rates of psychiatric disturbance in those with pre-existing psychiatric disease (358).

1.2.2.5. Tryptophan deficiency

Tryptophan levels are monitored by at least two distinct signal transduction pathways in mammalian species; sufficiency is monitored by mTOR (mammalian target of rapamycin) and deficiency by GCN2 (general control nonderepressible 2) (307, 359, 360). GCN2 is an amino acid sensor that binds uncharged tRNAs that accumulate when intracellular amino acids are depleted. Tryptophan deficiency results in GCN2-dependent phosphorylation and activation of the eukaryotic initiation factor 2 alpha (eIF2α), a GTP binding protein which plays a central role in initiating protein synthesis and cell growth (361). T lymphocytes are very sensitive to tryptophan shortage, which causes their arrest in the G1 phase of the cell cycle (362). Furthermore, tryptophan deficiency stress via GCN2 synergizes with proinflammatory cytokine production to increase innate immune responsiveness (363).

Severe dietary tryptophan restriction in laboratory animals has metabolic and immunological effects in the form of weight loss and B cell development arrest (364), as well as tendency towards cataract formation (365). Prolonged severe deficiency in tryptophan or niacin in humans causes pellagra, which is characterized by the “four D’s”: Dermatitis, diarrhoea, dementia and death (366, 367). Some disease states are known to correlate with altered tryptophan levels. For example, elevated tryptophan levels have been observed in

allergic diseases (368) and acute sleep deprivation (348, 349). Low tryptophan levels are seen in HIV/AIDS (369, 370), cardiovascular disease, major trauma, sepsis, and multiple organ failure, as well as severe AP (371-375). By way of contrast, excess circulating levels of tryptophan may cause systemic toxicity, which can more easily affect non-human mammals on account of a different form of TDO when they are administered a diet with high tryptophan content (376).

1.2.2.6. Tryptophan metabolism

Tryptophan is the precursor of many physiological important metabolites produced during the course of its degradation along 4 pathways; 3 of which are of quantitatively minor significance, whilst the kynurenine pathway accounts for ~95% of overall tryptophan degradation (377). The three quantitatively minor pathways (and their important products) involve: (1) hydroxylation (serotonin as neurotransmitter and gastrointestinal hormone, and melatonin in the pineal gland); (2) decarboxylation (trace amine called tryptamine); and (3) transamination (indole 3-pyruvate).

Approximately 1-2% of ingested tryptophan is metabolised by the serotonin pathway (337). The neurohormone melatonin is almost exclusively synthesised within the pineal gland and varies dramatically in a circadian fashion and plays an important neuroendocrine signalling role, conveying circadian and seasonal information to multiple organ systems. The rate-limiting step is in the synthesis of melatonin from serotonin is catalysed by the cytoplasmic enzyme arylamine *N*-acetyltransferase (AANAT; EC 2.3.1.5), an enzyme that displays circadian rhythm activity, with higher activity during the dark phase, as opposed to the light-phase (347). Melatonin is catabolised to kynuramines which are thought to have a role in promoting sexual behaviour (350). Trace amines including tryptamine are found at levels approximately 100-fold lower than traditional monoamines such as serotonin (378). Tryptamine is thought to play a neuromodulatory role, possibly as a neurotransmitter, and has some weak excitatory effects in small animals (378, 379). Transamination of tryptophan gives indole-3-pyruvate, which is a ligand of the aryl hydrocarbon receptor (AhR) with anti-inflammatory effects and, in clinical studies, reduces anxiety and promotes sleep (350, 380, 381), and is a precursor for kynurenic acid (382).

The major catabolic route of tryptophan in both the brain and the periphery, consists of metabolism along the kynurenine pathway which generates an array of biologically active indole-derived metabolites, collectively termed ‘kynurenines’, which have bioactive properties involved in excitatory neurotransmission (383), immune responses and inflammation (308, 350, 377, 384).

1.2.3. The kynurenine pathway

1.2.3.1. Discovery of the kynurenines

Half a century before the discovery of tryptophan, German chemist Justus Freiherr von Liebig in 1853 isolated a colourless acidic substance from dog urine, which he named 'kynurenic acid' (derived from '*kynos' – 'ouron'* acid) meaning 'dog' ('κῦων' or '*kynos*') and 'urine' ('οὖρον' or '*ouron*') in the original Ancient Greek. This is generally considered to be the first of the kynurenine pathway metabolites to be identified (although anthranilic acid was discovered 12 years prior), which are collectively termed the 'kynurenines'; a pathway that is conserved in insects, rodents and humans (385). By feeding dogs a protein-rich meat diet, Liebig later found he could increase urinary quantities of kynurenic acid sufficient to allow chemical analysis. The precursor of kynurenic acid, 'kynurenine', was discovered in 1925 by Japanese investigators Matsuoka and Yoshimatsu (386). Beadle and colleagues later determined kynurenine to be an intermediate between tryptophan and nicotinic acid in 1947 (387). Over the last century, particularly between 1930 to 1980 (**Figure 10**), many discoveries have been made in regard to the identity of metabolites and kynurenine pathway enzymes.

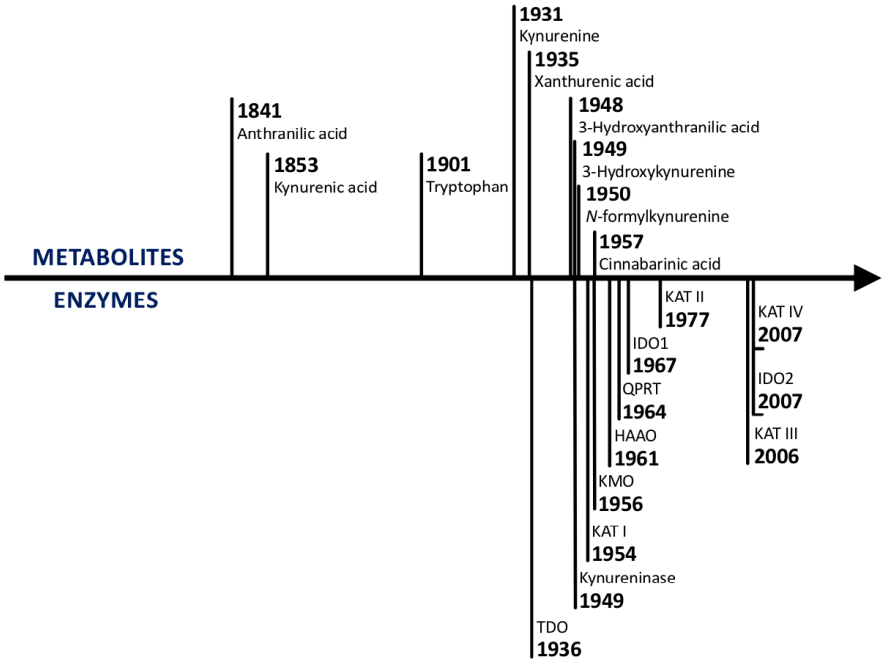

Figure 10. Discovery timeline for the kynurenine pathway

The publication dates of papers reporting the kynurenine pathway metabolites (top) and pathway enzymes (bottom) are shown with increasing time (x-axis) from left to right as shown by arrow. Abbreviations: HAAO: 3-Hydroxyanthranilate 3,4-dioxygenase; IDO: Indoleamine 2,3-dioxygenase; KAT: Kynurenine aminotransferase; KMO: Kynurenine 3-monooxygenase; QPRT: Quinolinic acid phosphoribosyltransferase; TDO: Tryptophan 2,3-dioxygenase.

The metabolites have importance throughout the various biological domains of life, and some can be seen in nature as biological pigments (**Figure 11**). The enzymes are of great importance as pathway catalysts.

Figure 11. **Kynurenines as biological pigments**

Left: The well camouflaged ***Misumena vatia* crab spider** seen here attacking a wasp, is famous for its colour change from white to yellow - the spider's yellow pigments are **kynurenine** and **3-hydroxykynurenine** (388).

Right: The red pigment in ***Trametes cinnabarina (Jacq.)*** fungus was isolated and named **cinnabarinic acid**; the metabolite derives its name from this fungus (389). Image sourced from www.mushroomobserver.org (01-may-2019).

1.2.3.2. The kynurenine pathway of tryptophan oxidation

A summary illustration of the current understanding of the metabolism of tryptophan is shown in **Figure 12**, with a focus upon the oxidative kynurenine pathway, detailing the main features. Before the 1980s, the 'kynurenines' were viewed as relatively innocuous precursors to nicotinamide adenine dinucleotide (NAD^+), and the focus of research in relation to the kynurenine pathway was on its role in the biosynthesis of nicotinamide and the CNS indoles, serotonin and melatonin. In 1981, it was discovered that quinolinic acid could excite neurons (NMDA-receptor agonist), and the following year kynurenic acid was found to block CNS glutamate receptors (350, 390, 391). Since that time, the kynurenine metabolites have increasingly been found to have physiological and pathological roles, particularly in the CNS. Kynurenines have been linked to several neurological and psychiatric disorders such as depression, schizophrenia, Huntington's disease (392). The majority of mammalian kynurenine pathway metabolism takes place in hepatocytes, which contain all the enzymes necessary for NAD^+ biosynthesis from tryptophan, and is responsible for ~90% overall tryptophan metabolism under physiological conditions (302, 377, 393). Because tryptophan and some of the kynurenines are able to cross the plasma membrane through specific transporters, they are able to exert metabolic modifications to the extracellular environment (394).

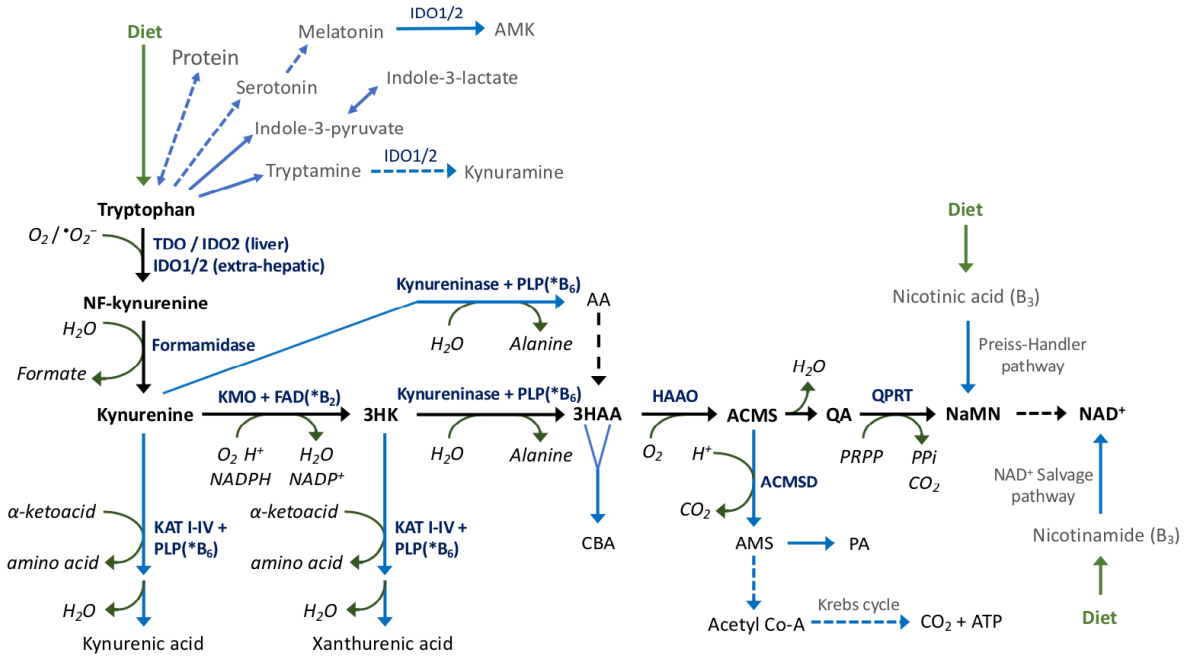

Figure 12. Tryptophan metabolism through the oxidative kynurenine pathway

Metabolites in black with black arrows denotes the main pathway. Compounds in italics are co-factors and by-products. Dotted arrow '---' denotes multi-step molecular transformation, whereas a solid arrow denotes direct transformation. A double ended arrow head denotes a bi-directional transformation. A double-tailed arrow denotes dimerization. Hydroxylation to serotonin and melatonin. Transamination to indole-3-pyruvate. Decarboxylation to tryptamine. Abbreviations: AA: Anthranilic acid; ACMS: 2-amino-3-carboxymuconic acid-6-semialdehyde (also known as 2-acroleyl-3-aminofumarate); AMK: *N*-acetyl-5-methoxykynuramine; AMS: 2-aminomuconic-6-semialdehyde; ATP: adenine triphosphate; B_3: vitamin B_3, nicotinic acid; B_6: vitamin B_6, pyridoxal; CBA: cinnabarinic acid; CO_2: carbon dioxide; FAD(*B_2): flavin-adenine dinucleotide (active form of riboflavin, B_2 vitamer); 3HAA: 3-hydroxyanthranilic acid; 3HAAO: 3-hydroxyanthranilic acid oxidase; IDO: indolamine 2,3-dioxygenase; KAT: kyurenine aminotransferase; KMO: kynurenine 3-monooxygenase; MAO: monoamine oxidase; NaMN: nicotinic acid mononucleotide; NAD^+: nicotinamide adenine dinucleotide (oxidized); O_2: oxygen; $^{\bullet}O_2^-$: superoxide anion; PLP(*B_6): pyridoxal 5'-phosphate (B_6 vitamer); PPi: inorganic pyrophosphate; PRPP: 5-phosphoribosyl-diphosphate; QA: quinolinic acid; QPRT: quinolinic acid phosphoribosyl transferase; TDO: tryptophan 2,3-dioxygenase.

1.2.3.3. Peripheral kynurenine metabolism and drug discovery

Outside of the liver and the brain, the kynurenine pathway metabolites and enzymes are widely distributed in many tissues. Tryptophan degradation in non-hepatic tissues is normally small (5-10%), but becomes considerably greater under conditions of immune activation, including pregnancy (377, 382). The extrahepatic kynurenine pathway does not include all the pathway enzymes, and the local expression of pathway enzymes determines which intermediates are produced in each site (377). The concentration of enzymes of the kynurenine pathway in peripheral tissues tend to be much higher than in the brain (308). Between males and females, both in humans and mice, there are baseline differences in KP metabolite concentrations (395). Excreted in the urine, investigators have sought to study the

association of KP metabolites and bladder tumours, finding a weak carcinogenic association with most metabolites (396).

Due to the close relationship between kynurenine metabolism and inflammatory responses, kynurenines are emerging as recognized players in a variety of common diseases outside of the nervous system, such as atherosclerosis (397), diabetes (398), cancer (399), obesity (400), as well as critical illness (401) and multiple organ dysfunction in acute pancreatitis (375). Where kynurenines have pathobiological roles this is anticipated to be a fruitful area for drug discovery (350).

1.2.4. Tryptophan oxidation

The initial and rate-limiting metabolizing step in the kynurenine pathway is the insertion of two oxygen atoms from atmospheric oxygen (O_2) into the indole ring of tryptophan, which opens the ring and thereby forms a substance called *N*-formyl-kynurenine (see Figures 11 and 12). This reaction is catalysed by only two classes of heme-dependent dioxygenases in human: namely, tryptophan 2,3-dioxygenase (TDO) and two forms of indoleamine 2,3-dioxygenase (IDO) (402, 403). In humans, TDO and IDOs are apoenzymes, and thus require binding by a cofactor to allow enzymatic activation (376, 404). Heme, or iron protoporphyrin, which is produced in cytosol and mitochondria, is the necessary cofactor for TDO and IDOs. A holoenzyme is a biochemically active compound formed by the combination of an apoenzyme (e.g. TDO) with the necessary coenzyme. In humans at healthy steady state, ~90% of absorbed tryptophan is metabolised within the liver through the hepatic kynurenine pathway (405). TDO is thought to contribute to ~70% of tryptophan oxidation, and thus IDO2 and other enzymes may contribute to a small proportion of hepatic oxidation of tryptophan (405).

1.2.4.1. Tryptophan 2,3-dioxygenase (TDO)

Discovered by Kotake and Masayama in 1936, TDO was originally assigned the ambiguous term ‘tryptophan pyrrole’ (EC 1.13.1.12) (406), but as it was shown to incorporate two oxygen atoms into tryptophan to form *N*-formyl-kynurenine, it was renamed as a dioxygenase ~20 years later (EC 1.13.11.11) (407). The *Tdo* gene is widely distributed across species from eukaryotes to bacteria and a few species possess two genes, but it is absent within the fungi kingdom (404). Most mammalian species constitutively express TDO in the liver, and its activity regulates plasma tryptophan concentrations, and thereby the supply of tryptophan to the brain under healthy basal conditions. There are, however, some mammals which lack TDO, namely gerbil and rabbit, which instead possess a compensatory higher IDO

activity (376, 377). The dominant role of TDO in tryptophan metabolism is apparent from the resulting biochemical phenotype of murine *Tdo* gene knockout, which elevates plasma tryptophan concentrations nearly 10-fold (347, 408). TDO is a 167 kDa tetrameric heme-containing cytosolic protein which has a very restricted substrate specificity, thought to be limited to the L-tryptophan enantiomer alone. TDO is predominantly expressed in the liver, whilst expression in the brain (347, 409, 410) and other tissues is relatively negligible (394). TDO has a short half-life of approximately 2 hours, and its gene expression and apoenzyme activity is readily and rapidly modifiable (377). A decrease in TDO activity could be caused by: (i) inhibition of apoenzyme synthesis; (ii) inactivation of the apoenzyme, by prevention of TDO conjugation with heme or allosteric inhibition; (iii): inhibition of the holoenzyme (apoenzyme and cofactor together) activity. In humans, but not all mammalian species, TDO can exist as an inactive heme-free apoenzyme, as well as a heme-containing holoenzyme (382). Review of the literature reveals several factors which have been demonstrated to regulate the production and activity of the TDO-heme holoenzyme:

i) (**+**) Substrate (**tryptophan**) activation - *TDO* mRNA induction (411)
ii) (**+**) *TDO* mRNA induction by **glucocorticoid** (377, 412-414)
iii) (**+**) Increase TDO enzyme activity by **histamine, tyrosine** & **phenylalanine** (414)
iv) (**~**) Altered TDO activity by **various hormones** (e.g. adrenaline, glucagon, insulin, thyroxine, progesterone, oestrogen) (377, 382, 415, 416)
v) (**-**) Feedback inhibition by **NADPH** (417) and hydroxykynurenines (**3HK**, **3HAA**) (418, 419)
vi) (**-**) TDO activity limited by inadequate cofactor supply (**heme** or **hypoxia**) (420)

1.2.4.2. Indoleamine 2,3-dioxygenases (IDOs)

1.2.4.2.1. Discovery of IDO1

Aware that TDO was not able catabolize the D-isoform of tryptophan, Kotake and Ito in 1937 reported an intriguing finding of D-kynurenine excretion in the urine of rabbits that had been fed the D-tryptophan enantiomer; a result which inferred the existence of an unknown TDO-like enzyme (406). This mystery was solved in 1967 when Osamu Hayaishi and colleagues in Japan discovered another tryptophan oxidising enzyme in the intestine of rabbits (406, 421). In contrast to TDO, this new enzyme had a broader substrate specificity for compounds containing indole rings, including both L- and D-tryptophan enantiomers, L- and D-5-hydroxytryptophan (serotonin) and several indolamines (377, 422). Thus, it was named 'indoleamine' dioxygenase, to reflect this broad substrate tolerance. Just as with TDO, IDO also uses oxygen (O_2) to in the oxidation of substrates, and not necessarily the superoxide

($^{\bullet}O_2^-$) reactive oxygen species, as was the prevailing theory until 2007 (423). IDO is a 41 kDa intracellular heme-containing cytosolic monomeric haemoprotein and, unlike TDO, is found in fungi too (404). Amongst mammals, IDO is expressed in various organs, with the liver (where TDO is abundantly found) being the notable exception, at least for the original enzyme (i.e. for IDO1). In humans, IDO is mostly found in the placenta, lung and alimentary canal (424, 425). It appears that mice have very high levels of IDO in epididymis (426), which has not been found in humans (425).

1.2.4.2.2. Function of IDO1

From a cellular perspective, IDO is found largely in macrophages in the periphery, but is also expressed in the CNS by astrocytes, microglia, infiltrating macrophages and DCs (347). There are many differences between properties of IDO and TDO which have been thoroughly compared in a recent review by Professor Badawy (351). In contrast with the liver TDO, the extrahepatic IDO is fully heme-saturated (382). Another important difference is the affinity each enzyme has for L-tryptophan. Specifically, TDO has a far higher capacity for binding tryptophan, but a lower binding affinity (K_M 190 μM for purified humane enzyme) for the kynurenine than IDO (K_M <50 μM) (351).

In the non-inflammatory healthy state, the contribution of IDO to tryptophan oxidation is minimal, but can be dramatically increased upon immune activation, transforming IDO into the main controller of tryptophan availability in immune-regulated pathological conditions (377). Small molecule inhibitors of IDO1 are emerging for novel cancer therapy adjuncts to help blunt tumour neovascularisation and restore immune-surveillance (427, 428).

1.2.4.2.3. Discovery of IDO2

For the remainder of the 20th centaury, only one form of IDO (EC 1.13.11.17) was known, which is often now referred to as IDO1 to distinguish it from a recently identified similar enzyme. Forty years after Hayaishi *et al.* discovered the first IDO, an adjacent gene on the mammalian chromosome homologous to IDO1 was reported in 2007 (429). This newly discovered gene was shown by three separate groups to encode a new enzyme able to oxidize tryptophan isoforms, and other indoleamine derivatives, and was therefore named indoleamine 2,3-dioxygenase-like protein, or IDO2, on account of its enzymatic activity and structural similarity to IDO1 (404, 430-433). The important differences between these apoenzymes, is that IDO1 has a far greater affinity for tryptophan than IDO2, and IDO2 is expressed in liver. Structurally, IDO1 and IDO2 share significant sequence homology at the amino acid level (43% identity for human IDOs) and a similar structure, with IDO2 having a slightly greater molecular

weight (47 kDa) (433-435). The biological importance of IDO2 in human health and disease is likely to be much less than that of IDO1 due to its lower affinity, and indeed up to 50% of individuals of European or Asian descent, and 25% of individual of African descent, are thought to lack functional *IDO2* alleles on account of single nucleotide polymorphisms (SNPs) which abolish IDO2 enzyme activity (431).

1.2.4.2.4. Role of IDO in inflammation

Under normal physiological conditions hepatic TDO will metabolize the majority of available tryptophan, but upon certain immune stimuli IDO expression is upregulated, which shifts tryptophan catabolism towards the kynurenine pathway in extrahepatic tissues with locoregional tryptophan consumption. Although IDO is also a hemoprotein, it exists in the active holoenzyme form (not as an apoenzyme), that cannot be further activated by heme. And unlike TDO, IDO activity can be inhibited by high tryptophan substrate concentrations (377). Interestingly IDO is not induced by glucocorticoid hormones which are known to induce *Tdo* gene expression in liver (347, 426). However, a number of other immunomodulatory mediators are known to induce *Ido1* transcription, such as lipopolysaccharide (LPS) and interferon type I and type II (436-438). Dexamethasone can further enhance the induction of IDO by interferon (439). IDO1 activity in the mouse lung can be increased more than 100-fold over basal levels by viral infection caused by influenza (440). By contrast, nitric oxide (NO) is known to inhibit IDO activity by a variety of mechanisms (352). Activation of IDO1 has many knock-on effects which include locoregional tryptophan depletion which blocks protein synthesis via GCN2 activation (360, 361, 363), inhibits the immunoregulatory kinases mTOR (360) and immunosuppressive effects of increased production of kynurenines by regulatory T cells (441) and dendritic cells (DCs) which significantly contribute to immune privilege and maternal tolerance towards the allogenic fetus (307, 361), and which foster a microenvironment that is defective in recognizing and eradicating cancer cells.

1.2.5. Kynurenine transamination and hydrolysis

After tryptophan is oxidized to form *N*-formyl-kynurenine (NF-Kyn), this product is hydrolysed by arylformamidase (also called kynurenine formamidase and known by abbreviations Afmid, FAM, FKF, KFase) (EC 3.5.1.9) to produce kynurenine with the release of formate (formic acid) (442, 443). The *Afmid* gene is predominantly expressed in the liver and kidney, but also by a wide range of tissues (377, 444, 445). As yet unidentified formamidase enzyme(s) may contribute to a small proportion of the hydrolysis of NF-Kyn,

accounting for <15% of total, although some experts are of the view that much of the hydrolysis happens spontaneously, especially under acidic conditions (442, 446).

1.2.5.1. Kynurenine

Kynurenine is the initial and most abundant of the kynurenines (405), providing pathway substrate for the downstream KP enzymes. Once formed, kynurenine may be further metabolised at the site of local production (e.g. in the liver as is the case of TDO / Afmid metabolism), or else enter the circulation where it is available for endothelial and peripheral blood cells, or diffusion into other tissues, or urinary excretion.

1.2.5.1.1. Kynurenine in the periphery

Within the circulation and tissues, kynurenine is transported across cell membranes by the large amino acid transporter SLC7A5 (LAT1). In the vasculature, kynurenine is involved in arterial blood pressure regulation, particularly upon immune challenge with IFNγ in an IDO1-dependant manner (447). Kynurenine suppresses binding to pyruvate dehydrogenase kinase (PDK1) or aryl hydrocarbon receptor (AhR) in T cells, DCs and other immune cells which serve modulate T cell responses (438). Dendritic cells (DCs) are converted into tolerogenic APCs that suppress effector T cells (Teff) responses and promote development of Foxp3-lineage T cells; namely, regulatory T cells (Tregs), thereby promoting immune tolerance (438). In the absence of inflammation, the brain receives ~60-80% of kynurenine from the periphery by competitive transport across the blood-to-brain barrier (via LAT1 transporters), with the remainder produced locally in the CNS (448, 449). In the event of a systemic immune stimulus however, such as a high dose of LPS, >98% of brain kynurenine comes from the periphery where tryptophan is catabolized by IDO to kynurenine (449).

1.2.5.1.2. Kynurenine in the mammalian brain

Within the brain, kynurenine is not known to have any direct electrophysiological effects on neuronal activity (383), but functions as an endogenous ligand of the aryl hydrocarbon receptor (AhR) and as a substrate for downstream metabolites and end-products, of which KA and QA have the greatest electrophysiological activity (382). In the periphery, kynurenine has been found to have several functions (**Table 10**), principally through the activation of the AhR. Specifically, kynurenine can affect immune tolerance, by increasing regulatory T cells (Tregs) differentiation and suppression of stimulatory T cell responses (450, 451). Additionally, kynurenine can affect bone remodelling and regulation of arterial blood pressure (397, 447).

KP metabolite	Source	Electrophysiological / CNS actions	Peripheral actions
Tryptophan (Trp)	Diet	• No electrophysiological effects but precursor of downstream kynurenines	• Systemic toxicity may be due to Trp or its metabolites (452)
N-formyl-kynurenine (NF-Kyn)	Trp	• No electrophysiological effects but precursor of downstream kynurenines	• Unknown • Serum levels increase in aging rodents (453)
Kynurenine (Kyn) (3-anthriloyl-L-alanine)	NFK	• No electrophysiological effects but precursor of downstream kynurenines • AhR agonist	• Blood pressure regulation (447) (397) • Immune tolerance by DC & T cell differentiation to Tregs by mechanisms including AhR (438) (450) • Suppression of T cell stimulatory response (451) • Tumour promotion by AhR (410) • Altered bone remodelling by AhR / RUNX2 (454)
Kynurenic acid (KA) (kynurenate)	Kyn, Diet	• NMDA antagonist (455) (456) • Kainate receptor antagonist (456) • AMPA receptor antagonist (456) • Nicotinic α7 receptor antagonist (457) (456)	• iNKT cell cytokine suppression by Gpr35 (458) • Adipose energy homeostasis by Gpr35 (459) • Inflammatory tumour progression by AhR (460) • ROS scavenging (461) • Altered bone remodelling by NMDA & AMPA receptors (454, 462) • Anti-inflammatory : reduces TNFα levels (463)
3-Hydroxykynurenine (3HK)	Kyn	• Cytotoxicity affecting specific neurones by generation of reactive oxygen species (e.g. striatal neurones) (464) (465) (466) • Antioxidant function in cerebral cortex (467)	• Suppression of T cell responses (451, 468, 469). • Lymphocyte cytotoxicity (T, B & NK cells) (451) • Protective UV light filter in human lens (470) • Generation of reactive oxygen species (470) (471) • Pro-apoptotic (HEK293, HAEC) (472) (473)
Anthranilic acid (AA) (anthranilate, 2-aminobenzoic acid)	Kyn	• None • Precursor for 3HAA & QA (383)	• Antioxidant (474) • Synthetic AA-derivative drugs have immuno-modulatory properties
Xanthurenic acid (XA) (4,8-dihydroxyquinoline-2-carboxylic acid, xanthurenate)	3HK	• Possible group II metabotropic glutamate receptor agonist (475). Possibly not (476). • Inhibits BH_4 synthesis – importance in serotonin synthesis (477) • Vesicular glutamate transport inhibitor (476) • Analgesia (478)	• Diabetogenic (insulin binding, beta cell toxicity & impaired insulin production) (398) • Inhibits BH_4 synthesis (477) • Antioxidant properties (479) • Pro-apoptotic (smooth muscle & epithelial) (480)
3-Hydroxy-AA (3HAA) (3-hydroxyanthranilate)	3HK, AA	• Antioxidant function in cerebral cortex (467) • Precursor for QA (383)	• Suppression of T cell stimulatory response (451) • Apoptosis of thymocytes & Th1 cells (481) • Generation of reactive oxygen species (471) • Suppression of iNOS induction (482) • Inhibits expansion & activation of all T-cells (483)
Cinnabarinic acid (CBA) (cinnavalininate)	3HAA x2	• Weak agonist of type 4 group metabotropic glutamate (mGluR4) receptor (484)	• CBA is an AhR ligand that stimulates IL22 production by CD4+ T cells (485) • mGluR4-CBA activation (484)
Picolinic acid (PA) (2-pyridinecarboxylate)	AMS	• Diverts metabolism away from excitotoxic QA	• Zinc binding ligand (486)
Quinolinic acid (QA) (quinolinate, pyridine-2,3-dicarboxylate)	ACMS	• Excitotoxic effect (487) • NMDA receptor agonist (487) • QA-Iron complexes cause lipid peroxidation (488)	• NAD^+ precursor • Altered bone remodelling by NMDA (454) • QA-Iron complexes are pro-oxidant (489) • Apoptosis of thymocytes & Th1 cells (481)
Nicotinic acid mononucleotide	Niacin, QA	• NAD^+ precursor	• NAD^+ precursor
Nicotinamide adenine dinucleotide (NAD^+)	NaMN	• Redox cofactors, cell viability and DNA repair	• Redox cofactors, cell viability and DNA repair

Table 10. Kynurenine pathway products of the oxidation of tryptophan in humans
Abbreviations: ACMS: 2-amino-3-carboxymucononic-6-semialdehyde (also known as 2-acroleyl-3-aminofumarate); AhR: aryl hydrocarbon receptor; AMPA: α-amino-3-hydroxy-5-methyl-4-isoxazolepropionic acid; AMS: 2-aminomuconic-6-semialdehyde; BH4: tetrahydrobiopterin; DCs: dendritic cells; Gpr35: G protein-coupled receptor 35; iNKT: invariant natural killer T cell; iNOS: inducible nitric oxide synthase; mGlu4: type 4 metabotropic glutamate; NAD^+: nicotinamide adenine dinucleotide (oxidized); NMDA: N-methyl-D-aspartate; ROS: reactive oxygen species.

1.2.5.1.3. Kynurenine in disease

In the clinical setting, increased circulating kynurenine with decreased tryptophan concentrations suggestive of IDO-mediated tryptophan catabolism has been observed during recovery after major trauma (374) in systemic lupus erythematosus (SLE) (490) and in obesity (400, 491). Equivalent tryptophan levels but increased kynurenine and kynurenic acid concentrations have been observed in human inflammatory bowel disease (492).

1.2.5.2. PLP Coenzyme (B_6 vitamer)

Both the transamination (to kynurenic acid) and hydrolysis (to anthranilic acid) of kynurenine require the B_6 vitamer coenzyme, pyridoxal 5′-phosphate (PLP). Pyridoxine is passively absorbed from the diet (e.g. meat, poultry, fish, vegetables and bananas) by the jejunum and ileum (493). The liver converts pyridoxine into the active form of vitamin B_6, PLP, by a process which is tightly regulated, even after a high dietary intake, and PLP is released into the plasma, strongly bound to albumin (494). Plasma PLP is dephosphorylated before uptake by tissues, cells or across the blood-to-brain barrier (495). Approximately 80% of total PLP body store resides in muscle tissues, bound to glycogen phosphorylase, where it is not readily released (496, 497). When intake of vitamin B_6 is low, or there is an increase in demand for PLP during inflammation, PLP is derived from much smaller liver and plasma stores, leaving plasma PLP concentrations susceptible to depletion during an immune response, including trauma, major surgery and myocardial infarction (496, 498). PLP is involved in >150 enzymatic reactions including metabolism of amino acids, neurotransmitters, nucleic acids, heme and lipids (495). Additionally, PLP has other effects, such as purinoceptor 2X (P2X) receptor antagonism and an inhibitor of some NADH-dependent enzymes (499-501). Plasma PLP levels are inversely associated with tissue-nonspecific alkaline phosphatase (ALP) and C-reactive protein (CRP), which are commonly measured in routine liver screen biochemistry. Physiologically, PLP deficiency is seen in pregnancy. Interested readers may wish to consult a comprehensive review of PLP by Ueland *et al.* (502).

1.2.5.3. Kynurenine transamination (to kynurenic acid)

1.2.5.3.1. Sources of kynurenic acid

Whilst kynurenic acid (KA) can be found in many commonly consumed components of the western diet (e.g. broccoli, honey, potatoes and alcohol-containing beverages (503-505)), it cannot easily pass through the blood-to-brain barrier due to its polar nature and apparent lack of efficacious transport processes. Therefore, KA found within the brain is mostly derived

by local neosynthesis from its brain-penetrable precursors kynurenine and/or tryptophan (506). Human and rodent genomes encode four kynurenine aminotransferase enzyme isoforms (KAT enzymes; E.C. 2.6.1.7) which irreversibly convert kynurenine to KA (377, 383) (**Tables 10 and 11**). KATs are dependent on the B_6 vitamer, pyridoxal 5′-phosphate (PLP), and an α-ketoacid co-substrate for kynurenine transamination. PLP serves as a coenzyme and is passively absorbed from the diet (e.g. meat, poultry, fish, vegetables and bananas) by the jejunum and ileum (493). Kynurenine is transiently converted to a ketoacid intermediate, which spontaneously cyclizes to form KA (507). Alternatively, KA may be generated by the effect of reactive oxygen species upon kynurenine (508, 509).

1.2.5.3.2. Kynurenic acid in the mammalian brain

In the brain, KAT II (also known as aminoadipate aminotransferase) is the dominant enzyme responsible for synthesis of kynurenic acid which is mostly produced by neurons, glial cells (e.g. astrocytes) and macrophages (510, 511). KA protects against neuronal excitotoxicity and has neuroprotective anti-epileptic and anxiolytic properties (512). Mechanistically, KA exerts an inhibitory effect on acetylcholine-regulated pathways via the neuronal cholinergic α7 nicotine receptors, exerting anti-glutaminergic properties, and also serves as a broad-spectrum endogenous glutamate receptor antagonist, which acts through three known targets (456, 457, 513, 514):

i) *N*-methyl-D-aspartate (NMDA) receptor antagonist by acting on a specific glycine-binding receptor site (455, 456, 515, 516)
ii) Kainate receptor antagonist (456)
iii) AMPA receptor antagonist (456).

Wirthgen and co-authors recently published a comprehensive review of the current understanding of the immunomodulatory effects of KA and its relation to pathological conditions, in the brain and peripherally (509). KA has often been found to be present at abnormally low levels in the serum of patients with disorders of the nervous system (e.g. affective psychosis, migraine and cluster headache) as compared to controls, but can be increased in other neurological conditions (509).

Enzyme (EC)	Gene (ID)	Main regulators	Enzyme Cofactor	Enzyme Substrate	Reaction type	Product (by-product)	Main human tissue expression
TDO (1.13.11.11)	*TDO2* (6999)	Trp(+), Glucocorticoid(+), NADPH(-) (377).	Heme	L-Trp, O_2 / $\cdot O_2^-$	Oxidation	NF-Kyn	Hepatic (517)
IDO1 (1.13.11.17)	*IDO1* (3620)	IFNγ(+), IFNα(+), LPS(+), PAF(+), NO(-), IL4(-), Trp(-), Dexamethasone(+) (368, 377, 439, 487, 518).	Heme	DL-Trp, various indolamines, O_2 / $\cdot O_2^-$	Oxidation	NF-Kyn	Extra-hepatic (placenta, lung, lymph node, intestine, others) (517)
IDO2 (1.13.11.52)	*IDO2* (169355)	IFNγ(+), IL10(+), LPS(+) (431).	Heme	DL-Trp, various indolamines, O_2 / $\cdot O_2^-$	Oxidation	NF-Kyn	Liver, intestine, placenta, brain, lung, kidney (431) (517)
FAM (3.5.1.9)	*AFMID* (125061)	Unknown (414).	No cofactor	NF-Kyn, H_2O	Amidase (amide hydrolysis)	Kyn (Formate)	Kidney, liver, many others (517)
KAT I KAT II KAT III KAT IV (2.6.1.7)	*CCBL1* (883) *AADAT* (51166) *CCBL2* (56267) *GOT2* (2806)	Oestrogens(-), hydrazine drugs(-) (377, 519).	PLP (Vit B_6)	Kyn, Broad specificity for amino acid and α-ketoacid (507)	Transamination & Cyclization	KA (amino acid)	I: Liver, brain, many others II: Brain, liver, many others III: Widely expressed IV: Heart, liver, brain, many others (517)
KAT I – IV (2.6.1.7)	As above	As above	As above	3HK, Broad specificity for amino acid and α-ketoacid (507)	As above	XA (amino acid)	As above
KYNU (3.7.1.3)	*KYNU* (8942)	Oestrogens(-), hydrazine drugs(-) (377, 519), IL1β(+) (520).	PLP (Vit B_6)	Kyn, H_2O	Hydrolysis	AA (L-alanine)	Liver, kidney, spleen, many others (517) (521)
KYNU (3.7.1.3)	As above	As above	As above	3HK, H_2O	Hydrolysis	3HAA (L-alanine)	As above
KMO (1.14.13.9)	*KMO* (8564)	LPS(+) (518, 522), IFNγ(+) (518, 523), TNFα(+) (518), IL1β(+) (520), PLP(-) (499).	NADPH FAD (Vit B_2)	Kyn, H^+, O_2	Hydroxylation	3HK (H_2O, $NADP^+$)	Liver, kidney, placenta, brain (glial cells), many others (517)
HAAO (1.13.11.6)	*HAAO* (23498)	Isoniazid (but not other hydrazine drugs) (519)	Fe^{2+}	3HAA, O_2	Oxidation	ACMS	Liver, kidney, intestine, many others (517)
ACMSD (4.1.1.45)	*ACMSD* (130013)	IFNγ(-) (524)	Zn^{2+}	ACMS, H^+	Decarboxylation	AMS (CO_2)	Kidney, liver (517)
QPRT (2.4.2.19)	*QPRT* (23475)	Unknown	Mg^{2+}	QA, PRPP	Phosphoribosyl transfer & Decarboxylation	NaMN (PPi, CO_2)	Kidney, liver, many others (517)

Table 11. Enzymes of the kynurenine pathway of tryptophan metabolism and NAD^+ synthesis in humans
Abbreviations: AADAT: aminoadipate aminotransferase; ACMS: 2-amino-3-carboxymuconic acid-6-semialdehyde (acroleyl aminofumarate); ACMSD: amino-carboxymuconate-semialdehyde decarboxylase; AMSD: 2-aminomuconate-semialdehyde dehydrogenase; EC: enzyme commission; FAD: flavin adenine dinucleotide; FAM: NF-Kyn formamidase; HAAO: 3-hydroyanthranilate 3,4-dioxygenase; 5HT: 5-hydroxytryptamine (also known as serotonin); IDO: Indoleamine 2,3-dioxygenase; KAT: kynurenine aminotransferase; KYNU: Kynureninase; KMO: Kynurenine 3-monooxygenase; NaMN: nicotinic acid mononucleotide; NF-Kyn: *N*-formyl-L-kynurenine; 2OG: 2-oxoglutarate; P5P: Pyridoxal 5'-phosphate; PPi: inorganic pyrophosphate; PRPP: 5-phosphoribosyl-diphosphate; QA: quinolinic acid; QPRT: quinolinic acid phosphoribosyl transferase; TDO: Tryptophan 2,3-dioxygenase; TNF: tumour necrosis factor. General literature with particular acknowledgement of the work of AAB Badawy (377) [Table 1]. www.brenda-enzymes.org [ref]; UniProtKB uniport.org. Entrez gene.

1.2.5.3.3. Kynurenic acid in peripheral tissues

In the periphery, KA can be sourced from the diet, or produced from kynurenine by the action of reactive oxygen species, or by the enzymatic activity of KAT I-IV by many tissues including liver, kidney, skeletal muscle (525), endothelium (526) and heart (527). Indeed, exercised skeletal muscle increases conversion of kynurenine to kynurenic acid resulting in accumulation of circulating kynurenic acid levels (459, 525). KA has specific functions outside of the nervous system, and is a selective agonist for the G protein-coupled receptor 35 (Gpr35) and the aryl hydrocarbon receptor (AhR). Gpr35 is predominantly expressed by leukocytes, particularly peripheral monocytes, and in alimentary tract crypts which are rich in proliferating gastrointestinal stem cells (528, 529). Expression of Gpr35 is thought to be involved in the pathogenesis of gastric adenocarcinoma (530) and of non-small-cell lung cancer (531). Of all the kynurenine pathway metabolites, only anthranilic acid in humans (but not mice or rats) has been shown to activate Gpr35, none of the other metabolites are Gpr35 ligands (463). The function of Gpr35 in leukocytes has been the focus of investigation for some authors. Kynurenic acid may be involved in the early stages of neutrophil and monocyte adhesion to surfaces coated with fibrinogen (529). KA reduces TNFα secretion by peripheral blood monocytes (463). Via Gpr35, KA deactivates the NLRP3 inflammasome in macrophages, thereby reducing production of IL1β (532). Inflammasome activation is protective in colitis, however, and thus KA-induced NLRP3 suppression appears to increases susceptibility to inflammatory bowel disease (532). Amongst IBD patients, elevated KA levels have been observed, further supporting the role of kynurenic acid as a contributory driver of the colitis disease process (458, 533). Elevated KA levels have also been positively correlated with systemic diseases such as chronic kidney disease and type 2 DM, with variable findings amongst different cancer groups (509). The contribution of Merle Mason from the University of Michigan Ann Arbor in isolating KATII as well as a multitude of tryptophan, kynurenine and KAT papers between 1950-1980 is noteworthy (534).

1.2.5.4. Kynurenine hydrolysis (to anthranilic acid)

As with KATs, kynureninase (EC 3.7.1.3) is also a PLP-dependent enzyme, which is required to perform hydrolysis of kynurenine, and its activity is severely impaired by deficiency in the B_6 vitamer (535). See Table 11 (above) for details regarding kynureninase (KYNU). Kynureninase in humans has two main substrates: kynurenine to make anthranilic acid (AA), and 3-hydroxykynurenine (3HK) to make 3-hydroxyanthranilic acid (3HAA). Alanine (L-Ala) is an additional product of this hydrolysis chemical reaction. In humans, kynureninase has a ~15-

20-fold higher affinity for 3HK than for kynurenine, favouring the generation of 3HAA over anthranilic acid (Figure 12, above) (536).

1.2.5.4.1. Discovery of anthranilic acid

The discovery of Anthranilic acid (AA) was made in 1841 by German chemist Carl Julius Fritzsche (1808-1871). He named the substance related to indigo, the natural plant dye compound, as '*Anthranilsäure*' – meaning coal (*anthrax*, Greek), indigo (*añil*, Spanish) and acid (säure, German) (537). AA is a white or yellow substance in solid form, but can have a bluish fluorescence in solution (537).

1.2.5.4.2. Known pathophysiological functions of anthranilic acid

It is able to cross the blood-to-brain barrier, apparently by passive diffusion, rather than via a transporter (506). With regards to diseases of the CNS, patients with Schizophrenia (538) and Parkinson's disease (539) have been found to have increased circulating AA plasma concentrations. As for systemic diseases, diabetes mellitus and rheumatoid arthritis have been found to be positively associated with AA levels. Circulating AA levels from serum of fasting diabetics have been found to be increased by an average 2.3-fold in type 1 diabetes mellitus (T1DM) compared to non-diabetic controls (540). Gestational diabetics have also been found to have elevated fasting serum AA levels as compared to normal glucose tolerance matched controls (541). In the synovial joint fluid, anthranilic acid levels were higher in rheumatoid arthritis than osteoarthritis patients (542).

1.2.6. Kynurenine hydroxylation (KMO / vitamin B_2 / 3HK)

1.2.6.1. Kynurenine 3-monooxygenase

Kynurenine 3-monooxygenase (KMO, EC 1.14.13.9), is a member of the monooxygenase superfamily, and a nicotinamide adenine dinucleotide phosphate (NADPH)-dependent flavin hydroxylase found in many tissues, that catalyses hydroxylation of kynurenine. Hydroxylation is the chemical process that results in the incorporation of a hydroxyl group (-OH) into a compound.

1.2.6.1.1. Discovery of KMO

Originally referred to as 'kynurenine-3-hydroxylase', KMO was discovered in RR Brown's laboratory in Wisconsin, USA in 1956 (543). The following year, the enzyme was determined to be dependent upon NADPH (authors used the term 'TPNH', meaning

triphosphopyridine nucleotide; an obsolete synonymous term for NADPH) (544). Ten years later, Hayaishi's laboratory in Japan discovered that KMO was a mitochondrial outer membrane protein (545), and the B_2 vitamer 'flavin adenine dinucleotide' (FAD) was found to be a necessary co-enzyme for KMO to function (546). Much more recently was it discovered that the C-terminal domain of KMO contains a membrane-targeting sequence that allows the enzyme to anchor into the mitochondrial outer membrane (547). The majority of the enzyme is located inside the mitochondrial membrane, and part of it sits outside, which is likely to be the site for substrate interaction (548). The expression of KMO is much higher in peripheral tissues (e.g. liver and kidney) than the brain (549).

1.2.6.1.2. Chemical activities of KMO

The chemical reaction catalysed by KMO is the incorporation of one atom of oxygen into kynurenine in the presence of NADPH as an electron donor (499). KMO is classified as a 'flavoenzyme' ('*flavus*', meaning yellow in Latin), referring to the necessary contribution of the yellow-coloured vitamin B_2 co-enzyme, FAD, with the 'flavin' functional group that facilitates electron transfer. The reaction catalysed by KMO and FAD is remarkably complex and has recently been studied in fantastic detail, by quantum mechanical calculations, showing that there are four successive transformations during the reaction process (550). Many KMO inhibitors have been engineered and can be found in the literature (551-553).

The production of 3-hydroxykynurenine (3HK) by KMO is the dominant route of kynurenine metabolism, and hydroxylation of kynurenine proceeds at a rate at least three fold that of transamination (to KA) at steady state (302, 554) (see Figure 10, above). Despite its key importance in the kynurenine-NAD^+ pathway, the activity of KMO, at least in mice, is not essential for life as *Kmo* deleted mice are overtly healthy (555). That said, there are differences in tissue expression and activity of KMO amongst different species evidenced by the finding that KMO inhibitors produce different biochemical effects in different species (551).

The *KMO* gene is located on human chromosome 1q42. Functionally relevant *KMO* single nucleotide polymorphisms have been identified which likely affect substrate binding (SNPs) and impair KMO activity (548). The B_6 vitamer, PLP, has been shown to inhibit KMO activity, most likely by blocking a phosphate binding site, as detailed above (in section 1.2.6.2.) (499). KMO is inducible by innate stimuli such as TLR4 agonist LPS (518, 522), and proinflammatory cytokines (e.g. IFNγ and TNFα) (518, 523). Under particular circumstances, KMO activity can be anti-inflammatory, such as the amelioration of experimental autoimmune gastritis, which is a Th17-driven disease model. Pro-inflammatory Th17 helper lymphocytes

express KMO, whose activity can be upregulated to catabolise kynurenine, an AhR agonist, and thus minimise elevated production of the IL-17 cytokine by Th17 cells (556).

KMO gene expression has been found to be increased in adipose tissues in obesity on account of the fat resident macrophages (400). In end stage renal failure (ESRF) 3HK plasma concentrations were ~3 fold higher than controls (557).

1.2.6.2. B_2 vitamer: Flavin adenine dinucleotide

The term 'vitamin B_2' encompasses three vitamers: riboflavin (7,8-dimethyl-10-ribitylisoalloxazine), flavin mononucleotide (FMN) and flavin adenine dinucleotide (FAD). Riboflavin is the precursor for the other two, and is enzymatically converted to FMN by riboflavin kinase, which by the action of FAD synthase catalysed to produce FAD (558). Dietary components rich in riboflavin include meat, poultry, fish, eggs, dairy and green vegetables (559). FAD is a redox-active coenzyme associated with various proteins. Deficiency of vitamin B_2 tends not to occur in isolation in humans, and so there is uncertainty with respect to the clinical manifestations of this deficiency (559). Mason helped to define the importance of vitamin B_2 in tryptophan metabolism (560). Riboflavin and the B_2 vitamers are relied upon by flavin-dependent proteins, of which there are 90 in humans, with the majority of such enzymes catalyse redox processes in primary metabolic pathways such as the Krebs cycle, oxidation and degradation of amino acids (561).

1.2.6.3. 3-Hydroxykynurenine

Originally isolated from pupae of the blowfly (*Calliphora erythrocephala*) in yellow crystalline form, 3-hydroxykynurenine (3HK) was first identified in mammalian biological systems in the mid-20th centaury (562). Along with kynurenine, 3HK is known as a yellow biological pigment in spiders and other insects (Figure 11, above). In humans, 3HK along with kynurenine and other KP metabolites can be found in the lens of the eye where it functions as one of many UV light filtering compounds (563). Another known physiological role for 3HK is its suppressive effect upon T-cell stimulatory responses (451, 468, 469).

Circulating 3HK shares the large neutral amino acid transporters used by kynurenine, to penetrate the blood-to-brain barrier (506) and thereafter enter into brain cells (564). This is not surprising since 3HK and kynurenine are both neutral alpha-amino acids (506). The biochemical effects of 3HK have been most closely studied in the brain, where both damaging (464-466) and protective effects have been reported (467). The hydroxykynurenines, 3HK and 3HAA, which share an *o*-aminophenol structure, are redox modulators which can enact strong anti-oxidant and pro-oxidant effects under certain conditions, which is likely due to the ease of

electron or H-atom abstraction (565). Prime examples, of this paradoxical redox effect is observed in the oxidation and reduction of haemoglobin by hydroxykynurenines (566), and in physiological and pathological roles in the human lens (471, 563, 567). Both hydroxykynurenines have been shown to function as antioxidant scavenging radicals, mostly likely due to their phenolic moiety – a term which refers to the presence of a hydroxyl group (-OH) bound to an aromatic hydrocarbon ring (**Figure 13**) (467, 479, 563).

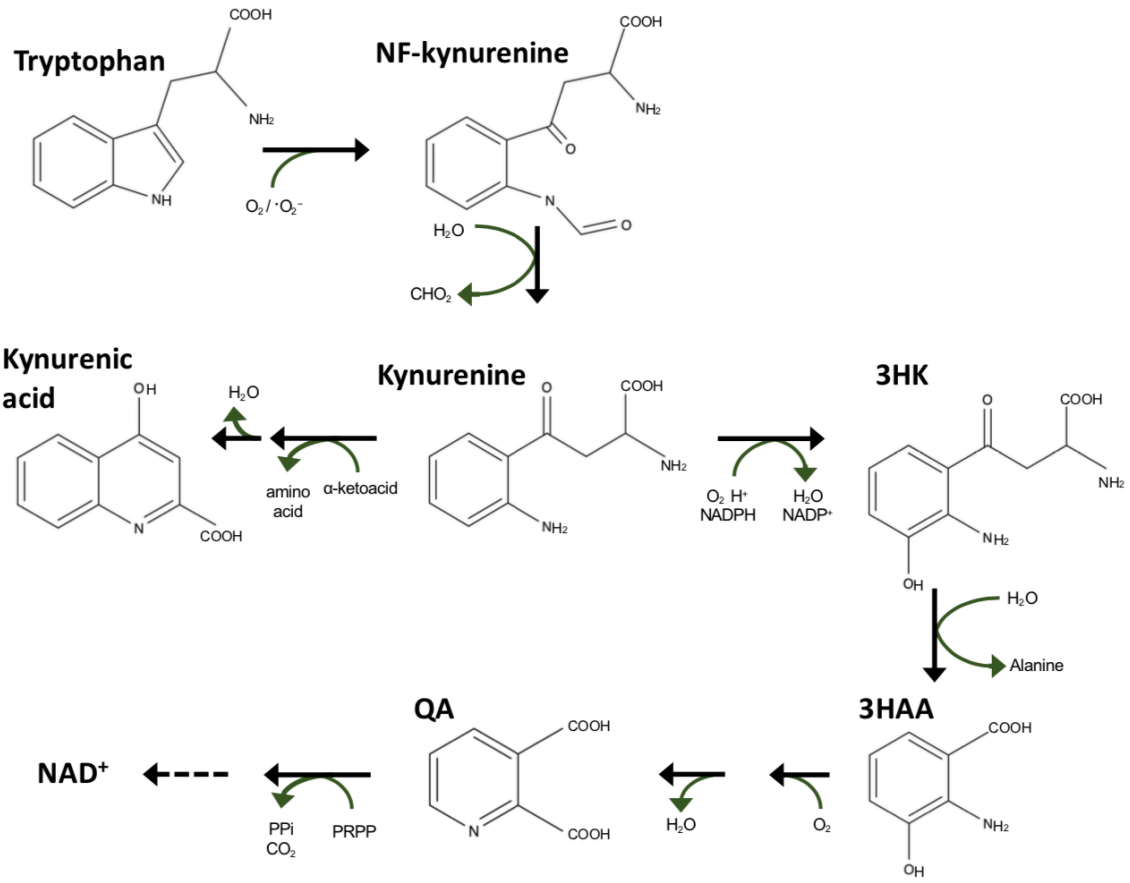

Figure 13. **Chemical structures of tryptophan and the kynurenine metabolites**
Dotted arrow '---' denotes multi-step molecular transformation, whereas a solid arrow denotes direct transformation. Abbreviations: CHO_2: formate; 3HAA: 3-hydroxyanthranilic acid; NAD^+: nicotinamide adenine dinucleotide (oxidized); O_2: molecular oxygen; $^{\cdot}O_2^-$: superoxide anion; PPi: inorganic pyrophosphate; PRPP: 5-phosphoribosyl-diphosphate; QA: quinolinic acid.

1.2.6.3.1 Autoxidation of 3HK and release of ROS during spontaneous transformation

In the presence of molecular oxygen, and under physiological conditions (i.e. pH and temperature), 3HK is readily autoxidized (shown under *in vitro* conditions) (465). Oxidation takes place when a molecule, atom or an ion lose an electron, which simultaneously causes

reduction (meaning gain of electrons) of oxygen-containing chemical species. Redox-active transition metals (e.g. Cu^{2+} and Fe^{3+}) strongly catalyse the oxidation of 3HK (471), and this oxidized 3HK can spontaneously form several compounds (464, 465, 471, 568-573). These compounds comprise xanthommatin (Xan) and hydroxy-xanthommatin (OHXan), and dihydroxy-quinolinequinone-carboxylic acid (DHQCA), as well as small quantities of other unidentified compounds (572, 574) (**Figure 14**). OHXan and Xan are products of self-dimerizing oxidised 3HK - requiring two molecules of 3HK to make a single molecule of Xan. During 3HK oxidation, molecular oxygen (O_2) gains electrons, making reactive oxygen species, which, as their name infers, are chemically more reactive than molecular oxygen which other-

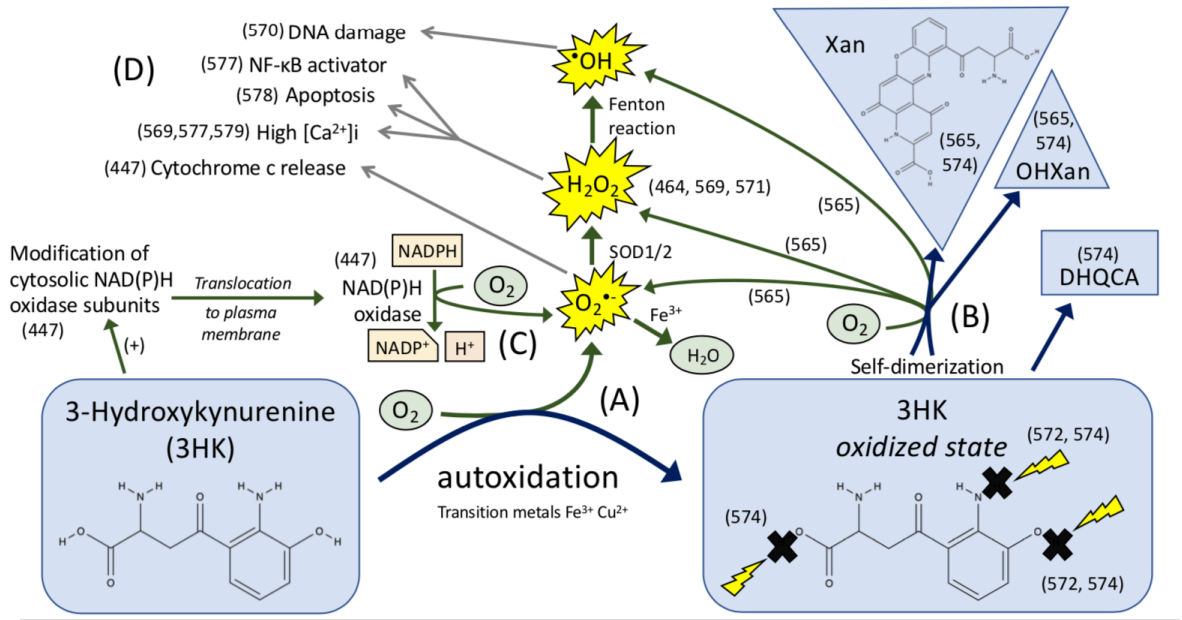

464: Okuda et al. 1996; **447**: Wang et al. 2014; **565**: Zhuravlev et al. 2018; **569**: Wei et al. 2000; **570**: Hiraku et al. 1995; **571**: Eastman et al. 1989; **572**: Vazquez et al. 2000; **573**: Colin-Gonnzalez. Etal. 2013; **574**: Ishii et al. 1992; **577**: Schmidt et al. 1995; **578**: Whittemore et al. 1995; **579**: Distelhorst et al. 1996.
DHQCA: 4,6-dihydroxyquinolinequinonecarboxylic acid; NAD(P)H: nicotinamide adenine dinucleotide phosphate oxidase; OHXan: hydroxy-xanthommatin; Xan: xanthommatin.

Figure 14. Cellular toxicity from 3-hydroxykynurenine-induced reactive oxygen species.
Three mechanisms known to cause redox stress (A-C): **A**: Autooxidation of 3-hydroxykynurenine (3HK) has been described by authors with H^+ abstraction postulated from the -OH group, -COOH group, or the $-NH_2$ group, in the presence of transition metals (Fe^{3+} or Cu^{2+}) giving rise to generation of superoxide ($O_2^{\bullet-}$), which subsequently produce hydrogen peroxide (H_2O_2) and hydroxyl radicals ($^{\bullet}OH$). **B**: Autooxidation can result in spontaneous production of metabolites besides oxidized 3HK, including DHQCA, and 3HK self-dimerization products xanthommatin (Xan) or hydroxy-xanthommatin (OHXan) which results in the production of various reactive oxygen species (ROS) when two molecules of 3HK combine. **C**: 3HK has also been shown to modify cytosolic NAD(P)H oxidase subunits, which promotes translocation to the plasma membrane for assembly to NAD(P)H oxidase which makes $O_2^{\bullet-}$. The observed effects of unchecked ROS caused by 3HK are listed in (**D**) and the specific targets of ROS are proximal in location to the site of ROS generation. Effects include mitochondrial membrane damage and cytosolic release of cytochrome c, high intracellular calcium concentrations by endoplasmic reticulum release, apoptosis, NF-κB activator, and DNA damage.

-wise would only react very slowly with biomolecules such as DNA, proteins and membranes (575, 576). Additionally, 3HK can react with, and chemically modify, cytosolic NAD(P)H oxidase subunits, which promotes translocation of subunits to the plasma membrane for construction of NAD(P)H oxidase which produces superoxide ($^{\cdot}O_2^-$) in the process of generating $NADP^+$ from NADPH (473). As well as producing other reactive oxygen species (ROS), superoxide ($^{\cdot}O_2^-$) can react with nitric oxide (e.g. in the vasculature) to form peroxynitrite, a reactive nitrogen species (RNS). Superoxide ($^{\cdot}O_2^-$) is rapidly converted to hydrogen peroxide (H_2O_2) by the enzymatic activity of superoxide dismutase enzymes 1 and 2. Unlike superoxide, H_2O_2 is not a free radical and has a much greater diffusion radius, and can readily diffuse across biological membranes. H_2O_2 can activate NF-κB by stimulating the phosphorylation of the IκB kinase complex, which is degraded, releasing NF-κB p50/p65 dimer to bind DNA (577). H_2O_2 reacts with metal cations (Fe^{2+} or Cu^+) to generate the highly reactive hydroxyl radical ($OH^{\cdot}$), termed the '*Fenton reaction*' (575). Hydrogen peroxide can cause neuronal apoptotic death, by mechanisms which include increase of intracellular free Ca^{2+} (578, 579). Oxidized 3HK can exert many damaging effects (573). These include the ability for oxidized 3HK to directly bind protein amino groups, 3HK-generated ROS can modify proteins, oxidise lipids, break DNA strand and modify nucleic acids, modify gene expression by activation of redox-sensitive transcription factors, induce cytochrome c release into the cytosol and induce apoptosis (473, 573). 3HK-induced cytotoxicity can be rescued by the use of free radical scavengers, caspase inhibitors and pharmacological closure of the mitochondrial permeability transition pore (580). Lastly, some of the damaging properties attributed to 3HK may be caused by its onward metabolites, for example, 3HAA which can also undergo autooxidation with the formation of ROS (350). Also, 3HK may potentiate the effects of other metabolites, such as quinolinic acid, and together can synergistically cause toxicity in the brain and aggravate excitotoxic nerve cell loss (581).

1.2.6.3.2 3HK in diseases

With regard to neurological disease, elevated levels of 3HK have been found in different parts of the brain in post-mortem brains of patients with Huntington's disease (582-584), Parkinson's disease (585), pneumococcal meningitis (586), and in AIDS-related dementia (587). Different types of neurons have different threshold levels for neurotoxicity to increased 3HK concentrations. Further specifics regarding 3HK in neurodegenerative diseases can be read in a thorough review of the topic by Colín-González *et al.* (573).

In relation to systemic human disease, elevated plasma 3HK concentrations have been found to confer an increased risk of acute coronary events over a 10-year period (588), and is

associated with incidence of obesity and diabetes mellitus (588, 589), and chronic renal failure (557) and severe acute pancreatitis (375). In an animal model of viral pneumonia, 3HK levels were elevated in lung homogenate (479). Additionally, along with 3HAA, 3HK appears to be an endogenous carcinogen, particularly with respect to bladder cancer by causing DNA damage through generation of H_2O_2 (570, 590).

A state of oxidative stress only exists, however, where there is an excessive production of ROS (such as by the aforementioned mechanisms – Figure 14) which saturate the cell's defence redox antioxidant systems. Furthermore, ROS are not always deleterious, and the literature supports a broader role for ROS, which include intracellular signalling mediators to regulate numerous physiological and biological responses. Examples include growth factor regulation, intracellular signalling, hypoxic signal transduction, autophagy, immune response and stem cell proliferation and differentiation (591, 592). 3HK can be eliminated by onward metabolism or transported out of a compartment using the large neutral amino acid transporter (564, 568, 573). Similar to kynurenine, 3HK in humans serves as a substrate for competing enzymes: kynureninase and KATs (Table 11). Humans do not make phenoxazinone synthases which catalyse the conversion of 3HK to XA in many forms of life (e.g. fungi, plants, bacteria and insects), rather humans rely on KATs to convert 3HK to XA. The majority of 3HK is metabolised by kynureninase to give 3-hydroxyanthranilate (3HAA) and amino acid L-alanine, by hydrolytic cleavage of the Cβ-Cγ bond (565). Indeed, mammalian kynureninase preferentially utilises 3HK over kynurenine as a substrate, which in the human liver has been reported to have an activity ratio of ~15-20:1 (593, 594). Kynureninase is heavily dependent upon coenzyme vitamin B_6 (PLP) (see 1.2.6.2.), and is exquisitely sensitive to lack of this vitamin; resulting in accumulation of 3HK when the supply of PLP is insufficient (535, 595, 596). And on replacement of PLP, plasma 3HK levels reduce (597).

1.2.7. 3HK transamination (to xanthurenic acid)

3HK has two primary metabolic fates (see **Figure 15**, below): either it is hydrolysed to 3HAA, or converted into the more chemically stable compound xanthurenic acid (XA) (598). On account of its yellow colour ('*xantho*' meaning 'yellow') and isolation from urine, 4,8-dihydroxyquinoline-2-carboxylic acid was named 'xanthurenic acid', and was first described by L Musajo in 1935 (599).

In humans, XA is formed by transamination of 3HK by KAT enzymes I-IV (E.C. 2.6.1.7), in the same way as KATs convert kynurenine into kynurenic acid with coenzyme PLP (see 1.2.5.2.). Intriguingly, mosquitoes have poorly functioning KAT enzymes with respect to 3HK transamination and do not possess kynureninase which is the major enzyme for 3HK

catabolism in most species (600). To prevent cytotoxic accumulation of 3HK, mosquitoes use two alanine glyoxalate aminotransferase enzymes (AGTs) to catalyse 3HK transamination to XA (601), which may give the additional benefit of antioxidant protection of the mosquito gut during ingestion of a blood meal (602).

The main biological functions of XA are listed in **Table 10** (above). XA can penetrate the blood-to-brain barrier and has a particular neurophysiological role with regard to glutamate neurophysiology. Some have reported XA as an agonist for group II metabotropic glutamate receptors ($mGluR_2$ and $mGluR_3$) (475), but these conclusions have been brought into question, and XA may instead modulate synaptic transmission by vesicular glutamate transport (VGLUT) inhibition (476). VGLUTs transport glutamate, an excitatory neurotransmitter, from the cytoplasm and into synaptic vesicles. As well as having apparent analgesic effects (478), XA may also limit serotonin biosynthesis by inhibiting production of the tryptophan hydroxylase cofactor tetrahydrobiopterin (BH_4) (477). In the periphery, XA has diabetogenic effects (insulin binding, beta cell toxicity with impaired insulin production) (398), pro-apoptotic effects (480), and also antioxidant properties (479, 602).

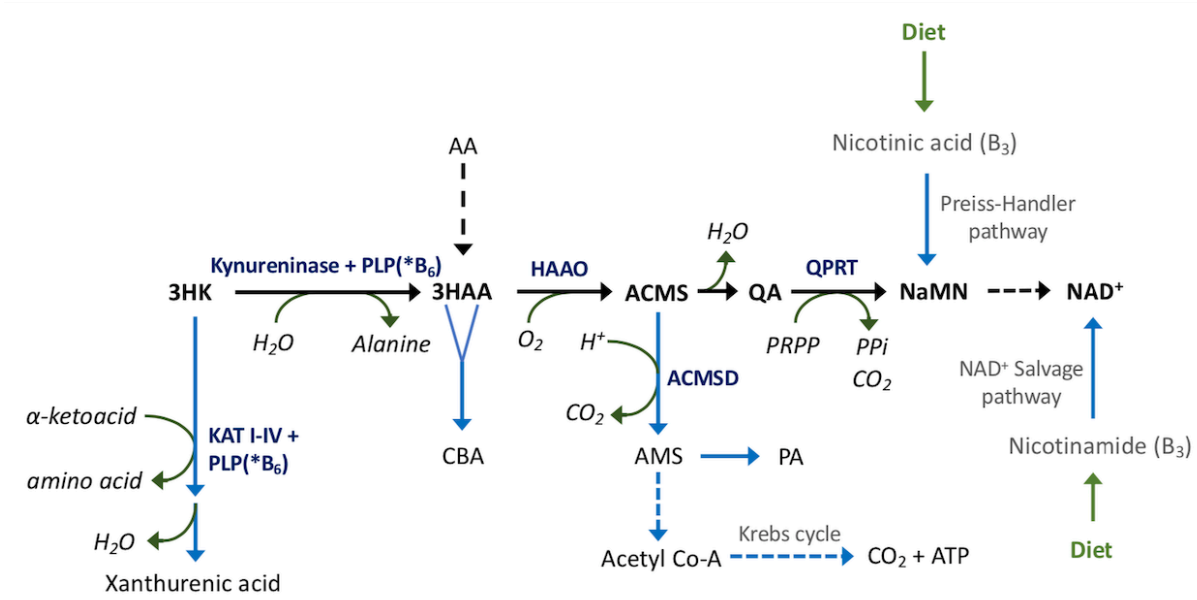

Figure 15. 3-Hydroxykynurenine catabolism and NAD+ biosynthesis

Metabolites in black with black arrows denotes the main pathway. Compounds in italics are co-factors and by-products. Dotted arrow '---' denotes multi-step molecular transformation, whereas a solid arrow denotes direct transformation. A double ended arrow head denotes a bi-directional transformation. A double-tailed arrow denotes dimerization. Abbreviations: ACMS: 2-amino-3-carboxymuconic acid-6-semialdehyde (also known as 2-acroleyl-3-aminofumarate); AMK: *N*-acetyl-5-methoxykynuramine; AMS: 2-aminomuconic-6-semialdehyde; ATP: adenine triphosphate; B_3: vitamin B_3, nicotinic acid; B_6: vitamin B_6, pyridoxal; CBA: cinnabarinic acid; CO_2: carbon dioxide; 3HAA: 3-hydroxyanthranilic acid; 3HAAO: 3-hydroxyanthranilic acid oxidase; KAT: kynurenine aminotransferase; MAO: monoamine oxidase; NaMN: nicotinic acid mononucleotide; NAD^+: nicotinamide adenine dinucleotide (oxidized); PLP(*B_6): pyridoxal 5'-phosphate (B_6 vitamer); PPi: inorganic pyrophosphate; PRPP: 5-phosphoribosyl-diphosphate; QA: quinolinic acid; QPRT: quinolinic acid phosphoribosyl transferase.

1.2.8. 3-Hydroxyanthranilic acid formation and onward metabolism (CA, ACMS, QA, PA)

3HK is converted by kynureninase and PLP into 3HAA (Figure 15). PLP deficiency causes increased 3HK due to impaired 3HK hydrolysis activity (595). 3HAA is structurally similar to 3HK (Figure 13, above) and shares many biochemical properties. 3HAA also has anti-oxidant (467, 479, 603), and pro-oxidant properties (471).

Two molecules of 3HAA are converted into one molecule of cinnabarinic acid by oxidative dimerization, which may occur by non-enzymatic and enzymatic processes (e.g. cinnabarinate synthase, ceruloplasmin, superoxide dismutase, catalase) (485, 604, 605). This red coloured compound '2-amino-3-oxo-3h-phenoxazine-1,9-dicarboxylic acid', was originally extracted from the red coloured fungus *Trametes cinnabarina (Jacq.)*, and its name, 'cinnabarinic acid' is a reference to this fungi (Figure 11, above) (389). Cinnabarinic acid is an endogenous ligand of the aryl hydrocarbon receptor which can drive IL-22 production (485), and is a weak agonist of type 4 group metabotropic glutamate receptors (mGluR4) (606).

Alternatively, 3HAA may be converted into 2-amino-3-carboxymuconic acid-6-semialdehyde (ACMS), also known as 2-acroleyl-3-aminofumarate, by 3-hydroxyanthraniliate 3,4-dioxygenase (HAAO; E.C. 1.13.11.6). This unstable compound sits at a junction in the kynurenine pathway (Figure 15) (377); ACMS can either proceed towards NAD^+ formation via quinolinic acid (QA) or form 2-aminomuconic-6-semialdehyde (AMS), the common precursor for picolinic acid and acetyl-CoA. Basal metabolic function favours the non-enzymatic cyclization of ACMS to QA (towards NAD^+ production), over the production of AMS (377).

Quinolinic acid (QA) (pyridine-2,3-dicarboxylic acid), was first identified as an tryptophan intermediate by LM Henderson (607). 3HAA-3,4-dioxygenase (HAAO; E.C. 1.13.11.6) (**Table 11**, above) is reportedly the most active kynurenine pathway enzyme and rapidly converts 3HAA into the unstable 2-amino-3-carboxymuconate semialdehyde (ACMS), which undergoes nonenzymic cyclization to form quinolinic acid (Figure 15) (377, 608, 609). The name quinolinic acid (QA) derives from quinoline, from which it can be produced through an oxidation reaction. And the term quinoline is derived from quinine, a medical alkaloid first isolated from the bark of a cinchona tree species. Unlike other KP metabolites, QA is a colourless solid substance, but has multiple physiological roles in the brain and the periphery (see **Table 10**, above). Because of its polar nature and lack of efficacious transport processes, similar to KA, QA cannot easily cross the blood-to-brain barrier, and accordingly all QA found in the brain is generated from oxidised 3HAA (506, 554, 610). In addition to providing substrate for NAD^+ production, QA has many excitotoxic effects in the brain (487): It is a powerful glutamate agonist and exerts an excitatory effect at the NMDA receptor located on primary

astrocytes (487, 554); QA-Iron complexes can cause lipid peroxidation (488); QA potentiates cytotoxic damage when present with 3HK (581); and QA may be pathologically important in an array of common and debilitating neurological and psychiatric diseases (554, 611). In the periphery, QA functions as an NAD^+ precursor but has other effects, such as altered bone remodelling by NMDA (454), pro-oxidant effects as QA-Iron complexes (489), and apoptosis of thymocytes and Th1 cells (481). QA metabolism proceeds towards NaMN and then NAD^+ biosynthesis.

Formation of picolinic acid (PA), also known as pyridine-2-carboxylic acid, diverts metabolism away from QA production (Figure 15). PA is a bidentate chelating ligand (meaning it binds with two sites) and facilitates zinc absorption from the intestine (377, 382, 486). Picolinic acid is formed by non-enzymatic cyclization of AMS. However, PA formation depends on the degree of the substrate saturation of the enzyme (ACMSD; E.C. 4.1.1.45) competing with this cyclization. Only when ACMSD is maximally saturated with ACMS is there sufficient quantity of AMS substrate to allow PA production to proceed faster than QA formation (377). AMS that is not converted into PA is available for 2-aminomuconic-6-semialdehyde dehydrogenase (AMSD) production of 2-aminomuconic acid, which is further metabolised to yield acetyl coenzyme A (Co-A) (377). Acetyl CoA is oxidised through the Krebs cycle (named after physician and biochemist Sir Hans A Krebs, 1900-1981, Nobel prize winner 1953).

1.2.9. Nicotinamide adenine dinucleotide (NAD^+)

Quinolinic acid is metabolised by quinolinic acid phosphoribosyl transferase (QPRT; EC 2.4.2.19) with 5-phosporibosyl-diphosphate (PRPP), by a phosphoribosyl transfer reaction followed by decarboxylation, to form nicotinic acid mononucleotide (NaMN); the substrate for nicotinic acid adenine dinucleotide (NAAD), which is converted into NAD^+ (367, 612, 613) (Figure 15, above). Nicotinic acid (also known as niacin), a form of vitamin B_3, can also be converted to NaMN and to NAD^+ by the Preiss-Handler pathway. Vitamin B_3 consists of three vitamers: nicotinamide, niacin (nicotinic acid) and nicotinamide riboside (see Figure 7 for chemical structure of nicotinic acid). Dietary nicotinamide can be used to produce NAD^+ by the salvage pathway (Figure 15). However, dietary tryptophan is more effective than dietary nicotinamide or nicotinic acid in elevating liver nicotinamide dinucleotides and urinary levels of *N*-methylnicotinamide (377). NAD^+ is an essential pyridine nucleotide that serves as an electron carrier in cellular metabolism. Beyond its role as a co-enzyme in redox reactions, NAD^+ is an important co-substrate for three classes of enzymes: Sirtuins (SIRTs), adenosine diphosphate (ADP)-ribose transferases (ARTs) and poly(ADP-ribose) polymerases (PARPs), the cyclic ADP-ribose (cADPR) synthases (367, 382). NAD^+ is consumed by these enzymes

and continuously degraded. To maintain stable cellular concentrations of NAD^+, organisms primarily use a NAD^+ salvage pathway but also rely on biosynthetic pathways. Without enough NAD^+, pellagra occurs, and this is why vitamin B_3 is referred to as the pellagra-preventing factor (367, 382). 60 mg of dietary tryptophan is considered to be roughly equivalent to 1mg of niacin (614), but there are wide individual variations on this approximate ratio (302). Daily niacin requirements of adults are ~15 mg. In the absence of niacin, a daily intake of ~1 g of tryptophan can meet this requirement. However, this necessitates an intake of ~100 g of protein, as the tryptophan content of most proteins is ~1% (419). For interested readers, review publications by A Badawy make for a thorough introduction on the topic of the kynurenine pathway of Tryptophan-NAD^+ metabolism (377).

1.3. Kynurenine pathway flux in acute inflammation

The acute phase response refers to an array of rapid host responses which involves dramatic leukocyte, humoral immunity, neuroendocrine and metabolic changes after a stressful physical stimulus. Collectively, these responses are generally protective and infer host survival advantage, when they are modest and short-lived. The acute phase components work in concert and biochemically interact in this multi-system organ response. The least well defined component of the acute phase response is arguably the metabolic changes which orchestrate nutrient/energy flux (615).

First described in 1942 by Sir David Cuthbertson (1900-1989, University of Glasgow), the ‘ebb’ and ‘flow’ phases of the acute stress response to injury and trauma are concepts which have been taught over the generations and still found in postgraduate textbooks more than 70-years later (e.g. Sabiston Textbook of Surgery, 20th Edition) (615-617). Broadly, the ‘ebb period’ denotes the early period of depressed metabolism and reduced energy expenditure after major injury, whilst the ‘flow period’ refers to a hypercatabolic phase (616). Contemporary scientific understanding of the metabolic response to injury includes altered metabolic rate, preference of certain macronutrients for energy substrate, stress hyperglycaemia, muscle wasting, changes in body composition and behaviour (615). Metabolism of macronutrients during critical illness is altered at several stages: digestive absorption, intracellular intermediate metabolism and substrate oxidation (615). Recently investigators have shown how transcriptional reprogramming in critical illness helps protect against the prooxidative effects of the inflammation by maintaining redox homeostasis (618).

In critical illness, particularly in the ‘flow’ phase, there is a robust phenotype of negative nitrogen balance which is under the influence of hormones and inflammatory mediators.

Proteins are dismantled by cellular proteasomes and the resulting peptides and amino acids are used in the synthesis of inflammatory mediators, gluconeogenesis (mainly alanine and glutamine) or oxidised and excreted as nitrogenous wastes (e.g. urea and ammonia) (615). Amino acid metabolism in critical illness, specifically tryptophan oxidation, in the so-called 'ebb' phase, is of particular interest and how this contributes to the acute phase response.

1.3.1. Flavin Adenine Dinucleotide (B_2) and Pyridoxal 5-Phosphate (B_6) in inflammation

Several of the kynurenine pathway enzymes are dependent upon B_2 (see section 1.2.6.2.) and B_6 (section 1.2.5.2) vitamers, as co-enzymes. Such reliance has been well demonstrated from B_2 (560) and B_6 (619) deficiency and supplementation studies with tryptophan loading. B_2 vitamer, flavin adenine dinucleotide (FAD), is required by KMO, whist B_6 vitamer, pyridoxal 5'-phosphate (PLP), is required by kynureninase and KATs (I-IV). In systemic inflammation and critical illness, several studies have consistently found that whilst red cell concentrations of FAD and PLP are preserved, plasma levels significantly drop (494, 620-627). Some investigators have sought to understand why and how plasma levels drop (e.g. redistribution of vitamers, including mobilisation to and consumption at sites of inflammation, or vitamer catabolism), and how erythrocytes maintain vitamer concentrations (495, 496, 625, 628, 629).

Riboflavin, which is a co-enzyme for 90 human proteins, has been found to have protective effects against sterile injury (630). PLP also has multiple inflammatory and immunomodulatory effects, and Ueland *et al.* have helpfully reviewed the vitamin B6-dependent inflammatory pathways; namely, the kynurenine pathway, the trans-sulfuration pathway (homocysteine metabolism), serine and glycine metabolism (300). Interestingly, vitamin B_6 supplementation has been shown to have cytoprotective effects by preventing oxygen radical generation and lipid peroxidation during hydrogen peroxide challenge (631). Sustained PLP deficiency in critically ill patients is associated with hyperglycaemia, a feature of the so-called 'ebb period' of the acute phase response (627).

1.3.2. Tryptophan, kynurenines and NAD^+ in inflammation

Systemic inflammation, and in particular AP, has been shown to cause disturbances of the serum amino acid profile in humans (632). Of the 23 amino acids studied, most were found to have statistically significant changes in serum concentrations between samples taken on hospital admission (day 0), day 5, or 6-weeks later (632).

Flux in the kynurenine pathway metabolites has been observed in the mesenteric lymph of rats with AP, and peripheral blood from humans with AP-associated multiple organ

dysfunction, with depletion of tryptophan and increases in 3HK (375, 633). The previous sections detail some of the modulatory effects of kynurenines on the immune system. Diverting kynurenine pathway metabolism can have protective effects, for example KMO inhibition was found to ameliorate multi-organ dysfunction in the early phase of experimental AP, suggesting a mechanistic role for 3HK in multiple organ dysfunction seen in critical illness (634). A whole raft of inflammatory mediators is known to modulate activity of KP enzymes: Glucocorticoid, platelet activating factor, nitric oxide, IL-1β, IL-4, IL-10, TNFα, IFNγ (**Table 11**, above). KMO inactivation is of particular interest given the cytotoxic effects of endogenous 3HK and 3HAA on peripheral tissues (473). Elevated 3HK levels are inversely related to decreased PLP levels in inflammation/injury (597). **Figure 16** provides an overview of the known effects of inflammation upon flux of the kynurenine pathway.

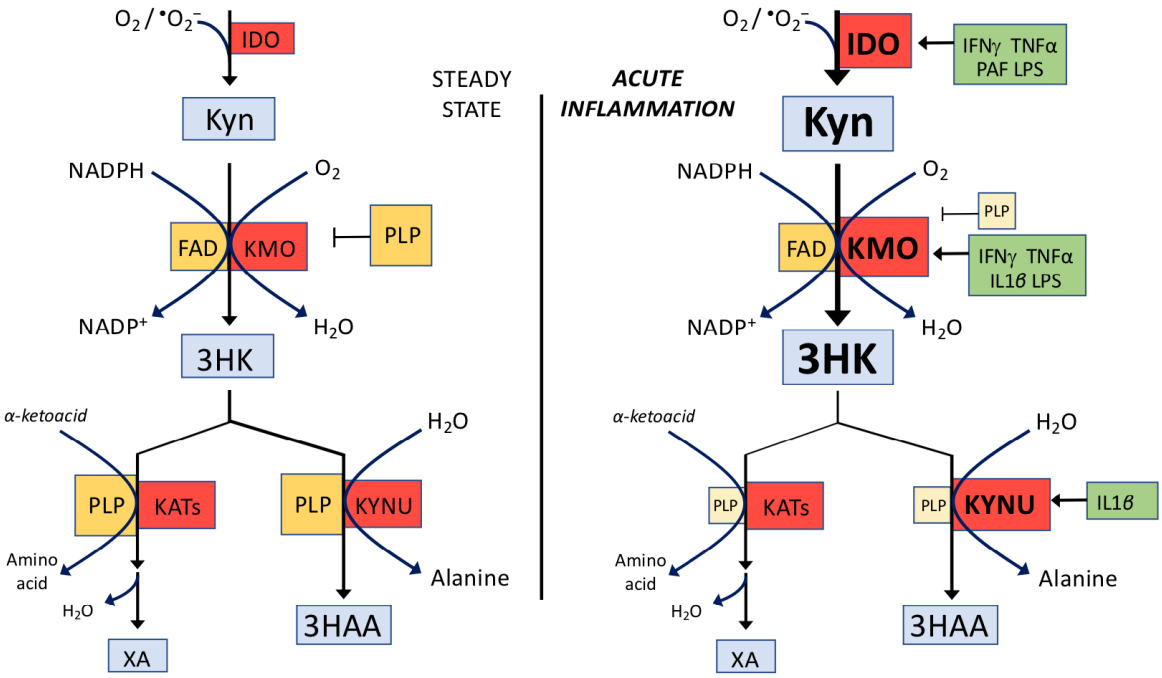

Figure 16. **Kynurenine pathway flux in systemic inflammation**

Enzymes depicted by red boxes (IDO, KMO, KATs, KYNU), Cytokines in green boxes (IFNγ, TNFα, PAF, LPS, IL-1β), metabolites in blue boxes (Kyn, 3HK, XA, 3HAA), vitamer co-enzymes in orange boxes (FAD, PLP).

Abbreviations: 3HAA: 3-hydroxyanthranilic acid; 3HK: 3-hydroxykynurenine; FAD: Flavin adenine dinucleotide; IDO: Indoleamine 2,3-dioxygenase; IFN: Interferon; IL-1β: Interleukin 1β; KAT: Kynurenine aminotransferase; KMO: Kynurenine 3-monooxygenase; Kyn: Kynurenine; KYNU: Kynureninase; LPS: Lipopolysaccharide; PAF: Platelet activating factor; PLP: Pyridoxal 5'-phosphate; TNF: Tumor necrosis factor; XA: Xanthurenic acid

1.4. Research aims

In light of the data that human AP severity correlates with increased plasma 3HK levels (375), and that using a severe, non-recovery model of experimental AP in mice with KMO deletion reduced multiple organ injury at 24-hrs (634), my hypothesis was formed to investigate the role of 3HK recovery phase of AP.

1.4.1. Overall hypothesis

Elevated levels of KMO product, 3-hydroxykynurenine, impairs survival in experimental AP, and suppression of 3HK improves recovery in experimental AP.

1.4.2. Research hypotheses

1) Inactivation of KMO activity, by *Kmo* genetic deletion, and thus abolition of 3HK levels, improves recovery in experimental AP [Experiment 1]
2) Conversely, elevated 3HK concentrations by genetic alteration, would impair AP recovery [Experiments 2 + 3]
3) Altered kynurenine levels by genetic alteration, would alter the systemic inflammatory response in AP in terms of the innate immune cellular response (blood and infiltrative leukocytes), non-cellular mediators (e.g. proinflammatory cytokines) and biochemical markers of end organ injury [Experiment 4]
4) Use of KMO inhibitor therapy for those mice with elevated 3HK levels, would provide protection against critical illness [Experiment 5]
5) Elevated 3HK synergises with proinflammatory mediators to potentiate cell death [Experiment 6].

2. MATERIALS AND METHODS

2.1. Genetically altered mice

Throughout the project, male mice were investigated. All experiments using animals are conducted in accordance with the Animals (Scientific Procedures) Act, 1986 governed by the UK Government Home Office, and after review from the University of Edinburgh research ethics committee and veterinary services (PPL: 60/4433). Genetically-altered mouse strains with a C57BL/6J background have been generated by our group for the study of kynurenine-3-monooxygenase (KMO). Specifically, we have developed a global KMO knockout mouse strain (referred to as KMO^{null}) engineered with FRT restriction sites flanking a transcription stop signal in exon 3 of *Kmo* and with integral loxP sites flanking key gene regions to give conditional (tissue-specific) knockout capability as needed; a wild-type control strain, created by crossing (and backcrossing) KMO^{null} mice with a FLP-deleter strain to excise the FRT-flanked stop signal to restore *Kmo* transcription ($KMO^{FRT\text{-}deleted}$, hereafter referred to as KMO^{wt}); and a hepatocyte-specific KMO knockout line where FLP-deleted KMO mice homozygous for loxP-flanked *Kmo* have been crossed with a Cre-recombinase expressing strain in which Cre expression (and therefore KMO inactivation) is driven by the albumin promoter and thus only occurs in liver tissue (hereafter referred to as $KMO^{alb\text{-}cre}$ mice). The latter have a KMO knockout biochemical phenotype in the blood plasma, but wild-type KMO expression in non-hepatic tissues. Genotyping is conducted by PCR of earmark clippings and only homozygous genotypes are used. Of these, only adult male mice, aged between 18 to 25 weeks old, and weighing ≥ 20 grams, are used. To compare outcomes between strains, mice from different lines are age-matched (≤ 14 days).

2.1.1. Genotyping

KMO^{null} (KMO knock out) and $KMO^{FRT\text{-}deleted}$ (FLPKMO, wild type) mice were generated in our laboratory (634). To create hepatocyte-restricted KMO knock out mice, $KMO^{FRT\text{-}deleted}$ mice were crossed with the *Albumin-Cre* B6.Cg-Tg (Alb-cre) 21Mgn/J mice. These mice were backcrossed for at least 6 generations to generate homozygous $KMO^{FRT\text{-}deleted}$ and Albumin cre positive mice. All mouse genotypes were confirmed by standard PCR-based genotyping of genomic DNA isolated from ear clips by Dr Xiaozheng Zhong (Senior Research Assistant, Mole Group). The following primer sequences were used for PCR genotyping: 5'-GCGGTCTGGCAGTAAAAACTATC-3' and 5'-GTGAAACAGCATTGCTGTCACTT-3' to yield a single PCR product of 100 base pairs representing albumin cre positive.

2.2. Analgesia

Pain is a major factor in clinical AP, and I had no reason to think that animals do not experience pain in experimental AP. Therefore, considerable efforts were taken to provide analgesia for experimental subjects throughout the disease course. The total dosing of animals in longitudinal studies was variable as it depended on cage-side pain scores and was protocol driven. Animal dosing in longitudinal studies is detailed in the appropriate results sections.

2.2.1. Parenteral analgesia

All operated mice were given pre-emptive analgesia whilst under general anaesthesia immediately before laparotomy with subcutaneous buprenorphine (0.05 mg/kg body weight, in 5% dextrose-DPBS wt/vol), and a further two doses (6-8 hrs and 20-24 hrs post-operatively). Additional doses of subcutaneous buprenorphine were given in accordance with prospectively defined criteria outlined in the cage-side clinical observation score sheet (Appendix 3).

2.2.2. Enteral analgesia

In anticipation of pain throughout the 7-day study period, animals were provided each morning (between 09:00 – 10:00 hrs) with oral Buprenorphine (0.01 mg) in a 0.5 mL dot of jelly, and consumption was monitored to allow consumption calculations. Jelly was not given on the day of cull to avoid post-prandial fluctuations in plasma glucose. Prior to experimentation, mice are supplied vehicle jelly dots (i.e. without Buprenorphine) to become accustomed to the jelly.

Protocol

1) Cut a half cube of concentrated stock jelly (Strawberry jelly, Hartley®) into small pieces and transfer into a stack of 60 ml medicine cups (preferably n = 4 cup stack to insulate users' hand).
2) Add 6 ml of hot water (just off boiling).
3) Stir until all jelly stock dissolved.
4) Cool to room temperature. To expedite this step, remove medicine cup from its stack and briefly place in freezer to allow rapid cooling.
5) Add 0.8 ml 0.3 mg/ml Buprenorphine (Vetergesic, Ceva Animal Health) and stir to mix. When making vehicle jelly, instead add 0.8 ml water at this step.
6) Aliquot 0.5 ml volumes into wells of a suitable plastic blister pack mold.
7) Use dental spatula (Medentra, #859-m9) to transfer 0.5 ml medicated jelly to petri dish for animal consumption.

2.3. Acute pancreatitis model

Transduodenal retrograde infusion of a bile acid salt solution to the pancreatic duct is a well-recognised model of AP, and is frequently reported to show evidence of injury at extra-pancreatic sites (eg. lung, kidney). Sodium taurocholic acid (Na-TCA), has been used for intraductal infusion by several research groups to successfully induce AP. Elevated plasma amylase levels and pancreatic histopathological changes are used to confirm presence of AP for 24-hr timepoint experiments. The control group consisted of a sham operation wherein the duodenal loop was handled and the pancreatic head and duodenal papilla were identified. The abdomen was left open for an equal length of time as the AP group. The protocol described is the final version (Protocol 9) resulting from preliminary work detailed in Results 3.1.

2.3.1. Materials – Retrograde biliopancreatic duct infusion

The materials used for surgical procedures, including induction of experimental AP, telemeter implantation, minipump implantation and *in vivo* tracer studies is listed in **Table 12**.

2.3.2. Protocol for induction of experimental acute pancreatitis

1) Prepare 2% sodium taurocholate (NaTCA) (wt/vol) in phosphate buffered saline (PBS) (37 mM) in 20 mL syringe.
2) Prepare analgesia for subcutaneous dosing (5% Dextrose, PBS, Buprenorphine).
3) Prepare clean surgical instruments using Enzystel instrument cleaner and Medistel instrument disinfectant.
4) Prepare 70% ethanol (in water) for disinfectant spray.
5) Set up equipment, including infusion pump.
6) Induce anaesthesia using vaporised Isofluorane (5%) in oxygen in the induction chamber of the anaesthetic rig.
7) Record the animal's weight (include details of any in-situ surgical devices such as skin clips or implants to allow body weight calculation).
8) Shave hair from the animal's operative site(s) and transfer the mouse to operating field on top of a pre-warmed heat mat.
9) Administer weight-adjusted dose of subcutaneous analgesia for pre-emptive post-operative analgesia (0.05 mg/kg body weight, in 5% dextrose-PBS wt/vol).
10) Apply a dot of protective Lacri-lube ointment to each eye.
11) Turn down the anaesthesia dose for maintenance at surgical depth (ie. 2-3%).

Equipment	Details
Infusion pump – PHD Ultra	Harvard Apparatus
5-0 Mersilk suture (round bodied, single ended)	Ethicon (W595)
5-0 steel suture	B Braun
7-0 Prolene suture (round bodied, double ended)	Ethicon (W8702)
Lacri-lube eye ointment	Allergan Ltd. (PL00426/0041)
Lacrimal cannula (26G x 1/18 in)	BD Visitec (Medguard Healthcare Ltd.) 581276
Polyethylene tubing, for infusion	General supplier
Colibri retractor (for laparotomy)	Fine Science Tools (17000-02)
Tissue scissors	Fine Science Tools (14095-11)
Skin scissors	Fine Science Tools (14072-10)
Guthrie retractor (liver retractor)	Fine Science Tools (17023-13)
Stainless steel micro serrefine microclamp (curved	Fine Science Tools (18055-06)
Forceps style clip applicator	Fine Science Tools (18057-14)
Tissue forceps	Fine Science Tools (11052-10 and 11152-10)
Autoclip wound clip system	Harvard Apparatus Ltd. (34-0557)
Isofluorane IsoFlo	Zoetis (Vm42058/4195)
Taurocholic acid sodium salt hydrate	Sigma-Aldrich (T4009-5G)
Glucose (Dextrose)	Sigma-Aldrich (G-8270)
Medistel	Tristel, MD311
Enzystel	Tristel, MD315
Phosphate Buffered Saline	Dulbecco's PBS, Gibco
Operating Microscope	Zeiss
Buprenorphine	Vetergesic, Ceva Animal Health

Table 12. Surgical materials

12) Prepare the skin with disinfectant (ie. 70% ethanol or Betadine) and arrange surgical drapes around the operative field
13) Arrange surgical microscope and don the sterile surgical gloves.
14) Using surgical scissors and forceps, open the abdomen and maintain wound edge retraction with a Colibri retractor.
15) Place a piece of gauze under liver edge and gently retract liver using Guthrie retractor to allow clear visualisation of the duodenal loop and bile duct.
16) Rotate the duodenal loop medially and identify the duodenal ampulla before placing a 7-0 Prolene stay suture through the duodenum proximal to the ampulla.
17) Puncture the duodenum with a 23G hypodermic needle just distal to the ampulla on the antimesenteric border.
18) Using a lacrimal cannula, cannulate the biliopancreatic duct.
19) Temporary occlude the proximal hepatic duct with a serrefine microclamp using forceps style clip applicator.

20) Infuse 50 µl sodium-taurocholic acid at a constant rate over 5 mins into the duct with an infusion pump.
21) Use a 'z' stich to close the duodenotomy with 7-0 Prolene.
22) Where appropriate, implant telemetry device (see methods 2.3.1.).
23) Give 0.5 ml intraperitoneal bolus of PBS.
24) Mass abdominal wall closure (all layers except skin) with 5-0 Mersilk.
25) Close skin with Autoclip skin clips.
26) Transfer to warm box (set 30^{o}C) for recovery from anaesthesia for half an hour.

Sham laparotomy

Sham laparotomy consists of an equivalent surgical wound incision length as AP subjects, handling of small bowel with visualisation of the pancreas, with time delay of abdominal wall closure (bearing in mind the length of time required for the AP group to cannulate the duct, complete 5 min infusion and suture close the duodenal puncture site). As with the AP, a 0.5 ml intraperitoneal bolus of PBS was given before mass closure with Mersilk and skin closure with autoclips.

2.4. Telemetry

2.4.1. Implantation of cardiometabolic telemeter (G2 HR E-mitter)

Large telemetry implants in small animals have been shown to delay recovery, and therefore small devices are preferable (635). Battery-free telemetry devices are smaller and lighter than those that containing batteries, these are instead powered by a plate positioned beneath the cage. The G2 HR E-mitter radio-telemetry device (Starr Life Sciences) is at present unique on the commercial market as the only battery-free telemeter that records heart rate. Additionally, this device also measures core body temperature (CBT) and locomotor activity (**Figure 17**).

1) At laparotomy, the G2 HR E-mitter telemetry device was implanted into the abdominal cavity and the two chest leads exteriorised through the abdominal wall using large bore needle and forceps.
2) The E-mitter leads were then tunnelled under the skin to the appropriate sites on the chest wall. Metal ferules are attached and crimped flat to act as receiver pads. Both leads are anchored to chest wall muscle with 5-0 steel suture.
3) Skin wounds are closed with wound Autoclip skin slips.

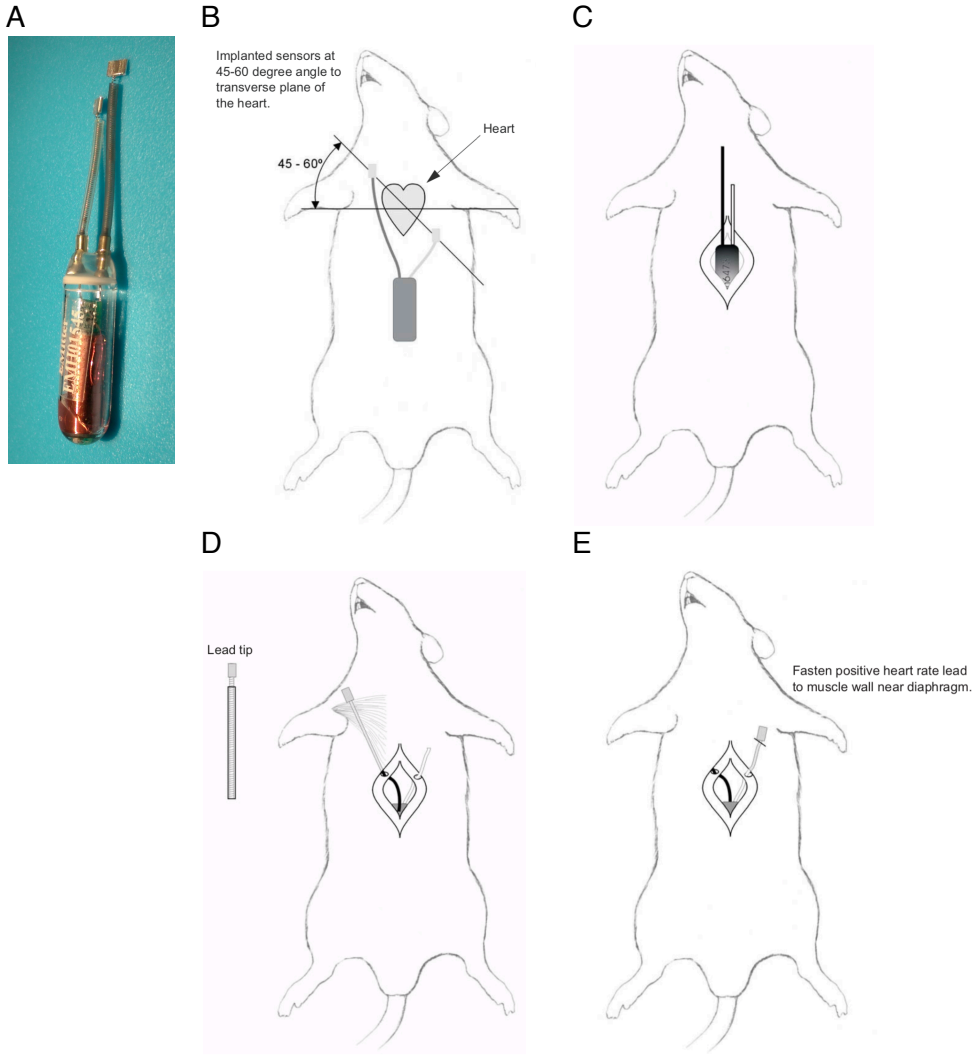

Figure 17: Surgically implantable telemetry devices – G2 HR Emitter
A: G2 HR E-Mitter device (referred to as 'cardiometabolic telemeter' in thesis to distinguish it from the other telemeter. B-E: Images reproduced from manufacturer's instruction manual. B: Picture depicts orientation of cardiac lead placement. C: Picture shows insertion of device within abdominal cavity. D: Lead is tunnelled subcutaneously to reach pectoral muscle. E: A separate pectoral incision is made to allow lead suture to pectoral muscle.

The original telemeter used, seen in Figure 17, involved a longer operation to implant chest leads. Later, a smaller telemeter device (**Figure 18**) was used as this was smaller and required invasive surgery to implant. Indeed, it required no more surgery than just a securing suture to the anterior abdominal wall than the AP or sham laparotomy and with hindsight was ideal for AP studies and preferable to the cardiometabolic device.

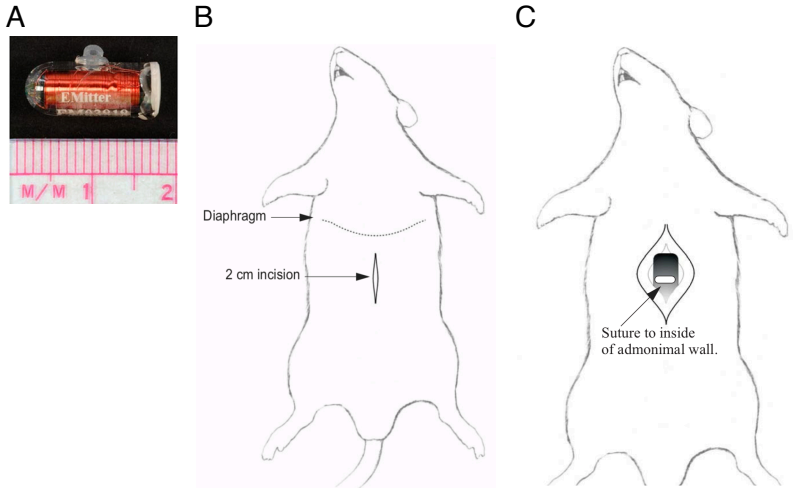

Figure 18: Surgically implantable telemetry devices – G2 E-mitter
A: G2 E-Mitter device (referred to as 'pill' or 'mini' telemeter to distinguish it from the other telemeter). B and C: Images reproduced from manufacturer's instruction manual. B: Picture depicts laparotomy incision (same size as that needed for pancreatic ductal infusion). C: Picture shows insertion of device within abdominal cavity and is secured to the anterior abdominal wall with a single suture.

2.4.2. Experimental design

Mice were singly housed and supplied vehicle jelly the day before surgery, in order to build their nest and become accustomed to the jelly. The next day, during the early light phase, two mice went either AP model or sham operation, and insertion of an E-mitter telemetry device (. After 30-mins in the warming box (30^0C air temperature), mice are housed on top of a telemetry receiver / energizer pad in a dedicated circadian room. Telemetry recording starts at the midpoint of the light phase on the day of surgery – termed zeitgeber time (ZT) 0-hr.

Mice are culled at set timepoints following ZT 0-hr, and this allows for a full telemetry dataset. For example, a 7-d experiment would be culled immediately following 168-hrs after ZT0 (**Figure 19**). Schedule 1 cull is performed by under terminal anaesthesia. An open cardiac puncture performed to acquire blood plasma. Fresh samples of lung, liver, kidney and body/tail of pancreas are frozen and stored along with plasma at -80^0C. Samples of lung, liver, kidney and head of pancreas are also fixed in 10% formalin. The total body weight at the start and end of the experiment is measured (to 2 d.p.), correcting for the mass of the E-mitter and remaining skin clips, to calculate change in body weight.

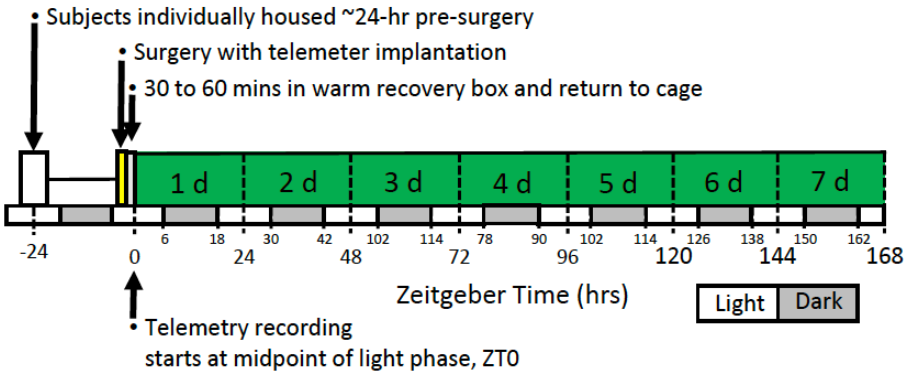

Figure 19. Experimental plan for 7-day recovery AP studies

The schematic demonstrates the time schedule for surgery (acute pancreatitis, AP; or sham operation), start of telemetry recording (at ZT 0-hr). Light and dark phase cycles are indicated along the timeline, with each 24-hr period consisting of a 6-hr light phase, 12-hr dark phase and 6-hr light phase.

2.4.3. Telemetry system installation and troubleshooting

Data acquisition was performed using the E-mitter system. PC with Windows operating system. Telemetry hardware with Vital View software. ER4000 receiver pads (Starr Life Sciences) (**Figure 20**). Telemetry data were recorded by a computer (Hewlett-Packard desktop computer, Windows 7 Enterprise) using VitalView animal monitoring software (version 5.0, STARR Life Sciences). The telemetry system was initially installed by the UK supplier company (Linton Instrumentation) using current software (v5.1) but failed to work as the application failed to detect the hardware. After testing a variety of new cables and computers to no avail, the software was replaced with an older version (v5.0); and the communication between the software and hardware was successfully established.

Figure 20. ER-4000 telemetry hardware

The caged telemetered mouse is housed on top of ER-4000.

2.4.4. Remote desktop

Install 'Microsoft Remote Desktop' for Mac OS X, version 8.0.38. This allows monitoring of mice remotely informing the investigator of extremes physiological data (e.g. hypothermia), which may warrant an unscheduled cage side clinical check.

2.4.5. Telemetry software setup

Calibration settings which accompany with each telemeter device issued by the manufacturer are entered into the VitalView software prior to each telemetry experiment. Settings for the smaller ('pill' or 'mini') telemeters are reproduced in **Table 13**. See Appendix 6.1. for the VitalView software setup.

	Low		**High**	
Telemeter ID	Temp.	Freq.	Temp.	Freq.
EM21	37.0	843.5	41.0	1005.0
EM22	37.0	853.4	41.0	1017.5
EM23	37.0	850.3	41.0	1019.5
EM24	37.0	842.0	41.0	1001.7
EM25	37.0	823.5	41.0	983.9
EM26	37.0	859.6	41.0	1027.4
EM27	37.0	847.4	41.0	1013.6
EM28	37.0	847.1	41.0	1016.7

Table 13. **Two-point calibration frequencies for mini-telemeters**

2.4.6. Processing ASCII files for downstream processing

Creation of ASCII files were converted to Comma-Separated-Value files. VitalView software (version 5.0) was used. Version 5.1 was originally tried but hardware installation problems arose which were eventually overcome by using version 5.0 of the software.

2.4.7. Telemetry data analysis

The original intention was to use the VitalView software to analyse the telemetry data. However, the analysis functions in the software were very limited and the data visualisations were of very poor quality. However, the data could easily be exported to be analysed elsewhere with a variety of options. Having discussed this problem with scientists from other disciplines who were familiar with time series data, it quickly became apparent that scientific Python computing modules offered a very attractive solution because its capabilities exceeded my requirements, it was open source with no financial costs, it was a very intuitive computer language with enormous online troubleshooting support (e.g. <www.stackoverflow.com>), and

it allowed complete transparency of my data analysis which would be easily reproduced and the code could be shared with other investigators.

2.4.8. Telemetry data visualisation and export in VitalView

Python scripts for visualising CSV file data outputs from VitalView are shown in Appendix 6.2. Python is a flexible computer language which can be used for any programming tasks and is a very popular language for data science due to the excellent and expanding scientific libraries. The installation of the *SciPy* stack was performed using the Anaconda Python distribution from Continuum Analytics (http://continuum.io/downloads.html). The *Jupyter* notebook interface was used (which has subsequently been superseded by JupyterLab). Data wrangling was performed with the Pandas library, calculations were performed using Numpy, and plotting was performed with Seaborn.

2.4.9. In-house check and re-calibration of G2 HR telemeters

One of the 'cardiometabolic' G2 HR telemeters (EM09) gave consistently lower temperature readings than the other devices, whilst giving equivalent heart rate and locomotor activity readings. This device had been a recently purchased from the company so did not qualify for recalibration which they offer at 1-year. To ascertain the calibration quality of all telemeters, an in-house quality control calibration was performed for every device individually using a single scientific thermometer for all readings (Fisher Scientific UK Ltd, Cat. #11735853):

1) Vitalview software was calibrated to the E-mitter with 2-point frequencies (Table 13)
2) A large waterbath was placed on top of the ER-4000 receiver containing warm water (>40^{o}C).
3) The telemeter was placed within a submerged open inner glass jar (to prevent water currents around the E-mitter)
4) Water was allowed to slowly cool and E-mitter temperature readings taken at each temperature integer (e.g. 39.0^{o}C, 38.0^{o}C, 37^{o}C) between 30 to 40^{o}C.
5) Step 4 was repeated 3 times for each device, recorded and a mean average calculated.

The smaller, mini-telemeters (G2 E-mitters) had temperature readings <1^{o}C from the waterbath themermometer and therefore in-house calibration was not applied as the differences were small and within limits of accuracy. However, the suspected mis-calibrated EM09 device was confirmed to be an outlier with respect to temperature readings (by 3.08^{o}C), and therefore a correction was applied to all temperature data from the G2 HR telemeters. Additionally, the difference (~3^{o}C) was consistant across the temperature range (30-40^{o}C). Appendix 3 (section 6.3.) documents the mean calibration differences at 37^{o}C which was used to correct the data.

2.4.10. COSINOR analysis of telemetry data

To determine circadian variations in telemetry parameter data, the open access circadian rhythm analysis software package, ChronosFit (Version 1.06), was used to fit a Cosinor curve with a 24-hr rhythm. The purpose of the Cosinor analysis was to fit a circadian trend curve to the physiological telemetry data points, a technique which has been used by other investigators studying the effects upon physiological data from systemic disease (636). The components of the Cosinor analysis are illustrated in Figure 25D: *mesor* (mean of the oscillation; called the *midline estimating statistic of rhythm*), *amplitude* (half the difference between the highest and lowest values), and *acrophase* (timing of the cosine maximum given the degrees, where 360^0 corresponds to a 24-hr cycle). The Cosinor curve is represented by the following function: C(t) = MESOR + amplitude cos(2 pi (t- acrophase)/ 24-h], where MESOR (mean of the oscillation), amplitude (half the difference between the highest and lowest values), and acrophase (timing of the cosine maximum given in degrees, where 360 degrees corresponded to a 24-h cycle).

2.4.11. Periodogram rhythm analysis

Chronos-Fit version 1.06 data analysis software program (Zuther *et al.* 2009) was used to analyse data. This program fits a cosinor curve to the measured data points and calculated the midline estimating statistic of rhythm (mesor; a rhythm-adjusted 24-h mean), amplitude (half of peak-to-trough of rhythmic change) and the acrophase (peak time of the rhythm).

2.5. Animal housing and welfare

2.5.1. Animal housing

Mice were housed in University of Edinburgh facilities with a 12:12-hr light-dark (LD) cycle. During experimentation, mice have access to both dry and wet diet (RM1; *Rat and Mouse No.1 Maintenance*, Special Diets Services) and water *ad libitum*. The RM1 standard feed used contains a variety of amino acids, including tryptophan (0.18%). Mice are individually housed, and environmental enrichment is standardised (nesting material, single tube). Because the circadian system is well known to drive daily rhythms in mammalian physiology and behaviour, we synchronise the timing of our experiments to the LD cycle. Telemetry recording starts at the midpoint of the light phase on the day of surgery (denoted *Zeitgeber Time zero*; 'ZT0'). In our institution, with a 07:00:00 – 19:00:00 light phase, ZT0 is therefore 13:00:00. The air temperature in the telemetry room is maintained at a mean 26.5^0C (range

24.0 – 29.2°C) and monitored at hourly intervals with a scientific thermometer data logger (SL52USB, Signatrol).

In an effort to maintain optimal animal welfare, I designed a specific clinical observation score sheet for this project in consultation with University of Edinburgh Veterinary colleagues (Appendix 6.4.). This clinical sheet lists defined humane-endpoints beyond which animals are culled, and is used for routine cage-side checks. Additionally, longitudinal telemetry readings (e.g. core body temperature) are also informative in relation to welfare (e.g. sustained profound hypothermia during the experiment is an indication to humanely cull an animal).

2.6. Animal cull and plasma processing

2.6.1. Humane cull procedure

Blood samples were taken by cardiac blood sampling under terminal anaesthesia, transferred to EDTA tubes (Microvette®,CB 300 K2E, Sarstedt) and centrifuged at 5,000 rpm for 3 mins, and plasma stored at -80°C. Histologically examined tissues (i.e. head and body of pancreas, half kidney, liver segment, lung) were fixed in 4% neutral- buffered formalin overnight before transfer into 70% aqueous ethanol prior to paraffin-embedding.

2.6.2. Blood plasma clinical chemistry

Plasma α-amylase, urea, creatinine, ALT, albumin and glucose concentrations were analysed using commercial kits from Alpha Laboratories Ltd. (Eastleigh, UK) adapted for use on the Cobas Fara centrifugal analyser (Roche Diagnostics Ltd., Welwyn Gareden City, UK). These were by senior biochemist Dr. Forbes Howie PhD, of the Shared University Reaserch Facilities (SuRF) at the Queen's Medical Research Institute, University of Edinburgh who was blinded to the treatments and mouse lines by the use of anonymising sample codes.

2.6.3. Plasma cytokine assay

Plasma cytokine levels were analysed using the Meso Scale Discovery (Rockville) V-PLEX Proinflammatory Panel1 mouse kit in accordance with MSD's instructions which are summarise in this protocol. An MSD calibration curve is shown in Appendix 10 (section 6.10). Samples were run in duplicate.

Protocol

1) Prepare wash buffer (PBS 0.05 % Tween-20).
2) Prepare calibration curve.

3) Prepare samples (1:1 dilution of plasma with Dilutent 41).
4) Wash MSD plate 3 x 150 µl per well wash buffer.
5) Add 50 µl per well of diluted plasma.
6) Incubate at room temperature, shaking gently for 2-hrs.
7) Meanwhile, prepare antibodies in Dilutent 45.
8) After 2-hrs, shake off wells.
9) Wash MSD plate 3 x 150 µl per well wash buffer.
10) Add antibodies mix to each well.
11) Incubate at room temperature, shaking gently for 2 hours.
12) Add 150 µl 2X Read Buffer T to each well.
13) Read on MSD plate reader.

2.7. Kmo gene expression

Isolation of total RNA and quantitative reverse transcription polymerase chain reaction (RT-PCR). Total RNA was isolated with RNeasy Mini Kit (Qiagen, 74106). The first-strand cDNA was synthesised from 0.5 µg of total RNA using kit (QuantiTect Reverse Transcription Kit, Qiagen) with G-Storm thermal cycler machine. RT-PCR was performed using cDNA and TaqMan probes.

Protocol – Preparation for RNA extraction

1) Prepare clean beads and dry prior to use, using protocols.
2) Label 2 ml eppendorf tubes (e.g. '1' – '9').
3) Prepare 1:100 dilution h β-mercaptoethanol (β-ME) in RLT buffer from RNeasy mini kit.
4) Prepare 70% ethanol in dH20.
5) Prepare fume hood and clean centrifuge.
6) Finally, transfer pre-prepared <20 mg tissue sections from -80°C storage to laboratory.

Protocol – RNA extraction

1) In hood, add 2 clean metal balls to each tube containing cut tissue [note: avoid tissue 'jumping' out tube by holding it at an angle].
2) Add 400 µl RLT (with β-ME) buffer and transfer to shaker (Qiagen TissueLyser).
3) Homogenise by 3 min shake (at 25 Hz) on shaker.

4) Centrifuge spin 3 mins at full speed (13,000 rpm = 16060 RCF, Biofuge fresco Hareaeus).
5) Aspirate lysate & transfer into new labelled eppendorf (labelled '1 to 9'). Keep balls for reuse.
6) Spin lysate 3 mins at full speed (16060 RCF)
7) Transfer 350 µl lysate into new labelled eppendorf, avoiding pellet aspiration.
8) Add 350 µl of 70% ethanol to lysate.
9) Invert all Eppendorf tubes together (x10) to mix immediately. Do not vortex.
10) Label the pink top of each RNeasy spin column.
11) Transfer 700 µl sample to corresponding RNeasy spin column (with collecting tube).
12) Spin 15 secs at 16060 RCF. Discard flow through.
13) In hood, wash 1: Add 700 µl RW1 buffer to RNeasy spin column.
14) Spin 16060 RCF for 15 secs. Discard flow through.
15) *Continue at lab bench*. Wash 2: Add 500 µl RPE buffer to RNeasy spin column.
16) Spin 16060 RCF for 15 secs. Discard flow through.
17) Wash 3: Add 500 µl RPE buffer to RNeasy spin column.
18) Spin for 2 mins at 16060 RCF.
19) Place column onto new 2 ml collection tube (supplied) & spin 16060 RCF for 60s.
20) Place RNeasy spin column in a new 1.5 ml collection tube (supplied).
21) Add 40 µl RNase free water (supplied) directly onto spin column membrane.
22) Arrange in centrifuge to prevent lids spinning, then spin 16060 RCF 60s to elute the RNA.
23) Use 1.3 µl from each on NanoDrop 1000 Spectrophotometer (ThermoScientific) to quantify RNA concentration of each sample.
24) Store RNA samples at -80^{o}C.

<u>Protocol – Preparation for reverse transcription</u>

1) Calculate volume of RNA needed (= *X* µl), referring to NanoDrop results from previous and calculate volume of RNase-free water needed for each sample (12 µl – *X* µl).

<u>Protocol – Reverse transcription</u>

1) Defrost RNase-free water on bench and thaw gDNA Wipeout buffer (from QuantiTect Reverse Transcription Kit, Qiagen) on ice.
2) Transfer RNA samples from -80^{o}C storage to laboratory on dry ice, and allow to thaw.
3) Add volume of RNase-free water into corresponding well of PCR plate.

4) Add volume of RNA solution from each sample to corresponding well of PCR plate, thus making up to 12 µl.
5) Add 2 µl gDNA Wipeout buffer to each well of PCR plate, thus making 14 µl per well.
6) Attach PCR flat cap lids (in separately cut column strips).
7) Mix PCR plate by vortex.
8) Spin down sample (briefly spin up to 1000 rpm on Rotina centrifuge 420R, and stop)
9) G-Storm PCR Machine: Template RNA generation: Incubate at 42 oC for 5 mins [use WIPE protocol: in Xiao folder]. Secure machine lid upon closing.
10) Prepare Mastermix using ratio in **Table 14**, making and extra ~10% to avoid running out. Mix and spine down matrix components once thawed.

Mastermix component	**Volume**
Quantiscript Reverse Transcriptase	1 µl
Quantiscript RT Buffer	4 µl
RT Primer Mix	1 µl

Table 14. Ratio of mastermix components

11) Add 6 µl of mastermix to 14 µl of tRNA to each plate well.
12) Mix PCR plate by vortex.
13) Spin down sample (briefly spin down).
14) G-Storm PCR Machine: Incubate 42^{o}C for 25 mins, and then at 95^{o}C for 3 mins, before cool to 4^{o}C at end of run [use CDNA protocol: in Xiao folder]. Secure lid upon closing.

Dilute all samples of cDNA

1) Briefly centrifuge plate to spin down contents.
2) Add 80 µl molecular water (RNase free) to make 100 µl stock of cDNA (from 500 ng total RNA).
3) Store dilute cDNA samples at -20^{o}C until ready for real-time PCR.

Protocol – Preparation for Real Time Polymerase Chain Reaction (RT-PCR)

1) Create PCR plate plan: Duplicates of 20 µl and x2 NTC ('no template control').

Protocol – RT-PCR

1) Make up enough 18S + Probe Mixture for each plate well, with ratio of:

a. 6 ul molecular H2O / RNase-free water
b. 10 µl TaqMan Fast Universal PCR Master Mix (2X), No AmpErase
c. 1 µl 18S VIC/MGB probe 20x (ThermoFisher Scientific, 4319413E)
d. 1 µl target probe 20x.

2) Add 2.2 x 18 µl of 18S/Target Mixture to tube for each sample (= 39.6 µl).
3) Add 2.2 x 18 µl of 18S/Target Mixture to tube for each sample (= 39.6 µl).
4) Add 2.2 x 2 µl cDNA to tube or molecular water for NTC (= 4.4 µl).
5) Add 20 µl sample to corresponding 2 wells in PCR plate.
6) Transfer plate to PCR machine (Applied Biosystems 7900HT Fast Real-Time PCR).

2.8. LC-MS/MS

I used high performance liquid chromatography – mass spec / mass spec (LC-MS/MS) to quantify concentrations of circulatory endogenous kynurenine metabolites, injected tracer compounds, and drug concentrations in the plasma, urine and tissue homogenates. The following describes the method I employed. Deuterated-5-Tryptophan was the default single internal standard used, and others were used only where specified in the results section. 0 ng (internal standard control), DB ('double blank' control, with no metabolites and no internal standards).

Equipment	**Supplier**
Oasis Hydrophilic Lipophilic Balanced (HLB) 96-well plate (10 mg Sorbent, 30 µm particle size)	Waters (#186000128)
Bovine Serum Albumin	Sigma
Collection plate	Masterblock®
Sciex 6500	Sciex
Borosilicate glass tube (13x100mm)	Fisherbrand (14-961-27)
Dri-Block DB-3 sample concentrator	Jencons (Scientific) Ltd.
SPE Dry tm 96 Dual	Argonaut
Centrifuge Heraeus Fresco 21	Thermo Scientific
Water (HPLC grade)	Fisher Scientific (W/0106/17)
L-tryptophan-(indole-d5) (D5-TRP)	Sigma-Aldrich
[^{13}C6]-L-Kynurenine (13C6-KYN)	Sigma-Aldrich
[U-Ring-13C6]-3-Hydroxykynureine (13C6-3HK)	Sigma-Aldrich
Kynurenic acid-3,5,6,7,8,-d5 (D5-KA)	Sigma-Aldrich
Acetonitrile (HPLC grade)	VWR Chemicals BDH (UN1648)
Methanol (HPLC grade)	Fisher Scientific (M/4000/17)
Phosphoric acid	BDH Anala R (10173BC)
Dulbecco's PBS	Gibco
Cryotube vials	ThermoScientific

Table 15. Equipment for LC-MS/MS

2.8.1.1. Preparation of calibration curve standard

The following 12 calibration standards were used routinely: 100 ng, 50 ng, 20 ng, 10 ng, 5 ng, 2 ng, 1 ng, 0.5 ng, 0.2 ng, 0.1 ng, 0 ng, Double Blank. The following compounds were used: L-Tryptophan, L-Kynurenine, Kynurenic acid, Anthranilic acid, 3-Hydroxy-DL-kynurenine, Xanthurenic acid, 2-hydroxykynurenic acid, Quinolinic acid. All compounds were sourced in powder form from Sigma Aldrich.

2.8.1.2. Preparation of plasma samples for extraction

1) Remove frozen plasma samples from -80°C storage, and thaw at room temperature.
2) Label one borosilicate glass tube for every sample and calibration standard.
3) Add 10 µl of the internal standard* (e.g. 5 µg/mL D5-Trp) to all tubes except Double Blank.
4) Add 100 µl of standard analyte mix to the calibration curve tubes.
5) Transfer glass tubes to Dri-block heater at 40°C, and evaporate to dryness.
6) Return all glass tubes to lab bench.
7) Add 100 µl of 4% phosphoric acid to all sample and calibration tubes, including Double Blank, and briefly vortex to mix.
8) Add 100 µl of mouse plasma to the corresponding glass tube and briefly vortex.
9) Add 100 µl of 1% Bovine Serum Albumin in PBS to each calibration standard tube and briefly vortex.

2.8.1.3. Preparation of extraction plate

1) Use a printed 96-well plate map to record with a unique identifier each well to be used for every sample and calibration standard.
2) Assemble the vacuum manifold and place an Oasis HLB 96-well plate on top. Do not place collection plate underneath at this stage.
3) Add 500 µl of Methanol to each well to be used, and vacuum to dryness.
4) Add 500 µl of high performance liquid chromatography (HPLC) water to each well to be used, and vacuum to dryness.

2.8.1.4. Sample extraction

1) Add all prepared sample to corresponding cartridge (i.e 100 µl plasma).
2) Subject manifold to vacuum (0.35 Bar) to dryness.

3) Add 500 µl of HPLC water, to wash each well, and subject manifold to vacuum to dryness.
4) Place Masterblock® 96-well collection plate inside vacuum manifold, underneath the plate.
5) Ensure the lid of the manifold is sealed.
6) Add 200 µl 80% methanol to elute the extract into the collection plate, and vacuum to dryness.
7) Transfer the collection plate to the SPE Dry Dual Sample Concentrator System.
8) Insert needles into collection plate (above elute) and set oxygen free nitrogen flow at 30 l/min at 60°C to dry down elute.
9) If not proceeding directly LC-MS/MS, secure cover film to collection plate and store at -20°C until processing.

2.8.1.5. Analyte resuspension

1) Add 70 µl of HPLC water and shake for 5 mins on KS 260 Basic Shaker (at 200 rpm).
2) Add 30 µl of methanol and shake for 5 mins on shaker (at 200 rpm).
3) Secure cover film to collection plate and placed into the LC-MS/MS autosampler.

Injection Volume	10 µl
Column	ACE Excel UHPLC C18 PFP 1.7 µm (2.1 x 100 mm)
Mobile Phase A	H_2O / 0.1% CH_2O_2
Mobile Phase B	CH_3OH / 0.1% CH_2O_2
Flow Rate	400 µl/min
Temperature	Oven 40°C

Table 16. Liquid chromatography settings - Shimadzu / QTRAP 6500+

CAD	-2
Ionspray voltage	4500 / -4500
Temperature	600
GS1	60
GS1	40
Spray voltage	5500
Turbospray / APCI	Turbospray
Entrance potential	10 / -10

Table 17. Mass spectrometry settings - Shimadzu / QTRAP 6500+

2.8.2. Tracer studies

Given the surprising finding of elevated concentrations of 3HK in Kmo$^{alb\text{-}cre}$ mice, I wanted to investigate the metabolism of 3HK. I performed pilot studies to determine a suitable concentration of tracer to allow detection by LC-MS/MS at 20 mins.

2.8.2.1. Protocol – preparation of intravenous tracer mix

1) Prepare 100 μg/mL L-tryptophan-(indole-d5) in PBS (A)
2) Prepare 100 μg/mL [U-Ring-^{13}C6]-3-Hydroxykynureine in PBS (B)
3) Mix 1:1 volume of (A) and (B) to give: 50 μg/ml D5-TRP and 50 μg/ml ^{13}C6-3HK in PBS.

2.8.2.2. Protocol – tracer mix injection and sample collection

1) A 0.3 ml syringe with the tracer mixture was prepared (50 μg/mL D5-TRP and 50 μg/mL ^{13}C6-3HK in PBS).
2) General anaesthesia induction was induced with 5% isoflurane gas in oxygen, which was reduced to ~2% isofluorane for maintenance.
3) A warming mat was used throughout and temperature of the mat checked at regular intervals.
4) Respiration was continuously monitored by the operator to ensure a regular rate and that anaesthesia not excessively deep or light, requiring adjustment of isofluorane.
5) Record the animal's weight and calculate the mixture volume for weight-adjusted injection.
6) Perform IV injection by tail vein (or penile vein where attempts to use tail vein fail).
7) Maintain animal under anaesthesia for 20 mins measured from tracer injection time point.
8) At 20 mins, open chest and perform cardiac puncture.
9) Transfer whole blood into EDTA tubes.
10) Aspirate urine and store at -80^{o}C.
11) Harvest lung, liver, kidney and spleen tissues, and transfer tissues into individual Cryotube vials and snap freeze in liquid nitrogen.
12) Centrifuge EDTA blood tubes for 3 mins at 5,000 rpm (detail) and store plasma at -80^{o}C.

2.8.2.3. LC-MS/MS Instrumentation method

Samples were then injected onto the LC-MS/MS system (10 µl). Shimadzu Nexera MP UHPLC with an AB SCIEX QTRAP 6500+ triple quadrupole system mass spectrometer, operated by Analyst® software (SCIEX, Cheshire, UK). The column used for analysis was an ACE Excel UHPLC silica column comprised of a C18 bonded to pentafluorophenyl (PFP) phase (C18-PFP) (1.7 µm, 2.1 x 100 mm, Advanced Chromatography Technologies Ltd., Aberdeen, Scotland). The sample was injected (10 µl); the column oven temperature was 40^0C. Two mobile phases were used 0.1% formic acid (Phase A) in water and 0.1% formic acid in methanol (Phase B) at a flow rate of 0.4 mL/min. Data processing was performed using MultiQuant™ Software, Version 3.0.2 (SCIEX, Cheshire, UK). All peaks analysed were individually assessed.

2.9. Flow cytometry

Dissociation of murine lung and liver samples was performed using the 'Lung Dissociation Kit, mouse' and 'Liver Dissociation Kit, mouse' kits by Miltenyi Biotec Ltd. Ex-vivo lung perfusion was performed using Phosphate buffered saline (PBS) via the right cardiac ventricle, with the aim of flushing out pulmonary erythrocytes. Liver perfusion was performed in situ by cannulation of the portal vein and PBS perfusion. Lung and liver organs were homogenized using the gentleMACS Dissociator (Miltenyi Biotec Ltd.) with organ-specific programs. I designed a single protocol for simultaneous lung and liver dissociation for flow cytometry applications. The modifications made to the original separate Miltenyi protocols were to maximise cellular yield, lyse erythrocytes, and optimize work-flow efficiency.

2.9.1. Preparation

Sodium citrate 3.8% (aqueous) was prepared in sterile water (wt/vol).

2.9.2. Blood preparation for flow cytometry

For analysis of the circulating blood innate immune cells population, blood was collected from cardiac puncture. Prepare 3.8% sodium citrate aqueous.

Equipment	**Manufacturer**
FACS DIVA software	BD
FACS tubes	BD
FlowJo software (Version 10.1r5)	TreeStar
gentleMACS™ Dissociator	Miltenyi Biotec
LSRFortessa™ cell analyser	BD
Nucleocounter	Chemometec
Rotina centrifuge 420R	Hettich
Reagents	**Manufacturer**
autoMACS® rinsing solution	Miltenyi Biotec (130-091-222)
Bovine Serum Albumin solution	Miltenyi Biotec
CD115-APC (clone CSF-1R)	BioLegend UK Ltd (135510)
CD3-PE (clone 17A2)	BioLegend UK Ltd (100205)
CD11b-BV421 (clone M1/70)	BioLengend UK Ltd (101236)
CD11c-PE/Cy7 (clone N418)	BioLegend UK Ltd (117318)
CD19-PE (clone 6D5)	BioLegend UK Ltd (115508)
CD45-AF700 (clone 30-F11)	BioLegend UK Ltd (103128)
CD64-APC (clone FcyRI)	BioLegend UK Ltd (139306)
Dulbecco's Modified Eagle Medium (DMEM)	Gibco
F4/80-APC (rat anti mouse APC Clone CI:A3-1)	AbD Serotec (MCA497APCT)
Fc-Block anti-CD16/CD32 (purified rat anti-mouse)	BD Biosciences (553142)
Fixable Viability Dye eFluor455UV	eBioscience (65-0868-14)
Fix/Lyse	eBioscience
Ly6C-FITC (clone HK1.4)	BioLegend UK Ltd (128006)
Ly6G-PerCP/Cy5.5 (clone 1A8)	BioLegend UK Ltd (127616)
MHCII-APC/Fire 750 (clone I-A/I-E)	BioLegend UK Ltd (107652)
Liver Dissociation Kit, mouse	Miltenyi Biotect (130-105-807)
Lung Dissociation Kit, mouse	Miltenyi Biotect (130-095-927)
NK1.1-PE (clone PK136)	BioLegend UK Ltd (108708)
Red cell lysing buffer Hybrid-Max	Sigma Aldrich (R7757-100ML)
SiglecF-PE-CF594 (clone E50-2440)	BD Bioscience (562757)
UltraComp eBeads	eBioscience (01-2222-41)
Table 18. Equipment for flow cytometry	

2.9.3. Protocol

Blood and organ harvest

1) Label the 6-well plates, and decant Dulbecco's Modified Eagle Medium (DMEM) medium into each well to be used.
2) Open chest and perform cardiac puncture to retrieve blood and decant into 1.5 mL Eppendorf tube.
3) Mix 50 µl whole blood with 50 µl sodium citrate (3.8% aqueous) and keep on ice.
4) Perfuse lungs with syringe with 2 ml PBS via right ventricle.
5) Surgically remove lungs and perform a second perfusion with another 2 ml PBS.

6) The lungs were transferred into a single well containing DMEM, in 6-well tissue culture plate, labelled “lung plate”.
7) Cannulate the portal vein and perform a 4ml PBS perfusion of liver in situ.
8) Excised and transfer the liver to a sterile petri dish and remove obvious non-hepatic tissue (i.e. connective tissue or gallbladder).
9) The left lobe of the liver was transferred into one well of a 6-well tissue culture plate containing Roswell park memorial institute (RPMI) media, labelled “liver plate”.
10) Kidney – place in labelled cryotube tube and snap freeze in liquid nitrogen.
11) Pancreas – place in labelled cryotube tube and snap freeze in liquid nitrogen.

Tissue Digestion

1) Warm Liver dissociation mix to 37^{o}C (from Liver Dissociation Kit, Miltenyi Biotec)
2) Tissue weights were recorded
3) For each liver sample, transfer tissue into an individual C Tube (Miltenyi Biotech) containing prewarmed dissociation mix.
4) For each lung sample, transfer tissue into an individual C Tube (Miltenyi Biotech)
5) Add enzyme mix into tube from kit (Lung Dissociation Kit mouse; Miltenyi Biotec).
6) Using a syringe and needle, repeatedly aspirate enzyme mix into tissue.
7) Cut tissue into small pieces with dissecting scissors, close tube and label appropriately (ie. Liv M1).

Blood processing

1) In lab, take 100 µl blood/ sodium citrate samples off ice
2) Add 50 µl anti-CD16/CD32 Fc-block (to give 1:500 final concentration Fc-block) and incubate for 10 mins 4^{o}C for 30 mins dark [making 150 µl]
3) Add 50 µl antibody stain mix (see below) at 4^{o}C for 30 mins dark [making 200 µl]
4) Add 500 µl Fix/Lyse solution (eBioscience) for 30 mins dark at room temperature
5) Store 4^{o}C for 30 mins dark until Flow cytometry

gentleMACS™

1) Attach C Tubes containing Lung in pairs to the gentleMACS™ Dissociator. Run program m_lung_01.01 (8s).
2) Attach C Tubes containing Liver in pairs to the gentleMACS™ Dissociator. Run program m_liver_03.01 (37s).
3) Incubate all samples at 37°C under continuous rotations for 30 mins.

4) Re-attach C Tubes containing Lung in pairs to the Dissociator and run program m_lung_02.01 (38s).
5) Re-attach C Tubes containing Liver in pairs to the Dissociator and run program m_liver_04.01 (37s).
6) Spin all C Tubes together (100 g for 60s) to concentrate the sample at the bottom of each tube.

Lung preparation

1) Label 15 ml Falcon to match each C Tube and place in large rack in line with corresponding C Tube.
2) Place a 70 μm SmartStrainer (Miltenyi Biotec) on top of 15 ml Falcon and decant 'clean PBS' through the SmartStrainer.
3) Discard the PBS used to pre-wet the strainer membrane, and replace strainer back onto of the same Falcon.
4) Re-suspend sample (flick) and pour cell suspension through SmartStrainer, collecting sample in the Falcon.
5) Wash each C Tube with 2.5 ml 1x Buffer S (close lid, invert x2), and decant this through corresponding strainer.
6) Using a separate rubber plunger (from 2 ml syringe) for each sample in turn, repeatedly press strainer membrane to encourage remaining cells on membrane through the strainer. Discard each plunger after use.
7) Wash C Tube with 2.5 ml 'clean PBS' (close lid, invert x2), and decant this through corresponding strainer.
8) Screw close lid of Falcon. Last check that Falcon tube is labelled appropriately. Discard SmartStrainers.

Liver preparation

1) Label 15 ml Falcon to match each C Tube and place in large rack in line with corresponding C Tube.
2) Place a 100 μm SmartStrainer (Miltenyi Biotec) on top of 15 ml Falcon and decant 'clean DMEM' through the SmartStrainer.
3) Discard the DMEM used to pre-wet the strainer membrane, and replace strainer back onto of the same Falcon.
4) Re-suspend sample and pour cell suspension through SmartStrainer, collecting sample in the Falcon.

5) Wash each C Tube with 2.5 ml DMEM (close lid, invert x2), and decant this through corresponding strainer.
6) Using a separate rubber plunger (from a 2 ml syringe) for each sample in turn, repeatedly press strainer membrane to encourage remaining cells on membrane through the strainer. Discard each plunger after use.
7) Wash C Tube with 2.5 ml DMEM (close lid, invert x2), and decant this through the corresponding strainer.
8) Screw close lid of Falcon. Last check that Falcon tube is labelled appropriately. Discard SmartStrainers.

Red cell lysis (organs)

1) Centrifuge all (liver, lung) samples together (300 x g for 10 mins). Meanwhile, label 96-well plate and place on ice to chill.
2) Aspirate supernatant without disturbing pellet.
3) Re-suspend pellet in residual by vortex.
4) Add 1 ml of red cell lysis buffer from stock. Keep at room temperature.
5) Remove any remaining large particles (connective debris) from the suspension using pipette tip, and gently mix for 5 mins.
6) Add 10 ml 'cold sterile PBS' (from fridge) to each, and centrifuge all samples together (300 x g for 5 mins).
7) Discard supernatant, and re-suspend cell pellet in residual fluid. Keep all samples on ice.

Cell counting

1) Label eppendorf tubes (x1 for each sample).
2) Decant required volume PEB buffer from stock (in fridge) into a 15 ml Falcon. Label Falcon tube: 'PEB'.
3) For Lung, add 600 µl PEB buffer to each sample and mix. Keep these stock samples on ice.
4) For Liver, add 700 µl PEB buffer to each sample and mix. Keep these stock samples on ice.
5) For Kidney, add 1100 µl PEB buffer to each sample and mix. Keep these stock samples on ice.
6) Transfer 40 µl of PEB buffer to an eppendorf tube. Do one for each sample.

7) Transfer 10 µl of cell suspension from stock to eppendorf tube. Label eppendorf tube. Do this for each sample.
8) In the cell counting room (Flow suite), add 50 µl Reagent A to each eppendorf tube, and mix.
9) Add 50 µl Reagent B, to each eppendorf tube, and mix.
10) In turn, aspirate the sample mix with a NucleoCassette and count cells with the NC-100 system.
11) Document the cell concentration for each sample from computer, and discard each NucleoCassette after use.
12) Complete a cell count for each sample in turn.
13) Use 2 million cells for each staining sample and 1 million for unstained compensation.

Cell staining

The following stain panel mixes were used for blood, lung and liver after considerable consultation with peers experienced in flow cytometry and my own preliminary experimentation.

Fluorophore	BV421	FITC	PE	PE	PE	PE-Cf594	APC	AF700	PE-Cy7	PerCP-Cy5.5	PEB buffer
Antibody	CD11b	Ly6C	CD3	CD19	NK1.1	SiglecF	CD115	CD45	CD11c	Ly6G	-
Vol. (µl) for 50 ul	1.0	0.7	1.0	1.0	1.0	1.0	1.0	1.0	0.7	1.0	40.6
Final conc.	1:200	1:285	1:200	1:200	1:200	1:200	1:200	1:200	1:285	1:200	-
Table 19: Blood (200 µl total volume [blood 50, citrate 50, Fc block 50, stain 50])											

Fluorophore	BV421	FITC	PE	PE	PE	PE-Cf594	APC	AF700	PE-Cy7	PerCP-Cy5.5	APC-Fire	Buffer
Antibody	CD11b	Ly6C	CD3	CD19	NK1.1	SiglecF	CD64	CD45	CD11c	Ly6G	MHCII	-
Vol. (µl) for 25 ul	0.25	0.33	0.33	0.33	0.33	0.25	0.5	0.5	0.25	0.5	0.33	21.1
Final conc.	1:400	1:300	1:300	1:300	1:300	1:400	1:200	1:200	1:400	1:200	1:300	-
Table 20: Lung (100 µl total volume [cells 50, Fc block 25, stain 25])												

Fluorophore	BV421	FITC	PE	PE	PE	PE-Cf594	APC	AF700	PE-Cy7	PerCP-Cy5.5	APC-Fire	Buffer
Antibody	CD11b	Ly6C	CD3	CD19	NK1.1	SiglecF	F4/80	CD45	CD11c	Ly6G	MHCII	-
Vol. (µl) for 25 ul	0.25	0.33	0.33	0.33	0.33	0.33	0.5	0.5	0.25	0.33	0.5	21.0
Final conc.	1:400	1:300	1:300	1:300	1:300	1:300	1:200	1:200	1:400	1:300	1:200	-
Table 21: Liver (100 µl total volume [cells 50, Fc block 25, stain 25])												

Flow cytometry

Single cell suspensions are analysed by flow cytometry using BD LSRFortessa™ instrument with BD FACSDiva™ software. Use of unstained cells, fluorescence minus one (FMO) controls, and stained beads (with +ve and -ve beads) were used with Flow cytometry staff to set up compensations with the lasers.

2.10. In-vivo drug studies

2.10.1. Drinking-water drug study protocol

Sonicator : Homogenisers Status US 70, MS 72. Philip Harris Scientific.

75 ml mini drinking bottle (Classic Pet Products: 0190)

2.10.2. Parenteral mini pump drug study protocol

Preparation of the drug solution (250 mg/mL)

1) Weigh required mass of GSK898 into an eppendorf tube.
2) Add volume required to make 500 mg/mL in Dimethyl sulphoxide (Sigma-Aldrich)
3) Add equal volume of sterile filtered PEG 400, thereby making 250 mg/mL solution.
4) Vortex mix.

Filling micro-osmotic pumps

1) Record the weight of an empty micro-osmotic Alzet Model 1002 [100 μl reservoir, 0.25 μl/hr, 14 days] pump (Charles River Ltd. 0004317) together with its flow moderator in a tissue culture hood, taking sterile precautions.
2) Fill the pump with drug solution using a 27G needle (GSK898, 250 mg/mL in DMSO : PEG) or vehicle solution (1 : 1, DMSO : PEG, no drug).
3) Fully insert flow moderator into body of pump.
4) Record the weight of the filled pump.
5) Place pumps in sterile 0.9% saline overnight at 37°C before implantation (to ensure pumps start immediately on implantation. In accordance with manufacturer's instructions).

Implantation of micro-osmotic pump

1) Induce general anaesthesia.
2) Administer weight-adjusted subcutaneous pre-emptive analgesia bolus away from surgical site.
3) Clipper hair to upper back.
4) Transfer animal to operative field.
5) Prepare skin with disinfectant (70% ethanol in water or Betadine)
6) Incise skin and dissect free a subcutaneous tissue pocket.
7) Insert pump into pocket.
8) Close with autoclip skin clips.

9) Allow recovery in warm box.

2.11. In-vitro studies

2.11.1. HMVEC-L Cell Passage

Materials

Reagents	Manufacturer	Cat number
EBM-2 MV BulletKit (CC-3156 & CC-4147)	Lonza	CC-3202
Trypsin-EDTA 0.05% (1x)	Gibco	25300-054
Table 22. Reagents for *in vitro* experiments		

Protocol

1) Make up Endothelial cell growth basal medium 2 (EBM-2) using EBM-2 BulletKit in accordance with manufactures' instructions.
2) Retrieve flask from incubator.
3) Aspirate off medium from flask and discard.
4) Wash cells with pre-warmed (37^{o}C) PBS (10 mL) and discard. Repeat & discard wash.
5) Add 5 ml pre-warmed Trypsin/EDTA to old flask.
6) Incubate at 37^{o}C for 3 mins and agitate flask to suspend cells.
7) Add 5 ml EBM-2 medium to flask (making 10 ml).
8) Transfer 10 ml cell suspension to falcon.
9) Spin 300g for 5 min.
10) Pour off supernatant from cell pellet.
11) Flick resuspend cells.
12) Add 1 ml EBM-2 medium and repeat resuspend cells.
13) Cell count (number of cells in 25 squares is X x10^4 per ml concentration).
14) Add 30 ml EBM-2 medium and split into 2 flasks.

2.11.2. Cell treatments

Equipment	**Manufacturer**	**Cat Number**
96-well flat bottom white plate (no lid)	Costar	3912
96-well flat bottom transparent plate + low evaporation lid	Costar	3595
Tecan Infinite M1000 plate reader	Tecan	
Reagents	**Manufacturer**	**Cat Number**
Caspase-Glo® 3/7 Assay	Promega Corporation	G8091
Human IL-1β (1 µg)	Miltenyi Biotec	130-093-895
Human IL-6 (25 µg)	Miltenyi Biotec	130-093-929
Human IL-10 (25 µg)	Miltenyi Biotec	130-093-948
Human TNF-alpha	Miltenyi Biotec	130-094-017
Staurosporine from Streptomyces sp.	Sigma-Aldrich	S5921-.1MG
DiOC6 (3) dye 100 mg	Thermo Fisher Scientific	D273
Dimethyl sulphoxide (DMSO)	Sigma-Aldrich	D8418-250ML
L-Tryptophan	Sigma-Aldrich	T0254-1G
L-Kynurenine	Sigma-Aldrich	K8625-25MG
IL-1 Receptor antagonist human	Sigma-Aldrich	SRP3327
Kynurenic acid	Sigma-Aldrich	K3375-1G
3-hydroxy-DL-kynurenine	Sigma-Aldrich	H1771-25MG
Xanthurenic acid	Sigma-Aldrich	D120804-1G
3-hydroxyanthranilic acid	Sigma-Aldrich	148776-250MG

Table 23. Cell treatments

2.11.3. Caspase 3/7 activity assay

Protocol

1) Seed HMVEC-L cells at 5 x 10^4 per well in a white flat-bottom 96-well plate.
2) Incubate 24 hrs at 37°C, 5% CO_2.
3) Aspirate and discard 20 µl supernatant from each well.
4) Add 20 µl of treatment mixture to designated well (DMSO 0.5% final concentration).
5) Gently mix contents of wells using plate shaker (at 150 rpm for 30 secs).
6) Incubate for 4 hours at 37°C, 5% CO_2.
7) Meanwhile, prepare the Caspase-Glo® reagent by adding Caspase-Glo® buffer to Caspase-Glo® substrate to make Caspase-Glo® reagent.
8) Remove 100 µl of supernatant from each well (store at -20 or -80 °C, as required)
9) Add 100 µl of Caspase-Glo® reagent to each well.
10) Gently mix contents of wells using plate shaker (at 150 rpm for 30 secs).
11) Incubate for 90 mins at 37°C, 5% CO_2.

12) Ensure plate reader (Tecan Infinite M1000) is switched on for >10 mins before use.
13) Transfer plate(s) to plate reader.
14) Read luminescence for each sample with the following settings: Attenuation OD1; Integration time 1000 ms.

2.12. Statistical analysis

2.12.1. Assessment of data variation

Conformity of data to the normal distribution was assessed by one-sample Kolmogorov-Smirnov with Lilliefors Significance Correction and Shapiro-Wilk tests. The Levene statistic was used to test homogeneity of variance between groups.

2.12.2. Statistical tests between groups

Two group data that were normally distributed were compared by unpaired *t*-test without assumption of equal variance (Welch), and non-parametric two-group data were compared by the Mann-Whitney U test. Multiple groups testing two categorical variables and a continuous variable were tested by two-way ANOVA. Multiple groups of normally distributed data were compared by ordinary one-way analysis of variance (ANOVA). Where significant, pairwise *post hoc* comparisons were performed by *post hoc* Tukey's multiple comparison tests if the data met the homogeneity of variance assumption, or by Games-Howell test where the data had unequal variances. Multiple groups of normally data that did not conform to the normal distribution were compared by Kruskal-Wallis one-way ANOVA test with *post hoc* pairwise comparisons made using the Dunn's approach. Comparison of survival curves was conducted with Log-rank (Mantel-Cox) test. All statistical tests were based on a two-sided α-value of 0.05, and *P* values ≤ 0.05 were considered statistically significant.

2.12.3. Power analyses

Power calculations were performed using G*Power (v3.1.9.4) software. A priori analysis was performed where suitable data were available, otherwise post hoc power calculations were performed. The following input parameters were routinely used: 2-tailed, α-error probability of 0.05, and power (1-β error probability) $\geq$ 0.9. Cohen's measures for the effect size d were determined with group means and standard deviations. Specific mention is given to power calculations in appropriate sections.

2.12.3. Statistical software packages

Data were analysed using IBM SPSS Statistics version 23.0 (IBM Corp., Armonk, NY, USA) and GraphPad Prism v7.0.

2.12.3. Statistical advice and resources

Statistical advice was taken from colleagues in the MRC Centre for Inflammation Research, University of Edinburgh, most helpfully my primary PhD supervisor. My main textbook was 'Statistics Explained: *Introductory Guide for Life Scientists*, 2nd Edition by Steve McKillop, Cambridge University Press [2012]. Online resources were also informative, in particular the helpful website authored by chartered statistician and retired biomedical academic, Dr MFW Festing <www.3rs-reduction.co.uk>.

3. RESULTS

3.1. Model optimization – Phase I – Telemetered AP recovery studies

3.1.1. Introduction

A rat model of biliary AP was first reported in 1980, describing the retrograde infusion of a bile acid, sodium taurocholate, into the distal biliopancreatic duct (12). More recently, this was modified as a mouse model (13) and has been adopted by other groups (14), including our own (106, 634). In this model, increasing concentrations of sodium taurocholate are associated with severity and multi-organ injury (134, 637). The reported infusion time employed by different groups is variable, and the preference of our lab was a 60-second infusion for severe injury studies, which others have used to good effect (134). Male mice alone were used. Although a limitation of this preliminary work, a mixture of *Kmo*^{wt} and *Kmo*^{null} mice were used (Table 21) as the preferred *Kmo*^{wt} litter stocks alone were insufficient. However, from previous work the *Kmo*^{null} mice were anticipated to be more resistant to lethality than *Kmo*^{wt} mice (634).

3.1.1.1. Initial choice of disease model protocol

The study of the resolution phase of an experimental severe inflammatory disease process, requires negotiating a fine balance between excessive lethality and too mild a disease model. The literature had reported a 95% survival rate at 7-days with 2% (wt/vol) sodium taurocholic acid (Na-TCA) (13), but at this concentration lung injury has been reported an being absent (638). Therefore, at the outset a dose higher than 2% was selected, whilst aiming to avoid the reported 60% lethality reported by one group using 5% sodium taurocholic acid (NaTCA) infusion (637). Additionally, we had chosen to use implantable radiotelemetry devices to study the physiological and sickness behaviour over the 7-day recovery interval, for scientific and welfare purposes, as agreed with veterinary colleagues. The extent to which a surgically implanted telemetry device (extended anaesthesia time and tissue injury) would contribute to sickness behaviour was unknown. We chose to use the cardiometabolic G2 HR telemeters (Starr Life Sciences) at the outset, as these measured core body temperature, locomotor activity and heart rate; all physiological parameters which alter with systemic inflammation.

The cardiometabolic telemeter implantation had to be implanted at the same time as the intraductal infusion because it would not be technically feasible to access the pancreas at subsequent laparotomy due to the size of the device, the chest leads which reduce mobility, and risk of bowel injury at re-laparotomy. The starting point for studying the early resolution phase of AP-associated multi-organ injury was therefore 100 µl 3% Na-TCA infused over 60-seconds, in conjunction with telemeter implantation.

3.1.1.2. Requirement to amend protocol

The high lethality encountered at the outset forced a revision to the protocol after consultation with veterinary colleagues due to Home Office restriction and ethical considerations. A stepwise logical approach was employed, testing key modifiable variables.

3.1.2. Aim

To determine a suitable protocol for studying the recovery of experimental AP for use with telemetry monitoring.

3.1.3. Results

With the use of **Protocol 1** [3% NaTCA, 100 µl, over 60s], 7 of 9 mice died (see **Figure 21**), leaving only two mice to survive the 7-day experimental period. This was a far higher lethality than anticipated, and after discussions with veterinary colleagues, the lethality of the model was investigated by trying to separate the surgery from the bile acid, by omitting the latter. Thus, **Protocol 2** consisted of the same volume and flow rate of infusate as in Protocol 1 (100 µl, over 60s), but using only PBS alone. There was no modification besides the omission of NaTCA. All six available mice survived 7 days (Figure 21). Therefore, it was concluded that it was not the surgical insult (i.e. tissue injury, anaesthesia and telemeter implantation) *per se* which was the cause of the lethality observed in Protocol 1, and that the lethality could be reduced by altering the infusate.

There were seemingly 3 modifiable components to the model with which may be responsible for severity: i) concentration of the chosen bile acid; ii) volume of infusate; iii) flow rate. The reason to consider more than just the bile concentration was that other research groups used far slower flow rates, and no other group reported faster infusion rates. I chose to modify the concentration as an initial variable, as the literature supports correlation of lethality with concentration. For **Protocol 3**, it was agreed with veterinary colleagues to use 1% NaTCA initially, using a concentration of bile acid that was lower than used in the literature to induce AP (2% is minimum), but keeping the infusate volume and flow rate consistent (100 µl, 60s). The first two mice tested with Protocol 3 died by ~30-hrs. It was concluded that the lethality might be modified by lessening the infusate volume or flow rate. As available animals and research time were increasingly limited, both the infusate volume and the flow rate were reduced, as other investigators had suggested that the ductal infusate dynamics may cause severe damage and rupture of the pancreatic ductal system which is of considerable importance in disease recovery studies. Specifically, Perides *et al.* state: "*We avoid flow rate higher than 10µl/min to avoid artifacts and injury due to rapid increase in intrapancreatic*

pressure" [Perides et al., Retrograde infusion of bile acids into the pancreatic duct to induce pancreatitis in rats and mice. *Pancreapedia: Exocrine Pancreas Knowledge Base*, DOI: 10.3998/panc.2011.8]. Furthermore, since lethality observed in Protocols 1-3 occurred ≤72-hrs, the next protocol was limited to 72-hr duration for expediency.

For **Protocol 4**, the same bile acid concentration as in Protocol 3 (1% TCA) was used but the infusate volume was halved, to 50 µl [used by other groups (13)], and the flow rate reduced by a factor of ten (over 5 mins = 300s; rate 0.167 µl/s). As both subjects survived, it was concluded that infusate volume and rate were preferable. However, as 1% NaTCA is not a concentration used by other groups to induce AP, a returned was made to the highest concentration used previously (3% NaTCA), but with the reduced infusion volume and flow rate. With **Protocol 5** (3% NaTCA, 50 µl, 300s) only 1 of 6 mice survived the 7-days. As with Protocol 1, this was an unworkable for recovery studies and therefore the concentration of NaTCA was reduced in **Protocol 6** (2% NaTCA, 50 µl, 300s) where the first two mice survived. As others had reported minimal lung injury with 2% model, I next tested the dose of 2.5%. With hindsight, lung injury with Protocol 6 could perhaps have been tested at this juncture, but as there was no consensus on how best to measure lung injury and efforts were focused on reaching a final infusion protocol as soon as possible, the lung assay option was overlooked. With **Protocol 7** (2.5% NaTCA, 50 µl, 300s) both subjects reached humane endpoints.

One supervisor suggested that sterile filtering the infusate may be give more consistent results by increasing the homogeneity of the infusate solution. Thus, **Protocol 8** (2.5% NaTCA, filtered, 50 µl, 300s) was tested, but still resulted in >50% 7-day lethality (n = 4 of 6 failed to survive 7-day). At this juncture, a pragmatic decision was taken to select the final choice of 2.0% NaTCA (37 mM), with sterile filtered, 50 µl infusion over 300s, (**Protocol 9**) for all of the AP studies. Survival results from the first experiment using Protocol 9 are included in **Table 24**. Further detail is Appendix 5, Table 66 (section 6.5). Survival curves of all protocol permutations are illustrated in **Figure 21**.

Protocol	Telemeter	[TCA] (wt./vol.)	Infusate vol.	Infusion rate	Mice available	Sterile filter used	Deaths (exp length)
P1	G2 HR	3.0 % (56 mM)	100 µl	100 µl/ min	9 (WT n=2, KMO n=7)	No	7 of 9 (168h)
P2	G2 HR	0% (0 mM)	100 µl	100 µl/ min	6 (WT n=3, KMO n=3)	No	0 of 6 (168h)
P3	G2 HR	1.0 % (19mM)	100 µl	100 µl/ min	2 (WT n=1, KMO n=1)	No	2 of 2 (168h)
P4	G2 HR	1.0 % (19mM)	50 µl	10 µl/ min	2 (WT n=2)	No	0 of 2 (72h)
P5	G2 HR	3.0 % (56 mM)	50 µl	10 µl/ min	6 (WT n=5, KMO n=1)	No	5 of 6 (168h)
P6	G2 HR	2.0 % (37mM)	50 µl	10 µl/ min	2 (WT n=2)	No	0 of 2 (168h)
P7	G2 HR	2.5 % (47mM)	50 µl	10 µl/ min	2 (WT n=2)	No	2 of 2 (168h)
P8	G2 HR	2.5 % (47mM)	50 µl	10 µl/ min	6 (WT n=5, KMO n=1)	Yes	4 of 6 (168h)
P9 - Final	G2 HR	2.0 % (37mM)	50 µl	10 µl/ min	6 (WT n=6)	Yes	5 of 6 (168h)

Table 24. Model optimization for telemetered AP 7-day recovery studies

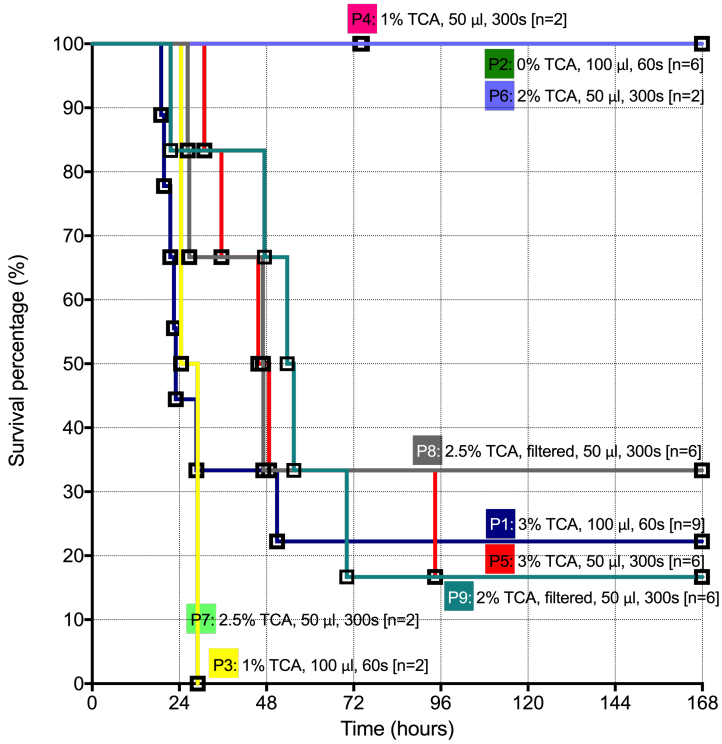

Figure 21. Infusion protocols towards optimization of telemetered AP model for recovery

P1: 3%TCA/PBS (56 mM) 100 µl over 60s, 7d;

P2: 0%TCA/PBS (0 mM) 100 µl, 60s, 7d;

P3: 1%TCA/PBS (19 mM) 100 µl, 60s, 7d;

P4: 1%TCA/PBS (19 mM) 50 µl, 300s, 3d;

P5: 3%TCA/PBS (56 mM) 50 µl, 300s, 7d;

P6: 2%TCA/PBS (37 mM), 50 µl, 300s, 7d;

P7: 2.5%TCA/PBS (47 mM), 50 µl over 300s, 7d;

P8: 2.5%TCA/PBS (47 mM), Filtered, 50 µl, 300s, 7d;

P9: 2.0% TCA/PBS (37 mM), Filtered, 50 µl, 300s, 7d: The final protocol taken forward for studies.

3.1.4. Conclusions

A final retrograde infusion of Na-TCA protocol was reached for use with telemetry, to study experimental AP and recovery over 7-days. The pancreatic injury and markers of the systemic inflammatory response at 24-hrs from this protocol are examined in section 3.6.

3.2. Experiment 1 – KMO deletion improves AP recovery

3.2.1. Animal welfare considerations

I defined critical illness humane endpoints in consultation with University of Edinburgh Named Veterinary Surgeons (NVS), as recognised by the UK Home Office. The humane endpoints indicating imminent death were: Unresponsiveness, severe laboured breathing and sustained profound hypothermia. All mice were given weight-adjusted pre-emptive analgesia under anaesthesia with buprenorphine subcutaneously, as well as two ealy post-operative doses (6-8 hrs and 20-24 hrs post-operatively). Daily oral post-operatively buprenorphine in jelly cubes was provided and consumption recorded.

Additional subcutaneous analgesia was administered if there were cage-side clinical signs that would trigger analgesia as recorded on the clinical score sheet Appendix 4 (section 6.4). In the absence of a humane endpoint being reached, any of the following signs observed during daily cage-side checks triggered a subcutaneous weight-adjusted dose of analgesia: 'Hunched posture', 'not inquisitive or alert', 'not eating or drinking', 'abdominal writhing'. See methods section (2.2.) for further detail.

3.2.2. Hypothesis

Absent 3HK, by KMO deletion (*Kmo*^{null}), is protective against multi-organ injury in a 7-day recovery AP model (with cardiometabolic telemeter) compared to wildtype.

3.2.3. Methods considerations

To measure the critical illness response to AP in mice and to monitor the recovery from systemic inflammation, we compared heart rate, temperature and locomotor activity between *Kmo*^{null} mice with AP and *Kmo*^{wt} mice with AP. Additional sham-operated control *Kmo*^{wt} mice underwent laparotomy and telemeter implantation, but without AP induction. Block randomisation was performed to ensure equal utilisation of specific telemeters between the three experimental groups to control for any variation in telemeter performance efficiency. This was done by random number generation in a spreadsheet (Excel by Microsoft) and sorting order by number order.

3.2.4. Results

3.2.4.1. Overview

The mean age, weight and length of anaesthesia did not differ significantly between the three groups: *Kmo*^{wt} sham, *Kmo*^{wt} AP and *Kmo*^{null} AP (**Table 25**). The mean duration of the

Group	No. / Sex	Rx	Mean age ± SEM (d)	Mean weight ± SEM (g)	Mean anaesthetic time ± SEM (min)
KMO^{wt}	6 / Male	Sham	143 ± 3.48	30.46 ± 0.70	46.2 ± 1.6
KMO^{wt}	6 / Male	AP	143 ± 0.73	28.86 ± 0.29	45.5 ± 2.0
KMO^{null}	6 / Male	AP	143 ± 2.03	30.46 ± 1.08	46.0 ± 1.1
1-way ANOVA			***p = 1.0, ns***	***p = 0.26, ns***	***p = 0.95, ns***

Table 25. Study subjects for experiment 1
SEM = Standard error of mean. ns = not significant.

experiment was significantly shorter (p = 0.01, KW 1-W ANOVA) in *Kmo^{wt}* AP group (69.4-hrs) compared to *Kmo^{wt}* Sham (168-hrs) and *Kmo^{null}* AP (147.5-hrs), since 5 of 6 *Kmo^{wt}* AP mice reached humane endpoints during the experiment.

3.2.3.2. Analgesia consumption

Whilst the mean subcutaneous buprenorphine dosing was equivalent between experimental groups (p = 0.179, KW 1-W ANOVA), the time-adjusted dosing was significantly higher (p = 0.008, KW 1-W ANOVA) in the *Kmo^{wt}* AP mice (0.111 μg/hr) due to the shortened experimental period and the peri-operative dosing given at the start of the experiment (**Table 26**). The mean oral buprenorphine dose consumed was significantly higher (p = 0.006, KW 1-W ANOVA) in the *Kmo^{wt}* Sham group (70 μg), which can be explained by an improved voluntary oral intake compared to AP mice, as well as longer survival (with daily oral analgesia supply). Therefore, because overall AP mice had reduced experimental times, there was no significant differences (p = 0.345, KW 1-W ANOVA) with time-adjusted oral buprenorphine consumption.

Mouse Line	Treatment	Number	Exp duration – mean (SD)	S/C Bup. Dose – mean (SD)	S/C Bup. Dose : Time adjusted – mean (SD)	Oral Bup. Dose – mean (SD)	Oral Bup. Dose : Time adjusted – mean (SD)
Kmo^{wt}	AP	N = 6	69.4 (50.9) hrs	5.500 (1.225) μg	0.111 (0.055) μg/hr	26.333 μg (23.51)	0.330 (0.181) μg/hr
Kmo^{wt}	Sham	N = 6	168.0 (0) hrs	4.500 (0.000) μg	0.027 (0.000) μg/hr	70.000 μg (00.00)	0.417 (0.000) μg/hr
Kmo^{null}	AP	N = 6	147.5 (50.2) hrs	4.625 (0.737) μg	0.044 (0.044) μg/hr	45.000 μg (35.07)	0.268 (0.209) μg/hr
1-way ANOVA between 3 groups			****p = 0.010, KW**	**ns p = 0.179, KW**	****p = 0.008, KW**	****p = 0.006, KW**	**ns p = 0.345, KW**

Table 26. Analgesia given during AP experiment 1
Columns: 'Exp duration – mean (SD)' denotes the mean number of hrs of experimented mice in the cohort with standard deviation (SD), with a maximum of 168-hrs. 'S/C Bup. Dose / group' denotes mean total dosing of subcutaneous buprenorphine of cohort. 'S/C Bup. Dose : Time adjusted' denotes the group's mean total dose per mouse divided by number of experimental hours for each mouse. 'Oral Bup. Dose – mean' denotes the group's mean total oral buprenorphine dose. 'Oral Bup. Dose : Time adjusted – mean' denotes the group's mean total oral dose per mouse divided by the number of experimental hours of each mouse. Oral buprenorphine single dose 0.01 mg. S/C buprenorphine single dose 0.05 mg/kg. KW: Kruskal-Wallis. ns = not significant; *p < 0.05; **p < 0.01.

3.2.3.3. Telemetry and humane endpoints

The telemetry data are shown in **Figures 22A** to **22D**. Sham-operated control *Kmo*^{wt} mice (n = 6) showed a disturbance in locomotor activity, including post-anaesthesia hyperactivity, in the first 24-hr period that reverted to a normal physiological crepuscular pattern by day 3 after surgery, with increased activity at the start of the dark phase (Figure 22B: dark phase depicted by vertical grey panels on timeline). Sham-operated *Kmo*^{wt} mice showed a much lesser degree of autonomic dysfunction by maintaining a stable oscillating core body temperature without significant hypothermic episodes (Figures 22A).

Kmo^{wt} mice with AP (n = 6) had repression of locomotor activity in the first 24-hrs similar to *Kmo*^{null} mice with AP (Figure 22D), but unlike *Kmo*^{null} mice, failed to recover over the subsequent 6 days due to significant hypothermia and reaching humane endpoints (Figure 22A). Five of the six *Kmo*^{wt} AP deteriorated with to critical illness and reached predefined humane endpoints requiring humane cull within the first 72-hrs. Specific signs in these mice were profound hypothermia (n = 5) and one of these additionally had severe labored breathing.

Critically ill mice heart had abnormal heart rates which were either profoundly bradycardic in 4 mice, with a mean heart rate of 217 b.p.m. (SEM 20 b.p.m) at the last data reading before cull, or conversely severely tachycardic (757 b.p.m.) in 1 mouse which exhibited severe labored breathing (Figure 22C). Telemetered *Kmo*^{null} mice with AP (n = 6) showed an initial reduction in locomotor activity equivalent to that observed in *Kmo*^{wt} mice with AP during the first 24-hrs (Figure 22D), which strengthened over the subsequent recovery period (Figure 22B). Furthermore, survival was significantly better in *Kmo*^{null} mice, with only 1 of 6 *Kmo*^{null} mice reaching a predefined humane endpoint throughout the 7-day experimental period. Specifically, this mouse had profound hypothermia (23.5^{o}C) and minimal response to gentle stimulation as humane endpoints.

3.2.3.4. Blood biochemistry & cytokines in humane endpoint mice confirmed multi-organ injury

In those mice which reached humane endpoints, blood sampling was performed at humane cull to confirm multiple organ failure and tissue injury, and results were compared with samples from *Kmo*^{wt} sham mice (samples taken at day 7). Specifically, alanine transaminase (ALT) indicating hepatocyte injury, lactate dehydrogenase (LDH) indicating diverse cellular injury, elevated urea indicating renal dysfunction, and a reduction in plasma albumin levels were measured and results were compatible with an acute phase response and vascular leakage (**Figure 23**).

Four of the 5 *Kmo*^{wt} AP mice which reached humane endpoints had sufficient plasma for cytokine assay in addition to biochemical assay. MSD V-Plex mouse assay confirmed elev-

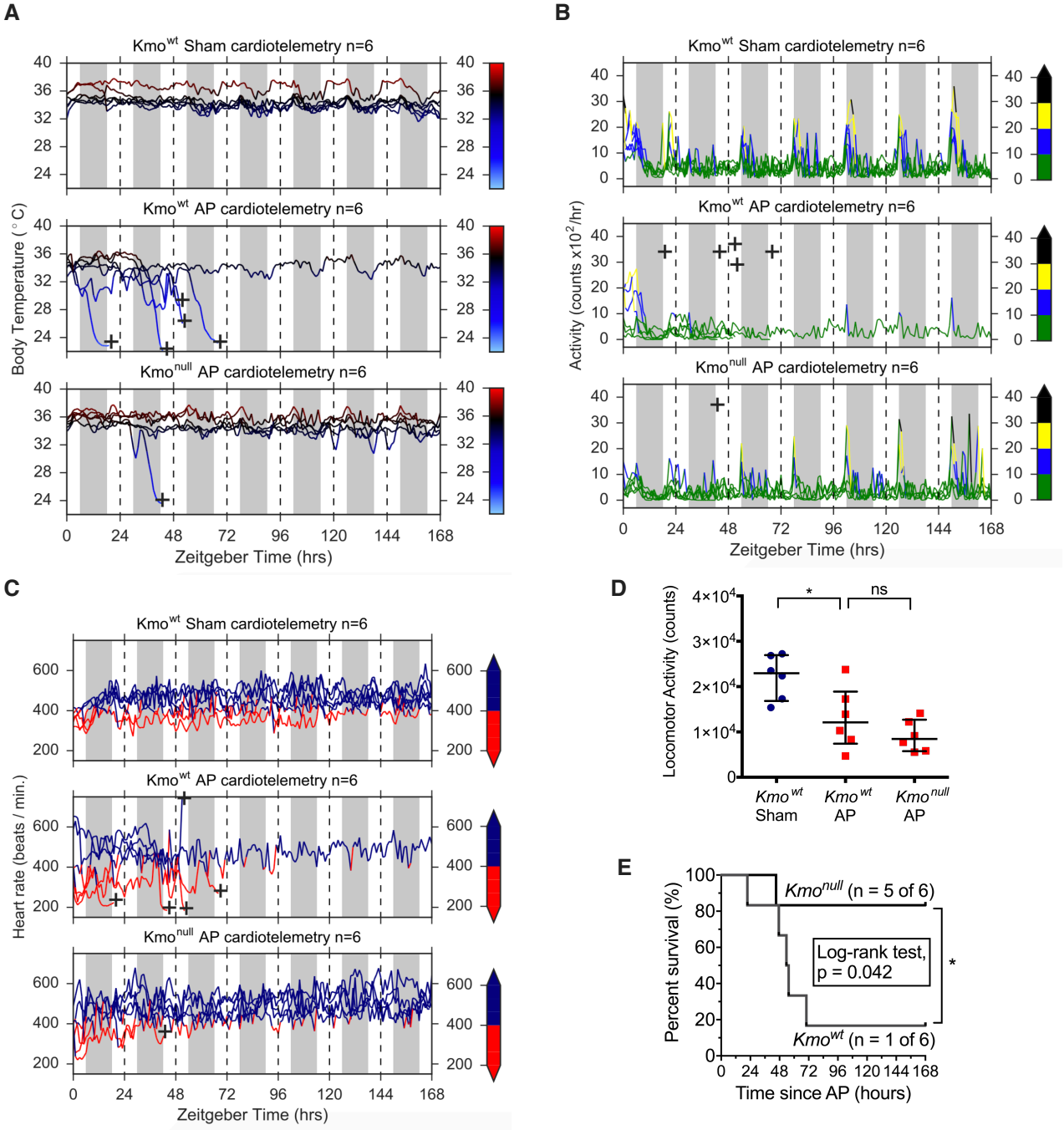

Figure 22. Experimental AP in telemetry-monitored mice can cause profound sickness behaviour but is ameliorated by *Kmo* deletion

Experimental 7-day recovery studies. *Kmo*^{wt} mice were randomized to sham operation (n = 6) or AP (n = 6). *Kmo*^{null} mice (n = 6) underwent AP alone. '**+**' symbol indicates the time when a mouse reached humane endpoint(s) and were culled under terminal anaesthesia. Humane endpoints were persistent hypothermia < 26°C, minimal response or severe labored breathing. Plots show 7-day AP survival curve (E), hourly mean core body temperature (A), heart rate (C) and locomotor activity (B) over 168-hrs. Vertical dark panels are the 12-hr dark phase intervals, with light phase in between. Telemetry recording started half-way through the light phase (Zeitgeber 0-hr) on the day of surgery (< 2hrs after recovery from anaesthesia for AP induction or sham laparotomy). Here *Kmo*^{wt} mice with AP had poor recovery, with 5 of 6 mice reaching humane endpoint(s). **A**: Temperature; **B**: Locomotor activity; **C**: Heart rate; **D**: Locomotor activity over 0-24-hrs; **E**: Survival. Profound sustained hypothermia (**A**), suppressed locomotor activity (**B**) and bradycardia (**C**) was more frequently observed in *Kmo*^{wt} as compared to *Kmo*^{null} mice with AP. Critical illness was most frequently observed on days 2 and 3 after AP induction in this telemetered model. Statistical tests were 1way-ANOVA *post-hoc* Tukey's (D) and log rank (E). ns = not significant ($p > 0.05$), *$p < 0.05$.

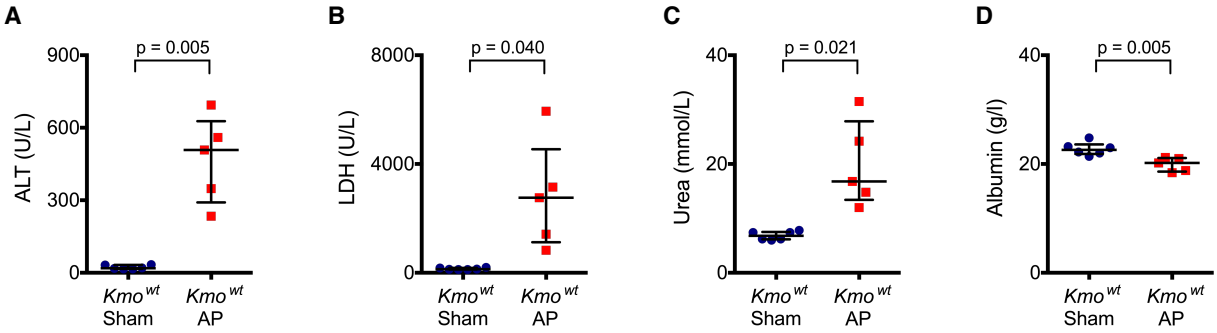

Figure 23. Biochemical analysis – experiment 1

A: alanine aminotransferase (ALT); B: Lactate dehydrogenase (LDH); C: Urea; D: Albumin. Statistical tests are depicted by p-values for *t*-tests. Primary data are recorded in Table 69, Appendix 6.6.

-ated concentrations of the pro-inflammatory cytokines interleukin 1β (IL-1β), interleukin 6 (IL-6) and tumour necrosis factor α (TNFα), compared to sham controls (**Figure 23**).

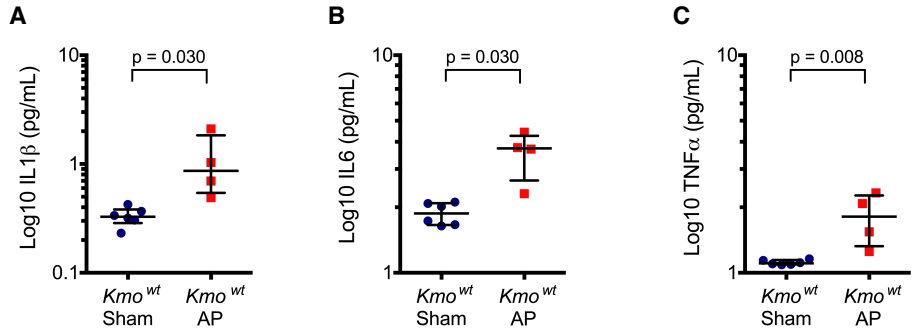

Figure 24. Plasma cytokines - experiment 1

A: Interleukin 1β (IL-1β); B: Interleukin 6 (IL-6); C: tumour necrosis factor α (TNFα).
Statistical tests are depicted by p-values for *t*-tests. Primary data are recorded in Table 70, Appendix 6.6.

3.2.3.5. Limitations

An alternative method when comparing blood results from critically ill mice with sham controls is to cull the paired mice that were randomised to sham and the disease model at the same timepoint (639). Whilst there are merits in such an approach by giving equal sampling timepoints, the main disadvantage in a telemetered study such as this is the lost opportunity to collect telemetry data-stream from controls.

3.2.4. Conclusions

Together, these data extend the concept that global *Kmo* gene blockade protects against AP-MODS, by demonstrating an impact on sickness behaviours as well as end organ dysfunction and demonstrating that the protection against AP-MODS in *Kmo*^{null} mice with AP persists for up to 7-days.

3.3. Experiment 2 – Hepatocyte-restricted *Kmo* knockout increases plasma 3HK

3.3.1. Background

Prior to joining the Mole lab in 2014, a novel mouse line was created by Dr. Xiaozhong Zheng (Senior Technical Assistant, Mole Group, University of Edinburgh) in 2013, in which *Kmo* gene deletion was conditional upon Cre recombinase, which restricted to cells with the *serum albumin (alb)* gene promotor (using cre-loxP technology), which is robustly hepatocyte-specific and highly efficient by adulthood (640, 641). Specifically, the $Kmo^{tm1c(KOMPWtsi/flox(ex5)}$ mouse strain which has loxP sites flanking exon 5 of the *Kmo* gene was crossed with a mouse strain that expresses *Cre* recombinase under the control of the promoter of the *Alb* gene (which encodes the protein serum albumin), B6.Cg-Tg (*Alb*-Cre) 21Mgn/J, which expresses Cre recombinase exclusively in hepatocytes. Offspring were further backcrossed for at least 6 generations to generate homozygous $Kmo^{FRT\text{-}deleted/alb\text{-}cre}$ mice (hereafter referred to as $Kmo^{alb\text{-}cre}$ mice). I undertook biochemical characterization of this novel mouse line by LC-MS/MS and confirmed genetic alteration by RT-qPCR. After conducting initial pancreatitis studies with this mouse line, and finding a disease phenotype (section 3.5, experiment 3), I undertook the tracer experiment to better understand this intriguing biochemical phenotype. After finishing work in the lab, Dr. Zheng extracted RNA from my frozen tissue samples which were sent to a commercial biotech RNA sequencing company (Novogene Limited, Hong Kong). The RNA sequencing data was generated and analysed by others in the research group, principally Miss Lucile Neyton and Professor Mole.

3.3.2. Hypotheses

1) *Kmo* gene deletion restricted to hepatocytes ($Kmo^{alb\text{-}cre}$) would show reduced expression of *Kmo* RNA in the liver compared to wildtype (Kmo^{wt}), but no difference in expression in kidney or spleen compared to Kmo^{wt}.
2) *Kmo* gene deletion restricted to hepatocytes ($Kmo^{alb\text{-}cre}$) would alter blood kynurenine biochemistry in a pattern similar with global Kmo deletion.
3) No difference between clearance of tracer 3HK ($^{13}C_6$-3HK) between mouse lines.
4) In light of the finding of elevated 3HK in $Kmo^{alb\text{-}cre}$ mice, this biochemical phenotype was anticipated to alter inflammatory gene regulation.

3.3.3. *Kmo* gene tissue expression – Hypothesis 1

I confirmed tissue specific loss in *Kmo* gene expression in $Kmo^{alb\text{-}cre}$ mice based on mRNA levels in liver, kidney and spleen. Data are tabulated in Tables 71 to 75 (Appendix 7) and displayed in **Figure 25** with 1-way ANOVA with *post-hoc* Tukey's tests.

Sample size and power calculations were assessed *post-hoc* from mean values and standard deviations using liver *Kmo* gene expression values [Log10(2^-ddCT)] between Kmo^{null} (mean = 2e-10 expression fold, SD = 0.776) and $Kmo^{alb\text{-}cre}$ (mean = 1.332 expression fold; SD = 0.157), giving an effect size d = 2.38 and power 0.96.

Figure 25. Gene expression of a novel hepatocyte-restricted *Kmo* knockout mouse line ($Kmo^{alb\text{-}cre}$)

RT-PCR tissue expression of *Kmo* gene in liver, kidney and spleen of wildtype (Kmo^{wt}), *Kmo* deleted (Kmo^{null}) and hepatocyte-restricted *Kmo* knockout ($Kmo^{alb\text{-}cre}$) mice (n = 5 per group). $Kmo^{alb\text{-}cre}$ mice have reduced *Kmo* in expression in whole liver tissue as compared to wildtype. Bars are mean ± s.e.m. Statistical tests shown are 1-way ANOVA with *post-hoc* Tukey's tests. Data are tabulated in Appendix 7.

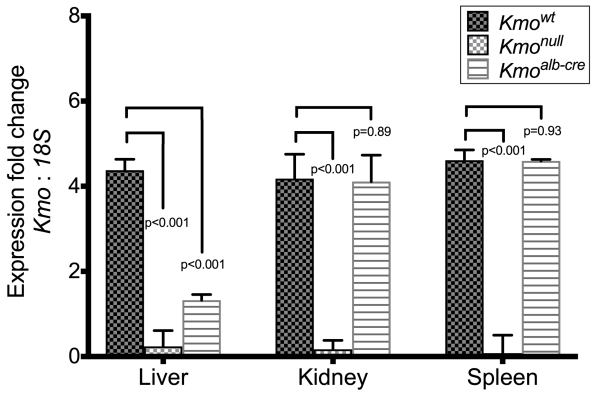

3.3.4. Kynurenine metabolites in three mouse lines – Hypothesis 2

Next, I compared steady-state kynurenine pathway metabolites of Kmo^{wt}, Kmo^{null} and $Kmo^{alb\text{-}cre}$ healthy mice (n = 6 male mice per group) by measuring upstream and downstream metabolite levels in plasma by liquid chromatography-tandem mass spectrometry using six adult male mice (**Figure 26**).

Effect and sample size were used to calculate power *post-hoc* from mean values and standard deviations using concentrations of kynurenine, the substrate of KMO enzyme, between Kmo^{null} (mean = 61.4 μM, SD = 20.3 μM) and $Kmo^{alb\text{-}cre}$ (mean = 24.8 μM; SD = 6.6 μM), giving an effect size d = 2.42 and the power 0.96.

Kmo^{wt}, Kmo^{null}, and $Kmo^{alb\text{-}cre}$ mice had equivalent (p = 0.075, one-way ANOVA) plasma [tryptophan] concentrations ~100 μM (Figure 26A). Kmo^{null} mice had a 21-fold (median 60.9 μM vs 2.8 μM, p = 0.002, Mann Whitney test) and $Kmo^{alb\text{-}cre}$ an 8-fold (median 23.4 μM vs 2.8 μM p = 0.002, Mann Whitney test) increase in plasma kynurenine at steady-state compared to Kmo^{wt} (Figure 26B). Kmo^{null} mice had an 18-fold (median 3.7 μM vs 0.2 μM, p = 0.001, *t*-test) increase in plasma anthranilic acid compared to Kmo^{wt}, and $Kmo^{alb\text{-}cre}$ had a 14-fold (median

2.7 µM *vs* 0.2 µM, p < 0.001, *t*-test) increase (Figure 26C). Plasma kynurenic acid was extremely elevated in *Kmo*^{null} mice had a 119-fold excess (median 13.9 µM *vs* 0.1 µM, p = 0.002, Mann Whitney test) and *Kmo*$^{alb\text{-}cre}$ a 51-fold increase (5.9 µM *vs* 0.1 µM, p = 0.002, Mann Whitney test) compared to *Kmo*^{wt} (Figure 26D).

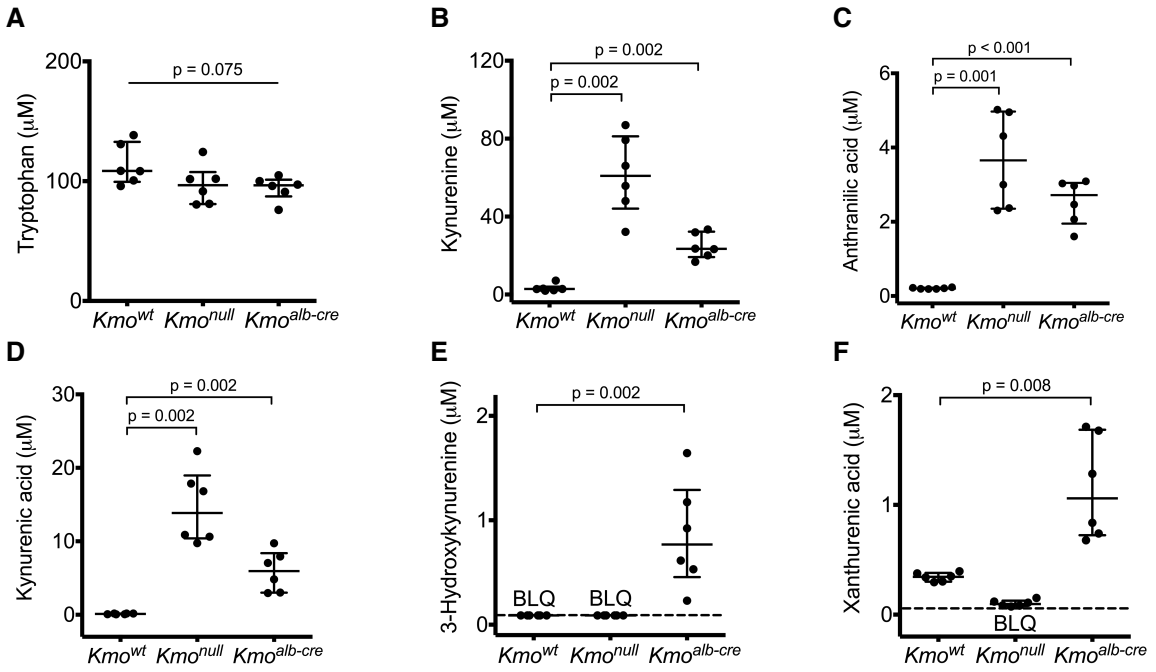

Figure 26: Biochemical characterization of the hepatocyte-restricted *Kmo* knockout mouse line (Kmo$^{alb\text{-}cre}$)
Steadystate plasma concentrations of kynurenine pathway metabolites measured by LC-MS/MS for Kmo^{wt}, Kmo^{null} and Kmo$^{alb\text{-}cre}$ mouse lines (n = 6 per group). **A**: Tryptophan; **B**: Kynurenine; **C**: Anthranilic acid; **D**: Kynurenic acid; **E**: 3-Hydroxykynurenine, with all samples in Kmo^{wt} and Kmo^{null} below limit of quantification (BLQ; --- 0.089 µM); **F**: Xanthurenic acid, with 3 of 6 samples in Kmo^{null} group BLQ (--- 0.049 µM). Plots show individual data and horizontal lines are median with interquartile range. Statistical tests are depicted by p-values: Group analysis by 1-way ANOVA (A) and pairwise tests shown are Welch's *t*-tests (C and F) or Mann Whitney U tests (B, D and E), depending on data conformity to normal or parametric distributions, as determined by normality tests.

Levels of the KMO product, 3-hydroxykynurenine, were below limit of detection (0.089 µM) at steady-state in *Kmo*^{wt} and *Kmo*^{null} mice. Unexpectedly, *Kmo*$^{alb\text{-}cre}$ mice had high levels of 3-hydroxykynurenine, greater than 8-fold higher (median 0.769 µM vs 0.089 µM, p = 0.002, Mann Whitney test) than *Kmo*^{wt} levels (Figure 26E). 3-Hydroxykynurenine can also be metabolised by KAT enzymes (I-IV) to form xanthurenic acid. *Kmo*$^{alb\text{-}cre}$ mice have a 11-fold increase (median 1.060 µM vs 0.100 µM, p < 0.001, *t*-test) and *Kmo*^{wt} a 3-fold increase (0.35 µM vs 0.10 µM, p = 0.003, *t*-test) in xanthurenic acid compared to *Kmo*^{null} mice (Figure 26F).

3.3.5. Kynurenine tracer study

To determine whether elevated [3HK] was in proportion to the elevated kynurenine (due to extrahepatic KMO activity) or whether there were any additional alterations in 3-hydroxykynurenine metabolism in *Kmo*$^{alb\text{-}cre}$ mice, a tracer study was performed (**Figure 27**).

I conducted preliminary work (not shown) to determine workable concentrations of tracer compounds for use at 20 min timepoint. Following which, I intravenously injected a premixed weight-adjusted (50 µg/g body weight) bolus of deuterated tryptophan-indole-d_5 and $^{13}C_6$-3-hydroxykynurenine, and sampled cardiac blood 20 mins after injection and measured native and deuterated metabolites in plasma. Equivalent concentrations of d_5-tryptophan indicated that tail vein injections were technically efficient (Figure 27A). D4-kynurenine tracer levels (metabolised from injected d_5-tryptophan) (Figure 27C) were highest with complete *Kmo* deletion (*Kmo*^{null}) and lowest in wildtype (*Kmo*^{wt}), and followed a similar profile to steady state endogenous kynurenine (Figure 27B). However, and unexpectedly, I detected higher $^{13}C_6$-3-hydroxykynurenine tracer levels in *Kmo*$^{alb\text{-}cre}$ mice compared to *Kmo*^{null} (4-fold lower) and *Kmo*^{wt} (10-fold lower) mice (Figure 27B). The tracer metabolite $^{13}C_6$-xanthurenic acid was highest in *Kmo*^{null} mice and relatively reduced in *Kmo*$^{alb\text{-}cre}$ mice (Figure 27D).

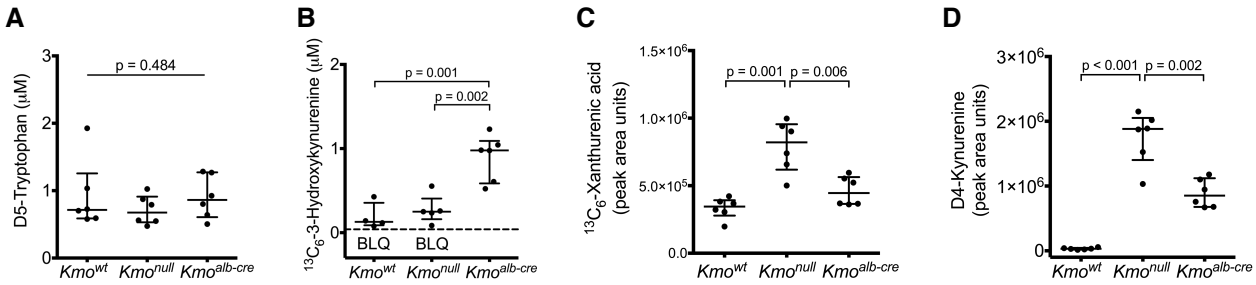

Figure 27: Kynurenine pathway metabolite tracer study

Plasma concentrations of tracer compounds and metabolites are shown 20 mins after weight-adjusted (50 µg/g) IV bolus containing deuterated tryptophan-indole-d5 (D5-TRP) and $^{13}C_6$-3-hydroxykynurenine ($^{13}C_6$-3HK). **A**: Comparable concentrations of D5-TRP indicates equivalent injection efficiency. **B**: $^{13}C_6$-3HK tracer levels were higher in *Kmo*$^{alb\text{-}cre}$ mice compared to *Kmo*^{null} (3.8-fold) and *Kmo*^{wt} (6.3-fold), reflecting reduced 3HK clearance in this line. For $^{13}C_6$-3HK, limit of detection was 0.0432 µM. **C**: In stark contrast to the low endogenous levels of pathway side-product Xanthurenic acid in *Kmo*^{null} mice, and high levels in *Kmo*$^{alb\text{-}cre}$ mice, the tracer metabolite $^{13}C_6$-Xanthurenic acid was highest in *Kmo*^{null} mice and relatively reduced in *Kmo*$^{alb\text{-}cre}$ mice. **D**: Tracer D5-Tryptophan was metabolised to D4-Kynurenine with highest levels in *Kmo*^{null} line. D4-Kynurenine levels were significantly lower in *Kmo*^{wt} ($p < 0.0001$, *t*-test) and in *Kmo*$^{alb\text{-}cre}$ ($p = 0.002$, *t*-test) when compared to *Kmo*^{null}. Individual data are shown and lines represent median values with interquartile range. Mice were adult males (n = 6 per group). Statistical tests are depicted by p-values: Group analysis by 1-way ANOVA (A) and pairwise tests shown are Welch's *t*-tests (B, C and D).

3.3.6. *Kmo*$^{alb\text{-}cre}$ versus *Kmo*^{null} transcriptomics

Given the intriguing biochemical phenotype of the three mouse strains with regards to circulating kynurenine metabolites, I was interested to know what effect altered chronic alterations in kynurenine pathway metabolism may have on peripheral tissues. The comparison between *Kmo*^{null} mice (with elevated kynurenine/KA but negligible 3HK) versus *Kmo*$^{alb\text{-}cre}$ (partial elevation of kynurenine/KA and very high 3HK levels) offers a particular tool to assess the biological effects of elevated 3HK concentrations. Computational RNA sequencing analysis revealed an array of significant ($p < 0.05$) transcriptional differences in liver tissue between *Kmo*$^{alb\text{-}cre}$ and *Kmo*^{null} mice at steady state (**Figure 28**). There was upregulation of TLR cascades, MyD88 cascade, NFkB induction, MAP kinase activation, TRAF6, cytokine signalling, interleukin signalling, cellular responses to stress, cellular responses to external stimuli, biological oxidations, RIP kinase. Transcriptomal upregulation of proinflammatory genes in *Kmo*$^{alb\text{-}cre}$ mice, which have elevated 3HK levels, suggest that these mice have a chronic proinflammatory state which may limit their capacity to adapt to insults (e.g. DAMPs/PAMPs) such as in AP.

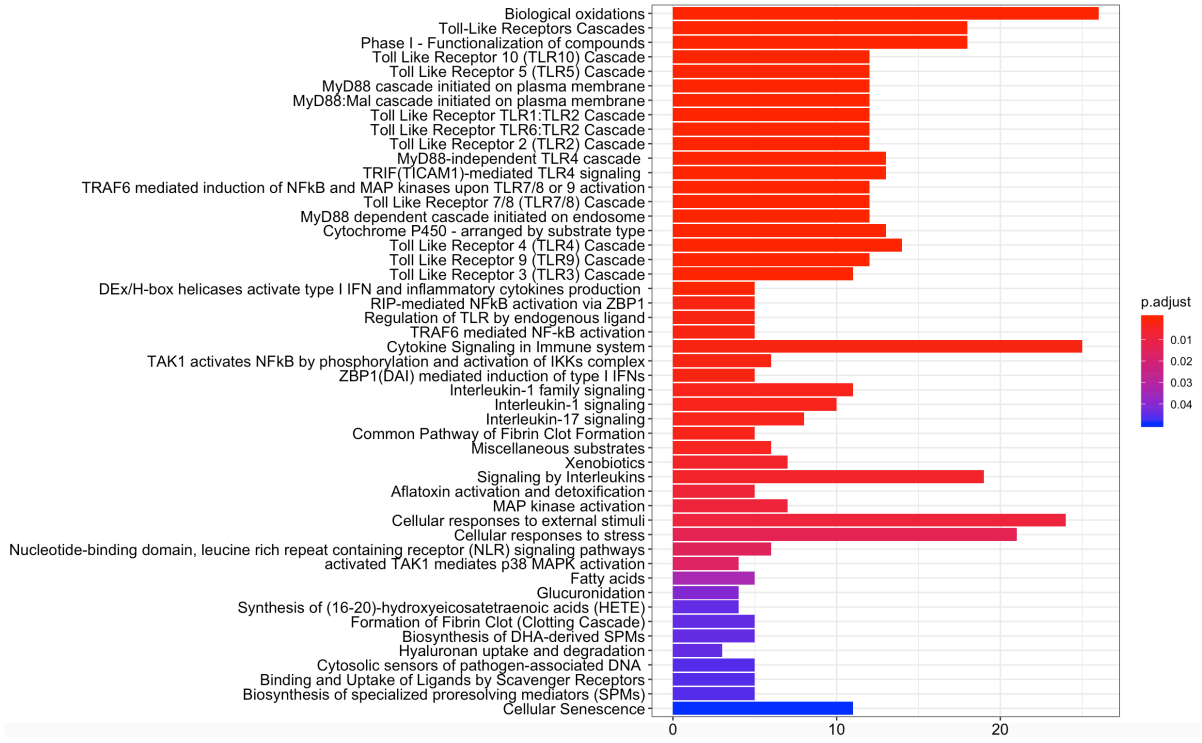

Figure 28. Barplot showing significant transcriptomic differences in liver tissue between *Kmo*$^{alb\text{-}cre}$ versus *Kmo*^{null}

Paired pathway analysis of differentially expressed genes in liver using a q-value threshold of 0.1 in Reactome software comparing *Kmo*$^{alb\text{-}cre}$ to *Kmo*^{null} (baseline).

3.3.7. Conclusions

I confirmed that *Kmo*$^{alb\text{-}cre}$ mice, with *Kmo* gene deletion restricted to hepatocytes using cre-loxP technology, had equivalent *Kmo* expression in spleen and kidney as *Kmo*^{wt} mice, but reduced expression in homogenised liver tissue. *Kmo* expression in livers from *Kmo*^{null} mice was lower than that in *Kmo*$^{alb\text{-}cre}$ mice, which was not surprising given the presence of non-hepatocyte cells within liver tissue which is the most likely explanation. Additionally, another plausible explanation is that the cre-loxP technology may lack 100% efficiency. However, this process is age-dependent with studies showing efficiency to be only 60% by 1 week, but it appears to be complete by 6 weeks (641), and all mice used in this work were adult. Analysis on a purified hepatocyte population was not performed since the equipment and protocols established for liver flow cytometry were designed to extract leukocytes from liver tissue.

Using LC-MS/MS, I detected an unanticipated elevation in plasma 3HK and XA levels. As this mouse line has elevated kynurenine and kynurenic acid concentrations (relative to Kmo^{wt}), which are potentially cytoprotective (as endogenous ligands of the AhR etc), this mouse line provides a useful tool alongside *Kmo*^{null} mice (which have very high levels of kynurenine and kynurenic acid), due to the stark contrast in circulating 3HK levels, whilst both having elevated kynurenine and kynureninc acid levels (relative to *Kmo*^{wt}). Lastly, *Kmo*$^{alb\text{-}cre}$ mice surprisingly had delayed clearance of trace 3HK ($^{13}C_6$-3HK), likely due to competition with amino acid transporter and metabolizing enzymes (KATs and kynureninase). Increased $^{13}C_6$-XA levels in Kmo^{null} likely represents uncompetitive metabolism by KATs due to the absence of endogenous 3HK in *Kmo*^{null}. These results suggest that Kmo$^{alb\text{-}cre}$ mice have such high circulating concentrations of endogenous 3HK that onward transport and metabolism are saturated. This suggests that further production of 3HK by pathway flux would quickly accumulate due to congested processes to eliminate 3HK, such as by onward catabolism or transport out of the compartment.

3.4. Model optimization – Phase II – Telemetered recovery studies

3.4.1. Background

The high lethality of *Kmo*^{wt} mice with the 2% Na-TCA (experiment 1) was a particular concern for both researchers and veterinary staff, for experimental and ethical reasons. The intention had been to experimentally compare mice at 7-days after AP using cardiometabolic telemeters in all recovery studies. However, repeated loss of study subjects during the experimental time interval would have a dramatic effect on the results, as those reaching humane endpoints would be the sickest. Furthermore, *Kmo*$^{alb\text{-}cre}$ mice with high circulating [3HK], would not be expected to have improved survival. Since the disease model could not be altered, and there was an option for a smaller telemeter device that could still record the two most reliable physiological parameters (core body temperature and locomotor activity), I proposed to switch the mini telemeter and therefore to provide some evidence supporting the hypothesis of a lesser systemic insult with a smaller implantable telemetry device.

3.4.2. Hypothesis

A smaller implantable device requiring less invasive surgery would cause a lesser insult, a finding shown by others previously (635), allowing a quicker return to baseline physiological parameters.

3.4.3. Results

Data shown are from *Kmo*^{wt} mice randomly allocated to sham laparotomy (with telemeter implantation), with n = 6 mini telemeters compared to n = 6 cardiotelemeter. Data listing the study subjects, weight loss and telemetry can be found in Appendix 8. **Figure 29** (below) shows earlier return to baseline physiological circadian profiles, with greater locomotor activity (29B) throughout the 7-day study period, and earlier return of circadian core body temperature profiling (29C). COSINOR analysis can be used to measure circadian oscillating rhythms by mathematically fitting a Cosine curve to the raw data (29D). The flatter core body profile observed in larger cardiometabolic telemeter (29C) was assessed by measuring daily COSINOR amplitude in all subjects. All amplitude measurements were significantly lower (60% reduction, $p < 0.001$, MWU) with the larger telemeters as compared to the mini pill telemeters (29D). The suppressed circadian body temperature was more marked initially, with associated impaired locomotor activity (Figures 29A and 29B), and return towards baseline physiological oscillations by days 3-4, with a significant ($p = 0.027$ *post hoc* Dunn's) reduction in temperature amplitude during days 1-2 with the larger cardiometabolic telemeter (29F).

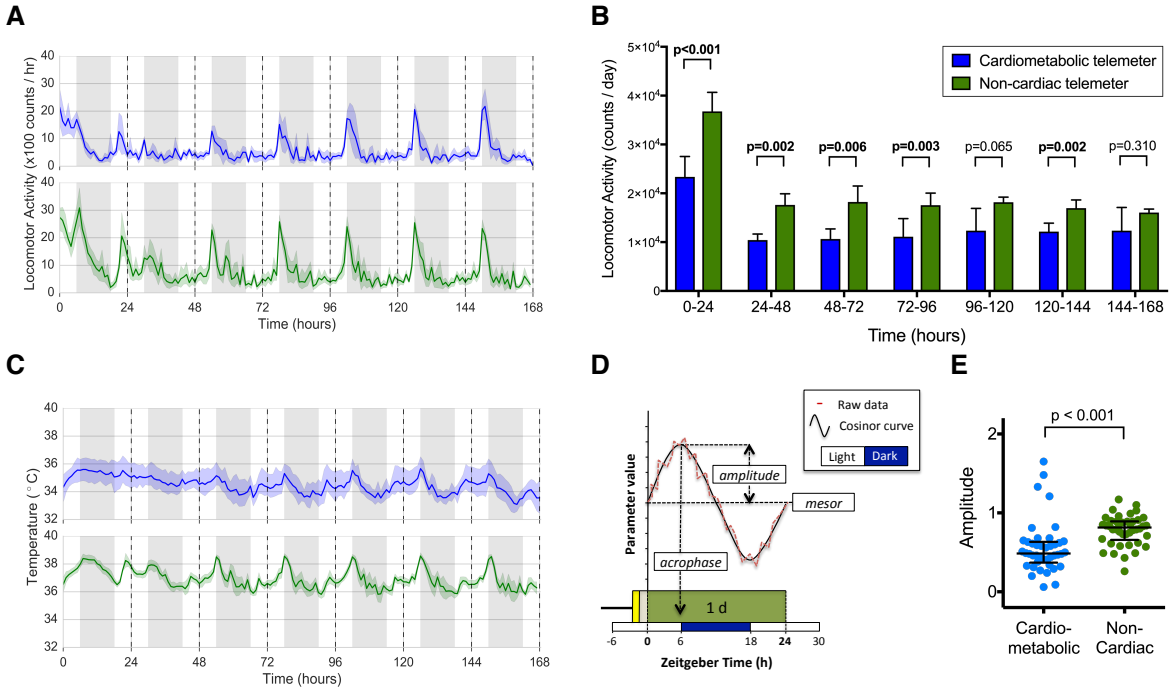

Figure 29. Physiological insult is reduced after non-cardiac telemeter implantation in *Kmo*^{wt} mice

Recovery from the less invasive non-cardiac telemeter (depicted by blue) is quicker than the larger G2 HR E-mitter cardiometabolic telemeter (depicted by green) in sham operated *Kmo*^{wt} mice. **A**: Rolling hourly mean locomotor activity (bold line) with 95% CI (shaded line) shows earlier plateau of normal circadian light-dark corpuscular locomotor activity of non-cardiac telemetered mice after 48-hrs (green) which is delayed in mice with larger cardiometabolic device (blue). **B**: Total daily activity levels are significantly higher in non-cardiac telemeter (green) as compared to mice with the larger device. Pairwise statistical analysis was performed by *t*-test, with significant differences marked in bold. **C**: Hourly mean core body temperatures are shown (bold line) with 95%CI (shaded line) showing higher mean core temperatures of more active mice with smaller non-cardiac telemeters, and reduced circadian light-dark oscillation of body temperature of mice in the first 48 hours after implantation of larger cardiometabolic telemeter. Cosinor analysis of circadian physiological behaviour comparing less invasive non-cardiac telemeter to cardiometabolic telemeter. **D**: Diagrammatic representation of cosinor analysis, with circadian parameters illustrated, including amplitude. **E**: Cosinor analysis revealed at 60% reduction in amplitude ($p < 0.001$, Mann Whitney U test) in circadian body temperature changes in cardiometabolic telemetered mice (median 0.484) compared to non-cardiac telemetered subjects throughout 7-days (median 0.815). **F**: The flattening of the body temperature amplitude which was significantly reduced in the first 2 days ($p = 0.0267$ *post* hoc Dunn's Kruskal Wallis test) resolved with time. Individual data are shown and horizontal lines are median with interquartile range.

3.4.4. Conclusions

The data confirm and help quantify the greater systemic insult to the mice with the larger telemeter device, supporting the decision to switch to the less invasive telemeter for 7-day AP recovery studies with the *Kmo*$^{alb\text{-}cre}$ line which, with elevated 3HK levels at baseline would be anticipated to have a worse recover profile that *Kmo*^{wt} mice.

3.5. Experiment 3 – Hepatocyte-restricted Kmo knockout out impairs recovery in AP

3.5.1. Background

Experiment 2 demonstrated elevated circulating concentration of 3HK in the novel *Kmo*$^{alb\text{-}cre}$ mouse line, and impaired onward clearance from the circulation of an intravenous 3HK tracer indicating 3HK elimination saturation. As this metabolite is considered to be contributory to multiple organ dysfunction in AP, as supported by elevated serum [3HK] in human severe AP which correlates with elevated C-reactive protein (CRP) levels (375) and protection against severe AP in rodent models (297, 634), my hypothesis was that mice with elevated [3HK] levels would have impaired recovery during a telemetered 7-day study period. Given that the *Kmo*^{wt} mice had poor 7-day recovery (Experiment 1) with AP using the cardiometabolic telemeter, and that confirmatory data (section 3.4) supported the notation that the larger cardiometabolic tracer had measurably impaired recovery after implantation, I chose to switch to the smaller telemeter device when comparing sickness behaviour and recovery over 7-days between the three related mouse lines (*Kmo*^{wt}, *Kmo*$^{alb\text{-}cre}$ and *Kmo*^{null}). Age-matched male mice from each colony were randomly assigned (by random number generation, between 0.00 to 1.00, with the lower number assigned to sham in Microsoft Excel) to sham or AP, where there were odd littermate numbers, a ratio of 2 AP: 1 sham was used, or 1:1 where even number of mice were available, until there was n=7 sham for each group.

3.5.2. Hypotheses

The *Kmo*$^{alb\text{-}cre}$ mice, with higher circulating [3HK], would display increased sickness behaviour and biochemical changes consistent with multiple organ injury.

3.5.3 Results

Details of study participants are fully listed in Appendix 9. Group sizes consisted of *Kmo*^{wt} (7 sham: 9 AP), *Kmo*^{null} (7 sham: 9 AP) and *Kmo*$^{alb\text{-}cre}$ (7 sham: 10 AP). Core body temperature and locomotor activity telemetry profiles shown in **Figure 30**. The key finding was of the high proportion of *Kmo*$^{alb\text{-}cre}$ AP mice reaching humane cull endpoints during this recovery study. With regards to *Kmo*^{wt} mice, in light of the Experiment 1 findings, it was unexpected that all mice would survive and not meet humane endpoints, however, this less invasive telemetry device might have made this model more akin to moderate AP, as opposed to severe AP, when extrapolated to the human situation.

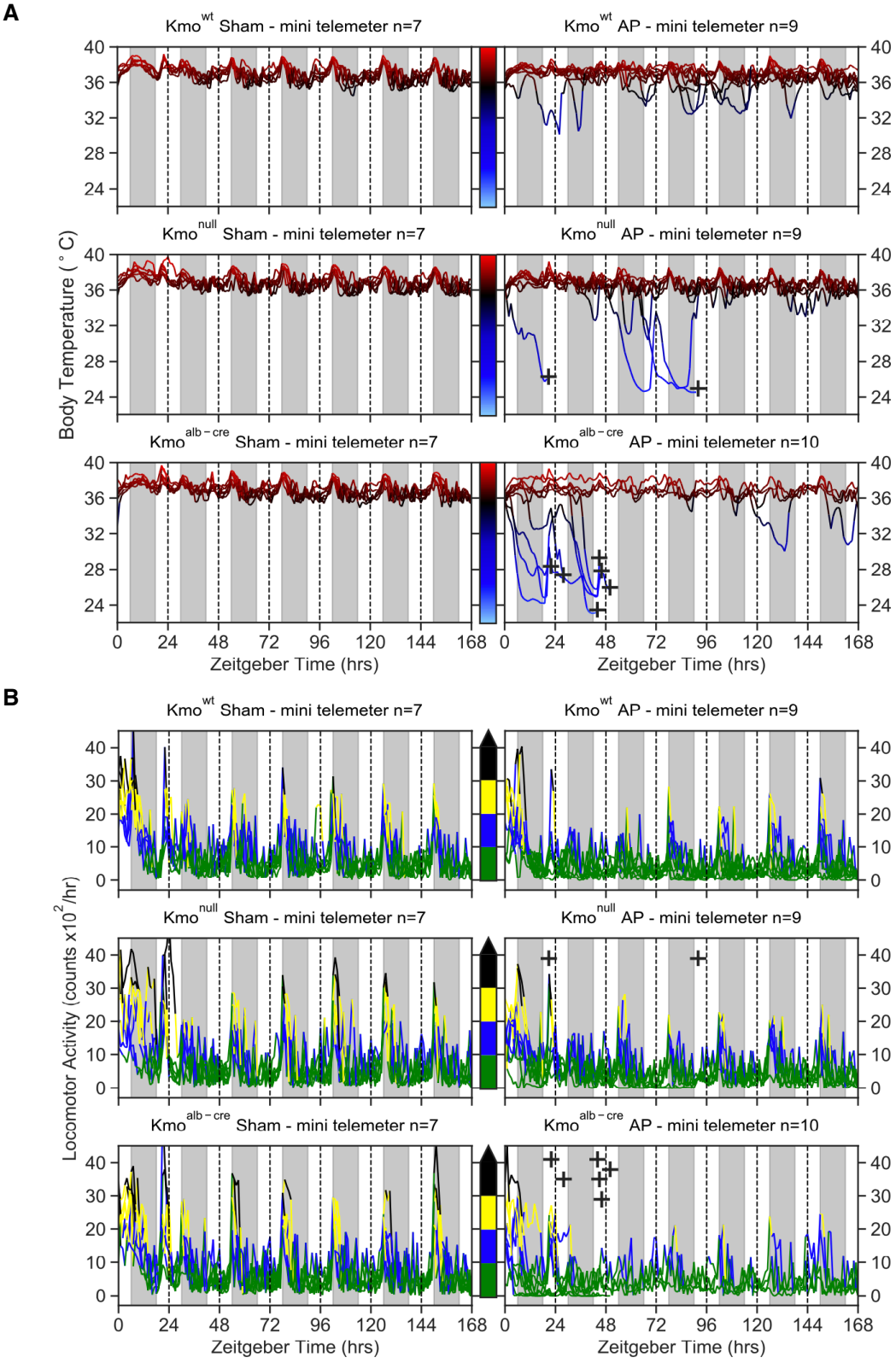

Figure 30: *Kmo*$^{alb\text{-}cre}$ mice were sicker and had worse survival to predefined humane endpoints in experimental AP compared to *Kmo*^{wt} and *Kmo*$^{alb\text{-}cre}$ mice.

Hourly mean core body temperatures (A) and locomotor activity (B) are shown for individual mice. A+B: Left side panels are sham surgery controls; Right side panels are AP. Top paired panels are *Kmo*^{wt} (n = 7 sham, n = 9 AP), middle panels are *Kmo*^{null} (n = 7 sham, n = 9 AP), and lowest paired panels are *Kmo*$^{alb\text{-}cre}$ (n = 7 sham, n = 10 AP).

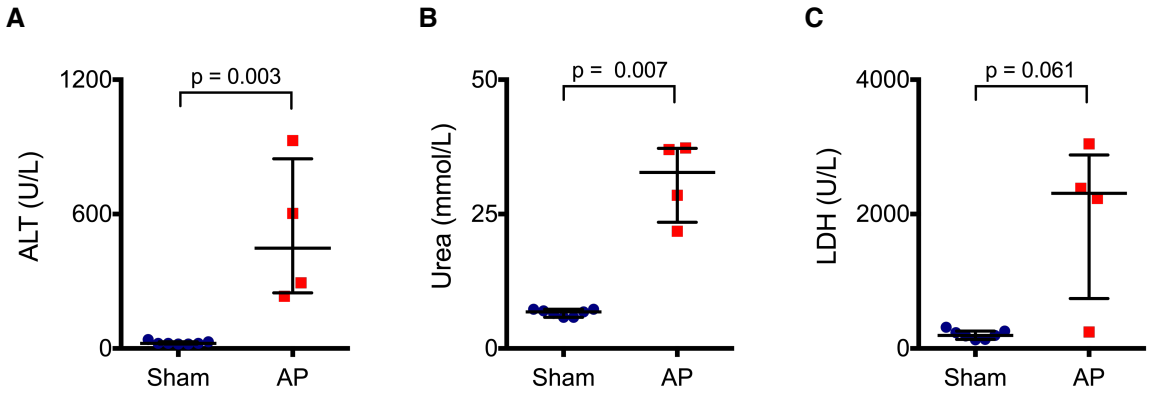

Figure 31: Biochemical evidence of multiple organ injury with AP in *Kmo$^{alb\text{-}cre}$*

Using the less invasive non-cardiac mini telemeters in AP Kmo$^{alb\text{-}cre}$ mice, those which reached humane endpoints are compared to matched mini telemetered Kmo$^{alb\text{-}cre}$ mice randomised to sham culled at 168-hrs.

A: ALT was significantly elevated in humane endpoint mice (p = 0.003, Mann Whitney test). **B**: Urea was significantly elevated in humane endpoint mice (p = 0.007, *t*-test). **C**: LDH was increased in 3 of 4 mice reaching humane endpoint but because of unequal intergroup data variance (Levene's test p = 0.009) *t*-test found no significant difference (p = 0.061, independent *t*-test without assumption of equal variance. Individual data are shown and horizontal lines are median with interquartile range.

Figure 31 shows biochemical evidence of multi-organ injury in *Kmo$^{alb\text{-}cre}$* mice reaching humane endpoints, as compared to recovered sham *Kmo$^{alb\text{-}cre}$*. **Figure 32** depicts the survival curves of the mouse lines and with statistical testing, showing a significantly impaired survival of *Kmo$^{alb\text{-}cre}$*. **Table 27** details the analgesia administered to the mice during the study, in line with the protocol.

Line	Treatment	Number	Exp duration – mean (SD)	S/C Bup. Dose – mean (SD)	S/C Bup. Dose : Time adjusted – mean (SD)	Oral Bup. Dose – mean (SD)	Oral Bup. Dose : Time adjusted – mean (SD)
Kmo^{wt}	Sham	N = 7	168.0 (0) hrs	4.393 (0.283) µg	0.026 (0.002) µg/hr	65.71 µg (11.34)	0.391 (0.062) µg/hr
Kmo^{wt}	AP	N = 9	168.0 (0) hrs	5.000 (0.750) µg	0.030 (0.004) µg/hr	61.11 µg (23.15)	0.364 (0.138) µg/hr
Kmo^{null}	Sham	N = 7	168.0 (0) hrs	4.500 (0.000) µg	0.027 (0.000) µg/hr	61.43 µg (22.68)	0.366 (0.135) µg/hr
Kmo^{null}	AP	N = 9	143.6 (51.4) hrs	4.667 (0.500) µg	0.049 (0.055) µg/hr	40.00 µg (33.54)	0.243 (0.195) µg/hr
Kmo$^{alb\text{-}cre}$	Sham	N = 7	168.0 (0) hrs	4.500 (0.000) µg	0.027 (0.000) µg/hr	68.57 µg (3.78)	0.408 (0.022) µg/hr
Kmo$^{alb\text{-}cre}$	AP	N = 10	91.9 (66.1) hrs	5.250 (0.791) µg	0.110 (0.078) µg/hr	28.30 µg (34.58)	0.183 (0.202) µg/hr
1-way ANOVA between 6 groups			****p = 0.002, KW**	***p = 0.019, KW**	****p = 0.006, KW**	***p = 0.020, KW**	***p = 0.022, KW**

Table 27. Analgesia given in AP experiment 3

Oral Buprenorphine single dose 0.01 mg. S/C Buprenorphine single dose 0.05 mg/kg.

KW: Kruskal-Wallis. *p < 0.05, **p < 0.01.

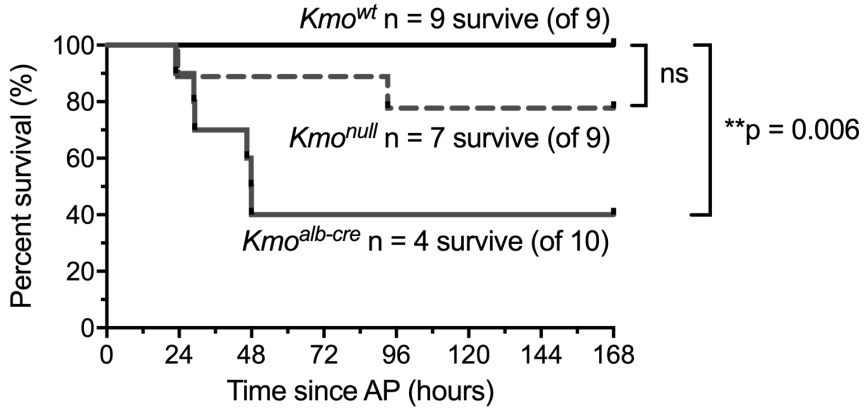

Figure 32. Impaired survival to humane endpoints in AP for Kmo$^{alb\text{-}cre}$ line in mini telemeter study.

Over 7-days, the 3 mouse lines with AP had statistically significant differences in survival to humane endpoint(s) ($p = 0.011$, 3-way log-rank (Mantel-Cox) test). *Kmo$^{alb\text{-}cre}$* mice with AP had a reduced survival (median of 48-hrs), and 40% 7-day recovery. The lower 7-day survival of *Kmo^{null}* compared to *Kmo^{wt}* did not significantly differ ($p = 0.145$). ns = not significant ($p > 0.05$).

One *Kmo^{null}* subject which reached humane endpoint at 23-hrs was found to have a leak from the duodenotomy closure, but was included for completeness.

3.5.4. Conclusions

These results demonstrated a significant impairment in survival in Kmo$^{alb\text{-}cre}$ mice after insult by experimental AP, with a tendency toward critical illness at early time points (<72 hours).

3.6. Experiment 4 – A comparison of early injury metrics at 24-hrs in recovery AP between differentially expressed KMO mouse lines

3.6.1. Introduction

Pairs of age-matched male mice from three groups were randomly assigned to AP or sham laparotomy treatment. The three mouse lines were wildtype *Kmo*^{wt} [genotype: FLP (HOM) or Acre(-)], *Kmo*$^{alb\text{-}cre}$ [geneotype: Acre(+)] and *Kmo*^{null} [geneotype: KMO (HOM)]. Randomisation was performed by computer generation (paired random number generation [between 0.00 to 1.00]: mouse with highest number was assigned to AP). AP treatment consisted of a retrograde biliopancreatic duct infusion with 50 µl 2% sodium taurocholic acid (Na-TCA) (in PBS) over 5 mins, for further detail see methods (section 2.3). These 24-hr experiments did not involve implantation of telemeters for both practical (limited numbers of telemetry systems) and experimental reasons (these were not 7-day recovery studies, but 24-hr timepoint chosen to minimise risk of death before end timepoint). Principally, subjects were used for either histology or flow cytometry experiments. Details of experimental subjects can be found in Appendix 10. Results of plasma biochemistry and cytokines, pancreas injury histology and flow cytometry of blood, lung digest and liver digest comparing sham to AP at 24-hrs post-surgery in *Kmo*^{wt}, *Kmo*$^{alb\text{-}cre}$ and *Kmo*^{null} are reported below.

3.6.2. Hypothesis

The null hypothesis was that there would be no statistically significant differences between mouse lines in any parameter measured. Samples sizes and power calculations detail in the corresponding sections.

3.6.3. Results – Biochemistry at 24-hr

Experimental subjects for biochemistry were all those mice used for 24-hr multi-organ histological experiments and flow cytometry experiments. Appendix 10, Table 88 lists all of the primary biochemical data. *Post-hoc* power analysis revealed sufficiently sized cohorts to power the experiment satisfactorily, with a power 0.95. Amylase was measured in all 90 mice at 24-hr, whilst the full biochemistry panel was measured in all but two of these (i.e. n = 88).

Initially, a two-way ANOVA was used to statistically test for clinical biochemistry differences with treatment (AP versus sham) across all 3 mouse lines, with null hypotheses of ‘no treatment effect’ and ‘no mouse line effect’ (Table 28). Next, an analysis was performed between AP groups of the 3 mouse lines to test the primary null hypothesis (section 3.6.2.).

These results are tablulated (**Tables 28 to 34**) and displayed (**Figure 33**) with statistical analysis between AP groups shown.

3.6.3.1. 2-way ANOVA on biochemistry

AP treatment effects on clinical biochemistry across mouse lines are shown in **Table 28**, revealing a statistically significant increase in amylase (log10 amylase) ($p < 0.001$), LDH ($p = 0.002$), and urea ($p = 0.008$). A statistically significant decrease in glucose ($p < 0.001$) and albumin ($p = 0.002$) with AP were also detected. Mean ALT concentrations were higher in AP than sham, but this was not significantly significant ($p = 0.214$).

Biochemistry	**Number** (Sham, AP)	**Mean Sham** (St. Dev)	**Mean AP** (St. Dev)	**Mean square**	**F-statistic**	**P-value**
Log10 amylase (U/L)	**45, 45**	**3.373 (0.095)**	**4.059 (0.398)**	**10.7**	**128.79**	**<0.001**
LDH (U/L)	**44, 44**	**211.4 (88.8)**	**403.5 (386.0)**	**818228.9**	**10.76**	**0.002**
Glucose (mmol/L)	**44, 44**	**16.7 (3.2)**	**12.5 (4.8)**	**386.2**	**22.38**	**<0.001**
Albumin (g/L)	**44, 44**	**26.3 (2.3)**	**24.8 (2.6)**	**51.5**	**9.91**	**0.002**
Urea (mmol/L)	**44, 44**	**6.1 (1.4)**	**8.8 (6.5)**	**155.6**	**7.46**	**0.008**
ALT (U/L)	44, 44	77.4 (79.7)	94.8 (59.7)	7057.6	1.57	n/s 0.214

Table 28. Treatment effect (AP versus sham) across 3 mouse lines on biochemistry, 2-way ANOVA

3.6.3.2. Amylase

Amylase results were converted from linear scale to log10 scale to allow data to be plotted meaningfully. There was no significant difference in log10 plasma amylase levels comparing AP groups across the 3 mouse lines (**Table 29**). There were significant increases in amylase with AP compared to sham across all three mouse lines: Kmo^{wt} ($p < 0.001$, GH), $Kmo^{alb\text{-}cre}$ ($p < 0.001$, GH) and Kmo^{null} ($p < 0.001$, GH).

Biochemistry Group size	**Rx**	**Median values (Std. deviation)**	**Normality testing**	**1-Way ANOVA**	**Post Hoc**	**Mean difference**
Amylase	**AP**	Log10 amylase	Passed	1-way	*Tukey post-hoc multiple testing*	
n = 16		Kmo^{wt} 3.927 g/l (0.384)		ANOVA	Kmo^{wt} AP vs Kmo^{null} AP, p = 0.965	0.036
n = 15		$Kmo^{alb\text{-}cre}$ 4.181 g/l (0.399)		p = 0.316	Kmo^{wt} AP vs $Kmo^{alb\text{-}cre}$ AP, p = 0.451	-0.176
n = 14		Kmo^{null} 3.859 g/l (0.407)			Kmo^{null} AP vs $Kmo^{alb\text{-}cre}$, p = 0.329	-0.212
Amylase	**Sham**	Log10 amylase	Passed	1-way	n/a	n/a
n = 16		Kmo^{wt} 3.355 g/l (0.060)		ANOVA		
n = 15		$Kmo^{alb\text{-}cre}$ 3.355 g/l (0.080)		p = 0.883		
n = 14		Kmo^{null} 3.333 g/l (0.115)				

Table 29. Amylase AP, 1-way ANOVA

3.6.3.3. Albumin and ALT

There was no significant difference in plasma albumin levels comparing AP groups across the 3 mouse lines (**Table 30**). Sham groups had a statistically significant difference in albumin levels, with a reduced albumin in $Kmo^{alb\text{-}cre}$ mice compared to Kmo^{wt}. Whilst biologica-

Biochemistry Group size	**Rx**	**Median values** **(Std. deviation)**	**Normality** **testing**	**1-Way** **ANOVA**	**Post Hoc**	**Mean** **difference**
Albumin	**AP**		Passed	1-way	*Tukey post-hoc multiple testing*	
n = 16		Kmo^{wt} 25.4 g/l (1.8)		ANOVA	Kmo^{wt} AP vs Kmo^{null} AP, p = 0.992	-0.1116
n = 14		$Kmo^{alb\text{-}cre}$ 23.8 g/l (3.3)		p = 0.056	Kmo^{wt} AP vs $Kmo^{alb\text{-}cre}$ AP, p = 0.094	1.917
n = 14		Kmo^{null} 25.3 g/l (2.0)			Kmo^{null} AP vs $Kmo^{alb\text{-}cre}$, p = 0.084	2.029
Albumin	**Sham**		Passed	**1-way**	*Tukey post-hoc multiple testing*	
n = 16		Kmo^{wt} 26.8 g/l (2.8)		**ANOVA**	Kmo^{wt} Sham vs Kmo^{null} Sham, p = 0.333	1.103
n = 14		$Kmo^{alb\text{-}cre}$ 25.1 g/l (1.2)		**p = 0.020**	**Kmo^{wt} Sham vs $Kmo^{alb\text{-}cre}$ Sham, p = 0.015**	2.253
n = 14		Kmo^{null} 26.3 g/l (1.8)			Kmo^{null} Sham vs $Kmo^{alb\text{-}cre}$ Sham, p = 0.326	1.15

Table 30. Albumin AP, 1-way ANOVA

-ally interesting, given the *alb-cre* genetic background of these mice, the difference was quantitatively small (<2 g/l) and therefore of no particular biological relevance in this context.

There was a significant difference in plasma ALT levels comparing AP groups across the 3 mouse lines with AP and sham (**Table 31**). Data was compared by Kruskal-Wallis test and *post-hoc* Dunn's tests due to non-parametric distributions. ALT was lowest in AP Kmo^{null} group (median 46.5 U/L, SD 34.0 U/L) which was lower (p = 0.001, Dunn's) than Kmo^{wt} (median 99.0 U/L, SD 55.1 U/L) and lower (p = 0.026, Dunn's) than $Kmo^{alb\text{-}cre}$ (median 86.0 U/L, SD 69.9 U/L). Similarly, after sham laparotomy, Kmo^{null} had lower ALT levels than Kmo^{wt}, but levels did not differ between the two genetically altered mouse lines (i.e. Kmo^{null} and $Kmo^{alb\text{-}cre}$).

Biochemistry Group size	**Rx**	**Median values** **(Std. deviation)**	**Normality** **testing**	**1-Way** **ANOVA**	**Post Hoc**	**Mean** **difference**
ALT	**AP**		Failed	**Kruskal-**	*Dunn's post-hoc multiple testing*	
n = 16		Kmo^{wt} 99.0 U/l (55.1)		**Wallis**	**Kmo^{wt} AP vs Kmo^{null} AP, p = 0.001**	**16.54**
n = 14		$Kmo^{alb\text{-}cre}$ 86.0 U/l (69.9)		**p = 0.001**	Kmo^{wt} AP vs $Kmo^{alb\text{-}cre}$ AP, p = 1.000	3.79
n = 14		Kmo^{null} 46.5 U/l (34.0)			**Kmo^{null} AP vs $Kmo^{alb\text{-}cre}$, p = 0.026**	**-12.75**
ALT	**Sham**		Failed	**Kruskal-**	*Dunn's post-hoc multiple testing*	
n = 16		Kmo^{wt} 91.0 U/l (70.5)		**Wallis**	**Kmo^{wt} Sham vs Kmo^{null} Sham, p < 0.001**	**18.78**
n = 14		$Kmo^{alb\text{-}cre}$ 49.0 U/l (22.7)		**p < 0.001**	Kmo^{wt} Sham vs $Kmo^{alb\text{-}cre}$ Sham, p = 0.181	8.817
n = 14		Kmo^{null} 30.0 U/l (112.2)			Kmo^{null} Sham vs $Kmo^{alb\text{-}cre}$ Sham, p = 0.120	-9.96

Table 31. ALT AP, 1-way ANOVA

3.6.3.4. LDH, Glucose and urea

There were no significant differences in plasma LDH (**Table 32**), glucose (**Table 33**) or urea (**Table 34**) levels between AP groups across the 3 mouse lines.

Biochemistry Group size	**Rx**	**Median values** **(Std. deviation)**	**Normality** **testing**	**1-Way** **ANOVA**	**Post Hoc**	**Mean** **difference**
LDH	**AP**		Failed	Kruskal-	*Dunn's post-hoc multiple testing*	
n = 16		Kmo^{wt} 254 U/l (440)		Wallis	Kmo^{wt} AP vs Kmo^{null} AP, p = 0.866	4.987
n = 14		$Kmo^{alb\text{-}cre}$ 312 U/l (472)		p = 0.432	Kmo^{wt} AP vs $Kmo^{alb\text{-}cre}$ AP, p = 1.000	-0.763
n = 14		Kmo^{null} 235 U/l (109)			Kmo^{null} AP vs $Kmo^{alb\text{-}cre}$, p = 0.709	-5.750
LDH	**Sham**		Failed	Kruskal-	n/a	n/a
n = 16		Kmo^{wt} 267 U/l (117)		Wallis		
n = 14		$Kmo^{alb\text{-}cre}$ 163 U/l (68.8)		p = 0.066		
n = 14		Kmo^{null} 169 U/l (36.2)				

Table 32. LDH AP, 1-way ANOVA

Biochemistry Group size	**Rx**	**Median values** **(Std. deviation)**	**Normality** **testing**	**1-Way** **ANOVA**	**Post Hoc**	**Mean** **difference**
Glucose	**AP**		Passed	1-way	*Tukey post-hoc multiple testing*	
n = 16		Kmo^{wt} 13.3 mmol/l (3.1)		ANOVA	Kmo^{wt} AP vs Kmo^{null} AP, p = 0.999	0.084
n = 14		$Kmo^{alb\text{-}cre}$ 10.7 mmol/l (6.3)		p = 0.739	Kmo^{wt} AP vs $Kmo^{alb\text{-}cre}$ AP, p = 0.759	1.277
n = 14		Kmo^{null} 14.2 mmol/l (5.0)			Kmo^{null} AP vs $Kmo^{alb\text{-}cre}$, p = 0.798	1.193
Glucose	**Sham**		Passed	1-way	n/a	n/a
n = 16		Kmo^{wt} 17.3 mmol/l (3.4)		ANOVA		
n = 14		$Kmo^{alb\text{-}cre}$ 16.6 mmol/l (2.9)		p = 0.386		
n = 14		Kmo^{null} 18.8 mmol/l (3.3)				

Table 33. Glucose AP, 1-way ANOVA

Biochemistry Group size	**Rx**	**Median values** **(Std. deviation)**	**Normality** **testing**	**1-Way** **ANOVA**	**Post Hoc**	**Mean** **difference**
Urea	**AP**		Failed	Kruskal-	*Dunn's post-hoc multiple testing*	
n = 16		Kmo^{wt} 6.65 mmol/l (3.8)		Wallis	Kmo^{wt} AP vs Kmo^{null} AP, p = 0.832	5.103
n = 14		$Kmo^{alb\text{-}cre}$ 6.15 mmol/l (10.2)		p = 0.451	Kmo^{wt} AP vs $Kmo^{alb\text{-}cre}$ AP, p = 1.000	-0.290
n = 14		Kmo^{null} 6.25 mmol/l (2.2)			Kmo^{null} AP vs $Kmo^{alb\text{-}cre}$, p = 0.798	-5.393
Urea	**Sham**		Failed	Kruskal-	n/a	n/a
n = 16		Kmo^{wt} 5.95 mmol/l (1.4)		Wallis		
n = 14		$Kmo^{alb\text{-}cre}$ 6.00 mmol/l (1.1)		p = 0.930		
n = 14		Kmo^{null} 5.50 mmol/l (1.8)				

Table 34. Urea AP, 1-way ANOVA

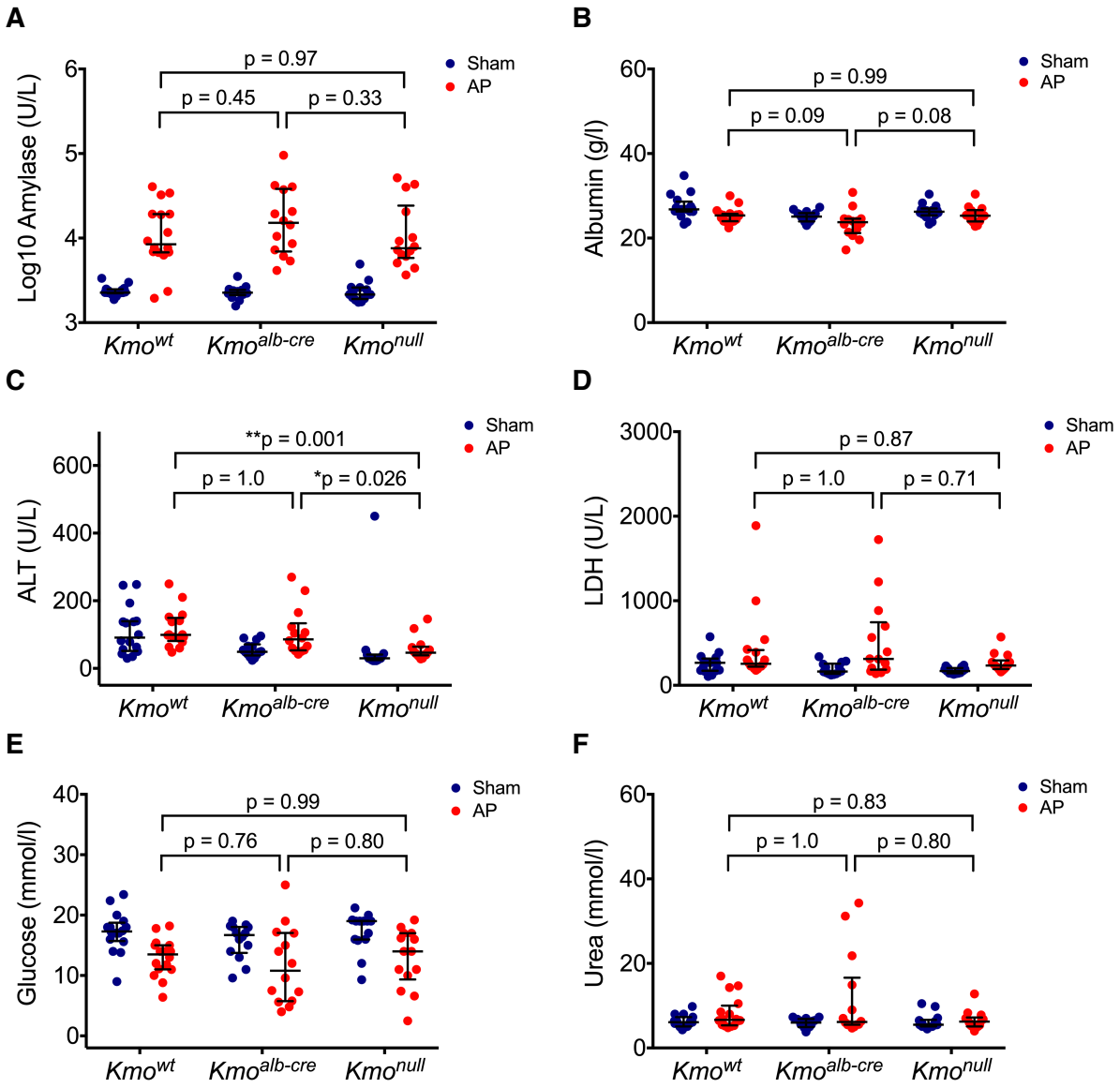

Figure 33. Plasma biochemistry 24h post sham laparotomy or AP in Kmo^{wt}, Kmo$^{alb\text{-}cre}$ and Kmo^{null}.

EDTA plasma at 24-hr post AP or Sham. Subjects: Kmo^{wt} n = 32 [16 sham: 16 AP]) and Kmo$^{alb\text{-}cre}$ n = 28 (14 sham: 14 AP); in all analyses except amylase, (i.e. B-F), Kmo^{null} n = 28 (14 sham: 14 AP), whilst in amylase analysis (A) there was an additional pair of Kmo^{null} that did not have all biochemical full testing [Kmo^{null} (15 sham: 15 AP)]. Male, age-matched Kmo^{wt}, Kmo$^{alb\text{-}cre}$, and Kmo^{null} mice were electronically randomised to AP or sham. Statistical annotations depict those ANOVAs with post-hoc testing between AP groups as calculated in Tables 26 to 31. **A**: Amylase results displayed on log10 scale for practical reasons due to wide variability in results amongst AP subjects. **B**: Albumin. **C**: Alanine aminotransferase (ALT). **D**: Lactate dehydrogenase (LDH). **E**: Glucose. **F**: Urea. Individual data are shown and horizontal lines are median with interquartile range. ns = not significant ($p > 0.05$); *$p < 0.05$, **$p < 0.01$.

3.6.4. Results – Cytokines at 24-hr

The cytokine data is detailed in Appendix 10, with the limits of detection for each cytokine for both V-PLEX plates (A and B) documented. In line with 3Rs principles, all efforts to maximise yield samples was made from the outset. As there were separate groups of mice used for multi-organ histological storage and other groups used for multi-organ flow cytometry, thus there were greater numbers of subjects with stored plasma available for measurement of circulating cytokine concentrations than for histology alone. Specifically, there was up to n = 11 for all groups. *Post-hoc* power calculations using n = 11 *Kmo*^{wt} data (sham and AP; using IL-1β), gave d = 1.672 and a satisfactory power (0.96).

Initially, a two-way ANOVA was used to statistically test for cytokine differences with treatment (AP versus sham) across all 3 mouse lines, with null hypotheses of 'no treatment effect' and 'no mouse line effect' (Table 32). Next, an analysis was performed between AP groups of the 3 mouse lines to test the primary null hypothesis (section 3.6.2.). These results are tablulated (Tables 33 to 42) and displayed (Figure 34) with statistical analysis between AP groups shown.

3.6.4.1. 2-way ANOVA on cytokines

AP treatment effects on cytokine plasma levels across mouse lines are shown in **Table 35**, revealing a statistically significant increase in IL-1β ($p < 0.001$), IL-2 ($p = 0.013$), IL-6 (log10) ($p < 0.001$), TNFα (log10) ($p = 0.016$), and KC/GRO ($p = 0.045$) with AP. There was no significant treatment effect upon IL-4 ($p = 0.50$), IL-5 ($p = 0.28$), IL-10 ($p = 0.08$), IL-12p70 ($p = 0.21$) or IFNγ ($p = 0.76$) levels across the mouse lines.

Cytokine (pg/ml)	**Number** (Sham, AP)	**Mean Sham** (pg/ml) (St. Dev)	**Mean AP** (pg/ml) (St. Dev)	**Mean square**	**F-statistic**	**P-value**
IL-1β	**36, 35**	**1.572 (0.42)**	**5.064 (5.22)**	**210.150**	**16.515**	**<0.001**
IL-2	**36, 35**	**2.331 (1.41)**	**3.991 (3.69)**	**46.829**	**6.491**	**0.013**
IL-4	36, 35	0.495 (0.61)	0.417 (0.39)	0.114	0.456	n/s 0.502
IL-5	36, 35	52.709 (40.60)	43.537 (25.99)	1448.941	1.181	n/s 0.281
IL-6 log10	**36, 35**	**1.912 (0.211)**	**2.554 (0.754)**	**7.177**	**25.579**	**<0.001**
IL-10	36, 35	18.030 (4.241)	79.536 (201.028)	63698.020	3.252	n/s 0.076
IL-12p70	36, 35	52.127 (36.488)	69.967 (77.673)	5397.865	1.572	n/s 0.214
IFNγ	36, 35	0.7318 (0.573)	0.685 (0.581)	0.034	0.097	n/s 0.757
TNFα Log10	**36, 35**	**1.002 (0.116)**	**1.176 (0.400)**	**0.530**	**6.139**	**0.016**
KC/GRO	**36, 35**	**36.870 (16.771)**	**364.109 (964.841)**	**1835719.19**	**4.180**	**0.045**

Table 35. Treatment effect (AP versus sham) across mouse lines on cytokines, 2-way ANOVA

3.6.4.2. IL-1β, IL-5, IL-6, IL-10, IFNγ, TNFα, KC/GRO

There was no significant difference in IL-1β (**Table 36**), IL-5 (**Table 37**), IL-6 (**Table 38**), IL-10 (**Table 39**), IFNγ (**Table 40**), TNFα (**Table 41**) or KC/GRO (**Table 42**) levels between AP groups across the 3 mouse lines.

Cytokine Group size	**Rx**	**Median values** **(Std. deviation)**	**Normality testing**	**1-Way ANOVA**	**Post Hoc**	**Mean difference**
IL-1β	**AP**		Failed	Kruskal-	*Dunn's post-hoc multiple testing*	
n = 11		Kmo^{wt} 2.91 pg/ml (1.4)		Wallis	Kmo^{wt} AP vs $Kmo^{alb\text{-}cre}$ AP, p = 0.515	-5.636
n = 11		$Kmo^{alb\text{-}cre}$ 4.01 pg/ml (8.0)		p = 0.186	Kmo^{wt} AP vs Kmo^{null} AP, p = 1.0	1.545
n = 11		Kmo^{null} 2.86 pg/ml (3.4)			$Kmo^{alb\text{-}cre}$ AP vs Kmo^{null} AP, p = 0.245	7.182
IL-1β	**Sham**		Failed	Kruskal-	n/a	n/a
n = 11		Kmo^{wt} 1.47 pg/ml (0.5)		Wallis		
n = 11		$Kmo^{alb\text{-}cre}$ 1.43 pg/ml (0.2)		p = 0.471		
n = 11		Kmo^{null} 1.63 pg/ml (0.5)				

Table 36. IL-1β AP, 1-way ANOVA

Cytokine Group size	**Rx**	**Median values** **(Std. deviation)**	**Normality testing**	**1-Way ANOVA**	**Post Hoc**	**Mean difference**
IL-5	**AP**		Failed	Kruskal-	*Dunn's post-hoc multiple testing*	
n = 11		Kmo^{wt} 49.5 pg/ml (23.6)		Wallis	Kmo^{wt} AP vs $Kmo^{alb\text{-}cre}$ AP, p = 1.000	3.455
n = 11		$Kmo^{alb\text{-}cre}$ 30.7 pg/ml (22.3)		p = 0.556	Kmo^{wt} AP vs Kmo^{null} AP, p = 0.931	4.182
n = 11		Kmo^{null} 26.7 pg/ml (33.4)			$Kmo^{alb\text{-}cre}$ AP vs Kmo^{null} AP, p = 1.000	0.727
IL-5	**Sham**		Failed	Kruskal-	n/a	n/a
n = 11		Kmo^{wt} 36.3 pg/ml (28.7)		Wallis		
n = 11		$Kmo^{alb\text{-}cre}$ 47.3 pg/ml (18.6)		p = 0.531		
n = 11		Kmo^{null} 34.8 pg/ml (57.7)				

Table 37. IL-5 AP, 1-way ANOVA

Cytokine Group size	**Rx**	**Median values** **(Std. deviation)**	**Normality testing**	**1-Way ANOVA**	**Post Hoc**	**Mean difference**
IL-6	**AP**		Failed	Kruskal-	*Dunn's post-hoc multiple testing*	
n = 11		Kmo^{wt} 2.10 pg/ml (0.66)		Wallis	Kmo^{wt} AP vs $Kmo^{alb\text{-}cre}$ AP, p = 0.121	-8.455
n = 11		$Kmo^{alb\text{-}cre}$ 2.72 pg/ml (0.92)		p = 0.066	Kmo^{wt} AP vs Kmo^{null} AP, p = 1.000	-0.273
n = 11		Kmo^{null} 2.19 pg/ml (0.50)			$Kmo^{alb\text{-}cre}$ AP vs Kmo^{null} AP, p = 0.142	0.142
IL-6	**Sham**		Passed	1-way	n/a	n/a
n = 11		Kmo^{wt} 2.05 pg/ml (0.26)		ANOVA		
n = 11		$Kmo^{alb\text{-}cre}$ 2.01 pg/ml (0.17)		p = 0.244		
n = 11		Kmo^{null} 1.82 pg/ml (0.20)				

Table 38. IL-6 AP, 1-way ANOVA

Cytokine Group size	**Rx**	**Median values** **(Std. deviation)**	**Normality testing**	**1-Way ANOVA**	**Post Hoc**	**Mean difference**
IL-10	**AP**		Failed	Kruskal-	*Dunn's post-hoc multiple testing*	
n = 11		Kmo^{wt} 18.4 pg/ml (16.1)		Wallis	Kmo^{wt} AP vs $Kmo^{alb\text{-}cre}$ AP, p = 0.627	-5.182
n = 11		$Kmo^{alb\text{-}cre}$ 19.8 pg/ml (322.9)		p = 0.201	Kmo^{wt} AP vs Kmo^{null} AP, p = 1.000	1.909
n = 11		Kmo^{null} 17.0 pg/ml (7.8)			$Kmo^{alb\text{-}cre}$ AP vs Kmo^{null}, p = 0.256	7.091
IL-10	**Sham**		Failed	Kruskal-	n/a	n/a
n = 11		Kmo^{wt} 15.6 pg/ml (5.8)		Wallis		
n = 11		$Kmo^{alb\text{-}cre}$ 16.4 pg/ml (3.9)		p = 0.075		
n = 11		Kmo^{null} 18.6 pg/ml (2.8)				

Table 39. IL-10 AP, 1-way ANOVA

Cytokine Group size	**Rx**	**Median values (Std. deviation)**	**Normality testing**	**1-Way ANOVA**	**Post Hoc**	**Mean difference**
IFNγ	**AP**		Failed	Kruskal-	*Dunn's post-hoc multiple testing*	
n = 11		Kmo^{wt} 0.38 pg/ml (0.78)		Wallis	Kmo^{wt} AP vs $Kmo^{alb\text{-}cre}$ AP, p = 1.0	1.545
n = 11		$Kmo^{alb\text{-}cre}$ 0.39 pg/ml (0.51)		p = 0.929	Kmo^{wt} AP vs Kmo^{null} AP, p = 1.0	1.045
n = 11		Kmo^{null} 0.45 pg/ml (0.51)			$Kmo^{alb\text{-}cre}$ AP vs Kmo^{null}, p = 1.0	-0.500
IFNγ	**Sham**		Failed	Kruskal-	n/a	n/a
n = 11		Kmo^{wt} 0.33 pg/ml (0.83)		Wallis		
n = 11		$Kmo^{alb\text{-}cre}$ 0.61 pg/ml (0.51)		p = 0.716		
n = 11		Kmo^{null} 0.48 pg/ml (0.41)				

Table 40. IFNγ AP, 1-way ANOVA

Cytokine Group size	**Rx**	**Median values (Std. deviation)**	**Normality testing**	**1-Way ANOVA**	**Post Hoc**	**Mean difference**
TNFα	**AP**	TNF log10	Failed	Kruskal-	*Dunn's post-hoc multiple testing*	
n = 11		Kmo^{wt} 0.980 pg/ml (0.516)		Wallis	Kmo^{wt} AP vs $Kmo^{alb\text{-}cre}$ AP, p = 0.308	-6.727
n = 11		$Kmo^{alb\text{-}cre}$ 1.097 pg/ml (0.442)		p = 0.197	Kmo^{wt} AP vs Kmo^{null} AP, p = 1.0	-0.636
n = 11		Kmo^{null} 1.012 pg/ml (0.134)			$Kmo^{alb\text{-}cre}$ AP vs Kmo^{null}, p = 0.419	6.091
TNFα	**Sham**	TNF log10	Failed	Kruskal-	n/a	n/a
n = 11		Kmo^{wt} 0.920 pg/ml (0.152)		Wallis		
n = 11		$Kmo^{alb\text{-}cre}$ 1.051 pg/ml (0.085)		p = 0.545		
n = 11		Kmo^{null} 1.004 pg/ml (0.114)				

Table 41. TNFα AP, 1-way ANOVA

Cytokine Group size	**Rx**	**Median values (Std. deviation)**	**Normality testing**	**1-Way ANOVA**	**Post Hoc**	**Mean difference**
KC/GRO	**AP**		Failed	Kruskal-	*Dunn's post-hoc multiple testing*	
n = xx		Kmo^{wt} 63.8 pg/ml (298.3)		Wallis	Kmo^{wt} AP vs $Kmo^{alb\text{-}cre}$ AP, p = 1.0	-3.455
n = xx		$Kmo^{alb\text{-}cre}$ 211.9 pg/ml (1633.0)		p = 0.430	Kmo^{wt} AP vs Kmo^{null} AP, p = 1.0	1.818
n = xx		Kmo^{null} 57.9 pg/ml 147.9)			$Kmo^{alb\text{-}cre}$ AP vs Kmo^{null}, p = 0.603	5.273
KC/GRO	**Sham**		Passed	1-way	n/a	n/a
n = xx		Kmo^{wt} 48.0 pg/ml (19.1)		ANOVA		
n = xx		$Kmo^{alb\text{-}cre}$ 33.0 pg/ml (10.8)		p = 0.102		
n = xx		Kmo^{null} 34.7 pg/ml (15.7)				

Table 42. KC/GRO AP, 1-way ANOVA

3.6.4.3. IL-2

There were significantly elevated levels of IL-2 in *$Kmo^{alb\text{-}cre}$* line compare with the *Kmo^{wt}* line in AP (mean rank difference -10.6, p = 0.03) on Dunn's *post-hoc* testing (**Table 43**).

Cytokine Group size	**Rx**	**Median values (Std. deviation)**	**Normality testing**	**1-Way ANOVA**	**Post Hoc**	**Mean difference**
IL-2	**AP**		Failed	**Kruskal-**	*Dunn's post-hoc multiple testing*	
n = 11		Kmo^{wt} 1.74 pg/ml (3.0)		**Wallis**	**Kmo^{wt} AP vs $Kmo^{alb\text{-}cre}$ AP, p = 0.030**	-10.64
n = 11		$Kmo^{alb\text{-}cre}$ 5.19 pg/ml (5.1)		**p = 0.036**	Kmo^{wt} AP vs Kmo^{null} AP, p = 0.626	-5.182
n = 11		Kmo^{null} 3.02 pg/ml (2.0)			$Kmo^{alb\text{-}cre}$ AP vs Kmo^{null} AP, p = 0.557	5.455
IL-2	**Sham**		Failed	Kruskal-	n/a	n/a
n = 11		Kmo^{wt} 0.72 pg/ml (1.8)		Wallis		
n = 11		$Kmo^{alb\text{-}cre}$ 3.07 pg/ml (1.3)		p = 0.097		
n = 11		Kmo^{null} 2.26 pg/ml (1.1)				

Table 43. IL-2 AP, 1-way ANOVA

3.6.4.4. IL-4

Kruskal-Wallis testing revealed a significantly elevated levels of IL-4 in *Kmo$^{alb\text{-}cre}$* line compare with the *Kmo^{null}* line in AP (mean rank difference 10.5, p = 0.03) on Dunn's *post-hoc* testing (**Table 44**).

Cytokine Group size	**Rx**	**Median values (Std. deviation)**	**Normality testing**	**1-Way ANOVA**	**Post Hoc**	**Mean difference**
IL-4	**AP**		Failed	**Kruskal-**	*Dunn's post-hoc multiple testing*	
n = 11		Kmo^{wt} 0.238 pg/ml (0.221)		**Wallis**	Kmo^{wt} AP vs Kmo$^{alb\text{-}cre}$ AP, p = 0.309	-6.682
n = 11		Kmo$^{alb\text{-}cre}$ 0.305 pg/ml (0.486)		**p = 0.035**	Kmo^{wt} AP vs Kmo^{null} AP, p = 1.000	3.818
n = 11		Kmo^{null} 0.127 pg/ml (0.448)			**Kmo$^{alb\text{-}cre}$ AP vs Kmo^{null} AP, p = 0.031**	10.50
IL-4	**Sham**		Failed	Kruskal-	n/a	n/a
n = 11		Kmo^{wt} 0.344 pg/ml (0.962)		Wallis		
n = 11		Kmo$^{alb\text{-}cre}$ 0.349 pg/ml (0.362)		p = 0.077		
n = 11		Kmo^{null} 0.170 pg/ml (0.175)				

Table 44. IL-4 AP, 1-way ANOVA

3.6.4.5. IL-12p70

There were significantly elevated levels of IL-12p70 in *Kmo$^{alb\text{-}cre}$* line compared to both the *Kmo^{wt}* line and the *Kmo^{null}* line on Dunn's *post-hoc* testing both in AP and sham (**Table 45**).

Cytokine Group size	**Rx**	**Median values (Std. deviation)**	**Normality testing**	**1-Way ANOVA**	**Post Hoc**	**Mean difference**
IL-12p70	**AP**		Failed	**Kruskal-**	*Dunn's post-hoc multiple testing*	
n = 11		Kmo^{wt} 22.7 pg/ml (83.9)		**Wallis**	**Kmo^{wt} AP vs Kmo$^{alb\text{-}cre}$ AP, p = 0.010**	**-11.59**
n = 11		Kmo$^{alb\text{-}cre}$ 81.0 pg/ml (96.9)		**p = 0.005**	Kmo^{wt} AP vs Kmo^{null} AP, p = 1.000	-0.818
n = 11		Kmo^{null} 22.7 pg/ml (37.2)			**Kmo$^{alb\text{-}cre}$ AP vs Kmo^{null} AP, p = 0.019**	**10.770**
IL-12p70	**Sham**		Failed	**Kruskal-**	*Dunn's post-hoc multiple testing*	
n = 11		Kmo^{wt} 31.4 pg/ml (55.6)		**Wallis**	**Kmo^{wt} Sham vs Kmo$^{alb\text{-}cre}$ Sham, p = 0.030**	**-10.32**
n = 11		Kmo$^{alb\text{-}cre}$ 55.8 pg/ml (24.1)		**p = 0.002**	Kmo^{wt} Sham vs Kmo^{null} Sham, p = 1.000	3.500
n = 11		Kmo^{null} 22.7 pg/ml (14.7)			**Kmo$^{alb\text{-}cre}$ Sham vs Kmo^{null} Sham, p = 0.002**	**13.82**

Table 45. IL-12p70 AP, 1-way ANOVA

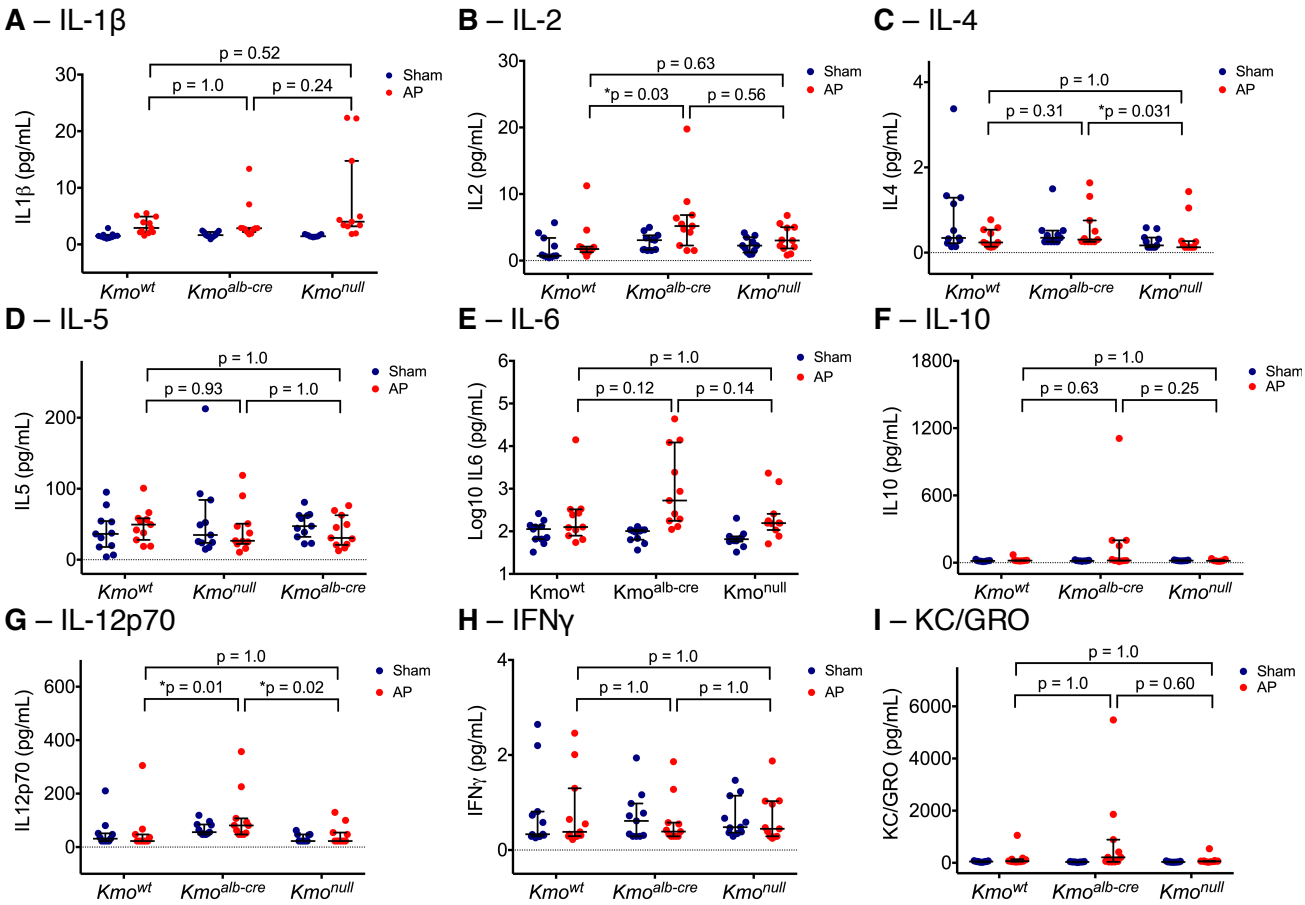

Figure 34. Plasma cytokines 24h post sham laparotomy or AP in *Kmo^{wt}*, *Kmo$^{alb\text{-}cre}$* and *Kmo^{null}*

EDTA plasma plasma cytokines levels were assessed in mice at 24-hrs after AP or sham in Kmo^{wt} n = 23 [12 sham: 11 AP]), Kmo$^{alb\text{-}cre}$ n = 24 (12 sham: 12 AP) and Kmo^{null} n = 24 (12 sham: 12 AP). One Kmo^{wt} AP mouse had insufficient blood for testing. IL-6 (E) and TNFα (J) results displayed on log10 scale for practical reasons due to wide linear variability in the results. Individual data are shown and horizontal lines are median with interquartile range. ns = not significant ($p > 0.05$); *$p < 0.05$. Stattisitical tests are those in Tables 33 to 42.

3.6.5. Results – Pancreas histology at 24-hr

An independent mouse histologist (Dr. J. Baily, formerly of the Centre for Cardiovascular Science, QMRI) experienced in scoring experimental AP, and blinded to the treatment groups, conducted the pancreas injury scoring. *Post-hoc* analysis on data from blinded histological scoring revealed an adequately powered experiment (d = 0.815, giving a power 0.93).

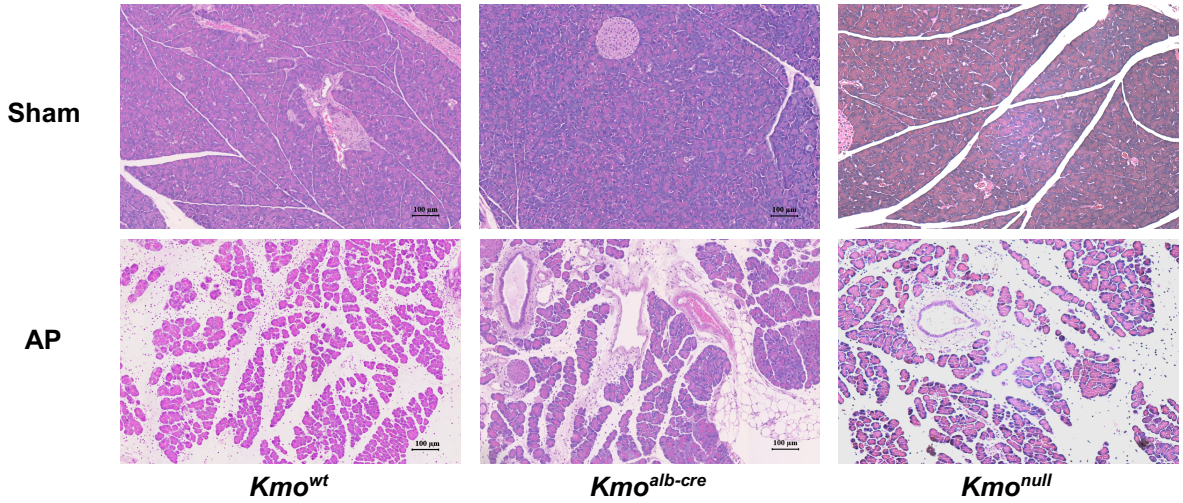

Figure 35. Histological pancreas injury scores

Composite histological pancreas injury scores (0 - 9) of mice at 24-hr: Kmo^{wt} (n=8 sham, n=8 AP), Kmo$^{alb\text{-}cre}$ (n=7 sham, n=7 AP) and Kmo^{null} (n=8 sham, n=8 AP). Example pancreatic head haematoxylin & eosin stain shows normal tissue morphology in sham control and features of acute inflammation in AP; PMN cell infiltrate, oedema and acinar necrosis. Subject ID: Kmo^{wt} sham (FK463), AP (FK496); Kmo$^{alb\text{-}cre}$ sham (Acre157), AP (Acre149); Kmo^{null} sham (K1151), Kmo^{null} AP (K1142). Unit distance on histological H&E images shown are 100 µm. Graph shows Individual data points and horizontal lines are median with interquartile range. Statistical analysis by Kruskal-Wallis ANOVA with post hoc Dunn's paired comparisons (failed normal data distribution testing). ns = not significant ($p > 0.05$); *$p < 0.05$, **$p < 0.01$.

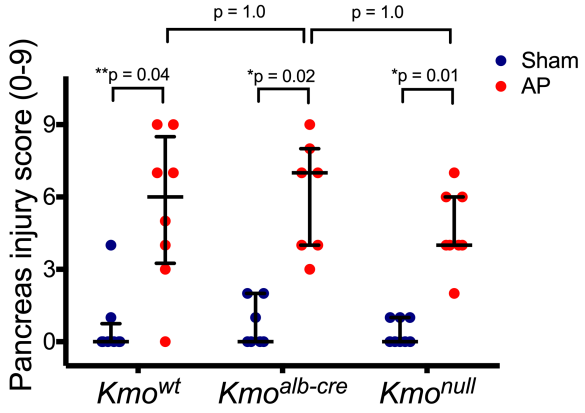

Appendix 10, Table 86 lists the scores for each subject, alongside plasma amylase results. Two-way ANOVA was used to statistically test for pancreas histological injury score differences with treatment (AP versus sham) across the 3 mouse lines. There were 46 mice electronically randomized to AP or sham: Kmo^{wt} (7 AP, 7 sham); Kmo$^{alb\text{-}cre}$ (8 AP, 8 sham); Kmo^{null} (8 AP, 8 sham). The AP treatment (2% NaTCA biliopancreatic duct infusion) produced a significant (F-statistic = 76.0, mean square 264.3, $p < 0.001$, 2-way ANOVA) increase in injury score from a sham laparotomy mean 0.57 units (Std dev. 0.99) to AP mean 5.35 units (Std dev. 2.39) on the 0 to 9 scoring scale. There was no significant difference across mouse line groups (F-statistic 0.829, mean square 2.88, $p = 0.444$, 2-way ANOVA). Kruskal-Wallis

one-way ANOVA (K-W statistic = 30.56, $p < 0.001$) was used to compare differences in pancreas injury score between groups comprised of data which failed normality testing. Post hoc Dunn's testing found no significant difference in pancreas injury scores between genetically altered mouse line groups in AP (**Figure 35**, above).

3.6.6. Results – Flow cytometry blood at 24-hr

Flow cytometry was performed on cardiac blood aspirated under anaesthesia, 24-hr following AP or sham in mice from the three mouse lines. Gating strategy for blood flow cytometry and the proportions of myeloid blood populations are shown in **Figure 36**. Firstly, a two-way ANOVA was used to statistically test blood flow cytometry population differences with treatment (AP versus sham) across the mouse lines, with null hypotheses of 'no treatment effect' and 'no mouse line effect' (Table 43). Appendix 10, Table 93 lists all of the blood flow cytometery data.

3.6.6.1. 2-way ANOVA on blood flow cytometry myeloid populations

AP treatment effects on blood leukocyte populations across mouse lines are shown in **Table 46**, revealing a statistically significant increase in proportion of circulating neutrophils (%CD45+) (F-statistic 23.99, $p < 0.001$, 2-way ANOVA), with a mean increase from 18.5% in sham laparotomy to 45.8%, across the mouse lines with AP. There was a significant decrease in eosinophil proportion of leukocytes after AP (F-statistic 6.38, $p = 0.017$, 2-way ANOVA), with a mean decrease from 2.4% in shams to 1.3% in AP. There was no significant treatment effect upon monocyte proportions (%CD45+) or Ly6C^{hi} monocyte (%monocytes).

Flow - blood	**Number** (Sham, AP)	**Mean Sham** (St. Dev)	**Mean AP** (St. Dev)	**Mean square**	**F-statistic**	**P-value**
Eosinophil (count, %CD45+)	18, 18	2.389 (1.042)	1.346 (1.308)	9.691	6.38	**0.017**
Neutrophil (count, %CD45+)	18, 18	18.511 (4.498)	45.75 (22.456)	6558.921	23.99	**<0.001**
Monocyte (count, %CD45+)	18, 18	4.889 (1.453)	5.020 (1.700)	0.151	0.59	n/s 0.810
L6C hi monocyte (count, %monocytes)	18, 18	40.606 (9.609)	45.667 (21.211)	230.512	0.77	n/s 0.389

Table 46. Treatment effect across mouse lines on blood flow cytometry myeloid, 2-way ANOVA

3.6.6.2. Blood eosinophils and neutrophils

There were no significant differences in eosinophil (**Table 47**) or neutrophil (**Table 48**) proprtions of blood leukocytes in AP between *Kmo*^{wt}, *Kmo*$^{alb\text{-}cre}$ or *Kmo*^{null}.

Flow - blood Group size	Rx	Median values (Std. deviation)	Normality testing	1-Way ANOVA	Post Hoc	Mean difference
Eosinophil	**AP**	%CD45+	Passed	1-way	*Tukey post-hoc multiple testing*	
n = 6		Kmo^{wt} 1.72 (1.44)		ANOVA	Kmo^{wt} AP vs $Kmo^{alb\text{-}cre}$ AP, p = 0.995	0.076
n = 6		$Kmo^{alb\text{-}cre}$ 1.40 (1.59)		p = 0.599	Kmo^{wt} AP vs Kmo^{null} AP, p = 0.626	0.728
n = 6		Kmo^{null} 0.58 (0.92)			$Kmo^{alb\text{-}cre}$ AP vs Kmo^{null} AP, p = 0.685	0.653
Eosinophil	**Sham**	%CD45+	Passed	1-way	n/a	n/a
n = 5		Kmo^{wt} 2.13 (0.91)		ANOVA		
n = 7		$Kmo^{alb\text{-}cre}$ 2.43 (0.75)		p = 0.984		
n = 6		Kmo^{null} 2.36 (1.53)				

Table 47. Blood Eosinophil AP, 1-way ANOVA

Flow - blood Group size	Rx	Median values (Std. deviation)	Normality testing	1-Way ANOVA	Post Hoc	Mean difference
Neutrophil	**AP**	%CD45+	Passed	1-way	*Tukey post-hoc multiple testing*	
n = 6		Kmo^{wt} 54.9 (25.5)		ANOVA	Kmo^{wt} AP vs $Kmo^{alb\text{-}cre}$ AP, p = 0.520	14.750
n = 6		$Kmo^{alb\text{-}cre}$ 27.9 (25.2)		p = 0.528	Kmo^{wt} AP vs Kmo^{null} AP, p = 0.699	10.800
n = 6		Kmo^{null} 43.9 (17.1)			$Kmo^{alb\text{-}cre}$ AP vs Kmo^{null} AP, p = 0.952	-3.950
Neutrophil	**Sham**	%CD45+	Failed	Kruskal-	n/a	n/a
n = 5		Kmo^{wt} 18.0 (6.4)		Wallis		
n = 7		$Kmo^{alb\text{-}cre}$ 17.6 (3.9)		p = 0.840		
n = 6		Kmo^{null} 18.6 (3.8)				

Table 48. Blood Neutrophil AP, 1-way ANOVA

3.6.6.3. Blood monocytes

There was no significant difference in blood monocyte proportions of leucocytes (**Table 49**), or the proportion of monocytes with $Ly6C^{hi}$ cell surface expression (**Table 50**) with AP across the mouse lines.

Flow - blood Group size	Rx	Median values (Std. deviation)	Normality testing	1-Way ANOVA	Post Hoc	Mean difference
Monocyte	**AP**	%CD45+	Passed	1-way	*Tukey post-hoc multiple testing*	
n = 6		Kmo^{wt} 4.62 (1.73)		ANOVA	Kmo^{wt} AP vs $Kmo^{alb\text{-}cre}$ AP, p = 0.958	0.287
n = 6		$Kmo^{alb\text{-}cre}$ 4.38 (1.20)		p = 0.852	Kmo^{wt} AP vs Kmo^{null} AP, p = 0.948	-0.322
n = 6		Kmo^{null} 5.23 (2.27)			$Kmo^{alb\text{-}cre}$ AP vs Kmo^{null} AP, p = 0.827	-0.610
Monocyte	**Sham**	%CD45+	Passed	1-way	n/a	n/a
n = 5		Kmo^{wt} 4.87 (1.62)		ANOVA		
n = 7		$Kmo^{alb\text{-}cre}$ 5.18 (1.34)		p = 0.205		
n = 6		Kmo^{null} 3.56 (1.25)				

Table 49. Blood Monocyte AP, 1-way ANOVA

Flow - blood Group size	Rx	Median values (Std. deviation)	Normality testing	1-Way ANOVA	Post Hoc	Mean difference
Ly6C hi	**AP**	%Monocytes	Failed	Kruskal-	*Dunn's post-hoc multiple testing*	
n = 6		Kmo^{wt} 44.7 (21.51)		Wallis	Kmo^{wt} AP vs $Kmo^{alb\text{-}cre}$ AP, p = 1.0	2.333
n = 6		$Kmo^{alb\text{-}cre}$ 43.5 (21.53)		p = 0.728	Kmo^{wt} AP vs Kmo^{null} AP, p = 1.0	2.167
n = 6		Kmo^{null} 29.9 (23.81)			$Kmo^{alb\text{-}cre}$ AP vs Kmo^{null} AP, p = 1.0	-0.167
Ly6C hi	**Sham**	%Monocytes	Passed	1-way	n/a	n/a
n = 5		Kmo^{wt} 38.0 (6.5)		ANOVA		
n = 7		$Kmo^{alb\text{-}cre}$ 42.6 (12.0)		p = 0.997		
n = 6		Kmo^{null} 42.5 (10.3)				

Table 50. Blood $Ly6^{hi}$ Monocytes AP, 1-way ANOVA

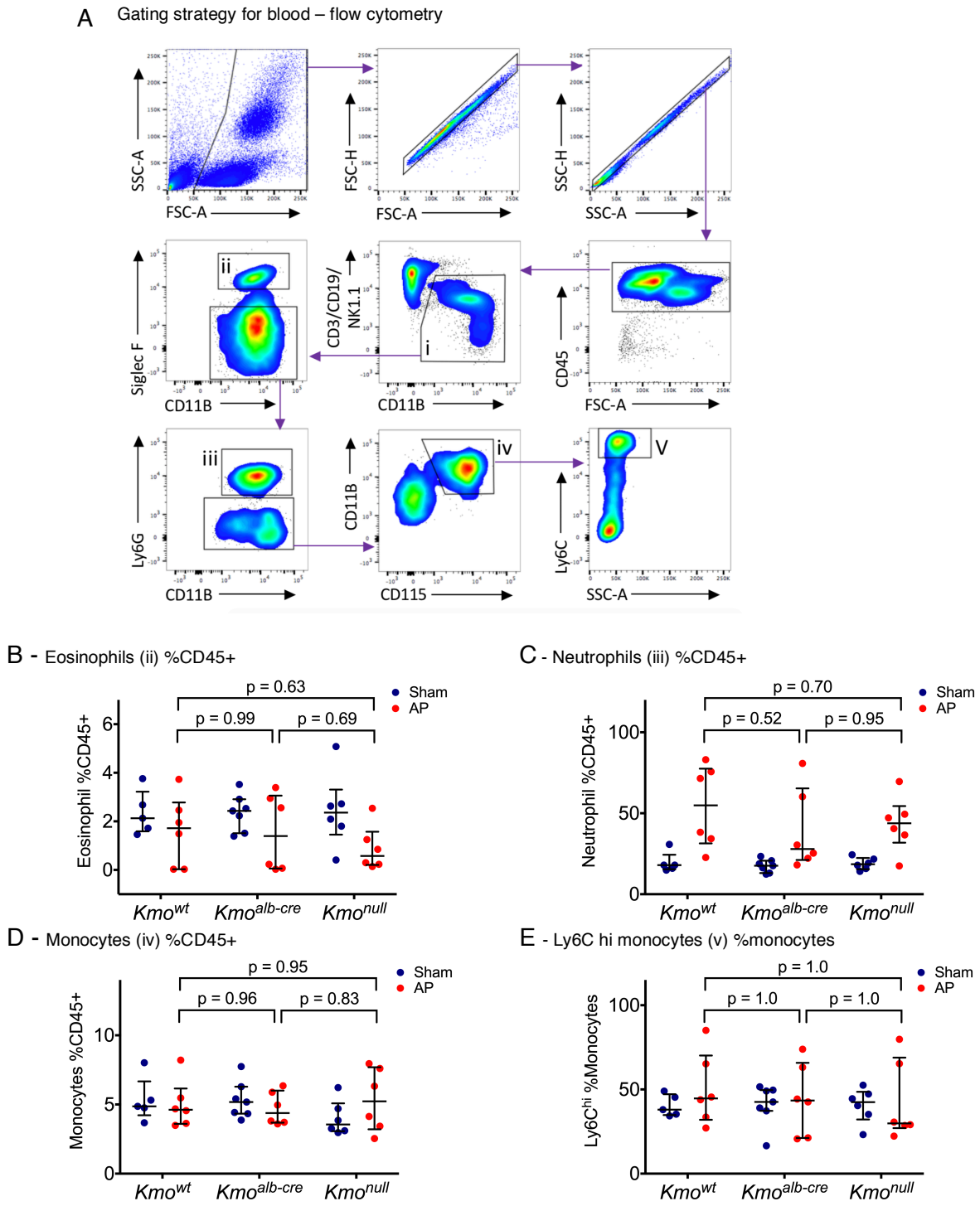

Figure 36. Flow cytometry used to quantify myeloid populations in blood

AP or sham at 24-hrs in Kmo^{wt} and Kmo$^{alb\text{-}cre}$ Kmo^{null} mice. **A**: Flow cytometry gating strategy for blood is shown. First, singlets are gated with side scatter to identify cell populations: CD45+ cells (leukocytes); Sink channel used to remove B cells (CD19+), T cells (CD3+) and NK cells (NK1.1+) from the analysis, leaving myeloid cell population (**i**); blood eosinophils (**ii**) are separated from the myeloid population using Siglec F; neutrophils are isolated as Ly6G+ (**iii**); blood monocyte population (**iv**) identified as CD115+; Ly6C^{hi} blood monocyte population (**v**). Results of blood cell populations are plotted, and statitistical analysis performed using post-hoc subgroup analysis where statistically significant 1-way ANOVA testing was determined. Immunophenotyping: **B**: Eosinophils (CD45+, CD11B+, CD3/CD19/NK1.1 neg, SiglecF hi) as %CD45+ cells; **C**: Neutrophils (CD45+, CD11B+, CD3/CD19/NK1.1 neg, Siglec F lo, Ly6G hi) as %CD45+ cells; **D**: Monocytes (CD45+, CD11B hi, CD3/CD19/NK1.1 neg, Siglec F lo, Ly6G neg, CD115 hi) as %CD45+ cells; **E**: Ly6C^{hi} monocytes as %monocytes. Individual data are shown and horizontal lines are median with interquartile range.

3.6.7. Results – Flow cytometry lung at 24-hr

Flow cytometry was performed on fresh lung digest at 24-hrs following AP or sham in mice from the three genetic lines. Lungs were homogenised into single cell suspensions by mechanical dissociation and enzymatic digestion using a commercial kit designed for lung leukocyte isolation. The gating strategy for flow cytometry of PBS-perfused lung digests and the proportions of myeloid populations are shown in **Figure 37**. Appendix 10, Table 95 lists all of the lung flow cytometery data. Two-way ANOVA was used to statistically test lung flow cytometry populations differences with treatment (**Table 51**).

3.6.7.1. 2-way ANOVA on lung flow cytometry myeloid populations

AP treatment effects on lung myeloid populations across mouse lines are shown in **Table 51**, revealing a statistically significant increase in the proportion of circulating neutrophils (%CD45+) (F-statistic 15.8, $p < 0.001$, 2-way ANOVA), with a mean increase from 7.7% with sham laparotomy to 25.5% in AP. There was a significant decrease in eosinophil proportion of leukocytes with AP (%CD45+) (F-statistic 11.0, $p = 0.002$, 2-way ANOVA), with a mean decrease from 3.9% in shams to 2.0% in AP. After gating out neutrophils, alveolar macrophages and eosinophils, the was a significant increase in infiltrative monocytes in the lung digests of AP mice, from a mean of 9.5% in shams to 12.1% of CD45+ cells in AP (F-statistic 4.8, $p = 0.035$, 2-way ANOVA). There was no significant treatment effect upon Ly6C^{hi} monocyte proportions (%monocytes).

Flow - lung	**Number** (Sham, AP)	**Mean Sham** (St. Dev)	**Mean AP** (St. Dev)	**Mean square**	**F-statistic**	**P-value**
Neutrophil (count, %CD45+)	**19, 19**	**7.745 (2.417)**	**25.457 (18.19)**	**2953.426**	**15.763**	**<0.001**
Eosinophil (count, %CD45+)	**19, 19**	**3.946 (1.433)**	**2.041 (1.954)**	**33.980**	**11.002**	**0.002**
Monocyte (count, %CD45+)	**19, 19**	**9.456 (2.158)**	**12.096 (4.434)**	**65.527**	**4.833**	**0.035**
Ly6C hi monocyte (count, %monocytes)	19, 19	25.74 (7.785)	31.06 (14.080)	259.619	1.827	n/s 0.186

Table 51. Treatment effect (AP versus sham) across mouse lines on lung flow cytometry, 2-way ANOVA

3.6.7.2. Lung neutrophils and eosinophils

There were no significant differences in neutrophil (**Table 52**) or eosinophil (**Table 53**) proprtions of PBS-perfused lung digest leukocytes in AP between *Kmo*^{wt}, *Kmo*$^{alb\text{-}cre}$ or *Kmo*^{null} mouse lines.

Flow - lung Group size	Rx	Median values (Std. deviation)	Normality testing	1-Way ANOVA	Post Hoc	Mean difference
Neutrophil n = 6 n = 7 n = 6	**AP**	%CD45+ Kmo^{wt} 24.52 (19.43) $Kmo^{alb\text{-}cre}$ 20.26 (23.10) Kmo^{null} 23.15 (12.92)	Passed	1-way ANOVA p = 0.074	*Tukey post-hoc multiple testing* Kmo^{wt} AP vs $Kmo^{alb\text{-}cre}$ AP, p = 0.965 Kmo^{wt} AP vs Kmo^{null} AP, p = 0.924 $Kmo^{alb\text{-}cre}$ AP vs Kmo^{null} AP, p = 0.990	 2.736 4.218 1.482
Neutrophil n = 6 n = 7 n = 6	**Sham**	%CD45+ Kmo^{wt} 7.65 (3.26) $Kmo^{alb\text{-}cre}$ 6.67 (2.01) Kmo^{null} 8.63 (1.83)	Passed	1-way ANOVA p = 0.410	n/a	n/a

Table 52. Lung Neutrophil AP, 1-way ANOVA

Flow - lung Group size	Rx	Median values (Std. deviation)	Normality testing	1-Way ANOVA	Post Hoc	Mean difference
Eosinophil n = 6 n = 7 n = 6	**AP**	%CD45+ Kmo^{wt} 3.54 (1.96) $Kmo^{alb\text{-}cre}$ 0.29 (2.37) Kmo^{null} 1.28 (1.57)	Failed	Kruskal- Wallis p = 0.780	*Dunn's post-hoc multiple testing* Kmo^{wt} AP vs $Kmo^{alb\text{-}cre}$ AP, p = 1.0 Kmo^{wt} AP vs Kmo^{null} AP, p = 1.0 $Kmo^{alb\text{-}cre}$ AP vs Kmo^{null} AP, p = 1.0	 0.56 2.25 1.69
Eosinophil n = 6 n = 7 n = 6	**Sham**	%CD45+ Kmo^{wt} 3.48 (0.91) $Kmo^{alb\text{-}cre}$ 4.34 (0.90) Kmo^{null} 4.50 (2.22)	Passed	1-way ANOVA p = 0.469	n/a	n/a

Table 53. Lung Eosinophil AP, 1-way ANOVA

3.6.7.3. Lung monocytes

Similarly, there was no significant difference in infiltrative (non-alveolar) monocytes proportions of CD45+ cells between AP groups across the 3 mouse lines (**Table 54**), nor was there any significant difference in Ly6C cell surface expression of monocytes (**Table 55**).

Flow - lung Group size	Rx	Median values (Std. deviation)	Normality testing	1-Way ANOVA	Post Hoc	Mean difference
Monocyte n = 6 n = 7 n = 6	**AP**	%CD45+ Kmo^{wt} 11.43 (3.83) $Kmo^{alb\text{-}cre}$ 11.40 (4.20) Kmo^{null} 9.33 (5.85)	Passed	1-way ANOVA p = 0.086	*Tukey post-hoc multiple testing* Kmo^{wt} AP vs $Kmo^{alb\text{-}cre}$ AP, p = 0.997 Kmo^{wt} AP vs Kmo^{null} AP, p = 0.922 $Kmo^{alb\text{-}cre}$ AP vs Kmo^{null} AP, p = 0.942	 0.184 1.043 0.860
Monocyte n = 6 n = 7 n = 6	**Sham**	%CD45+ Kmo^{wt} 8.80 (2.09) $Kmo^{alb\text{-}cre}$ 8.41 (2.36) Kmo^{null} 9.69 (2.39)	Passed	1-way ANOVA p = 0.989	n/a	n/a

Table 54. Lung Monocyte AP, 1-way ANOVA

Flow - lung Group size	Rx	Median values (Std. deviation)	Normality testing	1-Way ANOVA	Post Hoc	Mean difference
Ly6C hi n = 6 n = 7 n = 6	**AP**	%Monocytes Kmo^{wt} 28.65 (8.64) $Kmo^{alb\text{-}cre}$ 31.76 (17.32) Kmo^{null} 24.18 (16.19)	Failed	Kruskal- Wallis p = 0.701	*Dunn's post-hoc multiple testing* Kmo^{wt} AP vs $Kmo^{alb\text{-}cre}$ AP, p = 1.0 Kmo^{wt} AP vs Kmo^{null} AP, p = 1.0 $Kmo^{alb\text{-}cre}$ AP vs Kmo^{null} AP, p = 1.0	 0.119 2.500 2.381
Ly6C hi n = 6 n = 7 n = 6	**Sham**	%Monocytes Kmo^{wt} 23.49 (9.96) $Kmo^{alb\text{-}cre}$ 24.07 (8.79) Kmo^{null} 25.15 (4.63)	Passed	1-way ANOVA p = 0.830	n/a	n/a

Table 55. Lung $Ly6^{hi}$ Monocytes AP, 1-way ANOVA

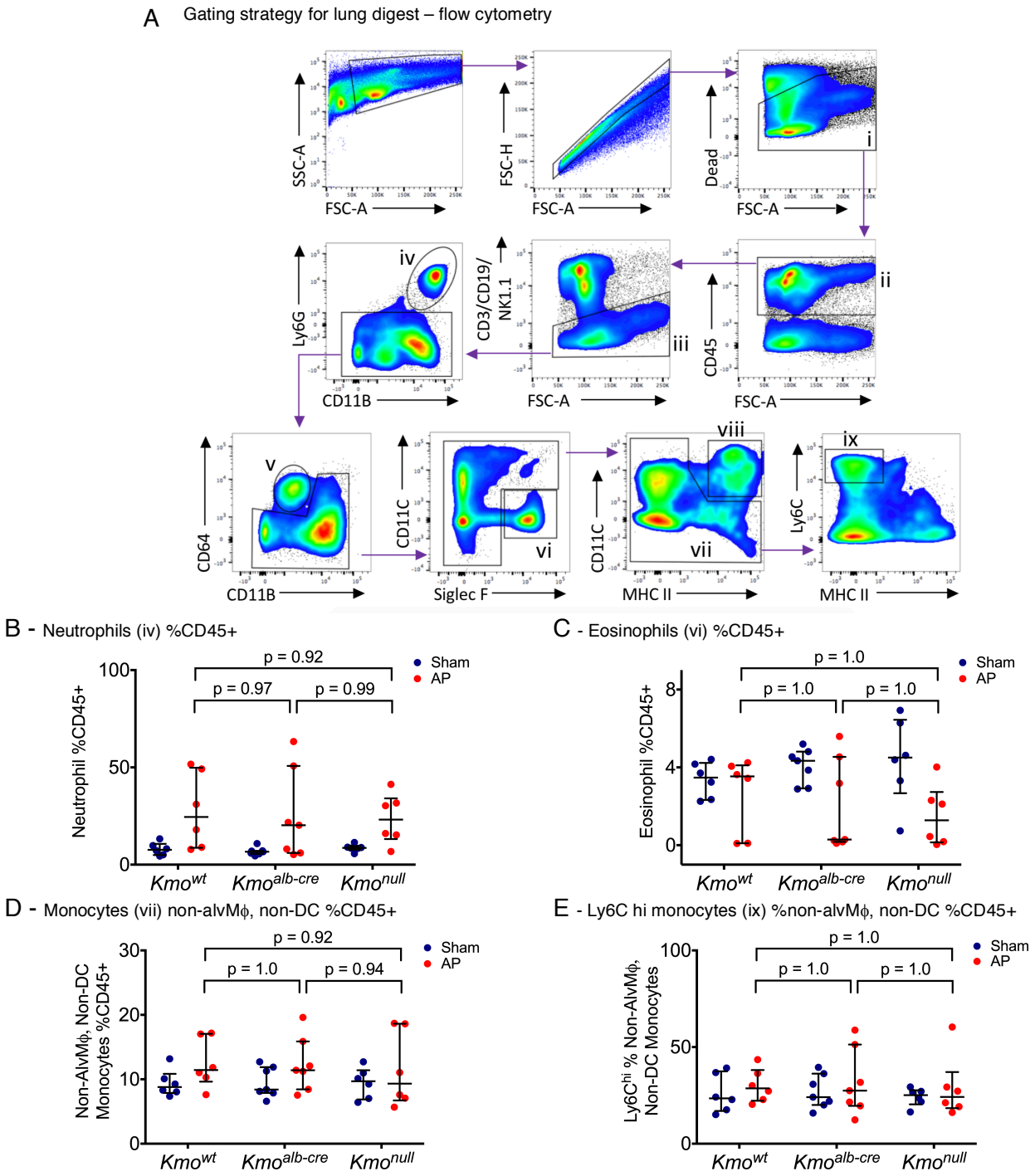

Figure 37. Flow cytometry used to quantify myeloid populations in lung digest

AP or sham at 24-hrs in Kmo^{wt} and Kmo$^{alb\text{-}cre}$ Kmo^{null} mice. **A**: Flow cytometry gating strategy for lung digest is shown. First, singlets are gated with side scatter to identify cell populations: Dead marker used to gate live cells (**i**); CD45+ cells (leukocytes) identified (**ii**); Sink channel used to remove B cells (CD19+), T cells (CD3+) and NK cells (NK1.1+) from the analysis, leaving myeloid cell population (**iii**); neutrophil population are isolated as Ly6G+ (**iv**); alveolar macrophages (**v**); eosinophils (**vi**); infiltrative monocytes (non-alveolar macrophages/ non-dendritic cells)(**vii**); lung dendritic cells (**viii**), Ly6C ^{hi} monocyte subpopulation (**ix**). Immunophenotyping: **B**: Neutrophils (non-dead, CD45+, CD3/CD19/NK1.1 neg, CD11B hi, Ly6G hi), **C**: Eosinophils (non-dead, CD45+, CD3/CD19/NK1.1 neg, Ly6G neg, CD64 lo, CD11C neg, Siglec-F hi). **D**: Infiltrative monocytes (non-dead, CD45+, CD3/CD19/NK1.1 neg, Ly6G neg, CD64 lo, non-CD11C/MHCII double pos); **E**: Ly6C^{hi} monocytes. Individual data are shown and horizontal lines are median with interquartile range.

3.6.8. Results – Flow cytometry liver at 24-hr

As with the lungs, flow cytometry was performed on fresh liver digests at 24-hrs following AP or sham in mice from the three genetic lines. Livers were homogenised into single cell suspensions by mechanical dissociation and enzymatic digestion using a commercial kit designed for liver leukocyte isolation. The gating strategy for flow cytometry of PBS-perfused liver digests and the proportions of myeloid populations are shown in **Figure 38**. Appendix 10, Table 97 lists all of the liver flow cytometery data.

3.6.8.1. 2-way ANOVA on liver flow cytometry myeloid populations

AP treatment effects on liver leukocyte populations across mouse lines are shown in **Table 56**, revealing a statistically significant increase in the proportion of circulating neutrophils (%CD45+) (F-statistic 20.3, $p < 0.001$, 2-way ANOVA), with a mean increase from 7.8% with sham laparotomy to 15.3% in AP, across the mouse lines with AP. There was a significant decrease in eosinophil proportion of leukocytes with AP (%CD45+) (F-statistic 29.0, $p < 0.001$, 2-way ANOVA), with a mean decrease from 4.9% in shams to 2.0% in AP. There was no significant treatment effect upon non-Kupffer/non-DC monocytes (%CD45+) or Ly6C^{hi} monocyte proportions (%monocytes).

Flow - liver	**Number** (Sham, AP)	**Mean Sham** (St. Dev)	**Mean AP** (St. Dev)	**Mean square**	**F-statistic**	**P-value**
Neutrophil (count, %CD45+)	**19, 18**	**7.86 (1.932)**	**15.32 (6.976)**	**515.212**	**20.308**	**<0.001**
Eosinophil (count, %CD45+)	**19, 18**	**4.86 (1.802)**	**2.05 (1.317)**	**70.344**	**29.008**	**<0.001**
Non-Kupffer/ non-DC monocytes (count, %CD45+)	19, 18	12.18 (4.45)	10.05 (2.41)	40.53	2.891	n/s 0.099
Ly6C^{hi} infiltrative monocytes (count, %monocytes)	19, 18	37.20 (7.23)	38.74 (10.19)	21.239	0.293	n/s 0.592

Table 56. Treatment effect (AP versus sham) across mouse lines on liver flow cytometry, 2-way ANOVA

3.6.8.2. Liver neutrophils and eosinophils

There was no significant difference in neutrophils (**Table 57**) or eosinophils (**Table 58**) proprtions of PBS-perfused liver digest leukocytes comparing AP groups across the 3 mouse lines: *Kmo*^{wt}, *Kmo*$^{alb\text{-}cre}$ or *Kmo*^{null}.

Flow - liver Group size	Rx	Median values (Std. deviation)	Normality testing	1-Way ANOVA	Post Hoc	Mean difference
Neutrophil	**AP**	%CD45+	Passed	1-way	*Tukey post-hoc multiple testing*	
n = 6		Kmo^{wt} 18.17 (8.90)		ANOVA	Kmo^{wt} AP vs $Kmo^{alb\text{-}cre}$ AP, p = 0.323	5.965
n = 6		$Kmo^{alb\text{-}cre}$ 11.96 (4.41)		p = 0.354	Kmo^{wt} AP vs Kmo^{null} AP, p = 0.702	3.245
n = 6		Kmo^{null} 13.07 (6.73)			$Kmo^{alb\text{-}cre}$ AP vs Kmo^{null} AP, p = 0.779	-2.720
Neutrophil	**Sham**	%CD45+	Passed	1-way	n/a	n/a
n = 6		Kmo^{wt} 7.43 (1.50)		ANOVA		
n = 7		$Kmo^{alb\text{-}cre}$ 7.20 (2.67)		p = 0.891		
n = 6		Kmo^{null} 8.17 (1.57)				

Table 57. Liver Neutrophil AP, 1-way ANOVA

Flow - liver Group size	Rx	Median values (Std. deviation)	Normality testing	1-Way ANOVA	Post Hoc	Mean difference
Eosinophil	**AP**	%CD45+	Passed	1-way	*Tukey post-hoc multiple testing*	
n = 6		Kmo^{wt} 2.24 (1.09)		ANOVA	Kmo^{wt} AP vs $Kmo^{alb\text{-}cre}$ AP, p = 0.945	0.248
n = 6		$Kmo^{alb\text{-}cre}$ 2.07 (1.60)		p = 0.494	Kmo^{wt} AP vs Kmo^{null} AP, p = 0.485	0.908
n = 6		Kmo^{null} 1.17 (1.27)			$Kmo^{alb\text{-}cre}$ AP vs Kmo^{null} AP, p = 0.676	0.660
Eosinophil	**Sham**	%CD45+	Passed	1-way	n/a	n/a
n = 6		Kmo^{wt} 4.88 (1.28)		ANOVA		
n = 7		$Kmo^{alb\text{-}cre}$ 6.38 (2.16)		p = 0.219		
n = 6		Kmo^{null} 4.67 (1.57)				

Table 58. Liver Eosinophil AP, 1-way ANOVA

3.6.8.3. Liver monocytes (non-Kupffer/ non-DC) and $Ly6C^{hi}$ monocytes

Similarly, there was no significant difference in infiltrative (non-Kupffer/non-DC) monocytes proportions of CD45+ cells in PBS-perfused liver digests between AP groups across the 3 mouse lines (**Table 59**). Nor was there any significant difference in Ly6C cell surface expression of these infiltrative monocytes (**Table 60**).

Flow - liver Group size	Rx	Median values (Std. deviation)	Normality testing	1-Way ANOVA	Post Hoc	Mean difference
Monocyte	**AP**	%CD45+	Passed	1-way	*Tukey post-hoc multiple testing*	
n = 6		Kmo^{wt} 11.84 (4.58)		ANOVA	Kmo^{wt} AP vs $Kmo^{alb\text{-}cre}$ AP, p = 0.918	-1.073
n = 6		$Kmo^{alb\text{-}cre}$ 11.23 (5.70)		p = 0.906	Kmo^{wt} AP vs Kmo^{null} AP, p = 0.999	-0.050
n = 6		Kmo^{null} 12.89 (3.63)			$Kmo^{alb\text{-}cre}$ AP vs Kmo^{null} AP, p = 0.925	1.023
Monocyte	**Sham**	%CD45+	Passed	1-way	n/a	n/a
n = 6		Kmo^{wt} 10.11 (3.16)		ANOVA		
n = 7		$Kmo^{alb\text{-}cre}$ 8.52 (1.84)		p = 0.818		
n = 6		Kmo^{null} 10.96 (2.51)				

Table 59. Liver Monocyte AP, 1-way ANOVA

Flow - liver Group size	Rx	Median values (Std. deviation)	Normality testing	1-Way ANOVA	Post Hoc	Mean difference
Ly6C hi	**AP**	%Monocytes	Passed	1-way	*Tukey post-hoc multiple testing*	
n = 6		Kmo^{wt} 34.70 (7.93)		ANOVA	Kmo^{wt} AP vs $Kmo^{alb\text{-}cre}$ AP, p = 0.857	-2.872
n = 6		$Kmo^{alb\text{-}cre}$ 38.67 (10.65)		p = 0.110	Kmo^{wt} AP vs Kmo^{null} AP, p = 0.109	-11.740
n = 6		Kmo^{null} 46.82 (9.31)			$Kmo^{alb\text{-}cre}$ AP vs Kmo^{null} AP, p = 0.260	-8.867
Ly6C hi	**Sham**	%Monocytes	Passed	1-way	n/a	n/a
n = 6		Kmo^{wt} 42.73 (9.76)		ANOVA		
n = 7		$Kmo^{alb\text{-}cre}$ 35.96 (5.74)		p = 0.948		
n = 6		Kmo^{null} 34.96 (7.22)				

Table 60. Liver $Ly6^{hi}$ Monocytes AP, 1-way ANOVA

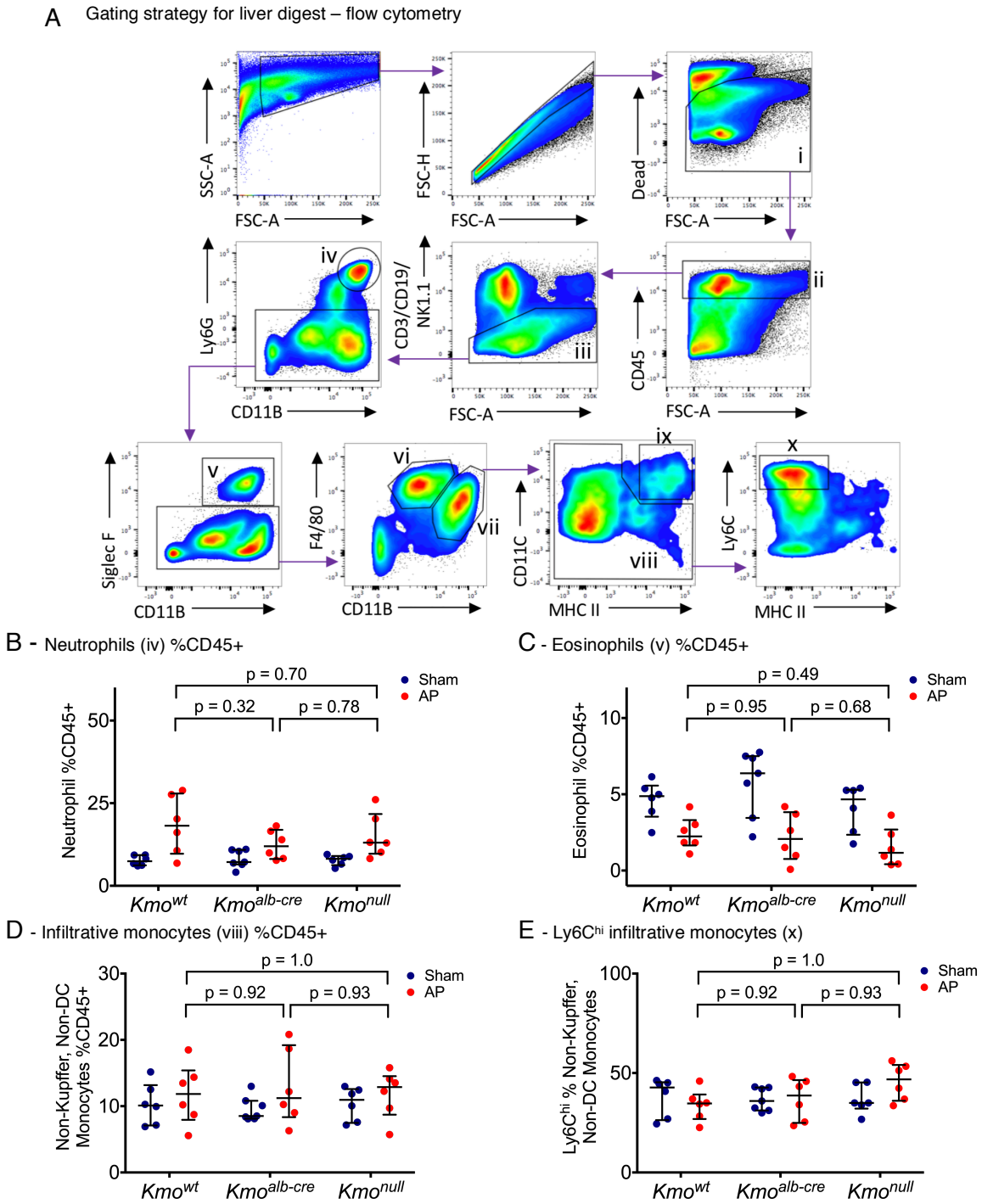

Figure 38. Flow cytometry used to quantify myeloid populations in liver digest

AP or sham at 24-hrs in Kmo^{wt} and Kmo$^{alb\text{-}cre}$ Kmo^{null} mice. **A**: Flow cytometry gating strategy for liver digest is shown. First, singlets are gated with side scatter to identify cell populations: Dead marker used to gate live cells (**i**); CD45+ cells (leukocytes) identified (**ii**); Sink channel used to remove B cells (CD19+), T cells (CD3+) and NK cells (NK1.1+) from the analysis, leaving myeloid cell population (**iii**); neutrophil population are isolated as Ly6G hi/ CD11B hi (**iv**); Eosinophils identified as Siglec F hi (**v**); Kupffer cell monocytes by F4/80 hi (**vi**); Infiltrative monocytes (non-Kupffer/ non-dendritic cells) (**vii**); liver dendritic cells (**ix**), Ly6C ^{hi} monocyte/ macrophage subpopulation (**x**). Immunophenotyping: **B**: Neutrophils (non-dead, CD45+, CD3/CD19/NK1.1 neg, CD11B hi, Ly6G hi); **C**: Eosinophils (non-dead, CD45+, CD3/CD19/NK1.1 neg, Ly6G neg, CD11B hi, Siglec-F hi); **D**: Infiltrative monocytes (non-dead, CD45+, CD3/CD19/NK1.1 neg, Ly6G neg, CD11B hi, non-CD11C/MHCII double pos); **E**: Ly6C^{hi} infiltrative monocytes. Individual data are shown and horizontal lines are median with interquartile range.

3.6.9. Results – Kynurenine metabolites at 24-hr

Two-way ANOVA was used to statistically test for changes in blood plasma kynurenine metabolites concentrations with treatment (AP versus sham) across the mouse lines on and is shown in **Table 61**. The only metabolite found to differ significantly was an associated increase in 3-hydroxykynrenine (F-statistic 4.8, p = 0.034, 2-way ANOVA) with AP treatment.

Kynurenine metabolites	Number (Sham, AP)	Mean Sham (μM) (St. Dev)	Mean AP (μM) (St. Dev)	Mean square	F-statistic	P-value
Tryptophan	23, 23	20950 (3634)	19611 (5153)	25690848	1.436	n/s 0.238
Kynurenine	23, 23	2371 (2654)	2945 (2411)	4065952.7	1.588	n/s 0.215
Kynurenic acid	23, 23	288.8 (489.3)	493.2 (561.2)	494660.2	3.294	n/s 0.077
Anthranilic acid	23, 23	66.6 (70.4)	75.2 (64.0)	887.6	0.421	n/s 0.520
3-Hydroxykyurenine	**23, 23**	**16.4 (29.3)**	**101.6 (243.8)**	**99892.9**	**4.801**	**0.034**
3-Hydroxy-anthranilic acid	23, 23	2.86 (3.99)	2.48 (2.01)	1.493	0.702	n/s 0.702
Xanthurenic acid	23, 23	101.6 (250.6)	162.9 (490.4)	53430.	0.417	n/s 0.522
Picolinic acid	23, 23	11.81 (3.78)	29.93 (53.64)	4574.9	4.076	n/s 0.050

Table 61. Treatment effect across mouse line groups on kynurenine metabolites, 2-way ANOVA

3.6.10. Conclusions - Experiment 4

The purpose of experiment 4 studies was to investigate for mechanistic insights which might explain the dramatic results seen in the previous experiment (#3); specifically, to investigate why *Kmo*$^{alb\text{-}cre}$ mice appeared more susceptible to severe sickness in experimental AP over 7-days using a recovery disease model. Specifically, these studies were designed to detect differences in the primary pancreatic injury (histology and amylase), activation of the cellular component of the innate immune response (blood flow cytometry), the humoral innate response (plasma cytokines), innate cellular organ infiltration (lung and liver flow cytometry) and end-organ dysfunction (LDH, ALT, albumin, urea, glucose), as well as to assess for flux in the kynurenine pathway. Unlike the results in experiment 3, however, which had shown a distinct difference in the response to AP by way of increased sickness behaviour by *Kmo*$^{alb\text{-}cre}$ mice, at 24-hrs in this recovery AP model, few significant differences were found between *Kmo*^{wt}, *Kmo*$^{alb\text{-}cre}$ and *Kmo*^{null} mouse lines. However, the following conclusions in relation to the effect of AP, and effect of mouse lines can be drawn from the data:

***Effects of AP**, compared to sham (24-hr in 2% NaTCA model)*

1) Elevated plasma amylase, LDH, and urea concentrations
2) Reduction in plasma glucose and albumin concentrations
3) Elevated pancreas injury histology score
4) Elevated plasma levels of IL-1β, IL-2, IL-6, TNFα, and KC/GRO
5) No difference in IL-4, IL-5, IL-10, IL-12p70 and IFNγ levels

6) Increased neutrophil proportions in blood, and lung and liver digests
7) Increased proportion of infiltrative monocytes in lung (but not liver), but no increase in Ly6C expression
8) Decreased proportion of eosinophils in blood, lung and liver. Likely secondary to neutrophilia
9) Increase in plasma 3HK concentrations, but not other kynurenine metabolites

Effects of mouse line *(other than kynurenine metabolite changes)*

1) No difference in amylase or pancreatic injury scores between mouse lines
2) *Kmo*^{null} mice had lower ALT levels that other mouse lines after surgery (regardless of sham or AP treatment)
3) *Kmo*$^{alb\text{-}cre}$ mice had elevated IL-2 and IL-4 levels in AP compared to other mouse lines, and had elevated IL-12p70 concentrations in both sham and AP
4) No differences in myeloid innate immune cell proportions due to mouse line

3.7. Experiment 5 – KMO inhibition prevents early critical illness in recovery AP

3.7.1. Background

The KMO inhibitor (KMOi) drug compound used in these studies, referred to as 'GSK898', was a kind gift from collaborators at GSK. This compound was found to have good oral bioavailability, having undergone PKPD (pharmacokinetic/pharmacodynamic) testing by the pharmaceutical laboratory. The particular data regarding the biochemical and PKPD properties of GSK898 were reviewed during in a joint drug discovery partnership with academia (DPAc) meeting between the Mole Group and GSK, but were not made available for publication in this thesis as they were the intellectual property of GlaxoSmithKline.

The compound became available during experiment number 3, when 7-day comparisons between *Kmo*^{wt}, *Kmo*^{null} and *Kmo*$^{alb\text{-}cre}$ mouse lines found impaired survival of the latter group with AP. Around this same time, I had conducted plasma kynurenine metabolite analysis and discovered that *Kmo*$^{alb\text{-}cre}$ mice had elevated circulating plasma 3HK levels (see experiment #2). After discussions with GSK collaborators, I decided to add-in a 'KMO inhibitor *Kmo*$^{alb\text{-}cre}$ AP' group, to test the efficacy of the drug in reducing sickness behaviour and survival. This was not unreasonable because when conducting telemetered experiements, staggering of groups is unavoidable, as there is a finite number of hardward units (i.e. no more than 8 mice). Further groups of AP mice were randomly assigned to either 'KMOi drinking water' or 'vehicle/normal drinking water' (using a random number generator function in Excel, Microsoft), making this add-in group scientifically justifiable. By way of explanation with regards to unavoidable group staggering, repeated use of the same telemeters in different groups is best practice, rather than using different telemeters for different groups which could bias telemeter data if one group of telemeters does not function well. Also, induction of pancreatitis and telemeter implantation is time consuming and only up to n = 4 mice can added on a single day, allowing adequate time for surgery and recovery from anaesthesia to start telemetry recording at 13:00hrs, which was half way through the 12-hr light phase. Accordingly, I used additional *Kmo*$^{alb\text{-}cre}$ mice of appropriate age from the breeding colony, randomising available *Kmo*$^{alb\text{-}cre}$ littermates in a 2:1 or 3:1 (Drug: Vehicle) ratio. The drug delivery was by drinking water, maintaining vehicle equivalence with previous groups in which all mice had *ad libitum* access to drinking water.

A pilot study was performed to ensure suitable drinking water GSK898 dosing (3HK concentrations by LC/MS-MS) for *Kmo*$^{alb\text{-}cre}$ mice. In this pilot study, male adult mice were randomised to 3-days drinking water with GSK898 at 0.25mg/ml or vehicle (drinking water without drug. This dose of GSK838 gave a mean 6.5-fold reduction in [3HK] (vehicle mean

0.441 μM, standard error of mean (SEM) 0.110 μM, range 0.180 to 0.715 μM; 0.25mg/ml GSK898 mean 0.068 μM, SEM 0.010 μM, range 0.046 to 0.085 μM) (p = 0.042, *t*-test Welch), or can be understood as an 85% reduction of vehicle [3HK] concentrations. These data are documented in Appendix 11 Table 99. As there was opportunity for further reduction in 3HK levels the concentration of the drug was therefore doubled. Therefore, the **drug concentration for the oral KMO inhibitor study was 0.5 mg/ml GSK898** (in filtered water). A sonicade device was used to aid dissolution of the compound in water. Higher concentrations might have been achievable with the use of solvents such as DMSO or PEG but adding such substances to the drug group would necessitate adding these to the vehicle group, and would have made void the drinking water group without such additives and was therefore not performed for the drinking water drug study. DMSO and PEG solvents are not biologically inert and are known to have effects on the immune system and thus their use (i.e. in minipump study and cytokine experiments described later) is minimised and with the use of solvent-added controls. Aqueous KMOi solution was protected from light to remove the possibility of photochemical degredation.

3.7.2. Hypotheses

Treatment with KMOi in AP, compared to vehicle, improves sickness behaviour and survival (to humane endpoints).

3.7.3. Results – Oral KMOi study

Details of the study participants are listed in Appendix 11 and all mice used in the KMOi studies were *Kmo*$^{alb\text{-}cre}$, the line with elevated steady-state 3HK levels. Briefly, the experiment consisted of n = 7 sham *Kmo*$^{alb\text{-}cre}$ mice (vehicle drinking water), n = 13 AP *Kmo*$^{alb\text{-}cre}$ mice (vehicle water), and n = 8 AP *Kmo*$^{alb\text{-}cre}$ mice (GSK898 drinking water 0.5 mg/ml).

3.7.3.1. Analgesia consumption

The mean subcutaneous buprenorphine dosing was significantly greater in the KMOi drinking water AP group which received the greatest mean dose (6.47 μg) (**Table 62**). However, the time-adjusted dosing was equivalent between groups (p = 0.096, 1-W ANOVA). This can be explained by longer survival of AP mice in the KMOi group compared to AP vehicle.

The mean oral buprenorphine dose consumed was significantly higher (p = 0.044, 1-W ANOVA) in the Sham group compared to the AP groups, which can be explained by an improved voluntary oral intake compared to AP mice, as well as longer survival (with daily oral analgesia supply). Therefore, because overall AP mice had reduced survival times, there were

Line	Treatment	Number	Exp duration – mean (SD)	S/C Bup. Dose – mean (SD)	S/C Bup. Dose : Time adjusted – mean (SD)	Oral Bup. Dose – mean (SD)	Oral Bup. Dose : Time adjusted – mean (SD)
$Kmo^{alb\text{-}cre}$	Sham + VDW	N = 7	168.0 (0) hrs	4.500 (0.000) μg	0.027 (0.000) μg/hr	68.57 (03.78) μg	0.408 (0.021) μg/hr
$Kmo^{alb\text{-}cre}$	AP + VDW	N = 13	98.1 (68.0) hrs	4.904 (0.998) μg	0.092 (0.069) μg/hr	32.54 (35.13) μg	0.205 (0.205) μg/hr
$Kmo^{alb\text{-}cre}$	AP + KMOiDW	N = 8	124.7 (46.3) hrs	6.469 (2.081) μg	0.067 (0.053) μg/hr	47.00 (21.92) μg	0.365 (0.072) μg/hr
1-way ANOVA between 3 groups			***p = 0.043, KW**	***p = 0.046, KW**	**ns p = 0.096, KW**	***p = 0.044, KW**	**ns p = 0.065, KW**

Table 62. Analgesia given in AP oral KMOi

VDW: Vehicle drinking water (filtered water); KMOiDW: KMO inhibitor drinking water. Oral Buprenorphine single dose 0.01 mg. S/C Buprenorphine single dose 0.05 mg/kg. KW: Kruskal-Wallis. *p < 0.05.

no significant differences (p = 0.065, 1-W ANOVA) with time-adjusted oral buprenorphine consumption.

3.7.3.2. Telemetry and humane endpoints

Sham-operated control *Kmo*$^{alb\text{-}cre}$ mice (n = 7) showed a higher activities levels throughout compared to AP, with a repeated normal physiological crepuscular pattern from 48-hrs onwards (**Figure 40A**, next page). Additionally, sham-operated mice established baseline oscillating core body temperature profiles after 48-hrs, and without significant hypothermic episodes seen with critically ill AP mice (**Figure 40B**, next page).

Unlike sham mice, the main finding with AP-treated mice was the tendency to develop of profound persistent hypothermia, which occurred earlier in vehicle mice (all occurred ~24 to 48-hrs), but mostly later in KMOi AP mice (Figure 40A). By the end of the 7-day experimental period, however, a similar proportion of mice in each AP group had deteriorated to predefined humane endpoints requiring humane cull (**Figure 39A**): Specifically, 5 of 8 with KMOi, and 9 of 13 vehicle mice were sacrified early. Whilst there was no significant difference in survival

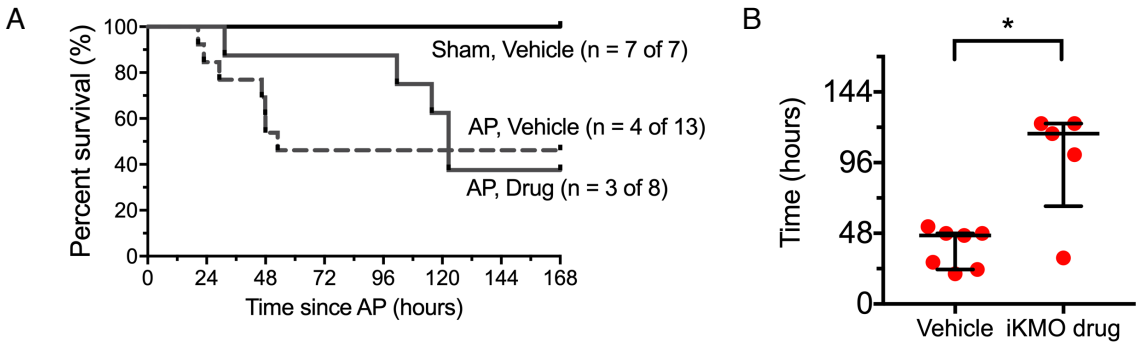

Figure 39. Survival in oral KMOi drug study

Oral drug 0.5mg/ml GSK898. **A**: Median survival of AP Vehicle = 52.9-hr. Median survival AP KMOi 112.6-hr. Log-rank (Mantel-Cox) between AP vehicle and AP drug p=0.810, chi square 0.05. Comparison of AP Vehicle to sham vehicle, p = 0.024, chi square 5.071; AP drug to sham vehicle 0.0143, chi square 6.00. **B**: Comparison of survival time to humane endpoint between AP vehicle and AP drug in non-survivors. T-test with Welch's correction for heterogenous data distribution p = 0.022. Individual data are shown and horizontal lines are median with interquartile range. ns = not significant (p > 0.05); *p < 0.05.

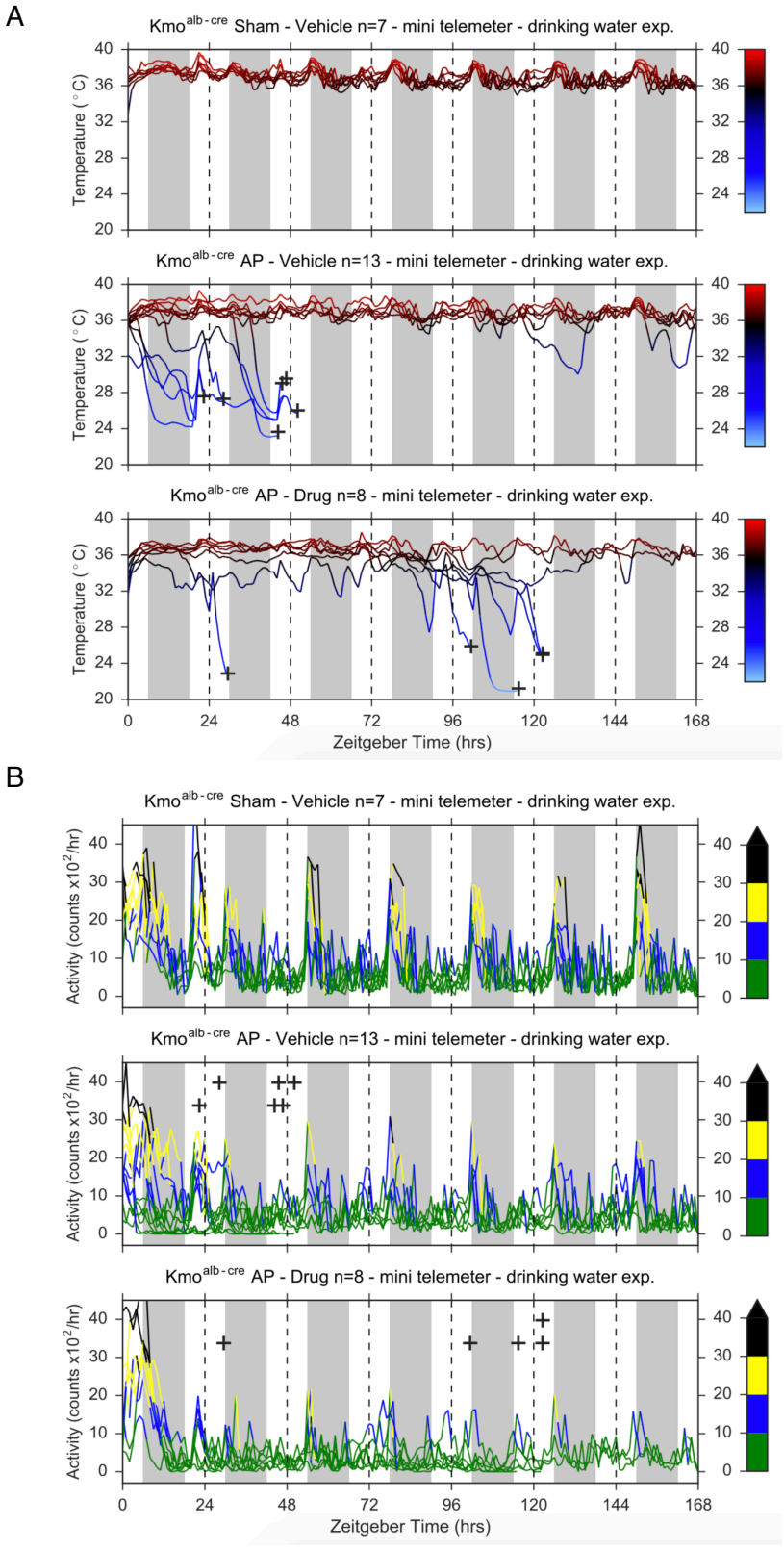

Figure 40. Telemetry in AP - vehicle drinking water versus GSK898 oral drug study. A: Core body temperature. **B**: Locomotor activity. '**+**' symbol represents timepoint of removal from study due to reaching humane cull endpoint.

curves at 7-days, it was notable that the vehicle mice died significantly earlier (median 53-hrs) than the KMOi group (median 113-hrs) (**Figure 39B**, above).

Oral KMOi consumption was monitored daily by recording drinking bottle weights. **Figure 41** shows daily mean KMOi drinking water fluid consumption (with standard error of the mean error bars) starting from 3-days prior to AP when the KMOi drinking water was introduced. It is noted that after AP, oral consumption of drinking water reduced compared to the pre-AP levels, for at least 5 days after AP. After 5-days mice tend to be drinking more or else have died. Since drug delivery was through the oral route, one explanation for the late deaths in the KMOi group could be that the plasma drug concentrations dropped below the threshold required for 3HK suppression, and thereby loosing a mechanism of protection against critical illness.

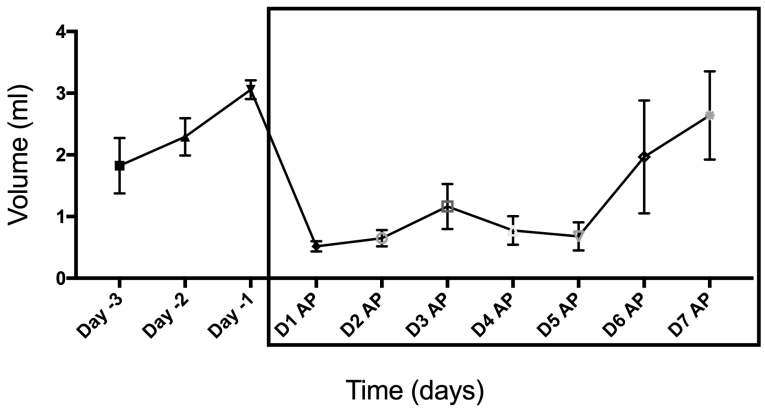

Figure 41. Oral KMO inhibitor drug consumption
Consumption of drugged drinking water at concentration of 0.5 mg/ml GSK898). Symbols are mean, error bars are standard error of the mean (SEM). Volume (y-axis) is volume of drugged water consumed per day.

3.7.4. Results – Mini pump KMOi study

Following the oral KMOi experiment, a parenteral study was designed to better evaluate whether inhibition of KMO provides protection against AP-MODS in the *Kmo*$^{alb\text{-}cre}$ mice, using a mini pump continuous drug administration technique. These animals underwent induction of AP and non-cardiac mini telemeter implantation 3 days after implantation of the Alzet 1002 osmotic pump [100 µl reservoir, 0.25 µl/hr, duration 14 days]. The pump contained KMO inhibitor drug (GSK898, 250 mg/ml, in 50:50 DMSO:PEG 400) or vehicle (50:50 DMSO:PEG 400). Manufacteurer documentation with the osmotic pumps listed 50:50 DMSO:PEG 400 as a compatible solvent mixture for the Alzet pumps. Given that the mini pump concentration was 500-fold greater than that used the oral drug study, a dual-solvent vehicle with both DMSO and PEG was employed.

3.7.4.1. Analgesia consumption

There were no significant differences in subcutaneous buprenorphine administration or oral buprenorphine dose consumption between AP groups treated with mini pump vehicle or KMOi (**Table 63**).

Line	Treatment	Number	Exp duration – mean (SD)	S/C Bup. Dose – mean (SD)	S/C Bup. Dose : Time adjusted – mean (SD)	Oral Bup. Dose – mean (SD)	Oral Bup. Dose : Time adjusted – mean (SD)
$Kmo^{alb\text{-}cre}$	AP + PumpV	N = 10	139.6 (59.8) hrs	4.175 (0.635) μg	0.050 (0.054) μg/hr	34.00 (35.14) μg	0.203 (0.209) μg/hr
$Kmo^{alb\text{-}cre}$	AP + PumpKi	N = 07	167.8 (0.45) hrs	4.286 (0.466) μg	0.026 (0.003) μg/hr	47.14 (32.51) μg	0.281 (0.194) μg/hr
MWU test between 2 groups			**ns p = 0.691**	**ns p = 0.842**	**ns p = 0.695**	**ns p = 0.678**	**ns p = 0.556**

Table 63. Analgesia given in AP mini pump

PumpV: Vehicle solution (DMSO/PEG); PKi: KMO inhibitor 250 mg/ml in DMSO/PEG. Oral Buprenorphine single dose 0.01 mg. S/C Buprenorphine single dose 0.05 mg/kg. MWU: Mann Whitney U test. ns: not significant.

3.7.4.2. Telemetry and humane endpoints

Two *Kmo*$^{alb\text{-}cre}$ mice with AP treated with vehicle reached the humane endpoint <30-hrs after AP and were humanely culled, whilst KMOi-treated mice all survived into the 7th day, albeit with one mouse reaching a humane endpoint at 166-hrs (see telemetry data overleaf in **Figure 42**). Plasma GKS898 drug levels (**Figure 43A**) and [3HK] levels (**Figure 43B**) were measured in all subjects at the time of euthanasia (at humane endpoint or after the standard 168-hr experiment endpoint), and a significant reduction in plasma [3HK] was confirmed in KMOi treated group ($p < 0.001$, Mann Whitney test). The two *Kmo*$^{alb\text{-}cre}$ mice in the vehicle group which reached the humane endpoints had elevated plasma [3HK] levels (**Figure 43B**), more than double that of surviving *Kmo*$^{alb\text{-}cre}$ mice, further supporting the concept of increased circulating [3HK] in critical illness. As there was no significant difference in survival between the two groups at the end of the experiment, nor was there a significant difference in injected analgesia volumes, a comparison in total body weight was made between those suriving mice treated with GSK898 versus vehicle. The KMOi-treated mice had less weight loss than vehicle-treated controls, suggesting improved recovery, particularly with regard to oral intake over the experimental period (**Figure 44**, below).

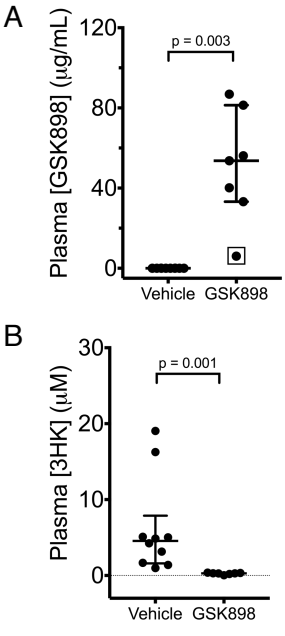

Figure 43. Plasma 3HK and drug levels with mini pump

Plasma [3HK] from blood sampled at time of cull (168-hrs or earlier if reached humane endpoint).

A: Log10 concentration of GSK898 drug in plasma. The outlier in GSK898 group represents, A436, the subject which reached humane endpoint at 166.8-hr.

B: Plasma 3HK concentrations. The two outliers in vehicle group represent A415 (endpoint 23.5-hr) and A450 (28.9-hr) showing an elevated 3HK levels in critical illness. Data nonparametric. Mann-Whitney U test p = 0.001. Individual data are shown and horizontal lines are median with interquartile range.

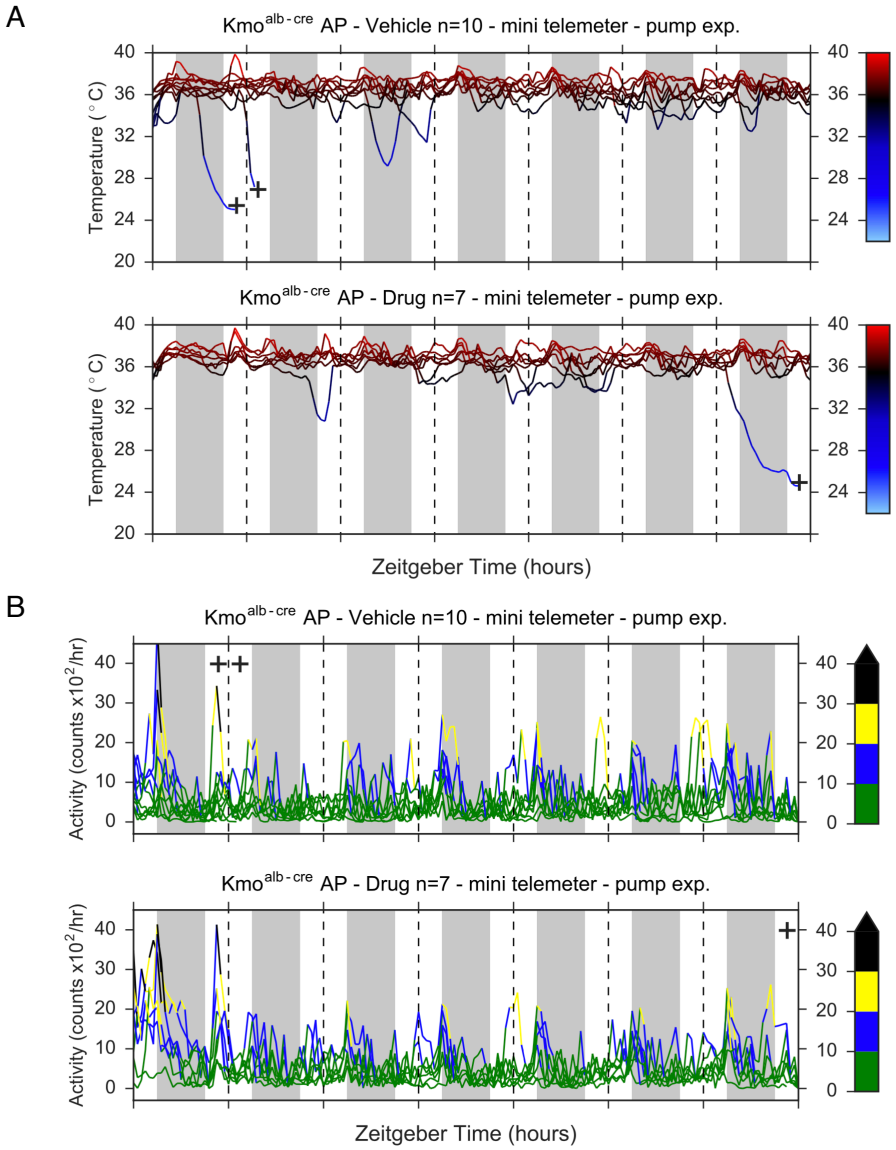

Figure 42. Telemetry in AP. Minipump study - vehicle versus GSK898

A: Core body temperature. **B**: Locomotor activity. **+** represents timepoint of removal from study due to reaching humane cull endpoint.

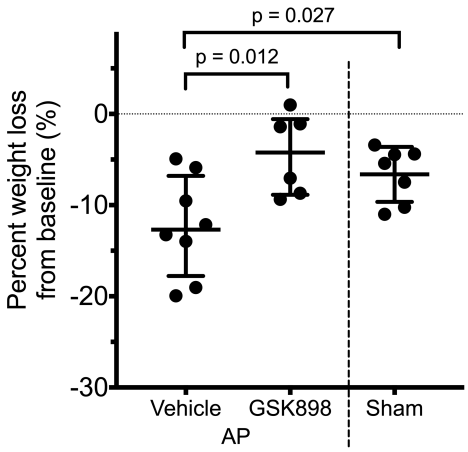

Figure 44. Minipump KMO inhibitor associated with reduced weight loss in 7-day AP in Kmo$^{alb\text{-}cre}$

Percentage of weight loss from baseline amongst 168-hr survivors in GSK898 minipump study. Vehicle survivors had mean 12.34% weight loss (SEM 1.94), compared to 4.44% (SEM 1.82) in drug treatment group, which was significant (p = 0.012, *t*-test).

3.8. Experiment 6 – 3HK synergies with IL1β to activate apoptosis *in vitro*

3.8.1. Background

As there appeared to be no significant differences in the cellular myeloid innate response (e.g. equivalent neutrophil counts in the blood and lungs) in the *Kmo*$^{alb\text{-}cre}$ as compared to *Kmo*^{wt} and *Kmo*^{null} lines (experiment #4), I wanted to investigated the potential mechanisms responsible for the apparent increased susceptibility to tissue injury of the *Kmo*$^{alb\text{-}cre}$ observed in AP recovery experiments, by exploring possible cytotoxic synergy between inflammatory cytokines and kynurenine pathway metabolites. The surprise finding of elevated circulating 3HK and XA in *Kmo*$^{alb\text{-}cre}$ mice at steady state, which appeared healthy, suggested that the toxic effects of 3HK (and potentially XA) are 'uncovered' by an acute inflammatory stressor. Since 3HAA has similar chemistry and redox activity as 3HK, I wanted to compare effects of this metabolite.

Because respiratory failure is the most common organ system for extra-pancreatic organ dysfunction in AP-MODS, and since the vascular endothelium is directly exposed to plasma kynurenines and cytokines, I used human lung vascular endothelial cells, HMVEC-L (Lonza). Cells were seeded (at 5,000 or 6,000 cells per well) and plated 24-hrs prior to treatment. Cells were treated for 4-hrs with the assigned treatment. This duration of agonist contact was determined from information from Sundquist *et al.* from Promega showing 'time dependence of caspase activities' from 1 to 7-hrs, and from my own preliminary work using this assay on HMVEC-L cells (not shown).
<www.promega.co.uk/resources/pubhub/cellnotes/timing-your-apoptosis-assays>.

Each data point represents a separate well. Control wells, including 0 ng/ml 'zero cytokines' wells, were performed in duplicate on each plate, giving twice the number as treatment wells. The treatment well results were performed in triplicate (i.e. three separate plates). Activation of apoptotic cell death pathways was measured using a caspase 3 and 7 luminometric assay (Promega). Cytokines IL-1β, IL-6 and IL-10 were co-cultured with HMVEC-L cells at titrated concentrations. I chose these cytokines because IL-1β (F-statistic 16.5, $p < 0.001$, 2-way ANOVA, Table 24, section 3.6) and IL-6 ($F = 25.6$, $p < 0.001$, 2-way ANOVA, Table 24) were robustly elevated in circulating plasma in my experimental AP model, and frequently reported in human AP studies, and IL-10 was chosen to compare any differences observed with proinflammatory cytokines with this anti-inflammatory mediator. All primary and control-converted data are available in Appendix 12.

3.8.2. Hypothesis

Potentially toxic hydroxykynurenines, 3HK and 3HAA, would induce endothelial cell caspase activation, and increasingly in the presence of pro-inflammatory cytokines (IL-1β, IL-6) but not anti-inflammatory cytokine IL-10.

3.8.3. Results

IL-6 or IL-10, alone or in combination with tryptophan, kynurenine, kynurenic acid, 3-hydroxykynurenine, anthranilic acid, or 3-hydroxyanthranilic acid, did not induce significant levels of caspase activity (**Table 64**). However, IL-1β at concentrations greater than or equal to 10 pg/ml co-administered with 3HK at 500 μM synergistically induced endothelial cell death (**Figure 45**). Comparative data between the 3 cytokines are displayed in **Figure 46**, having converted the luminescence values into a percentage proportion of positive (caspase activator, Staurosporin) and negative controls (cells, no caspase reagent).

3.8.4. Conclusions

These results suggest that the synergistic effects of IL-1β in the presence of elevated 3HK is particularly cytotoxic and is a strong activator of apoptotic cell death. Interestingly the other cytokines tested, whether proinflammatory (IL-6) or anti-inflammatory (IL-10), did not induce caspase activation. Additionally, other kynurenine metabolites, specifically XA (which found at elevated plasma concentrations in $Kmo^{alb\text{-}cre}$ mice, the mouse line more susceptible to critical illness in experimental AP) and 3HAA (which is chemically similar to 3HK) did not induce caspase. Together these data demonstrate that elevated circulating levels of IL-1β in AP-MODS potentiates the cytotoxic effects of 3HK with synergistic detrimental results.

	Caspase 3/7 activity / Luminescence % relative to controls								
	Cytokine			Metabolite					
[Metabolite]	IL-1β	IL-6	IL-10	Trp	Kyn	KA	3HK	3HAA	XA
100 µM	0	0	0	21.195	23.698	30.519	25.683	19.632	26.332
				17.913	20.237	21.793	21.082	14.066	18.538
				17.788	17.918	19.723	20.499	13.912	17.100
				23.509	27.571	35.354	21.139	16.120	21.701
				30.643	26.655	28.883	23.811	18.289	33.711
				29.112	25.591	25.391	20.421	24.785	28.119
	IL-1β 10 pg/ml	0	0	35.514	27.535	23.005	23.988	14.333	20.267
				32.328	33.183	32.915	30.645	20.734	30.849
				35.695	29.312	33.500	26.841	21.261	31.533
	IL-1β 100 pg/ml	0	0	38.882	37.724	35.996	30.133	26.455	25.362
				39.330	50.969	43.490	40.358	30.267	40.794
				50.050	42.474	49.365	41.057	35.489	42.847
	0	IL-6 100 ng/ml	0	20.256	19.644	28.781	26.495	18.218	26.574
				18.016	19.058	19.212	18.553	13.572	19.210
				16.952	19.973	17.214	19.926	13.432	16.238
	0	0	IL-10 100 ng/ml	24.268	23.482	29.424	26.816	21.625	26.135
				19.844	18.875	19.177	18.798	18.105	16.097
				18.250	19.458	17.775	20.604	12.872	17.989
500 µM	0	0	0	29.939	22.807	21.838	48.233	21.684	25.684
				19.705	20.760	16.065	31.577	15.121	16.789
				19.503	21.050	20.745	32.118	23.370	15.289
				29.864	25.148	28.087	9.685	9.774	20.694
				29.747	25.008	30.968	8.135	14.239	32.756
				29.542	27.644	32.593	12.004	9.729	26.700
	IL-1β 10 pg/ml	0	0	41.351	27.019	31.866	98.588	17.169	23.586
				25.410	51.645	37.911	135.570	23.938	35.941
				36.576	31.996	31.870	111.520	18.709	34.251
	IL-1β 100 pg/ml	0	0	43.597	34.865	63.397	138.641	35.302	30.029
				51.204	46.212	55.878	131.479	53.679	45.986
				52.846	41.243	54.120	122.378	33.948	44.596
	0	IL-6 100 ng/ml	0	22.634	30.844	25.480	26.629	27.511	22.302
				19.454	16.466	18.343	24.217	15.002	17.593
				20.750	21.566	19.095	27.196	23.385	15.410
	0	0	IL-10 100 ng/ml	22.687	22.276	23.150	27.573	26.204	25.170
				20.875	20.068	24.422	26.638	14.471	16.597
				20.973	22.513	23.944	24.434	17.515	15.753

Table 64. Comparison of relative endothelial caspase 3/7 activity with kynurenines and cytokines

Staurosporin 10 µM was used for positive control for caspase 3/7 activation. Negative control to gauge absence of luminescence took the form of a 'no caspase reagent' reading of wells containing cells, medium and DMSO to allow for cellular autofluorence.

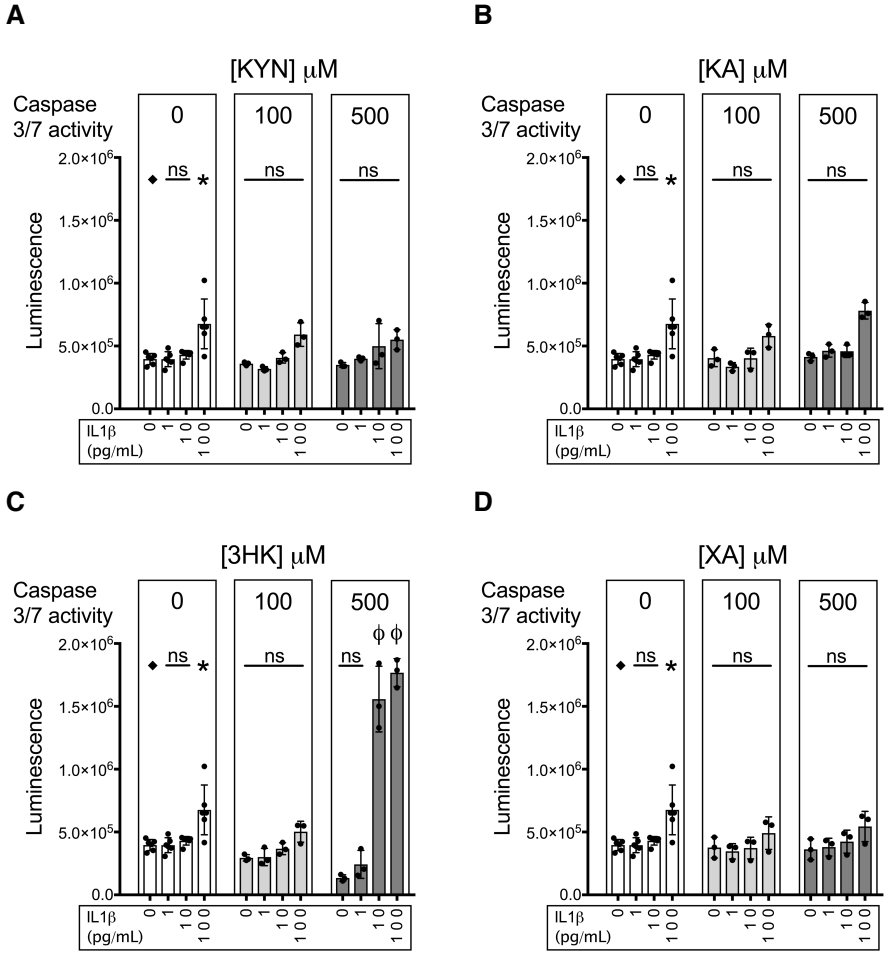

Figure 45: 3-Hydoxykynurenine in co-culture with IL1β synergistically induces endothelial apoptosis. Increasing concentrations of tryptophan catabolites were tested for endothelial cell (HMVEC-L in EBM2 medium) caspase activation in presence or absence of increasing IL1β doses. **C:** 3HK alone (at 500 μM) potentiated caspase 3/7 activity with IL-1β (≥10 pg/mL). Groups (n = 3 or 6, as shown) were compared by 1-way ANOVA with Dunnett's post-hoc test or Kruskal-Wallis with Dunn's test, as appropriate. Post-hoc tests were made against medium control (marked ◆: 0 μM metabolite, 0 pg/mL IL-1β). $p < 0.05^{*} < 0.001^{\Phi}$; ns = not significant.

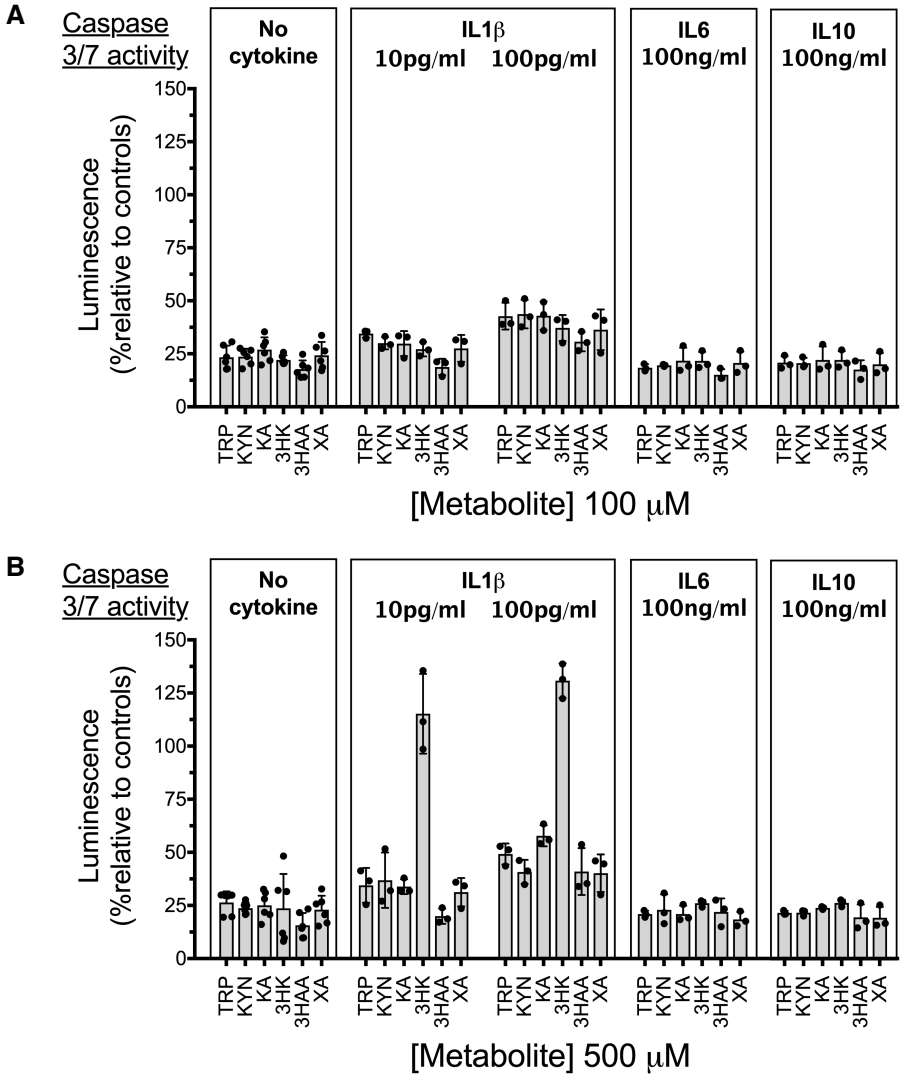

Figure 46: Comparison of cytokines IL-1β, IL-6, and IL-10 with kynurenine metabolites to potentiate endothelial cell apoptosis.

A comparison of caspase 3 and 7 activity in endothelial cells (HMVEC-L in EBM2 medium) comparing co-culture with kynurenine metabolites and cytokines IL-1β (low and high dose), IL-6 and IL-10 showing luminescence relative to controls for metabolites at 100 μM (**A**) and 500 μM (**B**). Staurosporin 10 μM was used for positive control for caspase 3/7 activation. Negative control to gauge absence of luminescence was a 'no caspase reagent' reading of wells containing cells, medium and DMSO. Whilst IL-1β had a pro-apoptotic effect with 3HK (as statistically confirmed in Figure 45), here no synergistic effect by IL-6 or IL-10 are observed, despite the use of high concentrations (100 ng/m).

4. DISCUSSION AND CONCLUSIONS

Acute pancreatitis is a sterile activator of the immune system. After pancreatic insult, there is release of DAMPS, cytokines, initiation of inflammatory signalling cascades, along with leukocyte and platelet activation and a neuro-endocrine stress response. This often gives rise to alterations in human physiology, which may arise far earlier than changes in the routine blood tests, which typically measure end-organ damage (e.g. creatinine, ALT), or radiological changes. Such altered physiological changes are characterized by the SIRS; whereby there are changes in bodily temperature, tachycardia, and an increased respiratory rate. Telemetry is an automated communications technology where measurements (*'metron'*) are made remotely (*'tele'*) and data are typically transferred through a wireless connection (e.g. radio waves). In biomedical research, telemetry is used to continuously record physiological parameters in unrestrained animals over prolonged time intervals, which is a different approach to the standard practice where large groups of animals are sacrificed at several timepoints. The literature contains many examples of interesting studies where telemetry has played a central role in sickness behaviour (636, 642). For scientific translational purposes, as well as welfare and standardising humane endpoint decision making (e.g. hypothermia <26^{o}C was our humane cull threshold), from the outset of the project we had planned to use telemetry monitoring animal physiological behaviour. Radiotelemetry devices have not been previously used in experimental AP, but would intuitively offer a useful adjunct in investigating the recovery phase. The design of studies involving telemetry requires an appreciation of the normal murine circadian physiological changes, how these may be perturbed by the experimental design, and how to minimise and control for such effects (e.g. timing of surgery) (643-645). Furthermore, circadian cycles are known to be important in health of critically ill patients (646, 647). Limited information exists regarding the physiological response after telemetry implantation, but it has been suggested that mice should be given '*sufficient time to adapt to bearing the transmitter before starting experiments*' (648). Given that our Na-TCA AP model involves opening the abdomen, it seemed logical to implant the intraperitoneal device at the same operation.

4.1. Model optimization – Phase I and II – for telemetered AP recovery studies

Large telemetry implants in small animals with batteries to monitor rodent physiology are problematic in that they are known to delay recover and require change of batteries (635). With the new battery-free telemeter technology used in this project, using a receiver pad

beneath the cage to provide electromagnetic current, I managed for the first time to capture the physiological changes of mice with AP.

With hindsight, lung injury with Protocol 6 could perhaps have been tested earlier, but as there was no consensus on how best to measure lung injury and efforts were focused on reaching a final infusion protocol as soon as possible, the lung assay option was overlooked with preference to test a higher dose of NaTCA as detailed in Protocol 7.

The impact of the telemeter device, in particular the larger cardiometabolic G2 HR device, is not without complication and from the data presented in sections 3.1, 3.3, and 3.5, there is compelling evidence that the added insult of the larger device which increased the systemic insult on these mice, increasing the tendency towards critical illness. This was not unforeseen, but was quantitatively unknown with respect to the degree to which critical illness would be poteniated in experimental AP. The added systemic insult from the larger cardiometabolic G2 HR telemeter likely made defining the protocol for recovery AP problematic. With the benefit of hindsight, I would rather have used the mini telemeter from the outset, and then perhaps 3% NaTCA infusate would have then worked satisfactorily, however, I suspect the high flow rate (100 μl over 60s), I may still have required adjustment.

4.2. Experiment 1 – KMO deletion improves AP recovery

Use of the radiotelemetry system, however, brought considerable advantages, allowing the investigator to remotely monitor mice. During the pilot model optimization phase I, I decided early on to adopt a protocol whereby should mice drop below 30^{o}C on a single occasion, but failed to meet humane endpoint criteria (see clinical score sheet - Appendix 3, section 6.3) they would be transferred to a warming chamber for ~30 mins, and receive a weight-adjusted subcutaneous bolus of warm saline, 5% dextrose and buprenorphine analgesia. Thereafter, where mice became hypothermic for a second time, they were not allowed to be re-warmed and would be culled if they reached a humane endpoint criterion, including hypothermia <26^{o}C, (as determined by telemetry). Using this system, I was better able to identify critically ill mice prior to their death, which allowed for tissue sampling under terminal anaesthesia, allowing confirmation of multi-organ dysfunction by biochemistry (Figure 23) and proinflammatory cytokine release (Figure 24).

The main finding of Experiment 1 was an improved survival difference with *Kmo^{null}*, as compared to *Kmo^{wt}*, with regards to protection against critical illness over a 7-day recovery study interval. This experiment conceptually extended the findings by my supervisor and collaborators (634) whereby the protective effects of KMO blockade now appeared to extend beyond the early 24-hour timepoint. The breeding colony of *Kmo^{null}* mice was very small at the

time of this experiment, and there were no age-matched *Kmo*^{null} mice available for a sham laparotomy group. However, a *Kmo*^{null} sham group would not have added to the findings of the experiment because the necessary sham group was that of the poorly surviving mouse line, which was the *Kmo*^{wt} mice.

4.3. Experiment 2 – Hepatocyte-restricted *Kmo* knockout increases plasma 3HK

The plasma kynurenine pathway metabolite profile in the *Kmo*$^{alb\text{-}cre}$ line, in particular the elevated [3HK] levels, had not been anticipated. Indeed, it may a first appear counter-intuitive that a partial KMO knockout (in terms of total bodily *Kmo* expression) would have elevated [3HK], as opposed to concentrations somewhere between that of wildtype (*Kmo*^{wt}) and full knockout (*Kmo*^{null}) mice. However, when considering the multi-compartment nature of mammalian metabolism, the results can be rationalised. Specifically, it is likely that a large proportion of bodily kynurenine is normally converted into 3HK within the (wildtype) hepatocytes, where it is intracellularly metabolised onwards (towards NAD^+ biosynthesis or else Acetyl CoA generation for the Krebs cycle). When hepatocyte kynurenine hydroxylation is blocked, as in *Kmo*$^{alb\text{-}cre}$ mice, kynurenine, which can more readily can cross membranes compartments, can pass into the circulation giving an abundant substrate for extra-hepatic KMO activity, and thus generating high quantities of plasma [3HK]. From the tracer study we can conclude that onward elimination of 3HK (e.g. metabolism or transportation) from the intravascular compartment is near saturation, as this would explain why $^{13}C_6$-3HK levels are higher in *Kmo*$^{alb\text{-}cre}$ than in *Kmo*^{wt} and *Kmo*^{null}.

One curious observation of these mice with high [3HK], is that they survive into adulthood and appear relatively healthy. However, RNA sequencing data (generated by my colleagues after I left the lab), indicate altered expression of pro-inflammatory genes in adult *Kmo*$^{alb\text{-}cre}$ mice at steadystate.

4.4. Experiment 3 – Hepatocyte-restricted *Kmo* knockout impairs AP recovery

Having established that the *Kmo*$^{alb\text{-}cre}$ line has a particular biochemical phenotype, with respect to the kynurenine pathway, and in particular high plasma [3HK], it was important to test this in the setting of AP, since elevated serum [3HK] in human AP patients is associated with increased disease severity with organ failure (375). The mini telemeter was used to monitor mice in these AP recovery studies, comparing sickness behaviour in *Kmo*$^{alb\text{-}cre}$ against *Kmo*^{wt}, and using *Kmo*^{null} as a 3HK negative control group.

From the data, a null hypothesis of '*no difference in critical illness and survival between these lines'* was rejected, due to the significant tendency towards critical illness and humane

endpoints in the *Kmo*$^{alb\text{-}cre}$ line. One observation which was not expected was the complete survival of the *Kmo*^{wt} mouse line, following the poor survival of *Kmo*^{wt} mice with AP and the more invasive cardiometabolic telemeter system in Experiment 1. However, given that the overall insult was reduced by switching to a less invasive telemeter, this telemetered AP model was a less severe disease model in terms of systemic injury, and in the case of *Kmo*^{wt} and *Kmo*^{null}, was generally under the threshold for critical illness as there was no significant difference in survival in AP between these two lines. The difference between cardiometabolic telemetered AP and mini telemetered AP, could conceptually be considered as moving from severe AP (using cardiometabolic telemeter) to moderate AP, when considered in terms of clinical terminology. That said, the finding of two deaths in *Kmo*^{null} mouse line during the study could be used against such a statement. In reality, researchers must be honest about the limitations in our disease models and the inherent disease severity variability which does exist despite our best efforts. One of these *Kmo*^{null} AP mice, culled ~24-hrs (K1217), was a surgical failure with a bile leak from the duodenotomy 'closure' site found at post mortem. Whilst it likely developed critical illness due to peritonitis secondary to leakage of enteric/bilious fluid content, it was not excluded for transparency reasons and the principal of '*intention-to-treat*'. There was another notable *Kmo*^{null} mouse which developed severe hypothermia with associated reduction in locomotor activity overnight, having appeared clinically well on cage side checks the evening before and the morning after. It is difficult to understand why that might have occurred and how it was able to spontaneously recover, but the telemetry trace is convincing with a simultaneous decline, and then recovery, in both locomotor and core temperature data readouts. This event highlights the benefits of telemetry recording, as without monitoring this transient episode would have passed unnoticed. *Kmo*$^{alb\text{-}cre}$ mice which reached humane endpoints were confirmed to have multiple organ injury by biochemical markers and cytokines, where there was sufficient blood sample for analysis (critically ill mice can yield very little blood due to cardiovascular changes).

4.5. Experiment 4 – Altered kynurenines did not alter early injury in recovery AP

There were little differences between mouse lines at 24-hrs but some discussion is required to give some wider context, technical detail and limitations. One particular strength of the 24-hr experiment was the controlled timepoint reached by all subjects, which was not feasible with the 7-day recover experiemnts due to the inherent disease variability and severity with subjects reaching humane endpoints before 168-hrs.

The data presented do raise some need for comment about the limitations of histological scoring by nature of examining a slice of the pancreas, however, often a large

cross-section of the pancreas is captured. Artefact changes in the pancreas may occur by suboptimal tissue fixation, which can be minimized by care to submerge the tissue in adequate volumes of fixative by the researcher. Interested readers can inspect histological injury score alongside plasma amylase concentrations in appendix 9, Table 53 and refer to cytokine levels (Table 56) to gauge systemic inflammatory insult. A noticeable outlier for histological assessment of pancreas injury was FK487 (wildtype, Kmo^{wt}, AP) which had a normal looking pancreas (in the section analysed) and low circulating cytokine levels (Table 56) comparable to that of sham laparotomy controls. These data would be expected in the sham group, however this mouse (FK487) did have an elevated amylase (7632 U/l) ~3-fold higher than shams and equivalent to another subject with clear histological changes (FK501, amylase 7740 U/l, maximal histology score 9/9). With regards to amylase, which usually is elevated in experimental AP, as can be seen in 'normal-amylase AP' in humans, occasionally a low amylase result is encountered despite having pancreatic inflammation. For example, FK486 (wildtype, AP) mouse with low amylase (1940 U/l) had a maximal histology injury score, and elevated IL-1β (3.7 pg/ml) and IL-6 (334.2 pg/ml). Creatinine was found to to have poor sensitivity (data not shown) for renal dysfunction as it was often undetected in mice which had reached humane endpoints, despite having high urea levels, and other markers of organ dysfunction (i.e. high ALT and LDH) and therefore creatinine was soon removed from the biochemical panel.

With respect to cytokines specifically, the sham laparotomy group were used as the control as opposed to steadystate healthy controls. The reason for omitting steady state controls on the assay was prinicipally for economic reasons and the MSD assay was not inexpensive and would have added very little scientific benefit.

Noteably, $Kmo^{alb\text{-}cre}$ mice were found to have elevated IL-12p70 in both sham and AP compared to other mouse linese. IL12 is a heterodimer cytokine produced by myeloid (i.e. monocytes, macrophages, neutrophils, DCs) and B cells. It is produced in response to microbial stimul and drives Th1 differentiation and IFN production (649). However, no differences in IFN were observed (Table 32 and 37). Additionally, $Kmo^{alb\text{-}cre}$ mice had elevated IL-2 and IL-4 in AP. The relevance of IL-4 here is questionable since overall, IL-4 levels did not appear to differ across mouse lines with AP (Table 32). However, IL-2 levels did appear to increase with AP (Table 32), and were more elevated in $Kmo^{alb\text{-}cre}$ mice compared to other mouse lines (Table 40). IL-2 is known for its role in lymphocyte proliferation, however elevated [3HK] levels are known to suppress T-cells (451). Most interestingly from Experiment 4 (section 3.6), we see that similar to humans with AP that have elevated blood [3HK], experimental AP is also associated with increased 3HK concentrations (Table 33).

4.6. Experiment 5 – KMO inhibition prevents early critical illness in recovery AP

Given the high concentrations of 3HK in *Kmo*$^{alb\text{-}cre}$ mice, in association with early lethality of these mice with AP, I performed KMO inhibitor (KMOi) studies. In answer a specific question raised by peers; '*why perform a KMOi study in the Kmo*$^{alb\text{-}cre}$ *AP mice with the mini telemeter rather than the use the drug in Kmo*^{wt} *mice with the cardiometabolic telemeter (after all humans are 'wildtype'!)*' the answer is 3-fold:

i) Firstly, this was a mechanistic question, as opposed to a mock clinical trial. The test was to determine whether the KMOi would reduce the early lethality phenotype observed in the *Kmo*$^{alb\text{-}cre}$ mouse line with AP, with reduced plasma [3HK]. Because the *Kmo*^{wt} mice had levels around the limit of detection, we would not have been able to demonstrate a reduction in plasma [3HK] levels, therefore the obvious first choice was the *Kmo*$^{alb\text{-}cre}$ line.

ii) Secondly, I did not have consistent data showing that *Kmo*^{wt} mice had elevated 3HK with 2% NaTCA, likely because substantial elevations of 3HK in *Kmo*^{wt} mice only appeared to occur with the onset of substantial multi-organ injury/ impending lethality, requiring a more severe injury challenge such as the addition of the invasive cardiometabolic telemeter or increased NaTCA concentrations (e.g. 5% NaTCA).

iii) By this point in the research, our Veterinary colleagues and I (working under Home Office licencing restrictions, 3Rs principles and ethical principles) were content with the lethality of the AP model using the mini telemeter which appeared to add very little, if any, further insult and severity to the model, as opposed to the cardiometabolic device which substantially synergised the severity of the AP model. If time and resources had allowed for an experiment using *Kmo*^{wt} mice and the severe model (i.e. AP with the cardiometabolic telemeter), it would have been carefully discussed and considered with Veterinary colleagues.

The drug is orally bioavailable and thus suitable to add to drinking water. Figure 36 shows similar 7-day survival, however the deaths in the drugged subjects were generally much later, indeed there was a significant delay in time to humane endpoint (Figure 36B). I had carefully recovered daily consumption of drugged water, and with a decrease in consumption of water in AP (Figure 37), arguably they dosing effect might have bear wearing off with time, meaning that the initial protection wore off.

To take things forwards, and circumvent the problem of impaired voluntary oral drinking water consumption in AP, I performed a parenteral, mini pump drug study. Again, this was performed in *Kmo*$^{alb\text{-}cre}$ mice. Interestingly in the minipump study (section 3.7, Figure 42B), we

see that the two vehicle-treated minipump mice that developed critical illness have elevated 3HK levels and were outliers with regards 3HK concentration data. There were not as many deaths in the *Kmo*$^{alb\text{-}cre}$ vehicle mini pump group as anticipated by the results from Experiment 3. There was one non-survivor amongst the mini pump KMO inhibitor treatment group, which was humanely culled at 166-hrs. Again, those reaching humane endpoint in the vehicle group did so at a much earlier time point than the KMOi drug-treated group. Comparing survivors between the drug and vehicle groups, there was a significant weight loss in the vehicle group.

4.7. Experiment 6 – Casepase 3/7 assay 3HK synergies with IL1β to activate apoptosis *in vitro*

3HK is known to have many deleteriorus cytotoxic effects (see section 1.2.6.3.), but *Kmo*$^{alb\text{-}cre}$ mice, with high circulating levels of [3HK], survive into adulthood and appear healthy. Therefore, I was lead to consider that elevated [3HK] levels may be more cytotoxic during inflammation as opposed to steadystate. I wanted to test the hypothesis that certain kynurenine metabolites may be more cytotoxic in co-culture with certain cytokines. I tested all available kynureine compounds, along with pro- (IL-1, IL-6) and anti-inflammatory cytokines (IL-10). Whilst did not specifically test activity of these cytokines, they were all freshly sourced from the supplier which undertakes in-house testing (Miltenyi Biotec). Compounds were dissolved with the use of DMSO, which required to be dissoclved in DMSO (0.5% final concentration) with controls. It was surprising that 3HK alone did not have significantly elevated caspase 3/7 actiivty after 4-hrs treatment, however, one explanation could be that the EBM-2 medium contained antioxidant which could have buffered the pro-oxidant effects.

4.8. Conclusions

The academic and pharmaceutical interest in the kynurenine pathway outside of the central nervous system is growing as increasingly researchers are finding the mechanistic relevance of the kynurenines in an increasing number of peripheral inflammatory and metabolic and diseases and the concept of metabolic support in critical illness is gaining traction (650). In my research, I found that KMO blockade in genetically-altered mice protects against critical illness and improves recovery in an experimental model of severe AP. I discovered a hepatocyte-specific role for KMO, where mice generated to lack *Kmo* solely in hepatocytes (*Kmo*$^{alb\text{-}cre}$) showed elevated plasma [3HK], reduced $^{13}C_6$-3-hydroxykynurenine tracer clearance, and transcriptomic alterations in key innate immunity pathways in liver tissue,

specifically modulating expression of canonical toll-like receptor pathway signalling genes, including MyD88, RIP kinase, MAP kinases and NF-κB. Although $Kmo^{alb\text{-}cre}$ mice with elevated 3HK mice did not significantly differ in pancreas injury metrics, multiple-organ neutrophilia infiltrate or routine biochemistry at an early timepoint (24-hr) using a less severe recovery model of AP, these mice succumbed fatally earlier and more readily to experimental AP over 7-days, thus indicating an impaired recovery and increased susceptibility for critical illness. Therapeutically reducing 3HK to undetectable levels through systemic blockade using a highly-specific KMO inhibitor rescues the phenotype, protecting against critical illness and early mortality in 7-day recovery experimental AP. In vitro, 3HK was the only kynurenine metabolite to induce cytotoxic insult, by way of caspase 3/7 activation, which required pro-inflammatiory cytokine, interleukin-1β, to potentiate this effect. These findings support the notion of a potential deleterious cytotoxic interaction between 3HK with innate immune mediators. The other kynurenine metabolites did not induce caspase activation.

Together, these findings establish the KMO product 3HK as a modulator of innate immunity that exhibits a complex interaction with inflammatory cytokines during critical illness to promote excess morbidity and death from multiple organ failure that may be rescued by systemic KMO blockade.

5. REFERENCES

1. Williams JA. The nobel pancreas: a historical perspective. Gastroenterology. 2013;144(6):1166-9.

2. Pannala R, Kidd M, Modlin IM. Acute pancreatitis: a historical perspective. Pancreas. 2009;38(4):355-66.

3. Tsuchiya R, Fujisawa N. On the etymology of "pancreas". Int J Pancreatol. 1997;21(3):269-72.

4. Whitcomb DC, Lowe ME. Human pancreatic digestive enzymes. Dig Dis Sci. 2007;52(1):1-17.

5. Dudeja V, Christein, JD., Jensen, EH., Vickers, SM. Exocrine Pancreas. Sabiston Textbook of Surgery: The Biological Basis of Modern Surgical Practice. 20th ed. Philadelphia, PA.: Elsevier Saunders; 2017. p. 1521.

6. Hegyi P, Pandol S, Venglovecz V, Rakonczay Z, Jr. The acinar-ductal tango in the pathogenesis of acute pancreatitis. Gut. 2011;60(4):544-52.

7. Navarro S. Historical review of our knowledge of acute pancreatitis. Gastroenterol Hepatol. 2018;41(2):143 e1- e10.

8. Gorelick FS, Lerch MM. Do Animal Models of Acute Pancreatitis Reproduce Human Disease? Cell Mol Gastroenterol Hepatol. 2017;4(2):251-62.

9. Lerch MM, Gorelick FS. Models of acute and chronic pancreatitis. Gastroenterology. 2013;144(6):1180-93.

10. Kui B, Balla Z, Vegh ET, Pallagi P, Venglovecz V, Ivanyi B, et al. Recent advances in the investigation of pancreatic inflammation induced by large doses of basic amino acids in rodents. Lab Invest. 2014;94(2):138-49.

11. Wan MH, Huang W, Latawiec D, Jiang K, Booth DM, Elliott V, et al. Review of experimental animal models of biliary acute pancreatitis and recent advances in basic research. HPB (Oxford). 2012;14(2):73-81.

12. Aho HJ, Koskensalo SM, Nevalainen TJ. Experimental pancreatitis in the rat. Sodium taurocholate-induced acute haemorrhagic pancreatitis. Scand J Gastroenterol. 1980;15(4):411-6.

13. Perides G, van Acker GJ, Laukkarinen JM, Steer ML. Experimental acute biliary pancreatitis induced by retrograde infusion of bile acids into the mouse pancreatic duct. Nat Protoc. 2010;5(2):335-41.

14. Ziegler KM, Wade TE, Wang S, Swartz-Basile DA, Pitt HA, Zyromski NJ. Validation of a novel, physiologic model of experimental acute pancreatitis in the mouse. Am J Transl Res. 2011;3(2):159-65.

15. Merry TL, Petrov MS. The rise of genetically engineered mouse models of pancreatitis: A review of literature. Biomol Concepts. 2018;9(1):103-14.

16. Schmidt J, Rattner DW, Lewandrowski K, Compton CC, Mandavilli U, Knoefel WT, et al. A better model of acute pancreatitis for evaluating therapy. Ann Surg. 1992;215(1):44-56.

17. Chan YC, Leung PS. Acute pancreatitis: animal models and recent advances in basic research. Pancreas. 2007;34(1):1-14.

18. Romac JM, Shahid RA, Swain SM, Vigna SR, Liddle RA. Piezo1 is a mechanically activated ion channel and mediates pressure induced pancreatitis. Nat Commun. 2018;9(1):1715.

19. Tepikin AV, Voronina SG, Gallacher DV, Petersen OH. Acetylcholine-evoked increase in the cytoplasmic Ca2+ concentration and Ca2+ extrusion measured simultaneously in single mouse pancreatic acinar cells. J Biol Chem. 1992;267(6):3569-72.

20. Moreau B, Straube S, Fisher RJ, Putney JW, Jr., Parekh AB. Ca2+-calmodulin-dependent facilitation and Ca2+ inactivation of Ca2+ release-activated Ca2+ channels. J Biol Chem. 2005;280(10):8776-83.

21. Petersen OH, Tepikin AV. Polarized calcium signaling in exocrine gland cells. Annu Rev Physiol. 2008;70:273-99.

22. Gerasimenko JV, Lur G, Sherwood MW, Ebisui E, Tepikin AV, Mikoshiba K, et al. Pancreatic protease activation by alcohol metabolite depends on Ca2+ release via acid store IP3 receptors. Proc Natl Acad Sci U S A. 2009;106(26):10758-63.

23. Streb H, Irvine RF, Berridge MJ, Schulz I. Release of Ca2+ from a nonmitochondrial intracellular store in pancreatic acinar cells by inositol-1,4,5-trisphosphate. Nature. 1983;306(5938):67-9.

24. Husain SZ, Prasad P, Grant WM, Kolodecik TR, Nathanson MH, Gorelick FS. The ryanodine receptor mediates early zymogen activation in pancreatitis. Proc Natl Acad Sci U S A. 2005;102(40):14386-91.

25. Gerasimenko JV, Sherwood M, Tepikin AV, Petersen OH, Gerasimenko OV. NAADP, cADPR and IP3 all release Ca2+ from the endoplasmic reticulum and an acidic store in the secretory granule area. J Cell Sci. 2006;119(Pt 2):226-38.

26. Gerasimenko JV, Gerasimenko OV, Petersen OH. The role of Ca2+ in the pathophysiology of pancreatitis. J Physiol. 2014;592(2):269-80.

27. Petersen OH, Gerasimenko OV, Gerasimenko JV. Pathobiology of acute pancreatitis: focus on intracellular calcium and calmodulin. F1000 Med Rep. 2011;3:15.

28. Chen JM, Ferec C. Genes, cloned cDNAs, and proteins of human trypsinogens and pancreatitis-associated cationic trypsinogen mutations. Pancreas. 2000;21(1):57-62.

29. Hegyi E, Sahin-Toth M. Genetic Risk in Chronic Pancreatitis: The Trypsin-Dependent Pathway. Dig Dis Sci. 2017;62(7):1692-701.

30. Aghdassi AA, John DS, Sendler M, Weiss FU, Reinheckel T, Mayerle J, et al. Cathepsin D regulates cathepsin B activation and disease severity predominantly in inflammatory cells during experimental pancreatitis. J Biol Chem. 2018;293(3):1018-29.

31. Szabo A, Sahin-Toth M. Increased activation of hereditary pancreatitis-associated human cationic trypsinogen mutants in presence of chymotrypsin C. J Biol Chem. 2012;287(24):20701-10.

32. Sherwood MW, Prior IA, Voronina SG, Barrow SL, Woodsmith JD, Gerasimenko OV, et al. Activation of trypsinogen in large endocytic vacuoles of pancreatic acinar cells. Proc Natl Acad Sci U S A. 2007;104(13):5674-9.

33. Gukovsky I, Pandol SJ, Mareninova OA, Shalbueva N, Jia W, Gukovskaya AS. Impaired autophagy and organellar dysfunction in pancreatitis. J Gastroenterol Hepatol. 2012;27 Suppl 2:27-32.

34. Petersen OH, Sutton R. Ca2+ signalling and pancreatitis: effects of alcohol, bile and coffee. Trends Pharmacol Sci. 2006;27(2):113-20.

35. Mooren F, Hlouschek V, Finkes T, Turi S, Weber IA, Singh J, et al. Early changes in pancreatic acinar cell calcium signaling after pancreatic duct obstruction. J Biol Chem. 2003;278(11):9361-9.

36. Kim JY, Kim KH, Lee JA, Namkung W, Sun AQ, Ananthanarayanan M, et al. Transporter-mediated bile acid uptake causes Ca2+-dependent cell death in rat pancreatic acinar cells. Gastroenterology. 2002;122(7):1941-53.

37. Hietaranta AJ, Singh VP, Bhagat L, van Acker GJ, Song AM, Mykoniatis A, et al. Water immersion stress prevents caerulein-induced pancreatic acinar cell nf-kappa b activation by attenuating caerulein-induced intracellular Ca2+ changes. J Biol Chem. 2001;276(22):18742-7.

38. Venglovecz V, Rakonczay Z, Jr., Ozsvari B, Takacs T, Lonovics J, Varro A, et al. Effects of bile acids on pancreatic ductal bicarbonate secretion in guinea pig. Gut. 2008;57(8):1102-12.

39. Wen L, Voronina S, Javed MA, Awais M, Szatmary P, Latawiec D, et al. Inhibitors of ORAI1 Prevent Cytosolic Calcium-Associated Injury of Human Pancreatic Acinar Cells and Acute Pancreatitis in 3 Mouse Models. Gastroenterology. 2015;149(2):481-92 e7.

40. Mukherjee R, Mareninova OA, Odinokova IV, Huang W, Murphy J, Chvanov M, et al. Mechanism of mitochondrial permeability transition pore induction and damage in the pancreas: inhibition prevents acute pancreatitis by protecting production of ATP. Gut. 2016;65(8):1333-46.

41. Halestrap AP, Richardson AP. The mitochondrial permeability transition: a current perspective on its identity and role in ischaemia/reperfusion injury. J Mol Cell Cardiol. 2015;78:129-41.

42. Odinokova IV, Sung KF, Mareninova OA, Hermann K, Evtodienko Y, Andreyev A, et al. Mechanisms regulating cytochrome c release in pancreatic mitochondria. Gut. 2009;58(3):431-42.

43. Kang R, Lotze MT, Zeh HJ, Billiar TR, Tang D. Cell death and DAMPs in acute pancreatitis. Mol Med. 2014;20:466-77.

44. Pandol SJ, Saluja AK, Imrie CW, Banks PA. Acute pancreatitis: bench to the bedside. Gastroenterology. 2007;132(3):1127-51.

45. Beutner G, Alanzalon RE, Porter GA, Jr. Cyclophilin D regulates the dynamic assembly of mitochondrial ATP synthase into synthasomes. Sci Rep. 2017;7(1):14488.

46. Shore ER, Awais M, Kershaw NM, Gibson RR, Pandalaneni S, Latawiec D, et al. Small Molecule Inhibitors of Cyclophilin D To Protect Mitochondrial Function as a Potential Treatment for Acute Pancreatitis. J Med Chem. 2016;59(6):2596-611.

47. Biczo G, Vegh ET, Shalbueva N, Mareninova OA, Elperin J, Lotshaw E, et al. Mitochondrial Dysfunction, Through Impaired Autophagy, Leads to Endoplasmic Reticulum Stress, Deregulated Lipid Metabolism, and Pancreatitis in Animal Models. Gastroenterology. 2018;154(3):689-703.

48. Frossard JL, Steer ML, Pastor CM. Acute pancreatitis. Lancet. 2008;371(9607):143-52.

49. Whitcomb DC, Gorry MC, Preston RA, Furey W, Sossenheimer MJ, Ulrich CD, et al. Hereditary pancreatitis is caused by a mutation in the cationic trypsinogen gene. Nat Genet. 1996;14(2):141-5.

50. Beer S, Zhou J, Szabo A, Keiles S, Chandak GR, Witt H, et al. Comprehensive functional analysis of chymotrypsin C (CTRC) variants reveals distinct loss-of-function mechanisms associated with pancreatitis risk. Gut. 2013;62(11):1616-24.

51. Geisz A, Sahin-Toth M. A preclinical model of chronic pancreatitis driven by trypsinogen autoactivation. Nat Commun. 2018;9(1):5033.

52. Geisz A, Hegyi P, Sahin-Toth M. Robust autoactivation, chymotrypsin C independence and diminished secretion define a subset of hereditary pancreatitis-associated cationic trypsinogen mutants. FEBS J. 2013;280(12):2888-99.

53. Dawra R, Sah RP, Dudeja V, Rishi L, Talukdar R, Garg P, et al. Intra-acinar trypsinogen activation mediates early stages of pancreatic injury but not inflammation in mice with acute pancreatitis. Gastroenterology. 2011;141(6):2210-7 e2.

54. Mareninova OA, Sendler M, Malla SR, Yakubov I, French SW, Tokhtaeva E, et al. Lysosome associated membrane proteins maintain pancreatic acinar cell homeostasis: LAMP-2 deficient mice develop pancreatitis. Cell Mol Gastroenterol Hepatol. 2015;1(6):678-94.

55. Chvanov M, De Faveri F, Moore D, Sherwood MW, Awais M, Voronina S, et al. Intracellular rupture, exocytosis and actin interaction of endocytic vacuoles in pancreatic acinar cells: initiating events in acute pancreatitis. J Physiol. 2018;596(13):2547-64.

56. Xiao AY, Tan ML, Wu LM, Asrani VM, Windsor JA, Yadav D, et al. Global incidence and mortality of pancreatic diseases: a systematic review, meta-analysis, and meta-regression of population-based cohort studies. Lancet Gastroenterol Hepatol. 2016;1(1):45-55.

57. Husain SZ, Srinath AI. What's unique about acute pancreatitis in children: risk factors, diagnosis and management. Nat Rev Gastroenterol Hepatol. 2017;14(6):366-72.

58. Petrov MS, Yadav D. Global epidemiology and holistic prevention of pancreatitis. Nat Rev Gastroenterol Hepatol. 2018.

59. McKay CJ, Evans S, Sinclair M, Carter CR, Imrie CW. High early mortality rate from acute pancreatitis in Scotland, 1984-1995. Br J Surg. 1999;86(10):1302-5.

60. Roberts SE, Williams JG, Meddings D, Goldacre MJ. Incidence and case fatality for acute pancreatitis in England: geographical variation, social deprivation, alcohol consumption and aetiology--a record linkage study. Alimentary pharmacology & therapeutics. 2008;28(7):931-41.

61. Toh SK, Phillips S, Johnson CD. A prospective audit against national standards of the presentation and management of acute pancreatitis in the South of England. Gut. 2000;46(2):239-43.

62. Roberts SE, Akbari A, Thorne K, Atkinson M, Evans PA. The incidence of acute pancreatitis: impact of social deprivation, alcohol consumption, seasonal and demographic factors. Alimentary pharmacology & therapeutics. 2013;38(5):539-48.

63. Mole DJ, Gungabissoon U, Johnston P, Cochrane L, Hopkins L, Wyper GM, et al. Identifying risk factors for progression to critical care admission and death among individuals with acute pancreatitis: a record linkage analysis of Scottish healthcare databases. BMJ Open. 2016;6(6):e011474.

64. Kim SB, Kim TN, Chung HH, Kim KH. Small Gallstone Size and Delayed Cholecystectomy Increase the Risk of Recurrent Pancreatobiliary Complications After Resolved Acute Biliary Pancreatitis. Dig Dis Sci. 2017;62(3):777-83.

65. Sadr Azodi O, Orsini N, Andren-Sandberg A, Wolk A. Effect of type of alcoholic beverage in causing acute pancreatitis. Br J Surg. 2011;98(11):1609-16.

66. Wolf A, Bernhardt J, Patrzyk M, Heidecke CD. The value of endoscopic diagnosis and the treatment of pancreas injuries following blunt abdominal trauma. Surg Endosc. 2005;19(5):665-9.

67. Marsoner K, Voetsch A, Lierzer C, Sodeck GH, Fruhwald S, Dapunt O, et al. Gastrointestinal complications following on-pump cardiac surgery-A propensity matched analysis. PLoS One. 2019;14(6):e0217874.

68. Parenti DM, Steinberg W, Kang P. Infectious causes of acute pancreatitis. Pancreas. 1996;13(4):356-71.

69. Sekimoto M, Takada T, Kawarada Y, Hirata K, Mayumi T, Yoshida M, et al. JPN Guidelines for the management of acute pancreatitis: epidemiology, etiology, natural history, and outcome predictors in acute pancreatitis. J Hepatobiliary Pancreat Surg. 2006;13(1):10-24.

70. Guo JJ, Jang R, Louder A, Cluxton RJ. Acute pancreatitis associated with different combination therapies in patients infected with human immunodeficiency virus. Pharmacotherapy. 2005;25(8):1044-54.

71. Pedersen SB, Langsted A, Nordestgaard BG. Nonfasting Mild-to-Moderate Hypertriglyceridemia and Risk of Acute Pancreatitis. JAMA Intern Med. 2016;176(12):1834-42.

72. Nitsche C, Maertin S, Scheiber J, Ritter CA, Lerch MM, Mayerle J. Drug-induced pancreatitis. Curr Gastroenterol Rep. 2012;14(2):131-8.

73. Sadr-Azodi O, Andren-Sandberg A, Orsini N, Wolk A. Cigarette smoking, smoking cessation and acute pancreatitis: a prospective population-based study. Gut. 2012;61(2):262-7.

74. Petrov MS, Yadav D. Global epidemiology and holistic prevention of pancreatitis. Nat Rev Gastroenterol Hepatol. 2019;16(3):175-84.

75. Bai HX, Lowe ME, Husain SZ. What have we learned about acute pancreatitis in children? J Pediatr Gastroenterol Nutr. 2011;52(3):262-70.

76. Frey CF, Zhou H, Harvey DJ, White RH. The incidence and case-fatality rates of acute biliary, alcoholic, and idiopathic pancreatitis in California, 1994-2001. Pancreas. 2006;33(4):336-44.

77. Cheng CL, Sherman S, Watkins JL, Barnett J, Freeman M, Geenen J, et al. Risk factors for post-ERCP pancreatitis: a prospective multicenter study. Am J Gastroenterol. 2006;101(1):139-47.

78. Badalov N, Baradarian R, Iswara K, Li J, Steinberg W, Tenner S. Drug-induced acute pancreatitis: an evidence-based review. Clin Gastroenterol Hepatol. 2007;5(6):648-61; quiz 4.

79. Misgar RA, Bhat MH, Rather TA, Masoodi SR, Wani AI, Bashir MI, et al. Primary hyperparathyroidism and pancreatitis. J Endocrinol Invest. 2020.

80. Rawla P, Bandaru SS, Vellipuram AR. Review of Infectious Etiology of Acute Pancreatitis. Gastroenterology Res. 2017;10(3):153-8.

81. Aerts R, Penninckx F. The burden of gallstone disease in Europe. Aliment Pharmacol Ther. 2003;18 Suppl 3:49-53.

82. Lowenfels AB, Lankisch PG, Maisonneuve P. What is the risk of biliary pancreatitis in patients with gallstones? Gastroenterology. 2000;119(3):879-80.

83. Lammert F, Gurusamy K, Ko CW, Miquel JF, Mendez-Sanchez N, Portincasa P, et al. Gallstones. Nat Rev Dis Primers. 2016;2:16024.

84. Venneman NG, Buskens E, Besselink MG, Stads S, Go PM, Bosscha K, et al. Small gallstones are associated with increased risk of acute pancreatitis: potential benefits of prophylactic cholecystectomy? Am J Gastroenterol. 2005;100(11):2540-50.

85. Acosta JM, Ledesma CL. Gallstone migration as a cause of acute pancreatitis. N Engl J Med. 1974;290(9):484-7.

86. Parniczky A, Kui B, Szentesi A, Balazs A, Szucs A, Mosztbacher D, et al. Prospective, Multicentre, Nationwide Clinical Data from 600 Cases of Acute Pancreatitis. PLoS One. 2016;11(10):e0165309.

87. Forsmark CE, Vege SS, Wilcox CM. Acute Pancreatitis. N Engl J Med. 2016;375(20):1972-81.

88. Perides G, Laukkarinen JM, Vassileva G, Steer ML. Biliary acute pancreatitis in mice is mediated by the G-protein-coupled cell surface bile acid receptor Gpbar1. Gastroenterology. 2010;138(2):715-25.

89. Lerch MM, Saluja AK, Runzi M, Dawra R, Saluja M, Steer ML. Pancreatic duct obstruction triggers acute necrotizing pancreatitis in the opossum. Gastroenterology. 1993;104(3):853-61.

90. Geyer N, Diszhazi G, Csernoch L, Jona I, Almassy J. Bile acids activate ryanodine receptors in pancreatic acinar cells via a direct allosteric mechanism. Cell Calcium. 2015;58(2):160-70.

91. Gerasimenko JV, Flowerdew SE, Voronina SG, Sukhomlin TK, Tepikin AV, Petersen OH, et al. Bile acids induce Ca2+ release from both the endoplasmic reticulum and acidic intracellular calcium stores through activation of inositol trisphosphate receptors and ryanodine receptors. J Biol Chem. 2006;281(52):40154-63.

92. Lerch MM, Weidenbach H, Hernandez CA, Preclik G, Adler G. Pancreatic outflow obstruction as the critical event for human gall stone induced pancreatitis. Gut. 1994;35(10):1501-3.

93. Elliott DW, Williams RD, Zollinger RM. Alterations in the pancreatic resistance to bile in the pathogenesis of acute pancreatitis. Ann Surg. 1957;146(4):669-81; discussion 81-2.

94. Lankisch PG, Apte M, Banks PA. Acute pancreatitis. Lancet. 2015;386(9988):85-96.

95. Saluja A, Dudeja V, Dawra R, Sah RP. Early Intra-Acinar Events in Pathogenesis of Pancreatitis. Gastroenterology. 2019;156(7):1979-93.

96. Whitcomb DC, LaRusch J, Krasinskas AM, Klei L, Smith JP, Brand RE, et al. Common genetic variants in the CLDN2 and PRSS1-PRSS2 loci alter risk for alcohol-related and sporadic pancreatitis. Nat Genet. 2012;44(12):1349-54.

97. Zator Z, Whitcomb DC. Insights into the genetic risk factors for the development of pancreatic disease. Therap Adv Gastroenterol. 2017;10(3):323-36.

98. Muller N, Sarantitis I, Rouanet M, de Mestier L, Halloran C, Greenhalf W, et al. Natural history of SPINK1 germline mutation related-pancreatitis. EBioMedicine. 2019;48:581-91.

99. Aoun E, Muddana V, Papachristou GI, Whitcomb DC. SPINK1 N34S is strongly associated with recurrent acute pancreatitis but is not a risk factor for the first or sentinel acute pancreatitis event. Am J Gastroenterol. 2010;105(2):446-51.

100. Mayerle J, Sendler M, Hegyi E, Beyer G, Lerch MM, Sahin-Toth M. Genetics, Cell Biology, and Pathophysiology of Pancreatitis. Gastroenterology. 2019;156(7):1951-68 e1.

101. Lankisch PG, Lowenfels AB, Maisonneuve P. What is the risk of alcoholic pancreatitis in heavy drinkers? Pancreas. 2002;25(4):411-2.

102. Samarasekera E, Mahammed S, Carlisle S, Charnley R, Guideline C. Pancreatitis: summary of NICE guidance. BMJ. 2018;362:k3443.

103. Munigala S, Conwell DL, Gelrud A, Agarwal B. Heavy Smoking Is Associated With Lower Age at First Episode of Acute Pancreatitis and a Higher Risk of Recurrence. Pancreas. 2015;44(6):876-81.

104. Sun J, Fu J, Zhong Y, Li L, Chen C, Wang X, et al. NRF2 mitigates acute alcohol-induced hepatic and pancreatic injury in mice. Food Chem Toxicol. 2018;121:495-503.

105. Bishehsari F, Magno E, Swanson G, Desai V, Voigt RM, Forsyth CB, et al. Alcohol and Gut-Derived Inflammation. Alcohol Res. 2017;38(2):163-71.

106. Fishman JE, Levy G, Alli V, Zheng X, Mole DJ, Deitch EA. The intestinal mucus layer is a critical component of the gut barrier that is damaged during acute pancreatitis. Shock. 2014;42(3):264-70.

107. Apte MV, Pirola RC, Wilson JS. Fatty acid ethyl esters--alcohol's henchmen in the pancreas? Gastroenterology. 2006;130(3):992-5.

108. Criddle DN, Murphy J, Fistetto G, Barrow S, Tepikin AV, Neoptolemos JP, et al. Fatty acid ethyl esters cause pancreatic calcium toxicity via inositol trisphosphate receptors and loss of ATP synthesis. Gastroenterology. 2006;130(3):781-93.

109. Criddle DN, Raraty MG, Neoptolemos JP, Tepikin AV, Petersen OH, Sutton R. Ethanol toxicity in pancreatic acinar cells: mediation by nonoxidative fatty acid metabolites. Proc Natl Acad Sci U S A. 2004;101(29):10738-43.

110. Huang W, Booth DM, Cane MC, Chvanov M, Javed MA, Elliott VL, et al. Fatty acid ethyl ester synthase inhibition ameliorates ethanol-induced Ca2+-dependent mitochondrial dysfunction and acute pancreatitis. Gut. 2014;63(8):1313-24.

111. Werner J, Laposata M, Fernandez-del Castillo C, Saghir M, Iozzo RV, Lewandrowski KB, et al. Pancreatic injury in rats induced by fatty acid ethyl ester, a nonoxidative metabolite of alcohol. Gastroenterology. 1997;113(1):286-94.

112. Mahajan A, Kadavigere R, Sripathi S, Rodrigues GS, Rao VR, Koteshwar P. Utility of serum pancreatic enzyme levels in diagnosing blunt trauma to the pancreas: a prospective study with systematic review. Injury. 2014;45(9):1384-93.

113. Sharbidre KG, Galgano SJ, Morgan DE. Traumatic pancreatitis. Abdom Radiol (NY). 2019.

114. Moore EE, Cogbill TH, Malangoni MA, Jurkovich GJ, Champion HR, Gennarelli TA, et al. Organ injury scaling, II: Pancreas, duodenum, small bowel, colon, and rectum. J Trauma. 1990;30(11):1427-9.

115. Tenner S, Baillie J, DeWitt J, Vege SS, American College of G. American College of Gastroenterology guideline: management of acute pancreatitis. Am J Gastroenterol. 2013;108(9):1400-15; 16.

116. Camargo CA, Jr., Greig PD, Levy GA, Clavien PA. Acute pancreatitis following liver transplantation. J Am Coll Surg. 1995;181(3):249-56.

117. Schrier RW, Bulger RJ. Steroid-induced pancreatitis. JAMA. 1965;194(5):564-5.

118. Economou M, Zissis, M. Infectious cases of acute pancreatitis. Annals of Gastroenterology. 2000;13(2):98-101.

119. Pappenheimer AM, Daniels JB, Cheever FS, Weller TH. Lesions caused in suckling mice by certain viruses isolated from cases of so called non-paralytic poliomyelitis and of pleurodynia. J Exp Med. 1950;92(2):169-90.

120. Watanabe T, Minaga K, Kamata K, Kudo M, Strober W. Mechanistic Insights into Autoimmune Pancreatitis and IgG4-Related Disease. Trends Immunol. 2018;39(11):874-89.

121. Okazaki K, Tomiyama T, Mitsuyama T, Sumimoto K, Uchida K. Diagnosis and classification of autoimmune pancreatitis. Autoimmun Rev. 2014;13(4-5):451-8.

122. Nesher G, Breuer GS, Temprano K, Moore TL, Dahan D, Baer A, et al. Lupus-associated pancreatitis. Semin Arthritis Rheum. 2006;35(4):260-7.

123. Chang CC, Chang YS, Wang SH, Lin SY, Chen YH, Chen JH. Primary Sjogren's syndrome and the risk of acute pancreatitis: a nationwide cohort study. BMJ Open. 2017;7(8):e014807.

124. P G. Scorpion venoms. New York: Springer; 2015. pages cm p.

125. Bartholomew C. Acute scorpion pancreatitis in Trinidad. Br Med J. 1970;1(5697):666-8.

126. Fletcher MD, Possani LD, Fletcher PL, Jr. Morphological studies by light and electron microscopy of pancreatic acinar cells under the effect of Tityus serrulatus venom. Cell Tissue Res. 1994;278(2):255-64.

127. Bartholomew C, Murphy JJ, McGeeney KF, Fitzgerald O. Exocrine pancreatic response to the venom of the scorpion, Tityus trinitatis. Gut. 1977;18(8):623-5.

128. Bartholomew C, McGeeney KF, Murphy JJ, Fitzgerald O, Sankaran H. Experimental studies on the aetiology of acute scorpion pancreatitis. Br J Surg. 1976;63(10):807-10.

129. Sankaran H, Deveney CW, Bartholomew C, Raghupathy E. Action of the venom of the scorpion Tityus trinitatis on pancreatic insulin secretion. Biochem Pharmacol. 1983;32(6):1101-4.

130. Bess MA, Edis AJ, van Heerden JA. Hyperparathyroidism and pancreatitis. Chance or a causal association? JAMA. 1980;243(3):246-7.

131. Tsuang W, Navaneethan U, Ruiz L, Palascak JB, Gelrud A. Hypertriglyceridemic pancreatitis: presentation and management. Am J Gastroenterol. 2009;104(4):984-91.

132. Ewald N, Hardt PD, Kloer HU. Severe hypertriglyceridemia and pancreatitis: presentation and management. Curr Opin Lipidol. 2009;20(6):497-504.

133. Noble MD, Romac J, Vigna SR, Liddle RA. A pH-sensitive, neurogenic pathway mediates disease severity in a model of post-ERCP pancreatitis. Gut. 2008;57(11):1566-71.

134. Lichtenstein A, Milani R, Jr., Fernezlian SM, Leme AS, Capelozzi VL, Martins MA. Acute lung injury in two experimental models of acute pancreatitis: infusion of saline or sodium taurocholate into the pancreatic duct. Critical care medicine. 2000;28(5):1497-502.

135. Sahar N, Ross A, Lakhtakia S, Cote GA, Neuhaus H, Bruno MJ, et al. Reducing the risk of post-ERCP pancreatitis using 4 French pancreatic plastic stents placed with common type guidewires - Results from a prospective multi-national registry. Dig Endosc. 2018.

136. Elmunzer BJ, Scheiman JM, Lehman GA, Chak A, Mosler P, Higgins PD, et al. A randomized trial of rectal indomethacin to prevent post-ERCP pancreatitis. N Engl J Med. 2012;366(15):1414-22.

137. Kubiliun NM, Adams MA, Akshintala VS, Conte ML, Cote GA, Cotton PB, et al. Evaluation of Pharmacologic Prevention of Pancreatitis After Endoscopic Retrograde Cholangiopancreatography: A Systematic Review. Clin Gastroenterol Hepatol. 2015;13(7):1231-9; quiz e70-1.

138. Alexandre M, Uduman AK, Minervini S, Raoof A, Shugrue CA, Akinbiyi EO, et al. Tobacco carcinogen 4-(methylnitrosamino)-1-(3-pyridyl)-1-butanone initiates and enhances pancreatitis responses. Am J Physiol Gastrointest Liver Physiol. 2012;303(6):G696-704.

139. Srinivasan P, Thrower EC, Loganathan G, Balamurugan AN, Subramanian VS, Gorelick FS, et al. Chronic Nicotine Exposure In Vivo and In Vitro Inhibits Vitamin B1 (Thiamin) Uptake by Pancreatic Acinar Cells. PLoS One. 2015;10(12):e0143575.

140. Srinivasan P, Subramanian VS, Said HM. Effect of the cigarette smoke component, 4-(methylnitrosamino)-1-(3-pyridyl)-1-butanone (NNK), on physiological and molecular parameters of thiamin uptake by pancreatic acinar cells. PLoS One. 2013;8(11):e78853.

141. Banks PA, Bollen TL, Dervenis C, Gooszen HG, Johnson CD, Sarr MG, et al. Classification of acute pancreatitis--2012: revision of the Atlanta classification and definitions by international consensus. Gut. 2013;62(1):102-11.

142. Lankisch PG, Burchard-Reckert S, Lehnick D. Underestimation of acute pancreatitis: patients with only a small increase in amylase/lipase levels can also have or develop severe acute pancreatitis. Gut. 1999;44(4):542-4.

143. Working Party of the British Society of G, Association of Surgeons of Great B, Ireland, Pancreatic Society of Great B, Ireland, Association of Upper GISoGB, et al. UK guidelines for the management of acute pancreatitis. Gut. 2005;54 Suppl 3:iii1-9.

144. Mole DJ, Olabi B, Robinson V, Garden OJ, Parks RW. Incidence of individual organ dysfunction in fatal acute pancreatitis: analysis of 1024 death records. HPB (Oxford). 2009;11(2):166-70.

145. Gloor B, Muller CA, Worni M, Martignoni ME, Uhl W, Buchler MW. Late mortality in patients with severe acute pancreatitis. Br J Surg. 2001;88(7):975-9.

146. Mutinga M, Rosenbluth A, Tenner SM, Odze RR, Sica GT, Banks PA. Does mortality occur early or late in acute pancreatitis? Int J Pancreatol. 2000;28(2):91-5.

147. Andersson B, Ansari D, Andersson E, Persson S, Andersson R. Fatal acute pancreatitis occurring outside of the hospital: clinical and social characteristics. World J Surg. 2010;34(10):2286-91.

148. Werlin SL, Kugathasan S, Frautschy BC. Pancreatitis in children. J Pediatr Gastroenterol Nutr. 2003;37(5):591-5.

149. Park A, Latif SU, Shah AU, Tian J, Werlin S, Hsiao A, et al. Changing referral trends of acute pancreatitis in children: A 12-year single-center analysis. J Pediatr Gastroenterol Nutr. 2009;49(3):316-22.

150. Sanchez-Ramirez CA, Larrosa-Haro A, Flores-Martinez S, Sanchez-Corona J, Villa-Gomez A, Macias-Rosales R. Acute and recurrent pancreatitis in children: etiological factors. Acta Paediatr. 2007;96(4):534-7.

151. Nydegger A, Heine RG, Ranuh R, Gegati-Levy R, Crameri J, Oliver MR. Changing incidence of acute pancreatitis: 10-year experience at the Royal Children's Hospital, Melbourne. J Gastroenterol Hepatol. 2007;22(8):1313-6.

152. Kandula L, Lowe ME. Etiology and outcome of acute pancreatitis in infants and toddlers. J Pediatr. 2008;152(1):106-10, 10 e1.

153. Pezzilli R, Morselli-Labate AM, Castellano E, Barbera C, Corrao S, Di Prima L, et al. Acute pancreatitis in children. An Italian multicentre study. Dig Liver Dis. 2002;34(5):343-8.

154. Teblick A, Peeters B, Langouche L, Van den Berghe G. Adrenal function and dysfunction in critically ill patients. Nat Rev Endocrinol. 2019;15(7):417-27.

155. Tran DD, Oe PL, de Fijter CW, van der Meulen J, Cuesta MA. Acute renal failure in patients with acute pancreatitis: prevalence, risk factors, and outcome. Nephrol Dial Transplant. 1993;8(10):1079-84.

156. Johnson CD, Abu-Hilal M. Persistent organ failure during the first week as a marker of fatal outcome in acute pancreatitis. Gut. 2004;53(9):1340-4.

157. Buter A, Imrie CW, Carter CR, Evans S, McKay CJ. Dynamic nature of early organ dysfunction determines outcome in acute pancreatitis. Br J Surg. 2002;89(3):298-302.

158. Dellinger EP, Forsmark CE, Layer P, Levy P, Maravi-Poma E, Petrov MS, et al. Determinant-based classification of acute pancreatitis severity: an international multidisciplinary consultation. Ann Surg. 2012;256(6):875-80.

159. Fan E, Brodie D, Slutsky AS. Acute Respiratory Distress Syndrome: Advances in Diagnosis and Treatment. JAMA. 2018;319(7):698-710.

160. Capelozzi VL, Allen TC, Beasley MB, Cagle PT, Guinee D, Hariri LP, et al. Molecular and Immune Biomarkers in Acute Respiratory Distress Syndrome: A Perspective From Members of the Pulmonary Pathology Society. Arch Pathol Lab Med. 2017;141(12):1719-27.

161. Akbarshahi H, Rosendahl AH, Westergren-Thorsson G, Andersson R. Acute lung injury in acute pancreatitis--awaiting the big leap. Respir Med. 2012;106(9):1199-210.

162. Kumar P, Gupta P, Rana S. Thoracic complications of pancreatitis. JGH Open. 2019;3(1):71-9.

163. Lambden S, Creagh-Brown BC, Hunt J, Summers C, Forni LG. Definitions and pathophysiology of vasoplegic shock. Crit Care. 2018;22(1):174.

164. Kellum JA, Prowle JR. Paradigms of acute kidney injury in the intensive care setting. Nat Rev Nephrol. 2018;14(4):217-30.

165. Nassar TI, Qunibi WY. AKI Associated with Acute Pancreatitis. Clin J Am Soc Nephrol. 2019.

166. Ranson JH, Pasternack BS. Statistical methods for quantifying the severity of clinical acute pancreatitis. J Surg Res. 1977;22(2):79-91.

167. Ranson JH, Rifkind KM, Roses DF, Fink SD, Eng K, Spencer FC. Prognostic signs and the role of operative management in acute pancreatitis. Surg Gynecol Obstet. 1974;139(1):69-81.

168. Imrie CW, Benjamin IS, Ferguson JC, McKay AJ, Mackenzie I, O'Neill J, et al. A single-centre double-blind trial of Trasylol therapy in primary acute pancreatitis. Br J Surg. 1978;65(5):337-41.

169. Osborne DH, Imrie CW, Carter DC. Biliary surgery in the same admission for gallstone-associated acute pancreatitis. Br J Surg. 1981;68(11):758-61.

170. Blamey SL, Imrie CW, O'Neill J, Gilmour WH, Carter DC. Prognostic factors in acute pancreatitis. Gut. 1984;25(12):1340-6.

171. Balthazar EJ, Ranson JH, Naidich DP, Megibow AJ, Caccavale R, Cooper MM. Acute pancreatitis: prognostic value of CT. Radiology. 1985;156(3):767-72.

172. Larvin M, McMahon MJ. APACHE-II score for assessment and monitoring of acute pancreatitis. Lancet. 1989;2(8656):201-5.

173. Knaus WA, Draper EA, Wagner DP, Zimmerman JE. APACHE II: a severity of disease classification system. Crit Care Med. 1985;13(10):818-29.

174. Fan ST, Lai EC, Mok FP, Lo CM, Zheng SS, Wong J. Prediction of the severity of acute pancreatitis. Am J Surg. 1993;166(3):262-8; discussion 9.

175. Ogawa M, Hirota M, Hayakawa T, Matsuno S, Watanabe S, Atomi Y, et al. Development and use of a new staging system for severe acute pancreatitis based on a nationwide survey in Japan. Pancreas. 2002;25(4):325-30.

176. Brown A, James-Stevenson T, Dyson T, Grunkenmeier D. The panc 3 score: a rapid and accurate test for predicting severity on presentation in acute pancreatitis. J Clin Gastroenterol. 2007;41(9):855-8.

177. Harrison DA, D'Amico G, Singer M. The Pancreatitis Outcome Prediction (POP) Score: a new prognostic index for patients with severe acute pancreatitis. Crit Care Med. 2007;35(7):1703-8.

178. Wu BU, Johannes RS, Sun X, Tabak Y, Conwell DL, Banks PA. The early prediction of mortality in acute pancreatitis: a large population-based study. Gut. 2008;57(12):1698-703.

179. Lankisch PG, Weber-Dany B, Hebel K, Maisonneuve P, Lowenfels AB. The harmless acute pancreatitis score: a clinical algorithm for rapid initial stratification of nonsevere disease. Clin Gastroenterol Hepatol. 2009;7(6):702-5; quiz 607.

180. Marshall JC, Cook DJ, Christou NV, Bernard GR, Sprung CL, Sibbald WJ. Multiple organ dysfunction score: a reliable descriptor of a complex clinical outcome. Crit Care Med. 1995;23(10):1638-52.

181. Vincent JL, Moreno R, Takala J, Willatts S, De Mendonca A, Bruining H, et al. The SOFA (Sepsis-related Organ Failure Assessment) score to describe organ dysfunction/failure. On behalf of the Working Group on Sepsis-Related Problems of the European Society of Intensive Care Medicine. Intensive Care Med. 1996;22(7):707-10.

182. Buxbaum J, Quezada M, Chong B, Gupta N, Yu CY, Lane C, et al. The Pancreatitis Activity Scoring System predicts clinical outcomes in acute pancreatitis: findings from a prospective cohort study. Am J Gastroenterol. 2018;113(5):755-64.

183. Wu BU, Batech M, Quezada M, Lew D, Fujikawa K, Kung J, et al. Dynamic Measurement of Disease Activity in Acute Pancreatitis: The Pancreatitis Activity Scoring System. Am J Gastroenterol. 2017;112(7):1144-52.

184. Bradley EL, 3rd. A clinically based classification system for acute pancreatitis. Summary of the International Symposium on Acute Pancreatitis, Atlanta, Ga, September 11 through 13, 1992. Arch Surg. 1993;128(5):586-90.

185. Schuster KM, Holena DN, Salim A, Savage S, Crandall M. American Association for the Surgery of Trauma emergency general surgery guideline summaries 2018: acute appendicitis, acute cholecystitis, acute diverticulitis, acute pancreatitis, and small bowel obstruction. Trauma Surg Acute Care Open. 2019;4(1):e000281.

186. Krishna SG, Hinton A, Oza V, Hart PA, Swei E, El-Dika S, et al. Morbid Obesity Is Associated With Adverse Clinical Outcomes in Acute Pancreatitis: A Propensity-Matched Study. Am J Gastroenterol. 2015;110(11):1608-19.

187. Abu Hilal M, Armstrong T. The impact of obesity on the course and outcome of acute pancreatitis. Obes Surg. 2008;18(3):326-8.

188. Navina S, Acharya C, DeLany JP, Orlichenko LS, Baty CJ, Shiva SS, et al. Lipotoxicity causes multisystem organ failure and exacerbates acute pancreatitis in obesity. Sci Transl Med. 2011;3(107):107ra10.

189. Gornik I, Gasparovic V, Gubarev Vrdoljak N, Haxiu A, Vucelic B. Prior statin therapy is associated with milder course and better outcome in acute pancreatitis--a cohort study. Pancreatology. 2013;13(3):196-200.

190. Premkumar R, Phillips AR, Petrov MS, Windsor JA. The clinical relevance of obesity in acute pancreatitis: targeted systematic reviews. Pancreatology. 2015;15(1):25-33.

191. Mayadas TN, Cullere X, Lowell CA. The multifaceted functions of neutrophils. Annu Rev Pathol. 2014;9:181-218.

192. Franco-Pons N, Gea-Sorli S, Closa D. Release of inflammatory mediators by adipose tissue during acute pancreatitis. J Pathol. 2010;221(2):175-82.

193. Lopez-Vicario C, Titos E, Walker ME, Alcaraz-Quiles J, Casulleras M, Duran-Guell M, et al. Leukocytes from obese individuals exhibit an impaired SPM signature. FASEB J. 2019;33(6):7072-83.

194. Bone RC, Balk RA, Cerra FB, Dellinger RP, Fein AM, Knaus WA, et al. Definitions for sepsis and organ failure and guidelines for the use of innovative therapies in sepsis. The ACCP/SCCM Consensus Conference Committee. American College of Chest Physicians/Society of Critical Care Medicine. Chest. 1992;101(6):1644-55.

195. Mittal R, Coopersmith CM. Redefining the gut as the motor of critical illness. Trends Mol Med. 2014;20(4):214-23.

196. Sharma D, Jakkampudi A, Reddy R, Reddy PB, Patil A, Murthy HVV, et al. Association of Systemic Inflammatory and Anti-inflammatory Responses with Adverse Outcomes in Acute Pancreatitis: Preliminary Results of an Ongoing Study. Dig Dis Sci. 2017;62(12):3468-78.

197. Mylona V, Koussoulas V, Tzivras D, Makrygiannis E, Georgopoulou P, Koratzanis G, et al. Changes in adaptive and innate immunity in patients with acute pancreatitis and systemic inflammatory response syndrome. Pancreatology. 2011;11(5):475-81.

198. Lord JM, Midwinter MJ, Chen YF, Belli A, Brohi K, Kovacs EJ, et al. The systemic immune response to trauma: an overview of pathophysiology and treatment. Lancet. 2014;384(9952):1455-65.

199. Oiva J, Mustonen H, Kylanpaa ML, Kyhala L, Kuuliala K, Siitonen S, et al. Acute pancreatitis with organ dysfunction associates with abnormal blood lymphocyte signaling: controlled laboratory study. Crit Care. 2010;14(6):R207.

200. Martinon F, Mayor A, Tschopp J. The inflammasomes: guardians of the body. Annu Rev Immunol. 2009;27:229-65.

201. Hoque R, Sohail M, Malik A, Sarwar S, Luo Y, Shah A, et al. TLR9 and the NLRP3 inflammasome link acinar cell death with inflammation in acute pancreatitis. Gastroenterology. 2011;141(1):358-69.

202. Kawai T, Akira S. The role of pattern-recognition receptors in innate immunity: update on Toll-like receptors. Nat Immunol. 2010;11(5):373-84.

203. Hoque R, Malik AF, Gorelick F, Mehal WZ. Sterile inflammatory response in acute pancreatitis. Pancreas. 2012;41(3):353-7.

204. Cheng Z, Abrams ST, Alhamdi Y, Toh J, Yu W, Wang G, et al. Circulating Histones Are Major Mediators of Multiple Organ Dysfunction Syndrome in Acute Critical Illnesses. Crit Care Med. 2019.

205. Cauwels A, Rogge E, Vandendriessche B, Shiva S, Brouckaert P. Extracellular ATP drives systemic inflammation, tissue damage and mortality. Cell Death Dis. 2014;5:e1102.

206. Scaffidi P, Misteli T, Bianchi ME. Release of chromatin protein HMGB1 by necrotic cells triggers inflammation. Nature. 2002;418(6894):191-5.

207. Marongiu L, Gornati L, Artuso I, Zanoni I, Granucci F. Below the surface: The inner lives of TLR4 and TLR9. J Leukoc Biol. 2019.

208. Chan JK, Roth J, Oppenheim JJ, Tracey KJ, Vogl T, Feldmann M, et al. Alarmins: awaiting a clinical response. J Clin Invest. 2012;122(8):2711-9.

209. Harris HE, Raucci A. Alarmin(g) news about danger: workshop on innate danger signals and HMGB1. EMBO Rep. 2006;7(8):774-8.

210. Kocsis AK, Szabolcs A, Hofner P, Takacs T, Farkas G, Boda K, et al. Plasma concentrations of high-mobility group box protein 1, soluble receptor for advanced glycation end-products and circulating DNA in patients with acute pancreatitis. Pancreatology. 2009;9(4):383-91.

211. Hreggvidsdottir HS, Ostberg T, Wahamaa H, Schierbeck H, Aveberger AC, Klevenvall L, et al. The alarmin HMGB1 acts in synergy with endogenous and exogenous danger signals to promote inflammation. J Leukoc Biol. 2009;86(3):655-62.

212. Sawa H, Ueda T, Takeyama Y, Yasuda T, Shinzeki M, Nakajima T, et al. Blockade of high mobility group box-1 protein attenuates experimental severe acute pancreatitis. World J Gastroenterol. 2006;12(47):7666-70.

213. Kang R, Zhang Q, Hou W, Yan Z, Chen R, Bonaroti J, et al. Intracellular Hmgb1 inhibits inflammatory nucleosome release and limits acute pancreatitis in mice. Gastroenterology. 2014;146(4):1097-107.

214. Burk AM, Martin M, Flierl MA, Rittirsch D, Helm M, Lampl L, et al. Early complementopathy after multiple injuries in humans. Shock. 2012;37(4):348-54.

215. Hornung V, Ablasser A, Charrel-Dennis M, Bauernfeind F, Horvath G, Caffrey DR, et al. AIM2 recognizes cytosolic dsDNA and forms a caspase-1-activating inflammasome with ASC. Nature. 2009;458(7237):514-8.

216. Speakman EA, Dambuza IM, Salazar F, Brown GD. T Cell Antifungal Immunity and the Role of C-Type Lectin Receptors. Trends Immunol. 2020;41(1):61-76.

217. Bartlett R, Stokes L, Sluyter R. The P2X7 receptor channel: recent developments and the use of P2X7 antagonists in models of disease. Pharmacol Rev. 2014;66(3):638-75.

218. Ramos HJ, Gale M, Jr. RIG-I like receptors and their signaling crosstalk in the regulation of antiviral immunity. Curr Opin Virol. 2011;1(3):167-76.

219. Lorne E, Dupont H, Abraham E. Toll-like receptors 2 and 4: initiators of non-septic inflammation in critical care medicine? Intensive Care Med. 2010;36(11):1826-35.

220. Sharif R, Dawra R, Wasiluk K, Phillips P, Dudeja V, Kurt-Jones E, et al. Impact of toll-like receptor 4 on the severity of acute pancreatitis and pancreatitis-associated lung injury in mice. Gut. 2009;58(6):813-9.

221. Xue J, Habtezion A. Carbon monoxide-based therapy ameliorates acute pancreatitis via TLR4 inhibition. J Clin Invest. 2014;124(1):437-47.

222. Kang R, Chen R, Xie M, Cao L, Lotze MT, Tang D, et al. The Receptor for Advanced Glycation End Products Activates the AIM2 Inflammasome in Acute Pancreatitis. J Immunol. 2016;196(10):4331-7.

223. Huang H, Evankovich J, Yan W, Nace G, Zhang L, Ross M, et al. Endogenous histones function as alarmins in sterile inflammatory liver injury through Toll-like receptor 9 in mice. Hepatology. 2011;54(3):999-1008.

224. Pendharkar SA, Singh RG, Chand SK, Cervantes A, Petrov MS. Pro-inflammatory cytokines after an episode of acute pancreatitis: associations with fasting gut hormone profile. Inflamm Res. 2018;67(4):339-50.

225. Samanta J, Singh S, Arora S, Muktesh G, Aggarwal A, Dhaka N, et al. Cytokine profile in prediction of acute lung injury in patients with acute pancreatitis. Pancreatology. 2018;18(8):878-84.

226. Ohmoto K, Yamamoto S. Serum interleukin-6 and interleukin-10 in patients with acute pancreatitis: clinical implications. Hepatogastroenterology. 2005;52(64):990-4.

227. Jakkampudi A, Jangala R, Reddy R, Mitnala S, Rao GV, Pradeep R, et al. Acinar injury and early cytokine response in human acute biliary pancreatitis. Sci Rep. 2017;7(1):15276.

228. Koussoulas V, Tzivras M, Karagianni V, Spyridaki E, Plachouras D, Giamarellou H, et al. Monocytes in systematic inflammatory response syndrome: differences between sepsis and acute pancreatitis. World J Gastroenterol. 2006;12(41):6711-4.

229. Gukovsky I, Gukovskaya AS, Blinman TA, Zaninovic V, Pandol SJ. Early NF-kappaB activation is associated with hormone-induced pancreatitis. Am J Physiol. 1998;275(6):G1402-14.

230. Norman JG, Fink GW, Franz MG. Acute pancreatitis induces intrapancreatic tumor necrosis factor gene expression. Arch Surg. 1995;130(9):966-70.

231. Vaquero E, Gukovsky I, Zaninovic V, Gukovskaya AS, Pandol SJ. Localized pancreatic NF-kappaB activation and inflammatory response in taurocholate-induced pancreatitis. Am J Physiol Gastrointest Liver Physiol. 2001;280(6):G1197-208.

232. Gukovskaya AS, Gukovsky I, Zaninovic V, Song M, Sandoval D, Gukovsky S, et al. Pancreatic acinar cells produce, release, and respond to tumor necrosis factor-alpha. Role in regulating cell death and pancreatitis. J Clin Invest. 1997;100(7):1853-62.

233. Brenner D, Blaser H, Mak TW. Regulation of tumour necrosis factor signalling: live or let die. Nat Rev Immunol. 2015;15(6):362-74.

234. Rakonczay Z, Jr., Hegyi P, Takacs T, McCarroll J, Saluja AK. The role of NF-kappaB activation in the pathogenesis of acute pancreatitis. Gut. 2008;57(2):259-67.

235. Zaninovic V, Gukovskaya AS, Gukovsky I, Mouria M, Pandol SJ. Cerulein upregulates ICAM-1 in pancreatic acinar cells, which mediates neutrophil adhesion to these cells. Am J Physiol Gastrointest Liver Physiol. 2000;279(4):G666-76.

236. Zhang H, Neuhofer P, Song L, Rabe B, Lesina M, Kurkowski MU, et al. IL-6 trans-signaling promotes pancreatitis-associated lung injury and lethality. J Clin Invest. 2013;123(3):1019-31.

237. Heinrich PC, Behrmann I, Haan S, Hermanns HM, Muller-Newen G, Schaper F. Principles of interleukin (IL)-6-type cytokine signalling and its regulation. Biochem J. 2003;374(Pt 1):1-20.

238. Hayashi T, Ishida Y, Kimura A, Iwakura Y, Mukaida N, Kondo T. IFN-gamma protects cerulein-induced acute pancreatitis by repressing NF-kappa B activation. J Immunol. 2007;178(11):7385-94.

239. Souza DG, Vieira AT, Soares AC, Pinho V, Nicoli JR, Vieira LQ, et al. The essential role of the intestinal microbiota in facilitating acute inflammatory responses. J Immunol. 2004;173(6):4137-46.

240. Shrivastava P, Bhatia M. Essential role of monocytes and macrophages in the progression of acute pancreatitis. World J Gastroenterol. 2010;16(32):3995-4002.

241. Orr SK, Butler KL, Hayden D, Tompkins RG, Serhan CN, Irimia D. Gene Expression of Proresolving Lipid Mediator Pathways Is Associated With Clinical Outcomes in Trauma Patients. Crit Care Med. 2015;43(12):2642-50.

242. Parker LC, Whyte MK, Dower SK, Sabroe I. The expression and roles of Toll-like receptors in the biology of the human neutrophil. J Leukoc Biol. 2005;77(6):886-92.

243. Gukovskaya AS, Vaquero E, Zaninovic V, Gorelick FS, Lusis AJ, Brennan ML, et al. Neutrophils and NADPH oxidase mediate intrapancreatic trypsin activation in murine experimental acute pancreatitis. Gastroenterology. 2002;122(4):974-84.

244. Bhatia M, Saluja AK, Hofbauer B, Lee HS, Frossard JL, Steer ML. The effects of neutrophil depletion on a completely noninvasive model of acute pancreatitis-associated lung injury. Int J Pancreatol. 1998;24(2):77-83.

245. Kono H, Rock KL. How dying cells alert the immune system to danger. Nat Rev Immunol. 2008;8(4):279-89.

246. McDonald B, Pittman K, Menezes GB, Hirota SA, Slaba I, Waterhouse CC, et al. Intravascular danger signals guide neutrophils to sites of sterile inflammation. Science. 2010;330(6002):362-6.

247. Manohar M, Verma AK, Venkateshaiah SU, Mishra A. Role of eosinophils in the initiation and progression of pancreatitis pathogenesis. Am J Physiol Gastrointest Liver Physiol. 2018;314(2):G211-G22.

248. Lopez-Font I, Gea-Sorli S, de-Madaria E, Gutierrez LM, Perez-Mateo M, Closa D. Pancreatic and pulmonary mast cells activation during experimental acute pancreatitis. World J Gastroenterol. 2010;16(27):3411-7.

249. Saeki K, Kanai T, Nakano M, Nakamura Y, Miyata N, Sujino T, et al. CCL2-induced migration and SOCS3-mediated activation of macrophages are involved in cerulein-induced pancreatitis in mice. Gastroenterology. 2012;142(4):1010-20 e9.

250. Demols A, Le Moine O, Desalle F, Quertinmont E, Van Laethem JL, Deviere J. CD4(+)T cells play an important role in acute experimental pancreatitis in mice. Gastroenterology. 2000;118(3):582-90.

251. Sendler M, Weiss FU, Golchert J, Homuth G, van den Brandt C, Mahajan UM, et al. Cathepsin B-Mediated Activation of Trypsinogen in Endocytosing Macrophages Increases Severity of Pancreatitis in Mice. Gastroenterology. 2018;154(3):704-18 e10.

252. Perides G, Weiss ER, Michael ES, Laukkarinen JM, Duffield JS, Steer ML. TNF-alpha-dependent regulation of acute pancreatitis severity by Ly-6C(hi) monocytes in mice. J Biol Chem. 2011;286(15):13327-35.

253. Wen HJ, Gao S, Wang Y, Ray M, Magnuson MA, Wright CVE, et al. Myeloid Cell-Derived HB-EGF Drives Tissue Recovery After Pancreatitis. Cell Mol Gastroenterol Hepatol. 2019.

254. Bedrosian AS, Nguyen AH, Hackman M, Connolly MK, Malhotra A, Ibrahim J, et al. Dendritic cells promote pancreatic viability in mice with acute pancreatitis. Gastroenterology. 2011;141(5):1915-26 e1-14.

255. Dabrowski A, Osada J, Dabrowska MI, Wereszczynska-Siemiatkowska U. Monocyte subsets and natural killer cells in acute pancreatitis. Pancreatology. 2008;8(2):126-34.

256. Qiu L, Zhou Y, Yu Q, Yu J, Li Q, Sun R. Decreased levels of regulatory B cells in patients with acute pancreatitis: association with the severity of the disease. Oncotarget. 2018;9(90):36067-82.

257. Pietruczuk M, Dabrowska MI, Wereszczynska-Siemiatkowska U, Dabrowski A. Alteration of peripheral blood lymphocyte subsets in acute pancreatitis. World J Gastroenterol. 2006;12(33):5344-51.

258. Duggal NA, Snelson C, Shaheen U, Pearce V, Lord JM. Innate and adaptive immune dysregulation in critically ill ICU patients. Sci Rep. 2018;8(1):10186.

259. Shi C, Hou C, Zhu X, Peng Y, Guo F, Zhang K, et al. New Predictor of Organ Failure in Acute Pancreatitis: CD4+ T Lymphocytes and CD19+ B Lymphocytes. Biomed Res Int. 2018;2018:1012584.

260. Wei X, Yao W, Li H, Qian J, Xie Y, Zhang Z, et al. B and NK Cells Closely Correlate with the Condition of Patients with Acute Pancreatitis. Gastroenterol Res Pract. 2019;2019:7568410.

261. Ueda T, Takeyama Y, Yasuda T, Takase K, Nishikawa J, Kuroda Y. Functional alterations of splenocytes in severe acute pancreatitis. J Surg Res. 2002;102(2):161-8.

262. Osada J, Wereszczynska-Siemiatkowska U, Dabrowski A, Dabrowska MI. Platelet activation in acute pancreatitis. Pancreas. 2012;41(8):1319-24.

263. Johnson CD, Kingsnorth AN, Imrie CW, McMahon MJ, Neoptolemos JP, McKay C, et al. Double blind, randomised, placebo controlled study of a platelet activating factor antagonist, lexipafant, in the treatment and prevention of organ failure in predicted severe acute pancreatitis. Gut. 2001;48(1):62-9.

264. Abdulla A, Awla D, Hartman H, Rahman M, Jeppsson B, Regner S, et al. Role of platelets in experimental acute pancreatitis. Br J Surg. 2011;98(1):93-103.

265. Abdulla A, Awla D, Jeppsson B, Regner S, Thorlacius H. CD40L is not involved in acute experimental pancreatitis. Eur J Pharmacol. 2011;659(1):85-8.

266. Wetterholm E, Linders J, Merza M, Regner S, Thorlacius H. Platelet-derived CXCL4 regulates neutrophil infiltration and tissue damage in severe acute pancreatitis. Transl Res. 2016;176:105-18.

267. Vanhorebeek I, Langouche L, Van den Berghe G. Endocrine aspects of acute and prolonged critical illness. Nat Clin Pract Endocrinol Metab. 2006;2(1):20-31.

268. Boonen E, Vervenne H, Meersseman P, Andrew R, Mortier L, Declercq PE, et al. Reduced cortisol metabolism during critical illness. N Engl J Med. 2013;368(16):1477-88.

269. Russell G, Lightman, S. The human stress response. Nat Rev Endocrinol. 2019.

270. Han X, Li B, Ye X, Mulatibieke T, Wu J, Dai J, et al. Dopamine D2 receptor signalling controls inflammation in acute pancreatitis via a PP2A-dependent Akt/NF-kappaB signalling pathway. Br J Pharmacol. 2017;174(24):4751-70.

271. Singer M, De Santis V, Vitale D, Jeffcoate W. Multiorgan failure is an adaptive, endocrine-mediated, metabolic response to overwhelming systemic inflammation. Lancet. 2004;364(9433):545-8.

272. Gloor B, Uhl W, Tcholakov O, Roggo A, Muller CA, Worni M, et al. Hydrocortisone treatment of early SIRS in acute experimental pancreatitis. Dig Dis Sci. 2001;46(10):2154-61.

273. Blaine SK, Milivojevic V, Fox H, Sinha R. Alcohol Effects on Stress Pathways: Impact on Craving and Relapse Risk. Can J Psychiatry. 2016;61(3):145-53.

274. Matikainen E, Juntunen J, Salmi T. Autonomic dysfunction in long-standing alcoholism. Alcohol Alcohol. 1986;21(1):69-73.

275. Nathan C, Ding A. Nonresolving inflammation. Cell. 2010;140(6):871-82.

276. Serhan CN. Treating inflammation and infection in the 21st century: new hints from decoding resolution mediators and mechanisms. FASEB J. 2017;31(4):1273-88.

277. Fullerton JN, O'Brien AJ, Gilroy DW. Lipid mediators in immune dysfunction after severe inflammation. Trends Immunol. 2014;35(1):12-21.

278. Schauer C, Janko C, Munoz LE, Zhao Y, Kienhofer D, Frey B, et al. Aggregated neutrophil extracellular traps limit inflammation by degrading cytokines and chemokines. Nat Med. 2014;20(5):511-7.

279. Folias AE, Penaranda C, Su AL, Bluestone JA, Hebrok M. Aberrant innate immune activation following tissue injury impairs pancreatic regeneration. PLoS One. 2014;9(7):e102125.

280. Yu S, Xie J, Xiang Y, Dai S, Yu D, Sun H, et al. Downregulation of TNF-alpha/TNF-R1 Signals by AT-Lipoxin A4 May Be a Significant Mechanism of Attenuation in SAP-Associated Lung Injury. Mediators Inflamm. 2019;2019:9019404.

281. Shi Z, Ye W, Zhang J, Zhang F, Yu D, Yu H, et al. LipoxinA4 attenuates acute pancreatitis-associated acute lung injury by regulating AQP-5 and MMP-9 expression, anti-apoptosis and PKC/SSeCKS-mediated F-actin activation. Mol Immunol. 2018;103:78-88.

282. Lankisch PG, Breuer N, Bruns A, Weber-Dany B, Lowenfels AB, Maisonneuve P. Natural history of acute pancreatitis: a long-term population-based study. Am J Gastroenterol. 2009;104(11):2797-805; quiz 806.

283. Das SL, Singh PP, Phillips AR, Murphy R, Windsor JA, Petrov MS. Newly diagnosed diabetes mellitus after acute pancreatitis: a systematic review and meta-analysis. Gut. 2014;63(5):818-31.

284. Doepel M, Eriksson J, Halme L, Kumpulainen T, Hockerstedt K. Good long-term results in patients surviving severe acute pancreatitis. Br J Surg. 1993;80(12):1583-6.

285. Lin SY, Hsu WH, Lin CC, Lin CL, Tsai CH, Kao CH. Effect of acute pancreatitis on the risk of developing osteoporosis: A nationwide cohort study. PLoS One. 2017;12(6):e0179358.

286. Tummala P, Tariq SH, Chibnall JT, Agarwal B. Clinical predictors of pancreatic carcinoma causing acute pancreatitis. Pancreas. 2013;42(1):108-13.

287. Skouras C, Hayes AJ, Williams L, Garden OJ, Parks RW, Mole DJ. Early organ dysfunction affects long-term survival in acute pancreatitis patients. HPB (Oxford). 2014;16(9):789-96.

288. Ventre C, Nowell S, Graham C, Kidd D, Skouras C, Mole DJ. Survival and new-onset morbidity after critical care admission for acute pancreatitis in Scotland: a national electronic healthcare record linkage cohort study. BMJ Open. 2018;8(12):e023853.

289. Moggia E, Koti R, Belgaumkar AP, Fazio F, Pereira SP, Davidson BR, et al. Pharmacological interventions for acute pancreatitis. Cochrane Database Syst Rev. 2017;4:CD011384.

290. Abu-Zidan FM, Windsor JA. Lexipafant and acute pancreatitis: a critical appraisal of the clinical trials. Eur J Surg. 2002;168(4):215-9.

291. Szentesi A, Toth E, Balint E, Fanczal J, Madacsy T, Laczko D, et al. Analysis of Research Activity in Gastroenterology: Pancreatitis Is in Real Danger. PLoS One. 2016;11(10):e0165244.

292. Lee PJ, Papachristou GI. New insights into acute pancreatitis. Nat Rev Gastroenterol Hepatol. 2019.

293. Huber W, Algul H, Lahmer T, Mayr U, Lehmann M, Schmid RM, et al. Pancreatitis cytosorbents (CytoSorb) inflammatory cytokine removal: A Prospective Study (PACIFIC). Medicine (Baltimore). 2019;98(4):e13044.

294. Marta K, Szabo AN, Pecsi D, Varju P, Bajor J, Godi S, et al. High versus low energy administration in the early phase of acute pancreatitis (GOULASH trial): protocol of a multicentre randomised double-blind clinical trial. BMJ Open. 2017;7(9):e015874.

295. Vervliet T, Yule DI, Bultynck G. Carbohydrate Loading to Combat Acute Pancreatitis. Trends Biochem Sci. 2018;43(10):741-4.

296. Singer M. Critical illness and flat batteries. Crit Care. 2017;21(Suppl 3):309.

297. Walker AL, Ancellin N, Beaufils B, Bergeal M, Binnie M, Bouillot A, et al. Development of a Series of Kynurenine 3-Monooxygenase Inhibitors Leading to a Clinical Candidate for the Treatment of Acute Pancreatitis. J Med Chem. 2017;60(8):3383-404.

298. Galloway P, McMillan DC, Sattar N. Effect of the inflammatory response on trace element and vitamin status. Ann Clin Biochem. 2000;37 (Pt 3):289-97.

299. Piro A, Tagarelli G, Lagonia P, Tagarelli A, Quattrone A. Casimir Funk: his discovery of the vitamins and their deficiency disorders. Ann Nutr Metab. 2010;57(2):85-8.

300. Zhang P, Tsuchiya K, Kinoshita T, Kushiyama H, Suidasari S, Hatakeyama M, et al. Vitamin B6 Prevents IL-1beta Protein Production by Inhibiting NLRP3 Inflammasome Activation. J Biol Chem. 2016;291(47):24517-27.

301. Mc MR, Oncley JL. The specific binding of L-tryptophan to serum albumin. J Biol Chem. 1958;233(6):1436-47.

302. Bender DA. Biochemistry of tryptophan in health and disease. Mol Aspects Med. 1983;6(2):101-97.

303. Lam H, Oh DC, Cava F, Takacs CN, Clardy J, de Pedro MA, et al. D-amino acids govern stationary phase cell wall remodeling in bacteria. Science. 2009;325(5947):1552-5.

304. Wu G. Amino acids: metabolism, functions, and nutrition. Amino Acids. 2009;37(1):1-17.

305. Ambrogelly A, Palioura S, Soll D. Natural expansion of the genetic code. Nat Chem Biol. 2007;3(1):29-35.

306. Richard DM, Dawes MA, Mathias CW, Acheson A, Hill-Kapturczak N, Dougherty DM. L-Tryptophan: Basic Metabolic Functions, Behavioral Research and Therapeutic Indications. Int J Tryptophan Res. 2009;2:45-60.

307. McGaha TL, Huang L, Lemos H, Metz R, Mautino M, Prendergast GC, et al. Amino acid catabolism: a pivotal regulator of innate and adaptive immunity. Immunol Rev. 2012;249(1):135-57.

308. Cervenka I, Agudelo LZ, Ruas JL. Kynurenines: Tryptophan's metabolites in exercise, inflammation, and mental health. Science. 2017;357(6349).

309. Radwanski ER, Last RL. Tryptophan biosynthesis and metabolism: biochemical and molecular genetics. Plant Cell. 1995;7(7):921-34.

310. Jimenez EC, Olivera BM, Gray WR, Cruz LJ. Contryphan is a D-tryptophan-containing Conus peptide. J Biol Chem. 1996;271(45):28002-5.

311. Notarangelo FM, Wang XD, Horning KJ, Schwarcz R. Role of d-amino acid oxidase in the production of kynurenine pathway metabolites from d-tryptophan in mice. J Neurochem. 2016;136(4):804-14.

312. Hopkins FG, Cole SW. A contribution to the chemistry of proteids: Part I. A preliminary study of a hitherto undescribed product of tryptic digestion. J Physiol. 1901;27(4-5):418-28.

313. Ehrenshaft M, Deterding LJ, Mason RP. Tripping up Trp: Modification of protein tryptophan residues by reactive oxygen species, modes of detection, and biological consequences. Free Radic Biol Med. 2015;89:220-8.

314. McMenamy RH. Binding of indole analogues to human serum albumin. Effects of fatty acids. J Biol Chem. 1965;240(11):4235-43.

315. Cynober LA. Plasma amino acid levels with a note on membrane transport: characteristics, regulation, and metabolic significance. Nutrition. 2002;18(9):761-6.

316. Le Floc'h N, Otten W, Merlot E. Tryptophan metabolism, from nutrition to potential therapeutic applications. Amino Acids. 2011;41(5):1195-205.

317. Parthasarathy A, Cross PJ, Dobson RCJ, Adams LE, Savka MA, Hudson AO. A Three-Ring Circus: Metabolism of the Three Proteogenic Aromatic Amino Acids and Their Role in the Health of Plants and Animals. Front Mol Biosci. 2018;5:29.

318. Herrmann KM. The Shikimate Pathway: Early Steps in the Biosynthesis of Aromatic Compounds. Plant Cell. 1995;7(7):907-19.

319. Herrmann KM, Weaver LM. The Shikimate Pathway. Annu Rev Plant Physiol Plant Mol Biol. 1999;50:473-503.

320. Dunn MF, Niks D, Ngo H, Barends TR, Schlichting I. Tryptophan synthase: the workings of a channeling nanomachine. Trends Biochem Sci. 2008;33(6):254-64.

321. Alkhalaf LM, Ryan KS. Biosynthetic manipulation of tryptophan in bacteria: pathways and mechanisms. Chem Biol. 2015;22(3):317-28.

322. Maeda H, Dudareva N. The shikimate pathway and aromatic amino Acid biosynthesis in plants. Annu Rev Plant Biol. 2012;63:73-105.

323. Merino E, Jensen RA, Yanofsky C. Evolution of bacterial trp operons and their regulation. Curr Opin Microbiol. 2008;11(2):78-86.

324. Losick R, Sonenshein AL. Molecular biology. Turning gene regulation on its head. Science. 2001;293(5537):2018-9.

325. Hubbard TD, Murray IA, Perdew GH. Indole and Tryptophan Metabolism: Endogenous and Dietary Routes to Ah Receptor Activation. Drug Metab Dispos. 2015;43(10):1522-35.

326. Yanofsky C, Horn V, Gollnick P. Physiological studies of tryptophan transport and tryptophanase operon induction in Escherichia coli. J Bacteriol. 1991;173(19):6009-17.

327. Nongonierma AB, FitzGerald RJ. Milk proteins as a source of tryptophan-containing bioactive peptides. Food Funct. 2015;6(7):2115-27.

328. Agus A, Planchais J, Sokol H. Gut Microbiota Regulation of Tryptophan Metabolism in Health and Disease. Cell Host Microbe. 2018;23(6):716-24.

329. Millward DJ. Identifying recommended dietary allowances for protein and amino acids: a critique of the 2007 WHO/FAO/UNU report. Br J Nutr. 2012;108 Suppl 2:S3-21.

330. Lazaris-Brunner G, Rafii M, Ball RO, Pencharz PB. Tryptophan requirement in young adult women as determined by indicator amino acid oxidation with L-[13C]phenylalanine. Am J Clin Nutr. 1998;68(2):303-10.

331. Kandasamy P, Gyimesi G, Kanai Y, Hediger MA. Amino acid transporters revisited: New views in health and disease. Trends Biochem Sci. 2018;43(10):752-89.

332. Segawa H, Fukasawa Y, Miyamoto K, Takeda E, Endou H, Kanai Y. Identification and functional characterization of a Na+-independent neutral amino acid transporter with broad substrate selectivity. J Biol Chem. 1999;274(28):19745-51.

333. Seymour RL, Ganapathy V, Mellor AL, Munn DH. A high-affinity, tryptophan-selective amino acid transport system in human macrophages. J Leukoc Biol. 2006;80(6):1320-7.

334. Bhutia YD, Babu E, Ganapathy V. Interferon-gamma induces a tryptophan-selective amino acid transporter in human colonic epithelial cells and mouse dendritic cells. Biochim Biophys Acta. 2015;1848(2):453-62.

335. Miyanokoshi M, Yokosawa T, Wakasugi K. Tryptophanyl-tRNA synthetase mediates high-affinity tryptophan uptake into human cells. J Biol Chem. 2018;293(22):8428-38.

336. Cheon CK, Lee BH, Ko JM, Kim HJ, Yoo HW. Novel mutation in SLC6A19 causing late-onset seizures in Hartnup disorder. Pediatr Neurol. 2010;42(5):369-71.

337. Gao J, Xu K, Liu H, Liu G, Bai M, Peng C, et al. Impact of the Gut Microbiota on Intestinal Immunity Mediated by Tryptophan Metabolism. Front Cell Infect Microbiol. 2018;8:13.

338. Zelante T, Iannitti RG, Cunha C, De Luca A, Giovannini G, Pieraccini G, et al. Tryptophan catabolites from microbiota engage aryl hydrocarbon receptor and balance mucosal reactivity via interleukin-22. Immunity. 2013;39(2):372-85.

339. Roager HM, Licht TR. Microbial tryptophan catabolites in health and disease. Nat Commun. 2018;9(1):3294.

340. Islam J, Sato S, Watanabe K, Watanabe T, Ardiansyah, Hirahara K, et al. Dietary tryptophan alleviates dextran sodium sulfate-induced colitis through aryl hydrocarbon receptor in mice. J Nutr Biochem. 2017;42:43-50.

341. Lamas B, Natividad JM, Sokol H. Aryl hydrocarbon receptor and intestinal immunity. Mucosal Immunol. 2018;11(4):1024-38.

342. Yano JM, Yu K, Donaldson GP, Shastri GG, Ann P, Ma L, et al. Indigenous bacteria from the gut microbiota regulate host serotonin biosynthesis. Cell. 2015;161(2):264-76.

343. Sjoerdsma A, Weissbach H, Udenfriend S. A clinical, physiologic and biochemical study of patients with malignant carcinoid (argentaffinoma). Am J Med. 1956;20(4):520-32.

344. Allegri G, Costa CV, Bertazzo A, Biasiolo M, Ragazzi E. Enzyme activities of tryptophan metabolism along the kynurenine pathway in various species of animals. Farmaco. 2003;58(9):829-36.

345. Gershon MD, Tack J. The serotonin signaling system: from basic understanding to drug development for functional GI disorders. Gastroenterology. 2007;132(1):397-414.

346. Clarke G, Grenham S, Scully P, Fitzgerald P, Moloney RD, Shanahan F, et al. The microbiome-gut-brain axis during early life regulates the hippocampal serotonergic system in a sex-dependent manner. Mol Psychiatry. 2013;18(6):666-73.

347. Ruddick JP, Evans AK, Nutt DJ, Lightman SL, Rook GA, Lowry CA. Tryptophan metabolism in the central nervous system: medical implications. Expert Rev Mol Med. 2006;8(20):1-27.

348. Eynard N, Flachaire E, Lestra C, Broyer M, Zaidan R, Claustrat B, et al. Platelet serotonin content and free and total plasma tryptophan in healthy volunteers during 24 hours. Clin Chem. 1993;39(11 Pt 1):2337-40.

349. Davies SK, Ang JE, Revell VL, Holmes B, Mann A, Robertson FP, et al. Effect of sleep deprivation on the human metabolome. Proceedings of the National Academy of Sciences of the United States of America. 2014;111(29):10761-6.

350. Stone TW, Darlington LG. Endogenous kynurenines as targets for drug discovery and development. Nat Rev Drug Discov. 2002;1(8):609-20.

351. Badawy AA. Tryptophan availability for kynurenine pathway metabolism across the life span: Control mechanisms and focus on aging, exercise, diet and nutritional supplements. Neuropharmacology. 2017;112(Pt B):248-63.

352. Yeung AW, Terentis AC, King NJ, Thomas SR. Role of indoleamine 2,3-dioxygenase in health and disease. Clin Sci (Lond). 2015;129(7):601-72.

353. Frick B, Schroecksnadel K, Neurauter G, Leblhuber F, Fuchs D. Increasing production of homocysteine and neopterin and degradation of tryptophan with older age. Clin Biochem. 2004;37(8):684-7.

354. Hargreaves KM, Pardridge WM. Neutral amino acid transport at the human blood-brain barrier. J Biol Chem. 1988;263(36):19392-7.

355. Curzon G, Friedel J, Knott PJ. The effect of fatty acids on the binding of tryptophan to plasma protein. Nature. 1973;242(5394):198-200.

356. Chaouloff F, Kennett GA, Serrurrier B, Merino D, Curzon G. Amino acid analysis demonstrates that increased plasma free tryptophan causes the increase of brain tryptophan during exercise in the rat. J Neurochem. 1986;46(5):1647-50.

357. Blomstrand E, Perrett D, Parry-Billings M, Newsholme EA. Effect of sustained exercise on plasma amino acid concentrations and on 5-hydroxytryptamine metabolism in six different brain regions in the rat. Acta Physiol Scand. 1989;136(3):473-81.

358. Bell C, Abrams J, Nutt D. Tryptophan depletion and its implications for psychiatry. Br J Psychiatry. 2001;178:399-405.

359. Peng W, Robertson L, Gallinetti J, Mejia P, Vose S, Charlip A, et al. Surgical stress resistance induced by single amino acid deprivation requires Gcn2 in mice. Sci Transl Med. 2012;4(118):118ra11.

360. Metz R, Rust S, Duhadaway JB, Mautino MR, Munn DH, Vahanian NN, et al. IDO inhibits a tryptophan sufficiency signal that stimulates mTOR: A novel IDO effector pathway targeted by D-1-methyl-tryptophan. Oncoimmunology. 2012;1(9):1460-8.

361. Munn DH, Sharma MD, Baban B, Harding HP, Zhang Y, Ron D, et al. GCN2 kinase in T cells mediates proliferative arrest and anergy induction in response to indoleamine 2,3-dioxygenase. Immunity. 2005;22(5):633-42.

362. Munn DH, Shafizadeh E, Attwood JT, Bondarev I, Pashine A, Mellor AL. Inhibition of T cell proliferation by macrophage tryptophan catabolism. J Exp Med. 1999;189(9):1363-72.

363. Liu H, Huang L, Bradley J, Liu K, Bardhan K, Ron D, et al. GCN2-dependent metabolic stress is essential for endotoxemic cytokine induction and pathology. Mol Cell Biol. 2014;34(3):428-38.

364. van Beek AA, Hugenholtz F, Meijer B, Sovran B, Perdijk O, Vermeij WP, et al. Frontline Science: Tryptophan restriction arrests B cell development and enhances microbial diversity in WT and prematurely aging Ercc1(-/Delta7) mice. J Leukoc Biol. 2017;101(4):811-21.

365. Raju TN, Kanth VR, Reddy PU. Influence of kynurenines in pathogenesis of cataract formation in tryptophan-deficient regimen in Wistar rats. Indian J Exp Biol. 2007;45(6):543-8.

366. Bogan KL, Brenner C. Nicotinic acid, nicotinamide, and nicotinamide riboside: a molecular evaluation of NAD+ precursor vitamins in human nutrition. Annu Rev Nutr. 2008;28:115-30.

367. Verdin E. NAD(+) in aging, metabolism, and neurodegeneration. Science. 2015;350(6265):1208-13.

368. Gostner JM, Becker K, Kofler H, Strasser B, Fuchs D. Tryptophan Metabolism in Allergic Disorders. Int Arch Allergy Immunol. 2016;169(4):203-15.

369. Fuchs D, Moller AA, Reibnegger G, Werner ER, Werner-Felmayer G, Dierich MP, et al. Increased endogenous interferon-gamma and neopterin correlate with increased degradation of tryptophan in human immunodeficiency virus type 1 infection. Immunol Lett. 1991;28(3):207-11.

370. Routy JP, Mehraj V, Vyboh K, Cao W, Kema I, Jenabian MA. Clinical Relevance of Kynurenine Pathway in HIV/AIDS: An Immune Checkpoint at the Crossroads of Metabolism and Inflammation. AIDS Rev. 2015;17(2):96-106.

371. Mangge H, Stelzer I, Reininghaus EZ, Weghuber D, Postolache TT, Fuchs D. Disturbed tryptophan metabolism in cardiovascular disease. Curr Med Chem. 2014;21(17):1931-7.

372. Logters TT, Laryea MD, Altrichter J, Sokolowski J, Cinatl J, Reipen J, et al. Increased plasma kynurenine values and kynurenine-tryptophan ratios after major trauma are early indicators for the development of sepsis. Shock. 2009;32(1):29-34.

373. Ploder M, Spittler A, Kurz K, Neurauter G, Pelinka LE, Roth E, et al. Accelerated tryptophan degradation predicts poor survival in trauma and sepsis patients. Int J Tryptophan Res. 2010;3:61-7.

374. Pellegrin K, Neurauter G, Wirleitner B, Fleming AW, Peterson VM, Fuchs D. Enhanced enzymatic degradation of tryptophan by indoleamine 2,3-dioxygenase contributes to the tryptophan-deficient state seen after major trauma. Shock. 2005;23(3):209-15.

375. Skouras C, Zheng X, Binnie M, Homer NZ, Murray TB, Robertson D, et al. Increased levels of 3-hydroxykynurenine parallel disease severity in human acute pancreatitis. Sci Rep. 2016;6:33951.

376. Badawy AA, Evans M. Animal liver tryptophan pyrrolases: Absence of apoenzyme and of hormonal induction mechanism from species sensitive to tryptophan toxicity. Biochem J. 1976;158(1):79-88.

377. Badawy AA. Kynurenine Pathway of Tryptophan Metabolism: Regulatory and Functional Aspects. Int J Tryptophan Res. 2017;10:1178646917691938.

378. Khan MZ, Nawaz W. The emerging roles of human trace amines and human trace amine-associated receptors (hTAARs) in central nervous system. Biomed Pharmacother. 2016;83:439-49.

379. Jones RS. Tryptamine: a neuromodulator or neurotransmitter in mammalian brain? Prog Neurobiol. 1982;19(1-2):117-39.

380. Bittinger MA, Nguyen LP, Bradfield CA. Aspartate aminotransferase generates proagonists of the aryl hydrocarbon receptor. Mol Pharmacol. 2003;64(3):550-6.

381. Politi V, De Luca G, Gallai V, Puca, Comin M. Clinical experiences with the use of indole-3-pyruvic acid. Adv Exp Med Biol. 1999;467:227-32.

382. Badawy AA. Tryptophan metabolism, disposition and utilization in pregnancy. Biosci Rep. 2015;35(5).

383. Schwarcz R, Bruno JP, Muchowski PJ, Wu HQ. Kynurenines in the mammalian brain: when physiology meets pathology. Nat Rev Neurosci. 2012;13(7):465-77.

384. Keszthelyi D, Troost FJ, Masclee AA. Understanding the role of tryptophan and serotonin metabolism in gastrointestinal function. Neurogastroenterology and motility : the official journal of the European Gastrointestinal Motility Society. 2009;21(12):1239-49.

385. Savvateeva E, Popov A, Kamyshev N, Bragina J, Heisenberg M, Senitz D, et al. Age-dependent memory loss, synaptic pathology and altered brain plasticity in the Drosophila mutant cardinal accumulating 3-hydroxykynurenine. J Neural Transm (Vienna). 2000;107(5):581-601.

386. Phillips RS. Structure and mechanism of kynureninase. Arch Biochem Biophys. 2014;544:69-74.

387. Beadle GW, Mitchell HK, Nyc JF. Kynurenine as an Intermediate in the Formation of Nicotinic Acid from Tryptophane by Neurospora. Proc Natl Acad Sci U S A. 1947;33(6):155-8.

388. Oxford GS, Gillespie RG. Evolution and ecology of spider coloration. Annu Rev Entomol. 1998;43:619-43.

389. Gripenberg J, Honkanen, E., Patoharju, O. Fungus Pigments Part V. Degradations of Cinnabarin. Acta Chem Scand. 1957;11(9):1485-92.

390. Stone TW, Perkins MN. Quinolinic acid: a potent endogenous excitant at amino acid receptors in CNS. Eur J Pharmacol. 1981;72(4):411-2.

391. Perkins MN, Stone TW. An iontophoretic investigation of the actions of convulsant kynurenines and their interaction with the endogenous excitant quinolinic acid. Brain Res. 1982;247(1):184-7.

392. Guidetti P, Schwarcz R. 3-Hydroxykynurenine and quinolinate: pathogenic synergism in early grade Huntington's disease? Adv Exp Med Biol. 2003;527:137-45.

393. Badawy AA. Tryptophan metabolism in alcoholism. Nutr Res Rev. 2002;15(1):123-52.

394. van Baren N, Van den Eynde BJ. Tryptophan-degrading enzymes in tumoral immune resistance. Front Immunol. 2015;6:34.

395. Leklem JE. Quantitative aspects of tryptophan metabolism in humans and other species: a review. Am J Clin Nutr. 1971;24(6):659-72.

396. Bryan GT, Brown RR, Price JM. Mouse Bladder Carcinogenicity of Certain Tryptophan Metabolites and Other Aromatic Nitrogen Compounds Suspended in Cholesterol. Cancer Res. 1964;24:596-602.

397. Song P, Ramprasath T, Wang H, Zou MH. Abnormal kynurenine pathway of tryptophan catabolism in cardiovascular diseases. Cell Mol Life Sci. 2017;74(16):2899-916.

398. Oxenkrug G. Insulin resistance and dysregulation of tryptophan-kynurenine and kynurenine-nicotinamide adenine dinucleotide metabolic pathways. Mol Neurobiol. 2013;48(2):294-301.

399. Ramapriyan R, Caetano MS, Barsoumian HB, Mafra ACP, Zambalde EP, Menon H, et al. Altered cancer metabolism in mechanisms of immunotherapy resistance. Pharmacol Ther. 2018.

400. Favennec M, Hennart B, Caiazzo R, Leloire A, Yengo L, Verbanck M, et al. The kynurenine pathway is activated in human obesity and shifted toward kynurenine monooxygenase activation. Obesity (Silver Spring). 2015;23(10):2066-74.

401. Zeden JP, Fusch G, Holtfreter B, Schefold JC, Reinke P, Domanska G, et al. Excessive tryptophan catabolism along the kynurenine pathway precedes ongoing sepsis in critically ill patients. Anaesth Intensive Care. 2010;38(2):307-16.

402. Booth ES, Basran J, Lee M, Handa S, Raven EL. Substrate Oxidation by Indoleamine 2,3-Dioxygenase: EVIDENCE FOR A COMMON REACTION MECHANISM. J Biol Chem. 2015;290(52):30924-30.

403. Batabyal D, Yeh SR. Human tryptophan dioxygenase: a comparison to indoleamine 2,3-dioxygenase. J Am Chem Soc. 2007;129(50):15690-701.

404. Ball HJ, Jusof FF, Bakmiwewa SM, Hunt NH, Yuasa HJ. Tryptophan-catabolizing enzymes - party of three. Front Immunol. 2014;5:485.

405. Badawy AA, Dougherty DM. Assessment of the Human Kynurenine Pathway: Comparisons and Clinical Implications of Ethnic and Gender Differences in Plasma Tryptophan, Kynurenine Metabolites, and Enzyme Expressions at Baseline and After Acute Tryptophan Loading and Depletion. Int J Tryptophan Res. 2016;9:31-49.

406. Yamamoto S, Hayaishi O. Tryptophan pyrrolase of rabbit intestine. D- and L-tryptophan-cleaving enzyme or enzymes. J Biol Chem. 1967;242(22):5260-6.

407. Hayaishi O. My life with tryptophan--never a dull moment. Protein Sci. 1993;2(3):472-5.

408. Kanai M, Funakoshi H, Takahashi H, Hayakawa T, Mizuno S, Matsumoto K, et al. Tryptophan 2,3-dioxygenase is a key modulator of physiological neurogenesis and anxiety-related behavior in mice. Mol Brain. 2009;2:8.

409. Haber R, Bessette D, Hulihan-Giblin B, Durcan MJ, Goldman D. Identification of tryptophan 2,3-dioxygenase RNA in rodent brain. J Neurochem. 1993;60(3):1159-62.

410. Opitz CA, Litzenburger UM, Sahm F, Ott M, Tritschler I, Trump S, et al. An endogenous tumour-promoting ligand of the human aryl hydrocarbon receptor. Nature. 2011;478(7368):197-203.

411. Knox WE, Mehler AH. The adaptive increase of the tryptophan peroxidase-oxidase system of liver. Science. 1951;113(2931):237-8.

412. Nakamura T, Shinno H, Ichihara A. Insulin and glucagon as a new regulator system for tryptophan oxygenase activity demonstrated in primary cultured rat hepatocytes. J Biol Chem. 1980;255(16):7533-5.

413. Danesch U, Gloss B, Schmid W, Schutz G, Schule R, Renkawitz R. Glucocorticoid induction of the rat tryptophan oxygenase gene is mediated by two widely separated glucocorticoid-responsive elements. EMBO J. 1987;6(3):625-30.

414. Knox WE. Two mechanisms which increase in vivo the liver tryptophan peroxidase activity: specific enzyme adaptation and stimulation of the pituitary adrenal system. Br J Exp Pathol. 1951;32(5):462-9.

415. Nakamura T, Niimi S, Nawa K, Noda C, Ichihara A, Takagi Y, et al. Multihormonal regulation of transcription of the tryptophan 2,3-dioxygenase gene in primary cultures of adult rat hepatocytes with special reference to the presence of a transcriptional protein mediating the action of glucocorticoids. J Biol Chem. 1987;262(2):727-33.

416. Badawy AA. Effects of pregnancy on tryptophan metabolism and disposition in the rat. Biochem J. 1988;255(1):369-72.

417. Cho-Chung YS, Pitot HC. Feedback control of rat liver tryptophan pyrrolase. I. End product inhibition of trytophan pyrrolase activity. J Biol Chem. 1967;242(6):1192-8.

418. Wagner C. Regulation of the tryptophan-nicotinic acid-DPN pathway in the rat. Biochemical and Biophysical Research Communications. 1964;17(6):668-73.

419. Badawy AA. Pellagra and alcoholism: a biochemical perspective. Alcohol Alcohol. 2014;49(3):238-50.

420. Elbers F, Woite C, Antoni V, Stein S, Funakoshi H, Nakamura T, et al. Negative Impact of Hypoxia on Tryptophan 2,3-Dioxygenase Function. Mediators Inflamm. 2016;2016:1638916.

421. Higuchi K, Hayaishi O. Enzymic formation of D-kynurenine from D-tryptophan. Arch Biochem Biophys. 1967;120(2):397-403.

422. Shimizu T, Nomiyama S, Hirata F, Hayaishi O. Indoleamine 2,3-dioxygenase. Purification and some properties. J Biol Chem. 1978;253(13):4700-6.

423. Werner ER, Werner-Felmayer G. Substrate and cofactor requirements of indoleamine 2,3-dioxygenase in interferon-gamma-treated cells: utilization of oxygen rather than superoxide. Curr Drug Metab. 2007;8(3):201-3.

424. Takikawa O. Biochemical and medical aspects of the indoleamine 2,3-dioxygenase-initiated L-tryptophan metabolism. Biochem Biophys Res Commun. 2005;338(1):12-9.

425. Yamazaki F, Kuroiwa T, Takikawa O, Kido R. Human indolylamine 2,3-dioxygenase. Its tissue distribution, and characterization of the placental enzyme. Biochem J. 1985;230(3):635-8.

426. Yoshida R, Nukiwa T, Watanabe Y, Fujiwara M, Hirata F, Hayaishi O. Regulation of indoleamine 2,3-dioxygenase activity in the small intestine and the epididymis of mice. Arch Biochem Biophys. 1980;203(1):343-51.

427. Prendergast GC, Malachowski WP, DuHadaway JB, Muller AJ. Discovery of IDO1 Inhibitors: From Bench to Bedside. Cancer Res. 2017;77(24):6795-811.

428. Prendergast GC, Mondal A, Dey S, Laury-Kleintop LD, Muller AJ. Inflammatory Reprogramming with IDO1 Inhibitors: Turning Immunologically Unresponsive 'Cold' Tumors 'Hot'. Trends Cancer. 2018;4(1):38-58.

429. Murray MF. The human indoleamine 2,3-dioxygenase gene and related human genes. Curr Drug Metab. 2007;8(3):197-200.

430. Ball HJ, Sanchez-Perez A, Weiser S, Austin CJ, Astelbauer F, Miu J, et al. Characterization of an indoleamine 2,3-dioxygenase-like protein found in humans and mice. Gene. 2007;396(1):203-13.

431. Metz R, Duhadaway JB, Kamasani U, Laury-Kleintop L, Muller AJ, Prendergast GC. Novel tryptophan catabolic enzyme IDO2 is the preferred biochemical target of the antitumor indoleamine 2,3-dioxygenase inhibitory compound D-1-methyl-tryptophan. Cancer Res. 2007;67(15):7082-7.

432. Yuasa HJ, Takubo M, Takahashi A, Hasegawa T, Noma H, Suzuki T. Evolution of vertebrate indoleamine 2,3-dioxygenases. J Mol Evol. 2007;65(6):705-14.

433. Ball HJ, Yuasa HJ, Austin CJ, Weiser S, Hunt NH. Indoleamine 2,3-dioxygenase-2; a new enzyme in the kynurenine pathway. Int J Biochem Cell Biol. 2009;41(3):467-71.

434. Fatokun AA, Hunt NH, Ball HJ. Indoleamine 2,3-dioxygenase 2 (IDO2) and the kynurenine pathway: characteristics and potential roles in health and disease. Amino Acids. 2013;45(6):1319-29.

435. Macchiarulo A, Camaioni E, Nuti R, Pellicciari R. Highlights at the gate of tryptophan catabolism: a review on the mechanisms of activation and regulation of indoleamine 2,3-dioxygenase (IDO), a novel target in cancer disease. Amino Acids. 2009;37(2):219-29.

436. Yoshida R, Hayaishi O. Induction of pulmonary indoleamine 2,3-dioxygenase by intraperitoneal injection of bacterial lipopolysaccharide. Proc Natl Acad Sci U S A. 1978;75(8):3998-4000.

437. Yoshida R, Imanishi J, Oku T, Kishida T, Hayaishi O. Induction of pulmonary indoleamine 2,3-dioxygenase by interferon. Proc Natl Acad Sci U S A. 1981;78(1):129-32.

438. Mellor AL, Lemos H, Huang L. Indoleamine 2,3-Dioxygenase and Tolerance: Where Are We Now? Front Immunol. 2017;8:1360.

439. Ozaki Y, Edelstein MP, Duch DS. The actions of interferon and antiinflammatory agents of induction of indoleamine 2,3-dioxygenase in human peripheral blood monocytes. Biochem Biophys Res Commun. 1987;144(3):1147-53.

440. Yoshida R, Urade Y, Tokuda M, Hayaishi O. Induction of indoleamine 2,3-dioxygenase in mouse lung during virus infection. Proc Natl Acad Sci U S A. 1979;76(8):4084-6.

441. Yan Y, Zhang GX, Gran B, Fallarino F, Yu S, Li H, et al. IDO upregulates regulatory T cells via tryptophan catabolite and suppresses encephalitogenic T cell responses in experimental autoimmune encephalomyelitis. J Immunol. 2010;185(10):5953-61.

442. Dobrovolsky VN, Bowyer JF, Pabarcus MK, Heflich RH, Williams LD, Doerge DR, et al. Effect of arylformamidase (kynurenine formamidase) gene inactivation in mice on enzymatic activity, kynurenine pathway metabolites and phenotype. Biochim Biophys Acta. 2005;1724(1-2):163-72.

443. Pabarcus MK, Casida JE. Kynurenine formamidase: determination of primary structure and modeling-based prediction of tertiary structure and catalytic triad. Biochim Biophys Acta. 2002;1596(2):201-11.

444. Pabarcus MK, Casida JE. Cloning, expression, and catalytic triad of recombinant arylformamidase. Protein Expr Purif. 2005;44(1):39-44.

445. Schuettengruber B, Doetzlhofer A, Kroboth K, Wintersberger E, Seiser C. Alternate activation of two divergently transcribed mouse genes from a bidirectional promoter is linked to changes in histone modification. J Biol Chem. 2003;278(3):1784-93.

446. Thomas SR, Stocker R. Redox reactions related to indoleamine 2,3-dioxygenase and tryptophan metabolism along the kynurenine pathway. Redox Rep. 1999;4(5):199-220.

447. Wang Y, Liu H, McKenzie G, Witting PK, Stasch JP, Hahn M, et al. Kynurenine is an endothelium-derived relaxing factor produced during inflammation. Nat Med. 2010;16(3):279-85.

448. Gal EM, Sherman AD. L-kynurenine: its synthesis and possible regulatory function in brain. Neurochem Res. 1980;5(3):223-39.

449. Kita T, Morrison PF, Heyes MP, Markey SP. Effects of systemic and central nervous system localized inflammation on the contributions of metabolic precursors to the L-kynurenine and quinolinic acid pools in brain. J Neurochem. 2002;82(2):258-68.

450. Mezrich JD, Fechner JH, Zhang X, Johnson BP, Burlingham WJ, Bradfield CA. An interaction between kynurenine and the aryl hydrocarbon receptor can generate regulatory T cells. J Immunol. 2010;185(6):3190-8.

451. Terness P, Bauer TM, Rose L, Dufter C, Watzlik A, Simon H, et al. Inhibition of allogeneic T cell proliferation by indoleamine 2,3-dioxygenase-expressing dendritic cells: mediation of suppression by tryptophan metabolites. J Exp Med. 2002;196(4):447-57.

452. Gross B, Ronen N, Honigman S, Livne E. Tryptophan toxicity--time and dose response in rats. Adv Exp Med Biol. 1999;467:507-16.

453. Refaey ME, McGee-Lawrence ME, Fulzele S, Kennedy EJ, Bollag WB, Elsalanty M, et al. Kynurenine, a Tryptophan Metabolite That Accumulates With Age, Induces Bone Loss. J Bone Miner Res. 2017;32(11):2182-93.

454. Michalowska M, Znorko B, Kaminski T, Oksztulska-Kolanek E, Pawlak D. New insights into tryptophan and its metabolites in the regulation of bone metabolism. J Physiol Pharmacol. 2015;66(6):779-91.

455. Kessler M, Terramani T, Lynch G, Baudry M. A glycine site associated with N-methyl-D-aspartic acid receptors: characterization and identification of a new class of antagonists. J Neurochem. 1989;52(4):1319-28.

456. Albuquerque EX, Schwarcz R. Kynurenic acid as an antagonist of alpha7 nicotinic acetylcholine receptors in the brain: facts and challenges. Biochem Pharmacol. 2013;85(8):1027-32.

457. Hilmas C, Pereira EF, Alkondon M, Rassoulpour A, Schwarcz R, Albuquerque EX. The brain metabolite kynurenic acid inhibits alpha7 nicotinic receptor activity and increases non-alpha7 nicotinic receptor expression: physiopathological implications. J Neurosci. 2001;21(19):7463-73.

458. Fallarini S, Magliulo L, Paoletti T, de Lalla C, Lombardi G. Expression of functional GPR35 in human iNKT cells. Biochem Biophys Res Commun. 2010;398(3):420-5.

459. Agudelo LZ, Ferreira DMS, Cervenka I, Bryzgalova G, Dadvar S, Jannig PR, et al. Kynurenic Acid and Gpr35 Regulate Adipose Tissue Energy Homeostasis and Inflammation. Cell Metab. 2018;27(2):378-92 e5.

460. DiNatale BC, Murray IA, Schroeder JC, Flaveny CA, Lahoti TS, Laurenzana EM, et al. Kynurenic acid is a potent endogenous aryl hydrocarbon receptor ligand that synergistically induces interleukin-6 in the presence of inflammatory signaling. Toxicol Sci. 2010;115(1):89-97.

461. Lugo-Huitron R, Blanco-Ayala T, Ugalde-Muniz P, Carrillo-Mora P, Pedraza-Chaverri J, Silva-Adaya D, et al. On the antioxidant properties of kynurenic acid: free radical scavenging activity and inhibition of oxidative stress. Neurotoxicol Teratol. 2011;33(5):538-47.

462. Lin TH, Yang RS, Tang CH, Wu MY, Fu WM. Regulation of the maturation of osteoblasts and osteoclastogenesis by glutamate. Eur J Pharmacol. 2008;589(1-3):37-44.

463. Wang J, Simonavicius N, Wu X, Swaminath G, Reagan J, Tian H, et al. Kynurenic Acid as a Ligand for Orphan G Protein-coupled Receptor GPR35. Journal of Biological Chemistry. 2006;281(31):22021-8.

464. Okuda S, Nishiyama N, Saito H, Katsuki H. Hydrogen peroxide-mediated neuronal cell death induced by an endogenous neurotoxin, 3-hydroxykynurenine. Proc Natl Acad Sci U S A. 1996;93(22):12553-8.

465. Eastman CL, Guilarte TR. The role of hydrogen peroxide in the in vitro cytotoxicity of 3-hydroxykynurenine. Neurochem Res. 1990;15(11):1101-7.

466. Nakagami Y, Saito H, Katsuki H. 3-Hydroxykynurenine toxicity on the rat striatum in vivo. Jpn J Pharmacol. 1996;71(2):183-6.

467. Leipnitz G, Schumacher C, Dalcin KB, Scussiato K, Solano A, Funchal C, et al. In vitro evidence for an antioxidant role of 3-hydroxykynurenine and 3-hydroxyanthranilic acid in the brain. Neurochem Int. 2007;50(1):83-94.

468. Platten M, Ho PP, Youssef S, Fontoura P, Garren H, Hur EM, et al. Treatment of autoimmune neuroinflammation with a synthetic tryptophan metabolite. Science. 2005;310(5749):850-5.

469. Taher YA, Piavaux BJ, Gras R, van Esch BC, Hofman GA, Bloksma N, et al. Indoleamine 2,3-dioxygenase-dependent tryptophan metabolites contribute to tolerance induction during allergen immunotherapy in a mouse model. J Allergy Clin Immunol. 2008;121(4):983-91 e2.

470. Korlimbinis A, Hains PG, Truscott RJ, Aquilina JA. 3-Hydroxykynurenine oxidizes alpha-crystallin: potential role in cataractogenesis. Biochemistry. 2006;45(6):1852-60.

471. Goldstein LE, Leopold MC, Huang X, Atwood CS, Saunders AJ, Hartshorn M, et al. 3-Hydroxykynurenine and 3-hydroxyanthranilic acid generate hydrogen peroxide and promote alpha-crystallin cross-linking by metal ion reduction. Biochemistry. 2000;39(24):7266-75.

472. Wilson K, Auer M, Binnie M, Zheng X, Pham NT, Iredale JP, et al. Overexpression of human kynurenine-3-monooxygenase protects against 3-hydroxykynurenine-mediated apoptosis through bidirectional nonlinear feedback. Cell Death Dis. 2016;7:e2197.

473. Wang Q, Zhang M, Ding Y, Wang Q, Zhang W, Song P, et al. Activation of NAD(P)H oxidase by tryptophan-derived 3-hydroxykynurenine accelerates endothelial apoptosis and dysfunction in vivo. Circ Res. 2014;114(3):480-92.

474. Chobot V, Hadacek F, Weckwerth W, Kubicova L. Iron chelation and redox chemistry of anthranilic acid and 3-hydroxyanthranilic acid: A comparison of two structurally related kynurenine pathway metabolites to obtain improved insights into their potential role in neurological disease development. J Organomet Chem. 2015;782:103-10.

475. Copeland CS, Neale SA, Salt TE. Actions of Xanthurenic acid, a putative endogenous Group II metabotropic glutamate receptor agonist, on sensory transmission in the thalamus. Neuropharmacology. 2013;66:133-42.

476. Neale SA, Copeland CS, Uebele VN, Thomson FJ, Salt TE. Modulation of hippocampal synaptic transmission by the kynurenine pathway member xanthurenic acid and other VGLUT inhibitors. Neuropsychopharmacology. 2013;38(6):1060-7.

477. Haruki H, Hovius R, Pedersen MG, Johnsson K. Tetrahydrobiopterin Biosynthesis as a Potential Target of the Kynurenine Pathway Metabolite Xanthurenic Acid. J Biol Chem. 2016;291(2):652-7.

478. Heyliger SO, Goodman CB, Ngong JM, Soliman KF. The analgesic effects of tryptophan and its metabolites in the rat. Pharmacol Res. 1998;38(4):243-50.

479. Christen S, Peterhans E, Stocker R. Antioxidant activities of some tryptophan metabolites: possible implication for inflammatory diseases. Proc Natl Acad Sci U S A. 1990;87(7):2506-10.

480. Malina HZ, Richter C, Mehl M, Hess OM. Pathological apoptosis by xanthurenic acid, a tryptophan metabolite: activation of cell caspases but not cytoskeleton breakdown. BMC Physiol. 2001;1:7.

481. Fallarino F, Grohmann U, Vacca C, Bianchi R, Orabona C, Spreca A, et al. T cell apoptosis by tryptophan catabolism. Cell Death Differ. 2002;9(10):1069-77.

482. Oh GS, Pae HO, Choi BM, Chae SC, Lee HS, Ryu DG, et al. 3-Hydroxyanthranilic acid, one of metabolites of tryptophan via indoleamine 2,3-dioxygenase pathway, suppresses inducible nitric oxide synthase expression by enhancing heme oxygenase-1 expression. Biochem Biophys Res Commun. 2004;320(4):1156-62.

483. Hayashi T, Mo JH, Gong X, Rossetto C, Jang A, Beck L, et al. 3-Hydroxyanthranilic acid inhibits PDK1 activation and suppresses experimental asthma by inducing T cell apoptosis. Proc Natl Acad Sci U S A. 2007;104(47):18619-24.

484. Fazio F, Lionetto L, Molinaro G, Bertrand HO, Acher F, Ngomba RT, et al. Cinnabarinic acid, an endogenous metabolite of the kynurenine pathway, activates type 4 metabotropic glutamate receptors. Mol Pharmacol. 2012;81(5):643-56.

485. Lowe MM, Mold JE, Kanwar B, Huang Y, Louie A, Pollastri MP, et al. Identification of cinnabarinic acid as a novel endogenous aryl hydrocarbon receptor ligand that drives IL-22 production. PLoS One. 2014;9(2):e87877.

486. Evans GW, Johnson PE. Characterization and quantitation of a zinc-binding ligand in human milk. Pediatr Res. 1980;14(7):876-80.

487. Guillemin GJ. Quinolinic acid, the inescapable neurotoxin. FEBS J. 2012;279(8):1356-65.

488. Stipek S, Stastny F, Platenik J, Crkovska J, Zima T. The effect of quinolinate on rat brain lipid peroxidation is dependent on iron. Neurochem Int. 1997;30(2):233-7.

489. Platenik J, Stopka P, Vejrazka M, Stipek S. Quinolinic acid-iron(ii) complexes: slow autoxidation, but enhanced hydroxyl radical production in the Fenton reaction. Free Radic Res. 2001;34(5):445-59.

490. Widner B, Sepp N, Kowald E, Ortner U, Wirleitner B, Fritsch P, et al. Enhanced tryptophan degradation in systemic lupus erythematosus. Immunobiology. 2000;201(5):621-30.

491. Carayol M, Leitzmann MF, Ferrari P, Zamora-Ros R, Achaintre D, Stepien M, et al. Blood Metabolic Signatures of Body Mass Index: A Targeted Metabolomics Study in the EPIC Cohort. J Proteome Res. 2017;16(9):3137-46.

492. Forrest CM, Youd P, Kennedy A, Gould SR, Darlington LG, Stone TW. Purine, kynurenine, neopterin and lipid peroxidation levels in inflammatory bowel disease. J Biomed Sci. 2002;9(5):436-42.

493. Salam RA, Zuberi NF, Bhutta ZA. Pyridoxine (vitamin B6) supplementation during pregnancy or labour for maternal and neonatal outcomes. Cochrane Database Syst Rev. 2015(6):CD000179.

494. Quasim T, McMillan DC, Talwar D, Vasilaki A, St JORD, Kinsella J. The relationship between plasma and red cell B-vitamin concentrations in critically-ill patients. Clin Nutr. 2005;24(6):956-60.

495. Ueland PM, McCann A, Midttun O, Ulvik A. Inflammation, vitamin B6 and related pathways. Mol Aspects Med. 2017;53:10-27.

496. Paul L, Ueland PM, Selhub J. Mechanistic perspective on the relationship between pyridoxal 5'-phosphate and inflammation. Nutr Rev. 2013;71(4):239-44.

497. Coburn SP, Lewis DL, Fink WJ, Mahuren JD, Schaltenbrand WE, Costill DL. Human vitamin B-6 pools estimated through muscle biopsies. Am J Clin Nutr. 1988;48(2):291-4.

498. Labadarios D, Brink PA, Weich HF, Visser L, Louw ME, Shephard GS, et al. Plasma vitamin A, E, C and B6 levels in myocardial infarction. S Afr Med J. 1987;71(9):561-3.

499. Breton J, Avanzi N, Magagnin S, Covini N, Magistrelli G, Cozzi L, et al. Functional characterization and mechanism of action of recombinant human kynurenine 3-hydroxylase. Eur J Biochem. 2000;267(4):1092-9.

500. Theriault O, Poulin H, Thomas GR, Friesen AD, Al-Shaqha WA, Chahine M. Pyridoxal-5'-phosphate (MC-1), a vitamin B6 derivative, inhibits expressed P2X receptors. Can J Physiol Pharmacol. 2014;92(3):189-96.

501. Minchiotti L, Ronchi S, Rippa M. Amino acid sequence around the pyridoxal 5'-phosphate binding sites of 6-phosphogluconate dehydrogenase. Biochim Biophys Acta. 1981;657(1):232-42.

502. Ueland PM, Ulvik A, Rios-Avila L, Midttun O, Gregory JF. Direct and Functional Biomarkers of Vitamin B6 Status. Annu Rev Nutr. 2015;35:33-70.

503. Turski MP, Kaminski P, Zgrajka W, Turska M, Turski WA. Potato- an important source of nutritional kynurenic acid. Plant Foods Hum Nutr. 2012;67(1):17-23.

504. Turska M, Rutyna R, Paluszkiewicz M, Terlecka P, Dobrowolski A, Pelak J, et al. Presence of kynurenic acid in alcoholic beverages - Is this good news, or bad news? Med Hypotheses. 2019;122:200-5.

505. Turski MP, Turska M, Paluszkiewicz P, Parada-Turska J, Oxenkrug GF. Kynurenic Acid in the digestive system-new facts, new challenges. Int J Tryptophan Res. 2013;6:47-55.

506. Fukui S, Schwarcz R, Rapoport SI, Takada Y, Smith QR. Blood-brain barrier transport of kynurenines: implications for brain synthesis and metabolism. J Neurochem. 1991;56(6):2007-17.

507. Han Q, Cai T, Tagle DA, Li J. Structure, expression, and function of kynurenine aminotransferases in human and rodent brains. Cell Mol Life Sci. 2010;67(3):353-68.

508. Blanco Ayala T, Lugo Huitron R, Carmona Aparicio L, Ramirez Ortega D, Gonzalez Esquivel D, Pedraza Chaverri J, et al. Alternative kynurenic acid synthesis routes studied in the rat cerebellum. Front Cell Neurosci. 2015;9:178.

509. Wirthgen E, Hoeflich A, Rebl A, Gunther J. Kynurenic Acid: The Janus-Faced Role of an Immunomodulatory Tryptophan Metabolite and Its Link to Pathological Conditions. Front Immunol. 2017;8:1957.

510. Moroni F, Cozzi A, Sili M, Mannaioni G. Kynurenic acid: a metabolite with multiple actions and multiple targets in brain and periphery. J Neural Transm (Vienna). 2012;119(2):133-9.

511. Amori L, Guidetti P, Pellicciari R, Kajii Y, Schwarcz R. On the relationship between the two branches of the kynurenine pathway in the rat brain in vivo. J Neurochem. 2009;109(2):316-25.

512. Stone TW, Stoy N, Darlington LG. An expanding range of targets for kynurenine metabolites of tryptophan. Trends Pharmacol Sci. 2013;34(2):136-43.

513. Vecsei L, Szalardy L, Fulop F, Toldi J. Kynurenines in the CNS: recent advances and new questions. Nature reviews Drug discovery. 2013;12(1):64-82.

514. Beggiato S, Tanganelli S, Fuxe K, Antonelli T, Schwarcz R, Ferraro L. Endogenous kynurenic acid regulates extracellular GABA levels in the rat prefrontal cortex. Neuropharmacology. 2014;82:11-8.

515. Szalardy L, Zadori D, Toldi J, Fulop F, Klivenyi P, Vecsei L. Manipulating kynurenic acid levels in the brain - on the edge between neuroprotection and cognitive dysfunction. Current topics in medicinal chemistry. 2012;12(16):1797-806.

516. Rozsa E, Robotka H, Vecsei L, Toldi J. The Janus-face kynurenic acid. J Neural Transm (Vienna). 2008;115(8):1087-91.

517. Fagerberg L, Hallstrom BM, Oksvold P, Kampf C, Djureinovic D, Odeberg J, et al. Analysis of the human tissue-specific expression by genome-wide integration of transcriptomics and antibody-based proteomics. Mol Cell Proteomics. 2014;13(2):397-406.

518. Chiarugi A, Calvani M, Meli E, Traggiai E, Moroni F. Synthesis and release of neurotoxic kynurenine metabolites by human monocyte-derived macrophages. J Neuroimmunol. 2001;120(1-2):190-8.

519. Bender DA. Inhibition in vitro of the enzymes of the oxidative pathway of tryptophan metabolism and of nicotinamide nucleotide synthesis by benserazide, carbidopa and isoniazid. Biochem Pharmacol. 1980;29(5):707-12.

520. Zunszain PA, Anacker C, Cattaneo A, Choudhury S, Musaelyan K, Myint AM, et al. Interleukin-1beta: a new regulator of the kynurenine pathway affecting human hippocampal neurogenesis. Neuropsychopharmacology. 2012;37(4):939-49.

521. Stone TW. Neuropharmacology of quinolinic and kynurenic acids. Pharmacol Rev. 1993;45(3):309-79.

522. Connor TJ, Starr N, O'Sullivan JB, Harkin A. Induction of indolamine 2,3-dioxygenase and kynurenine 3-monooxygenase in rat brain following a systemic inflammatory challenge: a role for IFN-gamma? Neurosci Lett. 2008;441(1):29-34.

523. Alberati-Giani D, Ricciardi-Castagnoli P, Kohler C, Cesura AM. Regulation of the kynurenine metabolic pathway by interferon-gamma in murine cloned macrophages and microglial cells. J Neurochem. 1996;66(3):996-1004.

524. Adams S, Teo C, McDonald KL, Zinger A, Bustamante S, Lim CK, et al. Involvement of the kynurenine pathway in human glioma pathophysiology. PLoS One. 2014;9(11):e112945.

525. Agudelo LZ, Femenia T, Orhan F, Porsmyr-Palmertz M, Goiny M, Martinez-Redondo V, et al. Skeletal muscle PGC-1alpha1 modulates kynurenine metabolism and mediates resilience to stress-induced depression. Cell. 2014;159(1):33-45.

526. Stazka J, Luchowski P, Wielosz M, Kleinrok Z, Urbanska EM. Endothelium-dependent production and liberation of kynurenic acid by rat aortic rings exposed to L-kynurenine. Eur J Pharmacol. 2002;448(2-3):133-7.

527. Baran H, Amann G, Lubec B, Lubec G. Kynurenic acid and kynurenine aminotransferase in heart. Pediatr Res. 1997;41(3):404-10.

528. Wang J, Simonavicius N, Wu X, Swaminath G, Reagan J, Tian H, et al. Kynurenic acid as a ligand for orphan G protein-coupled receptor GPR35. J Biol Chem. 2006;281(31):22021-8.

529. Barth MC, Ahluwalia N, Anderson TJ, Hardy GJ, Sinha S, Alvarez-Cardona JA, et al. Kynurenic acid triggers firm arrest of leukocytes to vascular endothelium under flow conditions. J Biol Chem. 2009;284(29):19189-95.

530. Okumura S, Baba H, Kumada T, Nanmoku K, Nakajima H, Nakane Y, et al. Cloning of a G-protein-coupled receptor that shows an activity to transform NIH3T3 cells and is expressed in gastric cancer cells. Cancer Sci. 2004;95(2):131-5.

531. Wang W, Han T, Tong W, Zhao J, Qiu X. Overexpression of GPR35 confers drug resistance in NSCLC cells by beta-arrestin/Akt signaling. Onco Targets Ther. 2018;11:6249-57.

532. Zheng X, Hu M, Zang X, Fan Q, Liu Y, Che Y, et al. Kynurenic acid/GPR35 axis restricts NLRP3 inflammasome activation and exacerbates colitis in mice with social stress. Brain Behav Immun. 2019.

533. Forrest CM, Gould SR, Darlington LG, Stone TW. Levels of purine, kynurenine and lipid peroxidation products in patients with inflammatory bowel disease. Adv Exp Med Biol. 2003;527:395-400.

534. Tobes MC, Mason M. Alpha-Aminoadipate aminotransferase and kynurenine aminotransferase. Purification, characterization, and further evidence for identity. J Biol Chem. 1977;252(13):4591-9.

535. Bender DA, Njagi EN, Danielian PS. Tryptophan metabolism in vitamin B6-deficient mice. Br J Nutr. 1990;63(1):27-36.

536. Lima S, Kumar S, Gawandi V, Momany C, Phillips RS. Crystal structure of the Homo sapiens kynureninase-3-hydroxyhippuric acid inhibitor complex: insights into the molecular basis of kynureninase substrate specificity. J Med Chem. 2009;52(2):389-96.

537. Sheibley F. Carl Julius Fritzsche and the discovery of Anthranilic Acid, 1841. J Chem Educ. 1943;20(3):115-7.

538. Oxenkrug G, van der Hart M, Roeser J, Summergrad P. Anthranilic Acid: A Potential Biomarker and Treatment Target for Schizophrenia. Ann Psychiatry Ment Health. 2016;4(2).

539. Oxenkrug G, van der Hart M, Roeser J, Summergrad P. Peripheral Tryptophan - Kynurenine Metabolism Associated with Metabolic Syndrome is Different in Parkinson's and Alzheimer's Diseases. Endocrinol Diabetes Metab J. 2017;1(4).

540. Oxenkrug G, van der Hart M, Summergrad P. Elevated anthranilic acid plasma concentrations in type 1 but not type 2 diabetes mellitus. Integr Mol Med. 2015;2(5):365-8.

541. Bentley-Lewis R, Huynh J, Xiong G, Lee H, Wenger J, Clish C, et al. Metabolomic profiling in the prediction of gestational diabetes mellitus. Diabetologia. 2015;58(6):1329-32.

542. Igari T, Tsuchizawa M, Shimamura T. Alteration of tryptophan metabolism in the synovial fluid of patients with rheumatoid arthritis and osteoarthritis. Tohoku J Exp Med. 1987;153(2):79-86.

543. FT de Castro JP, RR Brown. REDUCED TRIPHOSPHOPYRIDINENUCLEOTIDE REQUIREMENT FOR THE ENZYMATIC FORMATION OF 3-HYDROXYKYNURENINE FROM L-KYNURENINE. J Am Chem Soc. 1956;78(12):2904-5.

544. Saito Y, Hayaishi O, Rothberg S. Studies on oxygenases; enzymatic formation of 3-hydroxy-L-kynurenine from L-kynurenine. J Biol Chem. 1957;229(2):921-34.

545. Okamoto H, Yamamoto S, Nozaki M, Hayaishi O. On the submitochondrial localization of l-kynurenine-3-hydroxylase. Biochem Biophys Res Commun. 1967;26(3):309-14.

546. Okamoto H, Hayaishi O. Flavin adenine dinucleotide requirement for kynurenine hydroxylase of rat liver mitochondria. Biochem Biophys Res Commun. 1967;29(3):394-9.

547. Hirai K, Kuroyanagi H, Tatebayashi Y, Hayashi Y, Hirabayashi-Takahashi K, Saito K, et al. Dual role of the carboxyl-terminal region of pig liver L-kynurenine 3-monooxygenase: mitochondrial-targeting signal and enzymatic activity. J Biochem. 2010;148(6):639-50.

548. Holtze M, Saetre P, Engberg G, Schwieler L, Werge T, Andreassen OA, et al. Kynurenine 3-monooxygenase polymorphisms: relevance for kynurenic acid synthesis in patients with schizophrenia and healthy controls. J Psychiatry Neurosci. 2012;37(1):53-7.

549. Wonodi I, Schwarcz R. Cortical kynurenine pathway metabolism: a novel target for cognitive enhancement in Schizophrenia. Schizophr Bull. 2010;36(2):211-8.

550. Ozkilic Y, Tuzun NS. Mechanism of Kynurenine 3-Monooxygenase-Catalyzed Hydroxylation Reaction: A Quantum Cluster Approach. J Phys Chem A. 2019;123(14):3149-59.

551. Smith JR, Jamie JF, Guillemin GJ. Kynurenine-3-monooxygenase: a review of structure, mechanism, and inhibitors. Drug Discov Today. 2016;21(2):315-24.

552. Schwarcz R, Pellicciari R. Manipulation of brain kynurenines: glial targets, neuronal effects, and clinical opportunities. J Pharmacol Exp Ther. 2002;303(1):1-10.

553. Shave S, McGuire K, Pham NT, Mole DJ, Webster SP, Auer M. Diclofenac Identified as a Kynurenine 3-Monooxygenase Binder and Inhibitor by Molecular Similarity Techniques. ACS Omega. 2018;3(3):2564-8.

554. Lugo-Huitron R, Ugalde Muniz P, Pineda B, Pedraza-Chaverri J, Rios C, Perez-de la Cruz V. Quinolinic acid: an endogenous neurotoxin with multiple targets. Oxidative medicine and cellular longevity. 2013;2013:104024.

555. Giorgini F, Huang SY, Sathyasaikumar KV, Notarangelo FM, Thomas MA, Tararina M, et al. Targeted deletion of kynurenine 3-monooxygenase in mice: a new tool for studying kynurenine pathway metabolism in periphery and brain. J Biol Chem. 2013;288(51):36554-66.

556. Stephens GL, Wang Q, Swerdlow B, Bhat G, Kolbeck R, Fung M. Kynurenine 3-monooxygenase mediates inhibition of Th17 differentiation via catabolism of endogenous aryl hydrocarbon receptor ligands. Eur J Immunol. 2013;43(7):1727-34.

557. Pawlak K, Domaniewski T, Mysliwiec M, Pawlak D. The kynurenines are associated with oxidative stress, inflammation and the prevalence of cardiovascular disease in patients with end-stage renal disease. Atherosclerosis. 2009;204(1):309-14.

558. Barile M, Giancaspero TA, Leone P, Galluccio M, Indiveri C. Riboflavin transport and metabolism in humans. J Inherit Metab Dis. 2016;39(4):545-57.

559. Pinto JT, Zempleni J. Riboflavin. Adv Nutr. 2016;7(5):973-5.

560. Mason M. The metabolism of tryptophan in riboflavin-deficient rats. J Biol Chem. 1953;201(2):513-8.

561. Lienhart WD, Gudipati V, Macheroux P. The human flavoproteome. Arch Biochem Biophys. 2013;535(2):150-62.

562. Dalgliesh CE. The relation between pyridoxin and tryptophan metabolism, studied in the rat. Biochem J. 1952;52(1):3-14.

563. Luthra M, Balasubramanian D. 3-Hydroxykynurenine and 3-hydroxyanthranilic acid may act as endogenous antioxidants in the eye lens. Exp Eye Res. 1992;55(4):641-3.

564. Eastman CL, Guilarte TR, Lever JR. Uptake of 3-hydroxykynurenine measured in rat brain slices and in a neuronal cell line. Brain Res. 1992;584(1-2):110-6.

565. Zhuravlev AV, Vetrovoy OV, Savvateeva-Popova EV. Enzymatic and non-enzymatic pathways of kynurenines' dimerization: the molecular factors for oxidative stress development. PLoS Comput Biol. 2018;14(12):e1006672.

566. Tomoda A, Shirasawa E, Yoneyama Y. Reactions of oxy- and methemoglobin with tryptophan metabolites, 3-hydroxyanthranilic acid and 3-hydroxykynurenine. Hemoglobin. 1986;10(1):33-48.

567. Aquilina JA, Carver JA, Truscott RJ. Oxidation products of 3-hydroxykynurenine bind to lens proteins: relevance for nuclear cataract. Exp Eye Res. 1997;64(5):727-35.

568. Okuda S, Nishiyama N, Saito H, Katsuki H. 3-Hydroxykynurenine, an endogenous oxidative stress generator, causes neuronal cell death with apoptotic features and region selectivity. J Neurochem. 1998;70(1):299-307.

569. Wei H, Leeds P, Chen RW, Wei W, Leng Y, Bredesen DE, et al. Neuronal apoptosis induced by pharmacological concentrations of 3-hydroxykynurenine: characterization and protection by dantrolene and Bcl-2 overexpression. J Neurochem. 2000;75(1):81-90.

570. Hiraku Y, Inoue S, Oikawa S, Yamamoto K, Tada S, Nishino K, et al. Metal-mediated oxidative damage to cellular and isolated DNA by certain tryptophan metabolites. Carcinogenesis. 1995;16(2):349-56.

571. Eastman CL, Guilarte TR. Cytotoxicity of 3-hydroxykynurenine in a neuronal hybrid cell line. Brain Res. 1989;495(2):225-31.

572. Vazquez S, Garner B, Sheil MM, Truscott RJ. Characterisation of the major autoxidation products of 3-hydroxykynurenine under physiological conditions. Free Radic Res. 2000;32(1):11-23.

573. Colin-Gonzalez AL, Maldonado PD, Santamaria A. 3-Hydroxykynurenine: an intriguing molecule exerting dual actions in the central nervous system. Neurotoxicology. 2013;34:189-204.

574. Ishii T, Iwahashi H, Sugata R, Kido R. Formation of hydroxanthommatin-derived radical in the oxidation of 3-hydroxykynurenine. Arch Biochem Biophys. 1992;294(2):616-22.

575. Reczek CR, Chandel NS. ROS-dependent signal transduction. Curr Opin Cell Biol. 2015;33:8-13.

576. Winyard PG, Moody CJ, Jacob C. Oxidative activation of antioxidant defence. Trends Biochem Sci. 2005;30(8):453-61.

577. Schmidt KN, Amstad P, Cerutti P, Baeuerle PA. The roles of hydrogen peroxide and superoxide as messengers in the activation of transcription factor NF-kappa B. Chem Biol. 1995;2(1):13-22.

578. Whittemore ER, Loo DT, Watt JA, Cotman CW. A detailed analysis of hydrogen peroxide-induced cell death in primary neuronal culture. Neuroscience. 1995;67(4):921-32.

579. Distelhorst CW, Lam M, McCormick TS. Bcl-2 inhibits hydrogen peroxide-induced ER Ca2+ pool depletion. Oncogene. 1996;12(10):2051-5.

580. Chiarugi A, Meli E, Moroni F. Similarities and differences in the neuronal death processes activated by 3OH-kynurenine and quinolinic acid. J Neurochem. 2001;77(5):1310-8.

581. Guidetti P, Schwarcz R. 3-Hydroxykynurenine potentiates quinolinate but not NMDA toxicity in the rat striatum. Eur J Neurosci. 1999;11(11):3857-63.

582. Reynolds GP, Pearson SJ. Increased brain 3-hydroxykynurenine in Huntington's disease. Lancet. 1989;2(8669):979-80.

583. Pearson SJ, Reynolds GP. Increased brain concentrations of a neurotoxin, 3-hydroxykynurenine, in Huntington's disease. Neurosci Lett. 1992;144(1-2):199-201.

584. Thevandavakkam MA, Schwarcz R, Muchowski PJ, Giorgini F. Targeting kynurenine 3-monooxygenase (KMO): implications for therapy in Huntington's disease. CNS & neurological disorders drug targets. 2010;9(6):791-800.

585. Ogawa T, Matson WR, Beal MF, Myers RH, Bird ED, Milbury P, et al. Kynurenine pathway abnormalities in Parkinson's disease. Neurology. 1992;42(9):1702-6.

586. Bellac CL, Coimbra RS, Christen S, Leib SL. Pneumococcal meningitis causes accumulation of neurotoxic kynurenine metabolites in brain regions prone to injury. Neurobiol Dis. 2006;24(2):395-402.

587. Sardar AM, Bell JE, Reynolds GP. Increased concentrations of the neurotoxin 3-hydroxykynurenine in the frontal cortex of HIV-1-positive patients. J Neurochem. 1995;64(2):932-5.

588. Eussen SJ, Ueland PM, Vollset SE, Nygard O, Midttun O, Sulo G, et al. Kynurenines as predictors of acute coronary events in the Hordaland Health Study. Int J Cardiol. 2015;189:18-24.

589. Christensen MHE, Fadnes DJ, Rost TH, Pedersen ER, Andersen JR, Vage V, et al. Inflammatory markers, the tryptophan-kynurenine pathway, and vitamin B status after bariatric surgery. PLoS One. 2018;13(2):e0192169.

590. Allen MJ, Boyland E, Dukes CE, Horning ES, Watson JG. Cancer of the urinary bladder induced in mice with metabolites of aromatic amines and tryptophan. Br J Cancer. 1957;11(2):212-28.

591. Suzuki T, Yamamoto M. Stress-sensing mechanisms and the physiological roles of the Keap1-Nrf2 system during cellular stress. J Biol Chem. 2017;292(41):16817-24.

592. Holmstrom KM, Finkel T. Cellular mechanisms and physiological consequences of redox-dependent signalling. Nat Rev Mol Cell Biol. 2014;15(6):411-21.

593. Lima S, Khristoforov R, Momany C, Phillips RS. Crystal structure of Homo sapiens kynureninase. Biochemistry. 2007;46(10):2735-44.

594. Inada J, Okuno E, Kimura M, Kido R. Intracellular localization and characterization of 3-hydroxykynureninase in human liver. Int J Biochem. 1984;16(6):623-8.

595. Guilarte TR, Wagner HN, Jr. Increased concentrations of 3-hydroxykynurenine in vitamin B6 deficient neonatal rat brain. J Neurochem. 1987;49(6):1918-26.

596. Theofylaktopoulou D, Ulvik A, Midttun O, Ueland PM, Vollset SE, Nygard O, et al. Vitamins B2 and B6 as determinants of kynurenines and related markers of interferon-gamma-mediated immune activation in the community-based Hordaland Health Study. Br J Nutr. 2014;112(7):1065-72.

597. Midttun O, Ulvik A, Ringdal Pedersen E, Ebbing M, Bleie O, Schartum-Hansen H, et al. Low plasma vitamin B-6 status affects metabolism through the kynurenine pathway in cardiovascular patients with systemic inflammation. J Nutr. 2011;141(4):611-7.

598. Rossi F, Garavaglia S, Giovenzana GB, Arca B, Li J, Rizzi M. Crystal structure of the Anopheles gambiae 3-hydroxykynurenine transaminase. Proc Natl Acad Sci U S A. 2006;103(15):5711-6.

599. Glazer HS, Mueller JF, Thompson C, Hawkins VR, Vilter RW. A study of urinary excretion of xanthurenic acid and other tryptophan metabolites in human beings with pyridoxine deficiency induced by desoxypyridoxine. Arch Biochem Biophys. 1951;33(2):243-51.

600. Han Q, Beerntsen BT, Li J. The tryptophan oxidation pathway in mosquitoes with emphasis on xanthurenic acid biosynthesis. J Insect Physiol. 2007;53(3):254-63.

601. Han Q, Robinson H, Gao YG, Vogelaar N, Wilson SR, Rizzi M, et al. Crystal structures of Aedes aegypti alanine glyoxylate aminotransferase. J Biol Chem. 2006;281(48):37175-82.

602. Lima VL, Dias F, Nunes RD, Pereira LO, Santos TS, Chiarini LB, et al. The antioxidant role of xanthurenic acid in the Aedes aegypti midgut during digestion of a blood meal. PLoS One. 2012;7(6):e38349.

603. Thomas SR, Witting PK, Stocker R. 3-Hydroxyanthranilic acid is an efficient, cell-derived co-antioxidant for alpha-tocopherol, inhibiting human low density lipoprotein and plasma lipid peroxidation. J Biol Chem. 1996;271(51):32714-21.

604. Rao PV, Vaidyanahan CS. nzymic conversion of 3-hydroxyanthranilic acid into cinnabarinic acid. Partial purification and properties of ra-liver cinnabarinate synthase. Biochem J. 1966;99(2):317-22.

605. Le Roes-Hill M, Goodwin C, Burton S. Phenoxazinone synthase: what's in a name? Trends Biotechnol. 2009;27(4):248-58.

606. Fazio F, Lionetto L, Curto M, Iacovelli L, Copeland CS, Neale SA, et al. Cinnabarinic acid and xanthurenic acid: Two kynurenine metabolites that interact with metabotropic glutamate receptors. Neuropharmacology. 2017;112(Pt B):365-72.

607. Henderson LM. Quinolinic acid excretion by the rat receiving tryptophan. J Biol Chem. 1949;178(2):1005.

608. Foster AC, White RJ, Schwarcz R. Synthesis of quinolinic acid by 3-hydroxyanthranilic acid oxygenase in rat brain tissue in vitro. Journal of neurochemistry. 1986;47(1):23-30.

609. Nishizuka Y, Hayaishi O. Enzymic synthesis of niacin nucleotides from 3-hydroxyanthranilic acid in mammalian liver. J Biol Chem. 1963;238:483-5.

610. Foster AC, Miller LP, Oldendorf WH, Schwarcz R. Studies on the disposition of quinolinic acid after intracerebral or systemic administration in the rat. Experimental neurology. 1984;84(2):428-40.

611. Najjar S, Pearlman DM, Alper K, Najjar A, Devinsky O. Neuroinflammation and psychiatric illness. Journal of neuroinflammation. 2013;10:43.

612. Liu H, Woznica K, Catton G, Crawford A, Botting N, Naismith JH. Structural and kinetic characterization of quinolinate phosphoribosyltransferase (hQPRTase) from homo sapiens. J Mol Biol. 2007;373(3):755-63.

613. Gholson RK, Ueda I, Ogasawara N, Henderson LM. The Enzymatic Conversion of Quinolinate to Nicotinic Acid Mononucleotide in Mammalian Liver. J Biol Chem. 1964;239:1208-14.

614. Horwitt MK, Harvey, C.C., Rothwell, W.S., Cutler J.L., Haffron, D. Tryptophan-Niacin Relationships in Man. J Nutr. 1956;60(Suppl_1):1-43.

615. Preiser JC, Ichai C, Orban JC, Groeneveld AB. Metabolic response to the stress of critical illness. Br J Anaesth. 2014;113(6):945-54.

616. Cuthbertson DP. Post-shock metabolic response. The Lancet. 1942;239(6189):433-7.

617. Carson J, Al-Mousawi, A., Rodriguez, N.A., Finnerty, C.C., Herndon, D.N. Metabolism in Surgical Patients. In: Townsend CW, Beauchamp, R.D., Evers, B.M., Mattox, K., editor. Sabiston Textbook of Surgery: the biological basis of modern surgical practice2016.

618. Nalos M, Parnell G, Robergs R, Booth D, McLean AS, Tang BM. Transcriptional reprogramming of metabolic pathways in critically ill patients. Intensive Care Med Exp. 2016;4(1):21.

619. Yess N, Price JM, Brown RR, Swan PB, Linkswiler H. Vitamin B6 Depletion in Man: Urinary Excretion of Tryptophan Metabolites. J Nutr. 1964;84(3):229-36.

620. Ghashut RA, McMillan DC, Kinsella J, Talwar D. Erythrocyte concentrations of B1, B2, B6 but not plasma C and E are reliable indicators of nutrition status in the presence of systemic inflammation. Clin Nutr ESPEN. 2017;17:54-62.

621. Gray A, McMillan DC, Wilson C, Williamson C, O'Reilly DS, Talwar D. The relationship between plasma and red cell concentrations of vitamins thiamine diphosphate, flavin adenine dinucleotide and pyridoxal 5-phosphate following elective knee arthroplasty. Clin Nutr. 2004;23(5):1080-3.

622. McMillan DC, Maguire D, Talwar D. Relationship between nutritional status and the systemic inflammatory response: micronutrients. Proc Nutr Soc. 2019;78(1):56-67.

623. Molina-Lopez J, Florea D, Quintero-Osso B, de la Cruz AP, Rodriguez-Elvira M, Del Pozo EP. Pyridoxal-5'-phosphate deficiency is associated with hyperhomocysteinemia regardless of antioxidant, thiamine, riboflavin, cobalamine, and folate status in critically ill patients. Clin Nutr. 2016;35(3):706-12.

624. Huang YC, Chang HH, Huang SC, Cheng CH, Lee BJ, Cheng SY, et al. Plasma pyridoxal 5'-phosphate is a significant indicator of immune responses in the mechanically ventilated critically ill. Nutrition. 2005;21(7-8):779-85.

625. Ulvik A, Midttun O, Pedersen ER, Eussen SJ, Nygard O, Ueland PM. Evidence for increased catabolism of vitamin B-6 during systemic inflammation. Am J Clin Nutr. 2014;100(1):250-5.

626. Sakakeeny L, Roubenoff R, Obin M, Fontes JD, Benjamin EJ, Bujanover Y, et al. Plasma pyridoxal-5-phosphate is inversely associated with systemic markers of inflammation in a population of U.S. adults. J Nutr. 2012;142(7):1280-5.

627. Hou CT, Wu YH, Huang PN, Cheng CH, Huang YC. Higher plasma pyridoxal 5'-phosphate is associated with better blood glucose responses in critically ill surgical patients with inadequate vitamin B-6 status. Clin Nutr. 2011;30(4):478-83.

628. Cheng CH, Chang SJ, Lee BJ, Lin KL, Huang YC. Vitamin B6 supplementation increases immune responses in critically ill patients. Eur J Clin Nutr. 2006;60(10):1207-13.

629. Friso S, Jacques PF, Wilson PW, Rosenberg IH, Selhub J. Low circulating vitamin B(6) is associated with elevation of the inflammation marker C-reactive protein independently of plasma homocysteine levels. Circulation. 2001;103(23):2788-91.

630. Sanches SC, Ramalho LN, Mendes-Braz M, Terra VA, Cecchini R, Augusto MJ, et al. Riboflavin (vitamin B-2) reduces hepatocellular injury following liver ischaemia and reperfusion in mice. Food Chem Toxicol. 2014;67:65-71.

631. Kannan K, Jain SK. Effect of vitamin B6 on oxygen radicals, mitochondrial membrane potential, and lipid peroxidation in H2O2-treated U937 monocytes. Free Radic Biol Med. 2004;36(4):423-8.

632. Sandstrom P, Trulsson L, Gasslander T, Sundqvist T, von Dobeln U, Svanvik J. Serum amino acid profile in patients with acute pancreatitis. Amino Acids. 2008;35(1):225-31.

633. Mole DJ, McFerran NV, Collett G, O'Neill C, Diamond T, Garden OJ, et al. Tryptophan catabolites in mesenteric lymph may contribute to pancreatitis-associated organ failure. The British journal of surgery. 2008;95(7):855-67.

634. Mole DJ, Webster SP, Uings I, Zheng X, Binnie M, Wilson K, et al. Kynurenine-3-monooxygenase inhibition prevents multiple organ failure in rodent models of acute pancreatitis. Nat Med. 2016;22(2):202-9.

635. Helwig BG, Ward JA, Blaha MD, Leon LR. Effect of intraperitoneal radiotelemetry instrumentation on voluntary wheel running and surgical recovery in mice. J Am Assoc Lab Anim Sci. 2012;51(5):600-8.

636. Huitron-Resendiz S, Marcondes MC, Flynn CT, Lanigan CM, Fox HS. Effects of simian immunodeficiency virus on the circadian rhythms of body temperature and gross locomotor activity. Proc Natl Acad Sci U S A. 2007;104(38):15138-43.

637. Wittel UA, Wiech T, Chakraborty S, Boss B, Lauch R, Batra SK, et al. Taurocholate-induced pancreatitis: a model of severe necrotizing pancreatitis in mice. Pancreas. 2008;36(2):e9-21.

638. Laukkarinen JM, Van Acker GJ, Weiss ER, Steer ML, Perides G. A mouse model of acute biliary pancreatitis induced by retrograde pancreatic duct infusion of Na-taurocholate. Gut. 2007;56(11):1590-8.

639. Drechsler S, Weixelbaumer KM, Weidinger A, Raeven P, Khadem A, Redl H, et al. Why do they die? Comparison of selected aspects of organ injury and dysfunction in mice surviving and dying in acute abdominal sepsis. Intensive Care Med Exp. 2015;3(1):48.

640. Postic C, Shiota M, Niswender KD, Jetton TL, Chen Y, Moates JM, et al. Dual roles for glucokinase in glucose homeostasis as determined by liver and pancreatic beta cell-specific gene knock-outs using Cre recombinase. J Biol Chem. 1999;274(1):305-15.

641. Postic C, Magnuson MA. DNA excision in liver by an albumin-Cre transgene occurs progressively with age. Genesis. 2000;26(2):149-50.

642. Arras M, Glauser DL, Jirkof P, Rettich A, Schade B, Cinelli P, et al. Multiparameter telemetry as a sensitive screening method to detect vaccine reactogenicity in mice. PloS one. 2012;7(1):e29726.

643. Spani D, Arras M, Konig B, Rulicke T. Higher heart rate of laboratory mice housed individually vs in pairs. Laboratory animals. 2003;37(1):54-62.

644. Gordon CJ. Thermal physiology of laboratory mice: Defining thermoneutrality. J Therm Biol. 2012;37(8):654-85.

645. Gordon CJ. Quantifying the instability of core temperature in rodents. J Therm Biol. 2009;34(5):213-9.

646. Papaioannou V, Mebazaa A, Plaud B, Legrand M. 'Chronomics' in ICU: circadian aspects of immune response and therapeutic perspectives in the critically ill. Intensive Care Med Exp. 2014;2(1):18.

647. Seiver AJ, Szaflarski NL. Report of a case series of ultra low-frequency oscillations in cardiac output in critically ill adults with sepsis, systemic inflammatory response syndrome, and multiple organ dysfunction syndrome. Shock. 2003;20(2):101-9.

648. Cesarovic N, Jirkof P, Rettich A, Arras M. Implantation of radiotelemetry transmitters yielding data on ECG, heart rate, core body temperature and activity in free-moving laboratory mice. Journal of visualized experiments : JoVE. 2011(57).

649. Tait Wojno ED, Hunter CA, Stumhofer JS. The Immunobiology of the Interleukin-12 Family: Room for Discovery. Immunity. 2019;50(4):851-70.

650. Vincent JL. Metabolic support in sepsis and multiple organ failure: more questions than answers. Crit Care Med. 2007;35(9 Suppl):S436-40.

6. APPENDIX

6.1. Appendix 1 – Telemetry software setup

The following instructions should allow a new user to set up a new telemetry experiment.

1) Open VitalView icon in programs to open software application.
2) An error will appear ('Initialization error number 1'), click 'OK' to continue.
3) On the left side four options will appear: 'System Setup', 'Animal & Groups Setup'; 'Data Collection Monitor', and 'Data Load & Analysis'.
4) Select 'System Setup':
    a. Clipping limit default: Change lower limit temperature clipping from default 30oC to 20.0oC. No changes to Activity and Heart Rate.
    b. DP-24 DataPort Configuration: No changes.
    c. ER-4000 Configuration: '# of ER-4000's' change to 8 (alter to the number connected). No change to 'HR Oversample Buffer Size' or 'Temp. Oversample Buffer Size'. No change to 'COM Port' (keep at default 'COM1'). No change to 'Filter' (keep at default 4).
    d. Sample Timing Defaults: Keep at default interval 0hh, 1mm, 0ss.
    e. Data file defaults: Max File Size = 5.0M.
5) Select 'Animal & Group Setup':
    a. Temperature Calibration
        i. Select 'Temperature Calibration' (in bottom right corner)
        ii. Make a note of the serial number for each device (eg. EM015379) and assign it a code (eg. EM33).
        iii. Ensure 'Series 4000' is selected.
        iv. For each telemeter, enter the designated user friendly code name along with the factory supplied calibration frequency points for the high and low temperatures – these details are found on the individual packaging for each device. To illustrate, the frequencies of non-cardiac telemeters used in this work are listed in Table X.
        v. After all telemeters have been entered, save this information by selecting 'File' drop down menu (top left) and then select 'Exit' (bottom right) to return to 'Animal & Group Setup' screen.
    b. Add Animals to experiment
        i. First, click 'Group' drop down menu and select 'New' to create an experimental group and assign a suitable name (eg. '2017jul07_Pump').

ii. Next, click ‘Animal’ drop down menu and select ‘New’ to enter an animal into the experiment. A new window will appear (‘VitalView Animal Configuration’).
iii. In ‘Animal ID’ (top left) enter name of experimental subject. It simplifies matters to name this by the device code name and ER-4000 receiver plate number (ie. EM21/ER1).
iv. In ‘Group ID’ select the name of the group (from above – 5.b.i).
v. Next select from ‘Parameter’ the telemeter device and channel of interest from drop down menu (ie. ‘ER-4000 Temperature’) to replace default ‘TR-3000 Temperature’.
vi. From immediately below this, select the telemeter (ie. EM21)
vii. Select ‘Enable’ to highlight box.
viii. Under ‘Con’ select the corresponding ER-4000 plate for use with this selected telemeter (ie. ‘1’).
ix. Under ‘Chn’ select ‘1’ for temperature, ‘2’ for activity, ‘3’ for heart rate. Check clipping limits are acceptable (ie. 20.00 to 42.00 Deg for temperature).
x. To add activity counts, chose ‘ER-4000 Activity’ under drop down ‘parameter’ options. Select ‘Enable’. Select ‘1’ under ‘Con’ for ER-4000 #1, and chose channel ‘2’.
xi. Finally, an image icon can be selected (top left) at users’ preference.
xii. Click ‘OK’ (bottom left) to save changes.

c. Save ‘Animal & Group Setup’ changes by selecting ‘File’ drop down (top left) and choose ‘Save Configuration to File’. And exit to main menu by selecting ‘Exit’ from ‘File’ drop down menu in ‘Animal & Group setup’.

6) Start data recording
   a. In main menu, select ‘File’ drop down (top left) and choose ‘Start Data Collection’.
   b. The user will be given the choice of ‘Standard’ or ‘Test’. Select ‘Test’ initially to run checks.
   c. The software will check connection with each ER-4000 plate; ensure these are connected in series as per manual. Click ‘list is OK’ and select start time of test to run immediately.
   d. Save logfile as test, to allow identification (ie. ‘logfile_test2017jul07_Pump’)
   e. In the main menu, select ‘Data Collection Monitor’ to visualise live datastream.

f. In the main menu, select ‘File’ drop down (top left) and choose ‘Stop Data Collection’ to terminate test.

For the experiment (including delayed start), select ‘Start Data Collection’ from ‘File’ drop down in main menu, and choose ‘Standard’. Click ‘list is OK’ when prompted and select date time to start telemetry recording.

The following steps allow brief data inspection and export:

1) In main menu, select ‘Data Load & Analysis’, and select from ‘File’ drop down (top left) the option ‘Load from VitalView Data File’.
2) Choose experiment of interest (ie. ‘ .log’ file) and click ‘OK’ to load.
3) A new window will appear (‘Data Available From Selected Experiment’). Select one subject of interest (ie. EM21/ER1) and corresponding channels (i.e. temperature and activity).
4) Select ‘Special Span ?’ (bottom middle) and adjust date and time from the start and end of the experiment.
5) An alert will appear regarding the number of data points, select ‘Continue Load’ and the data will appear visually.
6) To export data, select from ‘File’ drop down in ‘Data Load & Analysis’ the option ‘Save To ASCII File’.
7) An alert will appear, relating to file format: Select ‘Old Format’ and save the file in the appropriate window.
8) An alert will appear: Select ‘Date/time in left-most column only’.

6.2. Appendix 2 – Python code

In[1]:	# Python packages import numpy as np; import pandas as pd; from __future__ import division import matplotlib as mpl; import matplotlib.pyplot as plt; %matplotlib inline; import seaborn as sns

In[2]:	dfA415 = pd.read_csv('/Users/alastairhayes/Documents/Telemetry/Data/A415/A415.csv')
	df1A415 = dfA415.drop(['time', 'ddmmyyyy'], axis=1)
	# Change datetime stamps from object dtype to datetime64 dtype
	df1A415.datetime = pd.to_datetime(df1A415.datetime, dayfirst=True)
	df1A415.ZT0 = pd.to_datetime(df1A415.ZT0, dayfirst=True)
	# Create column with accumulative activity
	ActSum_A415 = df1A415['act'].expanding(min_periods=1).sum()
	ActSum_A415.name = 'sumAct'
	# Create column with ZT
	tXA415 = df1A415.datetime; tYA415 = df1A415.ZT0
	deltaZTA415 = tXA415 - tYA415
	ZTA415 = deltaZTA415 / np.timedelta64(1, 'h')
	ZTA415.name = 'ZT'
	# Append ZT and sumAct series to df1 and drop useless column
	df2A415 = pd.concat([df1A415, ActSum_A415, ZTA415], axis=1)
	df3A415 = df2A415.drop(['ZT0'], axis=1)
	df4A415 = df3A415.set_index('ZT')
	# Set datetime as index and then separate telemetry parameters
	DTindexdfA415 = df3A415.set_index('datetime')
	df_tempA415 = DTindexdfA415['temp']
	df_actA415 = DTindexdfA415['act']
	df_ActSum_A415 = DTindexdfA415['sumAct']
	df_ZTA415 = DTindexdfA415['ZT']
	# Resample data at 60 min intervals (using mean for Temp and sum for Activity)
	s1A415 = df_tempA415.resample('60min').mean()
	s2A415 = df_actA415.resample('60min').sum()
	s3A415 = df_ActSum_A415.resample('60min').last()
	s4A415 = df_ZTA415.resample('60min').first()
	df5A415 = pd.concat([s1A415, s2A415, s3A415, s4A415], axis=1); df5A415.insert(3, 'Exp', 'Vehicle'); df5A415.insert(4, 'ID', 'A415')
	df5A415.head(1)

Figure 47. Python code for data wrangling

```
from matplotlib import gridspec                    #special function
sns.set_context("notebook"); sns.set_style("ticks");
fig = plt.figure(figsize=(10, 6))                  #Figure size
gs = gridspec.GridSpec(2, 1, height_ratios=[0.5,0.5]) #Ratio of upper and lower subplots
ax0 = plt.subplot(gs[0]);
#Data - KMO albcre, AP, Vehicle (n=10)
plt.plot(df5A415['ZT'][0:10080], df5A415['temp'][0:10080], linewidth=1.0, color='navy')
plt.plot(df5A416['ZT'][0:10080], df5A416['temp'][0:10080], linewidth=1.0, color='navy')
plt.plot(df5A421['ZT'][0:10080], df5A421['temp'][0:10080], linewidth=1.0, color='navy')
plt.plot(df5A422['ZT'][0:10080], df5A422['temp'][0:10080], linewidth=1.0, color='navy')
plt.plot(df5A432['ZT'][0:10080], df5A432['temp'][0:10080], linewidth=1.0, color='navy')
plt.plot(df5A439['ZT'][0:10080], df5A439['temp'][0:10080], linewidth=1.0, color='navy')
plt.plot(df5A440['ZT'][0:10080], df5A440['temp'][0:10080], linewidth=1.0, color='navy')
plt.plot(df5A449['ZT'][0:10080], df5A449['temp'][0:10080], linewidth=1.0, color='navy')
plt.plot(df5A450['ZT'][0:10080], df5A450['temp'][0:10080], linewidth=1.0, color='navy')
plt.plot(df5A451['ZT'][0:10080], df5A451['temp'][0:10080], linewidth=1.0, color='navy')
ax0.tick_params(labelsize=13)
plt.plot([24, 24], [20, 50], 'k--', lw=1); plt.plot([48, 48], [20, 50], 'k--', lw=1); plt.plot([72, 72], [20, 50], 'k--', lw=1); plt.plot([96,
96], [20, 50], 'k--', lw=1); plt.plot([120, 120], [20, 50], 'k--', lw=1); plt.plot([144, 144], [20, 50], 'k--', lw=1);
plt.ylabel('Temperature ($^\circ$C)', fontsize=14)
ax1 = plt.subplot(gs[1]);
#Data - KMO albcre, AP, GSK898 (n=7)
plt.plot(df5A411['ZT'][0:10080], df5A411['temp'][0:10080], linewidth=1.0, color='navy')
plt.plot(df5A420['ZT'][0:10080], df5A420['temp'][0:10080], linewidth=1.0, color='navy')
plt.plot(df5A430['ZT'][0:10080], df5A430['temp'][0:10080], linewidth=1.0, color='navy')
plt.plot(df5A431['ZT'][0:10080], df5A431['temp'][0:10080], linewidth=1.0, color='navy')
plt.plot(df5A436['ZT'][0:10080], df5A436['temp'][0:10080], linewidth=1.0, color='navy')
plt.plot(df5A438['ZT'][0:10080], df5A438['temp'][0:10080], linewidth=1.0, color='navy')
plt.plot(df5A452['ZT'][0:10080], df5A452['temp'][0:10080], linewidth=1.0, color='navy')
ax1.tick_params(labelsize=13)
plt.plot([24, 24], [20, 50], 'k--', lw=1); plt.plot([48, 48], [20, 50], 'k--', lw=1); plt.plot([72, 72], [20, 50], 'k--', lw=1); plt.plot([96,
96], [20, 50], 'k--', lw=1); plt.plot([120, 120], [20, 50], 'k--', lw=1); plt.plot([144, 144], [20, 50], 'k--', lw=1);
plt.ylabel('Temperature ($^\circ$C)', fontsize=14); plt.xlabel('Zeitgeber Time (hours)', fontsize=14)
#Titles
ax0.set_title('KMO alb-cre - AP - Vehicle n=10', fontsize=14)
ax1.set_title('KMO alb-cre - AP - GSK898 n=7', fontsize=14)
#Dark phase panels in upper left subplot
ax0.set_xticks([0, 24, 48, 72, 96, 120, 144, 168])
ax0.axvspan(6,18,color='k',alpha=0.2);ax0.axvspan(30,42,color='k',alpha=0.2);ax0.axvspan(54,66,color='k',alpha=0.2);ax
0.axvspan(78,90, color='k', alpha=0.2)
ax0.axvspan(102,114,color='k',alpha=0.2);ax0.axvspan(126,138,color='k',alpha=0.2);ax0.axvspan(150,162,color='k',alpha
=0.2)
ax0.yaxis.set_ticks(np.arange(22.0,42.01,3.0))
#Set upper subplot limits
ax0.set_ylim(25.0,40.0); ax0.set_xlim(0,168)
#Dark phase panels in upper middle subplot
```

```
ax1.set_xticks([0, 24, 48, 72, 96, 120, 144, 168])
ax1.axvspan(6,18,color='k',alpha=0.2);ax1.axvspan(30,42,color='k',alpha=0.2);ax1.axvspan(54,66,color='k',alpha=0.2);
ax1.axvspan(78,90,color='k',alpha=0.2);
ax1.axvspan(102,114,color='k',alpha=0.2);ax1.axvspan(126,138,color='k',alpha=0.2);ax1.axvspan(150,162, color='k',
alpha=0.2)
ax1.yaxis.set_ticks(np.arange(22.0,42.01,3.0))
#Set upper subplot limits
ax1.set_ylim(25.0,40.0); ax1.set_xlim(0,168)
sns.despine(top=False, right=False); plt.tight_layout()
plt.savefig('Test001.png', dpi=600)
```

Figure 48. Python code for visualisation of wrangling

6.3. Appendix 3 – G2 HR E-mitter in-house calibration

E-mitter	Waterbath temp. (°C)	Mean E-mitter temp. (°C) [of 3]	Difference (°C)
EM03s	37.0	36.75	0.25
EM04s	37.0	36.92	0.08
EM06s	37.0	33.93	3.08
EM09s	37.0	36.88	0.12

Table 65. In-house calibration of Recalibration of G2 HR E-mitters

6.4. Appendix 4 – Clinical score sheet

Clinical Observation Score Sheet (SOP–AH004, Appendix; V1.1) Effective date (dd-mmm-yy) – 11-mar-15

PPL: PL60 4433, Protocol No. 19b1	PIL (DM): PIL60/11249	PIL (AH): ID9077CFE	PIL (XZ): IF2C456F6	Page _____ of _____	
Mouse ID:	Exp. request #	Mouse Strain:	Mouse Gender:		
Date of E-mitter implantation (if applicable):		Weight at start of experiment:			
Date of intervention:		Type of intervention [SOP code(s)]:			

Instructions for use of this clinical score sheet

- For a mouse behaving normally, please enter a " **N** " in the boxes below.
- If the mouse is observed as being abnormal (i.e. a positive clinical finding) put a " **Y** " in the corresponding box.

Date of observation						
Day *(ie. post-operative day 0, 1 , 2 etc)*						
Time of observation						
Critical observations*						
Minimal or no response (Y / N)						
Severe labored breathing (Y / N)						
Major wound breakdown (Y / N)						
Prolonged bleeding (Y / N)						
Observations that trigger analgesia**						
Hunched posture (Y / N)						
Not inquisitive or alert (*enter 'N' if normal*)						
Not eating or drinking (*enter 'N' if normal*)						
Abdominal writhing (*enter 'N' if normal*)						
Mouse grimace scale – *Refer to MGS score over the page*						
Orbital tightening (Score 0, 1, 2, or 'unclear')						
Nose bulge (Score 0, 1, 2, or 'unclear')						
Cheek bulge (Score 0, 1, 2, or 'unclear')						
Ear position (Score 0, 1, 2, or 'unclear')						
Whisker change (Score 0, 1, 2, or 'unclear')						
General observations						
Ruffled haircoat (Y / N)						
Discharging or crusty nose (Y / N)						
Sunken eyes (Y / N)						
Discharging or crusty red eye (Y / N)						
Obvious diarrhoea (Y / N)						
Observer initials						
Notes (*eg. unpredicted/unexpected significant event or observation*)						

***Humane endpoints** (requiring cull by Schedule 1)

- Animal showing minimal or no response to external stimuli
- Animal showing severe labored breathing
- Animal with major wound breakdown (may consider x1 repair under GA)
- Animal with prolonged bleeding
- Animal with clear evidence of self-mutilation
- Sustained profound hypothermia (telemetry readout), despite warming

Date animal culled		
Cull method		
Actual severity* (indicate by tick √) **Refer to severity score over the page*	**Non-recovery**	
	Mild	
	Moderate	
	Severe	

****Administer Buprenorphine in accordance with the protocol** (SOP–AH003): Dilute 0.1ml Vetergesic (0.3mg/ml) in 1.9ml sterile water (i.e. 2ml of 0.015 mg/ml). Give weight adjusted dose subcutaneous to scruff. Give 8-12 hrs as required, and up to 48 hrs post-op; thereafter inform oncall (below).

Mouse weight	Dilute Vetergesic bolus volume and (dose) [s/c dose 0.05 mg/kg]
25 g	0.08 mls (0.00125 mg)
30 g	0.10 mls (0.0015 mg)
35 g	0.12 mls (0.00175 mg)

Analgesia prescription record for this rodent

Date	Time	Drug	Route	Dose	Initials
01-01-10	*17:00*	*Dilute Vetergesic*	*S/C*	*0.1ml or 0.0015mg*	*E.G*
		Dilute Vetergesic	S/C		
		Dilute Vetergesic	S/C		
		Dilute Vetergesic	S/C		

Please inform if concerns arise:

1st on call: Mr Alastair Hayes
alastair.hayes@ed.ac.uk 07971044186, 0131-237-9769

2nd : Dr Xiao Zheng	3rd : Mr Damian Mole
xzheng@staffmail.ed.ac.uk Mob: 07837514973	damian.mole@ed.ac.uk Mob: 07775801868

Figure 49. Clinical score sheet

6.5. Appendix 5 – Supplementary data of Model Optimization – Phase I

Line	ID	Cohort	Treatment	Survival status at end	Time of death (hrs)	Protocol	No.
Other - WT	ITGAX135	WT	3% TCA, 100 ul, 60s, U/F, G2HR	Survived	168.00	P1	1
Other - WT	ITGAX136	WT	3% TCA, 100 ul, 60s, U/F, G2HR	Lethal	22.53	P1	2
Kmo^{null}	K1044	Kmo^{null}	3% TCA, 100 ul, 60s, U/F, G2HR	Lethal	50.92	P1	3
Kmo^{null}	K1045	Kmo^{null}	3% TCA, 100 ul, 60s, U/F, G2HR	Lethal	21.50	P1	4
Kmo^{null}	K1046	Kmo^{null}	3% TCA, 100 ul, 60s, U/F, G2HR	Survived	168.00	P1	5
Kmo^{null}	K1047	Kmo^{null}	3% TCA, 100 ul, 60s, U/F, G2HR	Lethal	23.00	P1	6
Kmo^{wt}	K1052	Kmo^{null}	3% TCA, 100 ul, 60s, U/F, G2HR	Lethal	19.75	P1	7
Kmo^{wt}	K1053	Kmo^{null}	3% TCA, 100 ul, 60s, U/F, G2HR	Lethal	19.00	P1	8
Kmo^{wt}	K1050	Kmo^{null}	3% TCA, 100 ul, 60s, U/F, G2HR	Lethal	28.67	P1	9
Kmo^{wt}	FK372	WT	0% TCA, 100 ul, 60s, U/F, G2HR	Survived	168.00	P2	1
Kmo^{null}	K1056	Kmo^{null}	0% TCA, 100 ul, 60s, U/F, G2HR	Survived	168.00	P2	2
Kmo^{null}	K1059	Kmo^{null}	0% TCA, 100 ul, 60s, U/F, G2HR	Survived	168.00	P2	3
Kmo^{wt}	FK382	WT	0% TCA, 100 ul, 60s, U/F, G2HR	Survived	168.00	P2	4
Kmo^{null}	K1057	Kmo^{null}	0% TCA, 100 ul, 60s, U/F, G2HR	Survived	168.00	P2	5
Kmo^{wt}	FK374	WT	0% TCA, 100 ul, 60s, U/F, G2HR	Survived	168.00	P2	6
Kmo^{wt}	FK385	WT	1% TCA, 100 ul, 60s, U/F, G2HR	Survived	168.00	P3	1
Kmo^{null}	K1062	Kmo^{null}	1% TCA, 100 ul, 60s, U/F, G2HR	Survived	168.00	P3	2
Kmo^{wt}	FK391	WT	1% TCA, 50 ul, 300s, U/F, G2HR	Survived	72.00	P4	1
Kmo^{wt}	FK392	WT	1% TCA, 50 ul, 300s, U/F, G2HR	Survived	72.00	P4	2
Kmo^{wt}	FK393	WT	3% TCA, 50 ul, 300s, U/F, G2HR	Survived	168.00	P5	1
Kmo^{wt}	FK394	WT	3% TCA, 50 ul, 300s, U/F, G2HR	Lethal	48.73	P5	2
Kmo^{wt}	FK399	WT	3% TCA, 50 ul, 300s, U/F, G2HR	Lethal	30.88	P5	3
Kmo^{wt}	FK402	WT	3% TCA, 50 ul, 300s, U/F, G2HR	Lethal	94.43	P5	4
Kmo^{null}	K1106	Kmo^{null}	3% TCA, 50 ul, 300s, U/F, G2HR	Lethal	35.58	P5	5
Kmo^{wt}	FK429	WT	3% TCA, 50 ul, 300s, U/F, G2HR	Lethal	45.73	P5	6
Kmo^{wt}	FK420	WT	2% TCA, 50 ul, 300s, U/F, G2HR	Survived	168.00	P6	1
Kmo^{wt}	FK421	WT	2% TCA, 50 ul, 300s, U/F, G2HR	Survived	168.00	P6	2
Kmo^{wt}	FK434	WT	2.5% TCA, 50 ul, 300s, U/F, G2HR	Lethal	23.18	P7	1
Kmo^{wt}	FK435	WT	2.5% TCA, 50 ul, 300s, U/F, G2HR	Lethal	23.18	P7	2
Kmo^{wt}	FK436	WT	2.5% TCA, 50 ul, 300s, Filt., G2HR	Survived	168.00	P8	1
Kmo^{wt}	FK437	WT	2.5% TCA, 50 ul, 300s, Filt., G2HR	Survived	168.00	P8	2
Kmo^{null}	K1114	Kmo^{null}	2.5% TCA, 50 ul, 300s, Filt., G2HR	Lethal	26.70	P8	3
Kmo^{null}	FK449	WT	2.5% TCA, 50 ul, 300s, Filt., G2HR	Lethal	26.30	P8	4
$Kmo^{alb\text{-}cre}$ [-/-]	FKA126	WT	2.5% TCA, 50 ul, 300s, Filt., G2HR	Lethal	47.00	P8	5
$Kmo^{alb\text{-}cre}$ [-/-]	FKA127	WT	2.5% TCA, 50 ul, 300s, Filt., G2HR	Lethal	47.10	P8	6
Kmo^{wt}	FK459	WT	2.0% TCA, 50 ul, 300s, Filt., G2HR	Lethal	55.50	P9	1
Kmo^{wt}	FK460	WT	2.0% TCA, 50 ul, 300s, Filt., G2HR	Lethal	21.62	P9	2
Kmo^{wt}	FK468	WT	2.0% TCA, 50 ul, 300s, Filt., G2HR	Lethal	47.43	P9	3
Kmo^{wt}	FK473	WT	2.0% TCA, 50 ul, 300s, Filt., G2HR	Lethal	70.08	P9	4
Kmo^{wt}	FK506	WT	2.0% TCA, 50 ul, 300s, Filt., G2HR	Lethal	53.70	P9	5
Kmo^{wt}	FK507	WT	2.0% TCA, 50 ul, 300s, Filt., G2HR	Survived	168.00	P9	6

Table 66. Model optimization I.

Pilot work testing recovery in heart rate telemetered adult mice. U/F: unfiltered; Filt.: Filtered infusate.

6.6. Appendix 6 – Supplementary data of experiment 1 (cardiotelemeter study)

Line	**ID**	**Gene**	**Sex**	**DOB**	**Date**	**Age** (d)	**Rx**	**Telemeter**	**Weight** (g)	**Group**	**Anaesthetic** (min)
Kmo^{wt}	FK459	FK (HOM)	M	23/06/15	11/11/15	141	AP	EM-03s	28.63	WT/ AP	47
Kmo^{wt}	FK460	FK (HOM)	M	23/06/15	11/11/15	141	AP	EM-04s	29.35	WT / AP	44
Kmo^{wt}	FK468	FK (HOM)	M	15/07/15	07/12/15	145	AP	EM-03s	29.60	WT / AP	49
Kmo^{wt}	FK473	FK (HOM)	M	15/07/15	07/12/15	145	AP	EM-04s	27.84	WT / AP	43
Kmo^{wt}	FK506	FK (HOM)	M	20/09/15	10/02/16	143	AP	EM-09s	29.45	WT / AP	52
Kmo^{wt}	FK507	FK (HOM)	M	20/09/15	10/02/16	143	AP	EM-06s	28.28	WT / AP	38
Kmo^{wt}	FK508	FK (HOM)	M	20/09/15	11/02/16	144	Sham	EM-03s	27.90	WT / Sham	46
Kmo^{wt}	FK509	FK (HOM)	M	20/09/15	11/02/16	144	Sham	EM-04s	32.43	WT / Sham	47
Kmo^{wt}	FK520	FK (HOM)	M	02/11/15	14/03/16	133	Sham	EM-03s	31.65	WT / Sham	41
Kmo^{wt}	FK521	FK (HOM)	M	02/11/15	14/03/16	133	Sham	EM-04s	31.60	WT / Sham	43
$Kmo^{alb\text{-}cre}$	FKA123	Cre(-)	M	22/05/15	21/10/15	152	Sham	EM-09s	29.56	WT / Sham	52
$Kmo^{alb\text{-}cre}$	FKA128	Cre(-)	M	22/05/15	21/10/15	152	Sham	EM-06s	29.62	WT / Sham	48
Kmo^{null}	K1140	HOM	M	29/06/15	24/11/15	148	AP	EM-09s	32.60	Null / AP	50
Kmo^{null}	K1141	HOM	M	29/06/15	24/11/15	148	AP	EM-06s	31.75	Null / AP	46
Kmo^{null}	K1166	HOM	M	12/09/15	03/02/16	144	AP	EM-03s	32.93	Null / AP	47
Kmo^{null}	K1168	HOM	M	12/09/15	03/02/16	144	AP	EM-04s	29.57	Null / AP	42
Kmo^{null}	K1191	HOM	M	15/10/15	29/02/16	137	AP	EM-03s	25.81	Null / AP	46
Kmo^{null}	K1192	HOM	M	15/10/15	29/02/16	137	AP	EM-04s	30.11	Null / AP	45

Table 67. Study subjects – experiment 1

Line	**ID**	**Group**	**Exp. Length** (h)	**Start Weight** (g)	**End body weight** (g)	**Weight loss** (% start)
Kmo^{wt}	FK459	WT/ AP	55.5	28.63	25.02	12.609
Kmo^{wt}	FK460	WT / AP	21.6	29.35	28.90	1.533
Kmo^{wt}	FK468	WT / AP	47.4	29.60	25.19	14.899
Kmo^{wt}	FK473	WT / AP	70.1	27.84	24.67	11.386
Kmo^{wt}	FK506	WT / AP	53.7	29.45	26.53	9.915
Kmo^{wt}	FK507	WT / AP	168	28.28	25.91	8.380
Kmo^{wt}	FK508	WT / Sham	168	27.90	26.26	5.878
Kmo^{wt}	FK509	WT / Sham	168	32.43	29.03	10.484
Kmo^{wt}	FK520	WT / Sham	168	31.65	28.01	11.501
Kmo^{wt}	FK521	WT / Sham	168	31.60	29.30	7.278
$Kmo^{alb\text{-}cre}$	FKA123	WT / Sham	168	29.56	29.46	0.338
$Kmo^{alb\text{-}cre}$	FKA128	WT / Sham	168	29.62	27.97	5.571
Kmo^{null}	K1140	Null / AP	168	32.60	31.55	3.221
Kmo^{null}	K1141	Null / AP	45.12	31.75	28.27	10.961
Kmo^{null}	K1166	Null / AP	168	32.93	27.84	15.457
Kmo^{null}	K1168	Null / AP	168	29.57	26.22	11.329
Kmo^{null}	K1191	Null / AP	168	25.81	22.87	11.391
Kmo^{null}	K1192	Null / AP	168	30.11	24.79	17.669

Table 68. Outcomes of study subjects
Experiment length is 168 hours or less, where specified, due to mice reaching humane endpoint(s). The same scales instrument was used for every measurement.

6.6. Appendix 6 – Supplementary data of experiment 1 (cardiotelemeter study). Cont.

Line	ID	Group	Albumin (g/l)	ALT (U/l)	Amylase (U/l)	Creatinine (µmol/l)	Glucose (mmol/l)	LDH (U/l)	Urea (mmol/l)
Kmo^{wt}	FK459	WT/ AP	18.8	348	6960	<10	1.8	1420	12.0
Kmo^{wt}	FK460	WT / AP	20.2	694	18860	38	6.2	2760	24.2
Kmo^{wt}	FK468	WT / AP	18.4	508	3700	<10	0.6	5940	16.8
Kmo^{wt}	FK473	WT / AP	21.0	560	645	<10	4.0	3150	31.5
Kmo^{wt}	FK506	WT / AP	21.2	234	26140	<10	2.0	828	14.8
Kmo^{wt}	FK507	WT / AP	20.4	22	350	<10	10.6	120	6.8
Kmo^{wt}	FK508	WT / Sham	21.4	16	572	<10	9.2	128	7.4
Kmo^{wt}	FK509	WT / Sham	23.2	34	518	<10	14.2	198	6.2
Kmo^{wt}	FK520	WT / Sham	22.2	20	416	<10	12.0	120	6.2
Kmo^{wt}	FK521	WT / Sham	22.0	16	446	<10	13.2	120	7.8
$Kmo^{alb\text{-}cre}$	FKA123	WT / Sham	23.0	32	584	<10	12.6	174	6.0
$Kmo^{alb\text{-}cre}$	FKA128	WT / Sham	24.8	18	614	<10	10.8	136	7.4
Kmo^{null}	K1140	Null / AP	25.0	16	618	<10	16.6	166	10.4
Kmo^{null}	K1141	Null / AP	22.4	156	1184	14	0.8	1136	21.8
Kmo^{null}	K1166	Null / AP	23.8	16	426	<10	13.0	180	5.2
Kmo^{null}	K1168	Null / AP	22.0	14	414	<10	9.4	92	6.2
Kmo^{null}	K1191	Null / AP	22.8	72	1194	<10	11.6	194	6.8
Kmo^{null}	K1192	Null / AP	21.4	398	566	<10	6.2	456	6.4

Table 69. Biochemistry from experiment 1 subjects

Line	ID	Group	IFNγ (pg/ml) LOD = 0.0276	IL1β (pg/ml) LOD = 0.0618	IL2 (pg/ml) LOD = 0.154	IL4 (pg/ml) LOD = 0.0558	IL5 (pg/ml) LOD = 0.0505	IL6 (pg/ml) LOD = 0.556	IL10 (pg/ml) LOD = 0.350	IL12p70 (pg/ml) LOD = 22.682	KCGRO (pg/ml) LOD = 0.320	TNFα (pg/ml) LOD = 0.147
Kmo^{wt}	FK459	WT/ AP	1.7568	10.7794	6.7511	0.4434	1.2149	5048.9452	535.4282	69.8694	333.3103	119.8801
Kmo^{wt}	FK460	WT / AP	2.2794	126.3120	24.9114	5.9961	25.7080	26810.9542	797.8872	865.2830	6515.7199	212.7989
Kmo^{wt}	FK468	WT / AP	I/S	I/S	I/S	I/S	I/S	I/S	I/S	I/S	I/S	I/S
Kmo^{wt}	FK473	WT / AP	I/S	I/S	I/S	I/S	I/S	I/S	I/S	I/S	I/S	I/S
Kmo^{wt}	FK506	WT / AP	6.0403	3.0918	1.9556	0.3182	0.8505	5779.2782	72.3329	28.1512	1056.4771	34.8871
Kmo^{wt}	FK507	WT / AP	1.2129	4.9766	1.7986	0.9273	9.9952	203.1203	29.1542	<22.682	49.3533	17.8667
Kmo^{wt}	FK508	WT / Sham	0.9293	1.7043	2.4496	0.1917	10.2532	43.8162	29.4185	42.9806	23.8182	12.9753
Kmo^{wt}	FK509	WT / Sham	0.9590	2.0161	3.1719	1.8408	11.1699	46.1513	23.0893	55.3155	33.5665	12.2347
Kmo^{wt}	FK520	WT / Sham	1.0280	2.3307	0.8824	0.3085	2.9311	120.6068	28.6132	<22.682	56.2881	12.5529
Kmo^{wt}	FK521	WT / Sham	0.7547	2.0833	1.5192	BLQ	11.1215	129.3931	28.2643	<22.682	37.9779	14.4455
$Kmo^{alb\text{-}cre}$	FKA123	WT / Sham	0.6674	2.6588	1.6632	0.1029	3.1869	53.7508	28.1198	<22.682	32.5653	13.7827
$Kmo^{alb\text{-}cre}$	FKA128	WT / Sham	0.5116	2.1682	1.0876	0.1819	6.0296	104.0456	20.1513	<22.682	45.2230	12.3750
Kmo^{null}	K1140	Null / AP	0.8245	2.4331	1.8136	1.1120	6.4532	136.1978	22.1892	94.3316	45.2665	18.1821
Kmo^{null}	K1141	Null / AP	6.1805	314.6119	43.2671	10.8707	21.4628	27107.5944	9169.6493	1213.8133	6521.2530	2611.0276
Kmo^{null}	K1166	Null / AP	0.9279	2.9406	2.6171	0.7764	30.4867	84.4920	28.8176	<22.682	60.2789	23.5861
Kmo^{null}	K1168	Null / AP	5.4861	1.0027	2.7404	<0.0558	10.3892	99.8789	29.2142	<22.682	17.7348	16.1200
Kmo^{null}	K1191	Null / AP	0.1814	1.1456	0.3817	<0.0558	69.6805	89.5571	27.1922	<22.682	12.1530	12.7360
Kmo^{null}	K1192	Null / AP	142.0417	1.6475	5.6905	<0.0558	5.2332	1321.7306	83.5197	<22.682	59.3600	105.4563

Table 70. Cytokine panel from experiment 1 subjects
Plasma proinflammatory cytokines. BLQ: below level of quantification; I/S: insufficient sample. Quantification to 4 decimal places. LOD: limit of detection.

6.6. Appendix 6 – Supplementary data of experiment 1 (cardiotelemeter). Cont.

Line	ID	Group	IL1β (mmol/L)	Log10 IL1β	IL6 (mmol/L)	Log10 IL6	TNFα (mmol/L)	Log10 TNFα
Kmo^{wt}	FK459	WT/ AP	10.7794	1.0325951	5048.9452	3.7032007	119.8801	2.078747
Kmo^{wt}	FK460	WT / AP	126.3120	2.1014446	26810.9541	4.4283123	212.7989	2.327969
Kmo^{wt}	FK468	WT / AP	N/S	N/S	N/S	N/S	N/S	N/S
Kmo^{wt}	FK473	WT / AP	N/S	N/S	N/S	N/S	N/S	N/S
Kmo^{wt}	FK506	WT / AP	3.0918	0.4902157	5779.2782	3.7618736	34.8871	1.542665
Kmo^{wt}	FK507	WT / AP	4.9766	0.6969334	203.1203	2.3077533	17.8667	1.252045
Kmo^{wt}	FK508	WT / Sham	1.7043	0.2315338	43.8162	1.6416351	12.9753	1.113119
Kmo^{wt}	FK509	WT / Sham	2.0161	0.3045085	46.1513	1.6641843	12.2347	1.087593
Kmo^{wt}	FK520	WT / Sham	2.3307	0.3674899	120.6068	2.0813719	12.5529	1.098743
Kmo^{wt}	FK521	WT / Sham	2.0833	0.3187541	129.3931	2.1119111	14.4455	1.159732
$Kmo^{alb\text{-}cre}$	FKA123	WT / Sham	2.6588	0.4246881	53.7508	1.7303852	13.7827	1.139334
$Kmo^{alb\text{-}cre}$	FKA128	WT / Sham	2.1682	0.3360961	104.0456	2.0172238	12.3750	1.092544
Kmo^{null}	K1140	Null / AP	2.4331	0.3861596	136.1978	2.1341701	18.1821	1.259643
Kmo^{null}	K1141	Null / AP	314.6119	2.4977751	27107.5944	4.4330909	2611.0280	3.416812
Kmo^{null}	K1166	Null / AP	2.9406	0.4684302	84.4920	1.9268156	23.5862	1.372657
Kmo^{null}	K1168	Null / AP	1.0027	0.0011697	99.8789	1.9994738	16.1200	1.207364
Kmo^{null}	K1191	Null / AP	1.1456	0.0590417	89.5571	1.9520999	12.7360	1.105032
Kmo^{null}	K1192	Null / AP	1.6475	0.2168167	1321.7306	3.1211431	105.4536	2.023073

Table 71. Cytokines – Log10 from experiment 1 subjects
Plasma proinflammatory cytokines. BLQ: below level of quantification; I/S: insufficient sample.

6.7. Appendix 7 – Supplementary data of experiment 2 (kynurenines at steady state)

ID	Group	Sample ID	KMO ct values	Mean KMO ct (mKMO ct)	S18 Ct values	Mean S18 Ct value (mS18 ct)	dCt (mKMO ct-mS18 ct)	dCt[NULL]	ddCt (dCt – dCt[NULL])	X = 2^(-ddCt)	Result [Log10(X)]
FK638	WT	L1A	26.491524	26.0737295	17.375427	17.1179715	8.955758	22.5210942	-13.5653362	12121.9670	**4.08357310**
		L1B	25.655935		16.860516						
FK639	WT	L4A	25.750273	25.6537450	17.845621	18.0070135	7.6467315	22.5210942	-14.8743627	30035.1178	**4.47762934**
		L4B	25.557217		18.168406						
FK640	WT	L9A	25.802282	25.1661535	17.927431	17.1941625	7.971991	22.5210942	-14.5491032	23972.6737	**4.37971647**
		L9B	24.530025		16.460894						
FK641	WT	L10A	25.62061	25.1928610	17.534653	17.0126565	8.1802045	22.5210942	-14.3408897	20750.9491	**4.31703796**
		L10B	24.765112		16.490660						
FKA385	WT	L13A	24.826405	24.6895190	18.363405	18.0744515	6.6150675	22.5210942	-15.9060267	61403.2203	**4.78819115**
		L13B	24.552633		17.785498						
K1395	Null	L3A	38.764442	38.4380960	17.588780	17.652882	20.785214	22.5210942	-1.7358802	3.33082648	**0.52255201**
		L3B	38.11175		17.716984						
K1396	Null	L6B	38.692265	38.0679440	18.217247	17.8583165	20.2096275	22.5210942	-2.3114667	4.96387470	**0.69582081**
		L6B	37.443623		17.499386						
K1399	Null	L7A	43.453648	43.4536480	17.203716	16.8018895	26.6517585	22.5210942	4.1306643	0.05708817	**-1.2434539**
		L7B	Undet.		16.400063						
K1405	Null	L8A	38.717762	38.7177620	17.500837	16.9933235	21.7244385	22.5210942	-0.7966557	1.73706977	**0.23981726**
		L8B	Undet.		16.485810						
K1408	Null	L14A	41.551525	40.2431145	17.521530	17.008682	23.2344325	22.5210942	0.7133383	0.60990722	**-0.2147362**
		L14B	38.934704		16.495834						
A355	Alb-cre	L2A	36.057068	35.4064240	18.569155	18.0377530	17.3686710	22.5210942	-5.1524232	35.5659107	**1.55103393**
		L2B	34.755780		17.506351						
A356	Alb-cre	L5A	37.557556	37.4728240	18.974031	19.4750715	17.9977525	22.5210942	-4.5233417	22.9964889	**1.36166153**
		L5B	37.388092		19.976112						
A363	Alb-cre	L11A	35.652138	35.2122490	17.459753	17.0602005	18.1520485	22.5210942	-4.3690457	20.6639722	**1.31521381**
		L11B	34.772360		16.660648						
A364	Alb-cre	L12A	36.706715	36.2904950	17.447266	17.4540815	18.8364135	22.5210942	-3.6846807	12.8587696	**1.10919942**
		L12B	35.874275		17.460897						
A365W	Alb-cre	L15A	35.145283	35.7651815	17.919853	17.6437880	18.1213935	22.5210942	-4.3997007	21.1077471	**1.32444188**
		L15B	36.385080		17.367723						

Table 72. *Kmo* gene expression by RT-PCR: Liver raw data. Corrected to Kmo^{null}.

Undet.: undetermined. Experiment 2 subjects

6.7. Appendix 7 – Supplementary data of experiment 2 (kynurenines at steady state). Cont.

ID	Group	Sample ID	KMO ct values	Mean KMO ct (mKMO ct)	S18 Ct values	Mean S18 Ct value (mS18 ct)	dCt (mKMO ct-mS18 ct)	dCt[NULL]: mean dCt of NULL	ddCt (dCt – dCt[NULL])	X = 2^(-ddCt)	Result [Log10(X)]
FK638	WT	K1A	27.547320	26.3838540	17.188374	17.3015385	9.0823155	23.9648602	-14.8825447	30205.9408	**4.48009237**
		K1B	25.220388		17.414703						
FK639	WT	K4A	26.716719	26.3756145	16.416540	16.3022535	10.0733610	23.9648602	-13.8914992	15197.0028	**4.18175794**
		K4B	26.034510		16.187967						
FK640	WT	K9	26.583939	26.0058330	15.771565	15.1056265	10.9002065	23.9648602	-13.0646537	8567.47107	**3.93285265**
		K9	25.427727		14.439688						
FK641	WT	K10A	26.411232	25.8706485	19.269781	18.5983265	7.2723220	23.9648602	-16.6925382	105914.325	**5.0249547**
		K10B	25.330065		17.926872						
FKA385	WT	K13A	26.780682	26.6473250	16.613075	16.3112485	10.3360765	23.9648602	-13.6287837	12666.9687	**4.10267270**
		K13B	26.513968		16.009422						
K1395	Null	K3A	>45	Undet. (T/hold = 45)	19.73155	18.448718	26.551282	23.9648602	2.5864218	0.16649817	**-0.7785905**
		K3B	>45		17.165886						
K1396	Null	K6A	>45	Undet. (T/hold = 45)	23.664488	22.937664	22.062336	23.9648602	-1.9025242	3.73866758	**0.57271685**
		K6B	>45		22.21084						
K1399	Null	K7A	>45	Undet. (T/hold = 45)	22.224007	21.5975945	23.4024055	23.9648602	-0.5624547	1.47677977	**0.16931574**
		K7B	>45		20.971182						
K1405	Null	K8A	40.585644	40.898001	16.814274	16.4332255	24.4647755	23.9648602	0.4999153	0.70714830	**-0.1504895**
		K8B	41.210358		16.052177						
K1408	Null	K14A	>45	Undet. (T/hold = 45)	22.660158	21.656498	23.343502	23.9648602	-0.6213582	1.53832273	**0.18704746**
		K14B	>45		20.652838						
A355	Alb-cre	K2A	28.105637	27.661235	15.767592	15.1845165	12.4767185	23.9648602	-11.4881417	2872.6006	**3.45827525**
		K2B	27.216833		14.601441						
A356	Alb-cre	K5A	26.612507	26.377612	15.493902	15.2441345	11.1334775	23.9648602	-12.8313827	7288.38119	**3.86263108**
		K5B	26.142717		14.994367						
A363	Alb-cre	K11A	26.516200	25.779531	16.168610	15.464157	10.3153740	23.9648602	-13.6494862	12850.0486	**4.10890477**
		K11B	25.042862		14.759704						
A364	Alb-cre	K12A	26.062674	25.8070435	20.369268	19.565133	6.2419105	23.9648602	-17.7229497	216341.318	**5.33513947**
		K12B	25.551413		18.760998						
A365W	Alb-cre	K15A	28.009678	27.255933	18.06455	16.999927	10.256006	23.9648602	-13.7088542	13389.8688	**4.12677632**
		K15B	26.502188		15.935304						

Table 73. *Kmo* gene expression by RT-PCR: Kidney raw data. Corrected to Kmo^{null}

Experiment 2 subjects

6.7. Appendix 7 – Supplementary data of experiment 2 (kynurenines at steady state). Cont.

ID	Group	Sample ID	KMO ct values	Mean KMO ct (mKMO ct)	S18 Ct values	Mean S18 Ct value (mS18 ct)	dCt (mKMO ct-mS18 ct)	dCt[WT]: mean dCt of WT	ddCt (dCt – dCt[WT])	X = 2^(-ddCt)	Result [Log10(X)]
FK638	WT	S1A	31.736485	31.7355990	14.694613	14.818042	16.917557	27.9364357	-11.0188787	2074.97566	**3.31701301**
		S1B	31.734713		14.941471						
FK639	WT	S4A	29.995592	29.9517325	15.264813	14.9070865	15.044646	27.9364357	-12.8917897	7600.03159	**3.88081540**
		S4B	29.907873		14.54936						
FK640	WT	S9A	30.098242	30.161986	18.509748	18.5010165	11.6609695	27.9364357	-16.2754662	79323.8016	**4.89940352**
		S9B	30.225730		18.492285						
FK641	WT	S10A	30.127392	30.1308135	18.115622	18.167251	11.9635625	27.9364357	-15.9728732	64315.2482	**4.80831395**
		S10B	30.134235		18.21888						
FKA385	WT	S13A	29.484558	29.501504	17.03399	16.886976	12.614528	27.9364357	-15.3219077	40959.4210	**4.61235381**
		S13B	29.51845		16.739962						
K1395	Null	S3A	>45	Undet. (T/hold = 45)	14.212608	14.2057995	30.7942005	27.9364357	2.8577648	0.13795171	**-0.8602729**
		S3B	>45		14.198991						
K1396	Null	S6A	>45	Undet. (T/hold = 45)	16.199295	16.3192875	28.6807125	27.9364357	0.7442768	0.59696705	**-0.2240496**
		S6B	>45		16.43928						
K1399	Null	S7A	>45	Undet. (T/hold = 45)	17.473673	17.3311845	27.6688155	27.9364357	-0.2676202	1.20382042	**0.08056171**
		S7B	>45		17.188696						
K1405	Null	S8A	>45	Undet. (T/hold = 45)	19.552778	19.912213	25.087787	27.9364357	-2.8486487	7.20325361	**0.85752871**
		S8B	>45		20.271648						
K1408	Null	S14A	>45	Undet. (T/hold = 45)	17.55173	17.549337	27.450663	27.9364357	-0.4857727	1.40033568	**0.14623215**
		S14B	>45		17.546944						
A355	Alb-cre	S2A	30.6843	30.704777	15.337427	15.1862795	15.5184975	27.9364357	-12.4179382	5472.325	**3.73817188**
		S2B	30.725254		15.035132						
A356	Alb-cre	S5A	28.20303	28.265421	15.8438	15.6481855	12.6172355	27.9364357	-15.3192002	40882.6247	**4.61153877**
		S5B	28.327812		15.452571						
A363	Alb-cre	S11A	29.013552	29.158888	16.449436	16.659729	12.499159	27.9364357	-15.4372767	44369.3777	**4.64708334**
		S11B	29.304224		16.870022						
A364	Alb-cre	S12A	29.177818	29.1825415	16.303501	16.4892475	12.693294	27.9364357	-15.2431417	38783.1321	**4.58864288**
		S12B	29.187265		16.674994						
A365W	Alb-cre	S15A	30.824972	30.4486305	18.372221	17.7780685	12.670562	27.9364357	-15.2658737	39399.063	**4.59548589**
		S15B	30.072289		17.183916						

Table 74. *Kmo* gene expression by RT-PCR: Spleen raw data. Corrected to Kmo^{wt}

Experiment 2 subjects.

6.7. Appendix 7 – Supplementary data of experiment 2 (kynurenines at steady state). Cont.

Line	ID	Gene	Sex	DOB	Cull	Age	Group	Liver	Kidney	Spleen
Kmo^{wt}	FK638	FK (HOM)	M	29/10/16	08/02/17	102	WT	4.083573097	4.480092367	3.317013007
Kmo^{wt}	FK639	FK (HOM)	M	29/10/16	08/02/17	102	WT	4.477629339	3.932852647	3.880815397
Kmo^{wt}	FK640	FK (HOM)	M	29/10/16	14/02/17	108	WT	4.379716473	5.024954702	4.89940352
Kmo^{wt}	FK641	FK (HOM)	M	29/10/16	14/02/17	108	WT	4.317037964	4.181757944	4.80831395
$Kmo^{alb\text{-}cre}$	FKA385	Cre(-)	M	30/11/16	14/02/17	108	WT	4.788191149	4.102672698	4.612353808
Kmo^{null}	K1395	HOM	M	28/10/16	08/02/17	103	Null	0.522552009	-0.778590543	-0.860272925
Kmo^{null}	K1396	HOM	M	28/10/16	08/02/17	103	Null	0.695820811	0.572716852	-0.224049642
Kmo^{null}	K1399	HOM	M	16/11/16	14/02/17	90	Null	-1.243453856	0.169315736	0.080561708
Kmo^{null}	K1405	HOM	M	16/11/16	14/02/17	90	Null	0.239817262	-0.150489501	0.857528706
Kmo^{null}	K1408	HOM	M	16/11/16	14/02/17	90	Null	-0.214736225	0.187047456	0.146232154
$Kmo^{alb\text{-}cre}$	A355	Cre(+)	M	24/10/19	08/02/17	107	Alb-cre	1.551033934	3.458275246	3.738171883
$Kmo^{alb\text{-}cre}$	A356	Cre(+)	M	24/10/19	08/02/17	107	Alb-cre	1.361661532	3.862631079	4.61153877
$Kmo^{alb\text{-}cre}$	A363	Cre(+)	M	10/11/16	14/02/17	96	Alb-cre	1.315213808	4.108904772	4.647083338
$Kmo^{alb\text{-}cre}$	A364	Cre(+)	M	10/11/16	14/02/17	96	Alb-cre	1.109199415	5.335139471	4.58864288
$Kmo^{alb\text{-}cre}$	A365W	Cre(+)	M	10/11/16	14/02/19	96	Alb-cre	1.324441883	4.126776320	4.595485894

Table 75. *Kmo* gene expression by RT-PCR: Liver, kidney, spleen

Line	ID	Gene	Sex	DOB	Cull	Age (d)	Group	Trp (μM) LOD	Kyn (μM) LOD	KA (μM) LOD	AA (μM) LOD	3HK (μM) LOD	XA (μM) LOD
Kmo^{wt}	FK491	FK (HOM)	M	20/08/15	11/01/16	144	WT	100.659	7.149	0.067	0.193	BLQ	0.340
Kmo^{wt}	FK515	FK (HOM)	M	04/10/15	15/02/16	134	WT	130.970	1.931	0.069	0.190	BLQ	0.302
$Kmo^{alb\text{-}cre}$	FKA173	Cre (-)	M	12/11/15	24/03/16	133	WT	138.466	3.008	0.070	0.235	BLQ	0.296
$Kmo^{alb\text{-}cre}$	FKA174	Cre (-)	M	12/11/15	24/03/16	133	WT	108.399	2.855	0.163	0.220	BLQ	0.349
$Kmo^{alb\text{-}cre}$	FKA194	Cre (-)	M	27/12/15	18/05/16	143	WT	95.944	2.829	0.174	0.188	BLQ	0.395
Kmo^{wt}	FK529	FK (HOM)	M	02/01/16	12/07/19	192	WT	108.671	2.199	0.172	0.209	BLQ	0.376
Kmo^{null}	K1153	HOM	M	17/08/15	11/01/16	147	Null	102.040	32.169	10.624	2.369	BLQ	0.152
Kmo^{null}	K1163	HOM	M	27/08/15	11/01/16	137	Null	101.735	66.043	22.276	5.020	BLQ	0.109
Kmo^{null}	K1184	HOM	M	13/10/15	07/03/16	146	Null	124.350	79.267	9.747	4.309	BLQ	0.119
Kmo^{null}	K1195	HOM	M	15/10/15	07/03/16	144	Null	80.512	86.973	16.821	4.952	BLQ	0.084
Kmo^{null}	K1196	HOM	M	15/10/15	07/03/16	144	Null	81.072	48.035	10.878	2.304	BLQ	0.074
Kmo^{null}	K1226	HOM	M	27/01/16	30/06/16	155	Null	91.553	55.752	17.849	2.998	BLQ	0.082
$Kmo^{alb\text{-}cre}$	A166	Cre (+)	M	05/09/15	15/04/16	233	Alb-cre	91.063	31.912	7.047	3.032	1.173	1.283
$Kmo^{alb\text{-}cre}$	A172	Cre (+)	M	12/11/15	24/03/16	133	Alb-cre	100.025	23.559	4.828	2.465	0.923	1.711
$Kmo^{alb\text{-}cre}$	A193	Cre (+)	M	27/12/15	18/04/16	113	Alb-cre	97.126	33.379	7.928	3.090	1.643	1.676
$Kmo^{alb\text{-}cre}$	A210	Cre (+)	M	09/02/16	30/06/16	142	Alb-cre	104.897	20.056	3.028	2.970	0.230	0.678
$Kmo^{alb\text{-}cre}$	A224	Cre (+)	M	28/02/16	27/07/16	150	Alb-cre	76.022	23.296	9.736	2.066	0.614	0.837
$Kmo^{alb\text{-}cre}$	A225	Cre (+)	M	28/02/16	27/07/16	150	Alb-cre	96.036	16.775	2.952	1.604	0.531	0.739

Table 76. Steady state concentrations of kynurenine metabolites
Columns indicate which mouse line mice were derived from, arbitrary ID, genotype, sex, body weight, age at cull, experimental group, and plasma concentration of analyte according to LC-MS/MS analysis. Abbreviations: 3HK: 3-hydroxykynurenine; AA: anthranilic acid; KA: kynurenic acid; Kyn: kynurenine; Trp: tryptophan; XA: xanthurenic acid. Experiment 2.

6.7. Appendix 7 – Supplementary data of experiment 2 (kynurenines at steady state). Cont.

Line	**ID**	**Group**	**D5-TRP** (μM)	**D4-KYN** (PAU)	**13C6-3HK** (μM)	**13C6-XA** (PAU)
Kmo^{wt}	FK491	WT	0.702045302	14369	0.116826693	368300
Kmo^{wt}	FK515	WT	0.72675141	32786	BLQ	321869
$Kmo^{alb\text{-}cre}$	FKA173	WT	0.578992641	21110	BLQ	197558
$Kmo^{alb\text{-}cre}$	FKA174	WT	1.033833509	56875	0.426988747	421688
$Kmo^{alb\text{-}cre}$	FKA194	WT	1.925881678	29603	0.141156536	305167
KMO^{wt}	FK529	WT	0.591035076	40869	0.078898206	382113
Kmo^{null}	K1153	Null	0.548886553	1032544	0.085154451	501032
Kmo^{null}	K1163	Null	0.560021026	1525039	0.258070122	657516
Kmo^{null}	K1184	Null	0.791264456	2150600	0.553938393	901618
Kmo^{null}	K1195	Null	0.873411068	2018067	0.235434679	997133
Kmo^{null}	K1196	Null	0.474816018	1874645	BLQ	940961
Kmo^{null}	K1226	Null	1.025279557	1888389	0.249511231	739837
$Kmo^{alb\text{-}cre}$	A166	Alb-cre	0.801060881	757101	1.044141287	522774
$Kmo^{alb\text{-}cre}$	A172	Alb-cre	1.283857402	1177993	1.230742495	368609
$Kmo^{alb\text{-}cre}$	A193	Alb-cre	0.924448055	946110	0.981144372	595663
$Kmo^{alb\text{-}cre}$	A210	Alb-cre	0.504253082	671717	0.52183169	366370
$Kmo^{alb\text{-}cre}$	A224	Alb-cre	0.64063844	679186	0.606855802	553134
$Kmo^{alb\text{-}cre}$	A225	Alb-cre	1.268469846	1101418	0.976408741	361585

Table 77. Tracer metabolites in tracer study
Columns indicate which mouse line mice were derived from, arbitrary ID, experimental group, and plasma concentration of analyte or peak area units (PAU) according to LC-MS/MS analysis. Abbreviations: 13C6-3HK: $^{13}C_6$-3-hydroxykynurenine; 13C6-XA: 13C6-xanthurenic acid; D4-Kyn: deuterated-4-kynurenine; D5-Trp: deuterated-5-tryptophan.

6.8. Appendix 8 – Supplementary data of Model Optimization – Phase II

Line	ID	Gene	Sex	DOB	Date	Age (d)	Rx	Telemeter	Weight	Group	Anaesthetic (min)
Kmo^{wt}	FK502	FK (HOM)	M	20/09/15	09/02/16	142	Sham	EM-22	28.84	Pill	37
$Kmo^{alb\text{-}cre}$	FKA180	Cre(-)	M	19/12/15	20/04/16	123	Sham	EM-22	28.40	Pill	31
Kmo^{wt}	FK534	FK (HOM)	M	03/01/16	31/05/16	149	Sham	EM-23	27.12	Pill	37
Kmo^{wt}	FK535	FK (HOM)	M	03/01/16	31/05/16	149	Sham	EM-21	29.58	Pill	27
$Kmo^{alb\text{-}cre}$	FKA205	Cre(-)	M	28/01/16	16/06/16	140	Sham	EM-24	27.04	Pill	36
Kmo^{wt}	FK545	FK (HOM)	M	12/02/16	23/06/16	132	Sham	EM-25	27.85	Pill	34
$Kmo^{alb\text{-}cre}$	FKA123	Cre(-)	M	22/05/15	21/10/15	152	Sham	EM-09s	29.56	HR	52
$Kmo^{alb\text{-}cre}$	FKA128	Cre(-)	M	22/05/15	21/10/15	152	Sham	EM-06s	29.62	HR	48
Kmo^{wt}	FK508	FK (HOM)	M	20/09/15	11/02/16	144	Sham	EM-03s	27.90	HR	46
Kmo^{wt}	FK509	FK (HOM)	M	20/09/15	11/02/16	144	Sham	EM-04s	32.43	HR	47
Kmo^{wt}	FK520	FK (HOM)	M	02/11/15	14/03/16	133	Sham	EM-03s	31.65	HR	41
Kmo^{wt}	FK521	FK (HOM)	M	02/11/15	14/03/16	133	Sham	EM-04s	31.60	HR	43

Table 78. Model optimization II - Study subjects
Pilot work testing recovery telemetry profiles in cardiometabolic telemetered versus mini-pill telemetered mice.

Line	ID	Group	Exp. Length (h)	Weight (g)	End body weight (g)	Weight loss (% start)
Kmo^{wt}	FK502	Pill	180	28.84	29.54	2.427
$Kmo^{alb\text{-}cre}$	FKA180	Pill	180	28.40	26.94	5.141
Kmo^{wt}	FK534	Pill	180	27.12	25.18	7.153
Kmo^{wt}	FK535	Pill	180	29.58	26.86	9.195
$Kmo^{alb\text{-}cre}$	FKA205	Pill	180	27.04	25.70	4.956
Kmo^{wt}	FK545	Pill	180	27.85	25.23	9.408
$Kmo^{alb\text{-}cre}$	FKA123	HR	180	29.56	29.46	0.338
$Kmo^{alb\text{-}cre}$	FKA128	HR	180	29.62	27.97	5.571
Kmo^{wt}	FK508	HR	180	27.90	26.26	5.878
Kmo^{wt}	FK509	HR	180	32.43	29.03	10.484
Kmo^{wt}	FK520	HR	180	31.65	28.01	11.501
Kmo^{wt}	FK521	HR	180	31.60	29.30	7.278

Table 79. Model optimization II - Outcomes of study subjects (survival and weight loss)
Experiment length is 168 hours or less, where specified, due to mice reaching humane endpoint(s).

Line	ID	Group	Total activity (counts)	Telemeter
Kmo^{wt}	FK502	Pill	116840	EM-22
$Kmo^{alb\text{-}cre}$	FKA180	Pill	135839	EM-22
Kmo^{wt}	FK534	Pill	152427	EM-23
Kmo^{wt}	FK535	Pill	142834	EM-21
$Kmo^{alb\text{-}cre}$	FKA205	Pill	138721	EM-24
Kmo^{wt}	FK545	Pill	154782	EM-25
$Kmo^{alb\text{-}cre}$	FKA123	Cardio-telemeter	83679	EM-09s
$Kmo^{alb\text{-}cre}$	FKA128	Cardio-telemeter	82980	EM-06s
Kmo^{wt}	FK508	Cardio-telemeter	83375	EM-03s
Kmo^{wt}	FK509	Cardio-telemeter	91527	EM-04s
Kmo^{wt}	FK520	Cardio-telemeter	115905	EM-03s
Kmo^{wt}	FK521	Cardio-telemeter	114507	EM-04s

Table 80. Model optimization II – Outcomes of study subjects (telemetry)

6.9. Appendix 9 – Supplementary data of experiment 3 (*Kmo$^{alb\text{-}cre}$*)

Line	ID	Gene	Sex	DOB	Date	Age (d)	Rx	Telem.	Weight (g)	Group	Anaesthetic (min)	Comment
Kmo^{wt}	FK502	FK (HOM)	M	20/09/15	09/02/16	142	Sham	EM-22	28.84	WT / Sham	37	
Kmo^{wt}	FK503	FK (HOM)	M	20/09/15	09/02/16	142	AP	EM-21	29.10	WT/ AP	38	
Kmo^{wt}	FK504	FK (HOM)	M	20/09/15	09/02/16	142	AP	EM-23	31.18	WT/ AP	35	
Kmo$^{alb\text{-}cre}$	FKA177	Cre(-)	M	19/12/15	20/04/16	123	AP	EM-24	29.12	WT/ AP	32	
Kmo$^{alb\text{-}cre}$	FKA179	Cre(-)	M	19/12/15	20/04/16	123	AP	EM-23	29.68	WT/ AP	38	
Kmo$^{alb\text{-}cre}$	FKA180	Cre(-)	M	19/12/15	20/04/16	123	Sham	EM-22	28.40	WT/ Sham	31	
Kmo^{wt}	FK534	FK (HOM)	M	03/01/16	31/05/16	149	Sham	EM-23	27.12	WT/ Sham	37	
Kmo^{wt}	FK535	FK (HOM)	M	03/01/16	31/05/16	149	Sham	EM-21	29.58	WT/ Sham	27	
Kmo^{wt}	FK536	FK (HOM)	M	03/01/16	31/05/16	149	AP	EM-24	30.15	WT/ AP	38	
Kmo^{wt}	FK537	FK (HOM)	M	03/01/16	31/05/16	149	AP	EM-22	28.70	WT/ AP	30	
Kmo$^{alb\text{-}cre}$	FKA202	Cre(-)	M	28/01/16	16/06/16	140	AP	EM-21	26.77	WT/ AP	36	
Kmo$^{alb\text{-}cre}$	FKA205	Cre(-)	M	28/01/16	16/06/16	140	Sham	EM-24	27.04	WT/ Sham	36	
Kmo^{wt}	FK544	FK (HOM)	M	12/02/16	23/06/16	132	AP	EM-26	26.47	WT/ AP	35	
Kmo^{wt}	FK545	FK (HOM)	M	12/02/16	23/06/16	132	Sham	EM-25	27.85	WT/ Sham	34	
Kmo$^{alb\text{-}cre}$	FKA229	Cre(-)	M	28/02/16	01/08/16	155	Sham	EM-24	29.04	WT/ Sham	29	
Kmo$^{alb\text{-}cre}$	FKA230	Cre(-)	M	28/02/16	01/08/16	155	AP	27.86	27.86	WT/ AP	31	
Kmo^{null}	K1179	KMO (HOM)	M	13/10/15	03/03/16	142	AP	EM-22	33.20	Null/ AP	35	
Kmo^{null}	K1180	KMO (HOM)	M	13/10/15	03/03/16	142	Sham	EM-23	31.58	Null/ Sham	35	
Kmo^{null}	K1181	KMO (HOM)	M	13/10/15	03/03/16	142	AP	EM-21	33.38	Null/ AP	37	
Kmo^{null}	K1216	KMO (HOM)	M	25/01/16	01/06/16	128	Sham	EM-26	29.15	Null/ Sham	34	
Kmo^{null}	K1217	KMO (HOM)	M	25/01/16	01/06/16	128	AP	EM-25	dna	Null/ AP	33.	
Kmo^{null}	K1222	KMO (HOM)	M	27/01/16	01/06/16	126	AP	EM-27	30.85	Null/ AP	30	
Kmo^{null}	K1223	KMO (HOM)	M	27/01/16	01/06/16	126	Sham	EM-28	32.18	Null/ Sham	29	
Kmo^{null}	K1224	KMO (HOM)	M	27/01/16	16/06/16	141	Sham	EM-22	32.63	Null/ Sham	33	
Kmo^{null}	K1225	KMO (HOM)	M	27/01/16	16/06/16	141	AP	EM-23	31.93	Null/ AP	31	
Kmo^{null}	K1246	KMO (HOM)	M	09/03/16	28/07/16	141	AP	EM-27	31.41	Null/ AP	35	
Kmo^{null}	K1247	KMO (HOM)	M	09/03/16	28/07/16	141	Sham	EM-26	30.34	Null/ Sham	35	
Kmo^{null}	K1248	KMO (HOM)	M	09/03/16	28/07/16	141	AP	EM-25	31.40	Null/ AP	32	
Kmo^{null}	K1261	KMO (HOM)	M	17/04/16	08/09/16	144	AP	EM-21	32.38	Null/ AP	30	
Kmo^{null}	K1262	KMO (HOM)	M	17/04/16	08/09/16	144	AP	EM-26	32.20	Null/ AP	28	
Kmo^{null}	K1263	KMO (HOM)	M	17/04/16	08/09/16	144	Sham	EM-24	31.47	Null/ Sham	28	
Kmo^{null}	K1264	KMO (HOM)	M	17/04/16	08/09/16	144	Sham	EM-22	33.84	Null/ Sham	30	
Kmo$^{alb\text{-}cre}$	A226	Cre(+)	M	28/02/16	01/08/16	155	AP	EM-22	26.59	Acre/ AP	32	
Kmo$^{alb\text{-}cre}$	A227	Cre(+)	M	28/02/16	01/08/16	155	Sham	EM-23	27.36	Acre/ Sham	31	
Kmo$^{alb\text{-}cre}$	A234	Cre(+)	M	21/03/16	02/08/16	134	Sham	EM-28	30.55	Acre/ Sham	31	
Kmo$^{alb\text{-}cre}$	A235	Cre(+)	M	21/03/16	02/08/16	134	AP	EM-25	29.76	Acre/ AP	32	
Kmo$^{alb\text{-}cre}$	A238	Cre(+)	M	04/04/16	16/08/16	134	AP	EM-22	31.41	Acre/ AP	31	
Kmo$^{alb\text{-}cre}$	A241	Cre(+)	M	06/04/16	16/08/16	132	AP	EM-23	29.89	Acre/ AP	31	
Kmo$^{alb\text{-}cre}$	A243	Cre(+)	M	06/04/16	16/08/16	132	Sham	EM-21	27.60	Acre/ Sham	29	
Kmo$^{alb\text{-}cre}$	A244	Cre(+)	M	06/04/16	17/08/16	133	AP	EM-24	28.43	Acre/ AP	32	
Kmo$^{alb\text{-}cre}$	A246	Cre(+)	M	06/04/16	17/08/16	133	AP	EM-26	28.01	Acre/ AP	29	
Kmo$^{alb\text{-}cre}$	A252	Cre(+)	M	09/04/16	17/08/16	130	Sham	EM-25	27.37	Acre/ Sham	30	
Kmo$^{alb\text{-}cre}$	A253	Cre(+)	M	09/04/16	30/08/16	143	Sham	EM-24	28.00	Acre/ Sham	30	
Kmo$^{alb\text{-}cre}$	A265	Cre(+)	M	16/04/16	30/08/16	136	AP	EM-22	27.25	Acre/ AP	34	
Kmo$^{alb\text{-}cre}$	A270	Cre(+)	M	16/04/16	30/08/16	136	Sham	EM-21	27.93	Acre/ Sham	36	
Kmo$^{alb\text{-}cre}$	A272	Cre(+)	M	16/04/16	30/08/16	136	AP	EM-23	28.85	Acre/ AP	35	
Kmo$^{alb\text{-}cre}$	A280	Cre(+)	M	29/04/16	06/09/16	130	AP	EM-23	29.00	Acre/ AP	35	
Kmo$^{alb\text{-}cre}$	A281	Cre(+)	M	29/04/16	06/09/16	130	AP	EM-22	28.72	Acre/ AP	31	
Kmo$^{alb\text{-}cre}$	A282	Cre(+)	M	29/04/16	06/09/16	130	Sham	EM-25	29.54	Acre/ Sham	33	

Table 81. Study subjects – experiment 3
dna.: data not available. Subject K1217 was excluded as it was found to have a bile leak from the suture line and therefore critical illness attributed to surgical failure and biliary peritonitis.

6.9. Appendix 9 – Supplementary data of experiment 3 ($Kmo^{alb\text{-}cre}$). Cont.

Line	**ID**	**Group**	**Exp. Length** (h)	**Start Weight** (g)	**End body weight** (g)	**Weight loss** (% start)
Kmo^{wt}	FK502	WT / Sham	168.0	28.84	29.54	Gain 2.427
Kmo^{wt}	FK503	WT/ AP	168.0	29.10	27.57	5.258
Kmo^{wt}	FK504	WT/ AP	168.0	31.18	25.65	17.736
$Kmo^{alb\text{-}cre}$	FKA177	WT/ AP	168.0	29.12	25.96	10.852
$Kmo^{alb\text{-}cre}$	FKA179	WT/ AP	168.0	29.68	22.16	25.337
$Kmo^{alb\text{-}cre}$	FKA180	WT/ Sham	168.0	28.40	26.94	5.141
Kmo^{wt}	FK534	WT/ Sham	168.0	27.12	25.18	7.153
Kmo^{wt}	FK535	WT/ Sham	168.0	29.58	26.86	9.195
Kmo^{wt}	FK536	WT/ AP	168.0	30.15	26.82	11.045
Kmo^{wt}	FK537	WT/ AP	168.0	28.70	26.81	6.585
$Kmo^{alb\text{-}cre}$	FKA202	WT/ AP	168.0	26.77	24.07	10.086
$Kmo^{alb\text{-}cre}$	FKA205	WT/ Sham	168.0	27.04	25.70	4.956
Kmo^{wt}	FK544	WT/ AP	168.0	26.47	20.98	20.740
Kmo^{wt}	FK545	WT/ Sham	168.0	27.85	25.23	9.408
$Kmo^{alb\text{-}cre}$	FKA229	WT/ Sham	168.0	29.04	27.76	4.408
$Kmo^{alb\text{-}cre}$	FKA230	WT/ AP	168.0	27.86	23.06	17.229
Kmo^{null}	K1179	Null/ AP	168.0	33.20	31.80	4.217
Kmo^{null}	K1180	Null/ Sham	168.0	31.58	29.72	5.890
Kmo^{null}	K1181	Null/ AP	168.0	33.38	31.88	4.494
Kmo^{null}	K1216	Null/ Sham	168.0	29.15	26.82	7.993
Kmo^{null}	K1217	Null/ AP	23.5	29.15	28.82	1.132
Kmo^{null}	K1222	Null/ AP	168.0	30.85	25.48	17.407
Kmo^{null}	K1223	Null/ Sham	168.0	32.18	29.71	7.676
Kmo^{null}	K1224	Null/ Sham	168.0	32.63	32.65	Gain 0.061
Kmo^{null}	K1225	Null/ AP	168.0	31.93	30.90	3.226
Kmo^{null}	K1246	Null/ AP	168.0	31.41	28.70	8.628
Kmo^{null}	K1247	Null/ Sham	168.0	30.34	28.64	5.603
Kmo^{null}	K1248	Null/ AP	93.1	31.40	26.82	14.586
Kmo^{null}	K1261	Null/ AP	168.0	32.38	31.15	3.799
Kmo^{null}	K1262	Null/ AP	168.0	32.20	29.13	9.534
Kmo^{null}	K1263	Null/ Sham	168.0	31.47	30.65	2.606
Kmo^{null}	K1264	Null/ Sham	168.0	33.84	32.17	4.935
$Kmo^{alb\text{-}cre}$	A226	Acre/ AP	28.9	26.59	24.67	7.221
$Kmo^{alb\text{-}cre}$	A227	Acre/ Sham	168.0	27.36	26.16	4.386
$Kmo^{alb\text{-}cre}$	A234	Acre/ Sham	168.0	30.55	27.19	10.998
$Kmo^{alb\text{-}cre}$	A235	Acre/ AP	46.5	29.76	27.92	6.183
$Kmo^{alb\text{-}cre}$	A238	Acre/ AP	168.0	31.41	22.98	26.839
$Kmo^{alb\text{-}cre}$	A241	Acre/ AP	168.0	29.89	28.47	4.751
$Kmo^{alb\text{-}cre}$	A243	Acre/ Sham	168.0	27.60	26.66	3.406
$Kmo^{alb\text{-}cre}$	A244	Acre/ AP	168.0	28.43	24.10	15.230
$Kmo^{alb\text{-}cre}$	A246	Acre/ AP	48.0	28.01	25.11	10.353
$Kmo^{alb\text{-}cre}$	A252	Acre/ Sham	168.0	27.37	25.32	7.490
$Kmo^{alb\text{-}cre}$	A253	Acre/ Sham	168.0	28.00	26.75	4.464
$Kmo^{alb\text{-}cre}$	A265	Acre/ AP	22.8	27.25	27.68	Gain 1.578
$Kmo^{alb\text{-}cre}$	A270	Acre/ Sham	168.0	27.93	25.07	10.240
$Kmo^{alb\text{-}cre}$	A272	Acre/ AP	47.9	28.85	25.44	11.820
$Kmo^{alb\text{-}cre}$	A280	Acre/ AP	168.0	29.00	27.22	6.138
$Kmo^{alb\text{-}cre}$	A281	Acre/ AP	29.2	28.72	28.97	Gain 0.870
$Kmo^{alb\text{-}cre}$	A282	Acre/ Sham	168.0	29.54	27.94	5.416

Table 82. Outcomes of study subjects – experiment 3 (survival and weight loss)
Experiment length is 168 hours or less, where specified, due to mice reaching humane endpoint(s). The same scales instrument was used for every measurement. Subject K1217 was found to have a bile leak from the suture line and therefore critical illness attributed to surgical failure and biliary peritonitis – however, it was not excluded in line with intention to treat principles.

6.9. Appendix 9 – Supplementary data of experiment 3 ($Kmo^{alb\text{-}cre}$). Cont.

Line	**ID**	**Group**	**Exp. Length** (h)	**Amylase** (U/L)	**ALT** (U/L)	**Urea** (U/L)	**LDH** (U/L)	**Albumin** (g/L)	**Glucose** (mmol/L)
Kmo^{wt}	FK502	WT / Sham	168.0	618	18	7.5	168	26.3	12.8
Kmo^{wt}	FK503	WT/ AP	168.0	618	38	6.5	133	26.0	13.3
Kmo^{wt}	FK504	WT/ AP	168.0	515	105	10.0	235	26.8	11.3
$Kmo^{alb\text{-}cre}$	FKA177	WT/ AP	168.0	998	33	8.5	208	26.8	14.0
$Kmo^{alb\text{-}cre}$	FKA179	WT/ AP	168.0	710	63	19.8	620	24.0	8.0
$Kmo^{alb\text{-}cre}$	FKA180	WT/ Sham	168.0	605	20	7.0	165	28.5	13.8
Kmo^{wt}	FK534	WT/ Sham	168.0	598	28	5.8	130	29.0	14.8
Kmo^{wt}	FK535	WT/ Sham	168.0	650	13	10.5	140	30.3	13.8
Kmo^{wt}	FK536	WT/ AP	168.0	505	13	6.5	165	27.0	16.8
Kmo^{wt}	FK537	WT/ AP	168.0	738	15	9.3	173	27.5	12.0
$Kmo^{alb\text{-}cre}$	FKA202	WT/ AP	168.0	983	538	5.3	780	26.5	15.3
$Kmo^{alb\text{-}cre}$	FKA205	WT/ Sham	168.0	583	40	7.0	150	28.3	14.3
Kmo^{wt}	FK544	WT/ AP	168.0	85175	1678	6.5	2885	29.0	11.8
Kmo^{wt}	FK545	WT/ Sham	168.0	3575	58	6.8	265	29.0	13.5
$Kmo^{alb\text{-}cre}$	FKA229	WT/ Sham	168.0	513	28	6.0	130	27.8	11.5
$Kmo^{alb\text{-}cre}$	FKA230	WT/ AP	168.0	6075	1500	5.8	2250	27.3	7.8
Kmo^{null}	K1179	Null/ AP	168.0	613	48	8.5	180	28.0	13.5
Kmo^{null}	K1180	Null/ Sham	168.0	628	33	8.8	153	30.5	15.0
Kmo^{null}	K1181	Null/ AP	168.0	555	30	8.0	263	31.3	15.3
Kmo^{null}	K1216	Null/ Sham	168.0	468	20	5.8	133	28.5	18.5
Kmo^{null}	K1217	Null/ AP	23.5	26525	135	33.5	1463	33.8	5.3
Kmo^{null}	K1222	Null/ AP	168.0	2085	83	7.5	225	26.0	6.3
Kmo^{null}	K1223	Null/ Sham	168.0	475	13	6.5	118	27.8	11.3
Kmo^{null}	K1224	Null/ Sham	168.0	570	23	7.0	148	26.8	11.3
Kmo^{null}	K1225	Null/ AP	168.0	568	15	6.8	150	27.8	16.0
Kmo^{null}	K1246	Null/ AP	168.0	603	15	7.3	140	27.5	13.0
Kmo^{null}	K1247	Null/ Sham	168.0	560	20	9.0	163	30.3	14.8
Kmo^{null}	K1248	Null/ AP	93.1	I/S	I/S	I/S	I/S	I/S	I/S
Kmo^{null}	K1261	Null/ AP	168.0	663	23	7.8	215	28.0	16.5
Kmo^{null}	K1262	Null/ AP	168.0	3100	350	6.0	625	26.5	19.8
Kmo^{null}	K1263	Null/ Sham	168.0	683	20	7.3	145	29.5	12.0
Kmo^{null}	K1264	Null/ Sham	168.0	485	18	6.0	108	27.0	13.5
$Kmo^{alb\text{-}cre}$	A226	Acre/ AP	28.9	7325	603	37.3	2383	25.8	3.0
$Kmo^{alb\text{-}cre}$	A227	Acre/ Sham	168.0	755	40	6.8	235	28.5	15.8
$Kmo^{alb\text{-}cre}$	A234	Acre/ Sham	168.0	623	23	7.3	128	29.8	15.5
$Kmo^{alb\text{-}cre}$	A235	Acre/ AP	46.5	I/S	I/S	I/S	I/S	I/S	I/S
$Kmo^{alb\text{-}cre}$	A238	Acre/ AP	168.0	5275	248	8.3	508	19.3	4.0
$Kmo^{alb\text{-}cre}$	A241	Acre/ AP	168.0	673	35	6.5	138	26.0	16.5
$Kmo^{alb\text{-}cre}$	A243	Acre/ Sham	168.0	563	23	6.5	315	26.3	17.3
$Kmo^{alb\text{-}cre}$	A244	Acre/ AP	168.0	67325	25	9.0	328	23.0	10.3
$Kmo^{alb\text{-}cre}$	A246	Acre/ AP	48.0	I/S	I/S	I/S	I/S	I/S	I/S
$Kmo^{alb\text{-}cre}$	A252	Acre/ Sham	168.0	1773	20	5.8	135	26.5	17.3
$Kmo^{alb\text{-}cre}$	A253	Acre/ Sham	168.0	850	20	5.8	185	27.3	15.5
$Kmo^{alb\text{-}cre}$	A265	Acre/ AP	22.8	50050	233	28.5	3045	18.5	15.8
$Kmo^{alb\text{-}cre}$	A270	Acre/ Sham	168.0	1870	30	7.3	258	28.3	13.8
$Kmo^{alb\text{-}cre}$	A272	Acre/ AP	47.9	28025	928	21.8	2233	21.3	15.3
$Kmo^{alb\text{-}cre}$	A280	Acre/ AP	168.0	1293	43	7.3	293	28.0	16.0
$Kmo^{alb\text{-}cre}$	A281	Acre/ AP	29.2	13850	293	37.0	245	35.5	3.0
$Kmo^{alb\text{-}cre}$	A282	Acre/ Sham	168.0	663	23	6.8	193	25.8	7.5

Table 83. Outcomes of study subjects – experiment 3 (biochemistry at end point)
Experiment length is 168 hours or less, where specified, due to mice reaching humane endpoint(s). The same scales instrument was used for every measurement. Subject K1217 was excluded as it was found to have a bile leak from the suture line and therefore critical illness attributed to surgical failure and biliary peritonitis.

6.9. Appendix 9 – Supplementary data of experiment 3 ($Kmo^{alb\text{-}cre}$). Cont.

Group	Rx	Total group time (hrs)	Total s.c. dose / group	s.c. dose ($x10^5$) / exp time / group	Total oral dose (0.01 mg)	Oral dose ($x10^3$) / exp time / group
Kmo^{wt}	Sham	7 * 168 = **Total = 1176**	FK502 = 0.0015mg*3 FKA180 = 0.0015mg*3 FK534 = 0.0015mg*3 FK535 = 0.0015mg*3 FKA205= 0.00125mg*3 FK545 = 0.0015mg*3 FKA229 = 0.0015mg*3 **Total = 0.03075 mg**	0.03075 $x10^5$ / 1176 = **= 2.6147959**	1.FK502 = 7eaten 2.FKA180 = 7eaten 3.FK534 = 7eaten 4.FK535 = 7eaten 5.FKA205 = 7eaten 6.FK545 = 4eaten 7.FKA229 = 7eaten **Total = 46**	
Kmo^{wt}	AP	9 * 168 = **Total = 1512**	FK503 = 0.0015mg*3 FK504 = 0.0015mg*3 FKA177 = 0.0015mg*4 FKA179 = 0.0015mg*4 FK536 = 0.0015mg*3 FK537 = 0.0015mg*3 FKA202 = 0.0015mg*3 FK544 = 0.0015mg*3 FKA230 = 0.0015mg*4 **Total = 0.045 mg**	0.045 $x10^5$ / 1512 = **= 2.9761905**	FK503 = 7 eaten FK504 = 7 eaten FKA177 = 7 eaten FKA179 = 7 eaten FK536 = 7 eaten FK537 = 7 eaten FKA202 = 7 eaten FK544 = 0 eaten FKA230 = 6 eaten **Total = 55**	
Kmo^{null}	Sham	7 * 168 = **Total = 1176**	1.K1180 = 0.0015mg*3 2.K1216 = 0.0015mg*3 3.K1223 = 0.0015mg*3 4.K1224 = 0.0015mg*3 5.K1247 = 0.0015mg*3 6.K1263 = 0.0015mg*3 7.K1264 = 0.0015mg*3 **Total = 0.0315 mg**	0.0315 $x10^5$ / 1176 = **= 2.678571**	1.K1180 = 7eaten 2.K1216 = 7eaten 3.K1223 = 7eaten 4.K1224 = 7eaten 5.K1247 = 7eaten 6.K1263 = 7eaten 7.K1264 = 1eaten **Total = 43**	
Kmo^{null}	AP	K1179 = 168 K1181 = 168 K1217 = 23.5 K1222 = 168 K1225 = 168 K1246 = 168 K1248 = 93.1 K1261 = 168 K1262 = 168 **Total = 1292.6**	K1179 = 0.0015mg*3 K1181 = 0.0015mg*3 K1217 = 0.0015mg*3 K1222 = 0.0015mg*3 K1225 = 0.0015mg*3 K1246 = 0.0015mg*3 K1248 = 0.0015mg*4 K1261 = 0.0015mg*3 K1262 = 0.0015mg*3 **Total = 0.042 mg**	0.042 $x10^5$ / 1292.6 = **=3.249265**	K1179 = 7 eaten K1181= 7 eaten K1217 = 0 eaten K1222 = 6 eaten K1225 = 7 eaten K1246 = 7 eaten K1248 = 1 eaten K1261 = 1 eaten K1262 = 0 eaten **Total = 36**	
$Kmo^{alb\text{-}cre}$	Sham	7 * 168 = **Total = 1176**	A227 = 0.0015mg*3 A234 = 0.0015mg*3 A243 = 0.0015mg*3 A252 = 0.0015mg*3 A253 = 0.0015mg*3 A270 = 0.0015mg*3 A282 = 0.0015mg*3 **Total = 0.0315 mg**	0.0315 $x10^5$ / 1176 = **= 2.678571**	A227 = 7 eaten A234 = 6 eaten A243 = 7 eaten A252 = 7 eaten A253 = 7 eaten A270 = 7 eaten A282 = 7 eaten **Total = 48**	
$Kmo^{alb\text{-}cre}$	AP	A226 = 52.9 A235 = 46.5 A238 = 168 A241 = 168 A244 = 168 A246 = 48.0 A265 = 22.8 A272 = 47.9 A280 = 168 A281 = 29.2 **Total = 895.3**	A226 = 0.0015mg*4 A235 = 0.0015mg*4 A238 = 0.0015mg*3 A241 = 0.0015mg*3 A244 = 0.0015mg*3 A246 = 0.0015mg*4 A265 = 0.0015mg*3 A272 = 0.0015mg*4 A280 = 0.0015mg*3 A281 = 0.0015mg*4 **Total = 0.0525 mg**	0.0525 $x10^5$ / 895.3 = **= 5.8639562**	A226 = 0 eaten A235 = 0 eaten A238 = 7 eaten A241 = 6.3 eaten A244 = 7 eaten A246 = 1 eaten A265 = 0 eaten A272 = 0 eaten A280 = 7 eaten A281 = 0 eaten **Total = 28.3**	

Table 84. Analgesia given in AP experiment 3 - TOTAL
Columns from left to right: '**Mouse line**' denotes the mouse line. '**Rx**' denotes treatment: Sham laparotomy or experimental acute pancreatitis (AP). '**Total group time**' denotes the sum total number of hrs of experimented mice in the cohort (i.e. 168-hrs if survived entire 7-day period multiplied by 6 if all mice survived). Bup. = Buprenorphine. 1 dose s.c. Bup. = 0.05 mg/kg. 1 dose oral Bup. = 0.01 mg.

6.10. Appendix 10 – Supplementary data of 24h studies

Line	ID	Gene	Sex	DOB	Date	Age (d)	Rx	Weight (g)	Group	Anaesthetic (min)	Primary study
Kmo^{wt}	FK461	FK (HOM)	M	23/06/15	25/11/15	155	AP	29.56	WT	35	Histology + KP + cytokines
Kmo^{wt}	FK463	FK (HOM)	M	23/06/15	25/11/15	155	Sham	31.21	WT	35	Histology + KP + cytokines
Kmo$^{alb\text{-}cre}$	FKA143	Cre(-)	M	02/07/15	07/12/15	158	AP	32.67	WT	31	Histology + KP + cytokines
Kmo$^{alb\text{-}cre}$	FKA152	Cre(-)	M	12/07/15	07/12/15	148	Sham	29.56	WT	32	Histology + KP + cytokines
Kmo^{wt}	FK474	FK (HOM)	M	15/07/15	08/12/15	146	Sham	26.47	WT	31	Histology + KP + cytokines
Kmo^{wt}	FK475	FK (HOM)	M	15/07/15	08/12/15	146	AP	28.84	WT	32	Histology + KP + cytokines
Kmo^{wt}	FK485	FK (HOM)	M	20/08/15	07/01/16	140	Sham	28.98	WT	33	Histology + KP + cytokines
Kmo^{wt}	FK486	FK (HOM)	M	20/08/15	07/01/16	140	AP	24.92	WT	33	Histology + KP + cytokines
Kmo^{wt}	FK487	FK (HOM)	M	20/08/15	07/01/16	140	AP	28.62	WT	31	Histology + KP + cytokines
Kmo^{wt}	FK488	FK (HOM)	M	20/08/15	07/01/16	140	Sham	24.71	WT	30	Histology + KP + cytokines
Kmo^{wt}	FK489	FK (HOM)	M	20/08/15	10/01/16	143	Sham	27.46	WT	36	Histology + KP + cytokines
Kmo^{wt}	FK490	FK (HOM)	M	20/08/15	10/01/16	143	AP	28.47	WT	35	Histo + KP + cytokines + RNAseq
Kmo^{wt}	FK495	FK (HOM)	M	12/09/15	03/02/16	144	Sham	26.88	WT	32	Histology + KP + cytokines
Kmo^{wt}	FK496	FK (HOM)	M	12/09/15	03/02/16	144	AP	24.22	WT	32	Histo + KP + cytokines + RNAseq
Kmo^{wt}	FK500	FK (HOM)	M	20/09/15	08/02/16	141	Sham	29.15	WT	29	Histology + KP + cytokines
Kmo^{wt}	FK501	FK (HOM)	M	20/09/15	08/02/16	141	AP	31.07	WT	31	Histo + KP + cytokines + RNAseq
Kmo$^{alb\text{-}cre}$	FKA307	Cre(-)	M	20/06/16	07/11/16	140	AP	30.86	WT	25	Flow pilot M03A
Kmo^{wt}	FK592	FK (HOM)	M	13/06/16	07/11/16	147	Sham	29.60	WT	26	Flow pilot M04A
Kmo^{wt}	FK570	FK (HOM)	M	16/04/16	14/11/16	212	Sham	36.98	WT	27	Flow pilot + cytokines
Kmo^{wt}	FK571	FK (HOM)	M	16/04/16	14/11/16	212	AP	32.86	WT	29	Flow pilot + cytokines
Kmo^{wt}	FK572	FK (HOM)	M	16/04/16	14/11/16	212	Sham	34.22	WT	32	Flow pilot + cytokines
Kmo^{wt}	FK573	FK (HOM)	M	16/04/16	14/11/16	212	AP	31.84	WT	32	Flow pilot + cytokines
Kmo^{wt}	FK608	FK (HOM)	M	05/08/16	06/12/16	123	Sham	27.29	WT	28	Flow
Kmo^{wt}	FK609	FK (HOM)	M	05/08/16	06/12/16	123	AP	27.79	WT	25	Flow
Kmo^{wt}	FK616	FK (HOM)	M	27/08/16	12/12/16	107	AP	26.87	WT	27	Flow + cytokines
Kmo^{wt}	FK617	FK (HOM)	M	27/08/16	12/12/16	107	Sham	27.49	WT	27	Flow + cytokines
Kmo^{wt}	FK618	FK (HOM)	M	27/08/16	19/12/16	114	AP	26.17	WT	26	Flow + cytokines
Kmo^{wt}	FK619	FK (HOM)	M	27/08/16	19/12/16	114	Sham	25.97	WT	28	Flow + cytokines
Kmo^{wt}	FK622	FK (HOM)	M	14/09/16	16/01/17	124	Sham	27.88	WT	27	Flow
Kmo^{wt}	FK624	FK (HOM)	M	14/09/16	16/01/17	124	AP	28.08	WT	27	Flow
Kmo^{wt}	FK634	FK (HOM)	M	13/09/16	31/01/17	140	AP	30.20	WT	27	Flow
Kmo^{wt}	FK635	FK (HOM)	M	13/09/16	31/01/17	140	Sham	29.67	WT	27	Flow
Kmo$^{alb\text{-}cre}$	FKA331	Cre(-)	M	04/09/16	09/01/17	127	AP	24.91	WT	24	Flow
Kmo$^{alb\text{-}cre}$	FKA332	Cre(-)	M	04/09/16	09/01/17	127	Sham	27.24	WT	24	Flow
Kmo^{null}	K1142	KMO (HOM)	M	29/06/15	25/11/15	149	AP	30.07	Null	33	Histology + KP + cytokines
Kmo^{null}	K1143	KMO (HOM)	M	29/06/15	25/11/15	149	Sham	28.83	Null	34	Histology + KP + cytokines
Kmo^{null}	K1151	KMO (HOM)	M	17/08/15	07/01/16	143	Sham	28.27	Null	34	Histology + KP + cytokines
Kmo^{null}	K1152	KMO (HOM)	M	17/08/15	07/01/16	143	AP	32.30	Null	34	Histology + KP + cytokines
Kmo^{null}	K1159	KMO (HOM)	M	27/08/15	10/01/16	136	Sham	27.99	Null	31	Histology + KP + cytokines
Kmo^{null}	K1160	KMO (HOM)	M	27/08/15	10/01/16	136	AP	30.88	Null	32	Histology + KP + cytokines
Kmo^{null}	K1161	KMO (HOM)	M	27/08/15	10/01/16	136	AP	30.81	Null	31	Histology + KP + cytokines
Kmo^{null}	K1162	KMO (HOM)	M	27/08/15	10/01/16	136	Sham	29.04	Null	30	Histology + KP + cytokines
Kmo^{null}	K1169	KMO (HOM)	M	12/09/15	03/02/16	144	AP	30.25	Null	29	Histology + KP + cytokines
Kmo^{null}	K1170	KMO (HOM)	M	12/09/15	03/02/16	144	Sham	28.11	Null	29	Histology + KP + cytokines
Kmo^{null}	K1174	KMO (HOM)	M	01/10/15	16/02/16	138	Sham	29.99	Null	30	Histology + KP + cytokines
Kmo^{null}	K1175	KMO (HOM)	M	01/10/15	16/02/16	138	AP	31.39	Null	31	Histology + KP + cytokines
Kmo^{null}	K1182	KMO (HOM)	M	13/10/15	07/03/16	146	AP	32.52	Null	32	Histology + KP + cytokines
Kmo^{null}	K1183	KMO (HOM)	M	13/10/15	07/03/16	146	Sham	31.26	Null	30	Histology + KP + cytokines
Kmo^{null}	K1193	KMO (HOM)	M	15/10/15	07/03/16	144	AP	29.61	Null	31	Histology + KP + cytokines
Kmo^{null}	K1194	KMO (HOM)	M	15/10/15	07/03/16	144	Sham	28.56	Null	31	Histology + KP + cytokines
Kmo^{null}	K1312	KMO (HOM)	M	21/06/16	07/11/16	139	Sham	29.20	Null	28	Flow pilot (M02A)
Kmo^{null}	K1313	KMO (HOM)	M	21/06/16	07/11/16	139	AP	31.65	Null	28	Flow pilot (M01A)
Kmo^{null}	K1278	KMO (HOM)	M	27/04/16	16/11/16	203	AP	34.48	Null	28	Flow pilot + cytokines
Kmo^{null}	K1279	KMO (HOM)	M	27/04/16	16/11/16	203	Sham	30.84	Null	27	Flow pilot + cytokines
Kmo^{null}	K1296	KMO (HOM)	M	08/06/16	16/11/16	161	AP	30.81	Null	27	Flow + cytokines
Kmo^{null}	K1297	KMO (HOM)	M	08/06/16	16/11/16	161	Sham	31.29	Null	28	Flow + cytokines
Kmo^{null}	K1341	KMO (HOM)	M	28/07/16	06/12/16	131	AP	32.31	Null	27	Flow
Kmo^{null}	K1342	KMO (HOM)	M	28/07/16	06/12/16	131	Sham	31.71	Null	28	Flow
Kmo^{null}	K1343	KMO (HOM)	M	28/07/16	12/12/16	137	Sham	34.10	Null	30	Flow + cytokines
Kmo^{null}	K1344	KMO (HOM)	M	28/07/16	12/12/16	137	AP	31.73	Null	30	Flow + cytokines
Kmo^{null}	K1350	KMO (HOM)	M	06/08/16	19/12/16	135	AP	28.13	Null	27	Flow + cytokines
Kmo^{null}	K1351	KMO (HOM)	M	06/08/16	19/12/16	135	Sham	29.82	Null	30	Flow + cytokines

Kmo^{null}	K1369	KMO (HOM)	M	11/09/16	09/01/17	120	AP	31.78	Null	26	Flow
Kmo^{null}	K1370	KMO (HOM)	M	11/09/16	09/01/17	120	Sham	33.51	Null	26	Flow
Kmo^{null}	K1371	KMO (HOM)	M	11/09/16	16/01/17	127	AP	29.04	Null	27	Flow
Kmo^{null}	K1372	KMO (HOM)	M	11/09/16	16/01/17	127	Sham	34.27	Null	27	Flow
$Kmo^{alb\text{-}cre}$	A148	Cre(+)	M	12/07/15	07/12/15	153	Sham	28.98	Alb-cre	36	Histology + KP + cytokines
$Kmo^{alb\text{-}cre}$	A149	Cre(+)	M	12/07/15	07/12/15	153	AP	30.21	Alb-cre	34	Histology + KP + cytokines
$Kmo^{alb\text{-}cre}$	A150	Cre(+)	M	12/07/15	08/12/15	154	AP	28.42	Alb-cre	32	Histology + KP + cytokines
$Kmo^{alb\text{-}cre}$	A151	Cre(+)	M	12/07/15	08/12/15	154	Sham	27.32	Alb-cre	33	Histology + KP + cytokines
$Kmo^{alb\text{-}cre}$	A156	Cre(+)	M	26/07/15	21/12/15	148	AP	31.50	Alb-cre	36	Histology + KP + cytokines
$Kmo^{alb\text{-}cre}$	A157	Cre(+)	M	26/07/15	21/12/15	148	Sham	32.51	Alb-cre	34	Histology + KP + cytokines
$Kmo^{alb\text{-}cre}$	A163	Cre(+)	M	05/09/15	20/01/16	137	Sham	29.11	Alb-cre	32	Histology + KP + cytokines
$Kmo^{alb\text{-}cre}$	A164	Cre(+)	M	05/09/15	20/01/16	137	AP	29.77	Alb-cre	30	Histology + KP + cytokines
$Kmo^{alb\text{-}cre}$	A196	Cre(+)	M	16/01/16	01/06/16	137	AP	30.64	Alb-cre	29	Histology + KP + cytokines
$Kmo^{alb\text{-}cre}$	A197	Cre(+)	M	16/01/16	01/06/16	137	Sham	29.83	Alb-cre	29	Histology + KP + cytokines
$Kmo^{alb\text{-}cre}$	A201	Cre(+)	M	28/01/16	06/06/16	130	AP	26.33	Alb-cre	31	Histology + KP + cytokines
$Kmo^{alb\text{-}cre}$	A203	Cre(+)	M	28/01/16	06/06/16	130	Sham	30.46	Alb-cre	28	Histology + KP + cytokines
$Kmo^{alb\text{-}cre}$	A204	Cre(+)	M	28/01/16	06/06/16	130	Sham	29.58	Alb-cre	30	Histology + KP + cytokines
$Kmo^{alb\text{-}cre}$	A206	Cre(+)	M	28/01/16	06/06/16	130	AP	26.81	Alb-cre	30	Histology + KP + cytokines
$Kmo^{alb\text{-}cre}$	A313	Cre(+)	M	20/07/16	06/12/16	139	Sham	29.82	Alb-cre	27	Flow + cytokines
$Kmo^{alb\text{-}cre}$	A314	Cre(+)	M	20/07/16	06/12/16	139	AP	28.40	Alb-cre	27	Flow + cytokines
$Kmo^{alb\text{-}cre}$	A320	Cre(+)	M	12/08/16	12/12/16	122	Sham	28.91	Alb-cre	27	Flow + cytokines
$Kmo^{alb\text{-}cre}$	A322	Cre(+)	M	12/08/16	12/12/16	122	AP	29.89	Alb-cre	28	Flow + cytokines
$Kmo^{alb\text{-}cre}$	A327	Cre(+)	M	12/08/16	19/12/16	129	AP	28.20	Alb-cre	30	Flow + cytokines
$Kmo^{alb\text{-}cre}$	A328	Cre(+)	M	12/08/16	19/12/16	129	Sham	31.53	Alb-cre	30	Flow + cytokines
$Kmo^{alb\text{-}cre}$	A339	Cre(+)	M	22/09/19	09/01/17	109	Sham	27.68	Alb-cre	27	Flow
$Kmo^{alb\text{-}cre}$	A340	Cre(+)	M	22/09/19	09/01/17	109	AP	25.03	Alb-cre	26	Flow
$Kmo^{alb\text{-}cre}$	A341	Cre(+)	M	22/09/19	16/01/17	116	Sham	27.29	Alb-cre	28	Flow
$Kmo^{alb\text{-}cre}$	A342	Cre(+)	M	22/09/19	16/01/17	116	AP	25.82	Alb-cre	28	Flow
$Kmo^{alb\text{-}cre}$	A343	Cre(+)	M	22/09/19	31/01/17	131	AP	30.03	Alb-cre	27	Flow + cytokines
$Kmo^{alb\text{-}cre}$	A344	Cre(+)	M	22/09/19	31/01/17	131	Sham	27.85	Alb-cre	27	Flow + cytokines
$Kmo^{alb\text{-}cre}$	A345	Cre(+)	M	22/09/19	31/01/17	131	AP	26.95	Alb-cre	23	Flow + cytokines
$Kmo^{alb\text{-}cre}$	A346	Cre(+)	M	22/09/19	31/01/17	131	Sham	29.18	Alb-cre	25	Flow + cytokines

Table 85. 24h study subjects

AP = 2.0% filtered, in PBS, 50ul, 5min, clamp (1d). Sham = laparotomy with inspection of duodenal loop.

6.10. Appendix 10 – Supplementary data of 24h studies. Cont.

Line	ID	Rx	Group	Oedema	Infiltrate	Necrosis	Total	Comment	Amylase (U/L)	Log10 Amy
Kmo^{wt}	FK461	AP	WT	2	2	0	**4**		40600	4.61
Kmo^{wt}	FK463	Sham	WT	0	0	0	**0**		2160	3.33
$Kmo^{alb\text{-}cre}$	FKA143	AP	WT	1	1	1	**3**		6292	3.80
$Kmo^{alb\text{-}cre}$	FKA152	Sham	WT	0	0	0	**0**		2040	3.31
Kmo^{wt}	FK474	Sham	WT	0	0	0	**0**	A (detail below)	2212	3.34
Kmo^{wt}	FK475	AP	WT	3	2	2	**7**		6760	3.83
Kmo^{wt}	FK485	Sham	WT	0	0	0	**0**		2260	3.35
Kmo^{wt}	FK486	AP	WT	3	3	3	**9**		1940	3.29
Kmo^{wt}	FK487	AP	WT	0	0	0	**0**		7632	3.88
Kmo^{wt}	FK488	Sham	WT	1	3	0	**4**	B (detail below)	2256	3.35
Kmo^{wt}	FK489	Sham	WT	0	1	0	**1**		2272	3.36
Kmo^{wt}	FK490	AP	WT	2	2	3	**7**		9240	3.97
Kmo^{wt}	FK495	Sham	WT	0	0	0	**0**		2252	3.35
Kmo^{wt}	FK496	AP	WT	2	2	1	**5**		11680	4.07
Kmo^{wt}	FK500	Sham	WT	0	0	0	**0**		2300	3.36
Kmo^{wt}	FK501	AP	WT	3	3	3	**9**		7740	3.89
Kmo^{null}	K1142	AP	Null	2	1	1	**4**	C (detail below)	3660	3.56
Kmo^{null}	K1143	Sham	Null	0	1	0	**1**		2130	3.33
Kmo^{null}	K1151	Sham	Null	0	1	0	**1**		1852	3.27
Kmo^{null}	K1152	AP	Null	2	2	2	**6**	C (detail below)	7232	3.86
Kmo^{null}	K1159	Sham	Null	0	1	0	**1**		1740	3.24
Kmo^{null}	K1160	AP	Null	2	2	0	**4**		6080	3.78
Kmo^{null}	K1161	AP	Null	0	2	0	**2**	D (detail below)	7960	3.90
Kmo^{null}	K1162	Sham	Null	0	0	0	**0**		2152	3.33
Kmo^{null}	K1169	AP	Null	3	2	2	**7**		10140	4.01
Kmo^{null}	K1170	Sham	Null	0	0	0	**0**		2332	3.37
Kmo^{null}	K1174	Sham	Null	0	0	0	**0**		2452	3.39
Kmo^{null}	K1175	AP	Null	2	2	2	**6**	E (detail below)	6380	3.80
Kmo^{null}	K1182	AP	Null	2	1	1	**4**	C (detail below)	7060	3.85
Kmo^{null}	K1183	Sham	Null	0	0	0	**0**		2152	3.33
Kmo^{null}	K1193	AP	Null	2	1	1	**4**		43252	4.64
Kmo^{null}	K1194	Sham	Null	0	0	0	**0**		2600	3.41
$Kmo^{alb\text{-}cre}$	A148	Sham	Alb-cre	1	1	0	**2**		1980	3.30
$Kmo^{alb\text{-}cre}$	A149	AP	Alb-cre	3	2	2	**7**		7260	3.86
$Kmo^{alb\text{-}cre}$	A150	AP	Alb-cre	1	1	1	**3**		19332	4.29
$Kmo^{alb\text{-}cre}$	A151	Sham	Alb-cre	0	0	0	**0**		2392	3.38
$Kmo^{alb\text{-}cre}$	A156	AP	Alb-cre	3	2	2	**7**		20620	4.31
$Kmo^{alb\text{-}cre}$	A157	Sham	Alb-cre	0	0	0	**0**		2272	3.36
$Kmo^{alb\text{-}cre}$	A163	Sham	Alb-cre	1	1	0	**2**		2232	3.35
$Kmo^{alb\text{-}cre}$	A164	AP	Alb-cre	1	2	1	**4**		8600	3.93
$Kmo^{alb\text{-}cre}$	A196	AP	Alb-cre	3	3	3	**9**	F (detail below)	40496	4.61
$Kmo^{alb\text{-}cre}$	A197	Sham	Alb-cre	0	0	0	**0**		2344	3.37
$Kmo^{alb\text{-}cre}$	A201	AP	Alb-cre	3	3	2	**8**	C (detail below)	14304	4.16
$Kmo^{alb\text{-}cre}$	A203	Sham	Alb-cre	0	0	0	**0**		2256	3.35
$Kmo^{alb\text{-}cre}$	A204	Sham	Alb-cre	0	1	0	**1**		1576	3.20
$Kmo^{alb\text{-}cre}$	A206	AP	Alb-cre	2	1	1	**4**		95552	4.98

Table 86. Pancreas injury histology score at 24h with plasma amylase level

Oedema: 0 Absent; 1 focally increased between lobules; 2 diffusely increased between lobes; 3 acini disrupted and separated.
Inflammatory cell infiltrate: 0 Absent; 1 in ducts (around ductal margins); 2 in the parenchyma (in <50% of the lobules); 3 in the parenchyma (in >50% of the lobules).
Acinar necrosis: 0 Absent; 1 periductal necrosis (<= 5%*); 2 focal necrosis (5 to 20%*); 3 diffuse parenchymal necrosis (20-50%*).
*Refers to approximate % of cells involved per examined field.

Comments - A: Inflammatory infiltrate in omental fat rather than pancreas; B: Severe end-stage pancreas with loss of the majority of acinar tissue and retention of only residual ducts; C: With mild fat necrosis; D: Fat necrosis & inflame cell infiltrates but no acinar injury in section; E: With moderate fat necrosis; F: Cocco-bacillary bacteria present.

6.10. Appendix 10 – Supplementary data of 24h studies. Cont.

Line	ID	Rx	Group	Weight	**End body weight** (g)	**Weight loss** (% start)	Survived 24h
Kmo^{wt}	FK461	AP	WT	29.56	28.70	2.909	Y
Kmo^{wt}	FK463	Sham	WT	31.21	30.66	3.783	Y
$Kmo^{alb\text{-}cre}$	FKA143	AP	WT	32.67	32.43	0.735	Y
$Kmo^{alb\text{-}cre}$	FKA152	Sham	WT	29.56	28.91	2.199	Y
Kmo^{wt}	FK474	Sham	WT	26.47	26.46	0.038	Y
Kmo^{wt}	FK475	AP	WT	28.84	27.24	5.548	Y
Kmo^{wt}	FK485	Sham	WT	28.98	28.56	1.449	Y
Kmo^{wt}	FK486	AP	WT	24.92	24.19	2.929	Y
Kmo^{wt}	FK487	AP	WT	28.62	27.42	4.193	Y
Kmo^{wt}	FK488	Sham	WT	24.71	23.99	2.914	Y
Kmo^{wt}	FK489	Sham	WT	27.46	26.52	3.423	Y
Kmo^{wt}	FK490	AP	WT	28.47	27.49	3.442	Y
Kmo^{wt}	FK495	Sham	WT	26.88	26.23	2.418	Y
Kmo^{wt}	FK496	AP	WT	24.22	23.30	3.799	Y
Kmo^{wt}	FK500	Sham	WT	29.15	28.53	2.127	Y
Kmo^{wt}	FK501	AP	WT	31.07	30.14	2.993	Y
$Kmo^{alb\text{-}cre}$	FKA307	AP	WT	30.86	29.14	5.574	Y
Kmo^{wt}	FK592	Sham	WT	29.60	28.34	4.257	Y
Kmo^{wt}	FK570	Sham	WT	36.98	35.14	4.976	Y
Kmo^{wt}	FK571	AP	WT	32.86	31.00	5.660	Y
Kmo^{wt}	FK572	Sham	WT	34.22	32.85	4.004	Y
Kmo^{wt}	FK573	AP	WT	31.84	31.11	2.293	Y
Kmo^{wt}	FK608	Sham	WT	27.29	27.28	0.037	Y
Kmo^{wt}	FK609	AP	WT	27.79	25.95	6.621	Y
Kmo^{wt}	FK616	AP	WT	26.87	25.36	5.620	Y
Kmo^{wt}	FK617	Sham	WT	27.49	26.45	3.783	Y
Kmo^{wt}	FK618	AP	WT	26.17	24.83	5.120	Y
Kmo^{wt}	FK619	Sham	WT	25.97	24.91	4.082	Y
Kmo^{wt}	FK622	Sham	WT	27.88	27.53	1.255	Y
Kmo^{wt}	FK624	AP	WT	28.08	26.74	4.772	Y
Kmo^{wt}	FK634	AP	WT	30.20	MISSING	MISSING	Y
Kmo^{wt}	FK635	Sham	WT	29.67	MISSING	MISSING	Y
$Kmo^{alb\text{-}cre}$	FKA331	AP	WT	24.91	23.28	6.544	Y
$Kmo^{alb\text{-}cre}$	FKA332	Sham	WT	27.24	25.40	6.755	Y
Kmo^{null}	K1142	AP	Null	30.07	29.48	1.962	Y
Kmo^{null}	K1143	Sham	Null	28.83	28.72	0.382	Y
Kmo^{null}	K1151	Sham	Null	28.27	27.41	3.042	Y
Kmo^{null}	K1152	AP	Null	32.30	30.99	3.967	Y
Kmo^{null}	K1159	Sham	Null	27.99	28.12	-0.46	Y
Kmo^{null}	K1160	AP	Null	30.88	30.88	2.234	Y
Kmo^{null}	K1161	AP	Null	30.81	30.53	0.909	Y
Kmo^{null}	K1162	Sham	Null	29.04	28.41	2.169	Y
Kmo^{null}	K1169	AP	Null	30.25	28.90	4.463	Y
Kmo^{null}	K1170	Sham	Null	28.11	28.11	4.411	Y
Kmo^{null}	K1174	Sham	Null	29.99	30.42	-1.43	Y
Kmo^{null}	K1175	AP	Null	31.39	29.68	5.448	Y
Kmo^{null}	K1182	AP	Null	32.52	30.84	5.166	Y
Kmo^{null}	K1183	Sham	Null	31.26	29.90	4.351	Y
Kmo^{null}	K1193	AP	Null	29.61	28.40	4.086	Y
Kmo^{null}	K1194	Sham	Null	28.56	27.59	3.396	Y
Kmo^{null}	K1312	Sham	Null	29.20	28.28	3.151	Y
Kmo^{null}	K1313	AP	Null	31.65	29.77	5.940	Y
Kmo^{null}	K1278	AP	Null	34.48	32.14	6.787	Y
Kmo^{null}	K1279	Sham	Null	30.84	29.79	3.405	Y
Kmo^{null}	K1296	AP	Null	30.81	30.35	1.493	Y
Kmo^{null}	K1297	Sham	Null	31.29	29.80	4.762	Y
Kmo^{null}	K1341	AP	Null	32.31	29.79	7.799	Y
Kmo^{null}	K1342	Sham	Null	31.71	29.85	5.866	Y
Kmo^{null}	K1343	Sham	Null	34.10	31.74	6.921	Y
Kmo^{null}	K1344	AP	Null	31.73	29.53	6.934	Y
Kmo^{null}	K1350	AP	Null	28.13	27.04	3.875	Y
Kmo^{null}	K1351	Sham	Null	29.82	28.75	3.588	Y
Kmo^{null}	K1369	AP	Null	31.78	29.59	6.891	Y

Kmo^{null}	K1370	Sham	Null	33.51	31.03	7.401	Y
Kmo^{null}	K1371	AP	Null	29.04	27.33	5.888	Y
Kmo^{null}	K1372	Sham	Null	34.27	32.10	6.332	Y
$Kmo^{alb\text{-}cre}$	A148	Sham	Alb-cre	28.98	28.53	1.553	Y
$Kmo^{alb\text{-}cre}$	A149	AP	Alb-cre	30.21	29.82	1.291	Y
$Kmo^{alb\text{-}cre}$	A150	AP	Alb-cre	28.42	28.58	-0.56	Y
$Kmo^{alb\text{-}cre}$	A151	Sham	Alb-cre	27.32	26.85	1.720	Y
$Kmo^{alb\text{-}cre}$	A156	AP	Alb-cre	31.50	29.97	4.857	Y
$Kmo^{alb\text{-}cre}$	A157	Sham	Alb-cre	32.51	30.79	5.291	Y
$Kmo^{alb\text{-}cre}$	A163	Sham	Alb-cre	29.11	28.13	3.367	Y
$Kmo^{alb\text{-}cre}$	A164	AP	Alb-cre	29.77	28.78	3.325	Y
$Kmo^{alb\text{-}cre}$	A196	AP	Alb-cre	30.64	29.71	3.035	Y
$Kmo^{alb\text{-}cre}$	A197	Sham	Alb-cre	29.83	28.86	3.252	Y
$Kmo^{alb\text{-}cre}$	A201	AP	Alb-cre	26.33	26.86	-2.013	Y
$Kmo^{alb\text{-}cre}$	A203	Sham	Alb-cre	30.46	29.08	4.531	Y
$Kmo^{alb\text{-}cre}$	A204	Sham	Alb-cre	29.58	27.97	5.443	Y
$Kmo^{alb\text{-}cre}$	A206	AP	Alb-cre	26.81	26.36	1.678	Y
$Kmo^{alb\text{-}cre}$	A313	Sham	Alb-cre	29.82	28.78	3.488	Y
$Kmo^{alb\text{-}cre}$	A314	AP	Alb-cre	28.40	27.05	4.754	Y
$Kmo^{alb\text{-}cre}$	A320	Sham	Alb-cre	28.91	26.73	7.541	Y
$Kmo^{alb\text{-}cre}$	A322	AP	Alb-cre	29.89	28.96	3.111	Y
$Kmo^{alb\text{-}cre}$	A327	AP	Alb-cre	28.20	25.59	9.255	Y
$Kmo^{alb\text{-}cre}$	A328	Sham	Alb-cre	31.53	30.41	3.552	Y
$Kmo^{alb\text{-}cre}$	A339	Sham	Alb-cre	27.68	27.18	1.806	Y
$Kmo^{alb\text{-}cre}$	A340	AP	Alb-cre	25.03	23.79	4.954	Y
$Kmo^{alb\text{-}cre}$	A341	Sham	Alb-cre	27.29	25.76	5.606	Y
$Kmo^{alb\text{-}cre}$	A342	AP	Alb-cre	25.82	24.22	6.197	Y
$Kmo^{alb\text{-}cre}$	A343	AP	Alb-cre	30.03	MISSING	MISSING	Y
$Kmo^{alb\text{-}cre}$	A344	Sham	Alb-cre	27.85	MISSING	MISSING	Y
$Kmo^{alb\text{-}cre}$	A345	AP	Alb-cre	26.95	MISSING	MISSING	Y
$Kmo^{alb\text{-}cre}$	A346	Sham	Alb-cre	29.18	MISSING	MISSING	Y

Table 87. 24-hr exp. Outcome of study subjects – experiment 4 (weight loss)
The same scales instrument was used for every measurement.

6.10. Appendix 10 – Supplementary data of 24h studies. Cont.

Line	ID	Rx	Group	Albumin (g/L)	ALT (U/L)	Amylase (U/L)	Log10 Amylase	Creatinine (µmol/L)	Glucose (mmol/L)	LDH (U/L)	Urea (mmol/L)
Kmo^{wt}	FK461	AP	WT	24.0	63	40600	4.608526	8	15.0	228	6.8
Kmo^{wt}	FK463	Sham	WT	23.3	30	2160	3.334454	8	18.3	105	7.3
$Kmo^{alb\text{-}cre}$	FKA143	AP	WT	23.8	98	6292	3.798789	3	8.8	220	6.8
$Kmo^{alb\text{-}cre}$	FKA152	Sham	WT	26.3	35	2040	3.309630	3	16.8	120	5.0
Kmo^{wt}	FK474	Sham	WT	26.8	78	2212	3.344785	5	17.8	328	8.0
Kmo^{wt}	FK475	AP	WT	24.8	48	6760	3.829947	3	13.8	425	6.5
Kmo^{wt}	FK485	Sham	WT	27.5	138	2260	3.354108	8	20.0	575	5.8
Kmo^{wt}	FK486	AP	WT	25.3	90	1940	3.287802	3	10.8	193	6.3
Kmo^{wt}	FK487	AP	WT	23.8	60	7632	3.882638	3	17.8	198	8.5
Kmo^{wt}	FK488	Sham	WT	26.3	43	2256	3.353339	3	13.8	268	9.8
Kmo^{wt}	FK489	Sham	WT	26.3	193	2272	3.356408	5	16.5	388	5.8
Kmo^{wt}	FK490	AP	WT	26.5	93	9240	3.965672	8	12.8	300	6.5
Kmo^{wt}	FK495	Sham	WT	23.8	63	2252	3.352568	5	9.0	168	5.8
Kmo^{wt}	FK496	AP	WT	25.5	250	11680	4.067443	5	14.3	390	14.3
Kmo^{wt}	FK500	Sham	WT	27.0	100	2300	3.361728	5	16.0	265	4.3
Kmo^{wt}	FK501	AP	WT	24.0	93	7740	3.888741	5	14.0	225	5.3
Kmo^{wt}	FK570	Sham	WT	30.4	138	2500	3.397940	NT	17.6	270	6.4
Kmo^{wt}	FK571	AP	WT	25.8	210	19260	4.284656	NT	12.2	540	10.5
Kmo^{wt}	FK572	Sham	WT	29.0	248	3000	3.477121	NT	19.4	284	4.9
Kmo^{wt}	FK573	AP	WT	24.4	158	34100	4.532754	NT	14.6	262	4.8
Kmo^{wt}	FK608	Sham	WT	27.2	140	3340	3.523746	NT	14.0	176	5.1
Kmo^{wt}	FK609	AP	WT	22.4	100	18900	4.276462	NT	10.4	220	8.0
Kmo^{wt}	FK616	AP	WT	25.6	78	2340	3.369216	NT	11.8	246	5.1
Kmo^{wt}	FK617	Sham	WT	26.8	50	1880	3.274158	NT	17.2	170	6.1
Kmo^{wt}	FK618	AP	WT	28.4	100	6820	3.833784	NT	15.4	178	5.2
Kmo^{wt}	FK619	Sham	WT	31.0	134	2420	3.383815	NT	23.4	214	6.3
Kmo^{wt}	FK622	Sham	WT	34.8	56	2540	3.404834	NT	22.4	270	8.0
Kmo^{wt}	FK624	AP	WT	25.4	152	32440	4.511081	NT	6.4	1888	14.7
Kmo^{wt}	FK634	AP	WT	25.6	138	6900	3.838849	NT	18.2	300	5.5
Kmo^{wt}	FK635	Sham	WT	26.4	82	2380	3.376577	NT	17.4	180	6.3
$Kmo^{alb\text{-}cre}$	FKA331	AP	WT	30.0	141	19230	4.283979	NT	11.1	999	17.0
$Kmo^{alb\text{-}cre}$	FKA332	Sham	WT	25.2	246	2260	3.354108	NT	15.6	342	5.0
Kmo^{null}	K1142	AP	Null	23.0	70	3660	3.563481	3	16.0	195	6.8
Kmo^{null}	K1143	Sham	Null	26.5	28	2130	3.328380	5	16.0	143	6.3
Kmo^{null}	K1151	Sham	Null	25.0	25	1852	3.267641	5	18.5	138	5.5
Kmo^{null}	K1152	AP	Null	24.3	35	7232	3.859258	5	10.5	273	5.3
Kmo^{null}	K1159	Sham	Null	23.8	23	1740	3.240549	8	11.5	190	9.8
Kmo^{null}	K1160	AP	Null	26.5	55	6080	3.783904	3	17.3	273	7.0
Kmo^{null}	K1161	AP	Null	25.3	28	7960	3.900913	5	11.0	248	6.0
Kmo^{null}	K1162	Sham	Null	26.0	23	2152	3.332842	8	15.8	170	6.0
Kmo^{null}	K1169	AP	Null	25.0	30	10140	4.006038	10	10.0	210	6.5
Kmo^{null}	K1170	Sham	Null	26.8	23	2332	3.367729	8	15.8	130	4.5
Kmo^{null}	K1174	Sham	Null	25.5	450	2452	3.389520	8	16.8	190	10.5
Kmo^{null}	K1175	AP	Null	22.8	40	6380	3.804821	8	14.0	243	7.8
Kmo^{null}	K1182	AP	Null	27.0	45	7060	3.848805	10	18.0	218	6.8
Kmo^{null}	K1183	Sham	Null	26.5	25	2152	3.332842	10	19.3	230	6.5
Kmo^{null}	K1193	AP	Null	25.3	40	43252	4.636006	8	2.5	358	5.0
Kmo^{null}	K1194	Sham	Null	23.3	30	2600	3.414973	5	9.3	238	5.5
Kmo^{null}	K1278	AP	Null	NT	NT	4420	3.645422	NT	NT	NT	NT
Kmo^{null}	K1279	Sham	Null	NT	NT	1920	3.283301	NT	NT	NT	NT
Kmo^{null}	K1296	AP	Null	23.8	50	5080	3.705864	NT	17.2	176	4.0
Kmo^{null}	K1297	Sham	Null	26.0	54	1760	3.245513	NT	19.2	200	5.0
Kmo^{null}	K1341	AP	Null	30.4	62	51600	4.712650	NT	14.4	226	5.4
Kmo^{null}	K1342	Sham	Null	25.6	36	4920	3.691965	NT	19.0	140	5.1
Kmo^{null}	K1343	Sham	Null	26.6	44	2620	3.418301	NT	20.0	150	5.4
Kmo^{null}	K1344	AP	Null	25.4	118	20520	4.312177	NT	7.4	378	8.3
Kmo^{null}	K1350	AP	Null	24.0	146	40040	4.602494	NT	6.6	572	12.8
Kmo^{null}	K1351	Sham	Null	27.6	40	3180	3.502427	NT	19.0	144	5.0
Kmo^{null}	K1369	AP	Null	27.4	48	9200	3.963788	NT	19.2	186	4.8
Kmo^{null}	K1370	Sham	Null	30.4	30	1980	3.296665	NT	21.2	216	7.1

Kmo^{null}	K1371	AP	Null	26.0	40	2280	3.357935	NT	16.2	158	5.1
Kmo^{null}	K1372	Sham	Null	28.3	30	2180	3.338456	NT	19.2	168	5.1
$Kmo^{alb\text{-}cre}$	A148	Sham	Alb-cre	26.3	40	1980	3.296665	8	15.0	220	4.8
$Kmo^{alb\text{-}cre}$	A149	AP	Alb-cre	23.5	50	7260	3.860937	10	7.5	313	5.5
$Kmo^{alb\text{-}cre}$	A150	AP	Alb-cre	24.0	165	19332	4.286277	23	11.8	1223	34.3
$Kmo^{alb\text{-}cre}$	A151	Sham	Alb-cre	27.3	65	2392	3.378761	5	17.0	273	7.0
$Kmo^{alb\text{-}cre}$	A156	AP	Alb-cre	23.3	123	20620	4.314289	5	15.0	310	6.3
$Kmo^{alb\text{-}cre}$	A157	Sham	Alb-cre	25.0	48	2272	3.356408	8	15.5	215	7.3
$Kmo^{alb\text{-}cre}$	A163	Sham	Alb-cre	23.8	33	2232	3.348694	5	16.8	128	7.3
$Kmo^{alb\text{-}cre}$	A164	AP	Alb-cre	24.0	60	8600	3.934498	5	7.3	190	7.0
$Kmo^{alb\text{-}cre}$	A196	AP	Alb-cre	20.6	42	40496	4.607412	NT	4.0	884	21.8
$Kmo^{alb\text{-}cre}$	A197	Sham	Alb-cre	25.6	42	2344	3.369958	NT	9.6	338	6.8
$Kmo^{alb\text{-}cre}$	A201	AP	Alb-cre	17.2	52	14304	4.155458	NT	5.6	566	5.0
$Kmo^{alb\text{-}cre}$	A203	Sham	Alb-cre	23.0	66	2256	3.353339	NT	14.4	286	3.8
$Kmo^{alb\text{-}cre}$	A204	Sham	Alb-cre	24.0	24	1576	3.197556	NT	10.8	250	5.4
$Kmo^{alb\text{-}cre}$	A206	AP	Alb-cre	19.6	230	95552	4.980240	NT	4.8	1724	31.2
$Kmo^{alb\text{-}cre}$	A313	Sham	Alb-cre	25.8	86	2220	3.346353	NT	18.2	160	5.6
$Kmo^{alb\text{-}cre}$	A314	AP	Alb-cre	30.8	270	42040	4.623663	NT	19.2	700	14.9
$Kmo^{alb\text{-}cre}$	A320	Sham	Alb-cre	25.8	96	3520	3.546543	NT	18.8	166	5.0
$Kmo^{alb\text{-}cre}$	A322	AP	Alb-cre	21.4	104	6100	3.785330	NT	24.6	138	5.5
$Kmo^{alb\text{-}cre}$	A327	AP	Alb-cre	27.6	82	16060	4.205746	NT	13.8	262	6.0
$Kmo^{alb\text{-}cre}$	A328	Sham	Alb-cre	24.8	48	2480	3.394452	NT	18.0	150	5.5
$Kmo^{alb\text{-}cre}$	A339	Sham	Alb-cre	23.6	30	1820	3.260071	NT	13.2	122	6.4
$Kmo^{alb\text{-}cre}$	A340	AP	Alb-cre	24.4	66	5360	3.729165	NT	17.4	150	4.7
$Kmo^{alb\text{-}cre}$	A341	Sham	Alb-cre	25.2	50	2420	3.383815	NT	16.4	136	6.5
$Kmo^{alb\text{-}cre}$	A342	AP	Alb-cre	22.2	90	37460	4.573568	NT	5.8	396	9.0
$Kmo^{alb\text{-}cre}$	A343	AP	Alb-cre	24.6	54	10520	4.022016	NT	9.6	204	5.6
$Kmo^{alb\text{-}cre}$	A344	Sham	Alb-cre	26.8	54	2660	3.424882	NT	18.2	152	6.5
$Kmo^{alb\text{-}cre}$	A345	AP	Alb-cre	24.6	106	4140	3.617000	NT	17.2	168	5.5
$Kmo^{alb\text{-}cre}$	A346	Sham	Alb-cre	24.8	90	2160	3.334454	NT	18.4	136	4.7

Table 88. 24-hr exp. Outcome of study subjects – experiment 4 (biochemistry)
NT: not tested.

6.10. Appendix 10 – Supplementary data of 24h studies. Cont.

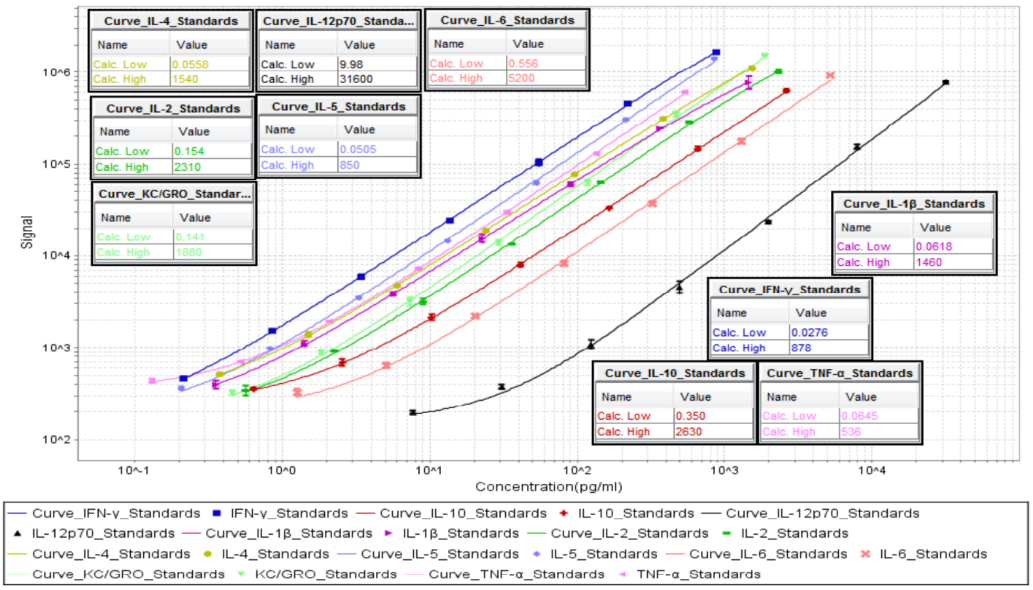

Figure 50: Calibration curves of MSD cytokine plate with limits of detection
From Plate A.

ID	Rx	Group	Plate	IFNγ (pg/ml)	IL1β (pg/ml)	IL2 (pg/ml)	IL4 (pg/ml)	IL5 (pg/ml)	IL6 (pg/ml)	IL10 (pg/ml)	IL12p70 (pg/ml)	KCGRO (pg/ml)	TNFα (pg/ml)	Notes
			LOD A	0.063	0.140	0.350	0.127	0.115	1.264	0.795	22.682	0.320	0.147	
			LOD B	0.290	0.253	1.519	0.254	1.158	10.545	0.757	47.170	0.335	0.630	
FK461	AP	WT	A	0.550	2.149	1.996	0.450	66.442	64.207	18.404	36.386	44.454	25.687	Used
FK463	Sham	WT	A	0.582	1.026	0.857	1.291	3.933	32.627	15.715	51.417	22.752	13.935	Used
FKA143	AP	WT	A	0.647	1.998	2.111	0.240	54.260	107.394	17.124	<22.682	28.459	9.558	Used
FKA152	Sham	WT	A	0.313	1.502	0.697	0.143	53.318	65.753	13.898	<22.682	26.094	8.319	Used
FK474	Sham	WT	A	0.733	1.534	0.554	1.146	6.612	261.370	17.414	35.407	78.943	12.540	Used
FK475	AP	WT	A	0.382	2.181	1.742	0.139	56.566	122.358	16.789	<22.682	63.789	8.277	Used
FK485	Sham	WT	A	0.334	1.136	0.428	0.296	17.998	137.643	12.399	<22.682	60.125	5.970	Used
FK486	AP	WT	A	2.009	3.740	4.581	0.772	19.135	334.182	20.096	<22.682	117.193	17.359	Used
FK487	AP	WT	A	0.222	1.541	0.672	0.174	18.820	54.701	13.978	<22.682	52.269	6.373	Used
FK488	Sham	WT	A	2.644	1.301	5.697	3.377	37.408	51.624	30.804	<22.682	49.243	17.433	Used
FK489	Sham	WT	A	0.326	1.469	0.722	0.140	19.913	112.916	10.943	<22.682	47.986	7.420	Used
FK490	AP	WT	A	0.288	3.903	1.246	0.136	37.932	244.068	17.544	<22.682	73.233	7.604	Used
FK495	Sham	WT	A	0.285	2.892	0.554	0.344	77.286	125.816	10.173	31.407	47.752	6.862	Used
FK496	AP	WT	A	0.311	2.341	1.251	<0.127	49.474	79.198	18.908	<22.682	39.677	7.321	Used
FK500	Sham	WT	A	0.258	1.689	0.697	0.222	54.501	182.239	12.818	<22.682	73.407	6.293	Used
FK501	AP	WT	A	1.299	5.511	2.011	0.216	41.835	327.471	16.667	<22.682	180.230	11.480	Used
FK570	Sham	WT	B	0.762	1.795	<1.519	<0.254	134.986	115.692	16.137	54.662	20.236	7.964	Not used
FK571	AP	WT	n/a	I/S	I/S	I/S	I/S	I/S	I/S	I/S	I/S	I/S	I/S	I/S
FK572	Sham	WT	B	0.811	1.194	2.181	0.325	30.959	65.742	19.736	80.618	35.451	9.824	Used
FK573	AP	WT	B	0.294	5.100	<1.519	0.238	100.743	267.855	21.608	67.186	135.878	10.708	Used
FK616	AP	WT	B	2.460	4.911	11.234	0.539	27.866	14034.698	70.950	305.011	1054.946	417.008	Used
FK617	Sham	WT	B	2.199	1.763	3.403	1.337	95.114	129.800	19.645	210.425	52.321	11.625	Used
FK618	AP	WT	B	0.332	2.907	1.558	0.584	58.296	126.112	21.229	<47.170	45.318	8.661	Used
FK619	Sham	WT	B	<0.290	1.370	4.181	0.520	36.317	71.495	15.643	<47.170	23.641	8.089	Used
K1142	AP	Null	A	0.963	2.866	2.229	<0.127	22.293	76.808	16.988	<22.682	55.481	8.937	Used
K1143	Sham	Null	A	1.144	1.634	2.263	<0.127	23.745	57.490	24.545	<22.682	34.651	9.919	Used
K1151	Sham	Null	A	0.348	1.434	1.907	<0.127	14.724	43.604	18.607	<22.682	23.315	10.097	Used
K1152	AP	Null	A	1.036	2.902	5.013	<0.127	26.735	155.033	17.019	<22.682	42.959	12.581	Used
K1159	Sham	Null	A	0.467	1.240	1.220	0.170	84.190	65.379	22.723	<22.682	70.489	9.220	Used

K1160	AP	Null	A	0.276	2.710	2.045	<0.127	89.994	107.465	17.696	<22.682	57.900	10.273	Used
K1161	AP	Null	A	0.472	2.681	0.818	<0.127	50.741	50.741	15.530	<22.682	20.466	6.813	Used
K1162	Sham	Null	A	0.383	0.922	0.929	<0.127	24.535	32.604	16.174	<22.682	25.931	9.959	Used
K1169	AP	Null	A	0.447	2.866	6.788	0.174	25.970	157.888	13.087	<22.682	47.260	12.534	Used
K1170	Sham	Null	A	0.670	2.409	2.258	<0.127	25.695	60.263	16.871	<22.682	42.363	10.492	Used
K1174	Sham	Null	A	0.367	2.438	0.974	<0.127	34.807	59.970	17.451	<22.682	37.844	9.803	Used
K1175	AP	Null	A	0.392	1.892	1.825	<0.127	47.157	155.535	12.337	<22.682	63.410	8.060	Used
K1182	AP	Null	A	0.248	1.789	1.001	<0.127	16.059	151.934	12.681	<22.682	65.962	7.606	Used
K1183	Sham	Null	A	0.482	1.495	2.820	0.354	49.041	203.046	22.232	<22.682	37.937	13.493	Used
K1193	AP	Null	A	1.030	13.360	4.893	1.432	25.210	1465.147	23.180	100.204	542.630	9.426	Used
K1194	Sham	Null	A	1.467	1.682	3.509	0.584	52.402	87.133	16.625	45.266	56.112	13.283	Used
K1278	AP	Null	B	<0.290	2.199	3.103	0.272	118.829	256.296	30.616	54.230	72.175	13.143	Used
K1279	Sham	Null	B	1.231	2.071	4.173	0.318	212.571	70.840	19.134	<47.170	25.189	12.097	Used
K1296	AP	Null	B	<0.290	2.856	3.023	<0.254	37.663	176.529	23.404	<47.170	41.727	16.461	Used
K1297	Sham	Null	B	<0.290	1.460	3.786	0.565	17.415	76.186	17.413	62.293	20.416	14.123	Used
K1343	Sham	Null	B	0.586	2.206	<1.519	<0.254	92.963	66.768	19.777	<47.170	22.079	5.446	Used
K1344	AP	Null	B	1.874	7.072	5.576	1.049	10.667	2330.471	36.678	129.890	86.539	17.245	Used
K1350	AP	Null	B	0.534	8.903	4.812	0.660	22.356	1251.897	497.509	89.675	489.979	40.719	N/U-surplus
K1351	Sham	Null	B	1.099	1.182	2.998	0.314	49.207	57.331	23.271	69.230	14.253	12.219	N/U-surplus
A148	Sham	Alb-cre	B	1.163	1.428	3.812	0.417	62.394	96.925	18.544	82.586	47.998	11.274	Used
A149	AP	Alb-cre	B	0.332	4.332	5.189	0.305	76.143	194.074	19.103	62.623	38.516	12.252	Used
A150	AP	Alb-cre	B	<0.290	4.937	6.381	<0.254	12.663	2436.790	150.709	107.406	212.329	33.507	Used
A151	Sham	Alb-cre	B	0.720	1.434	1.678	0.349	23.104	108.912	14.876	64.089	36.775	9.552	Used
A156	AP	Alb-cre	B	0.421	1.847	2.268	<0.254	49.631	111.187	10.034	<47.170	58.116	7.213	Used
A157	Sham	Alb-cre	B	<0.290	1.827	3.403	<0.254	44.209	101.364	15.807	55.761	48.387	9.116	Used
A163	Sham	Alb-cre	B	0.776	1.659	5.007	0.404	58.056	63.728	26.383	51.086	33.896	11.495	Used
A164	AP	Alb-cre	B	0.549	1.949	4.716	0.756	30.718	257.592	16.477	81.297	36.906	13.792	Used
A196	AP	Alb-cre	B	<0.290	22.362	4.265	<0.254	21.697	139276.387	1108.517	680.974	5477.826	238.829	Used
A197	Sham	Alb-cre	B	0.613	1.337	<1.519	<0.254	32.271	51.675	12.187	<47.170	27.019	7.072	Used
A201	AP	Alb-cre	B	1.278	3.384	5.483	0.331	45.496	528.060	19.237	92.981	211.932	12.202	Used
A203	Sham	Alb-cre	B	1.938	1.260	4.494	0.520	22.441	129.424	19.531	96.043	42.702	12.163	Used
A204	Sham	Alb-cre	B	0.310	1.615	1.640	<0.254	80.923	108.498	16.032	84.452	32.978	8.279	Used
A206	AP	Alb-cre	B	0.578	22.255	8.868	1.321	69.233	43433.935	199.695	357.291	1859.783	39.014	Used
A313	Sham	Alb-cre	B	<0.290	1.712	1.666	1.498	38.779	102.685	16.419	118.745	28.534	11.233	Used
A314	AP	Alb-cre	B	0.390	14.756	19.768	1.637	62.703	12180.191	199.750	225.793	887.832	45.804	Used
A320	Sham	Alb-cre	B	<0.290	1.357	3.160	0.517	63.735	36.492	15.642	<47.170	19.370	9.921	Used
A322	AP	Alb-cre	B	<0.290	3.206	<1.519	<0.254	20.911	129.797	19.942	52.969	34.195	10.062	Used
A327	AP	Alb-cre	B	1.859	3.402	6.843	0.501	29.509	176.045	17.960	<47.170	61.211	12.501	Used
A328	Sham	Alb-cre	B	0.980	1.376	3.065	<0.254	62.262	107.513	21.621	<47.170	32.282	12.446	Used
A343	AP	Alb-cre	B	<0.290	4.010	<1.519	0.265	16.527	864.951	29.314	<47.170	413.868	10.307	Used
A344	Sham	Alb-cre	B	0.337	1.834	<1.519	<0.254	47.296	68.604	19.766	52.982	14.431	13.750	Used
A345	AP	Alb-cre	B	0.762	2.429	1.829	<0.254	63.531	109.011	23.104	51.529	29.366	10.653	N/U-surplus
A346	Sham	Alb-cre	B	0.565	0.9265	3.103	<0.254	112.432	94.100	22.126	74.916	14.404	11.470	N/U-surplus

Table 89. 24-hr exp. Outcome of study subjects at 24h (cytokines)

I/S: insufficient sample. LOD: limit of detection. N/U: not used

ID	Rx	Group	Plate	IL6 (pg/ml)	Log10 IL6	TNFα (pg/ml)	Log10 TNFα
			LOD A	1.264		0.147	
			LOD B	10.545		0.630	
FK461	AP	WT	A	64.207	1.8076	25.687	1.4097
FK463	Sham	WT	A	32.627	1.5136	13.935	1.1441
FKA143	AP	WT	A	107.394	2.0310	9.558	0.9804
FKA152	Sham	WT	A	65.753	1.8179	8.319	0.9201
FK474	Sham	WT	A	261.370	2.4173	12.540	1.0983
FK475	AP	WT	A	122.358	2.0876	8.277	0.9179
FK485	Sham	WT	A	137.643	2.1388	5.970	0.7760
FK486	AP	WT	A	334.182	2.5240	17.359	1.2395
FK487	AP	WT	A	54.701	1.7380	6.373	0.8043
FK488	Sham	WT	A	51.624	1.7129	17.433	1.2414
FK489	Sham	WT	A	112.916	2.0528	7.420	0.8704
FK490	AP	WT	A	244.068	2.3875	7.604	0.8810

FK495	Sham	WT	A	125.816	2.0997	6.862	0.8365
FK496	AP	WT	A	79.198	1.8987	7.321	0.8646
FK500	Sham	WT	A	182.239	2.2606	6.293	0.7989
FK501	AP	WT	A	327.471	2.5152	11.480	1.0599
FK570	Sham	WT	B	115.692	2.0633	7.964	0.9011
FK571	AP	WT	n/a	I/S		I/S	
FK572	Sham	WT	B	65.742	1.8178	9.824	0.9923
FK573	AP	WT	B	267.855	2.4279	10.708	1.0297
FK616	AP	WT	B	14034.698	4.1472	417.008	2.6201
FK617	Sham	WT	B	129.800	2.1133	11.625	1.0654
FK618	AP	WT	B	126.112	2.1008	8.661	0.9376
FK619	Sham	WT	B	71.495	1.8543	8.089	0.9079
K1142	AP	Null	A	76.808	1.8854	8.937	0.9512
K1143	Sham	Null	A	57.490	1.7596	9.919	0.9965
K1151	Sham	Null	A	43.604	1.6395	10.097	1.0042
K1152	AP	Null	A	155.033	2.1904	12.581	1.0997
K1159	Sham	Null	A	65.379	1.8154	9.220	0.9647
K1160	AP	Null	A	107.465	2.0313	10.273	1.0117
K1161	AP	Null	A	50.741	1.7054	6.813	0.8333
K1162	Sham	Null	A	32.604	1.5133	9.959	0.9982
K1169	AP	Null	A	157.888	2.1983	12.534	1.0981
K1170	Sham	Null	A	60.263	1.7801	10.492	1.0209
K1174	Sham	Null	A	59.970	1.7779	9.803	0.9914
K1175	AP	Null	A	155.535	2.1918	8.060	0.9063
K1182	AP	Null	A	151.934	2.1817	7.606	0.8812
K1183	Sham	Null	A	203.046	2.3076	13.493	1.1301
K1193	AP	Null	A	1465.147	3.1659	9.426	0.9743
K1194	Sham	Null	A	87.133	1.9402	13.283	1.1233
K1278	AP	Null	B	256.296	2.4087	13.143	1.1187
K1279	Sham	Null	B	70.840	1.8503	12.097	1.0827
K1296	AP	Null	B	176.529	2.2468	16.461	1.2165
K1297	Sham	Null	B	76.186	1.8819	14.123	1.1499
K1343	Sham	Null	B	66.768	1.8246	5.446	0.7361
K1344	AP	Null	B	2330.471	3.3674	17.245	1.2367
K1350	AP	Null	B	1251.897	3.0976	40.719	1.6098
K1351	Sham	Null	B	57.331	1.7584	12.219	1.0870
A148	Sham	Alb-cre	B	96.925	1.9864	11.274	1.0521
A149	AP	Alb-cre	B	194.074	2.2880	12.252	1.0882
A150	AP	Alb-cre	B	2436.790	3.3868	33.507	1.5251
A151	Sham	Alb-cre	B	108.912	2.0371	9.552	0.9801
A156	AP	Alb-cre	B	111.187	2.0461	7.213	0.8581
A157	Sham	Alb-cre	B	101.364	2.0059	9.116	0.9598
A163	Sham	Alb-cre	B	63.728	1.8043	11.495	1.0605
A164	AP	Alb-cre	B	257.592	2.4109	13.792	1.1396
A196	AP	Alb-cre	B	139276.387	5.1439	238.829	2.3781
A197	Sham	Alb-cre	B	51.675	1.7133	7.072	0.8495
A201	AP	Alb-cre	B	528.060	2.7227	12.202	1.0864
A203	Sham	Alb-cre	B	129.424	2.1120	12.163	1.0850
A204	Sham	Alb-cre	B	108.498	2.0354	8.279	0.9180
A206	AP	Alb-cre	B	43433.935	4.6378	39.014	1.5912
A313	Sham	Alb-cre	B	102.685	2.0115	11.233	1.0505
A314	AP	Alb-cre	B	12180.191	4.0857	45.804	1.6609
A320	Sham	Alb-cre	B	36.492	1.5622	9.921	0.9966
A322	AP	Alb-cre	B	129.797	2.1133	10.062	1.0027
A327	AP	Alb-cre	B	176.045	2.2456	12.501	1.0969
A328	Sham	Alb-cre	B	107.513	2.0315	12.446	1.0950
A343	AP	Alb-cre	B	864.951	2.9370	10.307	1.0131
A344	Sham	Alb-cre	B	68.604	1.8363	13.750	1.1383
A345	AP	Alb-cre	B	109.011	2.0375	10.653	1.0275
A346	Sham	Alb-cre	B	94.100	1.9736	11.470	1.0596

Table 90. 24-hr exp. Plasma cytokines – Log10 data transformation
I/S: insufficient sample. LOD: limit of detection.

6.10. Appendix 10 – Supplementary data of 24h studies. Cont.

Line	**ID**	**Rx**	**Trp** (µg/ml) LOD 20 µg/l	**Kyn** (µg/l) LOD 10 µg/l	**KA** (µg/l) LOD 5 µg/l	**AA** (µg/l) LOD 1 µg/l	**3HK** (µg/l) LOD 1 µg/l	**3HAA** (µg/l) LOD 2 µg/l	**PA** (µg/l) LOD 10 µg/l	**XA** (µg/l) LOD 5 µg/l
Kmo^{wt}	FK461	AP	16950.18	115.867	<5	3.667	<1	2.340	<10	<5
Kmo^{wt}	FK463	Sham	18806.83	165.444	<5	4.356	8.356	<2	<10	<5
$Kmo^{alb\text{-}cre}$	FKA143	AP	21168.13	334.200	<5	4.667	<1	<2	<10	<5
$Kmo^{alb\text{-}cre}$	FKA152	Sham	26775.73	168.800	<5	1.667	<1	<2	<10	<5
Kmo^{wt}	FK474	Sham	20012.78	205.178	<5	4.222	6.311	<2	20.044	<5
Kmo^{wt}	FK475	AP	18108.83	216.266	<5	3.089	9.200	<2	<10	<5
Kmo^{wt}	FK485	Sham	23316.18	388.266	<5	4.378	26.067	<2	19.978	<5
Kmo^{wt}	FK486	AP	21022.86	1083.066	<5	2.556	52.689	<2	10.644	<5
Kmo^{wt}	FK487	AP	19951.80	175.822	<5	3.489	<1	<2	12.089	<5
Kmo^{wt}	FK488	Sham	18095.72	939.732	<5	4.111	19.578	<2	13.911	<5
Kmo^{wt}	FK489	Sham	24536.53	268.089	<5	4.756	<1	<2	15.844	<5
Kmo^{wt}	FK490	AP	25968.89	383.489	<5	5.867	8.422	<2	25.600	96.800
Kmo^{wt}	FK495	Sham	25489.06	540.399	7.178	8.489	30.844	21.15	21.800	286.000
Kmo^{wt}	FK496	AP	18640.06	237.422	<5	2.444	<1	<2	<10	<5
Kmo^{wt}	FK500	Sham	20932.93	165.400	<5	0.311	<1	<2	<10	<5
Kmo^{wt}	FK501	AP	16070.92	243.822	<5	0.978	<1	<2	<10	<5
Kmo^{null}	K1142	AP	21996.69	4970.528	899.355	101.200	<1	11.644	<10	<5
Kmo^{null}	K1143	Sham	18513.63	3783.996	514.288	81.533	<1	<2	<10	<5
Kmo^{null}	K1151	Sham	18954.87	3132.930	329.755	78.533	<1	<2	<10	<5
Kmo^{null}	K1152	AP	18438.89	3158.819	939.577	63.578	<1	<2	<10	<5
Kmo^{null}	K1159	Sham	22555.67	8650.014	2213.731	264.733	<1	<2	<10	<5
Kmo^{null}	K1160	AP	20962.27	5479.417	494.340	134.644	<1	<2	<10	<5
Kmo^{null}	K1161	AP	31471.52	5904.372	880.266	147.555	<1	3.111	<10	<5
Kmo^{null}	K1162	Sham	21037.69	4285.151	524.644	81.844	<1	<2	<10	<5
Kmo^{null}	K1169	AP	18783.4	3472.530	897.110	75.222	<1	<2	<10	<5
Kmo^{null}	K1170	Sham	18832.03	3187.841	233.155	61.244	<1	<2	<10	<5
Kmo^{null}	K1174	Sham	16611.21	10724.523	995.488	213.778	<1	<2	<10	<5
Kmo^{null}	K1175	AP	20334.62	6805.771	2276.220	202.244	<1	<2	<10	<5
Kmo^{null}	K1182	AP	20581.91	7601.304	960.288	150.022	<1	<2	<10	<5
Kmo^{null}	K1183	Sham	18396.76	2235.331	235.111	48.689	<1	<2	<10	<5
Kmo^{null}	K1193	AP	23594.60	5953.661	837.577	120.822	<1	<2	<10	<5
Kmo^{null}	K1194	Sham	16031.14	1731.132	437.422	43.978	<1	<2	<10	<5
$Kmo^{alb\text{-}cre}$	A148	Sham	18668.09	1291.999	<5	53.689	4.111	<2	<10	<5
$Kmo^{alb\text{-}cre}$	A149	AP	24984.62	2044.020	99.689	77.711	28.067	<2	<10	72.600
$Kmo^{alb\text{-}cre}$	A150	AP	11718.74	5481.283	1101.666	114.178	1030.399	<2	176.556	2323.200
$Kmo^{alb\text{-}cre}$	A151	Sham	28930.46	2728.997	165.155	113.844	<1	2.533	<10	63.800
$Kmo^{alb\text{-}cre}$	A156	AP	19848.40	3088.530	322.355	137.667	45.578	<2	10.200	6.600
$Kmo^{alb\text{-}cre}$	A157	Sham	20647.80	2793.886	433.044	124.400	88.822	<2	<10	1034.000
$Kmo^{alb\text{-}cre}$	A163	Sham	20106.49	2660.642	284.777	105.400	75.755	<2	<10	217.800
$Kmo^{alb\text{-}cre}$	A164	AP	22381.18	3408.797	310.933	173.666	72.022	<2	<10	134.200
$Kmo^{alb\text{-}cre}$	A196	AP	8247.792	2455.709	386.577	64.400	447.155	<2	87.067	336.600
$Kmo^{alb\text{-}cre}$	A197	Sham	28202.53	2500.553	219.088	143.733	96.000	<2	<10	644.600
$Kmo^{alb\text{-}cre}$	A201	AP	21116.76	2436.598	113.067	78.689	122.355	<2	<10	114.400
$Kmo^{alb\text{-}cre}$	A203	Sham	17890.18	731.866	<5	22.044	8.044	<2	<10	<5
$Kmo^{alb\text{-}cre}$	A204	Sham	18527.56	1253.977	<5	61.022	1.156	<2	<10	<5
$Kmo^{alb\text{-}cre}$	A206	AP	8722.236	2689.931	785.177	61.689	506.911	<2	206.200	587.400

Table 91. Concentrations of kynurenine metabolites in AP and sham at 24h
Columns indicate which mouse line mice were derived from, arbitrary ID, genotype, sex, body weight, age at cull, experimental group, and plasma concentration of analyte according to LC-MS/MS analysis. Abbreviations: 3HK: 3-hydroxykynurenine; AA: anthranilic acid; KA: kynurenic acid; Kyn: kynurenine; Trp: tryptophan; XA: xanthurenic acid.

6.10. Appendix 10 – Supplementary data of 24h studies. Cont.

Line	ID	Gene	Sex	Rx	Group	Flow Code	DOB	DOS	Age (d)	Exps
Kmo^{wt}	FK608	FK (HOM)	M	Sham	WT	M24	05/08/16	06/12/16	123	B,Lun,Liv
Kmo^{wt}	FK609	FK (HOM)	M	AP	WT	M23	05/08/16	06/12/16	123	B,Lun,Liv
Kmo^{wt}	FK616	FK (HOM)	M	AP	WT	M31	27/08/16	12/12/16	107	B,Lun,Liv
Kmo^{wt}	FK617	FK (HOM)	M	Sham	WT	M32	27/08/16	12/12/16	107	Lun,Liv
Kmo^{wt}	FK618	FK (HOM)	M	AP	WT	M45	27/08/16	19/12/16	114	B,Lun,Liv
Kmo^{wt}	FK619	FK (HOM)	M	Sham	WT	M46	27/08/16	19/12/16	114	B,Lun,Liv
Kmo^{wt}	FK622	FK (HOM)	M	Sham	WT	M64	14/09/16	16/01/17	124	B,Lun,Liv
Kmo^{wt}	FK624	FK (HOM)	M	AP	WT	M63	14/09/16	16/01/17	124	B,Lun,Liv
Kmo^{wt}	FK634	FK (HOM)	M	AP	WT	M73	13/09/16	31/01/17	140	B,Lun,Liv
Kmo^{wt}	FK635	FK (HOM)	M	Sham	WT	M74	13/09/16	31/01/17	140	B,Lun,Liv
$Kmo^{alb\text{-}cre}$	FKA331	Cre(-)	M	AP	WT	M53	04/09/16	09/01/17	127	B,Lun,Liv
$Kmo^{alb\text{-}cre}$	FKA332	Cre(-)	M	Sham	WT	M54	04/09/16	09/01/17	127	B,Lun,Liv
Kmo^{null}	K1296	KMO (HOM)	M	AP	Null	M13	08/06/16	16/11/16	161	B,Lun,Liv
Kmo^{null}	K1297	KMO (HOM)	M	Sham	Null	M14	08/06/16	16/11/16	161	B,Lun,Liv
Kmo^{null}	K1341	KMO (HOM)	M	AP	Null	M21	28/07/16	06/12/16	131	B,Lun,Liv
Kmo^{null}	K1342	KMO (HOM)	M	Sham	Null	M22	28/07/16	06/12/16	131	B,Lun,Liv
Kmo^{null}	K1343	KMO (HOM)	M	Sham	Null	M36	28/07/16	12/12/16	137	B,Lun,Liv
Kmo^{null}	K1344	KMO (HOM)	M	AP	Null	M35	28/07/16	12/12/16	137	B,Lun,Liv
Kmo^{null}	K1350	KMO (HOM)	M	AP	Null	M43	06/08/16	19/12/16	135	B,Lun,Liv
Kmo^{null}	K1351	KMO (HOM)	M	Sham	Null	M44	06/08/16	19/12/16	135	B,Lun,Liv
Kmo^{null}	K1369	KMO (HOM)	M	AP	Null	M51	11/09/16	09/01/17	120	B,Lun,Liv
Kmo^{null}	K1370	KMO (HOM)	M	Sham	Null	M52	11/09/16	09/01/17	120	B,Lun,Liv
Kmo^{null}	K1371	KMO (HOM)	M	AP	Null	M65	11/09/16	16/01/17	127	B,Lun,Liv
Kmo^{null}	K1372	KMO (HOM)	M	Sham	Null	M66	11/09/16	16/01/17	127	B,Lun,Liv
$Kmo^{alb\text{-}cre}$	A313	Cre(+)	M	Sham	Alb-cre	M26	20/07/16	06/12/16	139	B,Lun,Liv
$Kmo^{alb\text{-}cre}$	A314	Cre(+)	M	AP	Alb-cre	M25	20/07/16	06/12/16	139	B,Lun,Liv
$Kmo^{alb\text{-}cre}$	A320	Cre(+)	M	Sham	Alb-cre	M34	12/08/16	12/12/16	122	B,Lun,Liv
$Kmo^{alb\text{-}cre}$	A322	Cre(+)	M	AP	Alb-cre	M33	12/08/16	12/12/16	122	B,Lun,Liv
$Kmo^{alb\text{-}cre}$	A327	Cre(+)	M	AP	Alb-cre	M41	12/08/16	19/12/16	129	B,Lun,Liv
$Kmo^{alb\text{-}cre}$	A328	Cre(+)	M	Sham	Alb-cre	M48	12/08/16	19/12/16	129	B,Lun,Liv
$Kmo^{alb\text{-}cre}$	A339	Cre(+)	M	Sham	Alb-cre	M56	22/09/16	09/01/17	109	B,Lun,Liv
$Kmo^{alb\text{-}cre}$	A340	Cre(+)	M	AP	Alb-cre	M55	22/09/16	09/01/17	109	B,Lun,Liv
$Kmo^{alb\text{-}cre}$	A341	Cre(+)	M	Sham	Alb-cre	M62	22/09/16	16/01/17	116	B,Lun,Liv
$Kmo^{alb\text{-}cre}$	A342	Cre(+)	M	AP	Alb-cre	M61	22/09/16	16/01/17	116	Lun
$Kmo^{alb\text{-}cre}$	A343	Cre(+)	M	AP	Alb-cre	M71	22/09/16	31/01/17	131	B,Lun,Liv
$Kmo^{alb\text{-}cre}$	A344	Cre(+)	M	Sham	Alb-cre	M72	22/09/16	31/01/17	131	B,Lun,Liv
$Kmo^{alb\text{-}cre}$	A345	Cre(+)	M	AP	Alb-cre	M75	22/09/16	31/01/17	131	B,Lun,Liv
$Kmo^{alb\text{-}cre}$	A346	Cre(+)	M	Sham	Alb-cre	M76	22/09/16	31/01/17	131	B,Lun,Liv

Table 92. 24-hr exp. Outcome of study subjects – experiment 4 (flow cytometry)
WT = Sham (n = 7), AP (n = 7); KMO = Sham (n = 7), AP (n = 7); Alb-cre: Sham (n = 7), AP (n = 7).

6.10. Appendix 10 – Supplementary data of 24h studies. Cont.

ID	Rx	Group	Flow Code	CD45+ count	Eosino %CD45+	Neuts %CD45+	Neuts %Myeloid	Monos count	Ly6Chi count	% Ly6^{hi} monos	Comment
FK608	Sham	WT	M24	54463	1.46	16.0	55.8	4367	2142	49.0	
FK609	AP	WT	M23	32527	0.03	75.7	90.9	1183	538	45.5	
FK616	AP	WT	M31	56519	3.73	71.5	85.7	2649	2255	85.1	
FK617	Sham	WT	M32	*6347*	-	-	-	-	-	-	Excluded. A
FK618	AP	WT	M45	32730	1.95	22.7	69.6	1491	404	27.1	
FK619	Sham	WT	M46	52755	2.68	14.9	61.2	1940	685	35.3	
FKA331	AP	WT	M53	10409	1.49	38.3	53.7	854	287	33.6	
FKA332	Sham	WT	M54	53009	2.13	18.0	63.1	2579	979	38.0	
FK622	Sham	WT	M64	52185	1.72	18.0	62.8	2775	953	34.3	
FK624	AP	WT	M63	53198	0.02	83.1	91.7	2911	1898	65.2	
FK634	AP	WT	M73	56990	2.46	34.3	81.1	1990	874	43.9	
FK635	Sham	WT	M74	58524	3.76	30.8	73.5	2786	1265	45.4	
K1296	AP	Null	M13	22089	2.54	36.6	79.4	758	232	30.6	
K1297	Sham	Null	M14	22071	5.08	24.4	63.3	1373	318	23.2	
K1341	AP	Null	M21	53933	0.30	49.4	78.2	4289	3422	79.8	
K1342	Sham	Null	M22	54677	0.41	14.1	70.1	1622	768	47.3	
K1343	Sham	Null	M36	53868	1.80	15.9	67.4	1753	617	35.2	
K1344	AP	Null	M35	59271	0.23	69.6	78.8	3747	2445	65.3	
K1350	AP	Null	M43	28233	0.14	47.2	78.0	2147	625	29.1	
K1351	Sham	Null	M44	54018	2.63	19.2	66.9	1678	678	40.4	
K1369	AP	Null	M51	52057	1.25	40.5	78.6	2151	479	22.3	
K1370	Sham	Null	M52	52708	2.72	21.7	66.1	2032	1067	52.5	
K1371	AP	Null	M65	52663	0.85	17.5	76.2	1337	382	28.6	
K1372	Sham	Null	M66	52470	2.09	17.9	64.6	2467	1099	44.5	
A313	Sham	Alb-cre	M26	56538	2.53	18.8	64.2	2502	1290	51.6	
A314	AP	Alb-cre	M25	27689	0.07	80.8	90.0	1631	1206	73.9	
A320	Sham	Alb-cre	M34	53755	6.67	12.4	59.6	2332	1157	49.6	
A322	AP	Alb-cre	M33	32078	2.56	25.4	72.4	1154	492	42.6	
A327	AP	Alb-cre	M41	30935	0.23	30.4	75.8	1966	407	20.7	
A328	Sham	Alb-cre	M42	52558	1.51	13.1	57.4	2723	453	16.6	
A339	Sham	Alb-cre	M56	53082	2.91	23.4	59.6	4110	1749	42.6	
A340	AP	Alb-cre	M55	39709	2.95	18.1	64.3	1513	671	44.3	
A341	Sham	Alb-cre	M62	52632	2.43	16.3	56.3	3310	1236	37.3	
A342	*AP*	*Alb-cre*	*M61*	*5614*	-	-	-	-	-	-	Excluded. B.
A343	AP	Alb-cre	M71	11094	0.03	60.2	87.9	550	347	63.1	
A344	Sham	Alb-cre	M72	56549	3.52	17.6	61.1	3058	1501	49.1	
A345	AP	Alb-cre	M75	56391	3.39	22.2	71.1	2094	445	21.3	
A346	Sham	Alb-cre	M76	57200	2.23	20.7	72.1	2216	864	39.0	

Table 93. Blood flow cytometry

Comments - A: sample put on dry ice rather than wet ice, in error (excluded); B: cytometer wasted sample (excluded). n.c.: not calculated. Data: Blood flow analysis_current xls.

6.10. Appendix 10 – Supplementary data of 24h studies. Cont.

ID	Group	Code	Blood Neuts %CD45+	Blood Eosin %CD45+	Blood Mono %CD45+	Ly6Chi Monos %Monos	Comments
FK608	WT/Sham	M24	16.0	1.46	8.018	49.0	
FK617	*WT/Sham*	*M32*	*Excluded*	*Excluded*	*Excluded*	*Excluded*	*Excluded. A*
FK619	WT/Sham	M46	14.9	2.68	3.677	35.3	
FKA332	WT/Sham	M54	18.0	2.13	4.865	38.0	
FK622	WT/Sham	M64	18.0	1.72	5.318	34.3	
FK635	WT/Sham	M74	30.8	3.76	4.760	45.4	
FK609	WT/AP	M23	75.7	0.03	3.637	45.5	
FK616	WT/AP	M31	71.5	3.73	4.687	85.1	
FK618	WT/AP	M45	22.7	1.95	4.555	27.1	
FKA331	WT/AP	M53	38.3	1.49	8.204	33.6	
FK624	WT/AP	M63	83.1	0.02	5.472	65.2	
FK634	WT/AP	M73	34.3	2.46	3.492	43.9	
A313	Acre/Sham	M26	18.8	2.53	4.425	51.6	
A320	Acre/Sham	M34	12.4	1.39	4.338	49.6	
A328	Acre/Sham	M42	13.1	1.51	5.181	16.6	
A339	Acre/Sham	M56	23.4	2.91	7.743	42.6	
A341	Acre/Sham	M62	16.3	2.43	6.289	37.3	
A344	Acre/Sham	M72	17.6	3.52	5.408	49.1	
A346	Acre/Sham	M76	20.7	2.23	3.874	39.0	
A314	Acre/AP	M25	80.8	0.069	5.890	73.9	
A322	Acre/AP	M33	25.4	2.560	3.597	42.6	
A327	Acre/AP	M41	30.4	0.230	6.355	20.7	
A340	Acre/AP	M55	18.1	2.950	3.810	44.3	
A342	*Acre/AP*	*M61*	*(71.5)*	*Excluded*	*Excluded*	*Excluded*	*Excluded. B*
A343	Acre/AP	M71	60.2	0.027	4.958	63.1	
A345	Acre/AP	M75	22.2	3.390	3.713	21.3	
K1297	Null/Sham	M14	24.4	5.08	6.221	23.2	
K1342	Null/Sham	M22	14.1	0.41	2.967	47.3	
K1343	Null/Sham	M36	15.9	1.80	3.254	35.2	
K1351	Null/Sham	M44	19.2	2.63	3.106	40.4	
K1370	Null/Sham	M52	21.7	2.72	3.855	52.5	
K1372	Null/Sham	M66	17.9	2.09	4.702	44.5	
K1296	Null/AP	M13	36.6	2.54	3.432	30.6	
K1341	Null/AP	M21	49.4	0.30	7.952	79.8	
K1344	Null/AP	M35	69.6	0.23	6.322	65.3	
K1350	Null/AP	M43	47.2	0.14	7.605	29.1	
K1369	Null/AP	M51	40.5	1.25	4.132	22.3	
K1371	Null/AP	M65	17.5	0.85	2.539	28.6	

Table 94. Blood flow cytometry calculations

Comments - A: sample put on dry ice rather than wet ice, in error (excluded); B: cytometer wasted sample (excluded). n.c.: not calculated. Data: Blood flow analysis_current xls.

6.10. Appendix 10 – Supplementary data of 24h studies. Cont.

ID	Rx	Group	Code	Events	Live	L/ CD45+	L/45/ Myleoid	L/45/My / Neuts	L/45/My/ Eosino	Alv Macs	%Neuts [L/45]	NonDCs	Ly6C^{hi} Monos	Lung DCs	Comments
FK608	Sham	WT	M24	558718	242785	166449	63831	16290	3916	12256	9.79	21925	8079	6764	
FK609	AP	WT	M23	1110914	475434	277997	220870	143522	242	29209	51.60	30653	11139	9324	
FK616	AP	WT	M31	824957	410522	323117	192293	100262	13130	118945	31.0	38212	11477	9497	
FK617	Sham	WT	M32	657567	291811	229957	86186	30553	5189	14466	13.3	23188	9083	5813	
FK618	AP	WT	M45	486749	172592	133117	54137	15421	4827	13907	8.93	13722	3135	4191	
FK619	Sham	WT	M46	389115	170488	133859	45628	10895	5585	11139	8.14	12412	2834	3826	
FK622	Sham	WT	M64	285485	95892	71541	19016	5120	2316	3727	7.16	5269	1272	1134	
FK624	AP	WT	M63	143336	42059	24566	19868	12088	25	1602	49.20	4215	1833	584	
FK634	AP	WT	M73	606427	216954	146666	40890	11507	6218	5341	7.85	11164	2276	3117	
FK635	Sham	WT	M74	580486	194366	148375	33833	7548	5505	4175	5.09	11947	1801	2083	
FKA331	AP	WT	M53	829987	279097	143662	85166	25792	4949	16671	18.00	24451	6663	7141	
FKA332	Sham	WT	M54	457005	198121	142499	33162	6299	6287	4947	4.42	11849	2079	2441	
K1296	AP	Null	M13	304547	132419	97041	36474	15497	3898	3264	16.00	7382	1414	1532	
K1297	Sham	Null	M14	481390	152097	99197	34948	8300	6235	4714	8.37	10890	1789	2025	
K1312	Sham	Null	M02A	315199	132064	95388	26127	11655	1973	3438	12.2	6837	1853	1395	
K1313	AP	Null	M01A	548255	158891	96164	67457	39874	62	10487	41.5	12242	6801	2409	
K1341	AP	Null	M21	587271	292416	163185	90663	49507	728	14769	30.30	18035	10888	5270	
K1342	Sham	Null	M22	583224	240679	165000	49093	14545	1216	11783	8.82	15293	4492	4373	
K1343	Sham	Null	M36	647757	294662	210793	76223	18919	6989	14251	8.98	26789	7263	4695	
K1344	AP	Null	M35	2113229	672023	400738	329634	165456	158	38628	41.3	74572	20268	8407	
K1350	AP	Null	M43	549507	205537	135123	91035	42820	246	13394	31.7	25253	7401	5953	
K1351	Sham	Null	M44	374139	173342	132464	54395	15048	5818	13930	11.4	13405	2910	3732	
K1369	AP	Null	M51	557687	224047	143709	50703	22025	3037	10242	15.30	10158	1641	3596	
K1370	Sham	Null	M52	462645	209295	142780	43904	12051	9895	8846	8.44	9164	2181	2742	
K1371	AP	Null	M65	614019	209805	145614	33843	9811	3355	7268	6.74	8265	1751	2736	
K1372	Sham	Null	M66	543002	196689	145571	35712	8242	6720	6259	5.66	10228	2711	2086	
A313	Sham	Alb-cre	M26	682448	271858	15882	60902	17252	6888	9219	10.90	20184	7318	4747	
A314	AP	Alb-cre	M25	449091	238271	171452	147260	108516	405	10389	63.30	19277	11325	4467	
A320	Sham	Alb-cre	M34	739932	291390	212366	64014	15129	6127	10390	7.12	23961	9468	5536	
A322	AP	Alb-cre	M33	849278	304504	221297	74956	17820	7047	14066	8.05	17820	7337	5807	
A327	AP	Alb-cre	M41	542331	195636	106972	55285	21672	311	14196	20.3	12199	2633	4287	
A328	Sham	Alb-cre	M42	398911	192631	132271	45834	8826	3858	10649	6.67	15727	2493	4580	
A339	Sham	Alb-cre	M56	397996	151473	111161	31973	6584	4295	7822	5.92	8762	2109	2712	
A340	AP	Alb-cre	M55	487527	204654	145336	43955	8747	8118	10761	6.02	10954	2144	2892	
A341	Sham	Alb-cre	M62	610217	219598	145294	42908	10085	6599	8133	6.94	12216	3758	2851	
A342	AP	Alb-cre	M61	836330	268087	145505	118950	73842	242	10872	50.7	23087	11845	3108	
A343	AP	Alb-cre	M71	1395958	258104	150391	91085	32638	154	15188	21.7	29479	9364	5263	
A344	Sham	Alb-cre	M72	457488	175658	148385	32499	6697	7713	3694	4.51	9775	2147	1851	
A345	AP	Alb-cre	M75	624278	196758	151233	41441	8644	6872	6915	5.72	12761	1578	2492	
A346	Sham	Alb-cre	M76	549217	194242	150346	40066	8390	7232	5829	5.58	12223	2450	2484	

Table 95. Lung flow cytometry
File: lung flow analysis_current

6.10. Appendix 10 – Supplementary data of 24h studies. Cont.

ID	Group	Code	Lung Neuts %CD45+	Lung Eosin %CD45+	Lung non-Alv, Non-DCs %CD45+	Ly6Chi Monos %Monos - Lung	Comments
FK608	WT/Sham	M24	9.79	2.3527	13.172	36.848	
FK617	WT/Sham	M32	13.3	2.2565	10.084	39.171	
FK619	WT/Sham	M46	8.14	4.1723	9.272	22.833	
FKA332	WT/Sham	M54	4.42	4.4120	8.315	17.546	
FK622	WT/Sham	M64	7.16	3.2373	7.365	24.141	
FK635	WT/Sham	M74	5.09	3.7102	8.052	15.075	
FK609	WT/AP	M23	51.60	0.0871	11.026	36.339	
FK616	WT/AP	M31	31.03	4.0635	11.826	30.035	
FK618	WT/AP	M45	8.93	3.6261	10.308	22.847	
FKA331	WT/AP	M53	18.00	3.4449	17.020	27.250	
FK624	WT/AP	M63	49.20	0.1018	17.158	43.488	
FK634	WT/AP	M73	7.85	4.2396	7.612	20.387	
A313	Acre/Sham	M26	10.90	4.3370	12.709	36.256	
A320	Acre/Sham	M34	7.12	2.8851	11.283	39.514	
A328	Acre/Sham	M42	6.67	2.9167	11.890	15.852	
A339	Acre/Sham	M56	5.92	3.8638	7.882	24.070	
A341	Acre/Sham	M62	6.94	4.5418	8.408	30.763	
A344	Acre/Sham	M72	4.51	5.1980	6.588	21.964	
A346	Acre/Sham	M76	5.58	4.8102	8.130	20.044	
A314	Acre/AP	M25	63.30	0.2362	11.243	58.749	
A322	Acre/AP	M33	8.05	3.1844	12.080	41.173	
A327	Acre/AP	M41	20.26	0.2907	11.404	21.584	
A340	Acre/AP	M55	6.02	5.5857	7.537	19.573	
A342	Acre/AP	M61	50.70	0.1663	15.867	51.306	
A343	Acre/AP	M71	21.70	0.1024	19.602	31.765	
A345	Acre/AP	M75	5.72	4.5440	8.438	12.366	
K1297	Null/Sham	M14	8.37	6.2855	10.978	16.428	
K1342	Null/Sham	M22	8.82	0.7370	9.268	29.373	
K1343	Null/Sham	M36	8.98	3.3156	12.709	27.112	
K1351	Null/Sham	M44	11.40	4.3921	10.120	21.708	
K1370	Null/Sham	M52	8.44	6.9302	6.418	23.800	
K1372	Null/Sham	M66	5.66	4.6163	7.026	26.506	
K1296	Null/AP	M13	16.00	4.0169	7.607	19.155	
K1341	Null/AP	M21	30.30	0.4461	11.052	60.371	
K1344	Null/AP	M35	41.30	0.0394	18.609	27.179	
K1350	Null/AP	M43	31.70	0.1821	18.689	29.307	
K1369	Null/AP	M51	15.30	2.1133	7.068	16.155	
K1371	Null/AP	M65	6.74	2.3040	5.676	21.186	

Table 96. Lung flow cytometry calculations
File: lung flow analysis_current

6.10. Appendix 10 – Supplementary data of 24h studies. Cont.

ID	Rx	Group	Code	Events	Live1	L/ CD45+	L/45/ Myleoid	L/45/My / Neuts	L/45/My / Eosino	L/45/Myl/ Kupffers	L/45/Myl/ Infil monos	NonDC	Ly6C^{hi} infilt monos	%Ly6C^{hi} infilt monos	Notes
FKA307	AP	WT	M03A	355551	134834	42882	27665	9376	451	4492	5541	4624	1785	38.6	
FK592	Sham	WT	M04A	358210	152298	43813	15021	2072	1726	2629	2967	2510	982	39.1	
FK608	Sham	WT	M24	350214	162624	64609	24832	4031	2508	2687	8086	6243	2788	44.7	
FK609	AP	WT	M23	334562	170965	65828	27540	7017	718	5468	6722	5389	1853	34.4	
FK616	AP	WT	M31	249449	158614	113339	55057	32708	4737	953	6307	4188	1923	45.9	
FK617	Sham	WT	M32	506741	250841	124635	35239	10144	3104	2732	8628	6349	2937	46.3	
FK618	AP	WT	M45	414836	205948	82874	53094	5687	2499	13630	11912	9801	3432	35.0	
FK619	Sham	WT	M46	517256	242776	87185	48593	8137	4350	7676	13215	10645	2869	27.0	
FK622	Sham	WT	M64	674442	199401	72117	40210	4355	3881	13413	7403	6438	2903	45.1	
FK624	AP	WT	M63	307184	130810	94006	67030	25973	1719	1384	12664	10526	2981	28.3	
FK634	AP	WT	M73	860622	190234	76960	37873	12404	2030	9755	6720	5576	2062	37.0	
FK635	Sham	WT	M74	862496	191338	81518	34255	7573	3889	7521	8105	6956	2838	40.8	
FKA331	AP	WT	M53	2087156	162290	93915	65081	18990	1725	14186	17356	15062	3402	22.6	
FKA332	Sham	WT	M54	1804763	147207	70112	33779	4714	4314	9449	5016	4141	1013	24.5	
K1296	AP	Null	M13	720839	170349	86629	38728	11401	3145	7137	8423	7348	4125	56.1	
K1297	Sham	Null	M14	1004767	199449	76831	31699	5056	4150	6844	7728	5971	2701	45.2	
K1312	Sham	Null	M02A	647283	193144	41934	15175	1892	1139	3185	3886	3165	1032	32.6	
K1313	AP	Null	M01A	452003	163750	40681	21104	4564	148	3994	5602	4890	1562	31.9	
K1341	AP	Null	M21	327068	154996	68808	32276	7002	656	5161	9706	8414	4491	53.4	
K1342	Sham	Null	M22	402076	201027	77955	34882	6915	1368	5169	10108	8077	3663	45.4	
K1343	Sham	Null	M36	2195200	244377	96781	28038	9191	3961	806	6933	5260	1407	26.7	
K1344	AP	Null	M35	775897	377763	161227	71289	32679	618	2163	9230	8363	4286	51.2	
K1350	AP	Null	M43	479626	226509	83876	69937	21863	360	12524	10284	8609	3173	36.9	
K1351	Sham	Null	M44	976326	188248	84071	40620	4446	2145	9854	6374	5306	1855	35.0	
K1369	AP	Null	M51	616855	142550	77124	41046	10004	1065	10262	12188	10241	4340	42.4	
K1370	Sham	Null	M52	691771	192712	95401	38061	8124	5022	4478	11305	9061	3167	35.0	
K1371	AP	Null	M65	145121	53787	22320	10961	1838	532	2741	3015	2661	895	33.6	
K1372	Sham	Null	M66	108026	49039	21944	8307	1715	1153	683	2731	2292	778	33.9	
A313	Sham	Alb-cre	M26	318264	140377	55490	22635	5796	1912	2871	6005	4726	2033	43.0	
A314	AP	Alb-cre	M25	387452	193481	81990	41853	14861	2155	4296	10004	8185	3542	43.3	
A320	Sham	Alb-cre	M34	1410767	314482	108115	38365	11775	6893	1836	9052	6489	2725	42.0	
A322	AP	Alb-cre	M33	1046319	355058	165157	37240	12737	2492	2141	10402	7997	3665	45.8	
A327	AP	Alb-cre	M41	511355	250719	89679	67372	8928	704	22310	9196	7606	1931	25.4	
A328	Sham	Alb-cre	M42	693340	230502	89580	57479	3690	1979	16806	7255	5656	1833	32.4	
A339	Sham	Alb-cre	M56	451959	136867	83750	42271	5421	6171	6812	10881	8595	2580	30.0	
A340	AP	Alb-cre	M55	287749	78382	40684	20661	3365	1510	7121	3668	2821	961	34.1	
A341	Sham	Alb-cre	M62	533704	159075	51866	31373	3567	2974	9369	5228	4643	1983	42.7	
A342	*AP*	*Alb-cre*	*M61*	*19237*	*523*	*91*	-	-	-	-	-	-	-	-	*Excluded.*
A343	AP	Alb-cre	M71	845302	236074	75300	49842	12450	746	13576	14057	12206	2880	23.6	
A344	Sham	Alb-cre	M72	894484	226732	69424	37439	5001	5210	12606	5918	5170	1859	36.0	
A345	AP	Alb-cre	M75	694537	165695	80734	47357	11269	3383	7568	16806	14884	7187	48.3	
A346	Sham	Alb-cre	M76	809360	214213	85212	33452	9399	6603	2506	6916	5693	1777	31.2	

Table 97. Liver flow cytometry

Comment: Cytometer wasted sample and remainder insufficient (A342).

6.10. Appendix 10 – Supplementary data of 24h studies. Cont.

ID	Group	Code	Liver Neuts %CD45+	Liver Eosin %CD45+	Liver non-kupffer, Non-DCs %CD45+	Ly6C^{hi} Monos %Monos - Liver	Comments
FK608	WT/Sham	M24	6.24	3.88	12.52	44.66	
FK617	WT/Sham	M32	8.14	2.49	6.92	46.26	
FK619	WT/Sham	M46	9.33	4.99	15.16	26.95	
FKA332	WT/Sham	M54	6.72	6.15	7.15	24.46	
FK622	WT/Sham	M64	6.04	5.38	10.27	45.09	
FK635	WT/Sham	M74	9.29	4.77	9.94	40.80	
FK609	WT/AP	M23	10.66	1.09	10.21	34.38	
FK616	WT/AP	M31	28.86	4.18	5.56	45.92	
FK618	WT/AP	M45	6.86	3.02	14.37	35.02	
FKA331	WT/AP	M53	20.22	1.84	18.48	22.59	
FK624	WT/AP	M63	27.63	1.83	13.47	28.32	
FK634	WT/AP	M73	16.12	2.64	8.73	36.98	
A313	Acre/Sham	M26	10.45	3.45	10.82	43.02	
A320	Acre/Sham	M34	10.89	6.38	8.37	41.99	
A328	Acre/Sham	M42	4.12	2.21	8.10	32.41	
A339	Acre/Sham	M56	6.47	7.37	12.99	30.02	
A341	Acre/Sham	M62	6.88	5.73	10.08	42.71	
A344	Acre/Sham	M72	7.20	7.50	8.52	35.96	
A346	Acre/Sham	M76	11.03	7.75	8.12	31.21	
A314	Acre/AP	M25	18.13	2.63	12.20	43.27	
A322	Acre/AP	M33	7.71	1.51	6.30	45.83	
A327	Acre/AP	M41	9.96	0.79	10.25	25.39	
A340	Acre/AP	M55	8.27	3.71	9.02	34.07	
A342	Acre/AP	M61			Cytometer wasted	sample	*Excluded. A*
A343	Acre/AP	M71	16.53	0.99	18.67	23.59	
A345	Acre/AP	M75	13.96	4.19	20.82	48.29	
K1297	Null/Sham	M14	6.58	5.40	10.06	45.24	
K1342	Null/Sham	M22	8.87	1.75	12.97	45.35	
K1343	Null/Sham	M36	9.50	4.09	7.16	26.75	
K1351	Null/Sham	M44	5.29	2.55	7.58	34.96	
K1370	Null/Sham	M52	8.52	5.26	11.85	34.95	
K1372	Null/Sham	M66	7.82	5.25	12.45	33.94	
K1296	Null/AP	M13	13.16	3.63	9.72	56.14	
K1341	Null/AP	M21	10.18	0.95	14.11	53.38	
K1344	Null/AP	M35	20.27	0.38	5.72	51.25	
K1350	Null/AP	M43	26.07	0.43	12.26	36.86	
K1369	Null/AP	M51	12.97	1.38	15.80	42.38	
K1371	Null/AP	M65	8.23	2.38	13.51	33.63	

Table 98. Liver flow cytometry calculations

6.11. Appendix 11 – Supplementary data of experiment 5 (drug studies)

Group	[3HK] uM
A367 – 0.25mg/ml oral	0.084998
A368 – 0.25mg/ml oral	0.054414
A403 – 0.25mg/ml oral	0.084958
A405 – 0.25mg/ml oral	0.045746
A369 – Vehicle/ drinking water	0.715227
A370 – Vehicle/ drinking water	0.407366
A404 – Vehicle/ drinking water	0.179525
A406 – Vehicle/ drinking water	0.464352
KMOG11- 967 / drinking water	0.044601 (LOD)
KMOG11-997/ drinking water	0.044601 (LOD)
KMOG11-1027/ drinking water	0.044601 (LOD)
KMOG11-1057/ drinking water	0.044601 (LOD)

Table 99. Pilot work testing lower dose of GSK898 (0.25 mg/ml drinking water)

Line	ID	Sex	Weight	DOB	Age (d)	Telem	Gene	Start	Surgery Date	Finish	Rx
$Kmo^{alb\text{-}cre}$	A369	M	30.82	10/11/16	151	n/a	Cre(+)	10/04/17	n/a	14/04/17	Vehicle w.
$Kmo^{alb\text{-}cre}$	A370	M	31.52	10/11/16	151	n/a	Cre(+)	10/04/17	n/a	14/04/17	Vehicle w.
$Kmo^{alb\text{-}cre}$	A404	M	26.40	13/01/17	91	n/a	Cre(+)	10/04/17	n/a	14/04/17	Vehicle w.
$Kmo^{alb\text{-}cre}$	A406	M	26.48	13/01/17	91	n/a	Cre(+)	10/04/17	n/a	14/04/17	Vehicle w.
$Kmo^{alb\text{-}cre}$	A395	M	27.40	04/12/16	152	n/a	Cre(+)	05/05/17	n/a	09/05/17	0.5mg/ml w. (4d)
$Kmo^{alb\text{-}cre}$	A396	M	27.32	04/12/16	152	n/a	Cre(+)	05/05/17	n/a	09/05/17	0.5mg/ml w. (4d)
$Kmo^{alb\text{-}cre}$	A428	M	25.75	18/01/17	107	n/a	Cre(+)	05/05/17	n/a	09/05/17	0.5mg/ml w. (4d)
$Kmo^{alb\text{-}cre}$	A429	M	26.70	18/01/17	107	n/a	Cre(+)	05/05/17	n/a	09/05/17	0.5mg/ml w. (4d)
$Kmo^{alb\text{-}cre}$	A381	M	26.15	30/11/16	147	EM-21	Cre(+)	22/04/17	26/04/17	03/05/17	AP + 0.5mg/ml w.
$Kmo^{alb\text{-}cre}$	A383	M	28.71	30/11/16	147	EM-22	Cre(+)	22/04/17	26/04/17	01/05/17	AP + 0.5mg/ml w.
$Kmo^{alb\text{-}cre}$	A384	M	29.50	30/11/16	147	EM-24	Cre(+)	22/04/17	26/04/17	03/05/17	AP + 0.5mg/ml w.
$Kmo^{alb\text{-}cre}$	A388	M	29.41	30/11/16	148	EM-28	Cre(+)	23/04/17	27/04/17	02/05/17	AP + 0.5mg/ml w.
$Kmo^{alb\text{-}cre}$	A390	M	27.77	04/12/16	144	EM-25	Cre(+)	23/04/17	27/04/17	04/05/17	AP + 0.5mg/ml w.
$Kmo^{alb\text{-}cre}$	A391	M	27.44	04/12/16	144	EM-27	Cre(+)	23/04/17	27/04/17	01/05/17	AP + 0.5mg/ml w.
$Kmo^{alb\text{-}cre}$	A392	M	29.43	04/12/16	151	EM-21	Cre(+)	30/04/17	04/05/17	05/05/17	AP + 0.5mg/ml w.
$Kmo^{alb\text{-}cre}$	A393	M	29.41	04/12/16	151	EM-24	Cre(+)	30/04/17	04/05/17	10/05/17	AP + 0.5mg/ml w.
$Kmo^{alb\text{-}cre}$	A382	M	29.20	30/11/16	147	EM-23	Cre(+)	22/04/17	26/04/17	03/05/17	AP + vehicle w.
$Kmo^{alb\text{-}cre}$	A386	M	30.42	30/11/16	148	EM-26	Cre(+)	23/04/17	27/04/17	28/04/17	AP + vehicle w.
$Kmo^{alb\text{-}cre}$	A394	M	26.63	04/12/16	151	EM-23	Cre(+)	30/04/17	04/05/17	11/05/17	AP + vehicle w.
$Kmo^{alb\text{-}cre}$	A226	M	26.59	28/02/16	155	EM-22	Cre(+)	28/07/17	01/08/16	03/08/16	AP + vehicle w.
$Kmo^{alb\text{-}cre}$	A235	M	29.76	21/03/16	134	EM-25	Cre(+)	29/07/17	02/08/16	04/08/16	AP + vehicle w.
$Kmo^{alb\text{-}cre}$	A238	M	31.41	04/04/16	134	EM-22	Cre(+)	12/08/17	16/08/16	23/08/16	AP + vehicle w.
$Kmo^{alb\text{-}cre}$	A241	M	29.89	06/04/16	132	EM-23	Cre(+)	12/08/17	16/08/16	23/08/16	AP + vehicle w.
$Kmo^{alb\text{-}cre}$	A244	M	28.43	06/04/16	133	EM-24	Cre(+)	13/08/17	17/08/16	24/08/16	AP + vehicle w.
$Kmo^{alb\text{-}cre}$	A246	M	28.01	06/04/16	133	EM-26	Cre(+)	13/08/17	17/08/16	19/08/16	AP + vehicle w.
$Kmo^{alb\text{-}cre}$	A272	M	28.85	16/04/16	136	EM-23	Cre(+)	26/08/17	30/08/16	01/09/16	AP + vehicle w.
$Kmo^{alb\text{-}cre}$	A265	M	27.25	16/04/16	136	EM-22	Cre(+)	26/08/17	30/08/16	31/08/16	AP + vehicle w.
$Kmo^{alb\text{-}cre}$	A280	M	29.00	29/04/16	130	EM-23	Cre(+)	02/08/17	06/09/16	13/09/16	AP + vehicle w.
$Kmo^{alb\text{-}cre}$	A281	M	28.72	29/04/16	130	EM-22	Cre(+)	02/08/17	06/09/16	07/09/16	AP + vehicle w.
$Kmo^{alb\text{-}cre}$	A227	M	27.36	28/02/16	155	EM-23	Cre(+)	28/07/17	01/08/16	08/08/16	Sham + vehicle w.
$Kmo^{alb\text{-}cre}$	A234	M	30.55	21/03/16	134	EM-28	Cre(+)	29/07/17	02/08/16	09/08/16	Sham + vehicle w.
$Kmo^{alb\text{-}cre}$	A243	M	27.60	06/04/16	132	EM-21	Cre(+)	12/08/17	16/08/16	23/08/16	Sham + vehicle w.
$Kmo^{alb\text{-}cre}$	A252	M	27.37	09/04/16	130	EM-25	Cre(+)	13/08/17	17/08/16	24/08/16	Sham + vehicle w.
$Kmo^{alb\text{-}cre}$	A253	M	28.00	09/04/16	143	EM-24	Cre(+)	26/08/17	30/08/16	06/09/16	Sham + vehicle w.
$Kmo^{alb\text{-}cre}$	A270	M	27.93	16/04/16	136	EM-21	Cre(+)	26/07/17	30/08/16	06/09/16	Sham + vehicle w.
$Kmo^{alb\text{-}cre}$	A282	M	29.54	29/04/16	130	EM-23	Cre(+)	02/08/17	06/09/16	13/09/16	Sham + vehicle w.

Table 100. Drinking water drug study subjects
Experiment 5. Oral drug. 0.5mg/ml 898 drinking. Same scales instrument for all weight measurements.

6.11. Appendix 11 – Supplementary data of experiment 5 (drug studies). Cont.

Line	ID	Weight	Age (d)	Rx	Survival (h)	End weight (g)	Weight loss (%)
Kmo$^{alb\text{-}cre}$	A381	26.15	147	AP + 0.5mg/ml w.	168.0	26.77	-2.37
Kmo$^{alb\text{-}cre}$	A383	28.71	147	AP + 0.5mg/ml w.	122.6	23.74	17.31
Kmo$^{alb\text{-}cre}$	A384	29.50	147	AP + 0.5mg/ml w.	168.0	24.77	16.03
Kmo$^{alb\text{-}cre}$	A388	29.41	148	AP + 0.5mg/ml w.	122.6	23.74	19.28
Kmo$^{alb\text{-}cre}$	A390	27.77	144	AP + 0.5mg/ml w.	168.0	23.51	15.34
Kmo$^{alb\text{-}cre}$	A391	27.44	144	AP + 0.5mg/ml w.	101.5	25.23	8.05
Kmo$^{alb\text{-}cre}$	A392	29.43	151	AP + 0.5mg/ml w.	31.3	28.64	2.68
Kmo$^{alb\text{-}cre}$	A393	29.41	151	AP + 0.5mg/ml w.	115.8	23.64	19.62
Kmo$^{alb\text{-}cre}$	A382	29.20	147	AP + vehicle w.	168.0	25.70	11.99
Kmo$^{alb\text{-}cre}$	A386	30.42	148	AP + vehicle w.	20.5	29.75	2.20
Kmo$^{alb\text{-}cre}$	A394	26.63	151	AP + vehicle w.	168.0	25.92	2.67
Kmo$^{alb\text{-}cre}$	A226	26.59	155	AP + vehicle w.	52.9	24.67	7.22
Kmo$^{alb\text{-}cre}$	A235	29.76	134	AP + vehicle w.	46.5	27.92	6.18
Kmo$^{alb\text{-}cre}$	A238	31.41	134	AP + vehicle w.	168.0	22.98	26.84
Kmo$^{alb\text{-}cre}$	A241	29.89	132	AP + vehicle w.	168.0	28.47	4.75
Kmo$^{alb\text{-}cre}$	A244	28.43	133	AP + vehicle w.	168.0	24.10	15.23
Kmo$^{alb\text{-}cre}$	A246	28.01	133	AP + vehicle w.	48.0	25.11	10.35
Kmo$^{alb\text{-}cre}$	A272	28.85	136	AP + vehicle w.	47.8	25.44	11.820
Kmo$^{alb\text{-}cre}$	A265	27.25	136	AP + vehicle w.	23.4	27.68	Gain 1.578
Kmo$^{alb\text{-}cre}$	A280	29.00	130	AP + vehicle w.	168.0	27.22	6.138
Kmo$^{alb\text{-}cre}$	A281	28.72	130	AP + vehicle w.	29.2	28.97	Gain 0.870
Kmo$^{alb\text{-}cre}$	A227	27.36	155	Sham + vehicle w.	168.0	26.16	4.386
Kmo$^{alb\text{-}cre}$	A234	30.55	134	Sham + vehicle w.	168.0	27.19	10.998
Kmo$^{alb\text{-}cre}$	A243	27.60	132	Sham + vehicle w.	168.0	26.66	3.406
Kmo$^{alb\text{-}cre}$	A252	27.37	130	Sham + vehicle w.	168.0	25.32	7.490
Kmo$^{alb\text{-}cre}$	A253	28.00	143	Sham + vehicle w.	168.0	26.75	4.464
Kmo$^{alb\text{-}cre}$	A270	27.93	136	Sham + vehicle w.	168.0	25.07	10.240
Kmo$^{alb\text{-}cre}$	A282	29.54	130	Sham + vehicle w.	168.0	27.94	5.416

Table 101. Outcome of drinking water drug study subjects (survival and weight loss)
Experiment 5. Oral drug. 0.5mg/ml 898 drinking. Same scales instrument for all weight measurements.

Line	ID	Rx	Telem	Survival	Humane endpoint	Telemetry time (h)	Activity Total (counts)	Activity / hr
Kmo$^{alb\text{-}cre}$	A381	AP + 0.5mg/ml w.	EM-21	168.0	No	168.00	76879	457.6
Kmo$^{alb\text{-}cre}$	A383	AP + 0.5mg/ml w.	EM-22		**Yes**	122.55	49177	401.3
Kmo$^{alb\text{-}cre}$	A384	AP + 0.5mg/ml w.	EM-24	168.0	No	168.00	111941	666.3
Kmo$^{alb\text{-}cre}$	A388	AP + 0.5mg/ml w.	EM-28		**Yes**	122.58	57635	470.2
Kmo$^{alb\text{-}cre}$	A390	AP + 0.5mg/ml w.	EM-25	168.0	No	168.00	102015	607.2
Kmo$^{alb\text{-}cre}$	A391	AP + 0.5mg/ml w.	EM-27		**Yes**	101.42	39841	392.8
Kmo$^{alb\text{-}cre}$	A392	AP + 0.5mg/ml w.	EM-21		**Yes**	29.50	33106	1122.2
Kmo$^{alb\text{-}cre}$	A393	AP + 0.5mg/ml w.	EM-24		**Yes**	115.50	80817	699.7
Kmo$^{alb\text{-}cre}$	A382	AP + vehicle w.	EM-23	168.0	No	168.00	85083	506.4
Kmo$^{alb\text{-}cre}$	A386	AP + vehicle w.	EM-26		**Yes**	20.30	4341	213.8
Kmo$^{alb\text{-}cre}$	A394	AP + vehicle w.	EM-23	168.0	No	168.00	124634	741.9
Kmo$^{alb\text{-}cre}$	A226	AP + vehicle w.	EM-22		**Yes**	50.12	13136	262.1
Kmo$^{alb\text{-}cre}$	A235	AP + vehicle w.	EM-25		**Yes**	44.33	17651	398.2
Kmo$^{alb\text{-}cre}$	A238	AP + vehicle w.	EM-22	168.0	No	168.00	117908	701.8
Kmo$^{alb\text{-}cre}$	A241	AP + vehicle w.	EM-23	168.0	No	168.00	103024	613.2
Kmo$^{alb\text{-}cre}$	A244	AP + vehicle w.	EM-24	168.0	No	168.00	68024	404.9
Kmo$^{alb\text{-}cre}$	A246	AP + vehicle w.	EM-26		**Yes**	46.75	39641	847.9
Kmo$^{alb\text{-}cre}$	A272	AP + vehicle w.	EM-23		**Yes**	45.53	42421	931.7
Kmo$^{alb\text{-}cre}$	A265	AP + vehicle w.	EM-22		**Yes**	22.38	5089	227.4
Kmo$^{alb\text{-}cre}$	A280	AP + vehicle w.	EM-23	168.0	No	168.00	117205	697.6
Kmo$^{alb\text{-}cre}$	A281	AP + vehicle w.	EM-22		**Yes**	28.22	13095	464.0
Kmo$^{alb\text{-}cre}$	A227	Sham + vehicle w.	EM-23	168.0	No	168.00	155445	925.3
Kmo$^{alb\text{-}cre}$	A234	Sham + vehicle w.	EM-28	168.0	No	168.00	105159	625.9
Kmo$^{alb\text{-}cre}$	A243	Sham + vehicle w.	EM-21	168.0	No	168.00	160670	956.4
Kmo$^{alb\text{-}cre}$	A252	Sham + vehicle w.	EM-25	168.0	No	168.00	178645	1063.4
Kmo$^{alb\text{-}cre}$	A253	Sham + vehicle w.	EM-24	168.0	No	168.00	142455	847.9
Kmo$^{alb\text{-}cre}$	A270	Sham + vehicle w.	EM-21	168.0	No	168.00	147469	877.8
Kmo$^{alb\text{-}cre}$	A282	Sham + vehicle w.	EM-23	168.0	No	168.00	166382	990.4

Table 102. Outcome of drinking water drug study subjects (telemetry)
Experiment 5. Oral drug. 0.5mg/ml 898 drinking. Same scales instrument for all weight measurements.

6.11. Appendix 11 – Supplementary data of experiment 5 (drug studies). Cont.

Line	ID	Gene	Sex	DOB	Pump	Pump insert	AP Date	Cull	Age (d)	Rx	Weight (g)	Telem	Group
$Kmo^{alb\text{-}cre}$	A407	Cre(+)	M	13/01/17	A (898)	30/05/17	n/a	02/06/17	137	Drug	31.10	na	Acre/ Drug
$Kmo^{alb\text{-}cre}$	A408	Cre(+)	M	13/01/17	B (V)	30/05/17	n/a	02/06/17	137	Vehicle	30.12	na	Acre/ Vehicle
$Kmo^{alb\text{-}cre}$	A409	Cre(+)	M	13/01/17	C (898)	30/05/17	n/a	02/06/17	137	Drug	26.19	na	Acre/ Drug
$Kmo^{alb\text{-}cre}$	A433	Cre(+)	M	18/01/17	L (V)	09/06/17	n/a	12/06/17	132	Vehicle	26.02	na	Acre/ Vehicle
$Kmo^{alb\text{-}cre}$	A411	Cre(+)	M	13/01/17	D (898)	30/05/17	02/06/17	09/06/17	140	AP + Drug	29.63	EM-25	Acre/ AP/ Drug
$Kmo^{alb\text{-}cre}$	A420	Cre(+)	M	16/01/17	F (898)	30/05/17	02/06/17	09/06/17	137	AP + Drug	30.39	EM-28	Acre/ AP/ Drug
$Kmo^{alb\text{-}cre}$	A430	Cre(+)	M	18/01/17	H (898)	02/06/17	05/06/17	12/06/17	138	AP + Drug	26.23	EM-24	Acre/ AP/ Drug
$Kmo^{alb\text{-}cre}$	A431	Cre(+)	M	18/01/17	J (898)	02/06/17	05/06/17	12/06/17	138	AP + Drug	26.67	EM-21	Acre/ AP/ Drug
$Kmo^{alb\text{-}cre}$	A436	Cre(+)	M	03/03/17	M (898)	16/06/17	19/06/17	26/06/17	108	AP + Drug	26.82	EM-23	Acre/ AP/ Drug
$Kmo^{alb\text{-}cre}$	A438	Cre(+)	M	03/03/17	O (898)	16/06/17	19/06/17	26/06/17	108	AP + Drug	28.35	EM-24	Acre/ AP/ Drug
$Kmo^{alb\text{-}cre}$	A452	Cre(+)	M	27/04/17	X (898)	24/06/17	27/06/17	04/07/17	61	AP + Drug	21.88	EM-24	Acre/ AP/ Drug
$Kmo^{alb\text{-}cre}$	A415	Cre(+)	M	13/01/17	E (V)	30/05/17	02/06/17	03/06/17	140	AP + V	30.12	EM-26	Acre/ AP/ Vehicle
$Kmo^{alb\text{-}cre}$	A416	Cre(+)	M	13/01/17	G (V)	30/05/17	02/06/17	09/06/17	140	AP + V	29.12	EM-27	Acre/ AP/ Vehicle
$Kmo^{alb\text{-}cre}$	A421	Cre(+)	M	16/01/17	I (V)	02/06/17	05/06/17	12/06/17	140	AP + V	30.05	EM-22	Acre/ AP/ Vehicle
$Kmo^{alb\text{-}cre}$	A432	Cre(+)	M	18/01/17	K (V)	02/06/17	05/06/17	12/06/17	138	AP + V	26.88	EM-23	Acre/ AP/ Vehicle
$Kmo^{alb\text{-}cre}$	A439	Cre(+)	M	03/03/17	P (V)	16/06/17	19/06/17	26/06/17	105	AP + V	25.59	EM-21	Acre/ AP/ Vehicle
$Kmo^{alb\text{-}cre}$	A422	Cre(+)	M	16/01/17	S (V)	17/06/17	20/06/17	27/06/17	155	AP + V	29.92	EM-27	Acre/ AP/ Vehicle
$Kmo^{alb\text{-}cre}$	A440	Cre(+)	M	03/03/17	Q (V)	17/06/17	20/06/17	27/06/17	109	AP + V	26.37	EM-26	Acre/ AP/ Vehicle
$Kmo^{alb\text{-}cre}$	A449	Cre(+)	M	27/04/17	Y (V)	24/06/17	27/06/17	04/07/17	61	AP + V	24.76	EM-23	Acre/ AP/ Vehicle
$Kmo^{alb\text{-}cre}$	A450	Cre(+)	M	27/04/17	Z (V)	24/06/17	27/06/17	28/06/17	61	AP + V	24.21	EM-21	Acre/ AP/ Vehicle
$Kmo^{alb\text{-}cre}$	A451	Cre(+)	M	27/04/17	A2 (V)	24/06/17	27/06/17	04/07/17	61	AP + V	23.11	EM-22	Acre/ AP/ Vehicle

Table 103. Minipump drug study subjects
Drug: KMO inhibitor GSK898 250mg/ml in 50:50 DMSO:PEG; Vehicle: 50:50 DMSO:PEG, no drug.
Nb. A445 (pump R, 898) excluded due to operative failure and underwent schedule 1 cull (20/06/17).

Line	ID	Pump	Group	Weight (g)	End weight (g)	Weight loss (%)	Survival
$Kmo^{alb\text{-}cre}$	A411	D (898)	Acre/ AP/ Drug	29.63	27.54	7.05	168.0
$Kmo^{alb\text{-}cre}$	A420	F (898)	Acre/ AP/ Drug	30.39	29.96	1.41	168.0
$Kmo^{alb\text{-}cre}$	A430	H (898)	Acre/ AP/ Drug	26.23	26.49	Gain 0.99	168.0
$Kmo^{alb\text{-}cre}$	A431	J (898)	Acre/ AP/ Drug	26.67	24.35	8.70	168.0
$Kmo^{alb\text{-}cre}$	A436	M (898)	Acre/ AP/ Drug	26.82	22.19	17.26	166.8
$Kmo^{alb\text{-}cre}$	A438	O (898)	Acre/ AP/ Drug	28.35	28.04	1.09	168.0
$Kmo^{alb\text{-}cre}$	A452	X (898)	Acre/ AP/ Drug	21.88	19.83	9.37	168.0
$Kmo^{alb\text{-}cre}$	A415	E (V)	Acre/ AP/ Vehicle	30.12	28.96	3.85	23.5
$Kmo^{alb\text{-}cre}$	A416	G (V)	Acre/ AP/ Vehicle	29.12	25.05	13.98	168.0
$Kmo^{alb\text{-}cre}$	A421	I (V)	Acre/ AP/ Vehicle	30.05	28.57	4.93	168.0
$Kmo^{alb\text{-}cre}$	A432	K (V)	Acre/ AP/ Vehicle	26.88	25.30	5.88	168.0
$Kmo^{alb\text{-}cre}$	A439	P (V)	Acre/ AP/ Vehicle	25.59	22.20	13.25	168.0
$Kmo^{alb\text{-}cre}$	A422	S (V)	Acre/ AP/ Vehicle	29.92	23.95	19.95	168.0
$Kmo^{alb\text{-}cre}$	A440	Q (V)	Acre/ AP/ Vehicle	26.37	23.17	12.14	168.0
$Kmo^{alb\text{-}cre}$	A449	Y (V)	Acre/ AP/ Vehicle	24.76	22.40	9.53	168.0
$Kmo^{alb\text{-}cre}$	A450	Z (V)	Acre/ AP/ Vehicle	24.21	22.32	7.81	28.9
$Kmo^{alb\text{-}cre}$	A451	A2 (V)	Acre/ AP/ Vehicle	23.11	18.71	19.04	168.0

Table 104. Outcome of minipump drug study subjects (survival and weight loss)
Drug: KMO inhibitor GSK898 250mg/ml in 50:50 DMSO:PEG; Vehicle: 50:50 DMSO:PEG, no drug.
Nb. A445 (pump R, 898) excluded due to operative failure and underwent schedule 1 cull (20/06/17).

6.11. Appendix 11 – Supplementary data of experiment 5 (drug studies). Cont.

Line	ID	Pump	Group	Telem	Survival	Humane endpoint	Telemetry time	Activity Total	Activity / hr
$Kmo^{alb\text{-}cre}$	A411	D (898)	Acre/ AP/ Drug	EM-25	168.0	No	168.00	149803	**891.7**
$Kmo^{alb\text{-}cre}$	A420	F (898)	Acre/ AP/ Drug	EM-28	168.0	No	168.00	125734	**748.4**
$Kmo^{alb\text{-}cre}$	A430	H (898)	Acre/ AP/ Drug	EM-24	168.0	No	168.00	111544	**664.0**
$Kmo^{alb\text{-}cre}$	A431	J (898)	Acre/ AP/ Drug	EM-21	168.0	No	168.00	61034	**363.3**
$Kmo^{alb\text{-}cre}$	A436	M (898)	Acre/ AP/ Drug	EM-23	**166.8**	**Yes**	165.17	81721	**494.8**
$Kmo^{alb\text{-}cre}$	A438	O (898)	Acre/ AP/ Drug	EM-24	168.0	No	168.00	112290	**668.4**
$Kmo^{alb\text{-}cre}$	A452	X (898)	Acre/ AP/ Drug	EM-24	168.0	No	168.00	63091	**375.5**
$Kmo^{alb\text{-}cre}$	A415	E (V)	Acre/ AP/ Vehicle	EM-26	**23.5**	**Yes**	**21.43**	5974	**278.8**
$Kmo^{alb\text{-}cre}$	A416	G (V)	Acre/ AP/ Vehicle	EM-27	168.0	No	168.00	65485	**389.8**
$Kmo^{alb\text{-}cre}$	A421	I (V)	Acre/ AP/ Vehicle	EM-22	168.0	No	168.00	123059	**732.5**
$Kmo^{alb\text{-}cre}$	A432	K (V)	Acre/ AP/ Vehicle	EM-23	168.0	No	168.00	106879	**636.2**
$Kmo^{alb\text{-}cre}$	A439	P (V)	Acre/ AP/ Vehicle	EM-21	168.0	No	168.00	120473	**717.1**
$Kmo^{alb\text{-}cre}$	A422	S (V)	Acre/ AP/ Vehicle	EM-27	168.0	No	168.00	74368	**442.7**
$Kmo^{alb\text{-}cre}$	A440	Q (V)	Acre/ AP/ Vehicle	EM-26	168.0	No	168.00	81593	**485.7**
$Kmo^{alb\text{-}cre}$	A449	Y (V)	Acre/ AP/ Vehicle	EM-23	168.0	No	168.00	77597	**461.9**
$Kmo^{alb\text{-}cre}$	A450	Z (V)	Acre/ AP/ Vehicle	EM-21	**28.9**	**Yes**	**26.91**	11086	**426.4**
$Kmo^{alb\text{-}cre}$	A451	A2 (V)	Acre/ AP/ Vehicle	EM-22	168.0	No	168.00	26542	**158.0**

Table 105. Outcome of minipump drug study subjects (telemetry)
Drug: KMO inhibitor GSK898 250mg/ml in 50:50 DMSO:PEG; Vehicle: 50:50 DMSO:PEG, no drug

Line	ID	Pump	Group	Survival	[3HK] uM No IS	[Kyn] ng/ml IS=13C6Kyn	[GSK] ng/ml IS D5-Trp LOD 10ng/ml	3HAA 13C63HK	XA IS D5-Trp
$Kmo^{alb\text{-}cre}$	A411	D (898)	Acre/ AP/ Drug	168.0	0.2715	3224.24	34206.1	88.47	BLQ
$Kmo^{alb\text{-}cre}$	A420	F (898)	Acre/ AP/ Drug	168.0	0.2009	6206.58	46279.9	185.61	0.87
$Kmo^{alb\text{-}cre}$	A430	H (898)	Acre/ AP/ Drug	168.0	0.3775	3830.42	87936.1	156.65	2.14
$Kmo^{alb\text{-}cre}$	A431	J (898)	Acre/ AP/ Drug	168.0	0.2822	5884.33	35532.6	41.30	BLQ
$Kmo^{alb\text{-}cre}$	A436	M (898)	Acre/ AP/ Drug	**166.8**	0.0297	14008.72	3827.2	85.99	25.13
$Kmo^{alb\text{-}cre}$	A438	O (898)	Acre/ AP/ Drug	168.0	0.3336	6931.66	32148.5	47.89	0.87
$Kmo^{alb\text{-}cre}$	A452	X (898)	Acre/ AP/ Drug	168.0	0.2866	3463.10	111982.4	130.64	13.48
$Kmo^{alb\text{-}cre}$	A415	E (V)	Acre/ AP/ Vehicle	**23.5**	19.0379	4989.31	73.3	30.56	41.72
$Kmo^{alb\text{-}cre}$	A416	G (V)	Acre/ AP/ Vehicle	168.0	5.0223	2667.72	50.9	27.81	30.29
$Kmo^{alb\text{-}cre}$	A421	I (V)	Acre/ AP/ Vehicle	168.0	4.2415	5604.92	306.2	45.42	176.22
$Kmo^{alb\text{-}cre}$	A432	K (V)	Acre/ AP/ Vehicle	168.0	4.8599	3185.37	140.4	26.21	109.71
$Kmo^{alb\text{-}cre}$	A439	P (V)	Acre/ AP/ Vehicle	168.0	3.1421	3362.73	231.2	25.41	137.91
$Kmo^{alb\text{-}cre}$	A422	S (V)	Acre/ AP/ Vehicle	168.0	1.6650	5776.76	101.6	48.4	36.2
$Kmo^{alb\text{-}cre}$	A440	Q (V)	Acre/ AP/ Vehicle	168.0	5.0913	1174.14	125.5	21.72	21.93
$Kmo^{alb\text{-}cre}$	A449	Y (V)	Acre/ AP/ Vehicle	168.0	1.3855	1877.31	86.8	10	58.77
$Kmo^{alb\text{-}cre}$	A450	Z (V)	Acre/ AP/ Vehicle	**28.9**	16.2600	2005.70	145.3	53.51	11.92
$Kmo^{alb\text{-}cre}$	A451	A2 (V)	Acre/ AP/ Vehicle	168.0	0.9752	3458.32	90.0	26.15	22.27

Table 106. Outcome of minipump drug study subjects (3HK levels and drug levels)
Drug: KMO inhibitor GSK898 250mg/ml in 50:50 DMSO:PEG; Vehicle: 50:50 DMSO:PEG, no drug

6.12. Appendix 12 – Supplementary data of experiment 6 (*invitro* studies)

Interleukin-1β		**Caspase 3/7 activity / Luminescence (x10^5)**									
		Controls				**Metabolite**					
[Metabolite]	**[Cytokine]**	**Cytokine**	**+ve. Stauro.**	**No DMSO**	**No caspase**	**Trp**	**Kyn**	**KA**	**3HK**	**3HAA**	**XA**
		No Metabolite				Plate 1 Plate 2 Plate 3	Plate 1 Plate 2 Plate 3	Plate 1 Plate 2 Plate 3	Plate 1 Plate 2 Plate 3	Plate 1 Plate 2 Plate 3	Plate 1 Plate 2 Plate 3
		(P1, A) (P2, A) (P3, A) (P1, B) (P2, B) (P3, B)	(P1, F11) (P2, F11) (P3, F11) (P1, F12) (P2, F12) (P3, F12)	P1, H5 P1, H5 P3, H5	P1, H3 P2, H3 P3, H3						
100 µM	**0 pg/ml**	4.52084	13.78157	3.58971	0.00007	3.16975	3.71743	4.76679	2.85021	2.17355	2.92596
		3.54205	14.02375								
		4.13316	11.65738	3.79708	0.00070	4.16655	3.62444	3.92738	3.23780	2.48706	4.58372
		4.23459	13.18513								
		3.33285	13.16687	Error*	0.00049	3.91954	3.44549	3.41860	2.74952	3.33698	3.78585
		4.01575	15.26739								
100 µM	**1 pg/ml**	3.72346	As above			3.44454	3.11726	2.99124	2.74328	2.46221	2.75512
		3.86202									
		4.27233				3.13239	3.03451	3.64647	3.79803	3.17261	3.85693
		3.06752									
		3.95949				3.31009	3.37742	3.41638	2.49636	3.66511	3.77515
		4.84858									
100 µM	**10 pg/ml**	4.43283	As above			4.78843	3.71266	3.10181	3.23441	1.93265	2.73270
		3.63376									
		4.45128				4.39572	4.51193	4.47545	4.16686	2.81943	4.19463
		4.55265									
		4.31155				4.80572	3.94645	4.51023	3.61385	2.86270	4.24551
		4.43527									
100 µM	**100 pg/ml**	10.21961	As above			5.24249	5.08636	4.85346	4.06290	3.56704	3.41966
		5.99530									
		6.52227				5.34770	6.92992	5.91316	5.48743	4.11546	5.54658
		4.15998									
		6.52642				6.73819	5.71832	6.64607	5.52757	4.77803	5.76857
		7.14841									
500 µM	**0 pg/ml**	4.52084	As above			4.02666	3.39076	3.78702	1.30586	1.31768	2.79024
		3.54205									
		4.13316				4.04478	3.40050	4.21085	1.10663	1.93656	4.45393
		4.23459									
		3.33285				3.97750	3.72198	4.38820	1.61654	1.31019	3.59489
		4.01575									
500 µM	**1 pg/ml**	3.72346	As above			3.73670	3.82197	4.12373	2.04960	1.78012	2.98785
		3.86202									
		4.27233				5.08244	4.02719	5.14803	3.67496	1.82406	4.32427
		3.06752									
		3.95949				4.46899	4.12045	4.59708	1.54749	1.68085	4.07011
		4.84858									
500 µM	**10 pg/ml**	4.43283	As above			5.57546	3.64308	4.29660	13.29273	2.31496	3.18012
		3.63376									
		4.45128				3.45513	7.02186	5.15471	18.43147	3.25505	4.88688
		4.55265									
		4.31155				4.92433	4.30773	4.29088	15.01336	2.51909	4.61130
		4.43527									
500 µM	**100 pg/ml**	10.21961	As above			5.87821	4.70092	8.54789	18.69304	4.75989	4.04891
		5.99530									
		6.52227				6.96195	6.28324	7.59733	17.87523	7.29842	6.25252
		4.15998									
		6.52642				7.11467	5.55263	7.28606	16.47507	4.57057	6.00402
		7.14841									

Table 107. Endothelial cell caspase 3/7 study – interleukin 1 beta
17th May 2017. 6000 cells per well HMVEC-L. EBM-2. Read at 90mins

6.12. Appendix 12 – Supplementary data of experiment 7. Cont.

IL6		**Caspase 3/7 activity / Luminescence (x10^5)**									
		Controls				**Metabolite**					
[Metabolite]	**[Cytokine]**	**Cytokine**	**+ve Stauro.**	**No DMSO**	**No caspase**	**Trp**	**Kyn**	**KA**	**3HK**	**3HAA**	**XA**
		No Metabolite									
		Plate1 Plate 2 Plate 3	Plate 1 Plate 2 Plate 3	Plate 1 Plate 2 Plate 3	Plate 1 Plate 2 Plate 3	Plate 1 Plate 2 Plate 3	Plate 1 Plate 2 Plate 3	Plate 1 Plate 2 Plate 3	Plate 1 Plate 2 Plate 3	Plate 1 Plate 2 Plate 3	Plate 1 Plate 2 Plate 3
100 µM	**0 ng/ml**	1.45951	6.11164	1.41043	0.00014	1.29548	1.44843	1.86533	1.56973	1.19997	1.60943
		1.18422	6.98263	1.11637	0.00010	1.25091	1.41314	1.52177	1.47215	0.98227	1.29450
		1.20240	7.03619	1.13740	-0.00007	1.25158	1.26066	1.38773	1.44231	0.97883	1.20314
100 µM	**100 ng/ml**	1.30245	As above	As above	As above	1.23807	1.20071	1.75907	1.61936	1.11355	1.62422
		1.62154				1.25809	1.36754	1.34157	1.29555	0.94778	1.34147
		1.23227				1.19269	1.40536	1.21116	1.40198	0.94507	1.14247
500 µM	**0 ng/ml**	1.45951	As above	As above	As above	1.82984	1.39396	1.33475	2.94793	1.32535	1.56984
		1.18422				1.37598	1.44966	1.12185	2.20497	1.05591	1.17240
		1.20240				1.37222	1.48105	1.45962	2.25986	1. 64428	1.07568
500 µM	**100 ng/ml**	1.30245	As above	As above	As above	1.38340	1.88518	1.55738	1.62760	1.68145	1.36314
		1.62154				1.35846	1.14982	1.28088	1.69102	1.04758	1.22854
		1.23227				1.45994	1.51737	1.34351	1.91349	1.64534	1.08422

Table 108. Endothelial cell caspase 3/7 study – interleukin 6

Staurosporin 10 µM was used for positive control for caspase 3/7 activation. 5000 cells per well HMVEC-L. EBM-2. Read at 90mins.

6.12. Appendix 12 – Supplementary data of experiment 7. Cont.

IL10		**Caspase 3/7 activity / Luminescence (x10^5)**									
		Controls				**Metabolite**					
[Metabolite]	**[Cytokine]**	**Cytokine**	**+ve. Stauro.**	**No DMSO**	**No caspase**	**Trp**	**Kyn**	**KA**	**3HK**	**3HAA**	**XA**
		No Metabolite				Plate 1 Plate 2 Plate 3	Plate 1 Plate 2 Plate 3	Plate 1 Plate 2 Plate 3	Plate 1 Plate 2 Plate 3	Plate 1 Plate 2 Plate 3	Plate 1 Plate 2 Plate 3
		Plate1 Plate 2 Plate 3	Plate1 Plate 2 Plate 3	Plate 1 Plate 2 Plate 3	Plate1 Plate 2 Plate 3						
100 µM	**0 ng/ml**	1.45951	6.11164	1.41043	0.00014	1.29548	1.44843	1.86533	1.56973	1.19997	1.60943
		1.18422	6.98263	1.11637	0.00010	1.25091	1.41314	1.52177	1.47215	0.98227	1.29450
		1.20240	7.03619	1.13740	-0.00007	1.25158	1.26066	1.38773	1.44231	0.97883	1.20314
100 µM	**100 ng/ml**	1.53215	As above	As above	As above	1.48327	1.43523	1.79836	1.63900	1.32176	1.59740
		1.19456				1.38569	1.31803	1.33914	1.31265	1.26431	1.12407
		1.30182				1.28408	1.36905	1.25063	1.44970	0.90562	1.26572
500 µM	**0 ng/ml**	1.45951	As above	As above	As above	1.82984	1.39396	1.33475	2.94793	1.32535	1.56984
		1.18422				1.37598	1.44966	1.12185	2.20497	1.05591	1.17240
		1.20240				1.37222	1.48105	1.45962	2.25986	1. 64428	1.07568
500 µM	**100 ng/ml**	1.53215	As above	As above	As above	1.38668	1.36155	1.41497	1.68525	1.60162	1.53838
		1.19456				1.45768	1.40068	1.70539	1.86011	1.01055	1.15900
		1.30182				1.47567	1.58399	1.68472	1.71915	1.23237	1.10838

Table 109. Endothelial cell caspase 3/7 study – interleukin 10

Staurosporin 10 µM was used for positive control for caspase 3/7 activation. 5000 cells per well HMVEC-L. EBM-2. Read at 90mins

6.12. Appendix 12 – Supplementary data of experiment 7. Cont.

Name	Metabolite	Cytokine	+ve Control (Staurosporin)	-ve Control (No caspase)	Linear ($R=1^2$)	Count	% Caspase of Controls
TRP 500	TRP 500 µM	0	611164	14	$y = 6111.5x + 14$	182984	**29.9386403**
TRP 100	TRP 100 µM	0	611164	14	$y = 6111.5x + 14$	129548	**21.1951239**
TRP 500 + 100 ng/ml IL6	TRP 500 µM	100 ng/ml IL6	611164	14	$y = 6111.5x + 14$	138340	**22.6337233**
TRP 100 + 100 ng/ml IL6	TRP 100 µM	100 ng/ml IL6	611164	14	$y = 6111.5x + 14$	123807	**20.2557474**
TRP 500 + 100 ng/ml IL10	TRP 500 µM	100 ng/ml IL10	611164	14	$y = 6111.5x + 14$	138668	**22.6873926**
TRP 100 + 100 ng/ml IL10	TRP 100 µM	100 ng/ml IL10	611164	14	$y = 6111.5x + 14$	148327	**24.2678557**
KYN 500	KYN 500 µM	0	611164	14	$y = 6111.5x + 14$	139396	**22.8065123**
KYN 100	KYN 100 µM	0	611164	14	$y = 6111.5x + 14$	144843	**23.6977829**
KYN 500 + 100 ng/ml IL6	KYN 500 µM	100 ng/ml IL6	611164	14	$y = 6111.5x + 14$	188518	**30.8441463**
KYN 100 + 100 ng/ml IL6	KYN 100 µM	100 ng/ml IL6	611164	14	$y = 6111.5x + 14$	120071	**19.6444408**
KYN 500 + 100 ng/ml IL10	KYN 500 µM	100 ng/ml IL10	611164	14	$y = 6111.5x + 14$	136155	**22.2762006**
KYN 100 + 100 ng/ml IL10	KYN 100 µM	100 ng/ml IL10	611164	14	$y = 6111.5x + 14$	143523	**23.4817966**
KA 500	KA 500 µM	0	611164	14	$y = 6111.5x + 14$	133475	**21.8376831**
KA 100	KA 100 µM	0	611164	14	$y = 6111.5x + 14$	186533	**30.5193488**
KA 500 + 100 ng/ml IL6	KA 500 µM	100 ng/ml IL6	611164	14	$y = 6111.5x + 14$	155738	**25.4804876**
KA 100 + 100 ng/ml IL6	KA 100 µM	100 ng/ml IL6	611164	14	$y = 6111.5x + 14$	175907	**28.7806594**
KA 500 + 100 ng/ml IL10	KA 500 µM	100 ng/ml IL10	611164	14	$y = 6111.5x + 14$	141497	**23.1502904**
KA 100 + 100 ng/ml IL10	KA 100 µM	100 ng/ml IL10	611164	14	$y = 6111.5x + 14$	179836	**29.4235458**
3HK 500	3HK 500 µM	0	611164	14	$y = 6111.5x + 14$	294793	**48.2334942**
3HK 100	3HK 100 µM	0	611164	14	$y = 6111.5x + 14$	156973	**25.6825657**
3HK 500 + 100 ng/ml IL6	3HK 500 µM	100 ng/ml IL6	611164	14	$y = 6111.5x + 14$	162760	**26.6294690**
3HK 100 + 100 ng/ml IL6	3HK 100 µM	100 ng/ml IL6	611164	14	$y = 6111.5x + 14$	161936	**26.4946413**
3HK 500 + 100 ng/ml IL10	3HK 500 µM	100 ng/ml IL10	611164	14	$y = 6111.5x + 14$	168525	**27.5727726**
3HK 100 + 100 ng/ml IL10	3HK 100 µM	100 ng/ml IL10	611164	14	$y = 6111.5x + 14$	163900	**26.8160026**
3HAA 500	3HAA 500 µM	0	611164	14	$y = 6111.5x + 14$	132535	**21.6838747**
3HAA 100	3HAA 100 µM	0	611164	14	$y = 6111.5x + 14$	119997	**19.6323325**
3HAA 500 + 100 ng/ml IL6	3HAA 500 µM	100 ng/ml IL6	611164	14	$y = 6111.5x + 14$	168145	**27.5105948**
3HAA 100 + 100 ng/ml IL6	3HAA 100 µM	100 ng/ml IL6	611164	14	$y = 6111.5x + 14$	111355	**18.2182770**
3HAA 500 + 100 ng/ml IL10	3HAA 500 µM	100 ng/ml IL10	611164	14	$y = 6111.5x + 14$	160162	**26.2043688**
3HAA 100 + 100 ng/ml IL10	3HAA 100 µM	100 ng/ml IL10	611164	14	$y = 6111.5x + 14$	132176	**21.6251329**
XA 500	XA 500 µM	0	611164	14	$y = 6111.5x + 14$	156984	**25.6843655**
XA 100	XA 100 µM	0	611164	14	$y = 6111.5x + 14$	160943	**26.3321607**
XA 500 + 100 ng/ml IL6	XA 500 µM	100 ng/ml IL6	611164	14	$y = 6111.5x + 14$	136314	**22.3022171**
XA 100 + 100 ng/ml IL6	XA 100 µM	100 ng/ml IL6	611164	14	$y = 6111.5x + 14$	162422	**26.5741635**
XA 500 + 100 ng/ml IL10	XA 500 µM	100 ng/ml IL10	611164	14	$y = 6111.5x + 14$	153838	**25.1695983**
XA 100 + 100 ng/ml IL10	XA 100 µM	100 ng/ml IL10	611164	14	$y = 6111.5x + 14$	159740	**26.1353187**
TRP 500	TRP 500 µM	0	698263	10	$y = 6982.5x + 10$	137598	**19.704690**
TRP 100	TRP 100 µM	0	698263	10	$y = 6982.5x + 10$	125091	**17.913498**
TRP 500 + 100 ng/ml IL6	TRP 500 µM	100 ng/ml IL6	698263	10	$y = 6982.5x + 10$	135846	**19.453777**
TRP 100 + 100 ng/ml IL6	TRP 100 µM	100 ng/ml IL6	698263	10	$y = 6982.5x + 10$	125809	**18.016327**
TRP 500 + 100 ng/ml IL10	TRP 500 µM	100 ng/ml IL10	698263	10	$y = 6982.5x + 10$	145768	**20.874758**
TRP 100 + 100 ng/ml IL10	TRP 100 µM	100 ng/ml IL10	698263	10	$y = 6982.5x + 10$	138569	**19.843752**
KYN 500	KYN 500 µM	0	698263	10	$y = 6982.5x + 10$	144966	**20.759900**
KYN 100	KYN 100 µM	0	698263	10	$y = 6982.5x + 10$	141314	**20.236878**
KYN 500 + 100 ng/ml IL6	KYN 500 µM	100 ng/ml IL6	698263	10	$y = 6982.5x + 10$	114982	**16.465736**
KYN 100 + 100 ng/ml IL6	KYN 100 µM	100 ng/ml IL6	698263	10	$y = 6982.5x + 10$	136754	**19.058432**
KYN 500 + 100 ng/ml IL10	KYN 500 µM	100 ng/ml IL10	698263	10	$y = 6982.5x + 10$	140068	**20.068432**
KYN 100 + 100 ng/ml IL10	KYN 100 µM	100 ng/ml IL10	698263	10	$y = 6982.5x + 10$	131803	**18.874758**
KA 500	KA 500 µM	0	698263	10	$y = 6982.5x + 10$	112185	**16.065163**
KA 100	KA 100 µM	0	698263	10	$y = 6982.5x + 10$	152177	**21.792624**
KA 500 + 100 ng/ml IL6	KA 500 µM	100 ng/ml IL6	698263	10	$y = 6982.5x + 10$	128088	**18.342714**
KA 100 + 100 ng/ml IL6	KA 100 µM	100 ng/ml IL6	698263	10	$y = 6982.5x + 10$	134157	**19.211887**
KA 500 + 100 ng/ml IL10	KA 500 µM	100 ng/ml IL10	698263	10	$y = 6982.5x + 10$	170539	**24.422342**
KA 100 + 100 ng/ml IL10	KA 100 µM	100 ng/ml IL10	698263	10	$y = 6982.5x + 10$	133914	**19.177086**
3HK 500	3HK 500 µM	0	698263	10	$y = 6982.5x + 10$	220497	**31.577086**
3HK 100	3HK 100 µM	0	698263	10	$y = 6982.5x + 10$	147215	**21.081991**
3HK 500 + 100 ng/ml IL6	3HK 500 µM	100 ng/ml IL6	698263	10	$y = 6982.5x + 10$	169102	**24.216541**
3HK 100 + 100 ng/ml IL6	3HK 100 µM	100 ng/ml IL6	698263	10	$y = 6982.5x + 10$	129555	**18.552811**
3HK 500 + 100 ng/ml IL10	3HK 500 µM	100 ng/ml IL10	698263	10	$y = 6982.5x + 10$	186011	**26.638167**
3HK 100 + 100 ng/ml IL10	3HK 100 µM	100 ng/ml IL10	698263	10	$y = 6982.5x + 10$	131265	**18.797709**
3HAA 500	3HAA 500 µM	0	698263	10	$y = 6982.5x + 10$	105591	**15.120802**
3HAA 100	3HAA 100 µM	0	698263	10	$y = 6982.5x + 10$	098227	**14.066165**
3HAA 500 + 100 ng/ml IL6	3HAA 500 µM	100 ng/ml IL6	698263	10	$y = 6982.5x + 10$	104758	**15.001504**
3HAA 100 + 100 ng/ml IL6	3HAA 100 µM	100 ng/ml IL6	698263	10	$y = 6982.5x + 10$	094778	**13.572216**
3HAA 500 + 100 ng/ml IL10	3HAA 500 µM	100 ng/ml IL10	698263	10	$y = 6982.5x + 10$	101055	**14.471178**
3HAA 100 + 100 ng/ml IL10	3HAA 100 µM	100 ng/ml IL10	698263	10	$y = 6982.5x + 10$	126431	**18.105406**
XA 500	XA 500 µM	0	698263	10	$y = 6982.5x + 10$	117240	**16.789116**
XA 100	XA 100 µM	0	698263	10	$y = 6982.5x + 10$	129450	**18.537773**
XA 500 + 100 ng/ml IL6	XA 500 µM	100 ng/ml IL6	698263	10	$y = 6982.5x + 10$	122854	**17.593126**
XA 100 + 100 ng/ml IL6	XA 100 µM	100 ng/ml IL6	698263	10	$y = 6982.5x + 10$	134147	**19.210455**
XA 500 + 100 ng/ml IL10	XA 500 µM	100 ng/ml IL10	698263	10	$y = 6982.5x + 10$	115900	**16.597207**
XA 100 + 100 ng/ml IL10	XA 100 µM	100 ng/ml IL10	698263	10	$y = 6982.5x + 10$	112407	**16.096957**

TRP 500	TRP 500 µM	0	703619	-7	$y = 7036.3x - 7$	137222	**19.5030058**
TRP 100	TRP 100 µM	0	703619	-7	$y = 7036.3x - 7$	125158	**17.7884684**
TRP 500 + 100 ng/ml IL6	TRP 500 µM	100 ng/ml IL6	703619	-7	$y = 7036.3x - 7$	145994	**20.7496838**
TRP 100 + 100 ng/ml IL6	TRP 100 µM	100 ng/ml IL6	703619	-7	$y = 7036.3x - 7$	119269	**16.9515228**
TRP 500 + 100 ng/ml IL10	TRP 500 µM	100 ng/ml IL10	703619	-7	$y = 7036.3x - 7$	147567	**20.9732388**
TRP 100 + 100 ng/ml IL10	TRP 100 µM	100 ng/ml IL10	703619	-7	$y = 7036.3x - 7$	128408	**18.2503589**
KYN 500	KYN 500 µM	0	703619	-7	$y = 7036.3x - 7$	148105	**21.0496994**
KYN 100	KYN 100 µM	0	703619	-7	$y = 7036.3x - 7$	126066	**17.9175135**
KYN 500 + 100 ng/ml IL6	KYN 500 µM	100 ng/ml IL6	703619	-7	$y = 7036.3x - 7$	151737	**21.5658798**
KYN 100 + 100 ng/ml IL6	KYN 100 µM	100 ng/ml IL6	703619	-7	$y = 7036.3x - 7$	140536	**19.9739920**
KYN 500 + 100 ng/ml IL10	KYN 500 µM	100 ng/ml IL10	703619	-7	$y = 7036.3x - 7$	158399	**22.5126842**
KYN 100 + 100 ng/ml IL10	KYN 100 µM	100 ng/ml IL10	703619	-7	$y = 7036.3x - 7$	136905	**19.4579538**
KA 500	KA 500 µM	0	703619	-7	$y = 7036.3x - 7$	145962	**20.7451359**
KA 100	KA 100 µM	0	703619	-7	$y = 7036.3x - 7$	138773	**19.7234342**
KA 500 + 100 ng/ml IL6	KA 500 µM	100 ng/ml IL6	703619	-7	$y = 7036.3x - 7$	134351	**19.0949789**
KA 100 + 100 ng/ml IL6	KA 100 µM	100 ng/ml IL6	703619	-7	$y = 7036.3x - 7$	121116	**17.2140187**
KA 500 + 100 ng/ml IL10	KA 500 µM	100 ng/ml IL10	703619	-7	$y = 7036.3x - 7$	168472	**23.9442605**
KA 100 + 100 ng/ml IL10	KA 100 µM	100 ng/ml IL10	703619	-7	$y = 7036.3x - 7$	125063	**17.7749670**
3HK 500	3HK 500 µM	0	703619	-7	$y = 7036.3x - 7$	225986	**32.1181587**
3HK 100	3HK 100 µM	0	703619	-7	$y = 7036.3x - 7$	144231	**20.4991260**
3HK 500 + 100 ng/ml IL6	3HK 500 µM	100 ng/ml IL6	703619	-7	$y = 7036.3x - 7$	191349	**27.1955431**
3HK 100 + 100 ng/ml IL6	3HK 100 µM	100 ng/ml IL6	703619	-7	$y = 7036.3x - 7$	140198	**19.9259554**
3HK 500 + 100 ng/ml IL10	3HK 500 µM	100 ng/ml IL10	703619	-7	$y = 7036.3x - 7$	171915	**24.4335801**
3HK 100 + 100 ng/ml IL10	3HK 100 µM	100 ng/ml IL10	703619	-7	$y = 7036.3x - 7$	144970	**20.6041528**
3HAA 500	3HAA 500 µM	0	703619	-7	$y = 7036.3x - 7$	164428	**23.3695266**
3HAA 100	3HAA 100 µM	0	703619	-7	$y = 7036.3x - 7$	097883	**13.9121413**
3HAA 500 + 100 ng/ml IL6	3HAA 500 µM	100 ng/ml IL6	703619	-7	$y = 7036.3x - 7$	164534	**23.3845913**
3HAA 100 + 100 ng/ml IL6	3HAA 100 µM	100 ng/ml IL6	703619	-7	$y = 7036.3x - 7$	094507	**13.4323437**
3HAA 500 + 100 ng/ml IL10	3HAA 500 µM	100 ng/ml IL10	703619	-7	$y = 7036.3x - 7$	123237	**17.5154556**
3HAA 100 + 100 ng/ml IL10	3HAA 100 µM	100 ng/ml IL10	703619	-7	$y = 7036.3x - 7$	090562	**12.8716797**
XA 500	XA 500 µM	0	703619	-7	$y = 7036.3x - 7$	107568	**15.2885750**
XA 100	XA 100 µM	0	703619	-7	$y = 7036.3x - 7$	120314	**17.1000384**
XA 500 + 100 ng/ml IL6	XA 500 µM	100 ng/ml IL6	703619	-7	$y = 7036.3x - 7$	108422	**15.4099456**
XA 100 + 100 ng/ml IL6	XA 100 µM	100 ng/ml IL6	703619	-7	$y = 7036.3x - 7$	114247	**16.2377954**
XA 500 + 100 ng/ml IL10	XA 500 µM	100 ng/ml IL10	703619	-7	$y = 7036.3x - 7$	110838	**15.7533078**
XA 100 + 100 ng/ml IL10	XA 100 µM	100 ng/ml IL10	703619	-7	$y = 7036.3x - 7$	126572	**17.9894263**
TRP 500	TRP 500 µM	0	1348335	7	$y = 13483x + 7$	402666	**29.8641994**
TRP 100	TRP 100 µM	0	1348335	7	$y = 13483x + 7$	316975	**23.5087147**
TRP 500 + 10 pg/ml IL1β	TRP 500 µM	10 IL1β	1348335	7	$y = 13483x + 7$	557546	**41.3512571**
TRP 100 + 10 pg/ml IL1β	TRP 100 µM	10 IL1β	1348335	7	$y = 13483x + 7$	478843	**35.5140547**
TRP 500 + 100 pg/ml IL1β	TRP 500 µM	100 IL1β	1348335	7	$y = 13483x + 7$	587821	**43.5966773**
TRP 100 + 100 pg/ml IL1β	TRP 100 µM	100 IL1β	1348335	7	$y = 13483x + 7$	524249	**38.8817029**
KYN 500	KYN 500 µM	0	1348335	7	$y = 13483x + 7$	339076	**25.1478899**
KYN 100	KYN 100 µM	0	1348335	7	$y = 13483x + 7$	371743	**27.5707187**
KYN 500 + 10 pg/ml IL1β	KYN 500 µM	10 pg/ml IL1β	1348335	7	$y = 13483x + 7$	364308	**27.0192835**
KYN 100 + 10 pg/ml IL1β	KYN 100 µM	10 pg/ml IL1β	1348335	7	$y = 13483x + 7$	371266	**27.5353408**
KYN 500 + 100 pg/ml IL1β	KYN 500 µM	100 pg/ml IL1β	1348335	7	$y = 13483x + 7$	470092	**34.8650152**
KYN 100 + 100 pg/ml IL1β	KYN 100 µM	100 pg/ml IL1β	1348335	7	$y = 13483x + 7$	508636	**37.7237262**
KA 500	KA 500 µM	0	1348335	7	$y = 13483x + 7$	378702	**28.0868501**
KA 100	KA 100 µM	0	1348335	7	$y = 13483x + 7$	476679	**35.3535563**
KA 500 + 10 pg/ml IL1β	KA 500 µM	10 pg/ml IL1β	1348335	7	$y = 13483x + 7$	429660	**31.8662761**
KA 100 + 10 pg/ml IL1β	KA 100 µM	10 pg/ml IL1β	1348335	7	$y = 13483x + 7$	310181	**23.0048209**
KA 500 + 100 pg/ml IL1β	KA 500 µM	100 pg/ml IL1β	1348335	7	$y = 13483x + 7$	854789	**63.3970185**
KA 100 + 100 pg/ml IL1β	KA 100 µM	100 pg/ml IL1β	1348335	7	$y = 13483x + 7$	485346	**35.9963658**
3HK 500	3HK 500 µM	0	1348335	7	$y = 13483x + 7$	130586	**9.68471408**
3HK 100	3HK 100 µM	0	1348335	7	$y = 13483x + 7$	285021	**21.1387673**
3HK 500 + 10 pg/ml IL1β	3HK 500 µM	10 pg/ml IL1β	1348335	7	$y = 13483x + 7$	1329273	**98.5882964**
3HK 100 + 10 pg/ml IL1β	3HK 100 µM	10 pg/ml IL1β	1348335	7	$y = 13483x + 7$	323441	**23.9882815**
3HK 500 + 100 pg/ml IL1β	3HK 500 µM	100 pg/ml IL1β	1348335	7	$y = 13483x + 7$	1869304	**138.641029**
3HK 100 + 100 pg/ml IL1β	3HK 100 µM	100 pg/ml IL1β	1348335	7	$y = 13483x + 7$	406290	**30.1329823**
3HAA 500	3HAA 500 µM	0	1348335	7	$y = 13483x + 7$	131768	**9.77238003**
3HAA 100	3HAA 100 µM	0	1348335	7	$y = 13483x + 7$	217355	**16.1201513**
3HAA 500 + 10 pg/ml IL1β	3HAA 500 µM	10 pg/ml IL1β	1348335	7	$y = 13483x + 7$	231496	**17.1689535**
3HAA 100 + 10 pg/ml IL1β	3HAA 100 µM	10 pg/ml IL1β	1348335	7	$y = 13483x + 7$	193265	**14.3334569**
3HAA 500 + 100 pg/ml IL1β	3HAA 500 µM	100 pg/ml IL1β	1348335	7	$y = 13483x + 7$	475989	**35.3023808**
3HAA 100 + 100 pg/ml IL1β	3HAA 100 µM	100 pg/ml IL1β	1348335	7	$y = 13483x + 7$	356704	**26.4553141**
XA 500	XA 500 µM	0	1348335	7	$y = 13483x + 7$	279024	**20.6939850**
XA 100	XA 100 µM	0	1348335	7	$y = 13483x + 7$	292596	**21.7005859**
XA 500 + 10 pg/ml IL1β	XA 500 µM	10 pg/ml IL1β	1348335	7	$y = 13483x + 7$	318012	**23.5856263**
XA 100 + 10 pg/ml IL1β	XA 100 µM	10 pg/ml IL1β	1348335	7	$y = 13483x + 7$	273270	**20.2672254**
XA 500 + 100 pg/ml IL1β	XA 500 µM	100 pg/ml IL1β	1348335	7	$y = 13483x + 7$	404891	**30.0292220**
XA 100 + 100 pg/ml IL1β	XA 100 µM	100 pg/ml IL1β	1348335	7	$y = 13483x + 7$	341966	**25.3622339**
TRP 500	TRP 500 µM	0	1359531	70	$y = 13595x + 70$	404478	**29.7468187**
TRP 100	TRP 100 µM	0	1359531	70	$y = 13595x + 70$	416655	**30.6425156**
TRP 500 + 10 pg/ml IL1β	TRP 500 µM	10 pg/ml IL1β	1359531	70	$y = 13595x + 70$	345513	**25.4095623**
TRP 100 + 10 pg/ml IL1β	TRP 100 µM	10 pg/ml IL1β	1359531	70	$y = 13595x + 70$	439572	**32.3282089**

TRP 500 + 100 pg/ml IL1β	TRP 500 µM	100 pg/ml IL1β	1359531	70	$y = 13595x + 70$	696195	**51.2044869**
TRP 100 + 100 pg/ml IL1β	TRP 100 µM	100 pg/ml IL1β	1359531	70	$y = 13595x + 70$	534770	**39.3306363**
KYN 500	KYN 500 µM	0	1359531	70	$y = 13595x + 70$	340050	**25.0077234**
KYN 100	KYN 100 µM	0	1359531	70	$y = 13595x + 70$	362444	**26.6549467**
KYN 500 + 10 pg/ml IL1β	KYN 500 µM	10 pg/ml IL1β	1359531	70	$y = 13595x + 70$	702186	**51.6451637**
KYN 100 + 10 pg/ml IL1β	KYN 100 µM	10 pg/ml IL1β	1359531	70	$y = 13595x + 70$	451193	**33.1830085**
KYN 500 + 100 pg/ml IL1β	KYN 500 µM	100 pg/ml IL1β	1359531	70	$y = 13595x + 70$	628324	**46.2121368**
KYN 100 + 100 pg/ml IL1β	KYN 100 µM	100 pg/ml IL1β	1359531	70	$y = 13595x + 70$	692992	**50.9688856**
KA 500	KA 500 µM	0	1359531	70	$y = 13595x + 70$	421085	**30.9683707**
KA 100	KA 100 µM	0	1359531	70	$y = 13595x + 70$	392738	**28.8832659**
KA 500 + 10 pg/ml IL1β	KA 500 µM	10 pg/ml IL1β	1359531	70	$y = 13595x + 70$	515471	**37.9110702**
KA 100 + 10 pg/ml IL1β	KA 100 µM	10 pg/ml IL1β	1359531	70	$y = 13595x + 70$	447545	**32.9146745**
KA 500 + 100 pg/ml IL1β	KA 500 µM	100 pg/ml IL1β	1359531	70	$y = 13595x + 70$	759733	**55.8781170**
KA 100 + 100 pg/ml IL1β	KA 100 µM	100 pg/ml IL1β	1359531	70	$y = 13595x + 70$	591316	**43.4899595**
3HK 500	3HK 500 µM	0	1359531	70	$y = 13595x + 70$	110663	**8.13482898**
3HK 100	3HK 100 µM	0	1359531	70	$y = 13595x + 70$	323780	**23.8109599**
3HK 500 + 10 pg/ml IL1β	3HK 500 µM	10 pg/ml IL1β	1359531	70	$y = 13595x + 70$	1843147	**135.5702100**
3HK 100 + 10 pg/ml IL1β	3HK 100 µM	10 pg/ml IL1β	1359531	70	$y = 13595x + 70$	416686	**30.6447959**
3HK 500 + 100 pg/ml IL1β	3HK 500 µM	100 pg/ml IL1β	1359531	70	$y = 13595x + 70$	1787523	**131.4787050**
3HK 100 + 100 pg/ml IL1β	3HK 100 µM	100 pg/ml IL1β	1359531	70	$y = 13595x + 70$	548743	**40.3584406**
3HAA 500	3HAA 500 µM	0	1359531	70	$y = 13595x + 70$	193656	**14.2394998**
3HAA 100	3HAA 100 µM	0	1359531	70	$y = 13595x + 70$	248706	**18.2887826**
3HAA 500 + 10 pg/ml IL1β	3HAA 500 µM	10 pg/ml IL1β	1359531	70	$y = 13595x + 70$	325505	**23.9378448**
3HAA 100 + 10 pg/ml IL1β	3HAA 100 µM	10 pg/ml IL1β	1359531	70	$y = 13595x + 70$	281943	**20.7335785**
3HAA 500 + 100 pg/ml IL1β	3HAA 500 µM	100 pg/ml IL1β	1359531	70	$y = 13595x + 70$	729841	**53.6793674**
3HAA 100 + 100 pg/ml IL1β	3HAA 100 µM	100 pg/ml IL1β	1359531	70	$y = 13595x + 70$	411546	**30.2667157**
XA 500	XA 500 µM	0	1359531	70	$y = 13595x + 70$	445393	**32.7563810**
XA 100	XA 100 µM	0	1359531	70	$y = 13595x + 70$	458372	**33.7110702**
XA 500 + 10 pg/ml IL1β	XA 500 µM	10 pg/ml IL1β	1359531	70	$y = 13595x + 70$	488688	**35.9410077**
XA 100 + 10 pg/ml IL1β	XA 100 µM	10 pg/ml IL1β	1359531	70	$y = 13595x + 70$	419463	**30.8490622**
XA 500 + 100 pg/ml IL1β	XA 500 µM	100 pg/ml IL1β	1359531	70	$y = 13595x + 70$	625252	**45.9861714**
XA 100 + 100 pg/ml IL1β	XA 100 µM	100 pg/ml IL1β	1359531	70	$y = 13595x + 70$	554658	**40.793527**
TRP 500	TRP 500 µM	0	1346238.5	49	$y = 13462x + 49$	397750	**29.5424900**
TRP 100	TRP 100 µM	0	1346238.5	49	$y = 13462x + 49$	391954	**29.1119447**
TRP 500 + 10 pg/ml IL1β	TRP 500 µM	10 pg/ml IL1β	1346238.5	49	$y = 13462x + 49$	492433	**36.5758431**
TRP 100 + 10 pg/ml IL1β	TRP 100 µM	10 pg/ml IL1β	1346238.5	49	$y = 13462x + 49$	480572	**35.6947705**
TRP 500 + 100 pg/ml IL1β	TRP 500 µM	100 pg/ml IL1β	1346238.5	49	$y = 13462x + 49$	711467	**52.8463824**
TRP 100 + 100 pg/ml IL1β	TRP 100 µM	100 pg/ml IL1β	1346238.5	49	$y = 13462x + 49$	673819	**50.0497697**
KYN 500	KYN 500 µM	0	1346238.5	49	$y = 13462x + 49$	372198	**27.6444065**
KYN 100	KYN 100 µM	0	1346238.5	49	$y = 13462x + 49$	344549	**25.5905512**
KYN 500 + 10 pg/ml IL1β	KYN 500 µM	10 pg/ml IL1β	1346238.5	49	$y = 13462x + 49$	430773	**31.995543**
KYN 100 + 10 pg/ml IL1β	KYN 100 µM	10 pg/ml IL1β	1346238.5	49	$y = 13462x + 49$	394645	**29.3118407**
KYN 500 + 100 pg/ml IL1β	KYN 500 µM	100 pg/ml IL1β	1346238.5	49	$y = 13462x + 49$	555263	**41.2430545**
KYN 100 + 100 pg/ml IL1β	KYN 100 µM	100 pg/ml IL1β	1346238.5	49	$y = 13462x + 49$	571832	**42.4738523**
KA 500	KA 500 µM	0	1346238.5	49	$y = 13462x + 49$	438820	**32.5932997**
KA 100	KA 100 µM	0	1346238.5	49	$y = 13462x + 49$	341860	**25.3908037**
KA 500 + 10 pg/ml IL1β	KA 500 µM	10 pg/ml IL1β	1346238.5	49	$y = 13462x + 49$	429088	**31.8703759**
KA 100 + 10 pg/ml IL1β	KA 100 µM	10 pg/ml IL1β	1346238.5	49	$y = 13462x + 49$	451023	**33.4997772**
KA 500 + 100 pg/ml IL1β	KA 500 µM	100 pg/ml IL1β	1346238.5	49	$y = 13462x + 49$	728606	**54.1195216**
KA 100 + 100 pg/ml IL1β	KA 100 µM	100 pg/ml IL1β	1346238.5	49	$y = 13462x + 49$	664607	**49.3654732**
3HK 500	3HK 500 µM	0	1346238.5	49	$y = 13462x + 49$	161654	**12.0045313**
3HK 100	3HK 100 µM	0	1346238.5	49	$y = 13462x + 49$	274952	**20.4206656**
3HK 500 + 10 pg/ml IL1β	3HK 500 µM	10 pg/ml IL1β	1346238.5	49	$y = 13462x + 49$	1501336	**111.520354**
3HK 100 + 10 pg/ml IL1β	3HK 100 µM	10 pg/ml IL1β	1346238.5	49	$y = 13462x + 49$	361385	**26.8411826**
3HK 500 + 100 pg/ml IL1β	3HK 500 µM	100 pg/ml IL1β	1346238.5	49	$y = 13462x + 49$	1647507	**122.378398**
3HK 100 + 100 pg/ml IL1β	3HK 100 µM	100 pg/ml IL1β	1346238.5	49	$y = 13462x + 49$	552757	**41.0569009**
3HAA 500	3HAA 500 µM	0	1346238.5	49	$y = 13462x + 49$	131019	**9.72886644**
3HAA 100	3HAA 100 µM	0	1346238.5	49	$y = 13462x + 49$	333698	**24.7845045**
3HAA 500 + 10 pg/ml IL1β	3HAA 500 µM	10 pg/ml IL1β	1346238.5	49	$y = 13462x + 49$	251909	**18.7089585**
3HAA 100 + 10 pg/ml IL1β	3HAA 100 µM	10 pg/ml IL1β	1346238.5	49	$y = 13462x + 49$	286270	**21.2614025**
3HAA 500 + 100 pg/ml IL1β	3HAA 500 µM	100 pg/ml IL1β	1346238.5	49	$y = 13462x + 49$	457057	**33.9480018**
3HAA 100 + 100 pg/ml IL1β	3HAA 100 µM	100 pg/ml IL1β	1346238.5	49	$y = 13462x + 49$	477803	**35.4890804**
XA 500	XA 500 µM	0	1346238.5	49	$y = 13462x + 49$	359489	**26.7003417**
XA 100	XA 100 µM	0	1346238.5	49	$y = 13462x + 49$	378585	**28.1188531**
XA 500 + 10 pg/ml IL1β	XA 500 µM	10 pg/ml IL1β	1346238.5	49	$y = 13462x + 49$	461130	**34.2505571**
XA 100 + 10 pg/ml IL1β	XA 100 µM	10 pg/ml IL1β	1346238.5	49	$y = 13462x + 49$	424551	**31.5333531**
XA 500 + 100 pg/ml IL1β	XA 500 µM	100 pg/ml IL1β	1346238.5	49	$y = 13462x + 49$	600402	**44.5961224**
XA 100 + 100 pg/ml IL1β	XA 100 µM	100 pg/ml IL1β	1346238.5	49	$y = 13462x + 49$	576857	**42.8471252**

Table 110. Endothelial cell caspase 3/7 study – data conversion to relative percentage of controls
Staurosporin 10 µM was used for positive control for caspase 3/7 activation. Negative control to gauge absence of luminescence was a 'no caspase reagent' reading of wells containing cells, medium and DMSO.